

Environmental Chemistry for a Sustainable World 57

Inamuddin
Mohd Imran Ahamed
Eric Lichtfouse *Editors*


Water Pollution and Remediation: Photocatalysis

 Springer

Environmental Chemistry for a Sustainable World

Volume 57

Series Editors

Eric Lichtfouse , Aix-Marseille University, CNRS, IRD, INRAE, Coll France, CEREGE, Aix-en-Provence, France

Jan Schwarzbauer, RWTH Aachen University, Aachen, Germany

Didier Robert, CNRS, European Laboratory for Catalysis and Surface Sciences, Saint-Avold, France

Other Publications by the Editors

Books

Environmental Chemistry

<http://www.springer.com/978-3-540-22860-8>

Organic Contaminants in Riverine and Groundwater Systems

<http://www.springer.com/978-3-540-31169-0>

Sustainable Agriculture

Volume 1: <http://www.springer.com/978-90-481-2665-1>

Volume 2: <http://www.springer.com/978-94-007-0393-3>

Book series

Environmental Chemistry for a Sustainable World

<http://www.springer.com/series/11480>

Sustainable Agriculture Reviews

<http://www.springer.com/series/8380>

Journals

Environmental Chemistry Letters

<http://www.springer.com/10311>

More information about this series at <http://www.springer.com/series/11480>

Inamuddin • Mohd Imran Ahamed
Eric Lichtfouse
Editors


Water Pollution and Remediation: Photocatalysis

 Springer

Editors

Inamuddin
Department of Applied Chemistry
Aligarh Muslim University
Aligarh, India

Mohd Imran Ahamed
Department of Chemistry
Aligarh Muslim University
Aligarh, India

Eric Lichtfouse 
Aix-Marseille University, CNRS,
IRD, INRAE, Coll France, CEREGE
Aix-en-Provence, France

ISSN 2213-7114

ISSN 2213-7122 (electronic)

Environmental Chemistry for a Sustainable World

ISBN 978-3-030-54722-6

ISBN 978-3-030-54723-3 (eBook)

<https://doi.org/10.1007/978-3-030-54723-3>

© The Editor(s) (if applicable) and The Author(s), under exclusive license to Springer Nature Switzerland AG 2021

This work is subject to copyright. All rights are solely and exclusively licensed by the Publisher, whether the whole or part of the material is concerned, specifically the rights of translation, reprinting, reuse of illustrations, recitation, broadcasting, reproduction on microfilms or in any other physical way, and transmission or information storage and retrieval, electronic adaptation, computer software, or by similar or dissimilar methodology now known or hereafter developed.

The use of general descriptive names, registered names, trademarks, service marks, etc. in this publication does not imply, even in the absence of a specific statement, that such names are exempt from the relevant protective laws and regulations and therefore free for general use.

The publisher, the authors, and the editors are safe to assume that the advice and information in this book are believed to be true and accurate at the date of publication. Neither the publisher nor the authors or the editors give a warranty, expressed or implied, with respect to the material contained herein or for any errors or omissions that may have been made. The publisher remains neutral with regard to jurisdictional claims in published maps and institutional affiliations.

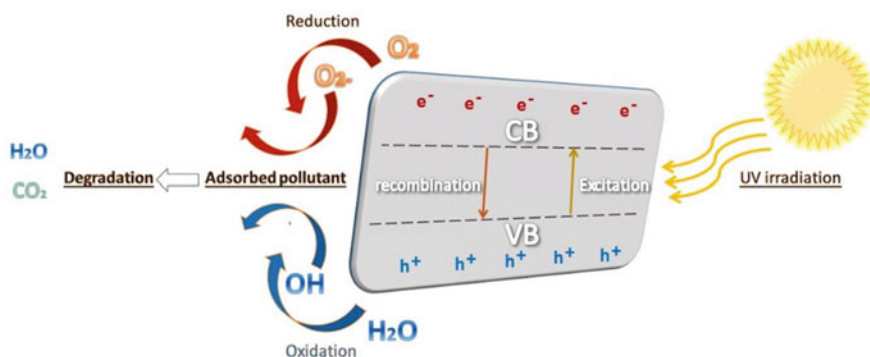
This Springer imprint is published by the registered company Springer Nature Switzerland AG
The registered company address is: Gewerbestrasse 11, 6330 Cham, Switzerland

Preface

Every 24 hours, enough sunlight touches the Earth to provide the energy for the entire planet for 24 years

Martha Maeda

Urbanization and industrialization are producing large volumes of wastewater containing various contaminants. If not treated properly, these contaminants induce adverse effects on health and socio-economic activities. Photocatalysis is a very promising light-driven technique for wastewater treatment. This book reviews advanced photocatalytic techniques for the removal of pollutants. In particular, chapters describe the basic mechanisms and types of photocatalysis and the advantages and disadvantages of photocatalysis for wastewater treatment, purification, and desalination. This book is an excellent reference guide for students, faculty, researchers, and professionals in the field of environmental science, photochemistry, semiconductors, and material science.



Chapter 1 by Kemacheevakul and Chuangchote details several photocatalysis-based technologies for remediation of organic pollutants in water, including (1) pharmaceuticals and personal care products, (2) persistent organic pollutants, and (3) organic dyes. Additionally, modifications of heterogeneous photocatalysts by doping, composites, and utilization of electrical potential in photocatalysis with various reactor configurations for wastewater treatment are also presented. Chapter 2 by Raizada et al. discusses the design and synthesis of visible-light responsive g-C₃N₄ photocatalysts in heterojunction with metal oxides of iron and copper for its insightful potential in water treatment and microbial disinfection. The major goal is to communicate benefits obtained by metal oxides heterojunction for improving photocatalytic degradation ability of g-C₃N₄. Chapter 3 by Shandilya et al. aims to explain basic knowledge of carbon quantum dots and their classification. Several top-down and bottom-up synthetic routes for the preparation of carbon quantum dots are discussed in detail. Followed by a brief discussion of up-conversion phenomena in carbon quantum dots. Further, their photocatalytic and antibacterial activity is also discussed in detail. Chapter 4 by Shandilya et al. concisely discusses the basic mechanism of photocatalysis, disadvantages of conventional methods, and general classification of azo dyes. Moreover, the advantages of exploring photocatalysis for azo dye removal are also discussed briefly. Binary, ternary, coupled semiconductor and carbon-supported material employed for the photodegradation of azo dyes are also discussed.

Chapter 5 by Merouani et al. details various experimental and theoretical signs of the progress of sonochemistry for the production of hydrogen. Factors influencing the sonochemical production of hydrogen are discussed in detail. The progress reported herein allows to determine some interesting tendencies and perspectives for this research but also highlights some needs for innovation. Chapter 6 by Chakma et al. provides a brief introduction of various sono-hybrid advanced oxidation processes for the treatment of recalcitrant pollutants. It mainly describes the synergistic mechanism of degradation process with the help of the physical and chemical effects of ultrasound and cavitation. The chapter also provides information about the influences of process parameters as well as the negative synergism in hybrid advanced oxidation processes. Chapter 7 by Ambaye discusses the recent applications of low dimensional nanostructured photocatalysts and their preparation, characterization, and efficiency for the disinfection of pathogenic microorganisms. It also highlights the processing mechanism of the photo-generated reactive oxygen species for the disinfection of pathogenic microorganisms and the effect of the chemical characteristics of the water matrix to apply on a large scale. Chapter 8 by Kapoor et al. provides necessary information on various membrane processes including developing processes forward osmosis and membrane distillation to enable the selection of an appropriate membrane process for water purification, desalination, wastewater treatment, and removal of toxic contaminants. The concept of decentralization of waste-water treatment is proposed to recover value and ensure a better environment. Chapter 9 by Chahkandi and Zargazi explains the importance of new applicable nanomaterials toward fundamentals of thermodynamics, kinetical reactions, recombination rate, and the usage methods of UV/Visible light sensitive

photocatalysts in water splitting, energy generation, and environmental concerns. The appropriate composited photocatalysts bring properties within the minimization of recombination rate and enhanced efficiency for applicable prospects and commercialization.

Chapter 10 by Zargazi and Chahkandi discusses the importance of doublet and triplet Bi-photocatalytic compounds, including appropriate and narrow bandgap activated by visible light, layered morphology to gain high separation photogenerated charges, having various morphologies from zero-dimensional to hierarchical structures effective in light-harvesting, and composition with other semiconductors to generate heterojunctions with high photocatalytic performance. Chapter 11 by Tripathi and Narayanan describes the characteristics and toxicity profile of tannery effluent. Various conventional and modern treatment methodologies have been discussed in detail. The major focus is given to the solar photocatalytic process, the influence of various factors, and the design of photocatalytic reactor systems. Chapter 12 by Patle et al. discusses ionic liquids and functionalized ionic liquids with the recent applications of the latter in the treatment of wastewater, particularly containing different dyes. Later, a case study on the photodegradation of organic dyes, namely methylene blue and Congo red using a polymer-supported ionic liquid Fe-porphyrin complex, is presented. Chapter 13 by Orbeci investigates the opportunity to use photocatalytic oxidation to remove chlorophenols and antibiotics from wastewater.

Aligarh, India

Inamuddin

Aligarh, India

Mohd Imran Ahamed

Aix-en-Provence, France

Eric Lichtfouse

Contents

| | | |
|----------|--|------------|
| 1 | Photocatalytic Remediation of Organic Pollutants in Water | 1 |
| | Patiya Kemacheevakul and Surawut Chuangchote | |
| 2 | Carbon Nitride/Metal Oxide Hybrids for Visible Light Harvesting and Water Remediation | 53 |
| | Pankaj Raizada, Vasudha Hasija, Pardeep Singh, and Vijay Kumar Thakur | |
| 3 | Metal and Carbon Quantum Dot Photocatalysts for Water Purification | 81 |
| | Pooja Shandilya, Pankaj Raizada, Anita Sudhaik, Adesh Saini, Reena Saini, and Pardeep Singh | |
| 4 | Photocatalytic Degradation of Azo Dyes in Water | 119 |
| | Pooja Shandilya, Pankaj Raizada, and Pardeep Singh | |
| 5 | Sonochemical Treatment of Textile Wastewater | 147 |
| | Slimane Merouani and Oualid Hamdaoui | |
| 6 | Degradation Mechanism of Pollutants Using Sono-hybrid Advanced Oxidation Processes | 189 |
| | Sankar Chakma, Prachi Upadhyay, and Bablu Alawa | |
| 7 | Photocatalytic Nanomaterials for Bacterial Disinfection | 215 |
| | Teklit Gebregiorgis Ambaye, Mentore Vaccari, and Eric D. van Hullebusch | |
| 8 | Role of Membranes in Wastewater Treatment | 247 |
| | Ashish Kapoor, Sivasamy Balasubramanian, Edward Kavitha, Elangovan Poonguzhali, and Sivaraman Prabhakar | |
| 9 | Nanomaterials for the Photoremediation of Pollutants | 283 |
| | Mohammad Chahkandi and Mahboobeh Zargazi | |

| | |
|--|------------|
| 10 Bismuth-Based Compounds as Visible Light Photocatalyst for Remediation and Water Splitting | 321 |
| Mahboobeh Zargazi and Mohammad Chahkandi | |
| 11 Solar Photocatalytic Treatment of Tannery Effluents | 359 |
| Alok Tripathi and Sheeba Narayanan | |
| 12 Functionalized Ionic Liquids for the Photodegradation of Dyes | 391 |
| Dipesh S. Patle, Vijay Khajone, Pundlik R. Bhagat, Arvind K. Jaiswal, and Sushil Kumar | |
| 13 Photocatalytic Degradation of Chlorophenols and Antibiotics from Wastewater | 411 |
| Cristina Orbeci, Constantin Bobiričă, and Liliana Bobiričă | |
| Index | 431 |

About the Editors

Inamuddin PhD, is an Assistant Professor at the Department of Applied Chemistry, Aligarh Muslim University, Aligarh, India. He has extensive research experience in multidisciplinary fields of analytical chemistry, materials chemistry, electrochemistry, renewable energy, and environmental science. He has published about 175 research articles in various international scientific journals, 18 book chapters, and 110 edited books with multiple well-known publishers. His current research interests include ion-exchange materials, a sensor for heavy metal ions, biofuel cells, supercapacitors, and bending actuators.

Mohd Imran Ahamed received his Ph.D. degree on the topic “Synthesis and characterization of inorganic-organic composite heavy metals selective cation-exchangers and their analytical applications,” from Aligarh Muslim University, Aligarh, India, in 2019. He has published several research and review articles in the journals of international recognition. His research works include ion-exchange chromatography, wastewater treatment and analysis, bending actuator, and electrospinning.

Eric Lichtfouse is a biogeochemist at Aix Marseille University who has invented carbon-13 dating, a molecular-level method allowing to study the dynamics of organic compounds in temporal pools of complex environmental media. He is the Chief Editor of the journal *Environmental Chemistry Letters* and the book series Sustainable Agriculture Reviews and Environmental Chemistry for a Sustainable World. He is the author of the book *Scientific Writing for Impact Factor Journals*, which includes an innovative writing tool: the Micro-Article.

Contributors

Bablu Alawa Department of Chemical Engineering, Indian Institute of Science Education and Research Bhopal, Bhopal, Madhya Pradesh, India

Teklit Gebregiorgis Ambaye Department of Civil, Environmental, Architectural Engineering and Mathematics, University of Brescia, Brescia, Italy
Department of Chemistry, Mekelle University, Mekelle, Ethiopia

Sivasamy Balasubramanian Department of Chemical Engineering, SRM Institute of Science and Technology, Kattankulathur, Tamil Nadu, India

Pundlik R. Bhagat School of Advance Science, Vellore Institute of Technology, Vellore, Tamil Nadu, India

Constantin Bobirică Department of Analytical Chemistry and Environmental Engineering, University Politehnica of Bucharest, Bucharest, Romania

Liliana Bobirică Department of Analytical Chemistry and Environmental Engineering, University Politehnica of Bucharest, Bucharest, Romania

Mohammad Chahkandi Department of Chemistry, Hakim Sabzevari University, Sabzevar, Iran

Sankar Chakma Department of Chemical Engineering, Indian Institute of Science Education and Research Bhopal, Bhopal, Madhya Pradesh, India

Surawut Chuangchote Research Center of Advanced Materials for Energy and Environmental Technology (MEET), King Mongkut's University of Technology Thonburi, Bangkok, Thailand

Department of Tool and Materials Engineering, Faculty of Engineering, King Mongkut's University of Technology Thonburi, Bangkok, Thailand

Oualid Hamdaoui Chemical Engineering Department, College of Engineering, King Saud University, Riyadh, Saudi Arabia

Vasudha Hasija School of Chemistry, Faculty of Basic Sciences, Shoolini University, Solan, Himachal Pradesh, India

Arvind K. Jaiswal Department of Chemical Engineering, Motilal Nehru National Institute of Technology, Allahabad, Prayagraj, Uttar Pradesh, India

Ashish Kapoor Department of Chemical Engineering, SRM Institute of Science and Technology, Kattankulathur, Tamil Nadu, India

Edward Kavitha Department of Chemical Engineering, SRM Institute of Science and Technology, Kattankulathur, Tamil Nadu, India

Patiya Kemacheevakul Department of Environmental Engineering, Faculty of Engineering, King Mongkut's University of Technology Thonburi, Bangkok, Thailand

Center of Excellence on Hazardous Substance Management (HSM), Bangkok, Thailand

Research Center of Advanced Materials for Energy and Environmental Technology (MEET), King Mongkut's University of Technology Thonburi, Bangkok, Thailand

Vijay Khajone School of Advance Science, Vellore Institute of Technology, Vellore, Tamil Nadu, India

Sushil Kumar Department of Chemical Engineering, Motilal Nehru National Institute of Technology, Allahabad, Prayagraj, Uttar Pradesh, India

Slimane Merouani Laboratory of Environmental Process Engineering, Department of Chemical Engineering, Faculty of Process Engineering, Salah Boubnider Constantine 3 University, Constantine, Algeria

Sheeba Narayanan Department of Chemical Engineering, National Institute of Technology, Tiruchirappalli, India

Cristina Orbeci Department of Analytical Chemistry and Environmental Engineering, University Politehnica of Bucharest, Bucharest, Romania

Dipesh S. Patle Department of Chemical Engineering, Motilal Nehru National Institute of Technology, Allahabad, Prayagraj, Uttar Pradesh, India

Elangovan Poonguzhali Department of Chemical Engineering, SRM Institute of Science and Technology, Kattankulathur, Tamil Nadu, India

Sivaraman Prabhakar Department of Chemical Engineering, SRM Institute of Science and Technology, Kattankulathur, Tamil Nadu, India

Pankaj Raizada School of Chemistry, Faculty of Basic Sciences, Shoolini University, Solan, HP, India

Himalayan Centre for Excellence in Nanotechnology, Shoolini University, Solan, HP, India

School of Biological Sciences, Faculty of Basic Sciences, Shoolini University, Solan, HP, India

Adesh Saini Himalayan Centre for Excellence in Nanotechnology, Shoolini University, Solan, Himachal Pradesh, India

School of Biological and Environmental Sciences, Faculty of Basic Sciences, Shoolini University, Solan, Himachal Pradesh, India

Reena Saini School of Biotechnology, Faculty of Applied Science and Biotechnology, Shoolini University, Solan, Himachal Pradesh, India

Pooja Shandilya School of Chemistry, Faculty of Basic Sciences, Shoolini University, Solan, HP, India

Himalayan Centre for Excellence in Nanotechnology, Shoolini University, Solan, HP, India

School of Biological Sciences, Faculty of Basic Sciences, Shoolini University, Solan, HP, India

Pardeep Singh School of Chemistry, Faculty of Basic Sciences, Shoolini University, Solan, HP, India

Himalayan Centre for Excellence in Nanotechnology, Shoolini University, Solan, HP, India

School of Biological Sciences, Faculty of Basic Sciences, Shoolini University, Solan, HP, India

Anita Sudhaik School of Chemistry, Faculty of Basic Sciences, Shoolini University, Solan, Himachal Pradesh, India

Vijay Kumar Thakur Biorefining and Advanced Materials Research Centre, Scotland's Rural College (SRUC), Edinburgh, UK

Alok Tripathi Department of Chemical Engineering, National Institute of Technology, Tiruchirappalli, India

Prachi Upadhyay Department of Chemical Engineering, Indian Institute of Science Education and Research Bhopal, Bhopal, Madhya Pradesh, India

Mentore Vaccari Department of Civil, Environmental, Architectural Engineering and Mathematics, University of Brescia, Brescia, Italy

Eric D. van Hullebusch Université de Paris, Institut de Physique du Globe de Paris, CNRS, Paris, France

Mahboobeh Zargazi Department of Chemistry, Faculty of Science, Ferdowsi University of Mashhad, Mashhad, Iran

Chapter 1

Photocatalytic Remediation of Organic Pollutants in Water



Patiya Kemacheevakul and Surawut Chuangchote

Contents

| | | |
|-------|---|----|
| 1.1 | Introduction | 2 |
| 1.2 | Photocatalysis | 3 |
| 1.2.1 | Type of Photocatalysis | 3 |
| 1.2.2 | Photocatalytic Process | 11 |
| 1.3 | Organic Pollutants in Water | 12 |
| 1.3.1 | Sources of Organic Pollutants in Wastewater | 12 |
| 1.3.2 | Major Groups of Organic Pollutants in Wastewater | 15 |
| 1.4 | Photocatalytic Remediation of Organic Pollutants in Water | 23 |
| 1.4.1 | Homogeneous Photocatalysis | 23 |
| 1.4.2 | Heterogeneous Photocatalysis | 25 |
| 1.5 | Modifications of Heterogeneous Photocatalysts | 29 |
| 1.5.1 | Doping | 30 |
| 1.5.2 | Composite of Semiconductors | 34 |
| 1.5.3 | Photoelectrodes in Photo-Electrocatalytic Process | 37 |
| 1.6 | Photocatalytic Reactors for Remediation of Organic Pollutants | 38 |
| 1.7 | Conclusions | 39 |
| | References | 40 |

P. Kemacheevakul

Department of Environmental Engineering, Faculty of Engineering, King Mongkut's University of Technology Thonburi, Bangkok, Thailand

Center of Excellence on Hazardous Substance Management (HSM), Bangkok, Thailand

Research Center of Advanced Materials for Energy and Environmental Technology (MEET), King Mongkut's University of Technology Thonburi, Bangkok, Thailand

e-mail: patiya.kem@kmutt.ac.th

S. Chuangchote (✉)

Research Center of Advanced Materials for Energy and Environmental Technology (MEET), King Mongkut's University of Technology Thonburi, Bangkok, Thailand

Department of Tool and Materials Engineering, Faculty of Engineering, King Mongkut's University of Technology Thonburi, Bangkok, Thailand

e-mail: surawut.chu@kmutt.ac.th

© The Editor(s) (if applicable) and The Author(s), under exclusive license to Springer Nature Switzerland AG 2021

Inamuddin et al. (eds.), *Water Pollution and Remediation: Photocatalysis*,

Environmental Chemistry for a Sustainable World 57,

https://doi.org/10.1007/978-3-030-54723-3_1

Abstract Water resource is the most precious resource for a human being that it is necessary to make the water resource to be clean and also non-toxic. Recently, water pollution becomes one of the most serious global issues, especially, water pollutions that contaminate various types of organic compounds, including pharmaceuticals and personal care products (PPCPs), persistent organic pollutants (POPs), and organic dyes. Photocatalysis as one of the advanced oxidation processes using reactive oxidative radicals or species to remediate the organic pollutants has drawn much attention recently.

Photocatalysis is a process which a chemical reaction is accelerated in the presence of a catalyst on exposure to light. The possibility to utilize solar energy as a free energy from nature to solve the environmental problems is the key significance of photocatalysis. Homogeneous photocatalysis has many advantages, e.g., high oxidation properties. It is, however, not popular in various photocatalytic applications, because it is difficult to separate the photocatalysts from the solution, the photocatalysts have low potential to reuse, purification of products is necessary, and almost homogeneous photocatalysts absorb narrowly light within the solar spectrum. It has been proven that heterogeneous photocatalysis is one of the most potential methods for treatment of organic pollutants in water. Anyhow, relatively large band gap energy causes some limitations of metal oxide-based heterogeneous photocatalysts. Modifications of the electronic band can be achieved by doping and composites of semiconductors. Another modification technique in heterogeneous photocatalysts is the utilization of electrical potential in photocatalysis. The coated semiconductor photocatalysts are used as photoelectrodes in photo-electrocatalytic applications. In addition, the photocatalytic reactor configuration for wastewater treatment by heterogeneous photocatalysis can be classified as two main groups, including fixed bed reactor and slurry type reactor. Apart from the conventional photocatalytic reactors, the combination of photocatalysis with another treatment process has also been developed to overcome the specific obstacles in each case, such as a photocatalytic membrane reactor.

Keywords Photocatalysis · Photocatalysts · Organic pollutants · Personal care products · Persistent organic pollutants · Organic dyes · Remediation · Ozonation · Fenton · Metal oxide

1.1 Introduction

Water resource is the most precious resource for a human being that it is necessary to make the water resource to be clean and also non-toxic. Anyway, due to urbanization, industrialization, and lack of people awareness to consider water as a crucial commodity, people in many countries are now facing problems related to water supply and security (Jayaswal et. al 2018; Meenakshisundaram 2019). Presently,

water pollution becomes one of the most serious global issues, especially, water pollutions that contaminate various types of organic compounds (Meenakshisundaram 2019), including pharmaceuticals and personal care products, persistent organic pollutants, and organic dyes.

In recent years, many researchers have developed the remediation techniques of organic pollutants in water. Photocatalysis, as one of the advanced oxidation processes (AOPs) using reactive oxidative radicals or species, particularly hydroxyl radicals, to remediate the organic pollutants, has drawn much attention recently. Various types of photocatalysis can be considered to be a green and effective strategy for solving global environmental and energy problems. The possibility to utilize solar energy as a free energy from nature to solve the environmental problems is the key significance of photocatalysis. In this chapter, the basic concept of photocatalysis, various organic pollutants in water, photocatalytic remediation of organic pollutants in water, and modifications of heterogeneous photocatalysts are discussed. Recent developments of photocatalytic reactors for remediation of organic pollutants are presented briefly.

1.2 Photocatalysis

Photocatalysis is a type of catalysis which a chemical reaction is accelerated in the presence of a catalyst (so-called photocatalyst) on exposure to light which is mostly described in term of photon ($h\nu$) – an elementary particle of light, where the photocatalyst participates in the chemical reaction without being consumed. Photocatalysis can be also defined as the acceleration of a photoreaction (e.g., photolysis) in the presence of a catalyst.

1.2.1 Type of Photocatalysis

Photocatalysis could be classified to be two types, i.e., homogeneous and heterogeneous photocatalysis, on the basis of appearances of the physical state of reactants.

Homogenous Photocatalysis

Homogeneous photocatalysis is the process that the photocatalyst is in the same phase (i.e., gas, solid, or liquid) with the reactant. The process of homogenous photocatalysis is driven under exposure to light which a molecular photocatalyst is promoted to the excited state (strong reductant and oxidant). Almost homogeneous photocatalysts can drive full redox reactions which most researchers use in water splitting to hydrogen and oxygen.

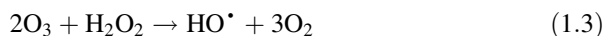
In homogeneous photocatalysis, the free radicals are produced by illumination of light over the homogeneous molecules of oxidizing agents such as hydrogen peroxide (H_2O_2) and ozone (O_3), which are dissolved in water or another medium (Stan et al. 2012). The commonly known processes are ozonation (UV/O_3), photo-Fenton processes (Fe^{2+} and $\text{Fe}^{2+}/\text{H}_2\text{O}_2$), $\text{UV}/\text{H}_2\text{O}_2$, and $\text{UV}/\text{H}_2\text{O}_2/\text{O}_3$.

Ozonation

Ozone, an unstable gas composed of three oxygen atoms (O_3) that is a strong greenhouse gas and variable in the troposphere, becomes one of the most powerful oxidants with an oxidation potential of 2.07 V (North 2015). Ozone is often used in water and wastewater treatments, municipal and industrial treatments, agriculture, chemical synthesis, drinking water disinfection, and food and beverage (Ikehata and Li 2018; Loeb et al. 2012). Ozone can be generated by promoting potential energy, e.g., ultraviolet irradiation or electric discharge, to gaseous oxygen molecules. In terms of the process of ozone, it can react and decompose into various oxidative species, e.g., hydroxyl radical (HO^\bullet) and hydrogen peroxide (H_2O_2), leading to the ozonation process.

Ozonation is the oxidation method which ozone involves in the process. It is extremely used for water treatment that enormous contaminants (e.g., color substances and heavy metals) contained in the water sources. Furthermore, outgrowths of ozonation are bacteria disinfection, odorous removal, taste generation, inorganic component conversions, and cutting of hardly biodegradable organic compounds (Arvanitoyannis and Kassaveti 2008). Ozonation can be more effective with UV radiation and oxidizing agents that increase radical formations.

UV/Ozone (UV/O_3) is one of the well-studied ozonation. Dissolved ozone molecules can absorb UV light (wavelength ~ 260 nm) by photolysis reaction, leading to the occurrence of hydrogen peroxide molecules (Eq. 1.1). Afterward, each mole of H_2O_2 will turn to absorb UV or react with O_3 , resulting in the generation of HO^\bullet as expressed in Eqs. (1.2) and (1.3) (Gong et al. 2008; Ikehata and Li 2018).



Ozonation has various advantages, such as the short half-life (~ 10 min) leading to the rapid reaction for degradation of organic molecules (Table 1.1). Anyway, unless at pH 10, the half-life of ozone in solution is less than 1 min that makes ozonation extensively consumes energy. The efficiency of this process depends on many

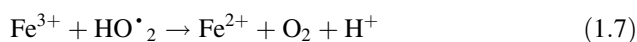
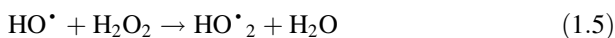
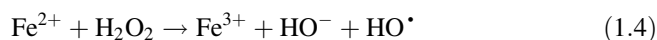
Table 1.1 Advantages and disadvantages of ozonation

| Advantage | Disadvantage |
|---|-------------------------|
| Efficient organic, inorganic, color, taste, and odor removals | High costs |
| Rapid reaction for degradation of organic molecules | Toxicity |
| No chemical contamination and residual effect | High-energy consumption |

variables such as UV light intensity, reactant constituent, the presence of scavenger species, pH, temperature, and type of organic target pollutants.

Photo-Fenton Process

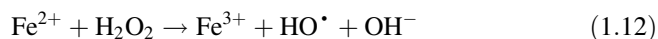
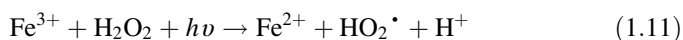
H₂O₂ is usually used as oxidizing agents because of its environmentally benign and uncomplicated characters. Various metal ions and their oxidative forms, such as Fe²⁺, Fe³⁺, Cu⁺, Cu²⁺, Ti³⁺, Ti⁴⁺, Cr²⁺, and Cr³⁺, can be used as a catalyst in H₂O₂-based processes. Notwithstanding, Fe²⁺ and Fe³⁺ are most frequently used, because other metal ions are toxic and relatively unavailable. Fenton is one of several processes that can enhance the oxidative potential of H₂O₂ which can be used for the degradation of organic compounds. Fenton uses Fe²⁺ [ferrous ions or iron (II)] as a catalyst under acidic conditions according to Eqs. (1.4)–(1.9) (Ameta et al. 2018a).



In Fenton reactions, hydroxyl radicals (HO[•]) and hydroxide anions (HO[−]), the oxidizing and extremely powerful species, can be generated to discharge one electron from an electron-rich organic substrates or any other species present in the medium to form hydroxide anions. HO[•] produced from the reactions can also attack and degrade a wide range of organic compounds. The efficiency of Fenton

oxidation depends on pH, concentrations of the pollutants and hydrogen peroxide, amount of ferrous ions, and temperature (Zheng et al. 2013; Ameta et al. 2018a).

In term of photocatalysis, photo-Fenton process is a combination of Fenton reactions and irradiation with light of suitable wavelength (180–400 nm) which can accelerate the formation of hydroxyl radicals and also increases the rate of degradation of organic pollutants. The continuous cycles of photo-Fenton process are shown in Eqs. (1.10)–(1.12). Fe^{2+} is generated through photoreduction of ferric ions (Fe^{3+}). The generated Fe^{2+} will turn to react with H_2O_2 resulting in more HO^\bullet formation.

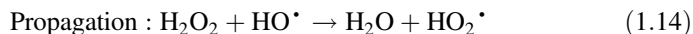


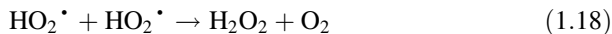
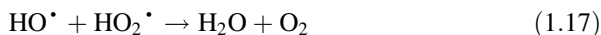
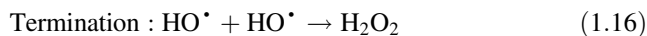
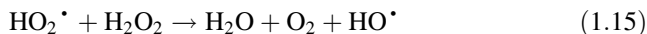
The efficiency of photo-Fenton process depends on pH, especially at pH 3, due to the soluble of hydroxy- Fe^{3+} complexes and $\text{Fe}(\text{OH})^{2+}$ leading to high catalytic activity (Ameta et al. 2018b).

UV/ H_2O_2

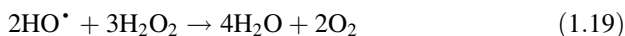
Normally, UV radiation can work simultaneously as a disinfectant, by physical inactivation of microorganisms (Mierzwa et al. 2018). UV radiation can be also used in UV/ H_2O_2 system for hemolytic cleavage of O-O bonds of H_2O_2 molecules, resulting in the production of hydroxyl radicals (HO^\bullet). The most application of UV/ H_2O_2 is uses for water and wastewater treatments.

UV/ H_2O_2 has three main reaction mechanisms of HO^\bullet production and recombination, which are initiation, propagation, and termination as shown in Eqs. (1.13)–(1.18). One mole of H_2O_2 theoretically produces two moles of HO^\bullet . The rate of HO^\bullet production strongly depends on the amount of H_2O_2 added, UV absorptivity of H_2O_2 , and characteristics of wastewater (Jamil et al. 2017; Mierzwa et al. 2018).





H_2O_2 molecules can act as a scavenger to consume HO^\bullet and subsequently produces oxygen and water molecules according to Eq. (1.19), so the demand concentration of H_2O_2 must be high to generate a sufficiently high concentration of HO^\bullet for decomposition and mineralization of organic target pollutants.



UV/ H_2O_2 / O_3

From ozonation discussed above, although UV absorptivity of O_3 is much higher than H_2O_2 , the self-decay rate of O_3 is approximately 1000 times higher than that of H_2O_2 . This limitation can be overcome by the addition of H_2O_2 into UV/ O_3 process for enhancement of the decomposition of O_3 , which is called “UV/ H_2O_2 / O_3 ” process.

Even though homogeneous photocatalysis has many advantages, e.g., high oxidation properties, it is, however, not popular in various photocatalytic applications. This is because it is difficult to separate the photocatalysts from the solution; the photocatalysts have a low potential to reuse; purification of products is necessary; and almost homogeneous photocatalysts absorb narrowly light within the solar spectrum (Karimian et al. 2015; Zhu and Wang 2017). In addition, the photocatalytic activity and stability of homogeneous photocatalysts are limited due to the instability inherent to the molecular nature of their structures (Limburg et al. 2016; Ye et al. 2016).

Heterogeneous Photocatalysis

Many years ago, heterogeneous photocatalysis was found by Fujishima and Honda due to an electrochemical photocatalysis of water at a semiconductor electrode. In heterogeneous photocatalysis, the catalyst is totally separate from the reactants. It occurs by emerging materials with supremacy properties (Klavarioti et al. 2009). On the basis of band gap energy – the differential energy between the valence band (the

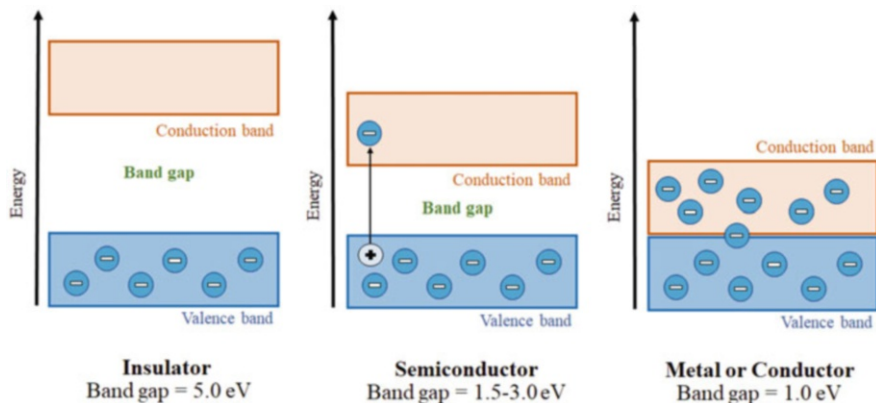


Fig. 1.1 Three basic categories of materials on the basis of band gap energy. In an insulator, there exists a large forbidden gap or band gap between the conduction band and valence band, so electrons cannot jump from the valence band to the conduction band. While the band gap in a semiconductor is narrower, so the energy provided at room temperature is sufficient to lift the electrons to the conduction band. In a metal or a conductor, there is no band gap, so the electrons can easily move in the space between the atoms

highest occupied molecular orbital, HOMO) and the conduction band (the lowest unoccupied molecular orbital, LUMO) – the materials are classified into three basic categories (Fig. 1.1). Normally, heterogeneous photocatalysts are semiconductor materials (i.e., metal oxides), because semiconductor can absorb light to activate the movement of electrons, which causes the generation of the reactive species. The reactive species in heterogeneous photocatalysis is used in a different way compared with those in homogeneous photocatalysts (Wu and Chang 2006). Heterogeneous photocatalysis occurs with several reactions, e.g., oxidation, dehydrogenation, metal deposition, water detoxification, and gaseous pollutant removals. Figure 1.2 shows an example of heterogeneous photocatalysis for hydrogen production from water.

Heterogeneous photocatalysis is generally carried out by utilizations of metal oxides as photocatalysts in the form of suspended phase or immobilized state (on other solid substrates). The illumination of light over the heterogeneous photocatalyst by photons with energy at least equal to its band gap energy can generate the electron–hole pairs. The photo-activated electrons are transferred from the valence band to the conduction band, leaving the positive holes in the valence band. Subsequently, the photo-activated electrons and holes can migrate from bulk to the surface of photocatalyst and react with some adsorbed substances on the surface to generate the free radicals (Srisasiwimon et al. 2018). Table 1.2 shows typical photocatalysts which are normally nanosized semiconductor materials with wide band gap energies (e.g., TiO_2 , ZnO , and SnO_2) (Bensebaa 2013; Yemmireddy and Hung 2017).

Fig. 1.2 Hydrogen production from water using heterogeneous powder photocatalysts. The photocatalysts are dispersed in a reactor with water. Sun or light shines at the dispersed photocatalysts, and then hydrogen is obtained (modified after (Kudo and Miseki 2009))

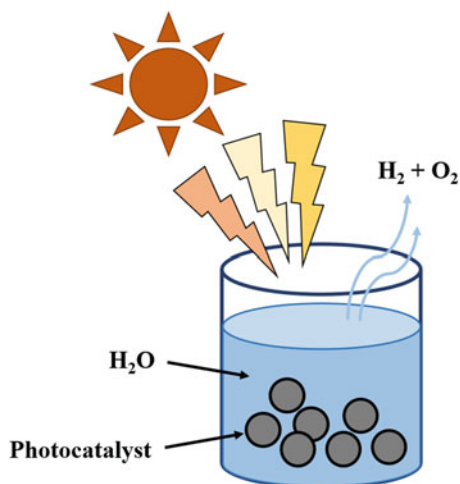


Table 1.2 Typical photocatalysts for photocatalysis

| Photocatalyst | Band gap (eV) | Spectral region |
|----------------------------|---------------|-----------------|
| ZnS | 3.80 | UV |
| SnO ₂ | 3.80 | UV |
| TiO ₂ (anatase) | 3.24 | UV |
| ZnO | 3.20 | UV |
| TiO ₂ (rutile) | 3.02 | UV and Visible |
| CdS | 2.40 | UV and Visible |
| Cu ₂ O | 2.20 | UV and Visible |

Oxidative Reactions

Typical photocatalysts, i.e., metal oxides (MO), such as oxides of titanium, zinc, tungsten, vanadium, chromium, and vanadium, can absorb photons to generate the photo-excited electrons and positive holes as expressed in Eq. (1.20). In the presence of water molecules, hydroxyl radicals (HO^\bullet) are produced by a reaction between positive holes and H_2O according to Eq. (1.21) (Fig. 1.3). Furthermore, H_2O_2 is possibly formed through the oxidative pathway, leading to the HO^\bullet generation from the cleavage of H_2O_2 under photolysis as shown in Eqs. (1.22)–(1.23) (Li et al. 2014).



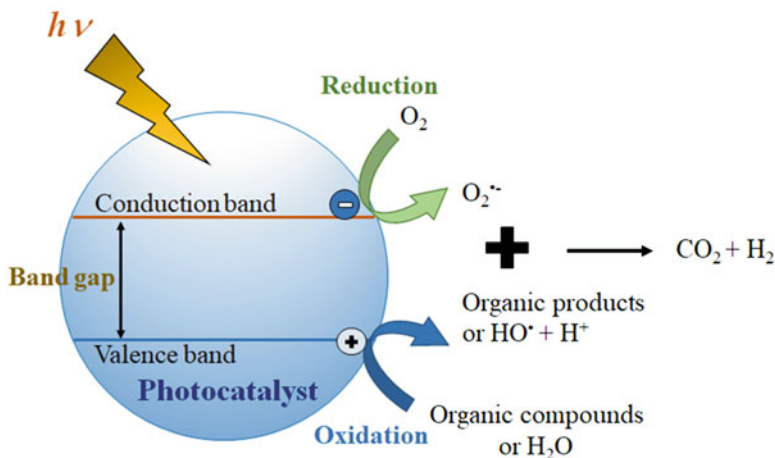
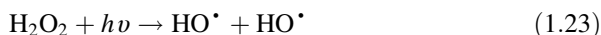
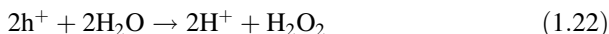


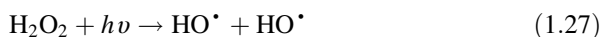
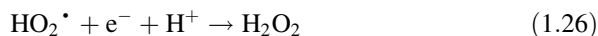
Fig. 1.3 Basic model of heterogeneous photocatalysis. The photocatalysts can absorb photons to generate the photo-excited electrons and positive holes. In the oxidation side, hydroxyl radicals (HO^\bullet) are produced by a reaction between the positive holes and water molecules. In the reduction side, the dissolved oxygen molecules can generate the short-lived superoxide anion radicals ($O_2^{\bullet -}$). HO^\bullet can be more generated from the other subsequently oxidation and reduction pathways. The radicals generated in photocatalysis are the key species to react with organic molecules in the photocatalytic applications



Reductive Reaction

The monovalent reduction of dissolved oxygen molecules which are adsorbed on the surface of photocatalyst can generate the short-lived free radicals in the form of superoxide anion radicals ($O_2^{\bullet -}$). Subsequently, the uncharged hydroperoxyl radicals (HO_2^\bullet) can be produced through protonation of $O_2^{\bullet -}$. Hydrogen peroxide (H_2O_2) is feasibly formed by protonation and reduction of HO_2^\bullet . Ultimately, the homolytic cleavage of H_2O_2 is also able to form more hydroxyl radicals (HO^\bullet) according to Eqs. (1.24–1.27) (Nosaka et al. 2002).





1.2.2 Photocatalytic Process

Photocatalytic process is normally described by heterogeneous photocatalysis. The process could be divided into four steps (Fig. 1.4): (I) light absorption for generation of electron–hole pair; (II) charge separation and migration of photogenerated carriers; (III) formation of hydroxyl radicals and superoxide ions via redox reactions; and (IV) photodecomposition of organic compounds via reaction with active species on the catalyst surface (Bensebaa 2013; Kudo and Miseki 2009).

For the first step (generation of electron–hole pair) as written above, the energy for photocatalysis reaction must be equal or exceed the band gap of photocatalysts (Nakata and Fujishima 2012). An electron (e^-) is activated to conduction band after the light absorption, so holes (h^+) are generated in the valence band.

For charge separation and migration of photogenerated carriers, this step strongly depends on the crystal structure, crystallinity, and particle size of photocatalysts. Low crystallinity leads to the increase of the amount of defects which operates as a trapping and a recombination center between photogenerated electrons and holes, causing a decrease in the photocatalytic activity. In addition, a small particle size creates the distance between photogenerated electrons (e^-) and holes (h^+) that

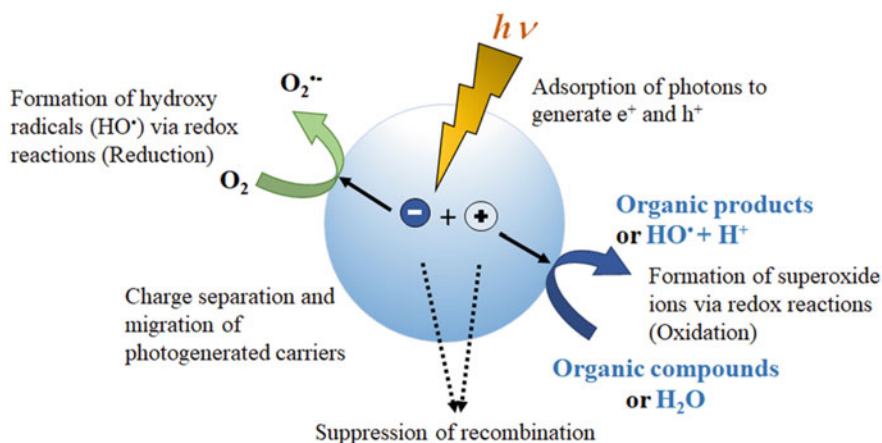


Fig. 1.4 Four steps of photocatalytic process: (I) light absorption for the generation of electron–hole pair; (II) charge separation and migration of photogenerated carriers; (III) formation of hydroxyl radicals and superoxide ions via redox reactions; and (IV) photodecomposition of organic compounds via reaction with active species on the catalyst surface

migrate to reaction sites on the surface, leading to decrease in the recombination probability.

For formation of hydroxyl radicals and superoxide ions via redox reactions, the oxidative reaction between holes and water molecules or other organic compounds leads to generation of HO^\bullet and H^+ (which can further form H_2O_2), while the reductive reaction between electron and O_2 molecules leads to generation of superoxide ions ($\text{O}_2^{\bullet-}$) (which can further form HO_2^\bullet , H_2O_2 , and HO^\bullet) (Sirelkhatim et al. 2015). However, this step is the surface chemical reactions, where the photogenerated electrons and holes can recombine with each other if the active sites for redox reactions do not exist on the surface, which depends on the surface character and surface area.

For the last step (photodecomposition of organic compounds via reaction with active species on the catalyst surface), radicals, ions, or molecules (HO^\bullet , $\text{O}_2^{\bullet-}$, OH^- , and H_2O_2) obtained from the reactions are key reactive oxygen species (ROS) in the initiation of other photocatalytic reactions which can react with the target organic compounds to degrade or otherwise convert them into harmless by-products or value-added chemicals or fuels (Payormhorm et al. 2017a; Payormhorm et al. 2017b). Recently, several catalysts have been progressed to produce good quality of photocatalysts like photoconversion processes such as solar to electricity, light to hydrogen, and light to mechanical works.

1.3 Organic Pollutants in Water

There are various types of pollutants in wastewater (e.g., organic pollutants, inorganic pollutants, pathogens, and radioactive pollutants). Organic pollutants are a main part of environmental pollution, which may cause an adverse effect on aquatic organisms even at low levels of exposure (Mao et al. 2017; Ahmad et al. 2018; Yu et al. 2019). Organic pollutants are found in various wastewater sources, e.g., domestic, industrial, and agricultural sectors.

Many kinds of organic pollutants, such as pharmaceuticals and personal care products (PPCPs), textile, food, beverage, persistent organic pollutants (POPs), insecticide, pesticide, oil, fertilizers, and chemical, are included in wastewater.

1.3.1 Sources of Organic Pollutants in Wastewater

Organic pollutants are found in three main wastewater sources which are domestic, industrial, and agricultural sectors. The examples of organic pollutants in wastewater from these three sectors are shown in Table 1.3.

Table 1.3 Example list of organic pollutants in wastewater from different sources

| Example of organic pollutant | | |
|------------------------------|---|---------------------|
| Domestic sector | Industrial sector | Agricultural sector |
| Human pharmaceuticals | Textile | Pesticides |
| Human feces | Organic dye-stuff | Herbicides |
| Human urine | Glue and adhesives | Organic fertilizers |
| Human hormones | Cellulose and paper | Crop residues |
| Toilet paper | Leather and bleaching agents | Veterinary drugs |
| Soaps | Biocides | Animal manure |
| Cosmetics | Petroleum | Animal urine |
| Dental cares | Food (e.g., carbohydrate, protein, lipid) | Animal hormones |
| Shampoos | Fermentation residues (e.g., brewers) | Animal feeds |
| Hair colors | Grains, winery waste | |
| Cleansing foams | Breweries liquid waste | |
| Deodorants | Distilleries liquid waste | |
| Fabric softener | Cleaning agents | |
| Cooking oil | Polychlorinated biphenyls (PCBs) | |
| Food residues | Pharmaceuticals | |
| Energy drinks | Soaps | |
| Insect repellents | Cosmetics | |
| Cleaning agents | Cooking oil | |
| Organic nutrients | Organic nutrients | |
| | Herbicides | |
| | Pesticides | |

Domestic Wastewater

Domestic wastewater is water derived from daily human activities in the residences, institutions, office buildings, commercial buildings, as well as healthcare and personal care facilities. Wastewater quantities from individual residences commonly depend on the water consumption rate per capita and population density. On the other hand, wastewater quantities from commercial sources are typically based on the land-use area or the number of guests (Metcalf and Eddy 1981). The domestic wastewater can be characterized by constituents of wastewater into four classes, which are grey water, yellow water, brown water, and black water.

Grey water is wastewater with small amounts of nutrients, pathogens, and suspended solids contamination, excluding toilet wastewater. It was called “grey water” because the color of wastewater will be gradually changed to grey during storage. The grey water is discharged from daily activities such as showering, hand washing, clothes washing, and dishwashing (Wang et al. 2010). General composition of grey water depends on lifestyles, personal hygiene of human, as well as climatic conditions. Showering wastewater is usually composed of soaps, dental cares, shampoos, cosmetics, hair color, and other personal care products. Clothes washing wastewater contains a group of nutrients (sodium, phosphorus, and

nitrogen), surfactants, foams, suspended solids, oil and greases, bacteria, and many others. Dishwashing and cooking wastewater generally consist of discarded food, nutrients, cooking oil, dishwashing soaps or liquids, and bacteria.

Yellow water contains human urine with or without flush water, which is presented in domestic wastewater approximately 1% by volume. Urine is a natural source of macronutrients. The presence of nitrogen, phosphorus, and potassium in conventional domestic wastewater mostly originates from urine.

Brown water is human feces, which may be included flush water and toilet papers. The significant constituents of brown water are organic matters, phosphorus, and infectious agents (Balkaya and Guneysu 2019). Furthermore, human feces and urine are also important sources of both metabolized and non-metabolized pharmaceutical residues after absorption and metabolization from human bodies.

Black water is a combination of yellow and brown waters; thus it is composed of human feces, urine, toilet papers, and flush water.

Industrial Wastewater

Apart from domestic wastewater, one of the important organic pollutant sources is industrial wastewater, such as textile, chemical, food, and beverage, which is a high concentration of various organic pollutants. Presently, a huge amount of industrial wastewater from several industries was released into rivers, lakes, and coastal areas. The results of this problem lead to be a serious pollution problem in water with negative effects to the ecosystem.

Nowadays, there are many types of organic pollutants in industrial wastewater based on different industries, such as leather, textile, metal processing, brewery and fermentation, food, pharmaceuticals, oil refining, cosmetics, soaps, pesticides, herbicides, cellulose and paper manufacturing, glue, and adhesives industries. The main source of organic pollutants in industrial wastewaters is produced from the chemical industry using organic substances for chemical reactions.

Agricultural Wastewater

Agricultural sector is also identified as one of the important sources for organic pollutants in wastewater that can affect ecology and the environment. Agricultural wastewater principally comes from by-products of anthropogenic activities in the agricultural area such as farmland, fertilizer, animal manure, and agrichemicals. Agricultural wastewater has been recognized as non-point source pollution, which is released from different agricultural activities. All types of agricultural activities produce a large number of organic pollutants (e.g., pesticides or herbicides), which subsequently discharge into surface water and penetrate to groundwater. Most agricultural wastewater is composed of sediment, nutrients, microorganism, and chemical, which is difficult to control because these substances usually discharge into surrounding natural water bodies during rainfall (Neumann et al. 2002).

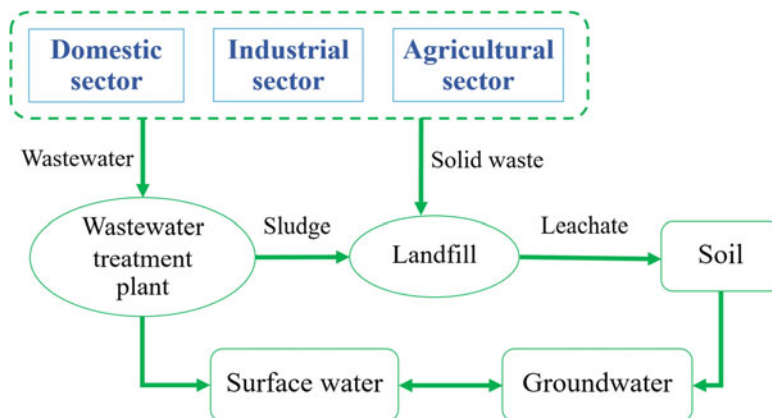


Fig. 1.5 General pathways of organic contamination in the environment. Note that organic pollutants from various wastewater sources can contaminate into the environment by both direct and indirect pathways

Moreover, agricultural wastewater with a high content of nutrients, especially nitrogen and phosphorus, can lead to eutrophication of water bodies.

Finally, organic pollutants from various wastewater sources can contaminate into the environment by both direct and indirect pathways. Figure 1.5 shows general pathways of organic contamination in the environment.

1.3.2 Major Groups of Organic Pollutants in Wastewater

Pharmaceuticals and Personal Care Products

Pharmaceuticals and personal care products are intentionally synthetic compounds with specific properties for human or animal healthcare and medical purposes. The molecular weight of pharmaceuticals and personal care products are typically ranging from 150 to 1000 Daltons (Awfa et al. 2018). Pharmaceuticals are the chemicals used in human and veterinary medicine, including antibiotics, hormones, stimulant drugs, beta-blockers, anti-inflammatories, antiarrhythmic agents, blood–lipid lowering agents, cancer therapeutics, diuretics, and many others (Chen et al. 2016; Fent et al. 2006). Pharmaceuticals and their metabolites can be released into the environment after incomplete absorption and excretion from the body of consumer, which are mainly presented in the dissolved phase (Prasad et al. 2019). Personal care products are products used for beauty and hygiene to enhance the quality of daily life, such as sunscreen, skincare products, body lotion, moisturizers, soaps, shampoo, dental care, lipstick, perfume, as well as mosquito repellent lotion and spray (Cizmas et al. 2015). The daily washing activities of human appear to be the main pathway to release the personal care products from the human body into sewerage

systems and aquatic environments. Furthermore, recreation activities such as swimming and other water sports can also contribute the personal care products' contamination in water (Yang et al. 2017). Example list of pharmaceuticals and personal care products with their physical and chemical properties is shown in Table 1.4.

The environmental contamination of pharmaceuticals and personal care products is caused by both intentional and unintentional discharge from many sources, including households, industries, hospitals, sewage treatment plants, livestock farms, and landfill leachate. The effluent discharge from sewage treatment plants and industries is identified to be the predominant sources (Awfa et al. 2018). Pharmaceuticals and personal care products are usually synthesized to be persistent, high chemical stability, and low biodegradability, which cannot be completely removed by conventional treatment processes. Although the occurrence of pharmaceuticals and personal care products in surface water, groundwater, tap water, as well as drinking water is frequently detected at a trace concentration (ranging from ng/L up to $\mu\text{g/L}$), the continuous exposure to these compounds can significantly lead to adverse effects on aquatic living organisms, terrestrial organisms, and balance of ecosystem (Jamil et al. 2017).

Many pharmaceuticals and personal care products behave as antimicrobial agents; thus the biological degradation processes that use microorganisms to break down organic pollutants in water seem to be ineffective to remove them. Physical treatment processes such as adsorption and membrane filtration can only transfer pharmaceuticals and personal care products from one medium to another medium without the destruction of them, leading to the formation of secondary contaminants in the form of spent adsorbents and concentrated water, respectively (Awfa et al. 2018). Nowadays, the chemical oxidation processes especially advanced oxidation processes, involving photo-Fenton, ozonation, UV/H₂O₂, and semiconductor photocatalysis, are accepted as the most promising potential treatment method for removals of pharmaceuticals and personal care products. Unfortunately, degradation of pharmaceuticals and personal care products by photo-Fenton and ozonation can form toxic by-products (Wang and Wang 2016). The low UV absorbance of hydrogen peroxide and scavenging effects of $\cdot\text{OH}$ by H₂O₂ are the main drawbacks, leading to high operating costs in the UV/H₂O₂ process (Guo et al. 2018). Semiconductor photocatalysis has been accepted as a cost-effective process for degradation and mineralization of pharmaceuticals and personal care products in water because this process can be operated at ambient condition by using low-cost available semiconductor photocatalysts and their modified forms, which can be activated by UV light, visible light, as well as natural sunlight. Furthermore, the immobilization of semiconductor photocatalysts on support material has been proved as a promising way to enhance the recycling ability of them, resulting in effective operating and maintenance cost (Klavarioti et al. 2009).

Table 1.4 Physical and chemical properties of pharmaceuticals and personal care products

| Class of pharmaceuticals and personal care products | Name of substance | Molecular formula | Molecular weight (g·mol ⁻¹) | Log K _{ow} | pK _a | Reference |
|---|---|--|---|---------------------|--------------------|--------------------|
| Analgesics /anti-inflammatories | Acetaminophen | C ₈ H ₉ NO ₂ | 151.2 | 0.46 | 9.38 | Kim et al. (2009) |
| | Antipyrine | C ₁₁ H ₁₂ N ₂ O | 188.2 | 0.38 | 1.40 | |
| | Diclofenac | C ₁₄ H ₁₁ Cl ₂ NO ₂ | 296.2 | 4.51 | 4.15 | |
| | Ethenzamide | C ₉ H ₁₁ NO ₂ | 165.2 | 0.77 | – | |
| | Fenopropfen | C ₁₅ H ₁₄ O ₃ | 242.3 | 3.90 | 7.30 | |
| | Indomethacin | C ₁₉ H ₁₆ ClNO ₄ | 357.8 | 4.27 | 4.50 | |
| | Isopropylantipyrine | C ₁₄ H ₁₈ N ₂ O | 230.3 | 1.94 | – | |
| | Ketoprofen | C ₁₆ H ₁₄ O ₃ | 254.3 | 3.12 | 4.45 | |
| | Mefenamic acid | C ₁₅ H ₁₅ NO ₂ | 241.3 | 5.12 | 4.20 | |
| | Acetaminophen | C ₈ H ₉ NO ₂ | 151.2 | 0.46 | 9.38 | Chen et al. (2016) |
| | Naproxen | C ₁₄ H ₁₄ O ₃ | 230.3 | 3.18 | 4.15 | |
| | Paracetamol | C ₁₆ H ₂₅ NO ₂ | 263.4 | 2.40 | 9.41 | |
| | Ceftiofur | C ₁₉ H ₁₇ N ₅ O ₇ S ₃ | 523.6 | – | – | Kim et al. (2009) |
| | Chlorotetracycline | C ₂₂ H ₂₃ ClN ₂ O ₈ | 478.9 | –0.62 | 3.30 | |
| | Clarithromycin | C ₃₈ H ₆₈ NO ₁₃ | 748.0 | 3.16 | 8.99 | |
| | Oxytetracycline | C ₂₂ H ₂₄ N ₂ O ₉ | 460.4 | –0.90 | 3.27 | |
| | Sulfadimethoxine | C ₁₂ H ₁₄ N ₄ O ₄ S | 310.3 | 1.63 | – | |
| Sulfadimidin | C ₁₂ H ₁₄ N ₄ O ₂ S | 278.3 | 0.89 | 7.59 | | |
| Sulfamethoxazole | C ₁₀ H ₁₁ N ₃ O ₃ S | 253.3 | 0.89 | 5.7 | | |
| Sulfamonomethoxine | C ₁₁ H ₁₂ N ₄ O ₃ S | 280.3 | 0.70 | | | |
| Tetracycline | C ₂₂ H ₂₄ N ₂ O ₈ | 444.4 | –1.30 | 3.30 | | |
| Trimethoprim | C ₁₄ H ₁₈ N ₄ O ₃ | 290.3 | 0.91 | 7.12 | Chen et al. (2016) | |
| Chloramphenicol | C ₁₁ H ₁₂ Cl ₂ N ₂ O ₅ | 323.1 | 1.14 | 9.61 | | |
| Penicillin G | C ₁₆ H ₁₈ N ₂ O ₄ S | 334.4 | 1.83 | 2.74 | | |

(continued)

Table 1.4 (continued)

| Class of pharmaceuticals and personal care products | Name of substance | Molecular formula | Molecular weight (g·mol ⁻¹) | Log K _{ow} | pK _a | Reference |
|---|---------------------|--|---|---------------------|-----------------|-------------------------|
| Beta-blockers | Erythromycin | C ₃₇ H ₆₇ NO ₁₃ | 733.9 | 3.06 | 8.88 | |
| | Roxithromycin | C ₄₁ H ₇₆ N ₂ O ₁₅ | 837.1 | 2.75 | 9.2 | |
| | Atenolol | C ₁₄ H ₂₂ N ₂ O ₃ | 266.3 | 0.16 | 9.6 | Chen et al. (2016) |
| Stimulant drug | Metoprolol | C ₁₅ H ₂₅ NO ₃ | 267.4 | 1.88 | 9.5 | |
| | Caffeine | C ₈ H ₁₀ N ₄ O ₂ | 194.2 | -0.07 | 10.4 | Chen et al. (2016) |
| Psychiatric drugs | Carbamazepine | C ₁₅ H ₁₂ N ₂ O | 236.3 | 2.45 | 2.3, 13.9 | Chen et al. (2016) |
| | Gabapentin | C ₉ H ₁₇ NO ₂ | 171.2 | -1.1 | 3.68, 10.7 | |
| Lipid regulators | Gemfibrozil | C ₁₅ H ₂₂ O ₃ | 250.3 | 4.77 | 4.7 | Chen et al. (2016) |
| | Bezafibrate | C ₁₉ H ₂₀ ClNO ₄ | 361.8 | 4.25 | 3.61 | |
| Contrast media | Iopromide | C ₁₈ H ₂₄ I ₃ N ₃ O ₈ | 791.1 | -2.1 | 10.62 | Chen et al. (2016) |
| | Iopamidol | C ₁₇ H ₂₂ I ₃ N ₃ O ₈ | 777.1 | -2.42 | 10.7 | |
| Diuretics | Furosemide | C ₁₂ H ₁₁ ClN ₂ O ₅ S | 330.7 | 2.03 | 4.7 | Chen et al. (2016) |
| | Hydrochlorothiazide | C ₇ H ₈ ClN ₃ O ₄ S ₂ | 297.7 | -0.07 | 7.9 | |
| Hormones | Estrone | C ₁₈ H ₂₂ O ₂ | 270.4 | - | 10.77 | Lewis and Archer (1979) |
| | 17β-estradiol | C ₁₈ H ₂₄ O ₂ | 272.4 | - | 10.71 | |
| | 2-methoxyestrone | C ₁₉ H ₂₄ O ₃ | 300.4 | - | 10.81 | |
| Antiarrhythmic agents | Disopyramide | C ₂₁ H ₂₉ N ₃ O | 339.5 | 2.58 | - | Kim et al. (2009) |
| | Metoprolol | C ₁₅ H ₂₅ NO ₃ | 267.4 | - | - | |
| Insect repellent | Propranolol | C ₁₆ H ₂₁ NO ₂ | 259.3 | 3.48 | 9.42 | |
| | Diethyltoluamide | C ₁₂ H ₁₇ NO | 191.3 | 2.18 | - | Kim et al. (2009) |
| Fragrances | Galaxolide | C ₁₈ H ₂₆ O | 258.4 | 5.90 | - | Prasad et al. (2019) |
| | Celestolide | C ₁₇ H ₂₄ O | 244.4 | 5.00 | - | |
| Sunscreen | Octocrylene | C ₂₄ H ₂₇ NO ₂ | 361.5 | 7.10 | - | Prasad et al. (2019) |

Persistent Organic Pollutants

Persistent organic pollutants are a group of toxic organic chemicals with long half-lives and persistence in the environment. Persistent organic pollutants have been mentioned to be toxic and harmful to human health and the environment. The commonly encountered persistent organic pollutants are organochlorine pesticides from agricultural discharge such as DDT, industrial chemicals such as polychlorinated biphenyls (PCBs), and industrial by-products, especially polychlorinated dibenzodioxins (PCDDs) and polychlorinated dibenzofurans (PCDFs) as known as dioxins. These pollutants are classified into three categories based on Stockholm Convention (Stockholm Convention 2019) as shown in Table 1.5.

Nowadays, the scientists, governments, and non-governmental organizations (NGOs) are very concerned about these pollutants because of their long persistence in the environment, long range transportability, high toxicity even at a low level of concentration, and accumulation in fatty tissues due to their high lipophilicity. Persistent organic pollutants are widely contaminated in air, water, soil, and migratory species which move across international regions. Moreover, persistent organic pollutants are found in even non-chemical areas such as the arctic regions (Teran et al. 2012). The resistance property of persistent organic pollutants under biological degradation is the main reason, causing bioaccumulation into animal bodies through food chains. The exposure of persistent organic pollutants creates various serious health problems such as cancer, allergies and hypersensitivity, hormone disruption, cardiovascular diseases, reproductive disorders, learning disabilities, and disruption of the immune system.

Therefore, it is very important to develop methods for mitigation and elimination of persistent organic pollutants. The existing remediation techniques include coagulation–flocculation–sedimentation, adsorption, membrane filtration, ozonation, and advanced oxidation processes (Kumari et al. 2020). Photocatalytic process is one solution to reduce these pollutants in the environment because of the high efficiency and fast degradation. However, a challenge of the elimination of persistent organic pollutants by-products should be concerned.

Organic Dyes

The industries in this century, whether they are the textile, paper, rubber, printing, plastics, cosmetics, dye intermediates, and so forth. All industries used dye as a component in the production to the desired color product. Nowadays, the organic dyes could be classified by two types which are natural and synthetic dyes. Firstly, the natural organic dyes are dyes extracted from organic compounds (contain carbon) which form the animal, minerals, and vegetable resources such as annatto (yellow to orange colors), henna plant (brown color), and tomatoes (orange or reddish colors). All of these dyes occur by natural which means they have no side effect from dyes and also can degrade by itself. Notwithstanding, natural dyes are not

Table 1.5 List of persistent organic pollutants in the Stockholm Convention (summarized from Stockholm Convention 2019)

| Annex | Persistent organic pollutant | Group |
|--|--|-----------------------------------|
| A (Elimination: elimination of production and use) | Aldrin | Pesticide |
| | Chlordane | Pesticide |
| | Chlordecone | Pesticide |
| | Endrin | Pesticide |
| | Dieldrin | Pesticide |
| | Heptachlor | Pesticide |
| | Lindane | Pesticide |
| | Mirex | Pesticide |
| | Toxaphene | Pesticide |
| | Alpha hexachlorocyclohexane | Pesticide |
| | Beta hexachlorocyclohexane | Pesticide |
| | Pentachlorophenol and its salts and esters | Pesticide |
| | Technical endosulfan and its related isomers | Pesticide |
| | Hexachlorobenzene | Pesticide and industrial chemical |
| | Pentachlorobenzene | Pesticide and industrial chemical |
| | Decabromodiphenyl ether | Industrial chemical |
| | Hexabromobiphenyl | Industrial chemical |
| | Hexabromocyclododecane | Industrial chemical |
| | Hexabromodiphenyl ether | Industrial chemical |
| | Heptabromodiphenyl ether | Industrial chemical |
| | Hexachlorobutadiene | Industrial chemical |
| | Polychlorinated biphenyls | Industrial chemical |
| | Polychlorinated naphthalenes | Industrial chemical |
| | Short chain chlorinated paraffins | Industrial chemical |
| Tetrabromodiphenyl ether | Industrial chemical | |
| Pentabromodiphenyl ether | Industrial chemical | |
| B (Restriction: restriction in production and use) | Dichlorodiphenyltrichloroethane | Pesticide |
| | Perfluorooctane sulfonic acid and its salts | Pesticide & Industrial chemical |
| | Perfluorooctane sulfonyl fluoride | Pesticide & Industrial chemical |
| C (Unintentional production: reduction of unintentional release) | Hexachlorobenzene | Unintentional production |
| | Hexachlorobutadiene | Unintentional production |
| | Pentachlorobenzene | Unintentional production |
| | Polychlorinated biphenyls | Unintentional production |

(continued)

Table 1.5 (continued)

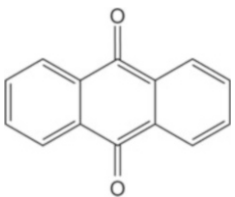
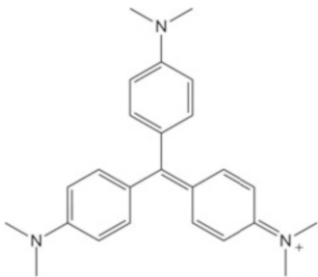
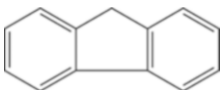
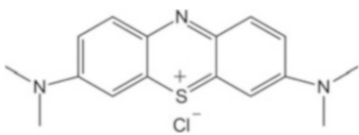
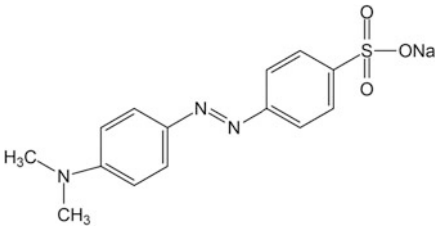
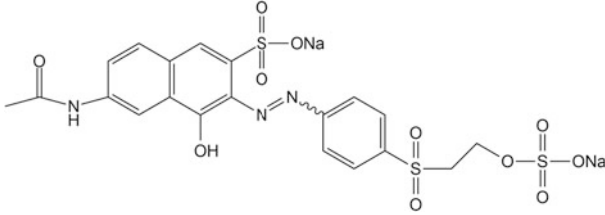
| Annex | Persistent organic pollutant | Group |
|-------|-----------------------------------|--------------------------|
| | Polychlorinated dibenzo-p-dioxins | Unintentional production |
| | Polychlorinated dibenzofurans | Unintentional production |
| | Polychlorinated naphthalenes | Unintentional production |

very in demand because of unendurability. Therefore, another type of dye which is synthetic organic dye became popular because of its lasting color pay-off and wide range of colors. Table 1.6 shows the examples of synthetic organic dyes. Synthetic organic dyes are manufactured from organic molecules. The resources for the synthesis of these dyes are chemicals, by-products of petroleum, and earth minerals (Ziarani et al. 2018).

Nevertheless, the disadvantage of dyes is not all of the dyes are eco-friendly, especially, synthetic organic dyes. Most of these dyes are very complex molecules, extremely toxic, chemical stability, and slow degradation (Reddy and Mohan 2016). Therefore, the discharge of organic dye containing in water is troublesome the environment, not only bad vision because of their color but also reduction of sunlight transmission (Crini and Badot 2008; Dinçer et al. 2007; Zhou et al. 2019). Moreover, these organic dyes also come with a risk substance, for instance, heavy metal (Zn, Pb, Cu, Cd, Co), amines, and aromatic compound (Zollinger 2003; Zhou et al. 2019). Therefore, these organic dyes are not only harmful to aquatic life but also mutagenic to humans. The health problems related to organic dyes are skin irritation, sneezing, sore eyes, carcinogenicity, dysfunction, and mutagenicity, including the brain, liver, kidney, central nervous and reproductive system, and others (Zhou et al. 2019).

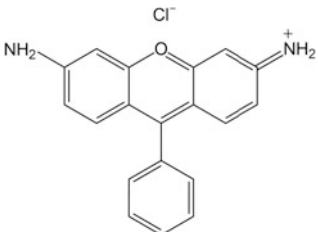
Presently, many researchers have been found and develop the solutions to treat organic dyes in water, for example, advanced oxidation processes (Andreozi et al. 1999; Ikehata et al. 2008), adsorption (Wu et al. 2001; Noll 1991), electro-oxidation (Särkkä et al. 2015; Recio et al. 2011), and reverse osmosis (Bodalo-Santoyo et al. 2003; Agenson et al. 2003). The solutions to treat these dyes are a challenging issue due to their high solubility and high persistence in the environment. Photocatalytic process is one of the interesting solutions for wastewater treatment because this process is non-toxic and it does not affect human life. Homogeneous or heterogeneous catalysts can be used as photocatalysts for the treatment of organic dyes in water (Mao et al. 2017; Bodson et al. 2016; Zhang et al. 2017; Mudassir et al. 2018; Qu et al. 2017).

Table 1.6 Examples of synthetic organic dyes

| Synthetic organic dye | Chemical structure |
|--------------------------------|--|
| Anthraquinone dye |  |
| Crystal violet |  |
| Fluorene |  |
| Methylene blue Thiazine dye |  |
| Methyl orange |  |
| Reactive orange 16 |  |

(continued)

Table 1.6 (continued)

| Synthetic organic dye | Chemical structure |
|-----------------------|---|
| Rhodamine |  |

1.4 Photocatalytic Remediation of Organic Pollutants in Water

In this section, photocatalytic organic pollutant treatments in water are categorized into two groups based on types of photocatalysis, i.e., homogenous and heterogeneous ones.

1.4.1 Homogeneous Photocatalysis

Homogeneous photocatalysis has attracted numerous attentions as a promising technology for remediation of organic pollutants in water.

Treatments of Pharmaceuticals and Personal Care Products

The combination of UV and hydrogen peroxide (UV/H₂O₂), ozonation (UV/O₃), and photo-Fenton has demonstrated their effectiveness in the degradation of pharmaceuticals and personal care products with initial concentration ranging from µg/L to ng/L as low as the commonly found levels in the environment. The completed removal of pharmaceuticals and personal care products, such as sulfamethoxazole, trimethoprim, bezafibrate, diclofenac, naproxen, ketoprofen, atenolol, metoprolol, propranolol, diazepam, carbamazepine, primidone (Kim et al. 2009), ofloxacin, ciprofloxacin, gemfibrozil, ibuprofen, sotalol, triclosan (De la Cruz et al. 2012), tylosin (He and Hua 2013), and enoxacin (Santoke et al. 2015) from water by UV/H₂O₂, has been reported by many researchers.

In the recent decade, the removal of some pharmaceuticals and personal care products, such as ketoprofen (Illés et al. 2014), caffeine, diethyltoluamide, cyclophosphamide (Kim and Tanaka 2010), mefenamic acid (Chang et al. 2012), and berberine (Qin et al. 2015), by UV/O₃ process, was performed. The degradation of pharmaceuticals and personal care products by UV/O₃ process has not been widely

applied in the large scale compared with other treatment methods in homogeneous photocatalysis, because of its high-energy requirement for both ozone generator and UV lamps (Kim and Tanaka 2011), resulting in higher operating costs. The removal efficiencies of pharmaceuticals and personal care products by different conditions of photo-Fenton systems have been reviewed (Wang and Wang 2016). Tetracycline with the initial concentration as high as 24 mg/L can be completely removed by photo-Fenton process. Moreover, bezafibrate, ibuprofen, and diclofenac with the trace initial concentration of millimolar level can also be completely removed by this process (Wang and Wang 2016).

Treatments of Persistent Organic Pollutants

Persistent organic pollutants, a group of hazardous pollutants, such as pesticides that are often found in agricultural wastewater, also continuously increased the environmental risks, so it is a challenge to solve this problem. A number of physical and chemical methods have been developed to treat persistent organic pollutants.

Degradation of persistent organic pollutants can be carried out by ozonation process. Atrazine has been reported to be degraded by catalytic ozonation with iron scraps (Li and Zhou 2019). Pesticide wastewater (Solís et al. 2019) and organophosphorus pesticide in water (Aimer et al. 2019) can be treated by ozonation.

Fenton or photo-Fenton is one of the alternative ways for remediation of persistent organic pollutants. $\text{Fe}^{\text{III}}(\text{OH})^{2+}$ under UV irradiation has been revealed to generate OH radicals which can further degrade 4-chlorophenol and other Cr (VI) phenolic compounds (e.g., 4-bromophenol, 4-nitrophenol, and phenol) (Kim et al. 2019). Among the typical iron salts, iron (III) nitrate can generate iron aquo complexes in aqueous and organic solutions, which are highly efficient and selective homogenous photocatalyst for degradation of cyclohexane into cyclohexanol and cyclohexanone up to 80 and nearly 100%, respectively (Iqbal et al. 2018). Fipronil, a pesticide, can be degraded via photo-Fenton catalysis (Singh et al. 2019). It has been found that the catalysis exhibited the highest degradation efficiency of 88.71% at pH 3 with an H_2O_2 concentration of 10 mM and the amount of catalyst of 1.5 g/L for 120 min reaction time (Singh et al. 2019). These show photo-Fenton is a promising technique due to the fast regeneration of Fe^{2+} and the less formation of iron sludge compared with the conventional Fenton process. Carbendazim can be degraded with a degradation efficiency of 96% within 15 min by Fenton process (da Costa et al. 2019). Moreover, modified Fenton processes (e.g., electro-Fenton) have been introduced (Méndez-Torres et al. 2019) with potential uses for degradations or removals of pesticide mixtures (Rosa Barbosa et al. 2018), organochlorine pesticide lindane (Dominguez et al. 2018), chlordimeform insecticide (Rezgui et al. 2018), and methoxychlor (Huang et al. 2018). It should be noted that the modified Fenton processes that use solid-state materials as the ferrous sources may also be considered as heterogeneous photocatalysis.

Normally, heterogeneous photocatalytic degradation of pesticides is a promising method because of the short time of treatment. However, it also needs more technical

and economic developments, because the main source of the system (UV irradiation) often requires a large amount of the electrical energy and the use of UV with ozone or hydrogen peroxide causes relatively high costs of the processes.

Treatments of Organic Dyes

Homogeneous photocatalysis has proved to be sufficiently effective alternatives for remediation of organic dyes in water, even though it has some limitations.

A few works have recently focused on the degradation of organic dyes by ozonation. For example, degradation of reactive red 24 from aqueous solution (Van et al. 2019), removal of methylene blue in wastewater (Ikhlaiq et al. 2019), organic dye removals with acid-treated clay catalysts (Boudissa et al. 2019), and degradation of azo dyes (El Hassani et al. 2019; Pérez et al. 2019; Pandian et al. 2018) have been reported with ozonation relations.

Azo dyes (Wang et al. 2019b; Innocenzi et al. 2019), acid orange 7 (AO7) (Wang et al. 2019b), reactive black 5 (RB5) (Wang et al. 2019b), reactive red 24 (Van et al. 2019), rhodamine B (Wang et al. 2019a), and methylene blue (Anantharaman et al. 2019; Ikhlaiq et al. 2019) have been studied to be decolorized by Fenton or photo-Fenton processes.

UV/H₂O₂ is an alternative way that is often found for photocatalytic remediation of organic dyes (e.g., methylene blue (Malvestiti et al. 2019), brilliant green (Rehman et al. 2018), and rhodamine B (Changchao et al. 2018)) in water.

In a comparison of Fenton and UV/H₂O₂ for dye degradation, increasing concentration of ferrous ions (that catalyze the Fenton reaction) can increase the generation of OH radicals from hydrogen peroxide up to an optimum level, while in UV/H₂O₂, the hydroxyl radicals generated are less due to the presence of photo-stable organic UV absorbers (ultimately, it reduces the efficiency of UV/H₂O₂ oxidation).

1.4.2 Heterogeneous Photocatalysis

Photocatalysts used in heterogeneous photocatalysis can be used as (1) powder and suspension forms and (2) coated forms on supporters or substrates.

Powder and Suspension Forms of Photocatalysts

Suspension of the small size photocatalysts, such as microparticles, nanoparticles, and other nanomaterials in other forms, in wastewater, is the traditional way to remove the organic contaminants via heterogeneous photocatalysis.

Treatments of Pharmaceuticals and Personal Care Products

Among various photocatalysts, photocatalytic removal of pharmaceuticals and personal care products in water using titanium dioxide (TiO_2) powder or nanoparticles, especially Degussa P25 – a commercially available TiO_2 – has been extensively investigated. Effects of photocatalyst amount, light source, and pH of the solution have also been studied to determine the optimum conditions for pharmaceuticals and personal care products removal over powder suspension in water. The examples are photocatalytic removal of crotamiton, clofibric acid, and sulfamethoxazole using TiO_2 under UV irradiation. Crotamiton is an antipruritic frequently detected in Japanese rivers. The removal efficiency of crotamiton is not affected by the initial pH of the solution in the range of 3–9, whereas the removal efficiencies of clofibric acid and sulfamethoxazole are significantly decreased when the initial pH is adjusted higher than 6.5, because of repulsive force between TiO_2 particle and these pollutants (Fukahori et al. 2012). Photocatalytic removal of ibuprofen, which is the common nonsteroidal anti-inflammatory drugs (NSAID) in the presence of TiO_2 powder suspended in the wastewater under UV/visible light irradiation is another example. Ibuprofen can be rapidly mineralized over TiO_2 . However, small amounts of intermediates in the form of oligomeric species can be detected during the photocatalytic reaction, leading to catalyst deactivation (Choina et al. 2013). The utilization of solar light, replacing an expensive and bio-hazardous UV light, as a light source is receiving considerable attention for photocatalytic removals of pharmaceuticals and personal care products, such as photocatalytic removals of amoxicillin over tungsten trioxide (WO_3) (Nguyen et al. 2019) and photocatalytic removals of caffeine over titanium dioxide (TiO_2) and zinc oxide (ZnO) nanoparticles (Ghosh et al. 2019).

Treatments of Persistent Organic Pollutants

In the case of elimination of persistent organic pollutants in water, photocatalysis using powder photocatalysts can be successfully applied for various target pollutants, such as diuron, alachlor, isoproturon, atrazine (Cruz et al. 2017), chlorpyrifos, cypermethrin, chlorothalonil (Affam and Chaudhuri 2013), rhodamine B, aldicarb, norfloxacin (Li et al. 2013), and perfluorooctanoic acid (Zhao et al. 2012). Photocatalytic mineralization of the representatives of aqueous persistent organic pollutants was performed, e.g., rhodamine B, aldicarb, and norfloxacin as representatives of color substances, pesticides, and antibiotics, respectively (Li et al. 2013). Under simulated sunlight irradiation, rhodamine B and norfloxacin can be decomposed, while aldicarb is difficult to be decomposed (Li et al. 2013). Perfluorooctanoic acid is a recent-found hazardous persistent organic pollutant. The shorter chain compounds of perfluorooctanoic acid are less bioaccumulative and produce a low level of environmental pollution; therefore photocatalytic degradation of perfluorooctanoic acid is increasingly interested as one of the alternative treatment processes. Photocatalytic degradation of perfluorooctanoic acid using

β -Ga₂O₃ photocatalyst powder suspended in perfluorooctanoic acid aqueous solution exhibited the degradation efficiency as high as 98.8% (Zhao et al. 2012).

Treatments of Organic Dyes

Photocatalytic degradation of dyes is the typical way to investigate the photocatalytic activity of synthesized photocatalysts. Before utilizations of the catalysts in other applications, the photocatalytic degradations of model dyes, e.g., methylene blue or methyl orange, are commonly done. Therefore, there are a large number of publications reported on this issue.

Powder suspension of titanium dioxide (TiO₂), zinc oxide (ZnO), and others has been extensively performed for photocatalytic removal of industrial organic pollutants in wastewater, especially dye-containing wastewater. Photocatalytic activity of ZnO nanoparticles for the decomposition of rhodamine B dye under UV illumination has been investigated. It was found that ZnO nanoparticles could degrade rhodamine B dye to 95% within 70 min. Photocatalytic degradation of azo dye in aqueous solutions under UV irradiation using nanostructured strontium titanate (Sr₂TiO₃) showed high photocatalytic activity compared with that of TiO₂ (Karimi et al. 2014). In addition, in photocatalytic degradation of dimethyl phthalate (DMP) (Jing et al. 2018) by TiO₂ particles, it was found that the photodegradation occurs at the surface of the photocatalysts more than in the homogenous phase.

Graphene–oxide hydrogel (zeolitic imidazolate framework) shows photocatalytic dye degradation ability with multiple cycles of uses because of its hydrophobic properties and high specific surface area (Mao et al. 2017). Amorphous photocatalysts of Zn-Al layered double hydroxide can be used for photocatalytic decoloration of methyl orange (Qu et al. 2017). SrSn(OH)₆ can be used for the degradation of rhodamine B (Luo et al. 2016). At low pH, SrSn(OH)₆ shows a good photocatalytic activity compared with commercial TiO₂ (P25), because the hexagonal phase of hydroxide stannate can create hydroxyl groups for degradation of rhodamine B. Many modifications of metal oxides, e.g., Ag/TiO₂ nanoparticles (Abdel Messih et al. 2017) and Nd₂Sn₂O₇ (Zinatloo-Ajabshir et al. 2019), have been developed for degradation various organic dyes. Some details of the modifications will be discussed in another session.

Even though the suspension of photocatalysts in wastewater is the efficient form for photocatalytic treatments of organic pollutants in water because of high surface contacts between the surface of heterogeneous photocatalysts and organic pollutants in water, the suspension form has major concerns about the recovery and reuse of the suspended materials and also the leak possibility to the environment of the photocatalysts. Therefore, the reuse strategies and leakage protections of the catalysts are ones of the challenges.

Coated Photocatalysts on Supporters or Substrates

Coating of a photocatalyst as a thin layer on supporting materials is an effective strategy to overcome the limitation of nanostructured photocatalyst powders involving the post-separation of slurry catalysts from the treated wastewater. Recent approaches for treatments of organic pollutants are as follows.

Treatments of Pharmaceuticals and Personal Care Products

Photocatalytic removal of pharmaceuticals and personal care products in water using photocatalysts coated on various support materials has been investigated, e.g., removal of salicylic acid, naproxen, diclofenac, and ibuprofen by TiO₂ (P25)/tetraethyl orthosilicate coated on glazed ceramics (Zhang et al. 2015); removal of ibuprofen by micro-TiO₂ on coated glass rings (Czech and Tysczuk-Rotko 2018); and removal of a wide variety of pharmaceuticals and personal care products and their metabolites [i.e., pharmaceuticals (carbamazepine, venlafaxine, fluoxetine, atenolol, sulfamethoxazole, ibuprofen, atorvastatin, and naproxen) and personal care products (triclosan and triclocarban)] by TiO₂ coated on quartz fiber filters (Arlos et al. 2016). Dip-coating technique is mostly used for the photocatalyst coatings in wide areas.

Treatments of Persistent Organic Pollutants

Photocatalytic removal of persistent organic pollutants in water is widely carried out using photocatalysts coated on solid substrates, especially glass substrates. The commercial TiO₂-coated glass microrods were applied to degrade phenol in water. The adherence of TiO₂ to glass microrods was proved to be good. The powder suspension of TiO₂ in bulk solution was not observed after experimental runs (Medina-Valtierra et al. 2006). Glass tubes and glass beads were used as supporting materials of TiO₂ thin film for degradation of paraquat in water. In the case of glass tubes, the photocatalytic activity of three different types of TiO₂ was compared, including commercial TiO₂ (P25), TiO₂ synthesized by hydrothermal method, and TiO₂ synthesized by sol-gel method. It was found that TiO₂ synthesized by hydrothermal method exhibited the highest paraquat herbicide removal efficiency (99%), followed by commercial TiO₂ (75%) and TiO₂ synthesized by sol-gel method (65%), respectively. The reason was that anatase phase of TiO₂ transformed to rutile phase during sol-gel preparation method with heat treatment above 400 °C (Lee et al. 2002). In the case of glass beads, paraquat can be efficiently degraded by N, S codoped TiO₂-coated glass beads under sunlight and visible light irradiation. The paraquat removal efficiencies could maintain after ten consecutive runs (Zahedi et al. 2015). Furthermore, photocatalytic removal of mixed pesticides (methyl parathion, dichlorvos, and lindane) in water using TiO₂-coated glass plates is presented in the

literature. All of the pesticides were completely removed, when the TiO_2 coated glass plates were used as a baffle wall of the reactor under solar light irradiation (Senthilnathan and Philip 2012).

Treatments of Organic Dyes

Photocatalyst-coated substrates can also be applied for degradation the organic dyes in water, which can form reactive oxygen species to individual or combination treatments. These coated substrates can be prepared by traditional coating techniques, such as pulsed laser deposition, spin coating, electron beam evaporation, spray pyrolysis, chemical bath deposition, sol-gel, dip-coating, and doctor blade. For instance, titanium dioxide-coated glass, ceramic tile, and stainless steel sheets can decolorize methylene blue and industrial dye wastewater up to 93% and can reuse up to 20 times with the same efficiencies (Sirirerkratana et al. 2019). TiO_2 layers immobilized on glass substrates by dip-coating technique for degradation of methyl orange were reported (Bouarioua and Zerdaoui 2017). It was found that three layers of TiO_2 are the best condition for the test with good adhesion and reproducibility. Besides, they claimed that immobilized TiO_2 can replace the suspension mode and eliminate the costly separation process of the catalysts (Bouarioua and Zerdaoui 2017). Other examples of photocatalyst-coated substrates for organic dye degradation are carbon-coated tungsten oxide (Tong et al. 2019), nebulizer spray-coated BiVO_4 thin films (Dhas et al. 2019), Fe ion-doped polyaniline film on tin-doped indium oxide (ITO)-coated glass substrate (Haspulat et al. 2013), and P-doped TiO_2 nanoparticles film coated on a ground glass substrate (Lv et al. 2011).

1.5 Modifications of Heterogeneous Photocatalysts

It has been proven that heterogeneous photocatalysis is one of the most potential methods for the treatment of organic pollutants in water. Relatively large band gap energy is a limitation of metal oxide-based heterogeneous photocatalysts, causing the requirement of UV light for activation. In addition, electron-hole recombination can also occur after the charge separation and migration of photogenerated carriers, resulting in the unsatisfactory photocatalytic activity to treat the target pollutants. The electronic band structure modifications and charge separation improvements of metal oxide-based photocatalysts have attracted significant attentions in the field of environmental treatments. Modifications of electronic band can be achieved by doping and composites of semiconductors. These enhance the photocatalytic activity of photocatalysts and shift the light absorption range toward visible region.

Another modification technique in heterogeneous photocatalysts is the utilization of electrical potential in photocatalysis. The coated semiconductor photocatalysts are used as the photoelectrodes in photo-electrocatalytic applications.

Table 1.7 Photocatalytic removal of pharmaceuticals and personal care products in water using modified photocatalysts

| Modification strategy | Photocatalyst | Organic pollutant | Reference |
|-----------------------|--|--------------------------|---------------------------------|
| Doping | Fe-doped TiO ₂ | Carbamazepine | Lin et al. (2017) |
| | | Ibuprofen | |
| | | Sulfamethoxazole | |
| | Bi-doped TiO ₂ | Ibuprofen | Bhatia and Dhir (2016) |
| | Ni-doped TiO ₂ | | |
| | N-doped TiO ₂ | Ciprofloxacin | Shetty et al. (2017) |
| | | Naproxen | |
| | | Paracetamol | |
| | S-doped TiO ₂ | Diclofenac | Yi et al. (2019) |
| | Pt-doped ZnO | Caffeine | Vaiano et al. (2019) |
| Ag-doped ZnO | | | |
| Au-doped ZnO | | | |
| Composite | Mg-ZnO-Al ₂ O ₃ | Caffeine | Elhalil et al. (2018) |
| | TiO ₂ /reduced graphene oxide | Carbamazepine | Lin et al. (2017) |
| | | Ibuprofen | |
| | | Sulfamethoxazole | |
| | Multi-walled carbon nanotubes-TiO ₂ -SiO ₂ | Acetaminophen | Czech and Tyszczyk-Rotko (2018) |
| ZnO-zeolite | Benzophenone caffeine | Jagannatha et al. (2019) | |
| Photoelectrode | TiO ₂ nanopore array | Tetracycline | Liu et al. (2009) |
| | TiO ₂ /SiO ₂ /Fe ₃ O ₄ | Diclofenac | Hu et al. (2011) |

Tables 1.7, 1.8 and 1.9 conclude several modification strategies for remediation of pharmaceuticals and personal care products, persistent organic pollutants, and organic dyes in water.

1.5.1 Doping

Doping of semiconductor photocatalysts with one or more foreign ions is one of the promising modification strategies to enhance the photocatalytic activity of photocatalyst under UV irradiation and shift the absorption wavelength to visible light. Metal doping displays a successful approach for modifications of photocatalysts with improved photonic efficiencies (Coronado et al. 2013). Metal-doped photocatalysts, such as Fe-doped TiO₂, Bi-doped TiO₂, Ni-doped TiO₂, Pt-doped ZnO, Ag-doped ZnO, and Au-doped ZnO, were published in the recent years (Lin et al. 2017; Bhatia and Dhir 2016; Vaiano et al. 2019). The nonmetal-doped photocatalysts are also available in the literature such as N-doped TiO₂ (Shetty et al. 2017) and S-doped TiO₂ (Yi et al. 2019). Doping can be done by

Table 1.8 Photocatalytic removal of persistent organic pollutants in water using modified photocatalysts

| Modification strategy | Photocatalyst | Organic pollutant | Reference |
|-----------------------|---|----------------------------|-------------------------------|
| Doping | Cu-doped TiO ₂ | Organophosphorus pesticide | Manga Raju et al. (2019) |
| | Fe-doped TiO ₂ | Diazinon pesticide | Phuong et al. (2019) |
| | C-doped TiO ₂ | Paraoxon pesticides | Rasoulnezhad et al. (2017) |
| | | Parathion pesticides | |
| | Fe-doped TiO ₂ | Diazinon | Tabasideh et al. (2017) |
| | Pd-doped In ₂ O ₃ | Atrazine | Aazam et al. (2018) |
| | Br-doped diamond | Methomyl pesticide | Costa et al. (2017) |
| Br-doped diamond | Insecticide propoxur | Guelfi et al. (2017) | |
| Composite | Polyaniline/FeZSM-5 | Herbicide glyphosate | Milojević-Rakić et al. (2018) |
| | MIL(Fe)/Fe-SPC composite | Thiamethoxam | Wei et al. (2018) |
| | Pd/ZnWO ₄ nanocomposite | Methylene blue | Chen et al. (2019a) |
| | TiO ₂ /Fe ₂ O ₃ nanocomposite | Diazinon | Mirmasoomi et al. (2017) |
| | ZnO nanorod/carboxylic graphene/polyaniline composite | Diuron | Anirudhan et al. (2018) |
| | Fe ₃ O ₄ /metal-organic framework nanocomposite | Diazinon | Sajjadi et al. (2019) |
| | TiO ₂ /ZrO ₂ nanocomposite | Herbicide chloridazon | Mbiri et al. (2018) |
| | Ag-ZnO composite | Imidacloprid | Kanwal et al. (2018) |
| | In, S-TiO ₂ /reduced graphene oxide nanocomposite | Pesticide atrazine | Khavar et al. (2018) |
| Photoelectrode | TiO ₂ /Ni photoelectrode | Dipterex pesticide | Fang et al. (2012) |
| | Porous coral-like WO ₃ /W photoelectrode | Perfluorooctanoic acid | Pan et al. (2019) |
| | Fluorine-doped tin oxide/WO ₃ /BiVO ₄ photoelectrodes | Phenol | Chatchai et al. (2009) |

several methods, such as impregnation, coprecipitation, ion implantation, and in situ synthesis methods (e.g., sol-gel, hydrothermal, and solvothermal).

Table 1.9 Photocatalytic removal of organic dyes in water using modified photocatalysts

| Modification strategy | Photocatalyst | Organic pollutant | Reference |
|-----------------------|--|----------------------------|-----------------------------|
| Doping | M-doped TiO ₂ nanoparticles (M=Cu, Zn) | Methyl orange | Khairy and Zakaria (2014) |
| | Fe-doped ZnO | Methyl orange | Saleh and Djaja (2014) |
| | Sr-doped NaTaO ₃ | Methylene blue | An et al. (2018) |
| | P- and Ag-doped TiO ₂ | <i>p</i> -Nitrophenol | Bodson et al. (2016) |
| | Fe ³⁺ Cr ³⁺ -codoped BaTiO ₃ | Azo dyes | Amaechi et al. (2019) |
| | Mg-doped ZnO | Methylene blue | Paula et al. (2019) |
| | GO-doped TiO ₂ | Rhodamine B | Zhang et al. (2017) |
| | Codoped or tri-doped g-C ₃ N ₄ | Rhodamine B methylene blue | Hasija et al. (2019) |
| Composite | NiO–ZnO–Ag nanocomposites | Methylene blue | Aydoghmish et al. (2019) |
| | Niobium oxides and different polymer matrices | Methylene blue | Heitmann et al. (2019) |
| | Tetraphenylporphyrin/WO ₃ /exfoliated graphite | Acid blue 25 (AB-25) | Malefane et al. (2019) |
| | Reduced graphene oxide-ZrO ₂ composite | Crystal violet | Ali et al. (2019) |
| | TiO ₂ /Bi ₂ O ₃ | Orange II | Ayekoe et al. (2016) |
| | WO ₃ /TiO ₂ /carbon fiber | Orange II | Balta et al. (2019) |
| | Zn ₃ (PO ₄) ₂ /BiPO ₄ | Rhodamine B | Naciri et al. (2019) |
| | BiFeWO ₆ /α-AgVO ₃ | Rhodamine B | Senthil et al. (2019) |
| | Graphene/ZnO | Methyl orange | Wang et al. (2019c) |
| | Nb/TiO ₂ | Rhodamine B | Ravishankar et al. (2019) |
| | BiOBr/BiOI/cellulose | Rhodamine B | Du et al. (2019) |
| | CdS/g-C ₃ N ₄ /metal–organic framework | Rhodamine B | Chen et al. (2019b) |
| | g-C ₃ N ₄ /TiO ₂ | Rhodamine B | Monga and Basu (2019) |
| | N-doped TiO ₂ /resin | Rhodamine B | Louangsouphom et al. (2019) |
| | CuS–CdS | Methylene blue | Mahanthappa et al. (2019) |
| | Methyl orange | Sun et al. (2019) | |

(continued)

Table 1.9 (continued)

| Modification strategy | Photocatalyst | Organic pollutant | Reference |
|-----------------------|---|--|-------------------------------|
| | MFe ₂ O ₄ -Ag ₂ O (M = Zn, Co, Ni) | | |
| | CdS/reduced graphene oxide | Methylene blue | Chen et al. (2019a) |
| | CeO ₂ /sugarcane bagasse | Methylene blue | Channei et al. (2017) |
| | BiVO ₄ -GO-PTFE | Remazol brilliant blue R methylene blue Rhodamine B | Dowla et al. (2017) |
| | ZnO/PMMA | Methylene blue | Di Mauro et al. (2017) |
| | Poly(methyl methacrylate)-TiO ₂ | Methylene blue | Mirhoseini and Salabat (2015) |
| | Fe ₂ O ₃ -loaded activated carbon fiber/polymer | Methylene blue | Kadirova et al. (2017) |
| Photoelectrode | Ag ₂ Mn ₈ O ₁₆ nanocrystals/ TiO ₂ nanotubes | Rhodamine B | Thabit et al. (2018) |
| | RuO ₂ /TiO ₂ photoelectrode | Reactive brilliant red X-3B | Fang et al. (2013) |

Treatments of Pharmaceuticals and Personal Care Products

The concentration of dopants is an important factor affecting removal efficiencies of pharmaceuticals and personal care products. One example is ibuprofen removal over transition metal-doped ZnO under solar light irradiation (Bhatia and Dhir 2016). The concentration of transition metal dopant was varied from 0.25% to 1% by weight. The 0.25 wt% Bi-doped TiO₂ exhibited the maximum removal efficiency, and the removal efficiencies decreased with increasing Bi content. On the other hand, the maximum removal efficiency over Ni-doped TiO₂ was observed at Ni content of 0.5 wt%, and the removal efficiencies decreased when Ni content was higher or lower than 0.5 wt%. Consequently, the optimum content of dopants should be considered case by case.

Treatments of Persistent Organic Pollutants

P-doped and Ag-doped TiO₂ photocatalysts for photocatalytic degradation of *p*-nitrophenol under UV light (Bodson et al. 2016), copper-doped anatase/brookite TiO₂ nanohybrids (Manga Raju et al. 2019), Fe-TiO₂/Bent-Fe photocatalyst for removal of diazinon pesticide (Phuong et al. 2019), degradation of paraoxon and parathion pesticides on carbon-doped TiO₂ nanorod thin films (Rasoulnezhad et al. 2017), degradation of diazinon by iron-doped TiO₂ nanoparticles (Tabasideh et al. 2017), Pd-doped In₂O₃ nanocomposites to degradation of atrazine (Aazam et al.

2018), degradation of methomyl pesticide boron-doped diamond electrode (Costa et al. 2017), and degradation of the insecticide propoxur by boron-doped diamond/air-diffusion cell (Guelfi et al. 2017) have been reported.

Treatments of Organic Dyes

Cu-doped and Zn-doped TiO₂ nanoparticles synthesized by sol–gel method were applied for methyl orange degradation (Khairy and Zakaria 2014). The small crystallite size and doping were found to cause an increase in the adsorption edge wavelength with decrease in band gap energy. Cu-doped TiO₂ showed the optimum photocatalytic activity for methyl orange degradation.

Magnesium- and iron-doped ZnO nanoparticles were fabricated to use for degradation of methyl orange and/or methylene blue under UV irradiation (Paula et al. 2019; Saleh and Djaja 2014). It was found that the various parameters, i.e., pH, dopant concentrations, and photocatalytic dosage, affected the photocatalytic activity, especially dopant concentration is the most important factor.

NaTaO₃ photocatalysts were synthesized with doping of Sr cations through crystallization in molten NaCl flux, resulting in an increase in the population of excited electrons. However, the reaction rate of the obtained photocatalysts showed less enhancement compared with the increase in electron population, which ascribed to a limited fraction of electrons overriding the energy gradient and returning back to the surface (An et al. 2018).

Doping of graphitic carbon nitride (g-C₃N₄) by various types of metals (Na, K, transition metals, and rare earth metals) and nonmetal materials (phosphorus, sulfur, oxygen, nitrogen, carbon, boron, and halogen) for photocatalytic remediation of organic dyes in water was reviewed (Hasija et al. 2019). It was shown that the photocatalytic activity for degradation of organic pollutants (rhodamine B and methylene blue) of the doped materials was successfully enhanced up to 50% compared with the bare ones, because of changes of band gaps of the materials.

Co-doping of two metal dopants or a metal ion with a nonmetal dopant for synergistic photocatalytic effects, i.e., the working together of two things to produce an effect greater than the sum of their individual effects, of the dopants is an alternative way to modify metal oxide photocatalysts (Sanitnon et al. 2019). For an example, ferroelectric Fe³⁺Cr³⁺ codoped BaTiO₃ nanopowders for the photocatalytic oxidation of azo dyes were fabricated (Amaechi et al. 2019). The photocatalytic activity of the powders was found to be maintained after three cycle uses, and the powders could be reused without generating any secondary residue.

1.5.2 Composite of Semiconductors

Composite (also called coupling) of two or more semiconductors is considered as an effective method for modification of photocatalysts, because the separation of photo-

excited electrons and holes was accelerated, resulting in improved photocatalytic performances.

Treatments of Pharmaceuticals and Personal Care Products

A large number of semiconductor composites have been developed as photocatalyst for the removal of pharmaceuticals and personal care products in water, such as Mg-ZnO-Al₂O₃ (Elhalil et al. 2018), TiO₂/reduced graphene oxide (Lin et al. 2017), MWCNT-TiO₂-SiO₂ (Czech and Tyszczyk-Rotko 2018), and ZnO-zeolite (Jagannatha et al. 2019).

Presently, the visible light-responsive photocatalytic removal of pharmaceuticals and personal care products by carbon–oxygen–titanium linkages in the composite system has attracted significant attention. Photocatalytic removal of 29 different pharmaceuticals and personal care products over carbonaceous TiO₂ composites was summarized (Awfa et al. 2018). The main carbonaceous materials included activated carbon, carbon nanotubes, and graphene. These materials can enhance the photocatalytic removal efficiency of pharmaceuticals and personal care products due to their high specific surface area and large electron storage capacity. Moreover, the carbonaceous materials can behave as a sensitizer to provide electrons for TiO₂ which can subsequently be activated by photons with suitable energy leading to higher photocatalytic performance (Awfa et al. 2018).

Treatments of Persistent Organic Pollutants

Highly photoactive metal oxides could be achieved by composite with two or more different materials of TiO₂, ZnO, SnO₂, SrTiO₂, WO₃, Cu₂O, and Fe₂O₃ with nonmetal elements such as N, S, C, and F for photocatalytic remediation of persistent organic pollutants. For example, a development of polyaniline/FeZSM-5 composites for the degradation of herbicide glyphosate was reported (Milojević-Rakić et al. 2018). The composites showed efficient green catalytic degradation of pesticide/herbicide pollutants in environmental remediation systems.

MIL(Fe)/Fe-doped nanospongy porous biocarbon (MIL(Fe)/Fe-SPC) composites were used for the degradation of thiamethoxam, pesticides, and other environmental pollutants (Wei et al. 2018).

Semiconductor composites with unique selective adsorption properties, such as Pd/ZnWO₄ nanocomposite (Chen et al. 2019a), TiO₂/Fe₂O₃ nanocomposite (Mirmasoomi et al. 2017), zinc oxide nanorod-incorporated carboxylic graphene/polyaniline composite (Anirudhan et al. 2018), Fe₃O₄/metal–organic framework nanocomposite (Sajjadi et al. 2019), TiO₂/ZrO₂ nanocomposite (Mbiri et al. 2018), Ag-ZnO composite (Kanwal et al. 2018), and In-S-TiO₂/reduced graphene oxide nanocomposite (Khavar et al. 2018) for degradation and detoxification of pesticides, were reported. High crystallinity, small particle size, high surface area, and well-defined porosity are important parameters to provide active sites for adsorption of

pollutants and facilitate the diffusions of pollutants and products away from the photoactive centers that assisted the effective performances of the photocatalysts.

Treatments of Organic Dyes

Many researchers have studied the photocatalytic remediation of organic dyes in water by composite materials. Degradation of methylene blue, methyl orange, acid blue 25 (AB-25), crystal violet dye, orange II azo dye, rhodamine B by NiO-ZnO-Ag nanocomposites (Aydoghmissi et al. 2019), tetraphenylporphyrin/WO₃/exfoliated graphite nanocomposite (Malefane et al. 2019), reduced graphene oxide-ZrO₂ composite (Ali et al. 2019), WO₃/TiO₂/carbon fiber composite (Balta et al. 2019), Zn₃(PO₄)₂/BiPO₄ composite (Naciri et al. 2019), BiFeWO₆/α-AgVO₃ composite (Senthil et al. 2019), graphene/ZnO composite (Wang et al. 2019c), Nb/TiO₂ composite (Ravishankar et al. 2019), BiOBr/BiOI/cellulose composite (Du et al. 2019), CdS/g-C₃N₄/metal-organic framework composite (Chen et al. 2019b), g-C₃N₄/TiO₂ composite (Monga and Basu 2019), CuS-CdS composite (Mahanthappa et al. 2019), MFe₂O₄-Ag₂O composite (M = Zn, Co, & Ni) (Sun et al. 2019), CdS/reduced graphene oxide composite (Chen et al. 2019a), and CeO₂/sugarcane bagasse composite (Channei et al. 2017) was developed and reported.

Carbon-metal oxide composites are another interesting photocatalysts. For example, graphene oxide-doped mesoporous TiO₂ photocatalysts for rhodamine B degradation were reported (Zhang et al. 2017). The obtained photocatalysts showed photodegradation efficiency up to 81% under visible light irradiation. In addition, the well dispersion of graphene oxide and mesoporous TiO₂ nanoparticles leads the good influences on the photocatalytic performance of the photocatalysts.

Additionally, semiconductors composited with polymers were also developed. For example, modification of niobium oxides and different polymer matrices, e.g., polypropylene (PP), poly(3-hydroxybutyrate) (PHB), and polyurethane (WPU), were proposed (Heitmann et al. 2019). Nano-/micro-scaled TiO₂/polyacrylamide beads for efficient photodegradation of organic dyes were reported (Mudassir et al. 2018). Nanoscale feature and high surface area of the TiO₂/polyacrylamide beads showed the superior degradation of organic dyes and enhanced rate constant of the reactions. The composite beads also showed interesting properties of efficient disinfections of *E. coli* and *S. aureus* under photocatalytic applications (Mudassir et al. 2018). Other several semiconductor/polymer composites for photocatalytic dye degradations are BiVO₄-GO-PTFE (Dowla et al. 2017), ZnO/PMMA (Di Mauro et al. 2017), poly(methyl methacrylate)/TiO₂ (Mirhoseini and Salabat 2015), and Fe₂O₃-loaded activated carbon fiber/polymer [polyester fiber or polyethylene pulp] (Kadirova et al. 2017).

1.5.3 Photoelectrodes in Photo-Electrocatalytic Process

Photo-electrocatalysis has become an attractive way to increase the catalytic efficiency of photocatalysis. Photo-electrocatalytic degradation of organic pollutants in water using photocatalyst-coated substrates as photoelectrodes has been developed.

Treatments of Pharmaceuticals and Personal Care Products

TiO₂ nanopore array for photo-electrocatalytic removal of tetracycline was reported (Liu et al. 2009). A comparative removal of diclofenac by magnetically attached TiO₂/SiO₂/Fe₃O₄ coated on graphite under UV irradiation with and without electric potential was performed by Hu et al. (2011). In the presence of +0.8 V, the removal efficiency of diclofenac was significantly higher than that of the conventional photocatalysis (Hu et al. 2011).

Treatments of Persistent Organic Pollutants

Photo-electrocatalytic remediation of persistent organic pollutants using TiO₂/Ni photoelectrode showed the reduction of chemical oxygen demand (COD) of water up to 82.6% (Fang et al. 2012). This method is more efficient than typical photocatalysis and typical electrochemical oxidations. A study of coral-like porous WO₃/W photoelectrode for degradation of perfluorooctanoic acid, a highly toxic persistent organic pollutant, was reported (Pan et al. 2019). The uniqueness of this research is the porous coral-like structure that has a suitable energy band position and strong oxidation ability, leading to a strong ability for photo-electrocatalytic degradation of perfluorooctanoic acid. Another example is the use of fluorine-doped tin oxide/WO₃/BiVO₄ photoelectrodes that showed that mixing of metal oxides on the BiVO₄ photocatalysts could enhance the charge separation (Chatchai et al. 2009). In the study of efficient photocatalytic degradation of phenol as a persistent organic pollutant substrate over Co₃O₄/BiVO₄ composite, the key factor for the high photocatalytic activity is the sequence of WO₃ and BiVO₄ layers (Long et al. 2006).

Treatments of Organic Dyes

Photoelectrodes made of Ag₂Mn₈O₁₆ nanocrystals/TiO₂ nanotubes were fabricated via anodization and annihilation methods and used for photocatalytic degradation of rhodamine B under solar-simulated light irradiation (Thabit et al. 2018). RuO₂/TiO₂ photoelectrodes for degradation of reactive brilliant red (X-3B) were also reported (Fang et al. 2013).

1.6 Photocatalytic Reactors for Remediation of Organic Pollutants

Photocatalytic reactor design is the major challenge in photocatalytic remediation of organic pollutants in water. The important key in photocatalytic reactor design consideration is that the large area of photocatalysts has to be illuminated efficiently. In general, the photocatalytic reactor configuration for wastewater treatment can be classified as two main groups, including fixed bed reactor and slurry type reactor (Ibhadon and Fitzpatrick 2013). Apart from the conventional photocatalytic reactor, the combination of photocatalysis with another treatment process has also been developed to overcome the specific obstacles in each case, such as a photocatalytic membrane reactor.

A wide variety of reactor configurations for removals of pharmaceuticals and personal care products have been reported in the literature. For example, removal of amoxicillin in water by a conventional slurry photocatalytic reactor under simulated solar light irradiation was performed (Nguyen et al. 2019). The optimal conditions for that study are an initial amoxicillin concentration of 1.0 μM , a photocatalyst amount of 0.104 g/L, and a pH of 4 (Nguyen et al. 2019). The continuous fixed bed photocatalytic reactor for the removal of paracetamol was developed (Borges et al. 2015). The reactor consists of TiO_2 -coated glass spheres placed in the glass tube. The synthetic wastewater was recirculated along with the system by a peristaltic pump during the irradiation of the simulated solar light. A submerged ceramic membrane photocatalytic reactor for amoxicillin removal was designed and reported (Li et al. 2019). The system is composed of two stainless steel rectangular tanks with the ceramic membrane fixed inside the tanks. The air compressor was connected to the top of the membrane for backwashing. The aeration pipe was installed at the bottom of the tanks to prevent the accumulating of photocatalyst powder on the membrane surface (Li et al. 2019).

A combination of conventional slurry or fixed bed photocatalytic reactors and membrane filtration for remediation of persistent organic pollutants in water has attracted considerable attention from researchers since the last decade. For example, a slurry bed photocatalytic membrane reactor for the removal of 32 different persistent organic pollutants was developed. The system is composed of a pre-filter unit, an irradiation unit with 32 UV lamps, and a photocatalyst recovery unit. A ceramic microfiltration membrane was used to separate photocatalysts (Benotti et al. 2009).

For organic dyes, a number of reactors (apart from conventional slurry-type ones) for remediation of organics dye in water have been created. A slurry-type reactor combined with an air sparging unit for degradation of methylene blue in water was reported (Abdellah et al. 2018). A fixed bed photocatalytic membrane reactor for degradation of 4BS dye was designed. N-doped TiO_2 was immobilized on a ceramic membrane, and then the membrane was installed between a reaction chamber and a separation chamber. A xenon lamp was used as a light source. The dye-containing aqueous solution was fed by a diaphragm pump (Wang et al. 2016). A photocatalytic reactor consisted of a UVA or UVC light source installed on the top of a chamber

was designed to decolorization of a synthetic (methylene blue-contained) wastewater and an actual (reactive purple-contained) dye wastewater. A pump was used to circulate the water on the 15° tiled TiO₂-coated substrates, i.e., glass, ceramic tile, and stainless steel sheets (Sirirerkratana et al. 2019). Two reactors – a batch reactor and a continuous reactor – were designed for degradation of acid violet 7 dye (AV7) using ZnO/polypyrrole powder photocatalysts. In the batch reactor, the powder photocatalysts were fixed on a rectangular glass plate, and the fixed glass was immersed in the dye solution. In a continuous annular reactor, the powders were supported on the inner wall of an external quartz ring that covered a UV lamp quartz tube (González-Casamachin et al. 2019).

1.7 Conclusions

Photocatalysis is a process which a chemical reaction is accelerated in the presence of a catalyst on exposure to light. Photocatalysis could be classified to be two types, i.e., homogeneous and heterogeneous photocatalysis, on the basis of appearances of the physical state of reactants. Ozonation (UV/O₃), photo-Fenton processes (Fe²⁺ and Fe²⁺/H₂O₂), UV/H₂O₂, and UV/H₂O₂/O₃ are examples of homogeneous photocatalysis, while photocatalysts in heterogeneous photocatalysis are typically semiconductor materials (i.e., metal oxides) which can be used in powder and suspension forms or coated forms on other substrates. Both homogeneous and heterogeneous photocatalytic processes have been utilized as alternative technologies for remediation of organic pollutants in water, including (i) pharmaceuticals and personal care products (synthetic compounds with specific properties for human or animal healthcare and medical purposes); (ii) persistent organic pollutants (organochlorine pesticides and industrial chemicals with long half-lives and persistence in the environment); and (iii) organic dyes (synthetic organic substances for colorants). Homogeneous photocatalysis has many advantages, e.g., high oxidation properties. It is, however, not popular in various photocatalytic applications, because it is difficult to separate the photocatalysts from the solution, the photocatalysts have low potential to reuse, purification of products is necessary, and almost homogeneous photocatalysts absorb narrowly light within the solar spectrum. It has been proven that heterogeneous photocatalysis is one of the most potential methods for the treatment of organic pollutants in water. Anyhow, relatively large band gap energy causes some limitations of metal oxide-based heterogeneous photocatalysts. Modifications of the electronic band can be achieved by doping and composites of semiconductors. Another modification technique in heterogeneous photocatalysts is the utilization of electrical potential in photocatalysis. The coated semiconductor photocatalysts are used as photoelectrodes in photo-electrocatalytic applications. In addition, the photocatalytic reactor configuration for wastewater treatment by heterogeneous photocatalysis can be classified as two main groups, including fixed bed reactor and slurry-type reactor. Apart from the conventional photocatalytic reactors, the combination of photocatalysis with another treatment process has also been

developed to overcome the specific obstacles in each case, such as a photocatalytic membrane reactor.

References

- Aazam E, Mohamed R, Hassan T (2018) Pd-doped In_2O_3 nanocomposites for the photocatalytic degradation of atrazine. *Desalin Water Treat* 101:216–222. <https://doi.org/10.5004/dwt.2018.21804>
- Abdel Messih MF, Ahmed MA, Soltan A, Anis SS (2017) Facile approach for homogeneous dispersion of metallic silver nanoparticles on the surface of mesoporous titania for photocatalytic degradation of methylene blue and indigo carmine dyes. *J Photochem Photobiol A Chem* 335:40–51. <https://doi.org/10.1016/j.jphotochem.2016.11.001>
- Abdellah MH, Nosier SA, El-Shazly AH, Mubarak AA (2018) Photocatalytic decolorization of methylene blue using TiO_2 /UV system enhanced by air sparging. *Alex Eng J* 57(4):3727–3735. <https://doi.org/10.1016/j.aej.2018.07.018>
- Affam AC, Chaudhuri M (2013) Degradation of pesticides chlorpyrifos, cypermethrin and chlorothalonil in aqueous solution by TiO_2 photocatalysis. *J Environ Manag* 130:160–165. <https://doi.org/10.1016/j.jenvman.2013.08.058>
- Agenson KO, Oh J-I, Uruse T (2003) Retention of a wide variety of organic pollutants by different nanofiltration/reverse osmosis membranes: controlling parameters of process. *J Membr Sci* 225 (1–2):91–103. <https://doi.org/10.1016/j.memsci.2003.08.006>
- Ahmad YH, Mohamed AT, Sliem MH, Abdullah AM, Al-Qaradawi SY (2018) Enhanced photocatalytic performance of WON@porous TiO_2 nanofibers towards sunlight-assisted degradation of organic contaminants. *RSC Adv* 8(57):32747–32755. <https://doi.org/10.1039/C8RA06477F>
- Aimer Y, Benali O, Groenen Serrano K (2019) Study of the degradation of an organophosphorus pesticide using electrogenerated hydroxyl radicals or heat-activated persulfate. *Sep Purif Technol* 208:27–33. <https://doi.org/10.1016/j.seppur.2018.05.066>
- Ali TT, Narasimharao K, Basahel SN, Mokhtar M, Alsharaeh EH, Mahmoud HA (2019) Template assisted microwave synthesis of rGO-ZrO₂ composites: efficient photocatalysts under visible light. *J Nanosci Nanotechnol* 19(8):5177–5188. <https://doi.org/10.1166/jnn.2019.16827>
- Amaechi IC, Hadj Youssef A, Rawach D, Claverie JP, Sun S, Ruediger A (2019) Ferroelectric Fe–Cr codoped BaTiO_3 nanoparticles for the photocatalytic oxidation of azo dyes. *ACS Appl Nano Materials* 2(5):2890–2901. <https://doi.org/10.1021/acsnanm.9b00336>
- Ameta RK, Chohadia A, Jain A, Punjabi PB (2018a) Chapter 3: Fenton and Photo-Fenton processes. In: Ameta SC, Ameta R (eds) *Advanced oxidation processes for waste water treatment*. Academic, pp 49–87. <https://doi.org/10.1016/B978-0-12-810499-6.00003-6>
- Ameta R, Solanki MS, Benjamin S, Ameta SC (2018b) Chapter 6: Photocatalysis. In: Ameta SC, Ameta R (eds) *Advanced oxidation processes for waste water treatment*. Academic, pp 135–175. <https://doi.org/10.1016/B978-0-12-810499-6.00006-1>
- An L, Kitta M, Iwase A, Kudo A, Ichikuni N, Onishi H (2018) Photoexcited electrons driven by doping concentration gradient: flux-prepared NaTaO_3 photocatalysts doped with strontium cations. *ACS Catal* 8(10):9334–9341. <https://doi.org/10.1021/acscatal.8b02437>
- Anantharaman A, Josephine BA, Teresita VM, Ajeesha T, George M (2019) Photo-Fenton activity of magnesium substituted cerium ferrite perovskites for degradation of methylene blue via sol-gel method. *J Nanosci Nanotechnol* 19(8):5116–5129. <https://doi.org/10.1166/jnn.2019.16819>
- Andreozzi R, Caprio V, Insola A, Marotta R (1999) Advanced oxidation processes (AOP) for water purification and recovery. *Catal Today* 53(1):51–59. [https://doi.org/10.1016/S0920-5861\(99\)00102-9](https://doi.org/10.1016/S0920-5861(99)00102-9)

- Anirudhan TS, Shainy F, Manasa Mohan A (2018) Fabrication of zinc oxide nanorod incorporated carboxylic graphene/polyaniline composite and its photocatalytic activity for the effective degradation of diuron from aqueous solutions. *Sol Energy* 171:534–546. <https://doi.org/10.1016/j.solener.2018.06.111>
- Arlon MJ, Hatat-Fraile MM, Liang R, Bragg LM, Zhou NY, Andrews SA, Servos MR (2016) Photocatalytic decomposition of organic micropollutants using immobilized TiO₂ having different isoelectric points. *Water Res* 101:351–361. <https://doi.org/10.1016/j.watres.2016.05.073>
- Arvanitoyannis IS, Kassaveti A (2008) 8 – Olive oil waste management: treatment methods and potential uses of treated waste. In: Arvanitoyannis IS (ed) *Waste management for the food industries*. Academic, Amsterdam, pp 453–568. <https://doi.org/10.1016/B978-012373654-3.50011-0>
- Awfa D, Ateia M, Fujii M, Johnson MS, Yoshimura C (2018) Photodegradation of pharmaceuticals and personal care products in water treatment using carbonaceous-TiO₂ composites: a critical review of recent literature. *Water Res* 142:26–45. <https://doi.org/10.1016/j.watres.2018.05.036>
- Aydoghmish SM, Hassanzadeh-Tabrizi SA, Saffar-Teluri A (2019) Facile synthesis and investigation of NiO–ZnO–Ag nanocomposites as efficient photocatalysts for degradation of methylene blue dye. *Ceram Int* 45(12):14934–14942. <https://doi.org/10.1016/j.ceramint.2019.04.229>
- Ayekoe PY, Robert D, Gone DL (2016) Preparation of effective TiO₂/Bi₂O₃ photocatalysts for water treatment. *Environ Chem Lett* 14(3):387–393. <https://doi.org/10.1007/s10311-016-0565-3>
- Balkaya N, Guneyso S (2019) *Recycling and reuse approaches for better sustainability*. Springer. ISBN 978-3-319-95888-0
- Balta Z, Bilgin Simek E, Berek D (2019) Solvothermal synthesis of WO₃/TiO₂/carbon fiber composite photocatalysts for enhanced performance under sunlight illumination. *Photochem Photobiol*. <https://doi.org/10.1111/php.13117>
- Benotti MJ, Stanford BD, Wert EC, Snyder SA (2009) Evaluation of a photocatalytic reactor membrane pilot system for the removal of pharmaceuticals and endocrine disrupting compounds from water. *Water Res* 43(6):1513–1522. <https://doi.org/10.1016/j.watres.2008.12.049>
- Bensebaa F (2013) Clean energy. In: *Interface science and technology*, vol 19. Elsevier, pp 279–383. <https://doi.org/10.1016/B978-0-12-369550-5.00005-7>
- Bhatia V, Dhir A (2016) Transition metal doped TiO₂ mediated photocatalytic degradation of anti-inflammatory drug under solar irradiations. *J Environ Chem Eng* 4(1):1267–1273. <https://doi.org/10.1016/j.jece.2016.01.032>
- Bodalo-Santoyo A, Gómez-Carrasco J, Gomez-Gomez E, Maximo-Martin F, Hidalgo-Montesinos A (2003) Application of reverse osmosis to reduce pollutants present in industrial wastewater. *Desalination* 155(2):101–108. [https://doi.org/10.1016/S0011-9164\(03\)00287-X](https://doi.org/10.1016/S0011-9164(03)00287-X)
- Bodson CJ, Heinrichs B, Tasseroul L, Bied C, Mahy JG, Man MWC, Lambert SD (2016) Efficient P- and Ag-doped titania for the photocatalytic degradation of waste water organic pollutants. *J Alloys Compd* 682:144–153. <https://doi.org/10.1016/j.jallcom.2016.04.295>
- Borges ME, Garcia DM, Hernandez T, Ruiz-Morales JC, Esparza P (2015) Supported photocatalyst for removal of emerging contaminants from wastewater in a continuous packed-bed photoreactor configuration. *Catalysts* 5(1):77–87. <https://doi.org/10.3390/catal5010077>
- Bouarioua A, Zerdaoui M (2017) Photocatalytic activities of TiO₂ layers immobilized on glass substrates by dip-coating technique toward the decolorization of methyl orange as a model organic pollutant. *J Environ Chem Eng* 5(2):1565–1574. <https://doi.org/10.1016/j.jece.2017.02.025>
- Boudissa F, Mirilà D, Arus V-A, Terkmani T, Semaan S, Proulx M, Nistor I-D, Roy R, Azzouz A (2019) Acid-treated clay catalysts for organic dye ozonation – thorough mineralization through optimum catalyst basicity and hydrophilic character. *J Hazard Mater* 364:356–366. <https://doi.org/10.1016/j.jhazmat.2018.09.070>
- Chang E, Liu T-Y, Huang C-P, Liang C-H, Chiang P-C (2012) Degradation of mefenamic acid from aqueous solutions by the ozonation and O₃/UV processes. *Sep Purif Technol* 98:123–129. <https://doi.org/10.1016/j.seppur.2012.02.020>

- Changchao Z, Feng C, Jintao Y, Mingqiang Z, Jianping S, Xiaoping J (2018) Enhanced UV/H₂O₂ process by expanded graphite: an effective method for rhodamine B dye decolorization. *Res Chem Intermed* 44(4):2425–2437. <https://doi.org/10.1007/s11164-017-3238-3>
- Channei D, Nakaruk A, Phanichphant S (2017) Photocatalytic degradation of dye using CeO₂/SCB composite catalysts. *Spectrochim Acta A Mol Biomol Spectrosc* 183:218–224. <https://doi.org/10.1016/j.saa.2017.04.063>
- Chatchai P, Murakami Y, Kishioka S-y, Nosaka AY, Nosaka Y (2009) Efficient photocatalytic activity of water oxidation over WO₃/BiVO₄ composite under visible light irradiation. *Electrochim Acta* 54(3):1147–1152. <https://doi.org/10.1016/j.electacta.2008.08.058>
- Chen Y, Vymazal J, Březinová T, Koželuh M, Kule L, Huang J, Chen Z (2016) Occurrence, removal and environmental risk assessment of pharmaceuticals and personal care products in rural wastewater treatment wetlands. *Sci Total Environ* 566:1660–1669. <https://doi.org/10.1016/j.scitotenv.2016.06.069>
- Chen F, Zou X, Chen C, Hu Q, Wei Y, Wang Y, Xiang B, Zhang J (2019a) Surfactant-free synthesis of homogeneous nano-grade cadmium sulfide grafted reduced graphene oxide composite as a high-activity photocatalyst in visible light. *Ceram Int* 45(11):14376–14383. <https://doi.org/10.1016/j.ceramint.2019.04.153>
- Chen Y, Zhai B, Liang Y, Li Y, Li J (2019b) Preparation of CdS/g-C₃N₄/MOF composite with enhanced visible-light photocatalytic activity for dye degradation. *J Solid State Chem* 274:32–39. <https://doi.org/10.1016/j.jssc.2019.01.038>
- Choina J, Kosslick H, Fischer C, Flechsig GU, Frunza L, Schulz A (2013) Photocatalytic decomposition of pharmaceutical ibuprofen pollutions in water over titania catalyst. *Appl Catal B Environ* 129:589–598. <https://doi.org/10.1016/j.apcatb.2012.09.053>
- Cizmas L, Sharma VK, Gray CM, McDonald TJ (2015) Pharmaceuticals and personal care products in waters: occurrence, toxicity, and risk. *Environ Chem Lett* 13(4):381–394. <https://doi.org/10.1007/s10311-015-0524-4>
- Coronado JM, Fresno F, Hernández-Alonso MD, Portela R (2013) Design of advanced photocatalytic materials for energy and environmental applications. Springer. <https://doi.org/10.1007/978-1-4471-5061-9>
- Costa DJ, Santos JC, Sanches-Brandao FA, Ribeiro WF, Salazar-Banda GR, Araujo MC (2017) Boron-doped diamond electrode acting as a voltammetric sensor for the detection of methomyl pesticide. *J Electroanal Chem* 789:100–107. <https://doi.org/10.1016/j.jelechem.2017.02.036>
- Crini G, Badot P-M (2008) Application of chitosan, a natural aminopolysaccharide, for dye removal from aqueous solutions by adsorption processes using batch studies: a review of recent literature. *Prog Polym Sci* 33(4):399–447. <https://doi.org/10.1016/j.progpolymsci.2007.11.001>
- Cruz M, Gomez C, Duran-Valle CJ, Pastrana-Martínez LM, Faria JL, Silva AM, Faraldos M, Bahamonde A (2017) Bare TiO₂ and graphene oxide TiO₂ photocatalysts on the degradation of selected pesticides and influence of the water matrix. *Appl Surf Sci* 416:1013–1021. <https://doi.org/10.1016/j.apsusc.2015.09.268>
- Czech B, Tyszczyk-Rotko K (2018) Visible-light-driven photocatalytic removal of acetaminophen from water using a novel MWCNT-TiO₂-SiO₂ photocatalysts. *Sep Purif Technol* 206:343–355. <https://doi.org/10.1016/j.seppur.2018.06.025>
- da Costa EP, Bottrel SEC, Starling MCV, Leão MM, Amorim CC (2019) Degradation of carbendazim in water via photo-Fenton in Raceway Pond Reactor: assessment of acute toxicity and transformation products. *Environ Sci Pollut Res* 26(5):4324–4336. <https://doi.org/10.1007/s11356-018-2130-z>
- De la Cruz N, Gimenez J, Esplugas S, Grandjean D, de Alencastro LF, Pulgarin C (2012) Degradation of 32 emergent contaminants by UV and neutral photo-Fenton in domestic wastewater effluent previously treated by activated sludge. *Water Res* 46(6):1947–1957. <https://doi.org/10.1016/j.watres.2012.01.014>
- Dhas CR, Arivukarasan D, Venkatesh R, Josephine AJ, Gnana Malar KCM, Santhoshi Monica SE, Subramanian B (2019) Influence of precursor aging time period on physical and photocatalytic

- properties of nebulizer spray coated BiVO₄ thin films. *Solid State Sci* 92:36–45. <https://doi.org/10.1016/j.solidstatesciences.2019.04.006>
- Di Mauro A, Cantarella M, Nicotra G, Pellegrino G, Gulino A, Brundo MV, Privitera V, Impellizzeri G (2017) Novel synthesis of ZnO/PMMA nanocomposites for photocatalytic applications. *Sci Rep* 7:40895. <https://doi.org/10.1038/srep40895>
- Diñçer AR, Güneş Y, Karakaya N, Güneş E (2007) Comparison of activated carbon and bottom ash for removal of reactive dye from aqueous solution. *Bioresour Technol* 98(4):834–839. <https://doi.org/10.1016/j.biortech.2006.03.009>
- Dominguez CM, Oturan N, Romero A, Santos A, Oturan MA (2018) Optimization of electro-Fenton process for effective degradation of organochlorine pesticide lindane. *Catal Today* 313:196–202. <https://doi.org/10.1016/j.cattod.2017.10.028>
- Dowla BMRU, Cho JY, Jang WK, Oh W-C (2017) Synthesis of BiVO₄-GO-PTFE nanocomposite photocatalysts for high efficient visible-light-induced photocatalytic performance for dyes. *J Mater Sci Mater Electron* 28(20):15106–15117. <https://doi.org/10.1007/s10854-017-7386-4>
- Du M, Du Y, Feng Y, Li Z, Wang J, Jiang N, Liu Y (2019) Advanced photocatalytic performance of novel BiOBr/BiOI/cellulose composites for the removal of organic pollutant. *Cellulose* 26(9):5543–5557. <https://doi.org/10.1007/s10570-019-02474-1>
- El Hassani K, Kalnina D, Turks M, Beakou BH, Anouar A (2019) Enhanced degradation of an azo dye by catalytic ozonation over Ni-containing layered double hydroxide nanocatalyst. *Sep Purif Technol* 210:764–774. <https://doi.org/10.1016/j.seppur.2018.08.074>
- Elhalil A, Elmoubarki R, Farnane M, Machrouhi A, Sadiq M, Mahjoubi F, Qourzal S, Barka N (2018) Photocatalytic degradation of caffeine as a model pharmaceutical pollutant on Mg doped ZnO-Al₂O₃ heterostructure. *Environ Nanotechnol Monit Manag* 10:63–72. <https://doi.org/10.1016/j.enmm.2018.02.002>
- Fang T, Yang C, Liao L (2012) Photoelectrocatalytic degradation of high COD dipterex pesticide by using TiO₂/Ni photo electrode. *J Environ Sci* 24(6):1149–1156. [https://doi.org/10.1016/S1001-0742\(11\)60882-6](https://doi.org/10.1016/S1001-0742(11)60882-6)
- Fang T, Liao L, Zhan S, Wu X (2013) Photoelectrocatalytic decolorization of reactive brilliant red X-3B. *Asian J Chem* 25(2):807–810. <https://doi.org/10.14233/ajchem.2013.12920>
- Fent K, Weston AA, Caminada D (2006) Ecotoxicology of human pharmaceuticals. *Aquat Toxicol* 76(2):122–159. <https://doi.org/10.1016/j.aquatox.2005.09.009>
- Fukahori S, Fujiwara T, Ito R, Funamizu N (2012) Photocatalytic decomposition of crotamiton over aqueous TiO₂ suspensions: determination of intermediates and the reaction pathway. *Chemosphere* 89(3):213–220. <https://doi.org/10.1016/j.chemosphere.2012.04.018>
- Ghosh M, Manoli K, Shen X, Wang JH, Ray AK (2019) Solar photocatalytic degradation of caffeine with titanium dioxide and zinc oxide nanoparticles. *J Photochem Photobiol A Chem* 377:1–7. <https://doi.org/10.1016/j.jphotochem.2019.03.029>
- Gong J, Liu Y, Sun X (2008) O₃ and UV/O₃ oxidation of organic constituents of biotreated municipal wastewater. *Water Res* 42(4–5):1238–1244. <https://doi.org/10.1016/j.watres.2007.09.020>
- González-Casamachin DA, De la Rosa JR, Lucio-Ortiz CJ, De Rio DADH, Martínez-Vargas DX, Flores-Escamilla GA, Guzman NED, Ovando-Medina VM, Moctezuma-Velazquez E (2019) Visible-light photocatalytic degradation of acid violet 7 dye in a continuous annular reactor using ZnO/PPy photocatalyst: synthesis, characterization, mass transfer effect evaluation and kinetic analysis. *Chem Eng J* 373:325–337. <https://doi.org/10.1016/j.cej.2019.05.032>
- Guelfi DRV, Gozzi F, Sirés I, Brillas E, Machulek A, de Oliveira SC (2017) Degradation of the insecticide propoxur by electrochemical advanced oxidation processes using a boron-doped diamond/air-diffusion cell. *Environ Sci Pollut Res* 24(7):6083–6095. <https://doi.org/10.1007/s11356-016-6416-8>
- Guo KH, Wu ZH, Yan SW, Yao B, Song WH, Hua ZC, Zhang XW, Kong XJ, Li XC, Fang JY (2018) Comparison of the UV/chlorine and UV/H₂O₂ processes in the degradation of PPCPs in simulated drinking water and wastewater: kinetics, radical mechanism and energy requirements. *Water Res* 147:184–194. <https://doi.org/10.1016/j.watres.2018.08.048>

- Hasija V, Raizada P, Sudhaik A, Sharma K, Kumar A, Singh P, Jonnalagadda SB, Thakur VK (2019) Recent advances in noble metal free doped graphitic carbon nitride based nanohybrids for photocatalysis of organic contaminants in water: a review. *Appl Mater Today* 15:494–524. <https://doi.org/10.1016/j.apmt.2019.04.003>
- Haspulat B, Gülce A, Gülce H (2013) Efficient photocatalytic decolorization of some textile dyes using Fe ions doped polyaniline film on ITO coated glass substrate. *J Hazard Mater* 260:518–526. <https://doi.org/10.1016/j.jhazmat.2013.06.011>
- He Y, Hua I (2013) Photochemical reactions of ibuprofen, naproxen, and tylosin. *ACS National Meetings* 350
- Heitmann AP, Rocha IC, Pereira IM, Oliveira LCA, de Oliveira Patrício PS (2019) Nanoparticles of niobium oxyhydroxide incorporated in different polymers for photocatalytic degradation of dye. *J Polym Res* 26(7):159. <https://doi.org/10.1007/s10965-019-1824-3>
- Hu XY, Yang J, Zhang JD (2011) Magnetic loading of $\text{TiO}_2/\text{SiO}_2/\text{Fe}_3\text{O}_4$ nanoparticles on electrode surface for photoelectrocatalytic degradation of diclofenac. *J Hazard Mater* 196:220–227. <https://doi.org/10.1016/j.jhazmat.2011.09.009>
- Huang Y, Yang Y, Wang X, Yuan X, Pi N, Yuan H, Liu X, Ni C (2018) Heterogeneous Fenton-like degradation of methoxychlor in water using two different FeS@hydrotalcites (LHDs) and $\text{Fe}_3\text{O}_4\text{@LHDs}$ catalysts prepared via an in situ growth method. *Chem Eng J* 342:142–154. <https://doi.org/10.1016/j.cej.2018.02.056>
- Ibhadon AO, Fitzpatrick P (2013) Heterogeneous photocatalysis: recent advances and applications. *Catalysts* 3(1):189–218. <https://doi.org/10.3390/catal3010189>
- Ikehata K, Li Y (2018) Chapter 5: Ozone-based processes. In: Ameta SC, Ameta R (eds) . Academic, *Advanced oxidation processes for waste water treatment*, pp 115–134. <https://doi.org/10.1016/B978-0-12-810499-6.00005-X>
- Ikehata K, Gamal El-Din M, Snyder SA (2008) Ozonation and advanced oxidation treatment of emerging organic pollutants in water and wastewater. *Ozone Sci Eng* 30(1):21–26. <https://doi.org/10.1080/01919510701728970>
- Ikhlaq A, Munir HMS, Khan A, Javed F, Joya KS (2019) Comparative study of catalytic ozonation and Fenton-like processes using iron-loaded rice husk ash as catalyst for the removal of methylene blue in wastewater. *Ozone Sci Eng* 41(3):250–260. <https://doi.org/10.1080/01919512.2018.1525276>
- Illés E, Szabó E, Takács E, Wojnárovits L, Dombi A, Gajda-Schranz K (2014) Ketoprofen removal by O_3 and O_3/UV processes: kinetics, transformation products and ecotoxicity. *Sci Total Environ* 472:178–184. <https://doi.org/10.1016/j.scitotenv.2013.10.119>
- Innocenzi V, Prisciandaro M, Centofanti M, Vegliò F (2019) Comparison of performances of hydrodynamic cavitation in combined treatments based on hybrid induced advanced Fenton process for degradation of azo-dyes. *J Environ Chem Eng* 7(3):103171. <https://doi.org/10.1016/j.jece.2019.103171>
- Iqbal MF, Tominaka S, Peng W, Takei T, Tsunoji N, Sano T, Ide Y (2018) Iron aquo complex as an efficient and selective homogeneous photocatalyst for organic synthetic reactions. *ChemCatChem* 10(20):4509–4513. <https://doi.org/10.1002/cctc.201801360>
- Jagannatha RB, Rani RS, Padaki M (2019) ZnO zeolite nanocomposite for photocatalytic elimination of benzophenone and caffeine. *ChemistrySelect* 4(6):1989–1993. <https://doi.org/10.1002/slct.201804006>
- Jamil TS, Roland H, Michael H, Jens-Uwe R (2017) Homogeneous photocatalytic processes for degradation of some endocrine disturbing chemicals under UV irradiation. *J Water Process Eng* 18:159–168. <https://doi.org/10.1016/j.jwpe.2017.04.005>
- Jayaswal K, Sahu V, Gurjar BR (2018) Chapter 2: Water pollution, human health and remediation. In: Bhattacharya S, Gupta A, Gupta A, Pandey A (eds) *Water remediation. Energy, environment, and sustainability*. Springer, Singapore, pp 11–27. https://doi.org/10.1007/978-981-10-7551-3_2

- Jing W, Li D, Li J, Li X, Wu Z, Liu Y (2018) Photodegradation of dimethyl phthalate (DMP) by UV-TiO₂ in aqueous solution: operational parameters and kinetic analysis. *Int J Environ Sci Technol* 15(5):969–976. <https://doi.org/10.1007/s13762-017-1471-3>
- Kadirova ZC, Hojamberdiev M, Katsumata K-I, Isobe T, Matsushita N, Nakajima A, Okada K (2017) Fe₂O₃-loaded activated carbon fiber/polymer materials and their photocatalytic activity for methylene blue mineralization by combined heterogeneous-homogeneous photocatalytic processes. *Appl Surf Sci* 402:444–455. <https://doi.org/10.1016/j.apsusc.2017.01.131>
- Kanwal M, Tariq SR, Chotana GA (2018) Photocatalytic degradation of imidacloprid by Ag-ZnO composite. *Environ Sci Pollut Res* 25(27):27307–27320. <https://doi.org/10.1007/s11356-018-2693-8>
- Karimi L, Zohoori S, Yazdanshenas ME (2014) Photocatalytic degradation of azo dyes in aqueous solutions under UV irradiation using nano-strontium titanate as the nanophotocatalyst. *J Saudi Chem Soc* 18(5):581–588. <https://doi.org/10.1016/j.jscs.2011.11.010>
- Karimian D, Yadollahi B, Mirkhani V (2015) Harvesting visible light for aerobic oxidation of alcohols by a novel and efficient hybrid polyoxometalate. *Dalton Trans* 44(4):1709–1715. <https://doi.org/10.1039/C4DT03299C>
- Khairy M, Zakaria W (2014) Effect of metal-doping of TiO₂ nanoparticles on their photocatalytic activities toward removal of organic dyes. *Egypt J Pet* 23(4):419–426. <https://doi.org/10.1016/j.ejpe.2014.09.010>
- Khavar AHC, Moussavi G, Mahjoub AR, Satari M, Abdolmaleki P (2018) Synthesis and visible-light photocatalytic activity of In, S-TiO₂@rGO nanocomposite for degradation and detoxification of pesticide atrazine in water. *Chem Eng J* 345:300–311. <https://doi.org/10.1016/j.ccej.2018.03.095>
- Kim I, Tanaka H (2010) Use of ozone-based processes for the removal of pharmaceuticals detected in a wastewater treatment plant. *Water Environ Res* 82(4):294–301. <https://doi.org/10.2175/106143009x12487095236630>
- Kim I, Tanaka H (2011) Energy consumption for PPCPs removal by O₃ and O₃/UV. *Ozone Sci Eng* 33(2):150–157. <https://doi.org/10.1080/01919512.2011.549427>
- Kim I, Yamashita N, Tanaka H (2009) Photodegradation of pharmaceuticals and personal care products during UV and UV/H₂O₂ treatments. *Chemosphere* 77(4):518–525. <https://doi.org/10.1016/j.chemosphere.2009.07.041>
- Kim D-h, Lee D, Monllor-Satoca D, Kim K, Lee W, Choi W (2019) Homogeneous photocatalytic Fe³⁺/Fe²⁺ redox cycle for simultaneous Cr(VI) reduction and organic pollutant oxidation: roles of hydroxyl radical and degradation intermediates. *J Hazard Mater* 372:121–128. <https://doi.org/10.1016/j.jhazmat.2018.03.055>
- Klavarioti M, Mantzavinos D, Kassinos D (2009) Removal of residual pharmaceuticals from aqueous systems by advanced oxidation processes. *Environ Int* 35(2):402–417. <https://doi.org/10.1016/j.envint.2008.07.009>
- Kudo A, Miseki Y (2009) Heterogeneous photocatalyst materials for water splitting. *Chem Soc Rev* 38(1):253–278. <https://doi.org/10.1039/B800489G>
- Kumari P, Bahadur N, Duméa LF (2020) Photo-catalytic membrane reactors for the remediation of persistent organic pollutants – a review. *Sep Purif Technol* 230:115878. <https://doi.org/10.1016/j.seppur.2019.115878>
- Lee J-C, Kim M-S, Kim B-W (2002) Removal of paraquat dissolved in a photoreactor with TiO₂ immobilized on the glass-tubes of UV lamps. *Water Res* 36(7):1776–1782. [https://doi.org/10.1016/S0043-1354\(01\)00378-5](https://doi.org/10.1016/S0043-1354(01)00378-5)
- Lewis K, Archer R (1979) pKa values of estrone, 17β-estradiol and 2-methoxyestrone. *Steroids* 34(5):485–499. [https://doi.org/10.1016/s0039-128x\(79\)80011-2](https://doi.org/10.1016/s0039-128x(79)80011-2)
- Li H, Zhou B (2019) Degradation of atrazine by catalytic ozonation in the presence of iron scraps: performance, transformation pathway, and acute toxicity. *J Environ Sci Health B* 54(5):432–440. <https://doi.org/10.1080/03601234.2019.1574175>
- Li K, Xiong J, Chen T, Yan L, Dai Y, Song D, Lv Y, Zeng Z (2013) Preparation of graphene/TiO₂ composites by nonionic surfactant strategy and their simulated sunlight and visible light

- photocatalytic activity towards representative aqueous POPs degradation. *J Hazard Mater* 250:19–28. <https://doi.org/10.1016/j.jhazmat.2013.01.069>
- Li M, Yin JJ, Wamer WG, Lo YM (2014) Mechanistic characterization of titanium dioxide nanoparticle-induced toxicity using electron spin resonance. *J Food Drug Anal* 22(1):76–85. <https://doi.org/10.1016/j.jfda.2014.01.006>
- Li Q, Jia R, Shao J, He Y (2019) Photocatalytic degradation of amoxicillin via TiO₂ nanoparticle coupling with a novel submerged porous ceramic membrane reactor. *J Clean Prod* 209:755–761. <https://doi.org/10.1016/j.jclepro.2018.10.183>
- Limburg B, Bouwman E, Bonnet S (2016) Rate and stability of photocatalytic water oxidation using [Ru(bpy)₃]²⁺ as photosensitizer. *ACS Catal* 6(8):5273–5284. <https://doi.org/10.1021/acscatal.6b00107>
- Lin L, Wang HY, Jiang WB, Mkaouer AR, Xu P (2017) Comparison study on photocatalytic oxidation of pharmaceuticals by TiO₂-Fe and TiO₂-reduced graphene oxide nanocomposites immobilized on optical fibers. *J Hazard Mater* 333:162–168. <https://doi.org/10.1016/j.jhazmat.2017.02.044>
- Liu Y, Gan X, Zhou B, Xiong B, Li J, Dong C, Bai J, Cai W (2009) Photoelectrocatalytic degradation of tetracycline by highly effective TiO₂ nanopore arrays electrode. *J Hazard Mater* 171(1–3):678–683. <https://doi.org/10.1016/j.jhazmat.2009.06.054>
- Loeb BL, Thompson CM, Drago J, Takahara H, Baig S (2012) Worldwide ozone capacity for treatment of drinking water and wastewater: a review. *Ozone Sci Eng* 34(1):64–77. <https://doi.org/10.1080/01919512.2012.640251>
- Long M, Cai W, Cai J, Zhou B, Chai X, Wu Y (2006) Efficient photocatalytic degradation of phenol over Co₃O₄/BiVO₄ composite under visible light irradiation. *J Phys Chem B* 110(41):20211–20216. <https://doi.org/10.1021/jp063441z>
- Louangsouphom B, Wang X, Song J, Wang X (2019) Low-temperature preparation of a N-TiO₂/macroporous resin photocatalyst to degrade organic pollutants. *Environ Chem Lett* 17(2):1061–1066. <https://doi.org/10.1007/s10311-018-00827-z>
- Luo Y, Chen J, Liu J, Shao Y, Li X, Li D (2016) Hydroxide SrSn(OH)₆: a new photocatalyst for degradation of benzene and rhodamine B. *Appl Catal B Environ* 182:533–540. <https://doi.org/10.1016/j.apcatb.2015.09.051>
- Lv Y, Yu L, Zhang X, Yao J, Zou R, Dai Z (2011) P-doped TiO₂ nanoparticles film coated on ground glass substrate and the repeated photodegradation of dye under solar light irradiation. *Appl Surf Sci* 257(13):5715–5719. <https://doi.org/10.1016/j.apsusc.2011.01.082>
- Mahanthappa M, Kottam N, Yellappa S (2019) Enhanced photocatalytic degradation of methylene blue dye using CuSCdS nanocomposite under visible light irradiation. *Appl Surf Sci* 475:828–838. <https://doi.org/10.1016/j.apsusc.2018.12.178>
- Malefane ME, Feleni U, Kuvarega AT (2019) Tetraphenylporphyrin/WO₃/exfoliated graphite nanocomposite for photocatalytic degradation of an acid dye under visible light irradiation. *New J Chem* 43:11348–11362. <https://doi.org/10.1039/C9NJ02747E>
- Malvestiti JA, Fagnani E, Simão D, Dantas RF (2019) Optimization of UV/H₂O₂ and ozone wastewater treatment by the experimental design methodology. *Environ Technol* 40(15):1910–1922. <https://doi.org/10.1080/09593330.2018.1432698>
- Manga Raju I, Rao S, KV DL, Divya G (2019) Poly 3-Thenoic acid sensitized, Copper doped anatase/brookite TiO₂ nanohybrids for enhanced photocatalytic degradation of an organophosphorus pesticide. *J Environ Chem Eng* 7(4):103211. <https://doi.org/10.1016/j.jece.2019.103211>
- Mao J, Ge M, Huang J, Lai Y, Lin C, Zhang K, Meng K, Tang Y (2017) Constructing multifunctional MOF@rGO hydro-/aerogels by the self-assembly process for customized water remediation. *J Mater Chem A* 5(23):11873–11881. <https://doi.org/10.1039/C7TA01343D>
- Mbiri A, Wittstock G, Taffa DH, Gatebe E, Baya J, Wark M (2018) Photocatalytic degradation of the herbicide chloridazon on mesoporous titania/zirconia nanopowders. *Environ Sci Pollut Res* 25(35):34873–34883. <https://doi.org/10.1007/s11356-017-1023-x>
- Medina-Valtierra J, García-Servín J, Frausto-Reyes C, Calixto S (2006) The photocatalytic application and regeneration of anatase thin films with embedded commercial TiO₂ particles

- deposited on glass microrods. *Appl Surf Sci* 252(10):3600–3608. <https://doi.org/10.1016/j.apsusc.2005.05.045>
- Meenakshisundaram S (2019) Environmental photocatalysis/photocatalytic decontamination. In: Martínez L, Kharissova O, Kharisov B (eds) *Handbook of ecomaterials*. Springer, Cham, pp 1625–1640. https://doi.org/10.1007/978-3-319-68255-6_65
- Méndez-Torres AM, Castro J, Fernández F, Garrido-Ramírez E, Escalona N, Gutiérrez C, Marco JF, Ureta-Zañartu MS (2019) Electrodes based on zeolites modified with cobalt and/or molybdenum for pesticide degradation. Part I: physicochemical characterization and efficiency of the electrodes for O₂ reduction and H₂O₂ production. *Electrocatalysis* 10(1):95–111. <https://doi.org/10.1007/s12678-018-0500-4>
- Metcalfe, Eddy (1981) *Wastewater engineering: Collection and pumping of wastewater*. McGraw-Hill. ISBN: 007041680X/9780070416802
- Mierzwa JC, Rodrigues R, Teixeira AC (2018) UV-hydrogen peroxide processes. In: *Advanced oxidation processes for waste water treatment*. Elsevier, pp 13–48. <https://doi.org/10.1016/B978-0-12-810499-6.00002-4>
- Milojević-Rakić M, Bajuk-Bogdanović D, Nedić Vasiljević B, Rakić A, Škrivanj S, Ignjatović L, Dondur V, Mentus S, Ćirić-Marjanović G (2018) Polyaniline/FeZSM-5 composites – synthesis, characterization and their high catalytic activity for the oxidative degradation of herbicide glyphosate. *Microporous Mesoporous Mater* 267:68–79. <https://doi.org/10.1016/j.micromeso.2018.03.019>
- Mirhoseini F, Salabat A (2015) Ionic liquid based microemulsion method for the fabrication of poly (methyl methacrylate)–TiO₂ nanocomposite as a highly efficient visible light photocatalyst. *RSC Adv* 5(17):12536–12545. <https://doi.org/10.1039/C4RA14612C>
- Mirmasoomi SR, Ghazi MM, Galedari M (2017) Photocatalytic degradation of diazinon under visible light using TiO₂/Fe₂O₃ nanocomposite synthesized by ultrasonic-assisted impregnation method. *Sep Purif Technol* 175:418–427. <https://doi.org/10.1016/j.seppur.2016.11.021>
- Monga D, Basu S (2019) Enhanced photocatalytic degradation of industrial dye by g-C₃N₄/TiO₂ nanocomposite: role of shape of TiO₂. *Adv Powder Technol* 30(5):1089–1098. <https://doi.org/10.1016/j.apt.2019.03.004>
- Mudassir MA, Hussain SZ, Khan M, Asma ST, Iqbal Z, Huma Z, Ullah N, Zhang H, Ansari TM, Hussain I (2018) Polyacrylamide exotemplate-assisted synthesis of hierarchically porous nanostructured TiO₂ macrobeads for efficient photodegradation of organic dyes and microbes. *RSC Adv* 8(52):29628–29636. <https://doi.org/10.1039/C8RA06197A>
- Naciri Y, Chennah A, Jaramillo-Páez C, Navío JA, Bakiz B, Taoufyq A, Ezahri M, Villain S, Guinneton F, Benlhachemi A (2019) Preparation, characterization and photocatalytic degradation of Rhodamine B dye over a novel Zn₃(PO₄)₂/BiPO₄ catalyst. *J Environ Chem Eng* 7(3):103075. <https://doi.org/10.1016/j.jece.2019.103075>
- Nakata K, Fujishima A (2012) TiO₂ photocatalysis: design and applications. *J Photochem Photobiol C: Photochem Rev* 13(3):169–189. <https://doi.org/10.1016/j.jphotochemrev.2012.06.001>
- Neumann M, Schulz R, Schafer K, Muller W, Mannheller W, Liess M (2002) The significance of entry routes as point and non-point sources of pesticides in small streams. *Water Res* 36(4):835–842. [https://doi.org/10.1016/s0043-1354\(01\)00310-4](https://doi.org/10.1016/s0043-1354(01)00310-4)
- Nguyen TT, Nam SN, Son J, Oh J (2019) Tungsten trioxide (WO₃)-assisted photocatalytic degradation of amoxicillin by simulated solar irradiation. *Sci Rep* 9:18. <https://doi.org/10.1038/s41598-019-45644-8>
- Noll KE (1991) *Adsorption technology for air and water pollution control*. CRC Press. ISBN 9780873713405
- North GR (2015) Climate and climate change | greenhouse effect. In: North GR, Pyle J, Zhang F (eds) *Encyclopedia of atmospheric sciences*, 2nd edn. Academic, Oxford, pp 80–86. <https://doi.org/10.1016/B978-0-12-382225-3.00470-9>

- Nosaka Y, Nakamura M, Hirakawa T (2002) Behavior of superoxide radicals formed on TiO₂ powder photocatalysts studied by a chemiluminescent probe method. *Phys Chem Chem Phys* 4 (6):1088–1092. <https://doi.org/10.1039/B108441K>
- Pan D, Xiao S, Chen X, Li R, Cao Y, Zhang D, Pu S, Li Z, Li G, Li H (2019) Efficient photocatalytic fuel cell via simultaneous visible-photoelectrocatalytic degradation and electricity generation on a porous coral-like WO₃/W photoelectrode. *Environ Sci Technol* 53 (7):3697–3706. <https://doi.org/10.1021/acs.est.8b05685>
- Pandian L, Rajasekaran R, Govindan P (2018) Synthesis, characterization and application of Cu doped ZnO nanocatalyst for photocatalytic ozonation of textile dye and study of its reusability. *Mater Res Express* 5(11):115505. <https://doi.org/10.1088/2053-1591/aadcdf>
- Paula CHR, Neto NFA, Garcia LMP, Nascimento RM, Paskocimas CA, Bomio MRD, Motta FV (2019) Increased degradation capacity of methylene blue dye using Mg-doped ZnO nanoparticles decorated by Ag⁰ nanoparticles. *J Electron Mater* 48(5):3017–3025. <https://doi.org/10.1007/s11664-019-07059-z>
- Payornhorm J, Chuangchote S, Laosiripojana N (2017a) CTAB-assisted sol-microwave method for fast synthesis of mesoporous TiO₂ photocatalysts for photocatalytic conversion of glucose to value-added sugars. *Mater Res Bull* 95:546–555. <https://doi.org/10.1016/j.materresbull.2017.08.016>
- Payornhorm J, Chuangchote S, Kiattitipong K, Chiarakorn S, Laosiripojana N (2017b) Xylitol and gluconic acid productions via photocatalytic-glucose conversion using TiO₂ fabricated by surfactant-assisted techniques: effects of structural and textural properties. *Mater Chem Phys* 196:29–36. <https://doi.org/10.1016/j.matchemphys.2017.03.058>
- Pérez A, Rodríguez JL, Galicia A, Chairez I, Poznyak T (2019) Recycling strategy for water contaminated with Reactive Black 5 in the presence of additives treated by simple ozonation. *Ozone Sci Eng* 41(1):46–59. <https://doi.org/10.1080/01919512.2018.1483816>
- Puong NM, Chu NC, Van Thuan D, Ha MN, Hanh NT, Viet HDT, Thu M, Thi N, Van Quan P, Truc T (2019) Novel removal of diazinon pesticide by adsorption and photocatalytic degradation of visible light-driven Fe-TiO₂/Bent-Fe photocatalyst. *J Chem* 2019:2678927. <https://doi.org/10.1155/2019/2678927>
- Prasad MNV, Vithanage M, Kapley A (2019) Pharmaceuticals and personal care products: waste management and treatment technology: emerging contaminants and micro pollutants. *Butterworth-Heinemann*. <https://doi.org/10.1016/C2017-0-03544-9>
- Qin W, Song Y, Dai Y, Qiu G, Ren M, Zeng P (2015) Treatment of berberine hydrochloride pharmaceutical wastewater by O₃/UV/H₂O₂ advanced oxidation process. *Environ Earth Sci* 73 (9):4939–4946. <https://doi.org/10.1007/s12665-015-4192-2>
- Qu J, He X, Li X, Ai Z, Li Y, Zhang Q, Liu X (2017) Precursor preparation of Zn–Al layered double hydroxide by ball milling for enhancing adsorption and photocatalytic decoloration of methyl orange. *RSC Adv* 7(50):31466–31474. <https://doi.org/10.1039/C7RA05316A>
- Rasoulnezhad H, Kavei G, Ahmadi K, Rahimipour MR (2017) Visible light photocatalytic degradation of paraoxon and parathion pesticides on carbon-doped TiO₂ nanorod thin films. *J Mater Sci Mater Electron* 28(24):18337–18347. <https://doi.org/10.1007/s10854-017-7780-y>
- Ravishankar TN, de O Vaz M, Ramakrishnappa T, Teixeira SR, Dupont J (2019) Ionic liquid-assisted hydrothermal synthesis of Nb/TiO₂ nanocomposites for efficient photocatalytic hydrogen production and photodecolorization of Rhodamine B under UV-visible and visible light illuminations. *Mater Today Chem* 12:373–385. <https://doi.org/10.1016/j.mtchem.2019.04.001>
- Recio F, Herrasti P, Sirés I, Kulak A, Bavykin D, Ponce-de-León C, Walsh F (2011) The preparation of PbO₂ coatings on reticulated vitreous carbon for the electro-oxidation of organic pollutants. *Electrochim Acta* 56(14):5158–5165. <https://doi.org/10.1016/j.electacta.2011.03.054>
- Reddy CN, Mohan SV (2016) Integrated bio-electrogenic process for bioelectricity production and cathodic nutrient recovery from azo dye wastewater. *Renew Energy* 98:188–196. <https://doi.org/10.1016/j.renene.2016.03.047>

- Rehman F, Sayed M, Khan JA, Shah NS, Khan HM, Dionysiou DD (2018) Oxidative removal of brilliant green by UV/S₂O₈²⁻, UV/HSO₅⁻ and UV/H₂O₂ processes in aqueous media: a comparative study. *J Hazard Mater* 357:506–514. <https://doi.org/10.1016/j.jhazmat.2018.06.012>
- Rezgui S, Amrane A, Fourcade F, Assadi A, Monser L, Adhoum N (2018) Electro-Fenton catalyzed with magnetic chitosan beads for the removal of Chlordimeform insecticide. *Appl Catal B Environ* 226:346–359. <https://doi.org/10.1016/j.apcatb.2017.12.061>
- Rosa Barbosa MP, Lima NS, de Matos DB, Alves Felisardo RJ, Santos GN, Salazar-Banda GR, Cavalcanti EB (2018) Degradation of pesticide mixture by electro-Fenton in filter-press reactor. *J Water Process Eng* 25:222–235. <https://doi.org/10.1016/j.jwpe.2018.08.008>
- Sajjadi S, Khataee A, Bagheri N, Kobya M, Şenocak A, Demirbas E, Karaoğlu AG (2019) Degradation of diazinon pesticide using catalyzed persulfate with Fe₃O₄@MOF-2 nanocomposite under ultrasound irradiation. *J Ind Eng Chem* 77:280–290. <https://doi.org/10.1016/j.jiec.2019.04.049>
- Saleh R, Djaja NF (2014) UV light photocatalytic degradation of organic dyes with Fe-doped ZnO nanoparticles. *Superlattice Microst* 74:217–233. <https://doi.org/10.1016/j.spmi.2014.06.013>
- Sanitnon P, Chiarakorn S, Chawengkijwanich C, Chuangchote S, Pongprayoon T (2019) Synergistic effects of zirconium and silver co-dopants in TiO₂ nanoparticles for photocatalytic degradation of an organic dye and antibacterial activity. *J Aust Ceram Soc*. <https://doi.org/10.1007/s41779-019-00368-w>
- Santoke H, Tong AYC, Mezyk SP, Johnston KM, Braund R, Cooper WJ, Peake BM (2015) UV Photodegradation of Enoxacin in water: kinetics and degradation pathways. *J Environ Eng ASCE* 141(10):7. [https://doi.org/10.1061/\(asce\)jee.1943-7870.0000954](https://doi.org/10.1061/(asce)jee.1943-7870.0000954)
- Särkkä H, Bhatnagar A, Sillanpää M (2015) Recent developments of electro-oxidation in water treatment—a review. *J Electroanal Chem* 754:46–56. <https://doi.org/10.1016/j.jelechem.2015.06.016>
- Senthil RA, Sun M, Pan J, Osman S, Khan A, Sun Y (2019) Facile fabrication of a new BiFeWO₆/α-AgVO₃ composite with efficient visible-light photocatalytic activity for dye-degradation. *Opt Mater* 92:284–293. <https://doi.org/10.1016/j.optmat.2019.04.046>
- Senthilnathan J, Philip L (2012) Elimination of pesticides and their formulation products from drinking water using thin film continuous photoreactor under solar radiation. *Sol Energy* 86(9):2735–2745. <https://doi.org/10.1016/j.solener.2012.06.011>
- Shetty R, Chavan VB, Kulkarni PS, Kulkarni BD, Kamble SP (2017) Photocatalytic degradation of pharmaceuticals pollutants using N-doped TiO₂ photocatalyst: identification of CFX degradation intermediates. *Indian Chem Eng* 59(3):177–199. <https://doi.org/10.1080/00194506.2016.1150794>
- Singh J, Sharma S, Aanchal, Basu S (2019) Synthesis of Fe₂O₃/TiO₂ monoliths for the enhanced degradation of industrial dye and pesticide via photo-Fenton catalysis. *J Photochem Photobiol A Chem* 376:32–42. <https://doi.org/10.1016/j.jphotochem.2019.03.004>
- Sirelkhatim A, Mahmud S, Seeni A, Kaus NHM, Ann LC, Bakhori SKM, Hasan H, Mohamad D (2015) Review on zinc oxide nanoparticles: antibacterial activity and toxicity mechanism. *Nano Micro Lett* 7(3):219–242. <https://doi.org/10.1007/s40820-015-0040-x>
- Sirirerkratana K, Kemacheevakul P, Chuangchote S (2019) Color removal from wastewater by photocatalytic process using titanium dioxide-coated glass, ceramic tile, and stainless steel sheets. *J Clean Prod* 215:123–130. <https://doi.org/10.1016/j.jclepro.2019.01.037>
- Solís RR, Gimeno O, Rivas FJ, Beltrán FJ (2019) Simulated solar driven photolytic ozonation for the oxidation of aqueous recalcitrant-to-ozone tritosulfuron. Transformation products and toxicity. *J Environ Manag* 233:513–522. <https://doi.org/10.1016/j.jenvman.2018.12.068>
- Srisasiwimon N, Chuangchote S, Laosiripojana N, Sagawa T (2018) TiO₂/lignin-based carbon composited photocatalysts for enhanced photocatalytic conversion of lignin to high value chemicals. *ACS Sustain Chem Eng* 6(11):13968–13976. <https://doi.org/10.1021/acssuschemeng.8b02353>

- Stan CD, Cretescu I, Pastravanu C, Poullos I, Drăgan M (2012) Treatment of pesticides in wastewater by heterogeneous and homogeneous photocatalysis. *Int J Photoenergy* 2012:194823. <https://doi.org/10.1155/2012/194823>
- Stockholm Convention. Available at: <http://www.pops.int/> (access: August 2019)
- Sun F, Zeng Q, Tian W, Zhu Y, Jiang W (2019) Magnetic MFe₂O₄-Ag₂O (M = Zn, Co, & Ni) composite photocatalysts and their application for dye wastewater treatment. *J Environ Chem Eng* 7(2):103011. <https://doi.org/10.1016/j.jece.2019.103011>
- Tabasideh S, Maleki A, Shahmoradi B, Ghahremani E, McKay G (2017) Sonophotocatalytic degradation of diazinon in aqueous solution using iron-doped TiO₂ nanoparticles. *Sep Purif Technol* 189:186–192. <https://doi.org/10.1016/j.seppur.2017.07.065>
- Teran T, Lamon L, Marcomini A (2012) Climate change effects on POPs' environmental behaviour: a scientific perspective for future regulatory actions. *Atmos Pollut Res* 3(4):466–476. <https://doi.org/10.5094/APR.2012.054>
- Thabit M, Liu H, Zhang J, Wang B (2018) Synthesis, characterization of Hollandite Ag₂Mn₈O₁₆ on TiO₂ nanotubes and their photocatalytic properties for Rhodamine B degradation. *Pol J Chem Technol* 20(2):85–91. <https://doi.org/10.2478/pjct-2018-0027>
- Tong M, Yang J, Jin Q, Zhang X, Gao J, Li G (2019) Facile preparation of amorphous carbon-coated tungsten trioxide containing oxygen vacancies as photocatalysts for dye degradation. *J Mater Sci* 54(15):10656–10669. <https://doi.org/10.1007/s10853-019-3645-y>
- Vaiano V, Jaramillo-Paez CA, Matarangolo M, Navio JA, Hidalgo MD (2019) UV and visible-light driven photocatalytic removal of caffeine using ZnO modified with different noble metals (Pt, Ag and Au). *Mater Res Bull* 112:251–260. <https://doi.org/10.1016/j.materresbull.2018.12.034>
- Van HT, Nguyen LH, Hoang TK, Tran TP, Vo AT, Pham T, Nguyen X (2019) Using FeO-constituted iron slag wastes as heterogeneous catalyst for Fenton and ozonation processes to degrade Reactive Red 24 from aqueous solution. *Sep Purif Technol* 224:431–442. <https://doi.org/10.1016/j.seppur.2019.05.048>
- Wang JL, Wang SZ (2016) Removal of pharmaceuticals and personal care products (PPCPs) from wastewater: a review. *J Environ Manag* 182:620–640. <https://doi.org/10.1016/j.jenvman.2016.07.049>
- Wang LK, Tay J-H, Tay STL, Hung Y-T (2010) *Environmental bioengineering*, vol 11. Springer. ISBN 978-1-60327-031-1
- Wang Z-b, Guan Y-j, Chen B, Bai S-l (2016) Retention and separation of 4BS dye from wastewater by the N-TiO₂ ceramic membrane. *Desalin Water Treat* 57(36):16963–16969. <https://doi.org/10.1080/19443994.2015.1082940>
- Wang C, Cao Y, Wang H (2019a) Copper-based catalyst from waste printed circuit boards for effective Fenton-like discoloration of Rhodamine B at neutral pH. *Chemosphere* 230:278–285. <https://doi.org/10.1016/j.chemosphere.2019.05.068>
- Wang D, Qiu S, Wang M, Pan S, Ma H, Zou J (2019b) Spectrophotometric determination of hydrogen peroxide in water by oxidative decolorization of azo dyes using Fenton system. *Spectrochim Acta A Mol Biomol Spectrosc* 221:117138. <https://doi.org/10.1016/j.saa.2019.117138>
- Wang L, Li Z, Chen J, Huang Y, Zhang H, Qiu H (2019c) Enhanced photocatalytic degradation of methyl orange by porous graphene/ZnO nanocomposite. *Environ Pollut* 249:801–811. <https://doi.org/10.1016/j.envpol.2019.03.071>
- Wei Y, Wang B, Cui X, Muhammad Y, Zhang Y, Huang Z, Li X, Zhao Z, Zhao Z (2018) Highly advanced degradation of thiamethoxam by synergistic chemisorption-catalysis strategy using MIL (Fe)/Fe-SPC composites with ultrasonic irradiation. *ACS Appl Mater Interfaces* 10(41):35260–35272. <https://doi.org/10.1021/acsami.8b12908>
- Wu C-H, Chang C-L (2006) Decolorization of Reactive Red 2 by advanced oxidation processes: comparative studies of homogeneity and heterogeneous systems. *J Hazard Mater* 128(2–3):265–272. <https://doi.org/10.1016/j.jhazmat.2005.08.013>

- Wu F-C, Tseng R-L, Juang R-S (2001) Kinetic modeling of liquid-phase adsorption of reactive dyes and metal ions on chitosan. *Water Res* 35(3):613–618. [https://doi.org/10.1016/S0043-1354\(00\)00307-9](https://doi.org/10.1016/S0043-1354(00)00307-9)
- Yang Y, Ok YS, Kim KH, Kwon EE, Tsang YF (2017) Occurrences and removal of pharmaceuticals and personal care products (PPCPs) in drinking water and water/sewage treatment plants: a review. *Sci Total Environ* 596:303–320. <https://doi.org/10.1016/j.scitotenv.2017.04.102>
- Ye S, Chen R, Xu Y, Fan F, Du P, Zhang F, Zong X, Chen T, Qi Y, Chen P (2016) An artificial photosynthetic system containing an inorganic semiconductor and a molecular catalyst for photocatalytic water oxidation. *J Catal* 338:168–173. <https://doi.org/10.1016/j.jcat.2016.02.024>
- Yemmireddy VK, Hung YC (2017) Using photocatalyst metal oxides as antimicrobial surface coatings to ensure food safety—opportunities and challenges. *Compr Rev Food Sci Food Saf* 16(4):617–631. <https://doi.org/10.1111/1541-4337.12267>
- Yi C, Liao Q, Deng W, Huang YW, Mao J, Zhang BP, Wu GP (2019) The preparation of amorphous TiO₂ doped with cationic S and its application to the degradation of DCFs under visible light irradiation. *Sci Total Environ* 684:527–536. <https://doi.org/10.1016/j.scitotenv.2019.05.338>
- Yu C, He H, Liu X, Zeng J, Liu Z (2019) Novel SiO₂ nanoparticle-decorated BiOCl nanosheets exhibiting high photocatalytic performances for the removal of organic pollutants. *Chin J Catal* 40:1212–1221. [https://doi.org/10.1016/S1872-2067\(19\)63359-0](https://doi.org/10.1016/S1872-2067(19)63359-0)
- Zahedi F, Behpour M, Ghoreishi SM, Khalilian H (2015) Photocatalytic degradation of paraquat herbicide in the presence TiO₂ nanostructure thin films under visible and sun light irradiation using continuous flow photoreactor. *Sol Energy* 120:287–295. <https://doi.org/10.1016/j.solener.2015.07.010>
- Zhang H, Zhang P, Ji Y, Tian J, Du Z (2015) Photocatalytic degradation of four non-steroidal anti-inflammatory drugs in water under visible light by P25-TiO₂/tetraethyl orthosilicate film and determination via ultra performance liquid chromatography electrospray tandem mass spectrometry. *Chem Eng J* 262:1108–1115. <https://doi.org/10.1016/j.cej.2014.10.019>
- Zhang J-J, Liu X, Ye T, Zheng G-P, Zheng X-C, Liu P, Guan X-X (2017) Novel assembly of homogeneous reduced graphene oxide-doped mesoporous TiO₂ hybrids for elimination of Rhodamine-B dye under visible light irradiation. *J Alloys Compd* 698:819–827. <https://doi.org/10.1016/j.jallcom.2016.12.279>
- Zhao B, Lv M, Zhou L (2012) Photocatalytic degradation of perfluorooctanoic acid with β-Ga₂O₃ in anoxic aqueous solution. *J Environ Sci* 24(4):774–780. [https://doi.org/10.1016/S1001-0742\(11\)60818-8](https://doi.org/10.1016/S1001-0742(11)60818-8)
- Zheng C, Zhao L, Zhou X, Fu Z, Li A (2013) Treatment technologies for organic wastewater. In: Elshorbagy W, Chowdhury RK (eds) *Water treatment*. IntechOpen, pp 249–286. <https://doi.org/10.5772/52665>
- Zhou Y, Lu J, Zhou Y, Liu Y (2019) Recent advances for dyes removal using novel adsorbents: a review. *Environ Pollut* 252(Pt A):352–365. <https://doi.org/10.1016/j.envpol.2019.05.072>
- Zhu S, Wang D (2017) Photocatalysis: basic principles, diverse forms of implementations and emerging scientific opportunities. *Adv Energy Mater* 7(23):1700841. <https://doi.org/10.1002/aenm.201700841>
- Ziarani GM, Moradi R, Lashgari N, Kruger HG (2018) Chapter 1: Introduction and importance of synthetic organic dyes. In: Ziarani GM, Moradi R, Lashgari N, Kruger HG (eds) *Metal-free synthetic organic dyes*. Elsevier, pp 1–7. <https://doi.org/10.1016/B978-0-12-815647-6.00001-7>
- Zinatloo-Ajabshir S, Morassaei MS, Salavati-Niasari M (2019) Eco-friendly synthesis of Nd₂Sn₂O₇-based nanostructure materials using grape juice as green fuel as photocatalyst for the degradation of erythrosine. *Compos Part B* 167:643–653. <https://doi.org/10.1016/j.compositesb.2019.03.045>
- Zollinger H (2003) *Color chemistry: syntheses, properties, and applications of organic dyes and pigments*. Wiley. <https://doi.org/10.1002/anie.200385122>

Chapter 2

Carbon Nitride/Metal Oxide Hybrids for Visible Light Harvesting and Water Remediation



Pankaj Raizada, Vasudha Hasija, Pardeep Singh, and Vijay Kumar Thakur

Contents

| | | |
|-------|--|----|
| 2.1 | Introduction | 54 |
| 2.2 | Synthetic Strategies for Fabrication of g-C ₃ N ₄ /Fe ₂ O ₃ | 58 |
| 2.2.1 | g-C ₃ N ₄ /Fe ₂ O ₃ Heterojunction Photocatalyst for Removal of Recalcitrant Pollutants | 60 |
| 2.3 | Synthetic Strategies for Fabrication of g-C ₃ N ₄ /Cu ₂ O | 63 |
| 2.3.1 | g-C ₃ N ₄ /Cu ₂ O Heterojunction Photocatalyst for Removal of Recalcitrant Pollutants | 66 |
| 2.4 | Conclusions | 70 |
| | References | 71 |

Abstract The flourishing global population, expanding industrialization, and climatic variations have led to depletion of already scarce resources. Among the multifarious energy crises, water body deterioration has emerged at the forefront, as there is currently no scalable provision means of conserving it. The accelerating energy demands have been so pressing that it is indispensable to utilize highly efficient solar energy-driven technologies for environment restoration. As a renewable solution, these advancements of tailored photocatalytic systems have gained immense research interest in the field of water purification. In the past decade, there has been exploitation of inherent properties of semiconductors as photocatalysts, which thereby led to the development of modern synthesis strategies and rational design for large-scale water remediation.

In this chapter, we reviewed value-added benefits offered by graphitic carbon nitride (g-C₃N₄) photocatalyst such as its cost-effectiveness, environmentally

P. Raizada (✉) · V. Hasija · P. Singh
School of Chemistry, Faculty of Basic Sciences, Shoolini University, Solan, Himachal Pradesh,
India

V. K. Thakur
Biorefining and Advanced Materials Research Centre, Scotland's Rural College (SRUC),
Edinburgh, UK

friendly nature, and expanded solar light absorption, promoting its usage as water pollutant eliminator. The expanded utilization of n-type semiconductor has proven to be in component due to drawbacks like large band gap, insufficient surface area, and rapid recombination of charge carriers. To overcome these limitations, we have presented in detail the potential abilities of metal oxides, ferrous oxide (Fe_2O_3), and cuprous oxide (Cu_2O) in heterojunction with g- C_3N_4 . A fruitful discussion on photocatalytic properties, green synthetic routes, and sustainability of g- C_3N_4 - Fe_2O_3 and g- C_3N_4 - Cu_2O heterostructure in the arena of water restoration and microbial disinfection is provided in this chapter.

Keywords g- C_3N_4 · Fe_2O_3 · Cu_2O · Photocatalysis · Heterojunction · Wastewater restoration · Bacterial disinfection

2.1 Introduction

The flourishing global population, expanding industrialization, and climate variations have led to pervasive depletion of already scarce resources. Environmental pollution and excessive utilization of renewable resources have posed a major challenge to scientific communities in the twenty-first century. The accelerating energy demands have been so pressing that it is indispensable to scrutinize highly efficient solar energy-driven technologies for environment restoration. The need for solar-inspired research primarily focusses as an alternative cost-effective energy resource in maintaining the standards of human life (Priya et al. 2016a, b; Gautam et al. 2016a, b, c; Kumar et al. 2019). Among the multifarious energy crises, water body deterioration has emerged at the forefront, as there is currently no scalable provision means of conserving it (Raizada et al. 2017a, b; Singh et al. 2017). Rapid discharge of inorganic pesticides, fertilizers, pollutants, and antibiotics decreases biochemical oxygen demand, lessening the survival of aquatic ecosystem (Singh et al. 2018; Gautam et al. 2016a, b, c). The increased public concerns regarding the rising levels of these pollutants have impelled the necessity to develop an innovative water remediation technique.

Various water treatment processes have been developed over the years but have limited large-scale application. These are as follows: (i) Adsorption on activated carbon and air stripping are chemically driven. (ii) Incineration leads to the formation of dioxins and furans due to incomplete combustion of organic pollutants. (iii) Filtration, membrane-assisted, and sedimentation methods result in the formation of heavy sludge and secondary pollutants. (iv) Biological treatment and coagulation accumulate pollutants, with formation of non-toxic secondary pollutants (Sudhaik et al. 2018a, b; Hasija et al. 2019a, b). Currently, the key drivers to eliminate the limitations of conventional methods are advanced oxidation technologies for effective removal of high load of pollutants (Pare et al. 2008; Hasija et al. 2019a, b). The mechanism of advanced oxidation technologies involves an interaction of photons

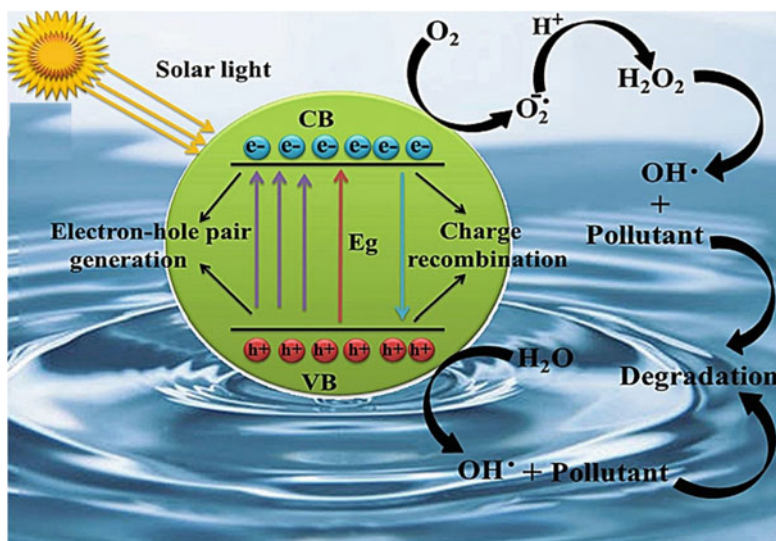


Fig. 2.1 Basic photocatalytic mechanism in a photocatalyst with band gap (E_g) involves excitation of electrons from valence band (VB) to conduction band (CB) upon solar light illumination for effective generation of reactive oxidative species superoxide ($O_2^{\cdot-}$) and hydroxyl radicals (OH^\cdot). (Reprinted with permission from Sharma et al. (2019) copyright©2019 Elsevier Ltd. All rights reserved)

possessing an appropriate energy level with chemical species, thereby releasing highly reactive oxidative species and free radicals, mainly hydroxyl radical (Singh et al. 2019a; Jamwal et al. 2015). Based on the principle of advanced oxidation technologies, photocatalysis has profusely sparked visible light-driven solar utilization strategy functional at ambient conditions to conquer the crisis of energy scarcity and severe environmental issues. This technology employs semiconductor metal oxide as photocatalyst which absorbs solar energy leading to excitation of electrons from valence band edge to the conduction band edge of the semiconductor, generating positive holes in valence band (Raizada et al. 2019a, b, c; Sharma et al. 2019; Singh et al. 2020; Dutta et al. 2019). The reactive oxidative species are formed on reaction of holes in valence band with hydroxide ions or water molecules, forming the exceptionally powerful, nonselective, oxidizing hydroxyl radical (Singh et al. 2013; Raizada et al. 2014a, b), whereas electrons in valence band reduce oxygen and form superoxide radical. The reactive oxidative species released during photocatalysis process significantly participates in photodegradation of the organic pollutants into carbon dioxide, water, and inorganic ions (Hasija et al. 2020; Sudhaik et al. 2018a, b; Singh et al. 2019b; Jiang et al. 2017). The detailed mechanism of photocatalysis has been described in Fig. 2.1 which involves the following steps of photocatalytic pathway: (1) illumination of photocatalyst with ultraviolet radiations UV, (2) photocatalyst absorbing the intruding photons with energy greater than or equal to their band gap potential, (3) charge carrier separation followed by diffusion

onto photocatalyst surface, and (4) fate of charge carriers either on recombination sites, surface reaction, or active sites.

The first demonstration early in 1972 by Fujishima and Honda commenced the era of photocatalysis by photoelectrochemical (PEC) water splitting via aid of titanium dioxide in the presence of ultraviolet light (Singh et al. 2014; Raizada et al. 2014a, b). Since then, varieties of semiconductors as photocatalysts have been reported, for instance ZnO, CaO, ZnWO₄, WO₃, ZrO₂, BiTiO₃, SrTiO₃, Fe₂O₃, Ag₂CO₃, BiOBr, BiOCl, CaFe₂O₄, MnFe₂O₄, ZnFe₂O₄, BiFe₂O₄, TaON, etc. (Raizada et al. 2014a, b, 2017a, b, 2019a, b, c; Priya et al. 2016a, b; Pan et al. 2012; Hua et al. 2019; Shandilya 2018a, b, 2019). The most ruggedly employed photocatalysts, TiO₂ and zinc oxide, are widely used owing to their flexible, biocompatible, and non-toxic nature (Raizada et al. 2019a, b, c). However, their photocatalytic performance is hindered by large band gap of 3.2 eV which is accompanied by decreased electron and hole pair separation, lowered migration ability, and poor solar light energy utilization potential (Lai et al. 2016). Metal oxides are pursued significantly for complete mineralization and photodegradation of pollutants from simulated water. They have been considered as a green, economical source due to its substantial properties of enhanced interfacial tension, with superior mechanical, optical, magnetic, and thermal characteristics. Its key features such high density and less size result in more reactive centers for attachment of pollutant groups and bacterial disinfection (Zhang et al. 2009; Pathania et al. 2014; Singh et al. 2017; Gautam et al. 2016a, b, c).

Very recently in 2006, “gold rush” attention has been accomplished by metal-free carbon, nitrogen-based n-type polymeric semiconductors, and graphitic carbon nitride (g-C₃N₄) (Zhou et al. 2018). The most communal carbon nitride allotrope is two-dimensional g-C₃N₄ consisting of triazine-based delocalized π -conjugated graphitic planes formed by covalently linked sp² hybridized nitrogen and carbon (Kroke et al. 2002). The inherent characteristic of g-C₃N₄ involving tunable band structure with optical midway band gap of 2.7 eV and positions of conduction band and valence band potentials located at -1.09 and $+1.56$ eV at pH 7, respectively, with visible light absorption of 450–460 nm (Wirnhier et al. 2013; Liebig et al. 1844). The peculiar properties of g-C₃N₄ include thermal stability up to 600 °C and high chemical resistance to acids, alkalis, or organic solvents Zhu et al. (2014). Additionally, its porous texture and larger guest-accessible surface area provide more active sites and suppressed recombination of photoexcited charge carriers. The band structure, morphology, electronic properties, optical absorption, facile fabrication, and its cost-effective, Earth-abundant, non-toxic nature provide insightful outlooks in the arena of solar energy conservation (Kessler et al. 2017; Zhao et al. 2015; Zhang et al. 2010). With such unique attributes, g-C₃N₄ is successfully contributing in various realms of environmental applications, including air purification, water splitting to produce oxygen and hydrogen, carbon dioxide reduction to hydrocarbon fuels, bacterial disinfection, and photodegradation of contaminants (Zuluaga et al. 2015; Bojdys et al. 2008; Zhang et al. 2018). The fabrication of visible light-driven photocatalyst is immensely opted by researchers to exploit inexhaustible abundant solar energy resource in photocatalysis process. For effective

fabrication of a robust photocatalyst, various synthesis methods have been followed. The most common methods are thermal polycondensation; physical vapor deposition (PVD); ionothermal, hard–soft templating; single-step nitridation; solvothermal/hydrothermal calcination; electrochemical sol–gel; ultrasonic-assisted exfoliation; etc. (Sudrajat 2018; Xiong et al. 2014; Rong et al. 2016; Chai et al. 2017). The myriads of a large number of facetious and innovative preparation techniques have subsequently progressed $g\text{-C}_3\text{N}_4$ as a promising visible light-responsive photocatalyst. Indeed, electronic and catalytic abilities of pristine $g\text{-C}_3\text{N}_4$ are moderately low due to wide band gap, small specific surface area, high photoexciton binding energy, low electrical conductivity, and decreased charge separation efficiency (Singh et al. 2013; Zhu et al. 2017). To surmount these limitations, enormous means have spurred underlining the unleashing importance of $g\text{-C}_3\text{N}_4$ as photocatalyst. In reference to advancements and developments to overcome shortcomings of pristine $g\text{-C}_3\text{N}_4$, countless research have focused on heterostructuring (coupling), nanoarchitecture design, and functionalization (doping) (Zhang et al. 2017a, b; Song et al. 2014; Raizada et al. 2019a, b, c). Among all the modification methods, accelerating advantages offered by coupling heterostructuring are known to be a competent method to tune the unique electronic and optical structure of $g\text{-C}_3\text{N}_4$. Typically, as depicted in Fig. 2.2, there are three types of conventional heterojunction photocatalysts: (type I) straddling gap, (type II) staggered gap, and (type III) broken gap (Low et al. 2017a, b). Thereafter, two new types of heterojunction came into light, i.e., Z-scheme direct and indirect heterojunction and surface heterojunction, to further improve photocatalytic activity (Low et al. 2017a, b; Gholipour et al. 2015; Nashim et al. 2013).

The synthesis of heterostructured nanocomposites by coupling one semiconductor with other refrains from recombining photogenerated charge carriers and equips the as-prepared photocatalyst with efficient novel characteristics exhibiting synergistic effects. Various reports reveal that combining $g\text{-C}_3\text{N}_4$ with another heterojunction photocatalysts fulfils several requirements, such as lowering of bandgap and absorption in visible light region with high thermal and chemical stability for long-term commercialized applications.

In this book chapter, we discuss design and synthesis of visible light-responsive $g\text{-C}_3\text{N}_4$ photocatalysts in heterojunction with metal oxides for its diverse potential in pollutant elimination and bacteria disinfection. A brief outlook is presented for synthesis of heterostructure of $g\text{-C}_3\text{N}_4$ –metal oxide via various methods. The synergistic effect is pronounced due to the wide band gaps, high dielectric constants, facetious separation, negligible agglomeration, and rapid electronic transitions. Herein, we have mainly presented an insightful description on the attributes offered by oxides of iron (Fe) and copper (Cu) in discipline of water purification.

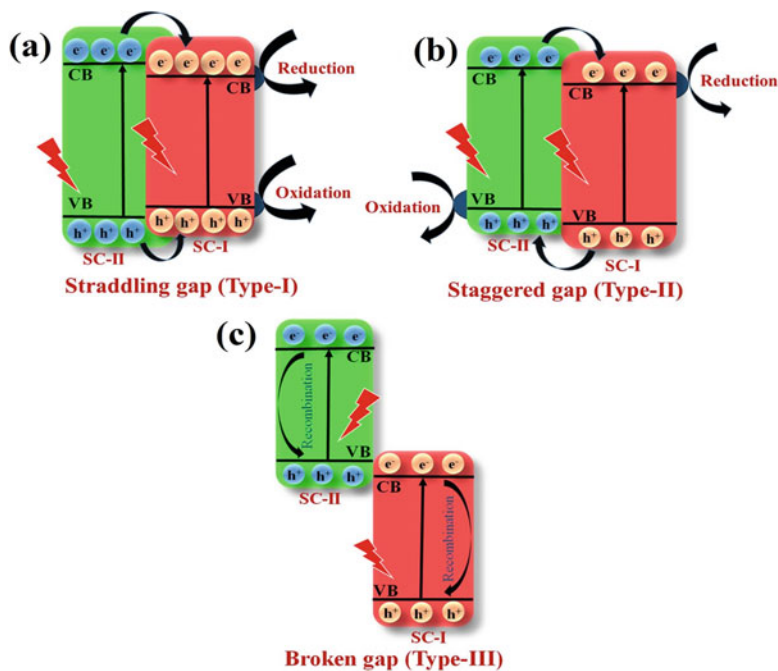


Fig. 2.2 Types of heterojunction depict transference of electrons and holes. (a) Straddling gap (type- I) involves migration of electrons from conduction band (CB) of semiconductor II (SC-II) to CB of semiconductor I (SC-I) and holes from valence band of SC-II to SC-I, (b) staggered gap (type II), and (c) broken gap (type III). (Reprinted with permission from Kumar et al. in (2019) copyright@2019 Elsevier Ltd. All rights reserved)

2.2 Synthetic Strategies for Fabrication of $g\text{-C}_3\text{N}_4/\text{Fe}_2\text{O}_3$

The value-added physicochemical properties of magnetic oxide nanocomposites include facile separation and optical, electrical, and magnetic properties which allow their practical applicability in realms of environment conservation. Specifically, their ability to exhibit confinement effect, with specific porous surface area, flexibility, equal size distribution, and good recyclability, makes them a suitable benign nanostructure (Ashik et al. 2018). Iron oxide exists in the following crystalline phases: hematite ($\alpha\text{-Fe}_2\text{O}_3$), magnetite (Fe_3O_4), wustite (FeO), and maghemite ($\gamma\text{-Fe}_2\text{O}_3$) (Medynska (2018)). Among them, hematite ($\alpha\text{-Fe}_2\text{O}_3$) has gained immense attention due to its cost-effective, non-toxic, and thermodynamically stable nature. Moreover, appropriate band gap of 2.2 eV and 600 nm absorption range makes $\alpha\text{-Fe}_2\text{O}_3$ a potential visible light-driven photocatalyst. The high chemical reactivity of $\alpha\text{-Fe}_2\text{O}_3$ is owed to its lower band-edge potential (2.48 eV) that improves its photodegradation ability (Li et al. (2017)). Another outstanding benefit accounts for its rapid processability, photostability, and easy separation forming solution via external magnetic field as claimed by Santhosh et al. (2019). The

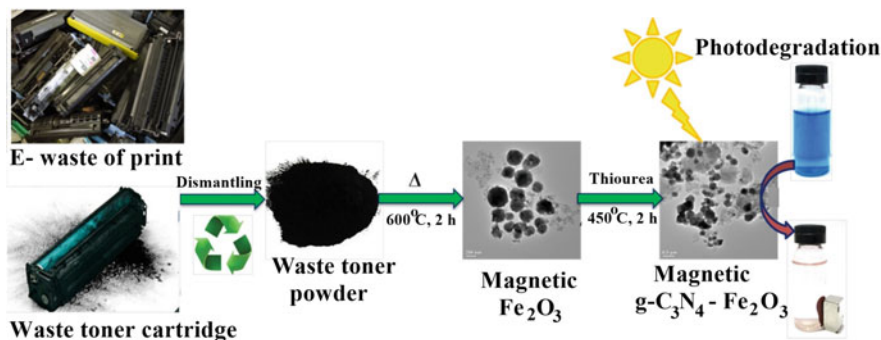


Fig. 2.3 Synthesis procedure of $g\text{-C}_3\text{N}_4/\text{Fe}_2\text{O}_3$ via waste toner powder. (Reprinted with permission from Babar et al. in (2019) copyright@2019 Elsevier Ltd. All rights reserved)

aforementioned spectacular features accentuate $\alpha\text{-Fe}_2\text{O}_3$ to significantly augment removal of recalcitrant pollutants from water bodies. Nevertheless, $\alpha\text{-Fe}_2\text{O}_3$ is accompanied with surface instability and rapid charge carrier recombination; therefore, heterojunction interface with a suitable band structure for spatial electron and hole pair separation is required (Christoforidis et al. (2016)). The explosive interests in the arena of hybrid nanocomposites in heterojunction with $g\text{-C}_3\text{N}_4$ have inevitably led to novel discoveries as discussed in the following section.

Development of photocatalytic nanocomposites with desirable magnetic and reusable properties has reached a boom, as evident from the literature. The method opted, persisting environmental conditions, and precursor type are significant aspects for achieving required characteristics of nanohybrid. The use of wide temperature range for appropriate designing of heterojunction between Fe_2O_3 and $g\text{-C}_3\text{N}_4$ has been widely taken into account. Wang et al. (2016a, b) performed calcination of precursors ferric nitrate ($\text{Fe}(\text{NO}_3)_3$) and melamine at 500°C in argon atmosphere to obtain nanorod $g\text{-C}_3\text{N}_4/\text{Fe}_2\text{O}_3$ heterojunction. Similar precursors were used by Li et al. (2017) and Yan et al. (2019) for the preparation of a synergistic hybrid $g\text{-C}_3\text{N}_4/\text{Fe}_2\text{O}_3$ composite via in situ calcination treatment at 550°C for 3 h. For the first time, an innovative, eco-friendly synthesis technique was followed by Babar et al. (2019) for dual purpose of e-waste management and wastewater treatment. A one-step calcination process involved exploitation of waste toner powder from printer cartridges which are an enriched source of Fe_2O_3 and thiourea as precursors. The smart strategy proceeded via crushing and mixing of 0.25 g of Fe_2O_3 (collected from cartridges) and 4.0 g of thiourea calcined at 450°C for 2 h and dried in oven at 80°C as presented in Fig. 2.3.

A stepwise procedure for fabrication of Fe_2O_3 /pronated (H)- C_3N_4 /reduced graphene oxide (rGO) was performed by Wang et al. (2018). The methods included calcination of melamine at 500°C , thermal treatment of $g\text{-C}_3\text{N}_4$ with nitric acid (HNO_3) at 353 K for synthesis of H- C_3N_4 , and annealing of iron trichloride hexahydrate ($\text{FeCl}_3 \cdot 6\text{H}_2\text{O}$) at 350°C for 10 min with further heating at 550°C for 4 h. For fabrication of ternary heterojunction, Hummers' method was opted in which

25 mg rGO is dispersed in 40 mg H-C₃N₄ with 0.25 g FeCl₃.6H₂O followed by stirring, ultracentrifugation, and drying on oven at 70 °C for 12 h. Feng et al. (2019) performed a pyrolysis approach for the synthesis of silver (Ag)-anchored g-C₃N₄/Fe₂O₃ to study photocatalytic and antibacterial activities. The process followed addition of 0.02 g laponite to 0.01 g FeNO₃.9H₂O with dropwise addition of 0.05 g silver nitrate (AgNO₃). The mixture was heated at 400 °C for 10 min in a muffle furnace to obtain Ag-mediated g-C₃N₄/Fe₂O₃. A ternary heterojunction comprising of Fe₂O₃-decorated ZnO/g-C₃N₄ was fabricated using precursors urea, zinc acetate dihydrate, and ferric oxyhydroxide (FeO (OH)). g-C₃N₄ was prepared by heating urea in a covered crucible at 550 °C followed by pyrolysis process, whereas a sol-gel method was employed for fabrication of nanocomposite by Balu et al. (2019). Ren et al. (2019) opted a one-step annealing process for synthesis of an octahedron hybrid with 3 g melamine and 0.3 g FeCl₃ controlled by polyvinylpyrrolidone. Wang et al. (2019) exemplified synergistic effect of incorporation of dopant manganese (Mn) in g-C₃N₄/Fe₂O₃ heterojunction. The procedure involved addition of 0.15 g manganese chloride (MnCl₂.4H₂O) to 2 g FeCl₃.6H₂O, thermal polymerization of precursors to form Mn-doped Fe₂O₃, and heating 10 g of urea at 550 °C in N₂ atmosphere for preparation of g-C₃N₄.

The usage of solvents at low temperature has proven to be a more economical synthesis strategy. Pant et al. (2017) performed facile one-step hydrothermal with precursors melamine, FeCl₃.4H₂O, and AgNO₃ and obtained Ag-mediated g-C₃N₄/Fe₂O₃. Xu et al. (2014) developed an ionic liquid system with precursors dicyanamide, FeCl₃, and 1-Butyl-3-methylimidazolium chloride via solvothermal process at low temperature. Theerthagiri et al. (2014) performed wet impregnation experiment utilizing precursors Fe (NO₃)₃.9H₂O and citric acid (1:3) with constant stirring and drying at 95 °C followed by addition of urea. The abovementioned discussions on synthesis strategies give a comparative overview of low- and high-temperature-driven methods.

2.2.1 g-C₃N₄/Fe₂O₃ Heterojunction Photocatalyst for Removal of Recalcitrant Pollutants

Among the countless properties exhibited by magnetic oxides, its large specific surface area with ample number of reactive sites makes it available for anchoring of pollutants. Additionally, its cost-effective nature and suitable bandgap of 2.2 eV with regeneration ability exhibit more pronouncing effect for photodegradation of pollutants. It is clearly apparent from review of literature that researchers have been constantly exploiting the inherent properties of Fe₂O₃ and g-C₃N₄ photocatalyst for water treatment purpose.

Babar et al. (2019) prepared g-C₃N₄/Fe₂O₃ from waste toner powder nanocomposite which exhibited 85% and 82% elimination of methyl orange dye and textile effluents, respectively. X-ray diffraction studies confirmed that on

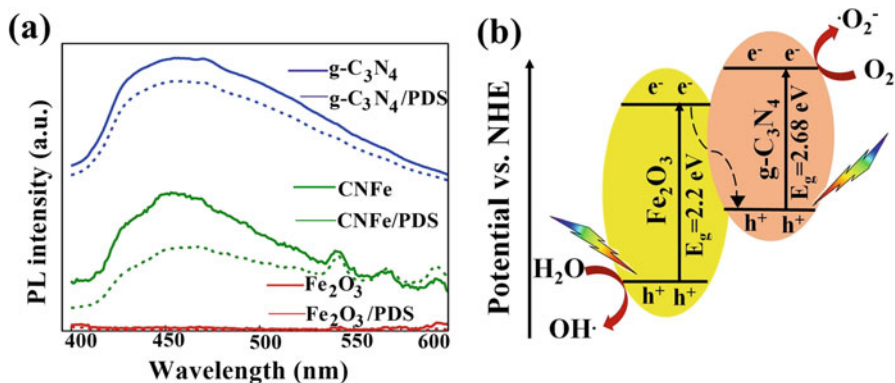


Fig. 2.4 (a) Photoluminescence (PL) spectra of $g\text{-C}_3\text{N}_4/\text{Fe}_2\text{O}_3$ photocatalyst with and without peroxydisulfate (PDS) under 320 nm excitation. (b) Mechanistic view depicting photogenerated electron-hole pair separation in $g\text{-C}_3\text{N}_4/\text{Fe}_2\text{O}_3$. (Reprinted with permission from Wang et al. in (2016a, b) copyright@2019 Elsevier Inc. All rights reserved)

incorporation of Fe_2O_3 , there was disappearance of 12.8° (100) diffraction peak which was attributed to $\Pi\text{-}\Pi$ interaction and van der Waals forces present in $g\text{-C}_3\text{N}_4$. Yan et al. (2019) improved photooxidation of bisphenol A via peroxydisulfate-mediated $g\text{-C}_3\text{N}_4/\text{Fe}_2\text{O}_3$ photocatalyst and was inferred that $\text{SO}_4^{\cdot -}$, OH^- and singlet oxygen are main reactive species responsible for 92.2% bisphenol A degradation within 60 min. On investigation of photoluminescence spectra as shown in Fig. 2.4a, it was observed that on addition of PDS, the PL intensity for $g\text{-C}_3\text{N}_4$ lowered by 15% only, whereas for $g\text{-C}_3\text{N}_4/\text{Fe}_2\text{O}_3$, it decreased to 42%. The decreased in intensity was attributed to electron scavenging nature of peroxydisulfate which increased the transport distance of photo-induced charge carriers. A supramolecular framework $g\text{-C}_3\text{N}_4/\text{Fe}_2\text{O}_3$ exhibited a high rhodamine B dye photodegradation ability on construction of a Z-scheme transfer pathway. The mechanistic details as shown in Fig. 2.4b revealed transference of reactive oxidative species to promote maximum electron-hole pair separation. Reactive species trapping experiment further exemplified transference of photogenerated electrons from conduction band (0.28 eV) of Fe_2O_3 to valence band (1.56 eV) of $g\text{-C}_3\text{N}_4$ which involved holes and electrons as major reactive species for 100% RhB removal under visible light by Wang et al. (2016a, b).

Liu et al. (2014) prepared a porous cross-linked nanostructure of $g\text{-C}_3\text{N}_4/\text{Fe}_2\text{O}_3$ as shown in Fig. 2.5 that was obtained via electrodeposition and chemical vapor deposition process. Results of scanning electron microscopy image depicted the change in morphology from needle-like Fe_2O_3 in Fig. 2.5a, b to cross-linked interconnected network with Fe_2O_3 nanoplatelets coating on $g\text{-C}_3\text{N}_4$ as illustrated in Fig. 2.5c, d. Balu et al. (2019) performed a photodegradation of tartrazine in aqueous solution that was investigated via ternary photocatalyst $\text{ZnO}/g\text{-C}_3\text{N}_4/\text{Fe}_2\text{O}_3$ under visible light irradiation depicting the trend of percentage photodegradation ability as follows: $g\text{-C}_3\text{N}_4$ (76.5%), ZnO (48.5%), $\text{Fe}_2\text{O}_3/g\text{-C}_3\text{N}_4$ (64%), and

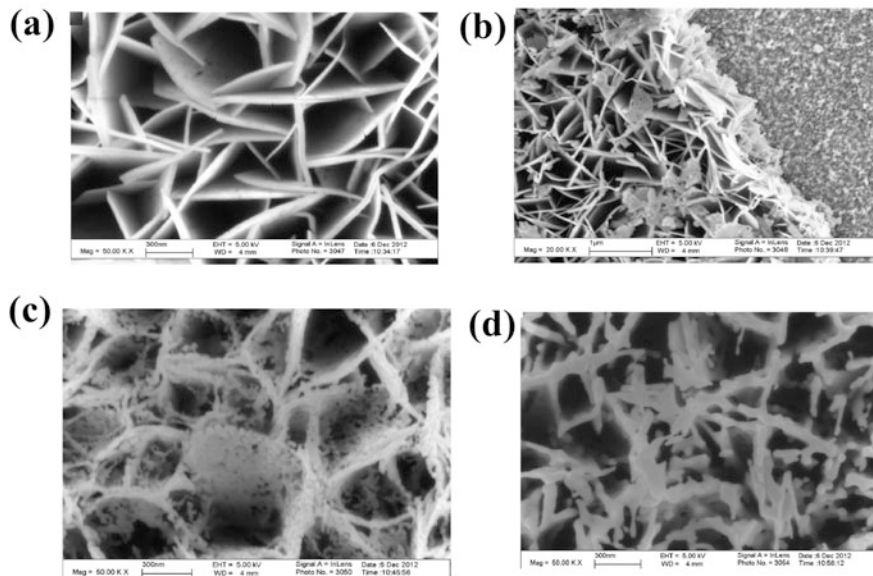
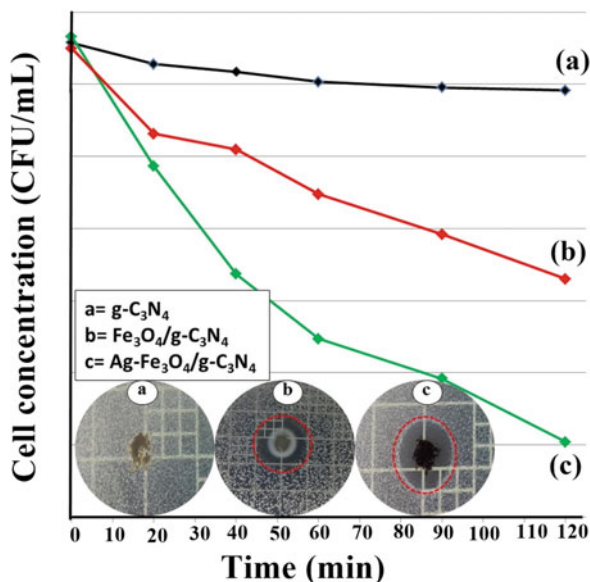


Fig. 2.5 Scanning electron microscope images of (a) Fe_2O_3 , (b) cross section of Fe_2O_3 , and (c, d) $\text{g-C}_3\text{N}_4/\text{Fe}_2\text{O}_3$ depict a morphology change from needle-like in bare Fe_2O_3 to cross-linked network in $\text{g-C}_3\text{N}_4/\text{Fe}_2\text{O}_3$. (Reprinted with permission from Liu et al. in (2019) copyright@2014 Elsevier Ltd. All rights reserved)

$\text{ZnO/g-C}_3\text{N}_4/\text{Fe}_2\text{O}_3$ (99.34%), respectively. A pseudo-first-order kinetic reaction is followed with a higher rate constant of $1.3 \times 10^{-1} \text{ min}^{-1}$. Analysis of regeneration cycle exemplified only 3.13 and 7.2% decrement in photocatalytic activity.

Researchers exemplified potential of Ag-mediated $\text{g-C}_3\text{N}_4/\text{Fe}_2\text{O}_3$ to degrade methylene blue dye and removal of *Escherichia coli* (*E. coli*) bacteria. Experimental results revealed minimum ability of $\text{g-C}_3\text{N}_4$ for antibacterial activity as shown in Fig. 2.6. Upon visible light irradiations the released reactive oxidative species caused cell membrane and protein lysis of bacteria with promoted antibacterial activity. The photodegradation capacity of methylene blue dye was performed by Pant et al. (2017) for bare $\text{g-C}_3\text{N}_4$, $\text{g-C}_3\text{N}_4/\text{Fe}_2\text{O}_3$, and Ag-mediated $\text{g-C}_3\text{N}_4/\text{Fe}_2\text{O}_3$ was 42%, 72% and 99%, respectively after 2 h of visible light irradiations. Theerthagiri et al. (2014) studied photodegradation activity of $\text{g-C}_3\text{N}_4/\text{Fe}_2\text{O}_3$ nanocomposite for commonly used colorant direct red 81 released from textile, leather, and plastic industries causing significant water pollution. The Brunauer–Emmett–Teller (BET) surface analysis revealed an increase in specific surface area from 13.4 to 28.8 m^2/g and a reduction in band gap from 2.7 to 2.4 eV for pristine $\text{g-C}_3\text{N}_4$ and 1.6 wt. % $\beta\text{-Fe}_2\text{O}_3$, respectively. The enlarged surface area and lowered band gap provided more catalytic surface area for degradation of various dyes (Christoforidis et al. 2016). Aldehyde functionalized $\text{g-C}_3\text{N}_4/\text{Fe}_2\text{O}_3$ resulted in 91.1% bisphenol A removal due to the formation of 3,4-dihydroxy benzaldehyde which decreased the probability of electron–hole pair distance in Z-scheme-driven photocatalytic system. The trapping

Fig. 2.6 Antibacterial activity of (a) bare g-C₃N₄, (b) Fe₃O₄/g-C₃N₄, and (c) Ag-Fe₃O₄/g-C₃N₄ photocatalyst against *Escherichia coli* (*E. coli*). Inset a, b, and c depict zone of inhibition for g-C₃N₄, Fe₃O₄/g-C₃N₄, and Ag-Fe₃O₄/g-C₃N₄ photocatalysts, respectively. (Reprinted with permission from Pant et al. in (2017) copyright©2017 Elsevier Ltd. All rights reserved)



experiment with various scavengers confirmed superoxide and holes as major and minor reactive species (Pan et al. 2019). The amount of phosphorus in agricultural waste and sewage has been estimated to be 15–20,000 mg/L; therefore, an effective photocatalyst g-C₃N₄/Fe₂O₃ has been synthesized via one-pot synthetic route for removal of phosphate (PO₄⁻³). The adsorption kinetics studies confirmed 92% reusability of g-C₃N₄/Fe₂O₃ with 76% PO₄⁻³ adsorption in 2 min by Gamshadzehi et al. (2019).

The versatile applicability of g-C₃N₄/Fe₂O₃ photocatalyst has been effectively examined by various characterization methods as discussed above (Zheng et al. 2012; Mohapatra et al. 2009). The potential properties of Fe₂O₃ make it a suitable candidate for elimination of unwanted microbes and pollutants from simulated water.

2.3 Synthetic Strategies for Fabrication of g-C₃N₄/Cu₂O

In the domain of semiconductor-based photocatalysts, cuprous oxide (Cu₂O) with crystal-facet tailored architecture and optimal band gap (2.0 eV) provides a meritorious arena in water remediation (Sun et al. 2018; Zhou et al. 2017). Its well-known merits include low-cost, non-toxic, and environment friendly nature, and it has gained research interests (Bai et al. 2015; Li et al. 2011, 2015a, b, 2016; McShane and Choi 2009; Qin et al. 2015; Chen et al. 2013; Peng et al. 2014; Raizada et al. 2020; Wang et al. 2016a, b). With outstanding physiochemical properties, it has various morphologies such as three-dimensional solid structures (McFadyen and

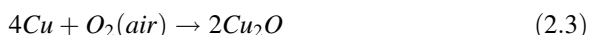
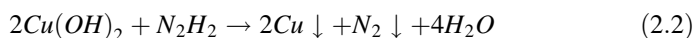
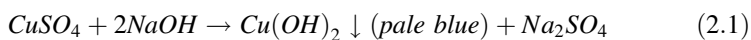
Matijevic 1973; Shang et al. 2014), mesoporous low-dimensional nanocomposites (Bernard and Fan 2006), thin films, and hollow porous structure (Mukherjee et al. 2016). Moreover, controllable size and shape emphasize on low and high indexed crystal facets (Zhang et al. 2014; Wang et al. 2013). Among all the structures, polyhedral Cu_2O are ideal semiconductors for maximum solar energy conversion and large surface for guest anchoring (Huang et al. 2014). This p-type semiconductor has been a potential candidate in the fields of water splitting, gas sensor, Li–Na-driven batteries, lubricants, and magnetic memory (Zhang et al. 2006; Dubale et al. 2016; Prucek et al. 2009; Pallecchi et al. 2010; Kim et al. 2016). However, its large scalable application has been restricted due to rapid transformation of crystal planes, recombination of charge carriers, and its highly oxidizable nature. To overcome the abovementioned problems, researchers have approached site-oriented doping and heterostructuring. Ievskaya et al. (2015) proposed an open-air deposition of Zn–Mg on thermally oxidized Cu_2O for purposes of solar cells and energy conversion. For the purpose of water splitting, $\text{Cu}_2\text{O}/\text{TiO}_2$ photocatalyst was synthesized via thermally driven hydrothermal method (Zhao et al. 2016). Photocatalytic ability for degradation of dyes rhodamine B and methyl orange was studied with as-synthesized $\text{Cu}_2\text{O}/\text{SnO}_2$ and $\text{InVO}_4\text{-Cu}_2\text{O-TiO}_2$ (Joshi et al. 2016; Kong et al. 2017). Chen et al. (2014) fabricated $\text{Cu}_2\text{O}/\text{g-C}_3\text{N}_4$ heterojunction through a facile one-step reduction method to enhance photocatalytic hydrogen production to 70% more than bare Cu_2O . In the following sections, we have given an outlook on synthesis of $\text{Cu}_2\text{O}/\text{g-C}_3\text{N}_4$ heterojunction for water purification purpose.

The advancements in structure of $\text{g-C}_3\text{N}_4/\text{Cu}_2\text{O}$ nanocomposites have been accomplished with various methodologies. To achieve the utmost photocatalytic performance, facet Cu_2O crystals have been prepared by high and low temperature and wet chemistry routes. The versatility of photodegradation exhibited by heterostructure $\text{g-C}_3\text{N}_4/\text{Cu}_2\text{O}$ was influenced by operational condition, selectivity of solvents, and controllable growth to inhibit aggregation. The most widely used synthetic approach is temperature-driven processes with the use of different solvents. The crucial vital factors are intimate contact between $\text{g-C}_3\text{N}_4$ and Cu_2O for efficient charge transfer, and other is maximized surface area for anchoring of pollutants.

High-temperature-driven fabrication process is most commonly employed for fabrication of heterostructure. Ji et al. (2018) explained chelation of Cu^{+2} in $\text{g-C}_3\text{N}_4$ obtained via calcination at 550 °C using precursors cyanoguanidine and copper acetate. Anchoring of p-type Cu_2O with n-type $\text{g-C}_3\text{N}_4$ has been successfully performed via precursors copper nitrate hexahydrate $\text{Cu}(\text{NO}_3)_2 \cdot 6\text{H}_2\text{O}$, urea, and sodium borohydride (NaBH_4). Reduction of Cu^{+2} is done by addition of NaBH_4 in calcined $\text{g-C}_3\text{N}_4$ by Anandan et al. (2017). Highly efficient photocatalyst was prepared by Zuo et al. (2017) in one-step redox anoxic calcination for removal of antibiotic chloramphenicol and carbamazepine. The superiority of this process is the use of attapulgite as a catalyst with inherent hydroxyl radical in structure to fasten the reaction. The released ammonia gas aids in easy reduction of Cu_2O and results in the formation of thin film of Cu^{+2} . Similarly, for inactivation of bacteria, $\text{g-C}_3\text{N}_4/\text{Cu}_2\text{O}$ nanocomposite was fabricated via thermal polycondensation of copper acetate with urea at 550 °C for 2 h with dropwise addition of sodium hydroxide as

performed by Liu et al. (2019). Chang and Tseng (2018) synthesized g-C₃N₄/Cu₂O crystals for CO₂ photoreduction under visible light irradiations. The method proceeded via pyrolysis of melamine at 550 °C, followed by dispersion of copper chloride (CuCl₂) in the presence of hydroxylamine hydrochloride. The mixture is kept in a temperature-controlled water bath at 30 °C, till color change is observed from light blue to clay orange. Yuan et al. (2018) similarly prepared g-C₃N₄/Cu₂O via 0.5 g calcined urea that was added in 0.37 g Cu (NO₃)₂ and pyrolyzed in a tubular furnace at 200 °C, till light gray powder was obtained.

Wet chemistry routes including hydrothermal, solvothermal, and chemical reduction methods utilize different solvent systems at low temperature for fabrication of sandwich-like g-C₃N₄/Cu₂O heterostructure. A facile one-step reduction process was followed for synthesis of CNCu using precursors urea and Cu (NO₃)₂ with hydrazinium hydrate (N₂H₄.H₂O). There was a stepwise process involving dispersion of mixture, ultrasonication, and oven drying at 60 °C for 6 h. The reduction mechanism was analyzed to be as follows as given in Eqs. (2.1, 2.2, and 2.3):



Bao and Chen (2017) clearly inferred that Cu⁺² undergo reduction under alkaline conditions to form Cu which on exposure to air forms Cu₂O. Similar precursors were used by Zhang et al. (2017a, b) for preparation of porous g-C₃N₄/Cu₂O, with NaBH₄ as reducing agent. A two-step reduction method was performed for suitable anchoring of Ag nanoparticles (NPs) on g-C₃N₄/Cu₂O to obtain maximum stability of nanocomposite. Typically, 30 mg thermally treated urea was added to 0.05 g Cu (NO₃)₂.3H₂O with dropwise addition of 1 mL of N₂H₄.H₂O, followed by constant stirring. The obtained ternary Ag- g-C₃N₄/Cu₂O was dried in vacuum oven at 40 °C for 2 h (Xi et al. 2019). The applicability of solvents is roughly in practice to make the synthesis process cost-effective on large scale. Tian et al. (2014) fabricated g-C₃N₄/Cu₂O p-n heterojunction using melamine and Cu (NO₃)₂ source in solvent glucose. A green synthesis approach was successfully opted for preparation of g-C₃N₄/Cu₂O as depicted in Fig. 2.7 to study antimicrobial activity. The practical use of citrus lemon green extract as solvent system makes the process chemical-free and reduces the perniciousness. The process involved was thermal condensation and calcination of 5 g melamine at 550 °C for 2 h to obtain g-C₃N₄. For preparation of g-C₃N₄/Cu₂O, different concentrations of Cu (NO₃)₂ were added in 1 g of g-C₃N₄ in 20 mL citrus leaf extract by Induja et al. (2019). Zhang et al. (2013) designed g-C₃N₄ coating onto octahedra facet Cu₂O core shells via solvothermal and chemisorption method. The purpose of this discussion is to highlight various facile strategies to synthesize CNCu, which are not time-consuming and based on green-chemistry approach.



Fig. 2.7 Green synthesis of $g\text{-C}_3\text{N}_4/\text{Cu}_2\text{O}$ via citrus leaves. (Reprinted with permission from Induja et al. (2019) copyright@2014 Elsevier Ltd. All rights reserved)

2.3.1 $g\text{-C}_3\text{N}_4/\text{Cu}_2\text{O}$ Heterojunction Photocatalyst for Removal of Recalcitrant Pollutants

The sole advantage offered by $g\text{-C}_3\text{N}_4$ as a surface is to prevent aggregation of Cu_2O NPs to enhance its metallic, optical, and catalytic properties as studied by Induja et al. (2019). Researchers have been exploiting these properties for elimination of organic and inorganic pollutants, bacterial pathogens, and other microbes. The role of various Cu_2O morphologies was studied by Chang and Tseng (2018) as depicted in Fig. 2.8 and claimed that cubic Cu_2O possessed wide band-gap than rhombic dodecahedral and sphere Cu_2O . Also, interaction between Cu_2O with $g\text{-C}_3\text{N}_4$ exhibited a stronger absorption blue shift of 614.9 nm, influenced by shapes of Cu_2O .

Zuo et al. (2018) further investigated the role of specific surface area in pollutant removal via N_2 -adsorption–desorption isotherm curve. According to the obtained results, the maximum surface area is $g\text{-C}_3\text{N}_4/\text{Cu}_2\text{O}$ ($219.2 \text{ m}^2/\text{g}^{-1}$) in molten state possessed ample channels for removal of MO dye. Mechanism of methyl orange photodegradation proceeded via migration of photogenerated electrons from Cu_2O toward conduction band of $g\text{-C}_3\text{N}_4$ and the simultaneous migration of holes from VB of $g\text{-C}_3\text{N}_4$ to VB of Cu_2O as demonstrated in Fig. 2.9.

In detail, Tian et al. (2014) exemplified the transfer of charge carriers in $g\text{-C}_3\text{N}_4/\text{Cu}_2\text{O}$ heterojunction upon visible light irradiation as depicted in Fig. 2.10. According to band potential values, $g\text{-C}_3\text{N}_4$ is an n-type semiconductor, and Cu_2O is a p-type semiconductor with band gap 2.87 and 2.0 eV, respectively, as shown in Fig. 2.10a. After the contact of both the semiconductors, there is generation of internal electric field until the fermi energy level reached an equilibrium point and eventually lead to heterojunction formation. Upon visible light irradiations as demonstrated in Fig. 2.10b, there was migration of h^+ from valence band of $g\text{-C}_3\text{N}_4$ (1.57 eV) to valence band of Cu_2O (1.3 eV) and transference of electrons from

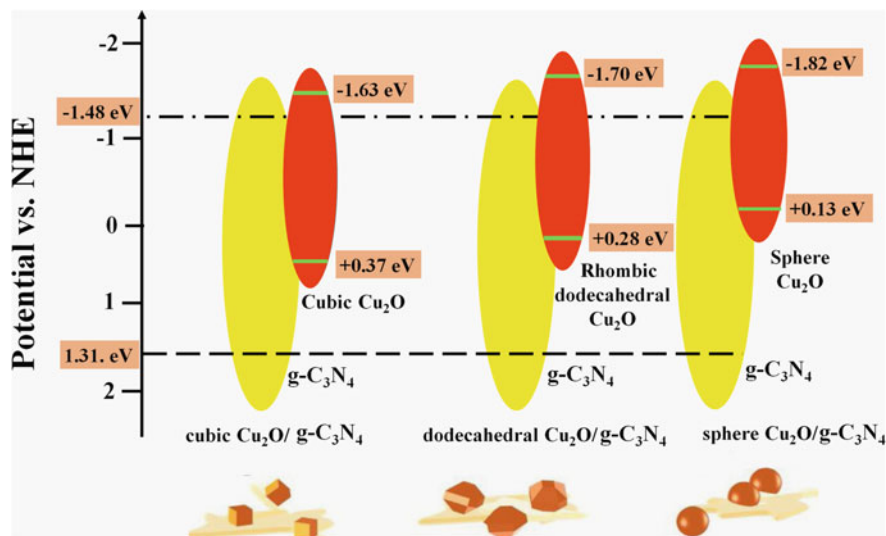


Fig. 2.8 Band structure variation cubic Cu_2O , rhombic dodecahedral, and sphere Cu_2O -coupled $\text{g-C}_3\text{N}_4$. (Reprinted with permission from Chang and Tseng in (2018) copyright@2018 Elsevier Ltd. All rights reserved)

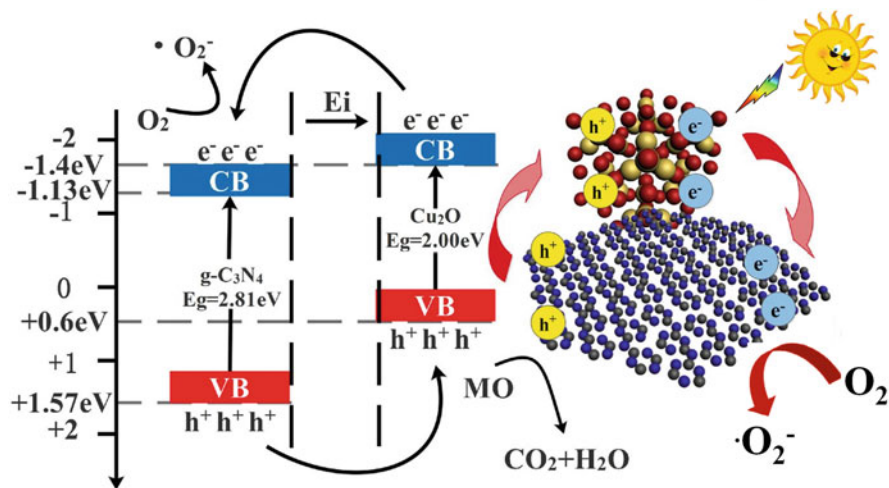


Fig. 2.9 Photocatalysis mechanism with transference of electrons from conduction band (CB) of Cu_2O to CB of $\text{g-C}_3\text{N}_4$ and simultaneous migration of holes from valence band (VB) of $\text{g-C}_3\text{N}_4$ to VB of Cu_2O . (Reprinted with permission from Zuo et al. in (2018) copyright@2018 Elsevier Ltd. All rights reserved)

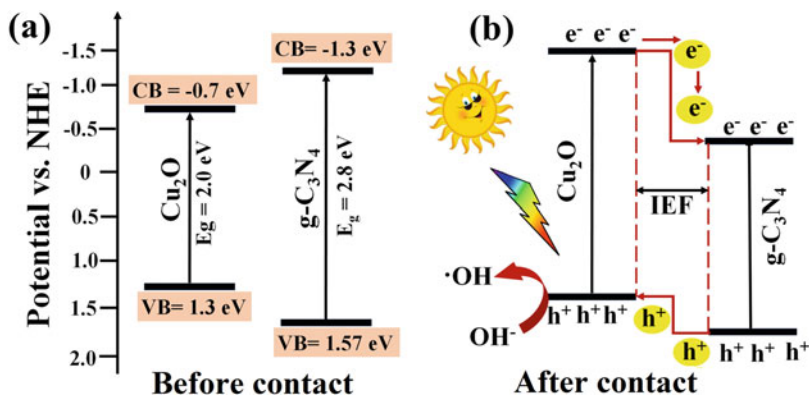


Fig. 2.10 Mechanistic illustration of g-C₃N₄/Cu₂O photocatalyst under visible light irradiation (a) before contact and (b) after contact with formation of internal electric field (IEF). (Reprinted with permission from Tian et al. in (2014) copyright©2014 Elsevier Inc. All rights reserved)

conduction band of Cu₂O (−0.7 eV) to conduction band of g-C₃N₄ (−1.13 eV). Successful formation of p–n heterojunction leads to efficient separation of electrons and holes and 95% degradation of methyl orange dye within 60 min.

Exploiting inherent properties of TiO₂ semiconductor, Min et al. (2017) synthesized universal TiO₂/g-C₃N₄/Cu₂O photocatalyst for 98.5% discoloration of RhB dye within 3 min and 100% removal of methylene blue and methyl orange dyes within 10 min of visible light irradiation. The homogenous distribution of TiO₂ and Cu₂O on the surface of g-C₃N₄ was established by transmission electron microscopy and scanning electron microscope/energy dispersive using X-ray analysis as displayed in Fig. 2.11.

Sudrajat (2017) performed abatement of atrazine via g-C₃N₄/Cu₂O photocatalyst. Anchoring of Cu₂O and valence state of Cu⁺² are estimated via X-ray photoelectron spectroscopy as demonstrated in Fig. 2.12 of 0.8% Cu₂O loading on g-C₃N₄. As shown in Fig. 2.12a, two symmetric prominent peaks at 932 and 952 eV confirm existence of Cu in +1 oxidation state. The characteristic peak at 284 eV is attributed to sp²-hybridized carbon in C–N–C lattice system of g-C₃N₄ in Fig. 2.12b. A weak additional peak as shown in Fig. 2.12c disappeared on loading of Cu, and this is assigned to the presence of amino group and tertiary N-atom. The diminishing of peak was attributed to association of Cu⁺¹ with amino moieties of g-C₃N₄.

Bao and Chen (2017) studied Z-scheme mechanism-assisted Cu₂O/Cu/g-C₃N₄ photocatalyst and observed that Cu⁰ acts as charge separation unit as the fermi level of Cu is lower than conduction band of g-C₃N₄. Hence, e[−] from conduction band of g-C₃N₄ migrates into metallic Cu to decrease recombination rate of electron–hole pair. The main reactive species involved in degradation of phenol and MO dye are hydroxyl and superoxide radicals detected using 5,5 dimethyl-1-pyrroline-N-oxide on the basis of electron spin radical trapping experiment. Similar work was carried out for elimination of methyl orange and methylene blue dyes from simulated water (Yan et al. 2017). Studies have revealed microbial disinfection activity of g-C₃N₄/

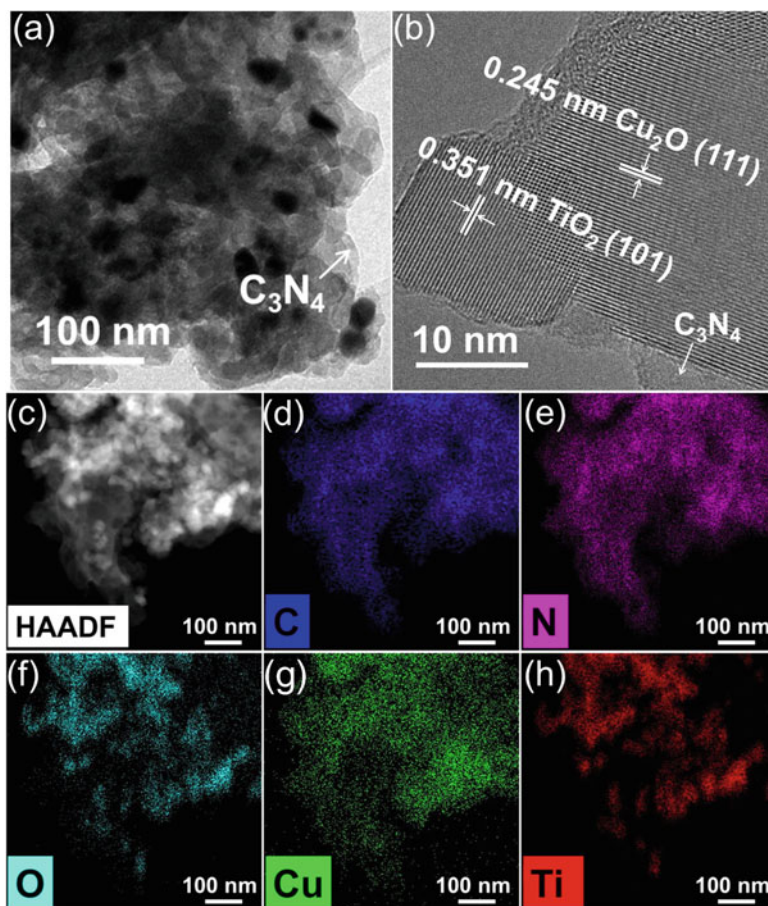


Fig. 2.11 (a) Transmission electron microscopy (TEM), (b) high-resolution transmission electron microscopy (HRTEM), (c–h) scanning transmission electron microscope/energy dispersive X-ray (STEM–EDX) mapping results of $\text{TiO}_2/\text{g-C}_3\text{N}_4/\text{Cu}_2\text{O}$. (Reproduced with permission from Min et al. in (2017) copyright@2017 Elsevier B.V. All rights reserved)

Cu_2O photocatalyst over Gram-negative bacterium and plant pathogen and observed that count of *E. coli* bacteria remained unchanged during photocatalytic experiment in the absence of light and in dark conditions, whereas excellent outcomes are obtained in case of $\text{g-C}_3\text{N}_4/\text{Cu}_2\text{O}$ -45%, resulting in inactivation of 7 log of *E. coli* in 120 min, higher than that of pristine Cu_2O . Similar behavior was observed by Liu et al. (2019) in case of fungus *Fusarium graminearum*, in which 89% of fungal elimination was observed within 5 h of visible irradiations, much higher than that of bare $\text{g-C}_3\text{N}_4$ and Cu_2O . Size control and structural alterations are opted to avoid aggregation of metal oxides using $\text{g-C}_3\text{N}_4$ as a promising surface support Rath et al. (2018).

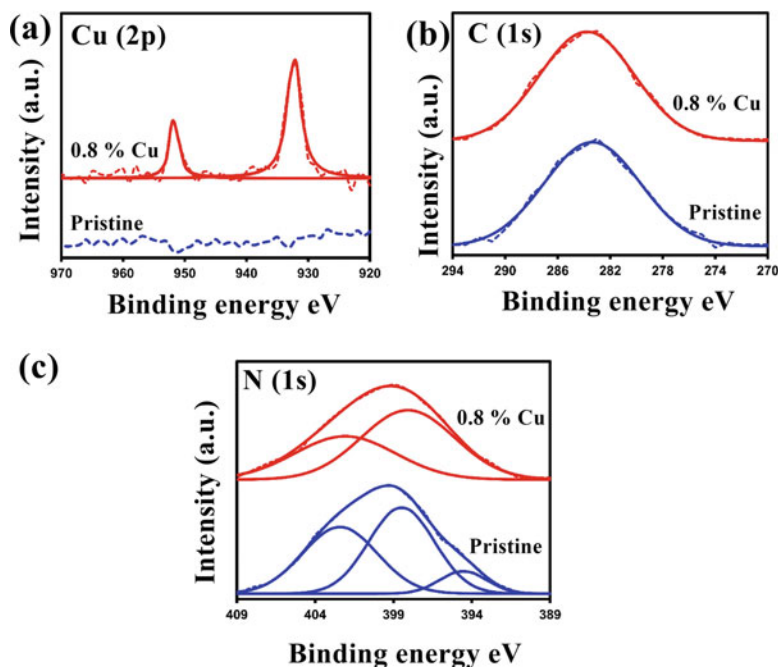


Fig. 2.12 XPS spectra of (a) Cu (2p), (b) C (1 s), (c) N (1 s) region in $g\text{-C}_3\text{N}_4/\text{Cu}_2\text{O}$ photocatalyst. (Reprinted with permission from Sudrajat in (2017) copyright@2017 Elsevier B.V. All rights reserved)

The above discussions well demonstrate that tailored architecture of heterostructure offers superior functionalities in photocatalytic degradation of pollutants, abatement of antibiotics, and microbial disinfection. The detailed description of the characterization techniques analogous to photocatalysis surmounts Cu_2O as a competent visible light-driven photocatalyst.

2.4 Conclusions

Benefiting from the feature of utilizing solar energy spectrum, photocatalysis ignites a boom in wastewater remediation technologies. With invaluable development in search of a novel visible light-driven photocatalyst, $g\text{-C}_3\text{N}_4$ was found to be widely used in large-scale applications. Exploiting the inherent properties of $g\text{-C}_3\text{N}_4$, it has significantly gained platform as a robustly efficient photocatalyst. Nevertheless, it is accompanied with certain limitations such as large band gap (2.7 eV), inefficient absorption of solar light, and rapid recombination of charge carriers. Hence, for designing a robustly active photocatalyst with improved properties, metal oxides have been well explored. $\alpha\text{-Fe}_2\text{O}_3$ possess outstanding photocatalytic ability with

band-edge potential (2.48 eV), porous surface area, flexible nature, and good magnetic separability and recyclability. Similarly, Cu_2O exists as crystal-facet tailored architecture with optimal band gap (2.0 eV) and low-cost, non-toxic, and environmentally friendly nature, thereby promoting a meritorious arena in water remediation. However, they are accompanied with thermal instability followed by aggregation into large composites, thereby losing the beauty of nanocomposite nature. Convincingly, it is suitable enough to fabricate a heterojunction with $\text{Fe}_2\text{O}_3/\text{Cu}_2\text{O}$ and g- C_3N_4 as a surface support to avoid aggregation of metal oxides and provide a combination of virtuous mechanical strength, large surface area, and arrogate band gap for generation of ROS. The aforementioned detailed discussion reiterates the indispensable contribution of Fe_2O_3 -g- C_3N_4 and Cu_2O -g- C_3N_4 nano-heterostructure photocatalytic system for pollutant elimination and microbial inactivation from water bodies. To achieve the ultimate goal of innovative synthesis for effective photocatalytic degradation, there is an advanced ongoing research.

References

- Anandan S, Wu JJ, Bahnemann D, Emeline A, Kumar M (2017) Crumpled $\text{Cu}_2\text{O}/\text{g-C}_3\text{N}_4$ nanosheets for hydrogen evolution catalysis. *Colloids Surf A Physicochem Eng Asp* 527:34–41. <https://doi.org/10.1016/j.colsurfa.2017.05.007>
- Ashik U, Kudo S, Hayashi J (2018) An overview of metal oxide nanostructures. *Synthesis of inorganic. Nanomaterials* 19–57. <https://doi.org/10.1016/B978-0-08-101975-7.00002-6>
- Babar S, Gavade N, Shinde H, Gore A, Mahajan P, Lee KH, Garadkar K (2019) An innovative transformation of waste toner powder into magnetic g- C_3N_4 - Fe_2O_3 photocatalyst: sustainable e-waste management. *J Environ Chem Eng*:103041. <https://doi.org/10.1016/j.jece.2019.103041>
- Bai S, Jiang J, Zhang Q, Xiong Y (2015) Steering charge kinetics in photocatalysis: intersection of materials syntheses, characterization techniques and theoretical simulations. *Chem Soc Rev* 44 (10):2893–2939. <https://doi.org/10.1039/C5CS00064E>
- Balu S, Velmurugan S, Palanisamy S, Chen S, Velusamy V, Yang T, Shafey E (2019) Synthesis of α - Fe_2O_3 decorated g- $\text{C}_3\text{N}_4/\text{ZnO}$ ternary Z-scheme photocatalyst for degradation of tartrazine dye in aqueous media. *J Taiwan Inst Chem Eng* 99:258–267. <https://doi.org/10.1016/j.jtice.2019.03.011>
- Bao Y, Chen K (2017) A novel Z-scheme visible light driven $\text{Cu}_2\text{O}/\text{Cu}/\text{g-C}_3\text{N}_4$ photocatalyst using metallic copper as a charge transfer mediator. *Mol Catal* 432:187–195. <https://doi.org/10.1016/j.mcat.2017.01.008>
- Bernard HB, Fan WY (2006) Shape evolution of Cu_2O nanostructures via kinetic and thermodynamic controlled growth. *J Phys Chem* 110(42):20801–20807. <https://doi.org/10.1021/jp061835k>
- Bojdys M, Müller J, Antonietti M, Thomas A (2008) Ionothermal synthesis of crystalline, condensed, graphitic carbon nitride. *Chem Eur J* 14:8177–8182. <https://doi.org/10.1002/chem.200800190>
- Chai B, Yan J, Wang C, Ren Z, Zhu Y (2017) Enhanced visible light photocatalytic degradation of Rhodamine B over phosphorus doped graphitic carbon nitride. *Appl Surf Sci* 391:376. <https://doi.org/10.1016/j.apsusc.2016.06.180>
- Chang PY, Tseng I (2018) Photocatalytic conversion of gas phase carbon dioxide by graphitic carbon nitride decorated with cuprous oxide with various morphologies. *J CO₂ Util* 26:511–521. <https://doi.org/10.1016/j.jcou.2018.06.009>

- Chen C, Yu C, Fu W (2013) Synthesis of graphite oxide (GO)/Cu₂O Nanocomposite and its catalytic performance under the ultrasound. *Nano* 8(03):1350032. <https://doi.org/10.1142/S179329201350032X>
- Chen J, Shen S, Guo P, Wang M, Wu P, Wang X, Guo L (2014) In-situ reduction synthesis of nano-sized Cu₂O particles modifying g-C₃N₄ for enhanced photocatalytic hydrogen production. *Appl Catal B* 152:335–341. <https://doi.org/10.1016/j.apcatb.2014.01.047>
- Christoforidis KC, Montini T, Bontempi E, Zafeirotas S, Jaen JD, Fornasiero P (2016) Synthesis and photocatalytic application of visible-light active β -Fe₂O₃/g-C₃N₄ hybrid nanocomposites. *Appl Catal B* 187:171–180. <https://doi.org/10.1016/j.apcatb.2016.01.013>
- Dubale A, Tamirat A, Chen HM, Berhe T, Pan CJ, Su W, Hwang B (2016) A highly stable CuS and CuS–Pt modified Cu₂O/CuO heterostructure as an efficient photocathode for the hydrogen evolution reaction. *J Mater Chem A* 4(6):2205–2216. <https://doi.org/10.1039/C5TA09464J>
- Dutta V, Singh P, Shandilya P, Sharma S, Raizada P, Saini AK, Sani AR (2019) Review on advances in photocatalytic water disinfection utilizing graphene and graphene derivatives-based nanocomposites. *J Environ Chem Eng* 7(3):103–132. <https://doi.org/10.1016/j.jece.2019.103132>
- Feng J, Shi Q, Li Y, Huang J, Li R, Hu X, Xie X (2019) Pyrolysis preparation of poly- γ -glutamic acid derived amorphous carbon nitride for supporting Ag and γ -Fe₂O₃ nanocomposites with catalytic and antibacterial activity. *Mater Sci Eng* 101:138–147. <https://doi.org/10.1016/j.msec.2019.03.096>
- Gamshadzei E, Nassiri M, Ershadifar H (2019) One-pot synthesis of microporous Fe₂O₃/g-C₃N₄ and its application for efficient removal of phosphate from sewage and polluted seawater. *Colloids Surf A Physicochem Eng Asp* 567:7–15. <https://doi.org/10.1016/j.colsurfa.2019.01.029>
- Gautam S, Shandilya P, Priya B, Singh VP, Raizada P, Rai R, Valente MA, Singh P (2016a) Superparamagnetic MnFe₂O₄ dispersed over graphitic carbon sand composite and bentonite as magnetically recoverable photocatalyst for antibiotic mineralization. *Sep Purif Technol* 172:498–511. <https://doi.org/10.1016/j.seppur.2016.09.006>
- Gautam S, Shandilya P, Singh P, Raizada P, Singh P (2016b) Model Solar photocatalytic mineralization of antibiotics using magnetically separable NiFe₂O₄ supported onto graphene sand composite and bentonite. *J Water Process Eng* 14:86–100. <https://doi.org/10.1016/j.jwpe.2016.10.008>
- Gautam S, Shandilya P, Singh VP, Raizada P, Singh P (2016c) Solar photocatalytic mineralization of antibiotics using magnetically separable NiFe₂O₄ supported onto graphene sand composite and bentonite. *J Water Process Eng* 14:86–100. <https://doi.org/10.1016/j.jwpe.2016.10.008>
- Gholipour M, Dinh C, Beland F, Do T (2015) Nanocomposite heterojunctions as sunlight-driven photocatalysts for hydrogen production from water splitting. *Nanoscale* 7(18):8187–8208. <https://doi.org/10.1039/C4NR07224C>
- Hasija V, Raizada P, Sudhaik A, Sharma K, Kumar A, Singh P, Jonnalagadda SB, Thakur VK (2019a) Recent advances in noble metal free doped graphitic carbon nitride based nanohybrids for photocatalysis of organic contaminants in water: a review. *Appl Mater Today* 15:494–524. <https://doi.org/10.1016/j.apmt.2019.04.003>
- Hasija V, Sudhaik A, Raizada P, Bandegharai AH, Singh P (2019b) Carbon quantum dots supported Ag/ZnO/phosphorus doped graphitic carbon nitride as Z-scheme photocatalysts for efficient photodegradation of 2,4-dinitrophenol. *J Environ Chem Eng* 7(4):103272. <https://doi.org/10.1016/j.jece.2019.103272>
- Hasija V, Raizada P, Sudhaik A, Singh P, Thakur VK, Parwaz AK (2020) Fabrication of Ag/AgI/WO₃ heterojunction anchored P and S co-doped graphitic carbon nitride as a dual Z scheme photocatalyst for efficient dye degradation. *Solid State Sci* 100:106095. <https://doi.org/10.1016/j.solidstatesciences.2019.106095>
- Hua S, Qu D, An L, Jiang W, Wen Y, Wang X, Sun Z (2019) Highly efficient p-type Cu₃P/n-type g-C₃N₄ photocatalyst through Z-scheme charge transfer route. *Appl Catal* 240:253–261. <https://doi.org/10.1016/j.apcatb.2018.09.010>

- Huang M, Rej S, Hsu S (2014) Facet-dependent properties of polyhedral nanocrystals. *Chem Commun* 50:1634–1644. <https://doi.org/10.1021/acsami.7b15828>
- Ievskaya Y, Hoyer R, Sadhanala A, Musselman K, MacManus J (2015) Fabrication of ZnO/Cu₂O heterojunctions in atmospheric conditions: improved interface quality and solar cell performance. *Sol Energy Mater Sol Cells* 135:43–48. <https://doi.org/10.1016/j.solmat.2014.09.018>
- Induja M, Sivaprakash K, Karthikeyan S (2019) Facile green synthesis and antimicrobial performance of Cu₂O nanospheres decorated g-C₃N₄ nanocomposite. *Mater Res* 112:331–335. <https://doi.org/10.1016/j.jssc.2014.01.011>
- Jamwal D, Kaur G, Raizada P, Singh P, Pathak D, Thakur P (2015) Twin-tail surfactant peculiarity in superficial fabrication of semiconductor quantum dots: toward structural, optical, and electrical features. *J Phys Chem C* 119(9):5062–5073. <https://doi.org/10.1021/jp510428z>
- Ji C, Yin SN, Sun S, Yang S (2018) An in-situ mediator-free route to fabricate Cu₂O/g-C₃N₄ type-II heterojunctions for enhanced visible-light photocatalytic H₂ generation. *Appl Surf Sci* 434:1224–1231. <https://doi.org/10.1016/j.apsusc.2017.11.233>
- Jiang L, Yuan X, Pan Y, Liang J, Zeng G, Wu Z, Wang H (2017) Doping of graphitic carbon nitride for photocatalysis. *Appl Catal* 217:388–406. <https://doi.org/10.1016/j.apcatb.2017.06.003>
- Joshi S, Ippolito SJ, Sunkara M (2016) Convenient architectures of Cu₂O/SnO₂ type II p–n heterojunctions and their application in visible light catalytic degradation of rhodamine B. *RSC Adv* 6(49):43672–43684. <https://doi.org/10.1039/C6RA07150C>
- Kessler FK, Zheng Y, Schwarz D, Merschjann C, Schnick W, Wang X, Bojdys M (2017) Functional carbon nitride materials-design strategies for electrochemical devices. *Nat Rev Mater* 2(6):17030. <https://doi.org/10.1038/natrevmats.2017.30>
- Kim AY, Kim MK, Cho K, Woo JY, Lee Y, Han SH, Lee JK (2016) One-step catalytic synthesis of CuO/Cu₂O in a graphitized porous C matrix derived from the Cu-based metal–organic framework for Li- and Na-ion batteries. *Appl Mater Interfaces* 8(30):19514–19523. <https://doi.org/10.1021/acsami.6b05973>
- Kong L, Zhang X, Wang C, Wan F, Li L (2017) Synergic effects of Cu_xO electron transfer co-catalyst and valence band edge control over TiO₂ for efficient visible-light photocatalysis. *Chin J Catal* 38(12):2120–2131. [https://doi.org/10.1016/S1872-2067\(17\)62959-0](https://doi.org/10.1016/S1872-2067(17)62959-0)
- Kroke E, Schwarz M, Bordon EH, Kroll P, Noll B, Norman (2002) A tri-s-triazine derivatives. Part I. From trichloro-tri-s-triazine to graphitic C₃N₄ structures. *New J Chem* 26:508–512. <https://doi.org/10.1039/B111062B>
- Kumar A, Raizada P, Singh P, Saini R, Saini A, Hosseini-Bandegharai A (2019) Perspective and status of polymeric graphitic carbon nitride based Z-scheme photocatalytic systems for sustainable photocatalytic water purification. *Chem Eng J* 14:123496. <https://doi.org/10.1016/j.cej.2019.123496>
- Lai C, Wang M, Zeng GM, Liu YG, Huang DL, Zhang C, Wang RZ, Xu P, Cheng M, Huang C (2016) Synthesis of surface molecular imprinted TiO₂/graphene photocatalyst and its highly efficient photocatalytic degradation of target pollutant under visible light irradiation. *Appl Surf Sci* 390:368–376. <https://doi.org/10.1016/j.apsusc.2016.08.119>
- Li H, Lei Y, Huang Y, Fang Y, Xu Y, Zhu L, Li X (2011) Photocatalytic reduction of carbon dioxide to methanol by Cu₂O/SiC nanocrystalline under visible light irradiation. *J Nat Gas Chem* 20(2):145–150. <https://doi.org/10.1021/la047979c>
- Li C, Hisatomi T, Watanabe O, Nakabayashi M, Shibata N, Domen K, Delaunay J (2015a) Positive onset potential and stability of Cu₂O based photocathodes in water splitting by atomic layer deposition of a Ga₂O₃ buffer layer. *Energy Environ Sci* 8(5):1493–1500. <https://doi.org/10.1039/C5EE00250H>
- Li X, Yu J, Low J, Fang Y, Xiao J, Chen X (2015b) Engineering heterogeneous semiconductors for solar water splitting. *J Mater Chem* 3(6):2485–2534. <https://doi.org/10.1039/C4TA04461D>
- Li X, Yu J, Jaroniec M (2016) Hierarchical photocatalysts. *Chem Soc Rev* 45(9):2603–2636. <https://doi.org/10.1039/C5CS00838G>
- Li Y, Li F, Wang XJ, Zhao J, Wei JN, Hao YJ, Liu Y (2017) Z-scheme electronic transfer of quantum-sized α -Fe₂O₃ modified g-C₃N₄ hybrids for enhanced photocatalytic hydrogen production. *Int J Hydrog Energy* 42(47):28327–28336. <https://doi.org/10.1016/j.ijhydene.2017.09.137>

- Liebig J, Ueber Mellon und Mellonverbindungen Justus Liebigs Ann (1844) Der Chemie 50:337–363. <https://doi.org/10.1002/jlac.18440500302>
- Liu Y, Yu YX, Zhang WD (2014) Photoelectrochemical study on charge transfer properties of nanostructured Fe₂O₃ modified by g-C₃N₄. Int J Hydrog Energy 39(17):9105–9113. <https://doi.org/10.1016/j.ijhydene.2014.03.248>
- Liu B, Wu Y, Zhang J, Han X, Shi H (2019) Visible-light-driven g-C₃N₄/Cu₂O heterostructures with efficient photocatalytic activities for tetracycline degradation and microbial inactivation. J Photochem Photobiol A 378:1–8. <https://doi.org/10.1016/j.jphotochem.2019.04.007>
- Low J, Jiang C, Cheng B, Wageh S, Ahmed A, Ghamdi A, Yu J (2017a) A review of direct Z-scheme photocatalysts. Small Methods 1(5):1700080. <https://doi.org/10.1002/smt.201700080>
- Low J, Yu J, Jaroniec M, Wageh S, Ghamdi A (2017b) Heterojunction photocatalysts. Adv Mater 29:20. <https://doi.org/10.1021/ja5044787>
- McFadyen P, Matijevic E (1973) Copper hydrous oxide sols of uniform particle shape and size. J Colloid Interface Sci 44(1):95–106. [https://doi.org/10.1016/0021-9797\(73\)90196-3](https://doi.org/10.1016/0021-9797(73)90196-3)
- McShane CM, Choi KS (2009) Photocurrent enhancement of n-type Cu₂O electrodes achieved by controlling dendritic branching growth. J Am Chem Soc 131(7):2561–2569. <https://doi.org/10.1021/ja806370s>
- Medynska ZA (2018) Metal oxide-based photocatalysis: fundamentals and prospects for application. Elsevier, Amsterdam
- Min Z, Wang X, Li Y, Jiang J, Li J, Qian D, Li J (2017) A highly efficient visible-light-responding Cu₂O-TiO₂/g-C₃N₄ photocatalyst for instantaneous discolorations of organic dyes. Mater Lett 193:18–21. <https://doi.org/10.1016/j.matlet.2017.01.083>
- Mohapatra SK, John SE, Banerjee S, Misra M (2009) Water photooxidation by smooth and ultrathin α -Fe₂O₃ nanotube arrays. Chem Mater 21(14):3048–3055. <https://doi.org/10.1021/cm8030208>
- Mukherjee I, Chatterjee S, Kulkarni NA (2016) Band gap tuning and room-temperature photoluminescence of a physically self-assembled Cu₂O nanocolumn array. J Phys Chem 120(2):1077–1082. <https://doi.org/10.1021/acs.jpcc.5b10597>
- Nashim A, Martha S, Parida KM (2013) Gd₂Ti₂O₇/In₂O₃: efficient visible-light-driven heterojunction-based composite photocatalysts for hydrogen production. ChemCatChem 5(8):2352–2359. <https://doi.org/10.1002/cctc.201300037>
- Pallecchi I, Pellegrino L, Banerjee N, Cantoni M, Gadaleta A, Siri AS, Marre D (2010) Cu₂O as a nonmagnetic semiconductor for spin transport in crystalline oxide electronics. Phys Rev 81(16):165311. <https://doi.org/10.1103/PhysRevB.81.165311>
- Pan C, Xu J, Wang Y, Li D, Zhu Y (2012) Dramatic activity of C₃N₄/BiPO₄ photocatalyst with core/shell structure formed by self-assembly. Adv Funct Mater 22(7):1518–1524. <https://doi.org/10.1002/adfm.201102306>
- Pan L, Cao S, Liu R, Chen H, Jiang F, Wang X (2019) Graphitic carbon nitride grown in situ on aldehyde-functionalized α -Fe₂O₃: all-solid-state Z-scheme heterojunction for remarkable improvement of photo-oxidation activity. J Colloid Interface Sci 548:284–292. <https://doi.org/10.1016/j.jcis.2019.04.035>
- Pant B, Park M, Lee JH, Kim HY, Park SJ (2017) Novel magnetically separable silver-iron oxide nanoparticles decorated graphitic carbon nitride nano-sheets: a multifunctional photocatalyst via one-step hydrothermal process. J Colloid Interface Sci 496:343–352. <https://doi.org/10.1016/j.jcis.2017.02.012>
- Pare B, Singh P, Jonnalagadda SB (2008) Visible light induced heterogeneous advanced oxidation process to degrade paracetamol dye in aqueous suspension of ZnO. Indian J Chem 47(6):830–835. <http://hdl.handle.net/123456789/2107>
- Pathania D, Sarita SP, Pathania D (2014) Preparation and characterization of nanoscale cadmium oxide using bovine serum albumin as green capping agent and its photocatalytic activity. Desalin Water Treat 52:3497–3503. <https://doi.org/10.1080/19443994.2013.803342>

- Peng B, Zhang S, Yang S, Wang H, Yu H, Zhang S, Peng F (2014) Synthesis and characterization of g-C₃N₄/Cu₂O composite catalyst with enhanced photocatalytic activity under visible light irradiation. *Mater Res* 56:19–24. <https://doi.org/10.1016/j.materresbull.2014.04.042>
- Priya B, Raizada P, Singh N, Thakur P, Singh P (2016a) Adsorptional photocatalytic mineralization of oxytetracycline and ampicillin antibiotics using Bi₂O₃/BiOCl supported on graphene sand composite and chitosan. *J Colloid Interface Sci* 479:271–283. <https://doi.org/10.1016/j.jcis.2016.06.067>
- Priya B, Shandilya P, Raizada P, Thakur P, Singh N, Singh P (2016b) Photocatalytic mineralization and degradation kinetics of ampicillin and oxytetracycline antibiotics using graphene sand composite and chitosan supported BiOCl. *J Mol Catal* 423:400–413. <https://doi.org/10.1016/j.molcata.2016.07.043>
- Prucek R, Kvitek L, Panacek A, Vancurova L, Soukupova J, Jancik D, Zboril R (2009) Polyacrylate-assisted synthesis of stable copper nanoparticles and copper (I) oxide nanocubes with high catalytic efficiency. *J Mater Chem* 19(44):8463–8469. <https://doi.org/10.1039/B913561H>
- Qin B, Zhao Y, Li H, Qiu L, Fan Z (2015) Facet-dependent performance of Cu₂O nanocrystal for photocatalytic reduction of Cr (VI). *Chin J Catal* 36(8):1321–1325. [https://doi.org/10.1016/S1872-2067\(15\)60877-4](https://doi.org/10.1016/S1872-2067(15)60877-4)
- Raizada P, Singh P, Kumar A, Pare B, Jonnalagadda SB (2014a) Zero valent iron-brick grain nanocomposite for enhanced solar-Fenton removal of malachite green. *Sep Purif Technol* 133:429–437. <https://doi.org/10.1016/j.seppur.2014.07.012>
- Raizada P, Singh P, Kumar A, Sharma G, Pare B, Jonnalagadda SB, Thakur P (2014b) Solar photocatalytic activity of nano-ZnO supported on activated carbon or brick grain particles: role of adsorption in dye degradation. *Appl Catal* 486:159–169. <https://doi.org/10.1016/j.apcata.2014.08.043>
- Raizada P, Kumari J, Shandilya P, Dhiman R, Singh VP, Singh P (2017a) Magnetically retrievable Bi₂WO₆/Fe₃O₄ immobilized on graphene sand composite for investigation of photocatalytic mineralization of oxytetracycline and ampicillin. *Process Saf Environ* 106:104–116. <https://doi.org/10.1016/j.psep.2016.12.012>
- Raizada P, Kumari J, Shandilya P, Singh P (2017b) Kinetics of photocatalytic mineralization of oxytetracycline and ampicillin using activated carbon supported ZnO/ZnWO₄. *Desalin Water Treat* 79:204–213. <https://doi.org/10.5004/dwt.2017.2083>
- Raizada P, Sudhaik A, Singh P (2019a) Photocatalytic water decontamination using graphene and ZnO coupled photocatalysts: a review. *Mater Sci Technol* 2(3):509–525. <https://doi.org/10.1016/j.mset.2019.04.007>
- Raizada P, Sudhaik A, Singh P, Shandilya P, Gupta VK, Hosseini A, Aggarwal S (2019b) Ag₃PO₄ modified phosphorus and sulphur co-doped graphitic carbon nitride as a direct Z-scheme photocatalyst for 2,4-dimethyl phenol degradation. *J Photochem Photobiol* 374:22–35. <https://doi.org/10.1016/j.jphotochem.2019.01.015>
- Raizada P, Sudhaik A, Singh P, Shandilya P, Saini AK, Gupta VK, Lim J, Jung H, Hosseini A (2019c) Fabrication of Ag₃VO₄ decorated phosphorus and sulphur co-doped graphitic carbon nitride as a high-dispersed photocatalyst for phenol mineralization and E. coli disinfection. *Sep Purif Technol* 212:887–900. <https://doi.org/10.1016/j.seppur.2018.12.007>
- Raizada P, Sudhaik A, Singh P, Shandilya P, Thakur P, Jung H (2020) Visible light assisted photodegradation of 2, 4-dinitrophenol using Ag₂CO₃ loaded phosphorus and sulphur co-doped graphitic carbon nitride nanosheets in simulated wastewater. *Arab J Chem* 13(1):3196–3209. <https://doi.org/10.1016/j.arabjc.2018.10.004>
- Rath PC, Saikia D, Mishra M, Kao HM (2018) Exceptional catalytic performance of ultrafine Cu₂O nanoparticles confined in cubic mesoporous carbon for 4-nitrophenol reduction. *Appl Surf Sci* 427:1217–1226. <https://doi.org/10.1016/j.apsusc.2017.08.097>
- Ren B, Xu Y, Zhang C, Zhang L, Zhao J, Liu Z (2019) Degradation of methylene blue by a heterogeneous Fenton reaction using an octahedron-like, high-graphitization carbon-doped

- Fe₂O₃ catalyst. *J Taiwan Inst Chem Eng* 97:170–177. <https://doi.org/10.1016/j.jtice.2019.01.017>
- Rong X, Qiu F, Rong J, Zhu X, Yan J, Yang D (2016) Enhanced visible light photocatalytic activity of W-doped porous g-C₃N₄ and effect of H₂O₂. *Mater Lett* 164:127–131. <https://doi.org/10.1021/am300835p>
- Santhosh C, Malathi A, Dhaneshvar E, Bhatnagar A, Grace AN, Madhavan J (2019) Iron oxide nanomaterials for water purification. In: *Nanoscale materials in water purification*. Elsevier, Amsterdam, pp 431–446. <https://doi.org/10.1016/B978-0-12-813926-4.00022-7>
- Shandilya P, Mittal D, Soni M, Raizada P, Hosseini A, Saini AK, Singh P (2018a) Fabrication of fluorine doped graphene and SmVO₄ based dispersed and adsorptive photocatalyst for abatement of phenolic compounds from water and bacterial disinfection. *J Clean Prod* 203:386–399. <https://doi.org/10.1016/j.jclepro.2018.08.271>
- Shandilya P, Mittal D, Soni M, Raizada P, Lim JH, Jeong DY, Dewedi RP, Saini AK, Singh P (2018b) Islanding of EuVO₄ on high-dispersed fluorine doped few layered graphene sheets for efficient photocatalytic mineralization of phenolic compounds and bacterial disinfection. *J Taiwan Inst Chem Eng* 93:528–542. <https://doi.org/10.1016/j.jtice.2018.08.034>
- Shandilya P, Mittal D, Sudhaik A, Soni M, Raizada P, Saini AK, Singh P (2019) GdVO₄ modified fluorine doped graphene nanosheets as dispersed photocatalyst for mitigation of phenolic compounds in aqueous environment and bacterial disinfection. *Sep Purif Technol* 210:804–816. <https://doi.org/10.1016/j.seppur.2018.08.077>
- Shang Y, Shao YM, Zhang DF, Guo L (2014) Recrystallization-induced self-assembly for the growth of Cu₂O superstructures. *Angew Chem Int Ed* 53(43):11514–11518. <https://doi.org/10.1002/anie.201406331>
- Sharma S, Dutta V, Singh P, Raizada P, Sani AR, Hosseini AB, Thakur VK (2019) Carbon quantum dot supported semiconductor photocatalysts for efficient degradation of organic pollutants in water: a review. *J Clean Prod* 228:755–769. <https://doi.org/10.1016/j.jclepro.2019.04.292>
- Singh P, Raizada P, Pathania D, Sharma G, Sharma P (2013) Microwave induced KOH activation of guava peel carbon as an adsorbent for congo red dye removal from aqueous phase. *Indian J Chem* 20(5):305–311. <http://nopr.niscair.res.in/handle/123456789/21463>
- Singh P, Raizada P, Kumari S, Kumar A, Pathania D, Thakur P (2014) Solar-Fenton removal of malachite green with novel Fe⁰-activated carbon nanocomposite. *Appl Catal* 476:9–18. <https://doi.org/10.1016/j.apcata.2014.02.009>
- Singh P, Gautam S, Shandilya P, Priya B, Singh VP, Raizada P (2017) Graphene bentonite supported ZnFe₂O₄ as super-paramagnetic photocatalyst for antibiotic degradation. *Adv Mater Lett* 8:229–238. <https://doi.org/10.5185/amlett.2017.1467>
- Singh P, Priya B, Shandilya P, Raizada P, Singh N, Pare B, Jonnalagadda SB (2019a) Photocatalytic mineralization of antibiotics using 60% WO₃/BiOCl stacked to graphene sand composite and chitosan. *Arab J Chem* 12(8):4627–4645. <https://doi.org/10.1016/j.arabjc.2016.08.005>
- Singh P, Sonu RP, Sudhaik A, Shandilya P, Thakur P, Agarwal S, Gupta VK (2019b) Enhanced photocatalytic activity and stability of AgBr/BiOBr/graphene heterojunction for phenol degradation under visible light. *J Saudi Chem Soc* 23(5):586–599. <https://doi.org/10.1016/j.jscs.2018.10.005>
- Singh P, Shandilya P, Raizada P, Sudhaik A, Sani AR, Hosseini A (2020) Review on various strategies for enhancing photocatalytic activity of graphene-based nanocomposites for water purification. *Arab J Chem* 13(1):3498–3520. <https://doi.org/10.1016/j.arabjc.2018.12.001>
- Song X, Tao H, Chen L, Sun Y (2014) Synthesis of Fe/g-C₃N₄ composites with improved visible light photocatalytic activity. *Mater Lett* 116:265. <https://doi.org/10.1016/j.matlet.2013.11.043>
- Sudhaik A, Raizada P, Shandilya P, Jeong DY, Lim JH, Singh P (2018a) Review on fabrication of graphitic carbon nitride based efficient nanocomposites for photodegradation of aqueous phase organic pollutants. *J Ind Eng Chem* 68:28–51. <https://doi.org/10.1016/j.jiec.2018.07.007>

- Sudhaik A, Raizada P, Shandilya P, Singh P (2018b) Magnetically recoverable graphitic carbon nitride and NiFe₂O₄ based magnetic photocatalyst for degradation of oxytetracycline antibiotic in simulated wastewater under solar light. *J Environ Chem Eng* 6(4):3874–3883. <https://doi.org/10.1016/j.jece.2018.05.039>
- Sudrajat H (2017) Reducing agent-free formation of Cu (I) nanoclusters on g-C₃N₄ for enhanced photocatalysis. *J Alloys Compd* 716:119–127. <https://doi.org/10.1016/j.jallcom.2017.04.302>
- Sudrajat H (2018) A one-pot solid-state route for realizing highly visible light active Na-doped g-C₃N₄ photocatalysts. *J Solid State Chem* 257:26. <https://doi.org/10.1016/j.jssc.2017.09.024>
- Sun S, Zhang X, Yang Q, Liang S, Zhang X, Yang Z (2018) Cuprous oxide (Cu₂O) crystals with tailored architectures: a comprehensive review on synthesis, fundamental properties, functional modifications and applications. *Prog Mater* 96:111–173. <https://doi.org/10.1016/j.pmatsci.2018.03.006>
- Theerthagiri J, Senthil RA, Priya A, Madhavan J, Michael RJV, Ashok M (2014) Photocatalytic and photoelectrochemical studies of visible-light active α -Fe₂O₃-g-C₃N₄ nanocomposites. *RSC Adv* 4(72):38222–38229. <https://doi.org/10.1039/C4RA04266B>
- Tian Y, Chang B, Fu J, Zhou B, Liu J, Xi F, Dong X (2014) Graphitic carbon nitride/Cu₂O heterojunctions: preparation, characterization, and enhanced photocatalytic activity under visible light. *J Solid State Chem* 212:1–6. <https://doi.org/10.1016/j.jssc.2014.01.011>
- Wang X, Liu C, Zheng BJ, Jiang YQ, Zhang L, Xie Z (2013) Controlled synthesis of concave Cu₂O microcrystals enclosed by high-index facets and enhanced catalytic activity. *J Mater Chem* 1:282–287. <https://doi.org/10.1039/C2TA00241H>
- Wang J, Li C, Cong J, Liu Z, Zhang H, Liang M, Yao J (2016a) Facile synthesis of nanorod-type graphitic carbon nitride/Fe₂O₃ composite with enhanced photocatalytic performance. *J Solid State Chem* 238:246–251. <https://doi.org/10.1016/j.jssc.2016.03.042>
- Wang Y, Zheng M, Liu S, Wang Z (2016b) Size control and growth process study of Au@ Cu₂O particles. *Nano Res Lett* 11(1):390. <https://doi.org/10.1186/s11671-016-1603-6>
- Wang S, Liu M, He S, Zhang S, Lv X, Song H, Chen D (2018) Protonated carbon nitride induced hierarchically ordered Fe₂O₃/HC₃N₄/rGO architecture with enhanced electrochemical sensing of nitrite. *Sensors Actuators B Chem* 260:490–498. <https://doi.org/10.1016/j.snb.2018.01.073>
- Wang N, Han B, Wen J, Liu M, Li X (2019) Synthesis of novel Mn-doped Fe₂O₃ nano-cube supported g-C₃N₄ photocatalyst for overall visible-light driven water splitting. *Colloids Surf A Physicochem Eng Asp* 567:313–318. <https://doi.org/10.1016/j.colsurfa.2019.01.053>
- Wirthier E, Mesch M, Senker J, Schnick W (2013) Formation and characterization of melam, melam hydrate, and a melam–melem adduct. *Chem Eur J* 19:2041–2049. <https://doi.org/10.1002/chem.201203340>
- Xi Q, Gao G, Jin M, Zhang Y, Zhou H, Wu C, Xu J (2019) Design of graphitic carbon nitride supported Ag–Cu₂O composites with hierarchical structures for enhanced photocatalytic properties. *Appl Surf Sci* 471:714–725. <https://doi.org/10.1016/j.apsusc.2016.05.162>
- Xiong T, Cen W, Zhang Y, Dong F (2014) Bridging the g-C₃N₄ interlayers for enhanced photocatalysis. *ACS Catal* 6:2462–2472. <https://doi.org/10.1021/acscatal.5b02922>
- Xu L, Xia J, Xu H, Yin S, Wang K, Huang L, Li H (2014) Reactable ionic liquid assisted solvothermal synthesis of graphite-like C₃N₄ hybridized α -Fe₂O₃ hollow microspheres with enhanced super-capacitive performance. *J Power Sources* 245:866–874. <https://doi.org/10.1016/j.jpowsour.2013.07.014>
- Yan X, Xu R, Guo J, Cai X, Chen D, Huang L, Tan S (2017) Enhanced photocatalytic activity of heterojunction coupled with Cu₂O/g-C₃N₄ reduced graphene oxide three-dimensional aerogel photocatalysis. *Mater Res* 96:18–27. <https://doi.org/10.1002/adma.201304173>
- Yan S, Shi Y, Tao Y, Zhang H (2019) Enhanced persulfate-mediated photocatalytic oxidation of bisphenol A using bioelectricity and a g-C₃N₄/Fe₂O₃ heterojunction. *Chem Eng* 359:933–943. <https://doi.org/10.1016/j.cej.2018.11.093>
- Yuan S, Cui P, Zhang Y, Zhang H, Huo L, Gao Y (2018) Popping of g-C₃N₄ mixed with cupric nitrate: facile synthesis of Cu-based catalyst for construction of CN bond. *Green Energy Environ* 3(4):368–374. <https://doi.org/10.1016/j.gee.2018.08.003>

- Zhang J, Liu J, Peng Q, Wang X, Li Y (2006) Nearly monodisperse Cu_2O and CuO nanospheres: preparation and applications for sensitive gas sensors. *Chem Mater* 18(4):867–871. <https://doi.org/10.1021/cm052256f>
- Zhang LW, Wang YJ, Cheng HY, Yao WQ, Zhu Y (2009) Synthesis of porous Bi_2WO_6 thin films as efficient visible light active photocatalysts. *Adv Mater* 21:1286–1290. <https://doi.org/10.1002/adma.200801354>
- Zhang J, Chen X, Takanahe K, Maeda K, Domen K, Epping J, Fu X, Antonietti M, Wang X (2010) Synthesis of a carbon nitride structure for visible light catalysis by copolymerization. *Angew Chem Int Ed* 49:441–444. <https://doi.org/10.1002/anie.200903886>
- Zhang Y, Wang Y, Jin J, Zhang J, Lin Z, Huang F, Yu J (2013) Efficient visible-light photocatalytic hydrogen evolution and enhanced photostability of core/shell $\text{CdS/g-C}_3\text{N}_4$ nanowires. *Appl Mater Interfaces* 5(20):10317–10324. <https://doi.org/10.1021/am403327g>
- Zhang L, Shi J, Liu M, Jing D, Guo L (2014) Photocatalytic reforming of glucose under visible light over morphology-controlled Cu_2O : efficient charge separation by crystal facet engineering. *ChemComm* 50(2):192–194. <https://doi.org/10.1039/C3CC46423G>
- Zhang Y, Gong H, Li G, Zeng H, Zhong L, Liu K, Cao H, Yan H (2017a) Synthesis of graphitic carbon nitride by heating mixture of urea and thiourea for enhanced photocatalytic H_2 production from water under visible light. *Int J Hydrog Energy* 42:143–151. <https://doi.org/10.1016/j.ijhydene.2016.11.040>
- Zhang P, Wang T, Zeng H (2017b) Design of $\text{Cu-Cu}_2\text{O/g-C}_3\text{N}_4$ nanocomponent photocatalysts for hydrogen evolution under visible light irradiation using water-soluble Erythrosine B dye sensitization. *Appl Surf Sci* 391:404–414. <https://doi.org/10.1016/j.apsusc.2016.05.162>
- Zhang G, Lin L, Li G, Zhang Y, Savateev A, Zafeiratos S, Wang X, Antonietti M (2018) Ionothermal synthesis of Triazine–Heptazine based copolymers with apparent quantum yields of 60% at 420 nm for solar hydrogen production from “sea water”. *Angew Chem Int Ed* 57:9372–9376. <https://doi.org/10.1002/anie.201804702>
- Zhao Z, Sun Y, Dong F (2015) Graphitic carbon nitride-based nanocomposites. *Nanoscale* 7(1):15–37. <https://doi.org/10.1039/C4NR03008G>
- Zhao K, Zhao S, Qi J, Yin H, Gao C, Khattak AM, Yu R (2016) Cu_2O clusters grown on TiO_2 nanoplates as efficient photocatalysts for hydrogen generation. *Inorg Chem* 3(4):488–493. <https://doi.org/10.1039/C5QI00284B>
- Zheng J, Kang M, Song G, Son S, Suh S, Kim C, Kang Y (2012) Morphology evolution of dendritic Fe wire array by electrodeposition, and photoelectrochemical properties of $\alpha\text{-Fe}_2\text{O}_3$ dendritic wire array. *CrystEngComm* 14(20):6957–6961. <https://doi.org/10.1039/C2CE26046H>
- Zhou X, Jin B, Luo J, Gu X, Zhang S (2017) Photoreduction preparation of Cu_2O @ polydopamine nanospheres with enhanced photocatalytic activity under visible light irradiation. *J Solid State Chem* 254:55–61. <https://doi.org/10.1016/j.jssc.2017.07.007>
- Zhou Z, Zhang Y, Shen Y, Liu S, Zhang Y (2018) Molecular engineering of polymeric carbon nitride: advancing applications from photocatalysis to biosensing and more. *Chem Soc Rev* 47:2298–2321. <https://doi.org/10.1039/C7CS00840F>
- Zhu J, Xiao P, Li H, Carabineiro S (2014) Graphitic carbon nitride: synthesis, properties, and applications in catalysis. *Appl Mater Interfaces* 6(19):16449–16465. <https://doi.org/10.1021/am502925j>
- Zhu B, Zhang J, Jiang C, Cheng B, Yu J (2017) First principle investigation of halogen-doped monolayer $\text{g-C}_3\text{N}_4$ photocatalyst. *Appl Catal* 207:27–34. <https://doi.org/10.1016/j.apcatb.2017.02.020>
- Zuluaga S, Liu L, Shafiq N, Rupich SM, Veyan J, Chabal Y, Thonhauser T (2015) Structural band-gap tuning in $\text{g-C}_3\text{N}_4$. *Phys Chem Chem Phys* 17:957–962. <https://doi.org/10.1039/C4CP05164E>
- Zuo S, Chen Y, Liu W, Yao C, Li X, Li Z, Liu X (2017) A facile and novel construction of attapulgite/ $\text{Cu}_2\text{O/g-C}_3\text{N}_4$ with enhanced photocatalytic activity for antibiotic degradation. *Ceram* 43(3):3324–3329. <https://doi.org/10.1016/j.ceramint.2016.11.173>

Zuo S, Xu H, Liao W, Yuan X, Sun L, Li Q, Xia D (2018) Molten-salt synthesis of g-C₃N₄-Cu₂O heterojunctions with highly enhanced photocatalytic performance. *Colloid Surf A* 546:307–315. <https://doi.org/10.1016/j.colsurfa.2018.03.013>

Chapter 3

Metal and Carbon Quantum Dot Photocatalysts for Water Purification



Pooja Shandilya, Pankaj Raizada, Anita Sudhaik, Adesh Saini, Reena Saini, and Pardeep Singh

Contents

| | | |
|-------|---|-----|
| 3.1 | Introduction | 82 |
| 3.2 | Classification of Carbon Quantum Dots | 85 |
| 3.3 | Method of Preparation of Carbon Quantum Dot-Modified Photocatalysts | 86 |
| 3.3.1 | Top-Down Method | 87 |
| 3.3.2 | Bottom-Up Approach | 93 |
| 3.4 | Photocatalytic Activity of Carbon Quantum Dot-Based Nanocomposites | 102 |
| 3.5 | Antibacterial Activity of Carbon Quantum Dot-Based Nanocomposites | 106 |
| 3.6 | Conclusion | 107 |
| | References | 108 |

Abstract Carbon quantum dots are zero-dimensional carbon nanomaterials having a size of less than 10 nm with sp^2 -/ sp^3 -hybridized carbon atom containing a variety of functional groups at basal plane and periphery. Carbon quantum dots are a new

P. Shandilya · P. Raizada · P. Singh (✉)

School of Chemistry, Faculty of Basic Sciences, Shoolini University, Solan, Himachal Pradesh, India

Himalayan Centre for Excellence in Nanotechnology, Shoolini University, Solan, Himachal Pradesh, India

A. Sudhaik

School of Chemistry, Faculty of Basic Sciences, Shoolini University, Solan, Himachal Pradesh, India

A. Saini

Himalayan Centre for Excellence in Nanotechnology, Shoolini University, Solan, Himachal Pradesh, India

School of Biological and Environmental Sciences, Faculty of Basic Sciences, Shoolini University, Solan, Himachal Pradesh, India

R. Saini

School of Biotechnology, Faculty of Applied Science and Biotechnology, Shoolini University, Solan, Himachal Pradesh, India

© The Editor(s) (if applicable) and The Author(s), under exclusive license to Springer Nature Switzerland AG 2021

Inamuddin et al. (eds.), *Water Pollution and Remediation: Photocatalysis*, Environmental Chemistry for a Sustainable World 57,

https://doi.org/10.1007/978-3-030-54723-3_3

class of carbonaceous material which are recently developed and attracted appreciable importance due to their superlative properties and significant applications in different fields. By virtue of their unique optical, electronic, and efficient light harvesting, tunable photoluminescence, and up-conversion property, carbon quantum dots displayed huge applications in bio-sensing, bio-imaging, drug delivery, photocatalysis, photovoltaics and optoelectronics. Today, contamination of water is one of the biggest and most alarming problems that demands an immediate solution, and non-availability of economical method for water treatment makes it more significant. The potential pollutants of water pollution are heavy metal ions, sewage, pesticide, pharmaceutical waste, and industrial waste. The most abundant carbon as photocatalytic nanomaterial could be a better choice among previously reported conventional photocatalyst and quantum dots.

The book chapter aims to demonstrate top-down method and bottom-up method for the fabrication of carbon quantum dots. Further, the basic mechanism of photocatalysis, disadvantages of conventional quantum dots, classification of carbon quantum dots, and the concept behind up-conversion phenomena were also reviewed. The photocatalytic degradation and antimicrobial application of carbon quantum dot-based photocatalyst were also explored. Lastly, conclusion and future perspective were considered and speculated. The design of photocatalytic system with high photo-efficiency is still challenging, and the area remains open to carry out future research.

Keywords Carbon quantum dots · Graphene quantum dots · Photocatalyst · Nanocomposites · Up-conversion · Water purification

3.1 Introduction

The need of a promising approach to meet the global energy requirement of the future generation as well decreasing environmental pollution by utilizing renewable solar energy is the most prominent method. The idea of bringing out an effective usage of solar energy makes scientists to explore such material which is capable of both energy conversion and environmental pollutant degradation (Chandel et al. 2019; Gautam et al. 2017; Zhu et al. 2017). The semiconductor photocatalysts become an evident material with immense potential for solving water pollution (Singh et al. 2014; Raizada et al. 2017a; Shandilya et al. 2018a). Thus, various semiconductor photocatalytic materials such as titanates (He et al. 2018; Kumar et al. 2019), vanadates (Adan et al. 2015), tungstates (Huang et al. 2014), zirconates (Chen et al. 2015), chalcogenides (Nie and Zhang 2017), oxyhalides (Sharma et al. 2019a; Priya et al. 2016a; Singh et al. 2016), ferrites (Sonu et al. 2019; Singh et al. 2019a, b), and borates (Huang et al. 2013) have been investigated. However, these materials are associated with certain limitations like inefficient solar light harvesting

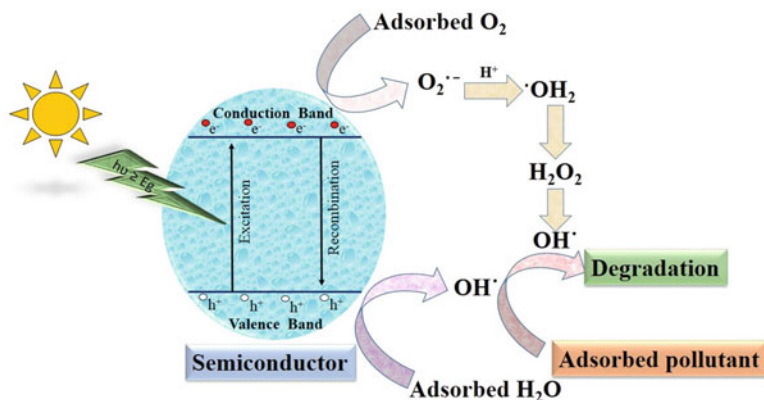


Fig. 3.1 Mechanistic view of semiconductor-based photocatalysis indicating generation of electron–hole pair under solar irradiation; the holes in the valence band oxidizes water molecule into hydroxyl radical, whereas the electron in the conduction band reduces oxygen into superoxide radical. The generated reactive oxygen species oxidizes adsorbed pollutant into innocuous product

due to wide band gap, complex synthetic procedure, high cost, high toxicity, and leaching.

The basic mechanism for photocatalytic reaction can be understood from Fig. 3.1. The electron–hole pair generation is mainly stimulated when light of certain frequency with energy greater than or equal to the band gap of semiconductor is made incident on its surface (Singh et al. 2018; Raizada et al. 2017b; Priya et al. 2016b; Gautam et al. 2016; Shandilya et al. 2019). The charge carrier generated may either recombine or assort individually to render hydroxyl radical in the valence band and superoxide radical in the conduction band (Singh et al. 2013). The electron exhibit a strong reductive potential of +0.5 to -1.5 V *w.r.t.* normal hydrogen electrode, whereas holes possess strong oxidative potential of +1.0 to +3 V *w.r.t.* normal hydrogen electrode. The reactive oxidation species is a strong oxidizing agent that can oxidize the pollutant into innocuous product. Further, electron reduces the oxygen into superoxide anion in the conduction band, and holes oxidize the water molecule into hydroxyl radical in the valence band (Raizada et al. 2014a, b, 2019a, b; Sudhaik et al. 2018a).

Both superoxide anion and hydroxyl radical are highly reactive oxidation species that can bang up all types of pollutant along with biomolecules and can be used to disinfect and deodorized air and water (Singh et al. 2017, 2018; Hasija et al. 2019a; Sudhaik et al. 2018b). The continuous attack by reactive oxidation species finally brings about the abasement of pollutant present in water. All impurities in water were oxidized by reactive oxidation species (OH^\cdot , $\text{O}_2^{\cdot-}$, and H_2O_2) generated during photocatalysis (Hasija et al. 2019b; Dutta et al. 2019; Raizada et al. 2019c, d).

However, ineffective utilization of solar spectrum due to wide band gap, higher rate of recombination of photogenerated charge carrier, difficulty in separation/recovery, complex synthetic procedure, high cost, high toxicity, and leaching are certain disadvantages possess by bare metal oxide-based semiconductor (Raizada

et al. 2016; Tian et al. 2014). One of the effective ways to minimize these limitations is to assemble carbon-coated nanostructure where the carbonaceous material enhances the charge carrier mobility by acting as an electron sink/acceptor. Further, the codoping of carbon framework with nitrogen and sulfur induces the surface defects which increase the delocalization of electron (Wu et al. 2007; Pang et al. 2015; Raizada et al. 2018). Thus, one of the prominent nanomaterials ruling nanotechnology is the metal-free carbon-based photocatalytic system employed for the degradation of pollutant from water. After oxygen, carbon is the second highest abundant element in the periodic table and also the major constituent of organic compound. The usage of the most abundant carbon as photocatalytic nanomaterial makes them more economical and advantageous in which carbon quantum dots acquire a significant attention.

Earlier, the survey was confined to CdSe/CdS and CdSe/ZnS and ZnSe/CdSe quantum dots. In these traditional quantum dots, cadmium is the chief constituent which leads to cytotoxicity due to the leakage of cadmium ions (Xu et al. 2010). Thus, scientists emphasize to develop cadmium-free quantum dots, for example, graphene quantum dots, carbon quantum dots, and silicon quantum dots (Al Awak et al. 2017). Quantum dots have been utilized in a variety of applications including bio-sensing, bio-imaging, and biomarkers and in medicine (Sharma et al. 2019b; Jamwal et al. 2015). However, potential cytotoxicity, environmental hazards, and tedious synthesis procedure were certain limitations that hindered the large-scale applicability of quantum dots. Conventional quantum dots like PbS, PbSe, HgTe, CdSe, InAs, and InP (Cademartiri et al. 2006; Moreels et al. 2007; Keuleyan et al. 2011; Guzelian et al. 1996; Micic et al. 1997) have various properties. However, metal-based quantum dots face major challenges of depositing on the support, recycling, and extremely hazardous nature which need to be addressed. Limitation of conventional quantum dots can be obviated by using organic quantum dots as an alternative; hence, many researchers nowadays are extensively working on it.

Currently, quantum-sized carbon has attracting much attention due to its tunable band gap with broader absorption range; good conductivity; strong photoluminescence emission; large-scale synthesis at low cost; less complex synthetic procedure; most abundant and thus inexpensive; high photostability; remarkable optical, electronic, and magnetic property; good biocompatibility; low toxicity; and high chemical stability that make them chemically inert (Chen et al. 2018b; Ma et al. 2017; Lim et al. 2015) (Fig. 3.2). All these properties make them widely utilized in different fields, for example, in optoelectronics, biosensor, drug delivery, bio-imaging, biomedical engineering, and photocatalysis (Luo et al. 2016; Namdari et al. 2017). Further, the excellent electronic property of carbon quantum dots makes them good electron donors and acceptors, resulting in their wide application in catalysis, semiconductor devices, and sensor (Fig. 3.3).

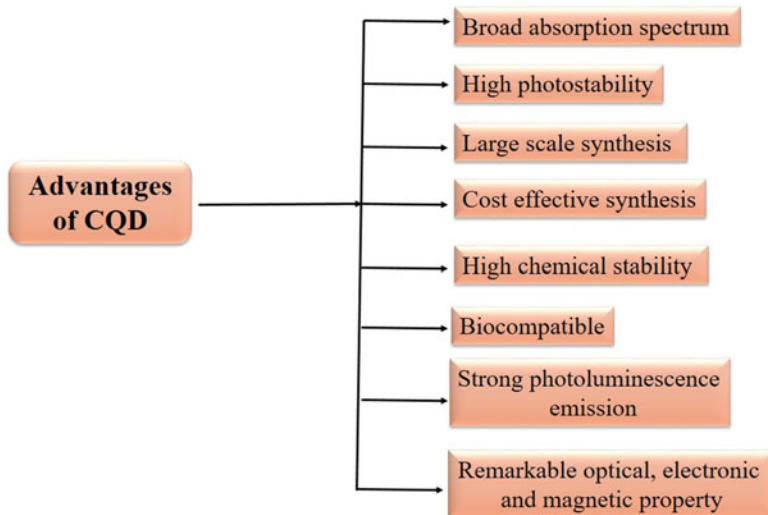


Fig. 3.2 Various advantages of carbon quantum dots

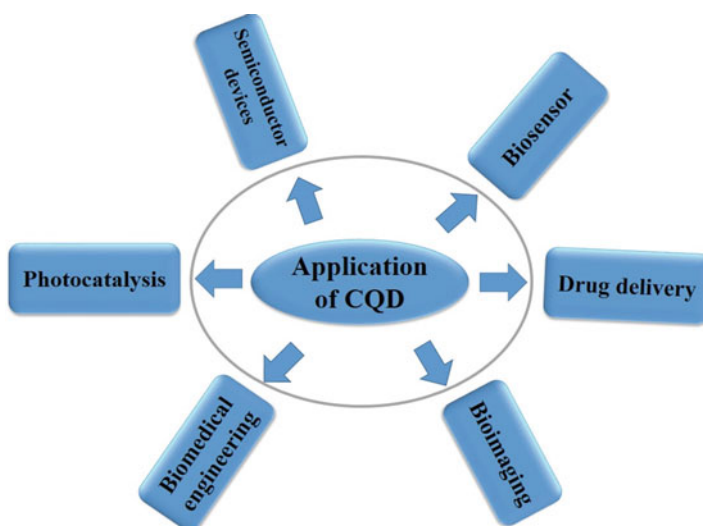


Fig. 3.3 Different applications of carbon quantum dots

3.2 Classification of Carbon Quantum Dots

Various allotropic forms of carbon are graphene, fullerene, carbon nanotubes, carbon onions, carbon nano-horns, and carbon quantum dots. On the basis of dimension, carbon nanomaterials are classified into zero-dimensional (carbon quantum dots,

fullerene, carbon onions, nano-diamonds), one-dimensional (carbon nanotubes, single-walled carbon nanotubes, carbon nanofibers), and two-dimensional materials (graphene, graphene nanoribbons, few layered graphenes) (Shandilya et al. 2018b).

Xu et al. (2004) firstly isolated carbon quantum dots from the crude soot while preparing single-walled carbon nanotubes (Xu et al. 2004). Sun et al. (2006) isolated carbon quantum dots from graphite powder and cement using laser ablation method (Sun et al. 2006). Pan et al. (2018) fabricated CdS/BiOCl heterojunction via selective deposition of CdS quantum dots on BiOCl nanosheets. Various characterization techniques indicate the uniform dispersion of CdS quantum dots. The photocatalytic performance was carried out against methyl orange and phenol, which shows 4.0 and 4.8 times higher efficiency of nanocomposites as compared to bare BiOCl. The increased visible light absorption and high migration efficiency of charge carrier are attributed for high efficiency. Due to the narrow band gap of CdS of 2.4 eV, CdS can be easily coupled with bismuth-based photocatalyst so as to inhibit rate of recombination by promoting charge carrier separation. Earlier, BiOI, BiOCl coupled with CdS quantum dots, and photocatalytic activity were evaluated against rhodamine B and methyl orange (Kandi et al. 2017; Liu et al. 2014).

There are many review articles published highlighting the synthetic approaches, properties, surface functionalization, and application of carbon quantum dots. Here, top-up and bottom-down approaches for the synthesis of carbon quantum dots with their advantages and disadvantages were reviewed. Then, the mechanism of some novel photocatalysts is also proposed followed by the general discussion of Z-scheme photocatalyst and later on the up-conversion phenomena of carbon quantum dots which are basically responsible for the higher photo-efficiency of nanocomposites by broadening the region of solar light absorption.

3.3 Method of Preparation of Carbon Quantum Dot-Modified Photocatalysts

Generally, there are two synthetic methods by which carbon quantum dots can be prepared: “bottom-up” and “top-down” approaches (Roy et al. 2015; Zhu et al. 2015). The main problems taken into account while synthesizing carbon quantum dots are agglomeration, surface functionalization, size control, and uniformity. The top-down approach includes the fragmentation of large based precursor (graphite, graphene, graphene oxide, carbon nanotube, carbon fiber) into carbon nanomaterial via arc discharge, laser ablation, electrochemical approach, acid oxidizing exfoliation, and ultrasonic exfoliation (Yuan et al. 2016). However, bottom-up approach includes hydrothermal/solvothermal method, microwave-assisted method, thermal pyrolytic route (oil bath), reverse micelle technique, template method, and substance oxidation (Zuo et al. 2016) (Fig. 3.4 and Table 3.1). Bottom-up approach is a template strategy which is used to construct carbon quantum dots by using citric

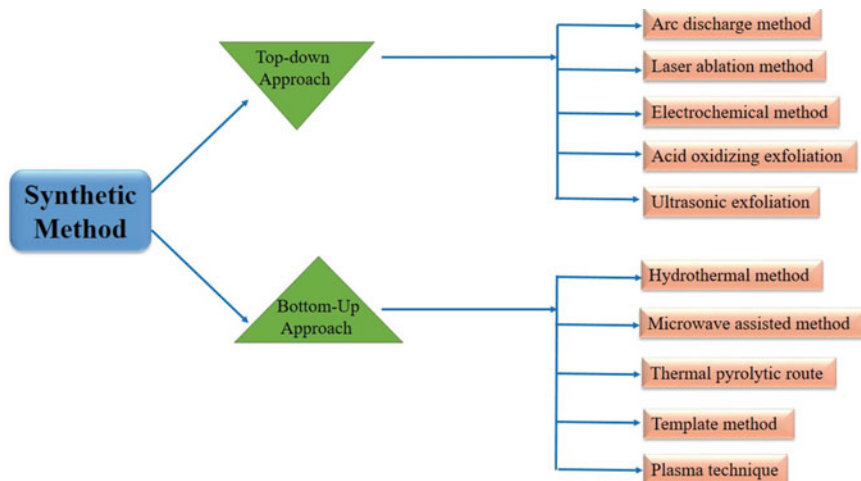


Fig. 3.4 Schematic diagram of various synthetic methods of top-down and bottom-up approach for the synthesis of carbon quantum dots

acid, glucose, xylose, and resin as carbonaceous materials (Yang et al. 2018; Tang et al. 2012).

3.3.1 Top-Down Method

Arc Discharge Method

In arc discharge method, a helium gas of 660 mbar pressure is electrically broken down to generate plasma using electric current at the anode and cathode. The pure graphite rod acts as the cathode which is 16 mm in diameter and 40 mm in length, while the anode is also made up of graphite rod which is 6 mm in diameter and 100 mm in length. The anode is further drilled to make a hole of 3.5 mm in diameter and 40 mm deep filled with carbon precursor along with catalysts. The arc discharge was generated by applying 100 A current and 30 V potential between the anode and cathode kept at a constant distance of 3 mm. Mixtures of metals, Ni–Co, Co–Y, and Ni–Y, in different atomic percentages were used as catalysts. The high-temperature plasma sublimes the carbon precursor. The carbon vapor moves toward the cathode where it cools down due to temperature gradient and is collected from the walls of the chamber (Journet et al. 1997). Xu et al. (2004) devised arc discharge method for the preparation of single-walled carbon nanotube exploiting soot which is condensed on the chamber walls.

Table 3.1 Advantages and disadvantages of synthetic method of carbon quantum dots

| Sr. no. | | Synthetic method | Advantages | Disadvantages | References |
|---------|--------------------|----------------------------------|---|--|---|
| 1. | Top-down approach | Arc discharge method | Most attainable method | Harsh condition, low quantum yield, composite method | Xu et al. (2004) and Journet et al. (1997) |
| | | Laser ablation method | Rapid, effective, varied size carbon quantum dots can be synthesized, effective technique | Low quantum yield, poor size control, large amount of carbon precursor is required | Xiao et al. (2017) and Liang et al. (2014) |
| | | Electrochemical method | Stable one-step method, size and nanostructure are controllable, hydrophilic carbon quantum dots can be synthesized, amount of carbon quantum dots can be increased by changing current density | Complex method | Bao et al. (2011) and Ahirwar et al. (2017) |
| | | Acid oxidizing exfoliation | Most accessible | Harsh condition, multistep process, poor control over size | Dong et al. (2012) and Zhu et al. (2010) |
| 2. | Bottom-up approach | Hydrothermal/solvothermal method | Hydrophilic carbon quantum dots can be synthesized, cost-effective, non-toxic method, and eco-friendly | Poor control over size | Zuo et al. (2016) and Sarkar et al. (2016) |
| | | Microwave-assisted method | Rapid, scalable, inexpensive, and eco-friendly method | Poor control over size | Qin et al. (2013) and Yang et al. (2013b) |
| | | Thermal pyrolytic route | Easy and simple method | Low quantum yield, high temperature requirement | Wang et al. (2011) and Liu et al. (2011) |
| | | Template method | Synthesized carbon quantum dots are bio-compatible and exhibit good colloidal stability | Low quantum yield, highly expensive method, time-consuming | Grun et al. (2000) and Lai et al. (2012) |

Laser Ablation Method

In laser ablation method, carbon precursors firstly absorb the high-energy laser pulse, and then electrons are removed through photoelectric and thermionic emission from the atom followed by generation of high electric field which produces strong repulsive forces and thus breaks down the carbon quantum dots (Xiao et al. 2017). Laser ablation method is a chemically simple and facile method and generates very little by-products. Also, laser ablation method does not require extreme temperature and pressure, and also there is no need of catalysts for the process to be carried out. Further, preparation of carbon quantum dots was done using carbon nanoparticles in organic solvent ethanol and acetone (Li et al. 2010a). Here, carbon nanomaterial was dissolved in organic solvent, with subsequent ultrasonication. The suspension was then conserved in a glass cell irradiated with laser followed by continuous magnetic stirring so as to avoid settling of nanoparticles. Other than carbon quantum dots, fluorescent carbon nanoparticles were also prepared by laser irradiation of carbon suspension in organic solvent (Hu et al. 2009).

Sun and co-worker (2006) also synthesize carbon dots by using laser ablation method in argon using water vapor. Carbon precursor was prepared by stepwise baking, curing, and annealing of the mixture of graphite powder and cement in an argon flow. The obtained sample was treated with aq. HNO_3 solution to oxidize surface carbon with refluxing for 12 h followed by surface passivation of carbon particle through organic species which exhibit luminescence property. Thus, the surface passivation of carbon precursor by organic molecule polyethylene glycol to prepare carbon quantum dots can activate the surface and become highly photoactive in visible and IR region (Wang et al. 2009). Not only carbon quantum dots but one-dimensional iron-based bimetallic magnetic nanoparticles such as FePt, FeCo, and FeNi were also synthesized by laser ablation method (Liang et al. 2014). Laser ablation method is mainly associated with low productivity problem which strongly depends upon laser power density and liquid medium. Because nanoparticles have strong absorption and scattering effects in liquid medium, determining their productivity is an important parameter.

Electrochemical Approach

Electrochemical method involves a nonselective top-down approach using various carbon precursors for the synthesis of carbon quantum dots. Electrochemical method is a unique method since the size of quantum dots can be adjusted by regulating potential. Ahirwar et al. (2017) synthesize graphene and graphene oxide quantum dots via electrochemical exfoliation method with 2–3 nm in size. The two electrodes used were made up of graphite which is dipped in the solution of electrolyte made up of combination of weak and strong electrolytes. Further, Devi et al. (2018) synthesize carbon quantum dots via electrochemical method using graphite electrode acting as the anode and cathode, respectively, and mixture of NaOH/EtOH as an electrolyte

solution. Depending upon applied current and time, different particle-sized carbon quantum dots are synthesized which is further confirmed by various spectroscopic techniques.

Deng et al. (2014) prepared carbon nanodots by one-pot electrochemical carbonization of alcohol under basic condition. Uniform carbon dots were prepared using low molecular weight alcohol. Herein, a three-electrode system is used where two platinum sheets were used as working and counter electrodes placed 3 cm apart, and calomel electrode was used as reference electrode. After electrolysis, the obtained mixture was evaporated at 800 °C until a yellow-colored powder was obtained followed by dialysis using dialysis membrane. Shinde and Pillai (2012) prepared uniform size graphene quantum dots from multi-walled carbon nanotube in nonaqueous solvent via electrochemical method. Due to high photostability, non-toxicity, and biocompatibility, graphene quantum dots are a promising candidate for various applications in nano-electronics and as biomarkers and chemosensors. The uniform-sized carbon dots can be further prepared from the bundle of carbon fiber using three-electrode system at constant potential (Bao et al. 2011). Here, carbon fiber was used as the working electrode, Pt sheet as the counter electrode, and Ag wire as the quasi-reference electrode, respectively. Among these methods, electrochemical method is a green method with large yield, less time-consuming, and operated at low temperature.

Further, zero-dimensional graphene quantum dots with sizes ranging from 3 to 5 nm were synthesized via electrochemical method (Li et al. 2011b). Firstly, the graphene film was prepared by direct filtration (pore size 220 nm) of colloidal suspension of reduced graphene oxide. Then, dried graphene was mechanically peeled to obtain graphene film, which is further treated with oxygen plasma for just 10 s to increase hydrophilicity. In the electrochemical preparation, three electrodes were used: a graphene film (working electrode), Pt wire (counter electrode), and Ag/AgCl (reference electrode). The mono-dispersed graphene quantum dots are much smaller in size (3–5 nm) as compared to graphene quantum dots (10 nm) synthesized by hydrothermal method (Li et al. 2008).

Other than carbon quantum dots, simple metal oxide or metal sulfide quantum dots were also synthesized by electrochemical method. Gopalakrishnan et al. synthesize MoS₂ luminescent quantum dots of sizes ranging from 2.5 to 6 nm from bulk solution using aqueous ionic liquid (Gopalakrishnan et al. 2015). Similarly, Valappil et al. (2017) synthesize transition metal dichalcogenides quantum dots WS₂ via electrochemical method with a wide application in optoelectronic devices. Earlier, various methods for the synthesis of quantum dots are available. Synthesis of potassium intercalation followed by ultrasonication is quite complicated and laborious; thus, it needs further purification for the removal of potassium ion (Lin et al. 2013). Another way is simple ultrasonication of WS₂ nanosheets but the size of the product cannot be determined easily.

Acid Oxidizing Exfoliation

In acid oxidizing exfoliation method, carbon quantum dots were synthesized by controlled oxidation using strong oxidizing acids such as H_2SO_4 and HNO_3 . Using harsh and drastic condition is necessary for the formulation of carbon quantum dots and one of the major disadvantages of acid oxidizing exfoliation method. Graphene quantum dots have promising application in nanotechnology and can be synthesized by chemical breakdown of graphene oxide (Zhu et al. 2010; Terrones et al. 2010). Peng et al. (2012) prepared graphene quantum dots in large scale by acid exfoliation followed by etching of carbon fibers having resin-rich surface. Different sized graphene quantum dots which can be accessed by easily varying the reaction temperature were observed.

Various strategies are focused on regulating the size of the carbonaceous material not more than 10 nm which is called carbon quantum dots that attributes to the quantum confinement effect. Liu et al. (2013) employed graphite nanoparticle as a starting material to prepare graphene and graphene oxide quantum dots as illustrated in Fig. 3.5. For the synthesis of graphene quantum dots, graphene nanoparticles were directly exfoliated and centrifuged at 4000 rpm for 30 min, and for graphene oxide quantum dots, modified hummer method is used followed by exfoliation. Various graphene layers well-adjusted by van der Waals forces and pi-pi interaction were exfoliated to obtain homogeneous and single-layered graphene quantum dots and graphene oxide quantum dots with high yield. Further, the exfoliation of graphite was also reported in various organic solvents (Hernandez et al. 2008).

Further, Peng et al. (2012) described graphene quantum dot synthesis through acid treatment and chemical exfoliation using carbon fibers as precursor, which produces graphene quantum dots with different sizes ranging from 1 to 4 nm. Dong et al. also detailed easy, cheap, and high yield approach to prepare graphene

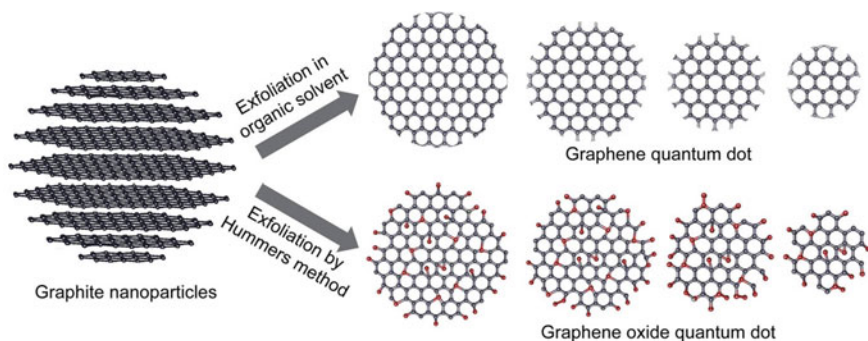


Fig. 3.5 Synthesis of graphene quantum dots and graphene oxide quantum dots via chemical exfoliation method. The exfoliation in organic solvent without an oxidizing agent yields a few layered graphene quantum dots, and the exfoliation by hummer's method in the presence of an oxidizing agent yields graphene oxide quantum dots using graphite nanoparticles as precursor (oxygen sites in graphene quantum dots are shown in red dots). (Reprinted with permission from Liu et al. (2013) copyright©2013, WILEY-VCH Verlag GmbH & Co. KGaA, Weinheim)

quantum dots employing CX-72 carbon black as the starting material by refluxing with conc. HNO_3 for 24 h (Dong et al. 2012). Single-layered graphene quantum dots can effectively penetrate the cell without any bio-conjugation which enables them to be utilized in bio-imaging and drug delivery, whereas multilayered graphene quantum dots exhibit broad solar absorption, rendering promising candidate in optoelectronic devices.

Ultrasonic Exfoliation

The synthesis of carbon quantum dots through ultrasonication can generate alternate waves in liquids of low and high pressure liable for the generation and collapsing of vacuum bubbles in the reaction medium. It also prevents agglomeration and creates strong hydrodynamic shear forces. Li et al. (2012) synthesize carbon quantum dot-based Cu_2O nanostructure via facile one-step ultrasonic treatment using glucose as carbon precursor in alkali medium. Higher productivity of nanostructure is due to the high light reflecting capability of Cu_2O and up-conversion photoluminescence of carbon quantum dots. IR light comprises nearly 53% of solar spectrum which has not been utilized effectively. For the first time, Li et al. (2012) demonstrated that carbon quantum dot-based Cu_2O photocatalytic system could harness the near-infrared region of the solar spectrum. The photocatalytic activity of nanostructure was evaluated against methyl blue. The spherical-shaped nanostructure protruding Cu_2O particle could be clearly seen in scanning electron microscope images in Fig. 3.6.

The ultrasonic waves had the potential to convert macroscopic carbonaceous material into nanoscale carbon quantum dots. Li et al. (2011a) synthesize water-soluble fluorescent carbon quantum dots by using hydrogen peroxide-assisted ultrasonic method using activated carbon as precursor. The hydrophilic character of carbon quantum dots was attributed to the occurrence of hydroxyl group. To prepare a suitable amount of activated carbon, an appropriate amount of H_2O_2 was added and subjected to 40 KHz ultrasonic treatment for 2 h at room temperature. The obtained suspension was then vacuum-filtered using 20 nm pore cellulose membrane. Park et al. (2014) described green synthesis based on carbon quantum dots using waste food via ultrasonic method at room temperature (Scheme 3.1). The usage of renewable resources for large-scale production of carbon quantum dots is a cost-effective method and useful in energy conversion and biomedical and industrial application. The synthetic procedure involves the following steps: dehydration, polymerization, carbonization, and passivation (Jeong et al. 2012). In a typical procedure, waste food and ethanol were mixed followed by ultrasonication to 45 min at 40 KHz. The obtained sample was centrifuged to separate heavy and agglomerated particle. The supernatant was then filtered twice through 0.22 μm membrane to separate carbon quantum dots and further dried at 45 $^\circ\text{C}$. The uniform spherical shape carbon quantum dots with average size of 4.6 nm were synthesized and further confirmed by high-resolution transmission electron microscope and atomic force microscopy images Fig. 3.7.

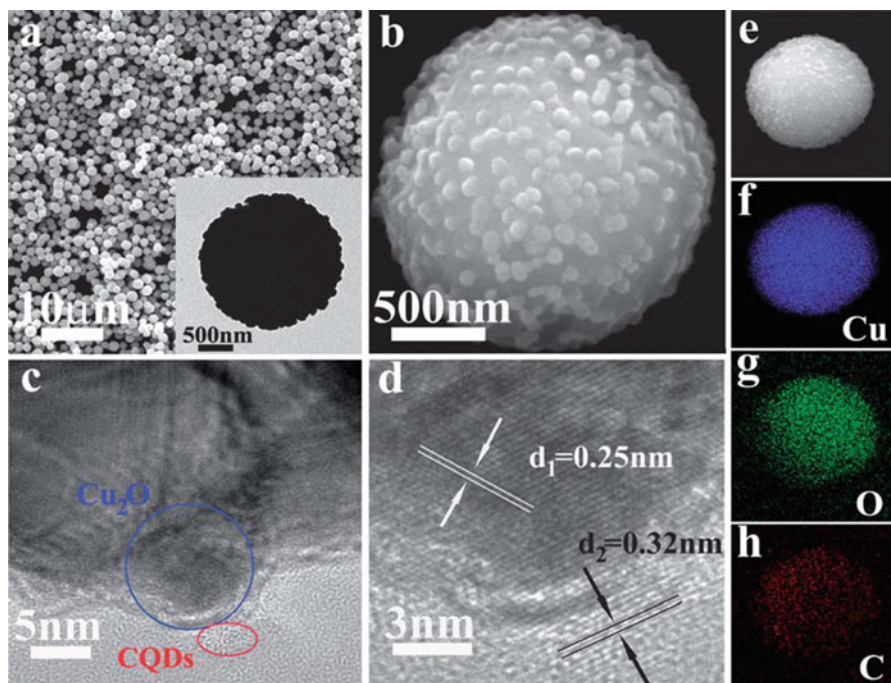
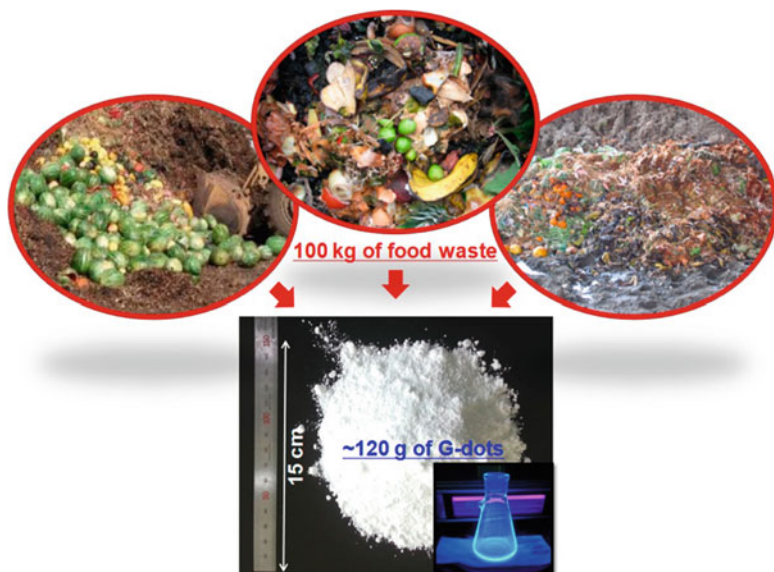


Fig. 3.6 (a–c) Spherical-shaped scanning electron microscopy images of carbon quantum dots/ Cu_2O composite at different resolutions: 10 nm, 500 nm, and 5 nm, respectively (inset of a). Transmission electron microscopy images of carbon quantum dots/ Cu_2O composite. (d) High-resolution transmission electron microscopy images of the carbon quantum dots/ Cu_2O prepared by one-step ultrasonic treatment with 0.25 nm and 0.32 nm d spacing values. (e) Scanning electron microscopy image of a single carbon quantum dots/ Cu_2O particle for energy-dispersive X-ray spectroscopy. (f–h) Element mapping data of Cu, O, and C elements throughout a single carbon quantum dots/ Cu_2O particle. (Reprinted with permission from Li et al. (2012) copyright@2012, The Royal Society of Chemistry)

3.3.2 Bottom-Up Approach

Hydrothermal Method

Chen et al. (2018a) develop green one-pot hydrothermal method for graphene quantum dot synthesis with a diameter ranging from 2.25 nm to 3.50 nm using starch as a natural polymer. Hydrothermal method is free from usage of any strong acid or metal impurities. The reaction mechanism during the synthesis follows hydrolyzation of starch mainly into glucose followed by ring closure to generate graphene quantum dots which is separated through centrifugation. Graphene is a promising building block for graphene quantum dot synthesis. Pan et al. (2010a) develop a hydrothermal method for piercing peroxidized graphene sheets into ultras-small graphene quantum dots. The graphene sheet is prepared by thermally reducing the graphene oxide.



Scheme 3.1 Schematic description of the large-scale synthesis of graphene dots by utilizing food waste. These nanodots represent the efficient transition from large food waste to valuable carbon-based nanomaterials. (Reprinted with permission from Park et al. (2014) copyright@2014, American Chemical Society)

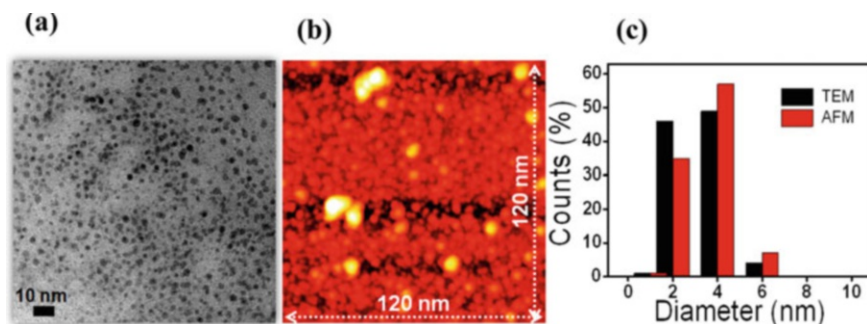


Fig. 3.7 (a) High-resolution transmission electron microscopy image of graphene dots at 10 nm resolution. (b) Atomic force microscopy image of graphene dots with a thickness of 120 nm. (c) Size distribution of graphene dots which indicates that the amount of graphene dots with a diameter of 2 nm was less than 45%, with a diameter of 4 nm is less than 60%, and with a diameter of 6 nm is less than 10% (*TEM* transmission electron microscopy, *AFM* atomic force microscopy). (Reprinted with permission from Park et al. (2014) copyright@2014, American Chemical Society)

Shen et al. (2018) prepared carbon quantum dots coupled with TiO_2 via hydrothermal method using glucose and citric acid as precursors. The heterojunction exhibits enhanced photocatalytic activity against phenol under ultraviolet light. Carbon quantum dots–glucose/ TiO_2 heterojunction was synthesized using glucose

and carbon quantum dots–citric acid/TiO₂ by using citric acid as precursor. Among these two heterojunctions, carbon quantum dots–glucose/TiO₂ has better crystalline property which is responsible for facile charge carrier migration and hence responsible for higher photocatalytic activity. Sarkar et al. (2016) prepared water-soluble carbon quantum dots from sucrose by using cost-effective and environment-friendly hydrothermal technique. Mixture of sucrose solution and ethanol was taken in Teflon autoclave and heated to 175–180 °C for 2 h and then cooled. The yellow-colored solution is obtained which is centrifuged at 16,000 rpm. Moreover, graphene quantum dots were also synthesized by a hydrothermal method using graphene sheets which are obtained by thermal oxidation of graphene oxide sheets at 200 °C (Pan et al. 2010a). The synthesized graphene quantum dots were used in organic photovoltaic devices.

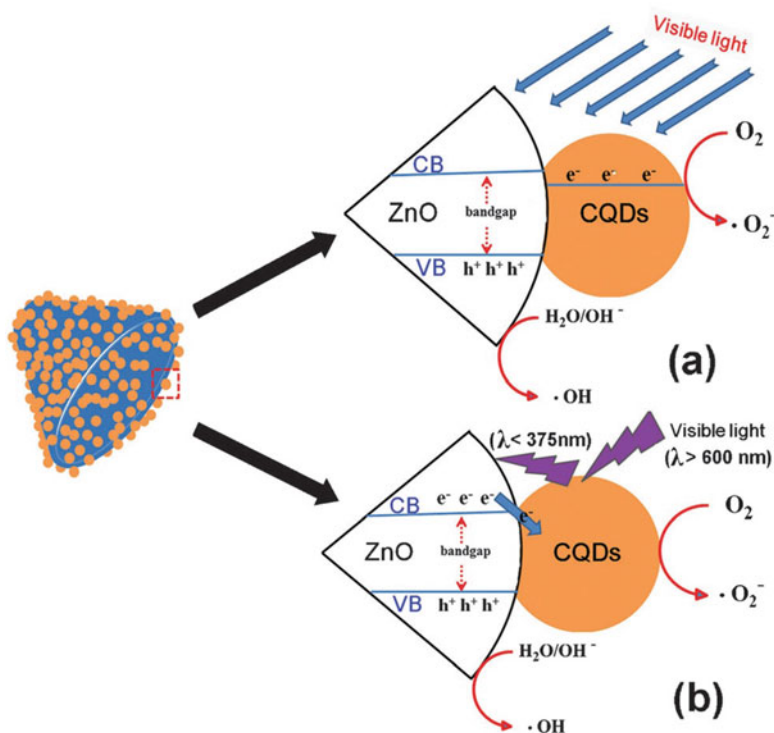
Mehta et al. (2014) devised a highly cost-effective and green hydrothermal technique to synthesize fluorescent quantum dots using plant-based precursor *Saccharum officinarum*. These quantum dots were used in cellular imaging of bacteria and yeast. Several green techniques have been devised for the preparation of carbon dots by utilizing inexpensive renewable precursor. Researchers developed green synthetic approach for the synthesis of carbon dots from watermelon peel and pomelo peel using hydrothermal method (Zhou et al. 2012a; Lu et al. 2012). Prasannan and Imae (2013) also reported the synthesis of fluorescent quantum dots by hydrothermal method at 180 °C using orange peel. Orange peel used mainly consists of various carbohydrates, glucose, fructose, sucrose, and cellulose, which are used as carbon sources. The morphology and chemical composition were characterized by various spectroscopic techniques. The carbon dots prepared were amorphous in nature with large quantity of functional group. Typically, orange waste was firstly washed with water and then in H₂SO₄ solution and again rinsed with water followed by drying in hot air oven at 150 °C for 10 h. The secured product was further treated with sodium hypochlorite solution and kept for 4 h at room temperature followed by washing with water several times till pH 7 is attained. Lastly, the oxidized orange peel was kept in autoclave for heating, followed by washing with dichloromethane to remove extra organic species followed by centrifugation. Hydrothermal carbonization is considered as a green and effective method avoiding the usage of strong toxic chemical.

Kapitonov et al. (2018) present a new method for carbon dot synthesis using hydrothermal method by choosing different precursors: berry juice, birch bark soot, glucose, and citric acid which are reported earlier. Various functional groups present on the surface of carbon dots are epoxy, carbonyl, hydroxyl, and carboxyl providing hydrophilic character to carbon dots. The carbon dots can be functionalized by doping with heteroatom to improve the surface property and also the quantum yield. Thus, nitrogen-doped carbon quantum dots were synthesized by hydrothermal method used for the selective sensor for the detection of Hg²⁺ (Liu et al. 2015), Fe³⁺ (Wu et al. 2013), and Ag⁺ (Li et al. 2017). Wang et al. (2018b) prepared nitrogen-doped carbon dots utilizing mandelic acid together with ethylenediamine as carbon and nitrogen source, respectively. The solution of mandelic acid and ethylenediamine were mixed ultrasonically at room temperature with subsequent

hydrothermal treatment followed by dialysis for 24 h. The obtained powder after dialysis was dried by adding ethanol and centrifuged at 10,000 rpm for 20 min.

Yu et al. (2012) synthesize ZnO/carbon quantum dot nanocomposites by using one-step hydrothermal method. The nanocomposites exhibit superior photoactivity under solar light for the decomposition of benzene and methanol, both toxic gases, and benzene binds by π - π interaction in conjugation between the two moieties. The higher efficiency of nanocomposites was attributed to the up-conversion emission by carbon quantum dots under visible region. ZnO loading on carbon quantum dots constructs a “dyad structure” where the electron is simultaneously transferred to carbon quantum dots’ surface and the hole remains at the ZnO surface (Scheme 3.2).

The simultaneous transfer of electron onto carbon quantum dots inhibits charge carrier recombination and increases the lifetime of electron-hole pair. The adsorbed O_2 on the surface of carbon quantum dots converts into superoxide radical anion, which is a strong oxidizing agent and easily oxidized the adsorbed toxic gases on the surface. The up-conversion of emission light means the conversion of longer



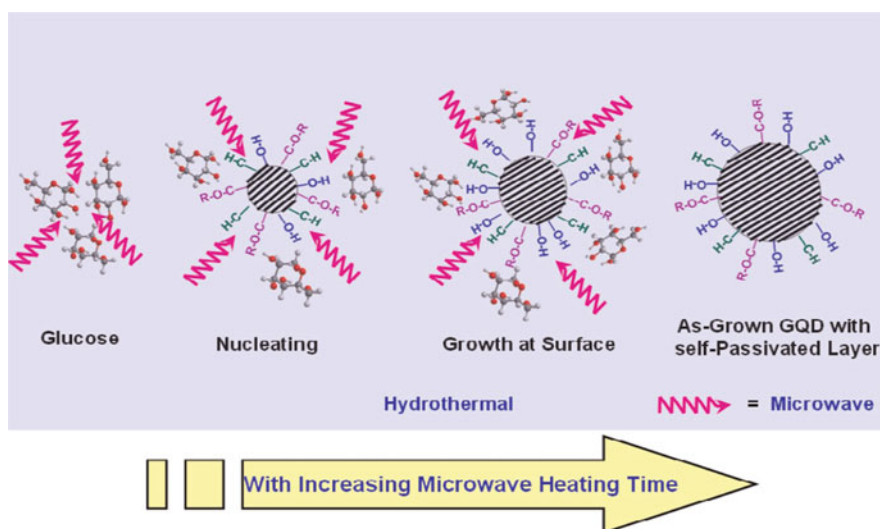
Scheme 3.2 Schematic model for the photocatalytic process of ZnO/carbon quantum dot composites under visible light. ZnO loading on carbon quantum dots constructs a “dyad structure” where electrons simultaneously migrate to the carbon quantum dot surface and holes remain at the ZnO surface. (CQDs carbon quantum dots). (Reprinted with permission from Yu et al. (2012) copyright@2012, The Royal Society of Chemistry)

wavelength visible light into short wavelength ultraviolet light which can now generate electron–hole pair on the surface of ZnO nanoparticle (Scheme 3.2b). As the band gap of ZnO is 3.3 eV which lies in ultraviolet region, therefore light of shorter wavelength can only initiate the excitation process.

Microwave Method

Microwave method is a low-cost, facile, rapid, and green method with high quantum yield efficiency in comparison to hydrothermal method (Yang et al. 2013b). Photoluminescent carbon dots were also synthesized by using flour as a source of carbon by microwave-assisted method (Qin et al. 2013). Tang et al. (2012) prepared water-soluble crystalline graphene quantum dots derived from glucose through microwave-facilitated hydrothermal method that utilizes the assets of both these methods (Scheme 3.3). Firstly, the glucose molecule is paralyzed followed by dehydration under hydrothermal method. The glucose solution was subjected to microwave oven at a different power of 280 to 700 W for a different period of time, 1–11 min. The transparent color of the solution changes to pale yellow which indicates the formation of graphene quantum dots. The microwave provides uniform heating responsible for consistent size distribution of graphene quantum dots.

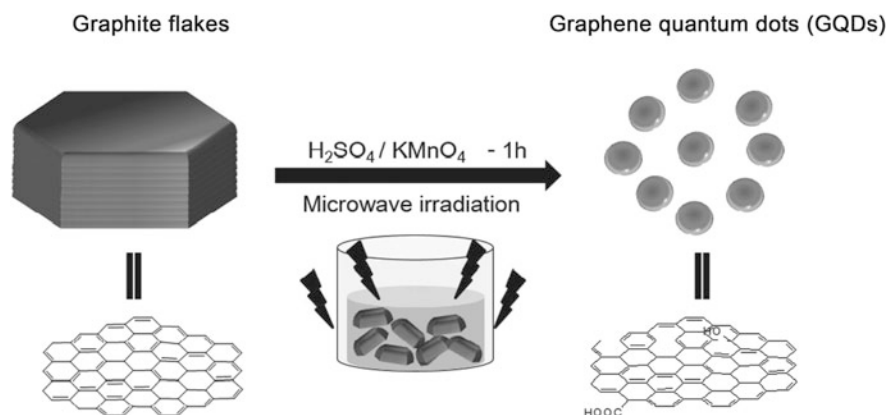
Zhu et al. (2009) also prepared carbon nanoparticle via microwave pyrolysis method which is a cheap and convenient method for large-scale production. For solution of polyethylene glycol and monosaccharide's glucose and fructose that



Scheme 3.3 Preparation of graphene quantum dots by microwave-assisted hydrothermal method using glucose as precursor followed by nucleation and microwave heating. (GQD graphene quantum dots). (Reprinted with permission from Tang et al. (2012) copyright@2012, American Chemical Society)

were heated in microwave oven of 500 W for 2–10 min, a yellow-colored solution changes to dark brown which indicates the formation of carbon nanoparticles. Microwave method was very less time-consuming as the nanoparticles were synthesized in just 10 min. Umrao et al. (2015) reported microwave carbonization followed by aromatization of acetyl acetone as a precursor to prepare graphene quantum dots having tunable size and surface functionalities. Graphene quantum dots can be modified for specific application by tailoring the size, surface, and band gap. Acetyl acetone is weakly acidic in nature, which is why dehydration and decomposition reaction under microwave irradiation proceed in a controlled manner followed by aldol condensation and cycloaddition reaction.

Further, doping of carbon quantum dots with heteroatom boron, nitrogen, sulfur, and fluorine is a potent approach for adjusting optical and electronic property of carbonaceous material. Kundu et al. (2015) also used one-step microwave technique for the preparation of codoped nitrogen, fluorine, and luminescent graphene quantum dots with average size of 2 nm by using multi-walled carbon nanotubes as precursor in ionic liquid. The coupling of ionic liquid with microwave technique enables ultrafast process and also increases the quantum yield to nearly 70%. Due to short reaction times, microwave irradiation method is extensively utilized for the preparation of carbon quantum dots. Graphite, a well-known precursor, comprised of stacked graphene sheets is one of the readily available and inexpensive materials for the synthesis of graphene quantum dots. Shin et al. (2014) synthesize graphene quantum dots via highly powered microwave irradiation using graphite under acidic condition followed by oxidative cleavage (Scheme 3.4). Carbon quantum dots can also be prepared by using amino acid as the starting material in the presence of acid or alkali. Histidine is dissolved in ortho-phosphoric acid followed by microwave irradiation to 700 W for nearly 3 min (Jiang et al. 2012). The resultant carbon



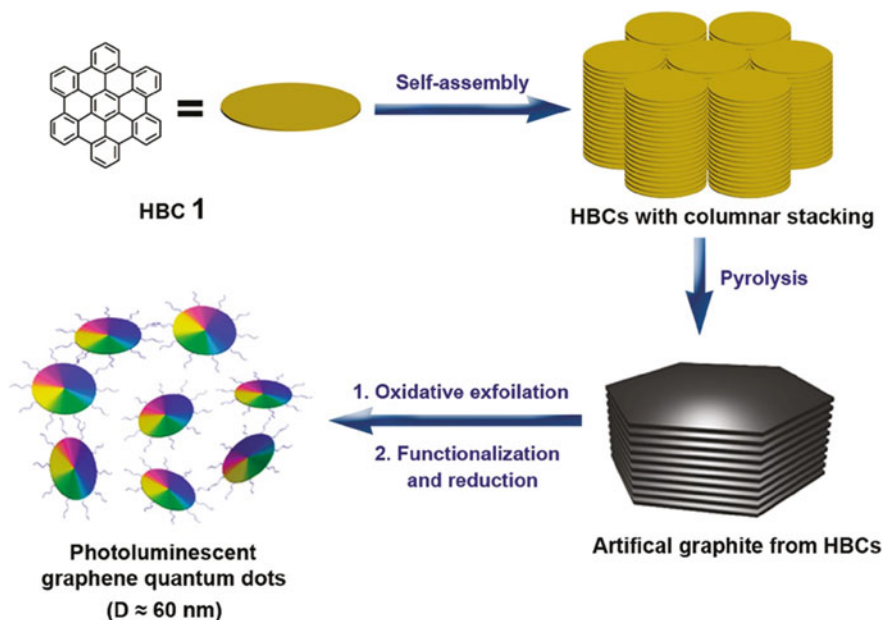
Scheme 3.4 Schematic representation of the fabrication of a few layered graphene quantum dots from multilayered graphite powder by one-pot microwave irradiation under acidic conditions. (Reprinted with permission from Shin et al. (2014) copyright©2013, Wiley-VCH Verlag GmbH & Co. KGaA, Weinheim)

quantum dots were dispersed and purified with ultrapure water using dialysis membrane to remove the impurities.

Pyrolytic Route

Liu et al. (2011) for the first time synthesized mono-dispersed disklike graphene quantum dots with 2–3 nm thickness and ~60 nm in diameter. The graphene quantum dots are synthesized by pyrolytic method using un-substituted hexa-peri-hexabenzocoronene as carbon source. The process involves various steps, carbonization, oxidation, surface functionalization, and reduction, as illustrated in Scheme 3.5.

Pan et al. (2010b) described the preparation carbon quantum dots via pyrolysis of ethylenediaminetetraacetic acid at low temperature. Typically, ethylenediaminetetraacetic acid was calcined at 400 °C for 2 h with a heating rate of 10 °C per minute in an inert atmosphere, and the product obtained is then dispersed in acetone followed by centrifugation. Ethylenediaminetetraacetic acid possesses stable carboxylate ion which persists during pyrolysis and enables carbon quantum dots to be hydrophilic and soluble in various polar organic solvents. Also, the highly sensitive and selective carbon dots were also prepared by pyrolysis of ethylenediaminetetraacetic acid, which is used as sensor for the detection of Hg^{2+} ion and biothiols (Zhou et al. 2012b). Guo et al. (2012) also prepared one-step

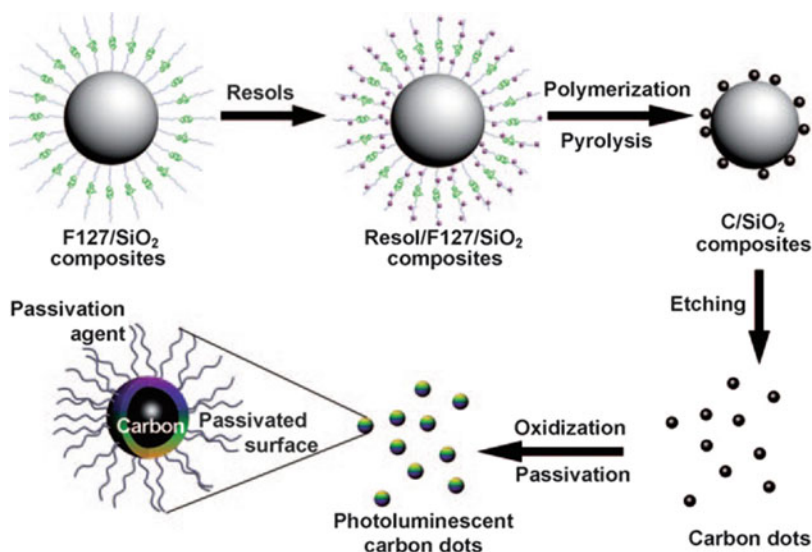


Scheme 3.5 Processing diagram for the preparation of photoluminescent graphene quantum dots using hexa-peri-hexabenzocoronene as carbon source. (HBC 1 hexa-peri-hexabenzocoronene). (Reprinted with permission from Liu et al. (2011) copyright©2011, American chemical society)

pyrolytic method for the synthesis of carbon dots by chemical unzipping of epoxy-enriched polystyrene photonic crystal.

Liu et al. (2009) reported novel route for the synthesis of nanosized carbon dots typically 1.5–2.5 nm. The preparation method includes polymerization, pyrolysis, oxidation, and surface passivation as illustrated in Scheme 3.6. Firstly, SiO₂ suspension was added to the aqueous solution amphiphilic triblock copolymer, and the sample was stirred overnight. Here, resols (i.e., phenol/formaldehyde resins) are used as carbon source. Further, high-temperature treatment removes silica carrier and generated nanosized carbon dots. Here, the surfactant-modified silica is utilized as carrier, anchors resols during polymerization, and also prevents aggregation of carbon dots during pyrolysis.

The surface-functionalized carbogenic nanoparticles with size less than 10 nm can be synthesized by thermal dissipation or by 4-aminoantipyrine route (Bourlinos et al. 2008). The organophilic nanoparticles were prepared by citrate route while, carbonization of 2-(2-aminoethoxy)-ethanol in another route prepare hydrophilic nanoparticles. In both these methods, amide linkage (–NH–CO–) ties the organic moiety to the core, and the precursor was pyrolyzed at 300 °C for 2 h. Wang et al. (2010) synthesize oil-soluble carbon dots by carbonization of carbon precursor and water-soluble carbon dots by simply altering the solvent and capping reagent. For oil-soluble carbon dot preparation, octadecane was used as the non-coordinating solvent, 1-hexadecylamine as the capping agent, and citric acid as the carbon source. The mixture of octadecane and 1-hexadecylamine was heated up to 300 °C under



Scheme 3.6 Processing diagram for the synthesis of multicolor photoluminescent carbon dots by polymerization, pyrolysis, oxidation, and surface passivation. Resols were used as carbon source. (Reprinted with permission from Liu et al. (2009) copyright©2009, Wiley-VCH Verlag GmbH & Co. KGaA, Weinheim)

inert atmosphere with addition of citric acid. The obtained product is purified with acetone several times. The oil-soluble carbon dots are appreciably soluble in organic solvents like toluene, hexane, and chloroform. Wang et al. (2011) synthesize amorphous carbon dots via pyrolytic method using anhydrous citric acid in the presence organosilicane as the coordinating solvent at 240 °C for 1 min. The ultrasmall carbon dot with a size of 0.9 nm was prepared with high quantum yield of 47%. Simple heating is required for the preparation of carbon dots from organosilicane as compared to other method where addition of polymer or inorganic compound is needed.

Template Method and Substance Oxidation

Mesoporous templates have been employed to confine the carbon dots in pores to gain a narrow size distribution, but effectively restricting the pore size of templates is challenging. In template method, carbon quantum dots are prepared by calcination using mesoporous template like silicon sphere or by etching to obtain nanosized carbon quantum dots. The uniform, spherical mesoporous silica was prepared using tetra-ethoxysilane as the precursor, *N*-hexadecylamine as the surfactant, and ammonia as the catalyst with particle size of 1.3 μm in diameter and pore size of 3.60 nm (Grun et al. 2000). Further, the nanosized hydrophilic carbon dots are synthesized by impregnated method by performing calcination of mesoporous silica with mixture of complex salts and citric acid solution (Zong et al. 2011). The mesoporous silica was used as support to prevent the aggregation of carbon dots, and also the small pore size of silica enables synthesis of nanosized carbon dots with sizes ranging from 1.5 nm to 2.5 nm.

Yang et al. (2013a) reported combination of copolymer pluronic and mesoporous silica as soft–hard template for the synthesis of mono-dispersed photoluminescence carbon dots. Soft–hard template method overcomes the disadvantages of using mesoporous silica alone and synthesizes carbon dots with narrow size distribution and well-defined morphology. The organic molecules with different aromatic framework like diaminebenzene, pyrene, 1,3,5-trimethylbenzene, and phenanthroline are used as carbon precursors. The use of different organic precursors is beneficial to modify the size, structure, composition, and photoluminescent property of carbon dots. Briefly, organic precursor was enwrapped into micelles of soft template with mesoporous silica followed by carbonization, template removal through etching, and passivation. Here, a soft template provides nano-space for the formation of nanosized carbon dots and mesoporous silica, while a hard template prevents aggregation of carbon dot particle. In another method free from catalysts, mesoporous silica was blended with polyethylene glycol and glycerol as carbon source (Lai et al. 2012). The majority of top-down techniques involve tedious methods and usage of extensively harsh chemicals which generate more chemical waste and high temperature for a prolonged time. On the other hand, bottom-up approach is a time-consuming process and complicated synthetic scheme and

requires costly and special equipment. Thus, there is an urgency of developing an adequate and cost-effective synthetic strategy for carbon quantum dot preparation.

3.4 Photocatalytic Activity of Carbon Quantum Dot-Based Nanocomposites

As per the previously reported literature, fabrication of carbon quantum dots, metal oxide, and metal sulfide-based carbon quantum dots has gained substantial attention. A remarkable efficiency is assigned because of broader range of solar spectrum. The aim of enhancing the photo-efficiency can be achieved by constructing a heterojunction system between the carbon quantum dots and the semiconductor. Li et al. (2010b) reported facile one-step electrochemical technique for uniform and mono-dispersed carbon quantum dots synthesized in alkaline medium with sizes ranging from 1.2 to 3.8 nm. Further, the design of carbon quantum dots is based on TiO₂ and SiO₂ nanocomposites by sol-gel strategy and utilized for the photodegradation of methyl blue. The complete photodegradation was observed in 25 min and 15 min for TiO₂/carbon quantum dots and SiO₂/carbon quantum dots, respectively. The excitation of TiO₂ and SiO₂ photocatalyst is due to the up-conversion process. Similarly, tetraethyl orthosilicate was added for the preparation of SiO₂/carbon quantum dots in a similar fashion. The photocatalytic activity was evaluated against methyl blue. The photodegradation analysis was carried out in 3100 mL conical flask containing 50 mgL⁻¹ dye solution with 10 mg nanocomposites, and 300 W halogen lamp was used as light source.

Deng et al. (2015) synthesize 2D BiOCl/carbon quantum dot composites by template-free coprecipitation method. The composites exhibit enhanced efficiency, and almost 100% removal of 2-nitrophenol was observed. The higher efficiency of the composites was attributed to excellent light absorption capacity in the visible region and effective electron-hole pair separation which slows the rate of recombination. Carbon dots/ZnO composites were also used for the photodegradation of various azo dyes under visible light using 250 W Xe lamp (Ding et al. 2016). The photodegradation follows the trend methyl blue > rhodamine B > methyl orange, respectively.

Feng et al. (2015) synthesized porous nanorods of carbon dots/ZnO by solvothermal deposition method. The photocatalytic activity was assessed against phenol under visible light. The pollutant was 94% degraded in 60 min. Further, Li et al. (2013) synthesized carbon dot/ZnO heterostructure via sol-gel method followed by spin coating method and evaluated the photo-efficiency against rhodamine B dye. Thirty percent of rhodamine B was photodegraded in 120 min using 18 W ultraviolet lamp. The heterostructure exhibit three times higher photo-efficiency as compared to base ZnO.

Besides ZnO, TiO₂ is also a promising photocatalyst to be utilized in photodegradation of various pollutants due to its high oxidizing ability and high

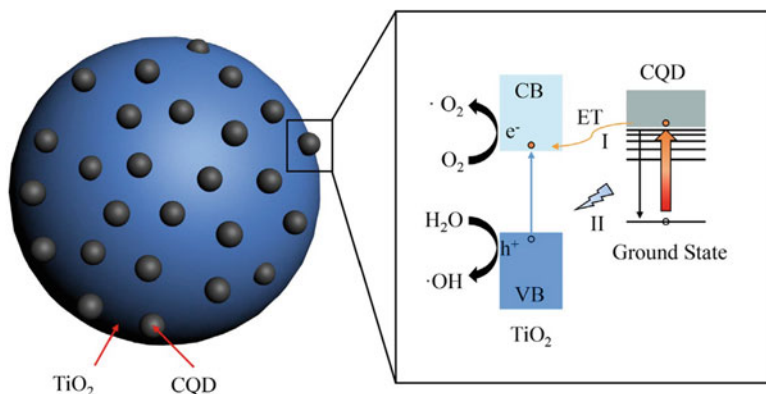


Fig. 3.8 Proposed mechanism for up-conversion photocatalytic process in carbon quantum dots/ TiO_2 , where high-energy photo emitted by carbon quantum dots generates the electron–hole pair over TiO_2 surface. (CQDs carbon quantum dots) (Reprinted with permission from Ke et al. (2017) copyright@2017, Published by Elsevier Inc.)

thermal and chemical stability. Nitrogen-doped carbon dot/ TiO_2 composites synthesized via hydrothermal method degraded 95% of rhodamine B in 30 min using 500 W Xe lamp (Zhang et al. 2013). Similarly, photodegradation analysis using carbon dot/ TiO_2 nanocomposites synthesized by hydrothermal method or sol–gel method was carried out by various researchers against methyl blue, methyl orange, and rhodamine B photodegradation (Saud et al. 2015; Wang et al. 2015; Li et al. 2010b, 2018a).

Ke et al. (2017) prepared carbon quantum dots via hydrothermal method and carbon quantum dots/ TiO_2 via sol–gel method, and photo-efficiency was observed against methyl blue dye under visible light. About 90% of methyl blue was degraded in just 120 min, and carbon quantum dots/ TiO_2 reveal nearly 3.6 times higher efficiency as compared to bare TiO_2 . On the other hand, the unique up-conversion property of carbon quantum dots which could convert low-energy photons into high-energy photons is utilized for the construction of heterojunction (Jia et al. 2012). Generally, conventional semiconductor quantum dots absorb high-energy photon and then emit low-energy photon which may be further thermally dissipated. But using carbonaceous-based quantum dots, low-energy photons convert into high-energy photons which is further utilized to generate charge carrier on the surface of TiO_2 (Fig. 3.8).

For carbon quantum dots/ TiO_2 composites that generate charge carrier under visible light irradiation, the photoinduced electron migrates to the conduction band of TiO_2 and further produces superoxide radical, whereas holes stay at ground state and generate hydroxyl radical. Some of the photoinduced electrons may recombine with holes in the ground state which emit photons of higher energy. That emitted photon of higher energy could excite the host TiO_2 and further generate electron–hole pair. Thus, up-conversion property of carbon quantum dots efficiently utilizes

solar energy and enhances the photo-efficiency. The carbon quantum dots were also loaded with Bi_2WO_6 and applied for the degradation of various organic pollutants.

Wang et al. (2018a) fabricated 0D and 2D carbon dots on Bi_2WO_6 nanosheets, and the photodegradation study was carried out on methyl orange and bisphenol A. The composites show three times higher efficiency as compared to Bi_2WO_6 alone. The excellent photocatalytic activity was ascribed to the up-conversion and electron reservoir property of carbon quantum dots. The high ability of charge carrier separation is further confirmed by density functional theory calculation. Further, electron spin resonance measurement and quenching experiment reveals hydroxyl radical, superoxide radical, and holes are the active species in photodegradation. Zhang et al. (2018) design nitrogen-doped carbon quantum dot-mediated $\text{Ag}_3\text{PO}_4/\text{BiVO}_4$, a Z-scheme photocatalyst, via solvothermal precipitation method. Tetracycline, an antibiotic, was used to assess the photocatalytic performance under visible light, and nearly 88.9% was degraded in just 30 min. The higher performance was due to the fabrication of Z-scheme photocatalyst which increases the effective utilization of solar light.

Zhang et al. (2017) fabricated carbon quantum dots/ Bi_2WO_6 nanocomposites and successfully studied photodegradation of rhodamine B and phenol and hydrogen production using solar light. Di et al. (2015a) design visible light-driven carbon quantum dots/ Bi_2WO_6 hybrid having a sphere-like structure. The competence was assessed against rhodamine B; ciprofloxacin, a colorless antibiotic agent; tetracycline hydrochloride; and bisphenol A, an endocrine interrupting agent. Further, electron spin resonance and trapping experiment studies explore that the active species were superoxide radical and holes, respectively. Other than Bi_2WO_6 , Bi_2MoO_6 having a band gap of 2.5–2.8 eV, high chemical stability, resistance to corrosion, and low cost is also of much importance. Di et al. (2015b) distributed carbon quantum dots having an average size of 7 nm over Bi_2MoO_6 via hydrothermal method and investigated the photodegradation of ciprofloxacin. The photo-efficiency was assessed using ciprofloxacin, bisphenol A, tetracycline hydrochloride, and methylene blue as targeted pollutant. The enhanced photo-efficiency is due to the more adsorption active species, visible light absorption, and slower rate of recombination.

Zhang et al. (2018) prepared carbon dot/ BiPO_4 photocatalytic system via hydrothermal followed by calcination method. The photocatalytic activity was assessed against indomethacin a nonsteroidal anti-inflammatory drug under solar light. The photocatalytic efficiency of nitrogen-doped carbon quantum dot/ BiPO_4 synthesized by ionic liquid-assisted solvothermal method was also tested against ciprofloxacin, enrofloxacin, tetracycline, and 4-chlorophenol, a colorless antibiotic, under ultraviolet radiation (Di et al. 2017). Zhang et al. (2018) prepared novel carbon quantum dots/ $\text{Bi}_2\text{O}_2\text{CO}_3$ using simple dynamic adsorption method and chosen methyl blue and phenol as targeted pollutants for degradation. Here, $\text{Bi}_2\text{O}_2\text{CO}_3$ photocatalyst exists in different morphological flower, porous ball, sponge, and slice-like structure. $\text{Bi}_2\text{O}_2\text{CO}_3$ has very unique layered structure consisting of CO_3^{2-} layer interwoven

among $[\text{Bi}_2\text{O}_2]^{2+}$ layers. The composites exhibit efficient photocatalytic performance, and nearly 94% and 61% of methyl blue and phenol were degraded within 2 h.

Wang et al. (2017) successfully loaded nitrogen-doped carbon dots onto the surface of g- C_3N_4 composites via polymerized method to design nitrogen-doped carbon dots/g- C_3N_4 photocatalysts. Graphitic carbon nitride is a visible light active metal-free photocatalyst with a band gap of 2.7 eV with various applications in CO_2 reduction, H_2 production, and pollutant degradation. The photocatalytic activity of nitrogen-doped carbon dots/g- C_3N_4 was remarkably higher as compared to g- C_3N_4 and was assessed against indomethacin under visible light. Novel carbon quantum dots/g- C_3N_4 metal-free nanocomposites were synthesized via electrostatic self-assembly method, facile low temperature process, and impregnation-thermal method (Jian et al. 2016; Hong et al. 2016; Zhang et al. 2016). Carbon quantum dots/g- C_3N_4 exhibits excellent electron transfer properties, and its photocatalytic activity was assessed against methyl blue, tetracycline hydrochloride, rhodamine B, and phenol under visible light. By using electrostatic self-assembly method, the size, composition, porosity, and surface functionality can be easily modified. An effective harvesting of solar light due to up-conversion process by carbon quantum dots is one of the reasons why carbon quantum dots/g- C_3N_4 is highly efficient.

Hu et al. (2019) synthesize mesoporous nitrogen-doped carbon quantum dot/BiOCl composites via solvothermal reduction method. The composites exhibit excellent photocatalytic activity against organic pollutant under visible region and near-infrared light. The photodegradation process is mainly dependent on holes and superoxide radical. Qu et al. (2019) fabricated graphene oxide/carbon dot/BiOI ternary nanocomposites by using simple one-step solvothermal method. The ternary nanocomposites exhibit excellent photocatalytic activity against the photodegradation of 4-chlorophenol in the visible region. The synergistic effect of nonmetallic graphene oxide, carbon nanodots, and BiOI is responsible for high efficiency. The photodegradation efficiency decreases in the order graphene oxide/carbon dot/BiOI > carbon dot/BiOI > graphene oxide/BiOI > BiOI, respectively, in 3 h under visible light.

Xie et al. (2018) construct graphene oxide/g- C_3N_4 /MoO₃ Z-scheme photocatalysts and photocatalytic activity against tetracycline antibiotic. The high efficiency is ascribed to the synergistic effect of Z-scheme heterojunction. Further, a ternary composite, carbon quantum dots/CdSe/reduced graphene oxide, is fabricated by hydrothermal method (Huo et al. (2017)). The optical and electronic properties were analyzed by transmission electron microscope, x-ray diffraction, and photo-electrochemical testing. The photocatalytic performance is investigated for the photodegradation of tetracycline hydrochloride. Although the carbon quantum dots have a promising application in nanotechnology and nanomedicine, a lot of work is still needed to be explored for the designing of smart materials.

3.5 Antibacterial Activity of Carbon Quantum Dot-Based Nanocomposites

Microbial pollution is the biggest and most challenging menace for individuals as overusing fluoroquinolone, chloramphenicol, and trimethoprim antibiotics makes multiple drug-resistant bacteria which are difficult to remove (Levy and Marshall 2004). With the advancement in nanoscience, antimicrobial nanomedicine also becomes a prominent field for the researcher to device some nanomaterial for microbial pollution. Previously, metals (Ag and Au) or metal oxide (CuO, ZnO and Fe₂O₃) nanoparticles were reported having antibacterial properties (Hoseinnejad et al. 2018; Pare et al. 2008, 2009; Raghunath and Perumal 2017). These earlier devised nanomaterials suffer with limitation of biological toxicity, generation of secondary pollutant, low efficiency, and poor degradation.

Recently, less toxic, environmental-friendly, and biocompatible carbonaceous materials have identified as promising antimicrobial agents. Li et al. (2018b) fabricated less toxic, biodegradable, and broad-spectrum antibacterial and antifungal carbon dots from vitamin C using electrochemical technique. Carbon dots displayed antibacterial activity, by destroying bacterial cell wall even at lower concentration. At the end, carbon dots are completely degraded into innocuous product in the visible region or at low temperature. The antibacterial activity of carbon dots is evaluated against Gram-positive (*Staphylococcus aureus* and *Bacillus subtilis*) and Gram-negative (*Bacillus* sp. WL-6 and *Escherichia coli*) bacteria, whereas their antifungal properties were evaluated against two pathogenic fungi, *Rhizoctonia solani* and *Pyricularia grisea*.

Kovacova et al. (2018) investigated the photocatalytic and antibacterial activity of hydrophobic carbon quantum dots/polyurethane nanocomposites synthesized by swell-encapsulation-shrink method. The nanocomposites had shown bactericidal effect against *Staphylococcus aureus* and *Escherichia coli* for 60 min of irradiation of blue light, whereas the photocatalytic degradation of Rose Bengal dye was observed for 180 min. Habiba et al. (2015) fabricated Ag nanoparticle-decorated graphene quantum dots via pulse laser method. The antibacterial activity of Ag-graphene quantum dots, bare graphene quantum dots, and Ag nanoparticle were compared. The symbiotic effect of Ag and graphene quantum dots in Ag-graphene quantum dot nanocomposites enhances the antibacterial property in comparison to Ag and graphene quantum dots.

Dong et al. (2017) employed carbon dots with other antibacterial agents such as H₂O₂, CH₃COOH, and Na₂CO₃. The photoactivated technology for antibacterial property is a rapidly growing field to prevent microbial pollution. Carbon quantum dot nanocomposites possess bactericidal property and can be utilized to remove photocatalyzed antimicrobial pollution. The antibacterial property of carbon-based nanocomposites can be easily tailored by surface modification. Liu et al. (2018) fabricated ZnO/graphene quantum dot nanocomposites using hydrothermal method and assessed their antibacterial property through minimum inhibitory concentration, and decreases in bacterial colony were counted by plate count method. The

antibacterial property was enhanced under ultraviolet photo-irradiation, which is attributed to the production of reactive oxidation species responsible for membrane damage as confirmed by paramagnetic resonance and fluorescence microscopic measurements. The ZnO/graphene quantum dot nanocomposites exhibit higher bactericidal effect as compared to ZnO and graphene quantum dots, which may be accounted due to the interfacial charge transfer from graphene quantum dots to ZnO surface that enhances the generation of reactive oxidation species.

3.6 Conclusion

Carbon quantum dots recently emerge as important nanomaterials among various available carbonaceous materials due to their unique properties. Carbon quantum dots are visible light-driven photocatalysts which exhibit special up-conversion phenomena in which they convert longer wavelength light into shorter wavelength with high-energy photon that is efficiently employed for the excitation of charge carrier from the surface of wide band gap semiconductor. The property of up-conversion validates carbon quantum dot usage as photosensitizer as well as photocatalyst. Besides their many applications in different fields, carbon quantum dot-based nanocomposites can also be efficiently used as antimicrobial agents. Carbon quantum dots displayed not only antibacterial but also antifungal property. The antibacterial activity of carbon quantum dot-based nanocomposites is basically due to the generation of reactive oxidation species which may cause oxidative stress as well as disruption of the cell membrane. The book chapter provides a basic review of various synthetic methods for the preparation of carbon quantum dot-based nanocomposites and utilization as photocatalyst. Though significant efforts have already been done on carbon quantum dots over the past 15 years, they are still facing many challenges. From the future prospective, understanding the concept behind up-conversion mechanism of carbon quantum dots, increasing yield of carbon quantum dots, optimization of synthetic procedure for better control over size, increasing photostability of carbon quantum dots, or minimizing photo-bleaching and green method to avoid chemical pollution need to be addressed before practical application. The literature survey reveals that studies were limited to certain basic pollutants like methylene blue, methyl orange, rhodamine B, and phenol. Thus, photodegradation by carbon quantum dots needs further extension to other pollutants as well, applying it to pollutants belonging in the real world. Lastly, photo-efficiency and separation of carbon quantum dots are also important issues, as no such photocatalyst is designed yet which shows high efficiency for degradation of pollutants. Despite the many challenges associated with carbon quantum dots, numerous opportunities are still waiting to explore endless potential to be employed in various technologies.

References

- Adan C, Marugan J, Obregon S, Colon G (2015) Photocatalytic activity of bismuth vanadate's under UV-A and visible light irradiation: inactivation of *Escherichia coli* vs oxidation of methanol. *Catal Today* 240:93–99. <https://doi.org/10.1016/j.cattod.2014.03.059>
- Ahirwar S, Mallick S, Bahadur D (2017) Electrochemical method to prepare graphene quantum dots and graphene oxide quantum dots. *ACS Omega* 2(11):8343–8353. <https://doi.org/10.1021/acsomega.7b01539>
- Al Awak MM, Wang P, Wang S, Tang Y, Sun YP, Yang L (2017) Correlation of carbon dots' light-activated antimicrobial activities and fluorescence quantum yield. *RSC Adv* 7(48):30177–30184. <https://doi.org/10.1039/C7RA05397E>
- Bao L, Zhang ZL, Tian ZQ, Zhang L, Liu C, Lin Y, Qi B, Pang DW (2011) Electrochemical tuning of luminescent carbon nanodots: from preparation to luminescence mechanism. *Adv Mater* 23(48):5801–5806. <https://doi.org/10.1002/adma.201102866>
- Bourlinos AB, Stassinopoulos A, Anglos D, Zboril R, Karakassides M, Giannelis EP (2008) Surface functionalized carbogenic quantum dots. *Small* 4(4):455–458. <https://doi.org/10.1002/sml.200700578>
- Cademartiri L, Montanari E, Calestani G, Migliori A, Guagliardi A, Ozin GA (2006) Size-dependent extinction coefficients of PbS quantum dots. *J Am Chem Soc* 128(31):10337–10346. <https://doi.org/10.1021/ja063166u>
- Chandel N, Sharma K, Sudhaik A, Raizada P, Hosseini-Bandegharai A, Thakur VK, Singh P (2019) Magnetically separable ZnO/ZnFeO₄ and ZnO/CoFe₂O₄ photocatalyst supported onto nitrogen doped graphene for photocatalytic degradation of toxic dyes. *Arab J Chem* 13(2):4324–4340. <https://doi.org/10.1016/j.arabjc.2019.08.005>
- Chen X, Wang J, Huang C, Zhang S, Zhang H, Li Z, Zou Z (2015) Barium zirconate: a new photocatalyst for converting CO₂ into hydrocarbons under UV irradiation. *Catal Sci Technol* 5(3):1758–1763. <https://doi.org/10.1039/C4CY01201A>
- Chen W, Li D, Tian L, Xiang W, Wang T, Hu W, Hu Y, Chen S, Chen J, Dai Z (2018a) Synthesis of graphene quantum dots from natural polymer starch for cell imaging. *Green Chem* 20(19):4438–4442. <https://doi.org/10.1039/C8GC02106F>
- Chen W, Lv G, Hu W, Li D, Chen S, Dai Z (2018b) Synthesis and applications of graphene quantum dots: a review. *Nanotechnol Rev* 7(2):157–185. <https://doi.org/10.1515/ntrev-2017-0199>
- Deng J, Lu Q, Mi N, Li H, Liu M, Xu M, Tan L, Xie Q, Zhang Y, Yao S (2014) Electrochemical synthesis of carbon nanodots directly from alcohols. *Chem Eur J* 20(17):4993–4999. <https://doi.org/10.1002/chem.201304869>
- Deng F, Lu X, Zhong F, Pei X, Luo X, Luo S, Dionysiou DD, Au C (2015) Fabrication of 2D sheet-like BiOCl/carbon quantum dot hybrids via a template-free coprecipitation method and their tunable visible-light photocatalytic activities derived from different size distributions of carbon quantum dots. *Nanotechnology* 27(6):065701. <https://doi.org/10.1088/0957-4484/27/6/065701>
- Devi NR, Kumar TV, Sundramoorthy AK (2018) Electrochemically exfoliated carbon quantum dots modified electrodes for detection of dopamine neurotransmitter. *J Electrochem Soc* 165(12):G3112–G3119. <https://doi.org/10.1149/2.0191812jes>
- Di J, Xia J, Ge Y, Li H, Ji H, Xu H, Zhang Q, Li H, Li M (2015a) Novel visible-light-driven CQDs/Bi₂WO₆ hybrid materials with enhanced photocatalytic activity toward organic pollutants degradation and mechanism insight. *Appl Catal B Environ* 168:51–61. <https://doi.org/10.1016/j.apcatb.2014.11.057>
- Di J, Xia J, Ji M, Li H, Xu H, Li H, Chen R (2015b) The synergistic role of carbon quantum dots for the improved photocatalytic performance of Bi₂MoO₆. *Nanoscale* 7(26):11433–11443. <https://doi.org/10.1039/C5NR01350J>
- Di J, Xia J, Chen X, Ji M, Yin S, Zhang Q, Li H (2017) Tunable oxygen activation induced by oxygen defects in nitrogen doped carbon quantum dots for sustainable boosting photocatalysis. *Carbon* 114:601–607. <https://doi.org/10.1016/j.carbon.2016.12.030>

- Ding D, Lan W, Yang Z, Zhao X, Chen Y, Wang J, Zhang X, Zhang Y, Su Q, Xie E (2016) A simple method for preparing ZnO foam/carbon quantum dots nanocomposite and their photocatalytic applications. *Mater Sci Semicond Process* 47:25–31. <https://doi.org/10.1016/j.mssp.2016.02.004>
- Dong Y, Chen C, Zheng X, Gao L, Cui Z, Yang H, Guo C, Chi Y, Li CM (2012) One-step and high yield simultaneous preparation of single-and multi-layer graphene quantum dots from CX-72 carbon black. *J Mater Chem* 22(18):8764–8766. <https://doi.org/10.1039/C2JM30658A>
- Dong X, Al Awak M, Tomlinson N, Tang Y, Sun YP, Yang L (2017) Antibacterial effects of carbon dots in combination with other antimicrobial reagents. *PLoS One* 12(9):0185324. <https://doi.org/10.1371/journal.pone.0185324>
- Dutta V, Singh P, Shandilya P, Sharma S, Raizada P, Saini AK, Gupta VK, Hosseini-Bandegharaei A, Agarwal S, Rahmani-Sani A (2019) Review on advances in photocatalytic water disinfection utilizing graphene and graphene derivatives-based nanocomposites. *J Environ Chem Eng* 7(3):103132. <https://doi.org/10.1016/j.jece.2019.103132>
- Feng C, Deng XY, Ni XX, Li WB (2015) Fabrication of carbon dots modified porous ZnO nanorods with enhanced photocatalytic activity. *Acta Phys-Chim Sin* 31(12):2349–2357. <https://doi.org/10.3866/PKU.WHXB201510281>
- Gautam S, Shandilya P, Singh VP, Raizada P, Singh P (2016) Solar photocatalytic mineralization of antibiotics using magnetically separable NiFe₂O₄ supported onto graphene sand composite and bentonite. *J Water Process Eng* 14:86–100. <https://doi.org/10.1016/j.jwpe.2016.10.008>
- Gautam S, Shandilya P, Priya B, Singh VP, Raizada P, Rai R, Valente MA, Singh P (2017) Superparamagnetic MnFe₂O₄ dispersed over graphitic carbon sand composite and bentonite as magnetically recoverable photocatalyst for antibiotic mineralization. *Sep Purif Technol* 172:498–511. <https://doi.org/10.1016/j.seppur.2016.09.006>
- Gopalakrishnan D, Damien D, Li B, Gullappalli H, Pillai VK, Ajayan PM, Shaijumon MM (2015) Electrochemical synthesis of luminescent MoS₂ quantum dots. *Chem Commun* 51(29):6293–6296. <https://doi.org/10.1039/C4CC09826A>
- Grun M, Büchel G, Kumar D, Schumacher K, Bidlingmaier B, Unger KK (2000) Rational design, tailored synthesis and characterisation of ordered mesoporous silicas in the micron and submicron size range. *Stud Surf Sci Catal* 128:155–165. [https://doi.org/10.1016/S0167-2991\(00\)80019-1](https://doi.org/10.1016/S0167-2991(00)80019-1)
- Guo X, Wang CF, Yu ZY, Chen L, Chen S (2012) Facile access to versatile fluorescent carbon dots toward light-emitting diodes. *Chem Commun* 48(21):2692–2694. <https://doi.org/10.1039/C2CC17769B>
- Guzelian AA, Banin U, Kadavanich AV, Peng X, Alivisatos AP (1996) Colloidal chemical synthesis and characterization of InAs nanocrystal quantum dots. *Appl Phys Lett* 69(10):1432–1434. <https://doi.org/10.1063/1.117605>
- Habiba K, Bracho-Rincon DP, Gonzalez-Feliciano JA, Villalobos-Santos JC, Makarov VI, Ortiz D, Avalos JA, Gonzalez CI, Weiner BR, Morell G (2015) Synergistic antibacterial activity of PEGylated silver–graphene quantum dots nanocomposites. *Appl Mater Today* 1(2):80–87. <https://doi.org/10.1016/j.apmt.2015.10.001>
- Hasija V, Raizada P, Sudhaik A, Sharma K, Kumar A, Singh P, Jonnalagadda SB, Thakur VK (2019a) Recent advances in noble metal free doped graphitic carbon nitride based nanohybrids for photocatalysis of organic contaminants in water: a review. *Appl Mater Today* 15:494–524. <https://doi.org/10.1016/j.apmt.2019.04.003>
- Hasija V, Sudhaik A, Raizada P, Hosseini-Bandegharaei A, Singh P (2019b) Carbon quantum dots supported AgI/ZnO/phosphorus doped graphitic carbon nitride as Z-scheme photocatalyst for efficient photodegradation of 2, 4-dinitrophenol. *J Environ Chem Eng* 7(4):103272. <https://doi.org/10.1016/j.jece.2019.103272>
- He DC, Fu QM, Ma ZB, Zhao HY, Tu YF, Tian Y, Zhou D, Zheng G, Lu HB (2018) Facile synthesis and photocatalytic activity of ZnO/zinc titanate core–shell nanorod arrays. *Mater Res Express* 5(2):025006. <https://doi.org/10.1088/2053-1591/aaa938>

- Hernandez Y, Nicolosi V, Lotya M, Blighe FM, Sun Z, De S, McGovern IT, Holland B, Byrne M, Gun'Ko YK, Boland JJ (2008) High-yield production of graphene by liquid-phase exfoliation of graphite. *Nat Nanotechnol* 3(9):563. <https://doi.org/10.1038/nnano.2008.215>
- Hong Y, Meng Y, Zhang G, Yin B, Zhao Y, Shi W, Li C (2016) Facile fabrication of stable metal-free CQDs/g-C₃N₄ heterojunctions with efficiently enhanced visible-light photocatalytic activity. *Sep Purif Technol* 171:229–237. <https://doi.org/10.1016/j.seppur.2016.07.025>
- Hoseinnejad M, Jafari SM, Katouzian I (2018) Inorganic and metal nanoparticles and their antimicrobial activity in food packaging applications. *Crit Rev Microbiol* 44(2):161–181. <https://doi.org/10.1080/1040841X.2017.1332001>
- Hu SL, Niu KY, Sun J, Yang J, Zhao NQ, Du XW (2009) One-step synthesis of fluorescent carbon nanoparticles by laser irradiation. *J Mater Chem* 19(4):484–488. <https://doi.org/10.1039/B812943F>
- Hu W, Che G, Che H, Hu H, Jiang E, Ruan X, Zhang X, Liu C, Dong H (2019) Construction of mesoporous NCQDs–BiOCl composites for photocatalytic degrading organic pollutants in water under visible and near-infrared light. *J Environ Eng* 145(6):04019031. [https://doi.org/10.1061/\(ASCE\)EE.1943-7870.0001532](https://doi.org/10.1061/(ASCE)EE.1943-7870.0001532)
- Huang H, He Y, Lin Z, Kang L, Zhang Y (2013) Two novel Bi-based borate photocatalysts: crystal structure, electronic structure, photoelectrochemical properties, and photocatalytic activity under simulated solar light irradiation. *J Phys Chem C* 117(44):22986–22994. <https://doi.org/10.1021/jp4084184>
- Huang H, Liu K, Chen K, Zhang Y, Zhang Y, Wang S (2014) Ce and F comodification on the crystal structure and enhanced photocatalytic activity of Bi₂WO₆ photocatalyst under visible light irradiation. *J Phys Chem C* 118(26):14379–14387. <https://doi.org/10.1021/jp503025b>
- Huo P, Guan J, Zhou M, Ma C, Liu X, Yan Y, Yuan S (2017) Carbon quantum dots modified CdSe loaded reduced graphene oxide for enhancing photocatalytic activity. *J Ind Eng Chem* 50:147–154. <https://doi.org/10.1016/j.jiec.2017.02.008>
- Jamwal D, Kaur G, Raizada P, Singh P, Pathak D, Thakur P (2015) Twin-tail surfactant peculiarity in superficial fabrication of semiconductor quantum dots: toward structural, optical, and electrical features. *J Phys Chem C* 119(9):5062–5073. <https://doi.org/10.1021/jp510428z>
- Jeong J, Jung J, Choi M, Kim JW, Chung SJ, Lim S, Lee H, Chung BH (2012) Color tunable photoluminescent fullerene nanoparticles. *Adv Mater* 24(15):1999–2003. <https://doi.org/10.1002/adma.201104772>
- Jia X, Li J, Wang E (2012) One-pot green synthesis of optically pH-sensitive carbon dots with upconversion luminescence. *Nanoscale* 4(18):5572–5575. <https://doi.org/10.1039/C2NR31319G>
- Jian X, Liu X, Yang HM, Li JG, Song XL, Dai HY, Liang ZH (2016) Construction of carbon quantum dots/proton-functionalized graphitic carbon nitride nanocomposite via electrostatic self-assembly strategy and its application. *Appl Surf Sci* 370:514–521. <https://doi.org/10.1016/j.apsusc.2016.02.119>
- Jiang J, He Y, Li S, Cui H (2012) Amino acids as the source for producing carbon nanodots: microwave assisted one-step synthesis, intrinsic photoluminescence property and intense chemiluminescence enhancement. *Chem Commun* 48(77):9634–9636. <https://doi.org/10.1016/j.apsusc.2016.02.119>
- Journet C, Maser WK, Bernier P, Loiseau A, La Chapelle ML, Lefrant DS, Deniard P, Lee R, Fischer JE (1997) Large-scale production of single-walled carbon nanotubes by the electric-arc technique. *Nature* 388(6644):756. <https://doi.org/10.1038/41972>
- Kandi D, Martha S, Thirumurugan A, Parida K (2017) Modification of BiOI microplates with CdS QDs for enhancing stability, optical property, electronic behaviour toward rhodamine B decolourization, and photocatalytic hydrogen evolution. *J Phys Chem C* 121(9):4834–4849. <https://doi.org/10.1021/acs.jpcc.6b11938>
- Kapitonov AN, Egorova MN, Tomskaya AE, Smagulova SA, Alekseev AA (2018) Hydrothermal synthesis of carbon dots and their luminescence. *AIP* 2041:030003. <https://doi.org/10.1063/1.5079363>

- Ke J, Li X, Zhao Q, Liu B, Liu S, Wang S (2017) Upconversion carbon quantum dots as visible light responsive component for efficient enhancement of photocatalytic performance. *J Colloid Interface Sci* 496:425–433. <https://doi.org/10.1016/j.jcis.2017.01.121>
- Keuleyan S, Lhuillier E, Brajuskovic V, Guyot-Sionnest P (2011) Mid-infrared HgTe colloidal quantum dot photodetectors. *Nat Photonics* 5(8):489. <https://doi.org/10.1038/nphoton.2011.142>
- Kovacova M, Markovic ZM, Humpolicek P, Micusik M, Svajdlenkova H, Kleinova A, Danko M, Kubat P, Vajdak J, Capakova Z, Lehocky M (2018) Carbon quantum dots modified polyurethane nanocomposite as effective photocatalytic and antibacterial agents. *ACS Biomater Sci Eng* 4(12):3983–3993. <https://doi.org/10.1021/acsbiomaterials.8b00582>
- Kumar A, Raizada P, Singh P, Saini R, Saini A, Hosseini-Bandegharaei A (2019) Perspective and status of polymeric graphitic carbon nitride based Z-scheme photocatalytic systems for sustainable photocatalytic water purification. *Chem Eng J*:123496. <https://doi.org/10.1016/j.cej.2019.123496>
- Kundu S, Yadav RM, Narayanan TN, Shelke MV, Vajtai R, Ajayan PM, Pillai VK (2015) Synthesis of N, F and S co-doped graphene quantum dots. *Nanoscale* 7(27):11515–11519. <https://doi.org/10.1039/C5NR02427G>
- Lai CW, Hsiao YH, Peng YK, Chou T (2012) Facile synthesis of highly emissive carbon dots from pyrolysis of glycerol; gram scale production of carbon dots/mSiO₂ for cell imaging and drug release. *J Mater Chem* 22(29):14403–14409. <https://doi.org/10.1039/C2JM32206D>
- Levy SB, Marshall B (2004) Antibacterial resistance worldwide: causes, challenges and responses. *Nat Med* 10(12s):122. <https://doi.org/10.1038/nm1145>
- Li X, Wang X, Zhang L, Lee S, Dai H (2008) Chemically derived, ultrasoft graphene nanoribbon semiconductors. *Sci* 319(5867):1229–1232. <https://doi.org/10.1126/science.1150878>
- Li X, Wang H, Shimizu Y, Pyatenko A, Kawaguchi K, Koshizaki N (2010a) Preparation of carbon quantum dots with tunable photoluminescence by rapid laser passivation in ordinary organic solvents. *Chem Commun* 47(3):932–934. <https://doi.org/10.1039/C0CC03552A>
- Li H, He X, Kang Z, Huang H, Liu Y, Liu J, Lian S, Tsang CHA, Yang X, Lee ST (2010b) Water-soluble fluorescent carbon quantum dots and photocatalyst design. *Ange Chem Int Ed* 49(26):4430–4434. <https://doi.org/10.1002/anie.200906154>
- Li H, He X, Liu Y, Yu H, Kang Z, Lee ST (2011a) Synthesis of fluorescent carbon nanoparticles directly from active carbon via a one-step ultrasonic treatment. *Mater Res Bull* 46(1):147–151. <https://doi.org/10.1016/j.materresbull.2010.10.013>
- Li Y, Hu Y, Zhao Y, Shi G, Deng L, Hou Y, Qu L (2011b) An electrochemical avenue to green-luminescent graphene quantum dots as potential electron-acceptors for photovoltaics. *Adv Mater* 23(6):776–780. <https://doi.org/10.1002/adma.201003819>
- Li H, Liu R, Liu Y, Huang H, Yu H, Ming H, Lian S, Lee ST, Kang Z (2012) Carbon quantum dots/Cu₂O composites with protruding nanostructures and their highly efficient (near) infrared photocatalytic behavior. *J Mater Chem* 22(34):17470–17475. <https://doi.org/10.1039/C2JM32827E>
- Li Y, Zhang BP, Zhao JX, Ge ZH, Zhao XK, Zou L (2013) ZnO/carbon quantum dots heterostructure with enhanced photocatalytic properties. *Appl Surf Sci* 279:367–373. <https://doi.org/10.1016/j.apsusc.2013.04.114>
- Li J, Zuo G, Qi X, Wei W, Pan X, Su T, Zhang J, Dong W (2017) Selective determination of Ag⁺ using Salecan derived nitrogen doped carbon dots as a fluorescent probe. *Mater Sci Eng C* 77:508–512. <https://doi.org/10.1016/j.msec.2017.04.007>
- Li G, Wang F, Liu P, Chen Z, Lei P, Xu Z, Li Z, Ding Y, Zhang S, Yang M (2018a) Polymer dots grafted TiO₂ nanohybrids as high performance visible light photocatalysts. *Chemosphere* 197:526–534. <https://doi.org/10.1016/j.chemosphere.2018.01.071>
- Li H, Huang J, Song Y, Zhang M, Wang H, Lu F, Huang H, Liu Y, Dai X, Gu Z, Yang Z (2018b) Degradable carbon dots with broad-spectrum antibacterial activity. *ACS Appl Mater Interfaces* 10(32):26936–26946. <https://doi.org/10.1021/acsami.8b08832>

- Liang Y, Liu P, Yang G (2014) Fabrication of one-dimensional chain of iron-based bimetallic alloying nanoparticles with unique magnetizations. *Cryst Growth Des* 14(11):5847–5855. <https://doi.org/10.1021/cg501079a>
- Lim SY, Shen W, Gao Z (2015) Carbon quantum dots and their applications. *Chem Soc Rev* 44(1):362–381. <https://doi.org/10.1039/C4CS00269E>
- Lin L, Xu Y, Zhang S, Ross IM, Ong AC, Allwood DA (2013) Fabrication of luminescent monolayered tungsten dichalcogenides quantum dots with giant spin-valley coupling. *ACS Nano* 7(9):8214–8223. <https://doi.org/10.1021/nn403682r>
- Liu R, Wu D, Liu S, Koynov K, Knoll W, Li Q (2009) An aqueous route to multicolor photoluminescent carbon dots using silica spheres as carriers. *Angew Chem Int Ed* 48(25):4598–4601. <https://doi.org/10.1002/anie.200900652>
- Liu R, Wu D, Feng X, Muellen K (2011) Bottom-up fabrication of photoluminescent graphene quantum dots with uniform morphology. *J Am Chem Soc* 133(39):15221–15223. <https://doi.org/10.1021/ja204953k>
- Liu F, Jang MH, Ha HD, Kim JH, Cho YH, Seo TS (2013) Facile synthetic method for pristine graphene quantum dots and graphene oxide quantum dots: origin of blue and green luminescence. *Adv Mater* 25(27):3657–3662. <https://doi.org/10.1002/adma.201300233>
- Liu B, Xu W, Sun T, Chen M, Tian L, Wang J (2014) Efficient visible light photocatalytic activity of CdS on (001) facets exposed to BiOCl. *New J Chem* 38(6):2273–2277. <https://doi.org/10.1039/C4NJ00257A>
- Liu Y, Liao M, He X, Liu X, Kou X, Xiao D (2015) One-step synthesis of highly luminescent nitrogen-doped carbon dots for selective and sensitive detection of mercury (ii) ions and cellular imaging. *Anal Sci* 31(10):971–977. <https://doi.org/10.2116/analsci.31.971>
- Liu J, Rojas-Andrade MD, Chata G, Peng Y, Roseman G, Lu JE, Millhauser GL, Saltikov C, Chen S (2018) Photo-enhanced antibacterial activity of ZnO/graphene quantum dot nanocomposites. *Nanoscale* 10(1):158–166. <https://doi.org/10.1039/C7NR07367D>
- Lu W, Qin X, Liu S, Chang G, Zhang Y, Luo Y, Asiri AM, Al-Youbi AO, Sun X (2012) Economical, green synthesis of fluorescent carbon nanoparticles and their use as probes for sensitive and selective detection of mercury (II) ions. *Anal Chem* 84(12):5351–5357. <https://doi.org/10.1021/ac3007939>
- Luo Z, Qi G, Chen K, Zou M, Yuwen L, Zhang X, Huang W, Wang L (2016) Microwave-assisted preparation of white fluorescent graphene quantum dots as a novel phosphor for enhanced white-light-emitting diodes. *Adv Funct Mater* 26(16):2739–2744. <https://doi.org/10.1002/adfm.201505044>
- Ma M, Hu X, Zhang C, Deng C, Wang X (2017) The optimum parameters to synthesize bright and stable graphene quantum dots by hydrothermal method. *J Mater Sci Mater Electron* 28(9):6493–6497. <https://doi.org/10.1007/s10854-017-6337-4>
- Mehta VN, Jha S, Kailasa SK (2014) One-pot green synthesis of carbon dots by using Saccharum officinarum juice for fluorescent imaging of bacteria (*Escherichia coli*) and yeast (*Saccharomyces cerevisiae*) cells. *Mater Sci Eng C* 38:20–27. <https://doi.org/10.1016/j.msec.2014.01.038>
- Micic OI, Cheong HM, Fu H, Zunger A, Sprague JR, Mascarenhas A, Nozik AJ (1997) Size-dependent spectroscopy of InP quantum dots. *J Phys Chem B* 101(25):4904–4912. <https://doi.org/10.1021/jp9704731>
- Moreels I, Lambert K, De Mynck D, Vanhaecke F, Poelman D, Martins JC, Allan G, Hens Z (2007) Composition and size-dependent extinction coefficient of colloidal PbSe quantum dots. *Chem Mater* 19(25):6101–6106. <https://doi.org/10.1021/cm071410q>
- Namdari P, Negahdari B, Eatemadi A (2017) Synthesis, properties and biomedical applications of carbon-based quantum dots: an updated review. *Biomed Pharmacother* 87:209–222. <https://doi.org/10.1016/j.biopha.2016.12.108>
- Nie L, Zhang Q (2017) Recent progress in crystalline metal chalcogenides as efficient photocatalysts for organic pollutant degradation. *Inorg Chem Front* 4(12):1953–1962. <https://doi.org/10.1039/C7QI00651A>

- Pan D, Zhang J, Li Z, Wu M (2010a) Hydrothermal route for cutting graphene sheets into blue-luminescent graphene quantum dots. *Adv Mater* 22(6):734–738. <https://doi.org/10.1002/adma.200902825>
- Pan D, Zhang J, Li Z, Wu C, Yan X, Wu M (2010b) Observation of pH-, solvent, spin-, and excitation-dependent blue photoluminescence from carbon nanoparticles. *Chem Commun* 46(21):3681–3683. <https://doi.org/10.1039/C000114G>
- Pan J, Liu J, Zuo S, Khan UA, Yu Y, Li B (2018) Synthesis of cuboid BiOCl nanosheets coupled with CdS quantum dots by region-selective deposition process with enhanced photocatalytic activity. *Mater Res Bull* 103:216–224. <https://doi.org/10.1016/j.materresbull.2018.03.043>
- Pang Q, Tang J, Huang H, Liang X, Hart C, Tam KC, Nazar LF (2015) A nitrogen and sulfur dual-doped carbon derived from polyrhodanine@ cellulose for advanced lithium–sulfur batteries. *Adv Mater* 27(39):6021–6028. <https://doi.org/10.1002/adma.201502467>
- Pare B, Jonnalagadda SB, Tomar H, Singh P, Bhagwat VW (2008) ZnO assisted photocatalytic degradation of acridine orange in aqueous solution using visible irradiation. *Desalination* 232(1-3):80–90. <https://doi.org/10.1016/j.desal.2008.01.007>
- Pare B, Singh P, Jonnalagadda SB (2009) Artificial light assisted photocatalytic degradation of lissamine fast yellow dye in ZnO suspension in a slurry batch reactor. *Indian J Chem A* 48:1364–1369. <http://nopr.niscair.res.in/handle/123456789/6122>
- Park SY, Lee HU, Park ES, Lee SC, Lee JW, Jeong SW, Kim CH, Lee YC, Huh YS, Lee J (2014) Photoluminescent green carbon nanodots from food-waste-derived sources: large-scale synthesis, properties, and biomedical applications. *ACS Appl Mater Interfaces* 6(5):3365–3370. <https://doi.org/10.1021/am500159p>
- Peng J, Gao W, Gupta BK, Liu Z, Romero-Aburto R, Ge L, Song L, Alemany LB, Zhan X, Gao G, Vithayathil SA (2012) Graphene quantum dots derived from carbon fibers. *Nano Lett* 12(2):844–849. <https://doi.org/10.1021/nl2038979>
- Prasanna A, Imae T (2013) One-pot synthesis of fluorescent carbon dots from orange waste peels. *Ind Eng Chem Res* 52(44):15673–15678. <https://doi.org/10.1021/ie402421s>
- Priya B, Shandilya P, Raizada P, Thakur P, Singh N, Singh P (2016a) Photocatalytic mineralization and degradation kinetics of ampicillin and oxytetracycline antibiotics using graphene sand composite and chitosan supported BiOCl. *J Mol Catal A Chem* 423:400–413. <https://doi.org/10.1016/j.molcata.2016.07.043>
- Priya B, Raizada P, Singh N, Thakur P, Singh P (2016b) Adsorptional photocatalytic mineralization of oxytetracycline and ampicillin antibiotics using Bi₂O₃/BiOCl supported on graphene sand composite and chitosan. *J Colloid Interface Sci* 479:271–283. <https://doi.org/10.1016/j.jcis.2016.06.067>
- Qin X, Lu W, Asiri AM, Al-Youbi AO, Sun X (2013) Microwave-assisted rapid green synthesis of photoluminescent carbon nanodots from flour and their applications for sensitive and selective detection of mercury (II) ions. *Sens Actuator B Chem* 184:156–162. <https://doi.org/10.1016/j.snb.2013.04.079>
- Qu S, Xiong Y, Zhang J (2019) Fabrication of GO/CDots/BiOI nanocomposites with enhanced photocatalytic 4-chlorophenol degradation and mechanism insight. *Sep Purif Technol* 210:382–389. <https://doi.org/10.1016/j.seppur.2018.08.027>
- Raghunath A, Perumal E (2017) Metal oxide nanoparticles as antimicrobial agents: a promise for the future. *Int J Antimicrob Agents* 49(2):137–152. <https://doi.org/10.1016/j.ijantimicag.2016.11.011>
- Raizada P, Singh P, Kumar A, Sharma G, Pare B, Jonnalagadda SB, Thakur P (2014a) Solar photocatalytic activity of nano-ZnO supported on activated carbon or brick grain particles: role of adsorption in dye degradation. *Appl Catal A Gen* 486:159–169. <https://doi.org/10.1016/j.apcata.2014.08.043>
- Raizada P, Singh P, Kumar A, Pare B, Jonnalagadda SB (2014b) Zero valent iron-brick grain nanocomposite for enhanced solar-Fenton removal of malachite green. *Sep Purif Technol* 133:429–437. <https://doi.org/10.1016/j.seppur.2014.07.012>

- Raizada P, Priya B, Thakur P, Singh P (2016) Solar light induced photodegradation of oxytetracycline using Zr doped TiO₂/CaO based nanocomposite. *Indian J Chem* 55 (07):803–809. <http://nopr.niscair.res.in/handle/123456789/35068>
- Raizada P, Kumari J, Shandilya P, Singh P (2017a) Kinetics of photocatalytic mineralization of oxytetracycline and ampicillin using activated carbon supported ZnO/ZnWO₄. *Desalin Water Treat* 79:204–213. <https://doi.org/10.5004/dwt.2017.20831>
- Raizada P, Kumari J, Shandilya P, Dhiman R, Singh VP, Singh P (2017b) Magnetically retrievable Bi₂WO₆/Fe₃O₄ immobilized on graphene sand composite for investigation of photocatalytic mineralization of oxytetracycline and ampicillin. *Process Saf Environ* 106:104–116. <https://doi.org/10.1016/j.psep.2016.12.012>
- Raizada P, Sudhaik A, Singh P, Shandilya P, Thakur P, Jung H (2018) Visible light assisted photodegradation of 2, 4-dinitrophenol using Ag₂CO₃ loaded phosphorus and sulphur co-doped graphitic carbon nitride nanosheets in simulated wastewater. *Arab J Chem* 13:3196–3209. <https://doi.org/10.1016/j.arabjc.2018.10.004>
- Raizada P, Sudhaik A, Singh P, Shandilya P, Gupta VK, Hosseini-Bandegharai A, Agrawal S (2019a) Ag₃PO₄ modified phosphorus and sulphur co-doped graphitic carbon nitride as a direct Z-scheme photocatalyst for 2, 4-dimethyl phenol degradation. *J Photochem Photobiol A* 374:22–35. <https://doi.org/10.1016/j.jphotochem.2019.01.015>
- Raizada P, Sudhaik A, Singh P (2019b) Photocatalytic water decontamination using graphene and ZnO coupled photocatalysts: a review. *Mater Sci Energy Technol* 2(3):509–525. <https://doi.org/10.1016/j.msct.2019.04.007>
- Raizada P, Sudhaik A, Singh P, Hosseini-Bandegharai A, Thakur P (2019c) Converting type II AgBr/VO into ternary Z Scheme photocatalyst via coupling with phosphorus doped g-C₃N₄ for enhanced photocatalytic activity. *Sep Purif Technol* 227:115692. <https://doi.org/10.1016/j.seppur.2019.115692>
- Raizada P, Sudhaik A, Singh P, Shandilya P, Saini AK, Gupta VK, Lim JH, Jung H, Hosseini-Bandegharai A (2019d) Fabrication of Ag₃VO₄ decorated phosphorus and sulphur co-doped graphitic carbon nitride as a high-dispersed photocatalyst for phenol mineralization and *E. coli* disinfection. *Sep Purif Technol* 212:887–900. <https://doi.org/10.1016/j.seppur.2018.12.007>
- Roy P, Chen PC, Periasamy AP, Chen YN, Chang HT (2015) Photoluminescent carbon nanodots: synthesis, physicochemical properties and analytical applications. *Mater Today* 18(8):447–458. <https://doi.org/10.1016/j.mattod.2015.04.005>
- Sarkar S, Banerjee D, Ghorai UK, Chattopadhyay KK (2016) Hydrothermal synthesis of carbon quantum dots and study of its photoluminescence property. In: 2016 international conference on microelectronics. Computing and Communication (MicroCom) (1–3). IEEE. <https://doi.org/10.1109/MicroCom.2016.7522521>
- Saud PS, Pant B, Alam AM, Ghouri ZK, Park M, Kim HY (2015) Carbon quantum dots anchored TiO₂ nanofibers: effective photocatalyst for waste water treatment. *Ceram Int* 41 (9):11953–11959. <https://doi.org/10.1016/j.ceramint.2015.06.007>
- Shandilya P, Mittal D, Soni M, Raizada P, Lim JH, Jeong DY, Dewedi RP, Saini AK, Singh P (2018a) Islanding of EuVO₄ on high-dispersed fluorine doped few layered graphene sheets for efficient photocatalytic mineralization of phenolic compounds and bacterial disinfection. *J Taiwan Inst Chem E* 93:528–542. <https://doi.org/10.1016/j.jtice.2018.08.034>
- Shandilya P, Mittal D, Soni M, Raizada P, Hosseini-Bandegharai A, Saini AK, Singh P (2018b) Fabrication of fluorine doped graphene and SmVO₄ based dispersed and adsorptive photocatalyst for abatement of phenolic compounds from water and bacterial disinfection. *J Clean Prod* 203:386–399. <https://doi.org/10.1016/j.jclepro.2018.08.271>
- Shandilya P, Mittal D, Sudhaik A, Soni M, Raizada P, Saini AK, Singh P (2019) GdVO₄ modified fluorine doped graphene nanosheets as dispersed photocatalyst for mitigation of phenolic compounds in aqueous environment and bacterial disinfection. *Sep Purif Technol* 210:804–816. <https://doi.org/10.1016/j.seppur.2018.08.077>
- Sharma K, Dutta V, Sharma S, Raizada P, Hosseini-Bandegharai A, Thakur P, Singh P (2019a) Recent advances in enhanced photocatalytic activity of bismuth oxyhalides for efficient

- photocatalysis of organic pollutants in water: a review. *J Ind Eng Chem* 78(25):1–20. <https://doi.org/10.1016/j.jiec.2019.06.022>
- Sharma S, Dutta V, Singh P, Raizada P, Sani AR, Bandegharai AH, Thakur VK (2019b) Carbon quantum dot supported semiconductor photocatalysts for efficient degradation of organic pollutants in water: a review. *J Clean Prod* 228:755–769. <https://doi.org/10.1016/j.jclepro.2019.04.292>
- Shen T, Wang Q, Guo Z, Kuang J, Cao W (2018) Hydrothermal synthesis of carbon quantum dots using different precursors and their combination with TiO₂ for enhanced photocatalytic activity. *Ceram Int* 44(10):11828–11834. <https://doi.org/10.1016/j.ceramint.2018.03.271>
- Shin Y, Lee J, Yang J, Park J, Lee K, Kim S, Park Y, Lee H (2014) Mass production of graphene quantum dots by one-pot synthesis directly from graphite in high yield. *Small* 10(5):866–870. <https://doi.org/10.1002/sml.201302286>
- Shinde DB, Pillai VK (2012) Electrochemical preparation of luminescent graphene quantum dots from multiwalled carbon nanotubes. *Chem Eur J* 18(39):12522–12528. <https://doi.org/10.1002/chem.201201043>
- Singh P, Raizada P, Pathania D, Kumar A, Thakur P (2013) Preparation of BSA-ZnWO₄ nanocomposites with enhanced adsorptional photocatalytic activity for methylene blue degradation. *Int J Photoenergy* 2013:7. <https://doi.org/10.1155/2013/726250>
- Singh P, Raizada P, Kumari S, Kumar A, Pathania D, Thakur P (2014) Solar-Fenton removal of malachite green with novel FeO-activated carbon nanocomposite. *Appl Catal A Gen* 476:9–18. <https://doi.org/10.1016/j.apcata.2014.02.009>
- Singh P, Priya B, Shandilya P, Raizada P, Singh N, Pare B, Jonnalagadda SB (2016) Photocatalytic mineralization of antibiotics using 60% WO₃/BiOCl stacked to graphene sand composite and chitosan. *Arab J Chem* 12:4627–46445. <https://doi.org/10.1016/j.arabjc.2016.08.005>
- Singh P, Gautam S, Shandilya P, Priya B, Singh VP, Raizada P (2017) Graphene bentonite supported ZnFe₂O₄ as super-paramagnetic photocatalyst for antibiotic degradation. *Adv Mater Lett* 8(3):229–238. <https://doi.org/10.5185/amlett.2017.1467>
- Singh P, Shandilya P, Raizada P, Sudhaik A, Rahmani-Sani A, Hosseini-Bandegharai A (2018) Review on various strategies for enhancing photocatalytic activity of graphene based nanocomposites for water purification. *Arab J Chem* 13:3498–3520. <https://doi.org/10.1016/j.arabjc.2018.12.001>
- Singh P, Raizada P, Sudhaik A, Shandilya P, Thakur P, Agarwal S, Gupta VK (2019a) Enhanced photocatalytic activity and stability of AgBr/BiOBr/graphene heterojunction for phenol degradation under visible light. *J Saudi Chem Soc* 23(5):586–599. <https://doi.org/10.1016/j.jscs.2018.10.005>
- Singh P, Sharma K, Hasija V, Sharma V, Sharma S, Raizada P, Thakur VK (2019b) Systematic review on applicability of magnetic iron oxides–integrated photocatalysts for degradation of organic pollutants in water. *Mater Today Chem* 14:100–186. <https://doi.org/10.1016/j.mtchem.2019.08.005>
- Sonu DV, Sharma S, Raizada P, Bandegharai AH, Gupta VK, Singh P (2019) Review on augmentation in photocatalytic activity of CoFe₂O₄ via heterojunction formation for photocatalysis of organic pollutants in water. *J Saudi Chem Soc* 23(8):1119–1136. <https://doi.org/10.1016/j.jscs.2019.07.003>
- Sudhaik A, Raizada P, Shandilya P, Singh P (2018a) Magnetically recoverable graphitic carbon nitride and NiFe₂O₄ based magnetic photocatalyst for degradation of oxytetracycline antibiotic in simulated wastewater under solar light. *J Environ Chem Eng* 6(4):3874–3883. <https://doi.org/10.1016/j.jece.2018.05.039>
- Sudhaik A, Raizada P, Shandilya P, Jeong DY, Lim JH, Singh P (2018b) Review on fabrication of graphitic carbon nitride based efficient nanocomposites for photodegradation of aqueous phase organic pollutants. *J Ind Eng Chem* 67:28–51. <https://doi.org/10.1016/j.jiec.2018.07.007>
- Sun YP, Zhou B, Lin Y, Wang W, Fernando KS, Pathak P, Meziari MJ, Harruff BA, Wang X, Wang H, Luo PG (2006) Quantum-sized carbon dots for bright and colourful photoluminescence. *J Am Chem Soc* 128(24):7756–7757. <https://doi.org/10.1021/ja062677d>

- Tang L, Ji R, Cao X, Lin J, Jiang H, Li X, Teng KS, Luk CM, Zeng S, Hao J, Lau SP (2012) Deep ultraviolet photoluminescence of water-soluble self-passivated graphene quantum dots. *ACS Nano* 6(6):5102–5110. <https://doi.org/10.1021/nn300760g>
- Terrones M, Botello-Méndez AR, Campos-Delgado J, Lopez-Urias F, Vega-Cantú YI, Rodríguez-Macías FJ, Elías AL, Muñoz-Sandoval E, Cano-Márquez AG, Charlier JC, Terrones H (2010) Graphene and graphite nanoribbons: morphology, properties, synthesis, defects and applications. *Nano Today* 5(4):351–372. <https://doi.org/10.1016/j.nantod.2010.06.010>
- Tian J, Zhao Z, Kumar A, Boughton RI, Liu H (2014) Recent progress in design, synthesis, and applications of one-dimensional TiO₂ nanostructured surface heterostructures: a review. *Chem Soc Rev* 43(20):6920–6937. <https://doi.org/10.1039/C4CS00180J>
- Umrao S, Jang MH, Oh JH, Kim G, Sahoo S, Cho YH, Srivastva A, Oh IK (2015) Microwave bottom-up route for size-tunable and switchable photoluminescent graphene quantum dots using acetylacetone: new platform for enzyme-free detection of hydrogen peroxide. *Carbon* 81:514–524. <https://doi.org/10.1016/j.carbon.2014.09.084>
- Valappil MO, Anil A, Shaijumon M, Pillai VK, Alwarappan S (2017) A single-step electrochemical synthesis of luminescent WS₂ quantum dots. *Chem Eur J* 23(38):9144–9148. <https://doi.org/10.1002/chem.201701277>
- Wang X, Cao L, Lu F, Meziani MJ, Li H, Qi G, Zhou B, Harruff BA, Kermarrec F, Sun YP (2009) Photoinduced electron transfers with carbon dots. *Chem Commun* 25:3774–3776. <https://doi.org/10.1039/B906252A>
- Wang F, Pang S, Wang L, Li Q, Kreiter M, Liu CY (2010) One-step synthesis of highly luminescent carbon dots in noncoordinating solvents. *Chem Mater* 22(16):4528–4530. <https://doi.org/10.1021/cm101350u>
- Wang F, Xie Z, Zhang H, Liu CY, Zhang YG (2011) Highly luminescent organosilane-functionalized carbon dots. *Adv Funct Mater* 21(6):1027–1031. <https://doi.org/10.1021/cm101350u>
- Wang W, Ni Y, Xu Z (2015) One-step uniformly hybrid carbon quantum dots with high-reactive TiO₂ for photocatalytic application. *J Alloys Compd* 622:303–308. <https://doi.org/10.1016/j.jallcom.2014.10.076>
- Wang F, Chen P, Feng Y, Xie Z, Liu Y, Su Y, Zhang Q, Wang Y, Yao K, Lv W, Liu G (2017) Facile synthesis of N-doped carbon dots/g-C₃N₄ photocatalyst with enhanced visible-light photocatalytic activity for the degradation of indomethacin. *Appl Catal B Environ* 207:103–113. <https://doi.org/10.1016/j.apcatb.2017.02.024>
- Wang J, Tang L, Zeng G, Deng Y, Dong H, Liu Y, Wang L, Peng B, Zhang C, Chen F (2018a) 0D/2D interface engineering of carbon quantum dots modified Bi₂WO₆ ultrathin nanosheets with enhanced photoactivity for full spectrum light utilization and mechanism insight. *Appl Catal B Environ* 222:115–123. <https://doi.org/10.1016/j.apcatb.2017.10.014>
- Wang Y, Chang X, Jing N, Zhang Y (2018b) Hydrothermal synthesis of carbon quantum dots as fluorescent probes for the sensitive and rapid detection of picric acid. *Anal Methods* 10(23):2775–2784. <https://doi.org/10.1039/C8AY00441B>
- Wu G, Nishikawa T, Ohtani B, Chen A (2007) Synthesis and characterization of carbon-doped TiO₂ nanostructures with enhanced visible light response. *Chem Mater* 19(18):4530–4537. <https://doi.org/10.1021/cm071244m>
- Wu ZL, Zhang P, Gao MX, Liu CF, Wang W, Leng F, Huang CZ (2013) One-pot hydrothermal synthesis of highly luminescent nitrogen-doped amphoteric carbon dots for bioimaging from bombyx mori silk–natural proteins. *J Mater Chem B* 1(22):2868–2873. <https://doi.org/10.1039/C3TB20418A>
- Xiao J, Liu P, Wang CX, Yang GW (2017) External field-assisted laser ablation in liquid: an efficient strategy for nanocrystal synthesis and nanostructure assembly. *Prog Mater Sci* 87:140–220. <https://doi.org/10.1016/j.pmatsci.2017.02.004>
- Xie Z, Feng Y, Wang F, Chen D, Zhang Q, Zeng Y, Lv W, Liu G (2018) Construction of carbon dots modified MoO₃/g-C₃N₄ Z-scheme photocatalyst with enhanced visible-light photocatalytic

- activity for the degradation of tetracycline. *Appl Catal B Environ* 229:96–104. <https://doi.org/10.1016/j.apcatb.2018.02.011>
- Xu X, Ray R, Gu Y, Ploehn HJ, Gearheart L, Raker K, Scrivens WA (2004) Electrophoretic analysis and purification of fluorescent single-walled carbon nanotube fragments. *J Am Chem Soc* 126(40):12736–12737. <https://doi.org/10.1021/ja040082h>
- Xu M, Deng G, Liu S, Chen S, Cui D, Yang L, Wang Q (2010) Free cadmium ions released from CdTe-based nanoparticles and their cytotoxicity on *phaeodactylum tricornutum*. *Metallomics* 2 (7):469–473. <https://doi.org/10.1039/C005387M>
- Yang Y, Wu D, Han S, Hu P, Liu R (2013a) Bottom-up fabrication of photoluminescent carbon dots with uniform morphology via a soft-hard template approach. *Chem Commun* 49 (43):4920–4922. <https://doi.org/10.1039/C3CC38815H>
- Yang Z, Li Z, Xu M, Ma Y, Zhang J, Su Y, Gao F, Wei H, Zhang L (2013b) Controllable synthesis of fluorescent carbon dots and their detection application as nanoprobes. *Nano-Micro Lett* 5 (4):247–259. <https://doi.org/10.1007/BF03353756>
- Yang P, Zhu Z, Chen M, Chen W, Zhou X (2018) Microwave-assisted synthesis of xylan-derived carbon quantum dots for tetracycline sensing. *Opt Mater* 85:329–336. <https://doi.org/10.1016/j.optmat.2018.06.034>
- Yu H, Zhang H, Huang H, Liu Y, Li H, Ming H, Kang Z (2012) ZnO/carbon quantum dots nanocomposites: one-step fabrication and superior photocatalytic ability for toxic gas degradation under visible light at room temperature. *New J Chem* 36(4):1031–1035. <https://doi.org/10.1039/C2NJ20959D>
- Yuan F, Li S, Fan Z, Meng X, Fan L, Yang S (2016) Shining carbon dots: synthesis and biomedical and optoelectronic applications. *Nano Today* 11(5):565–586. <https://doi.org/10.1016/j.nantod.2016.08.006>
- Zhang YQ, Ma DK, Zhang YG, Chen W, Huang SM (2013) N-doped carbon quantum dots for TiO₂-based photocatalysts and dye-sensitized solar cells. *Nano Energy* 2(5):545–552. <https://doi.org/10.1016/j.nanoen.2013.07.010>
- Zhang H, Zhao L, Geng F, Guo LH, Wan B, Yang Y (2016) Carbon dots decorated graphitic carbon nitride as an efficient metal-free photocatalyst for phenol degradation. *Appl Catal B Environ* 180:656–662. <https://doi.org/10.1016/j.apcatb.2015.06.056>
- Zhang Z, Zheng T, Xu J, Zeng H, Zhang N (2017) Carbon quantum Dots/Bi₂WO₆ composites for efficient photocatalytic pollutant degradation and hydrogen evolution. *Nano* 12(07):1750082. <https://doi.org/10.1142/S1793292017500825>
- Zhang Q, Chen P, Zhuo M, Wang F, Su Y, Chen T, Yao K, Cai Z, Lv W, Liu G (2018) Degradation of indometacin by simulated sunlight activated CDs-loaded BiPO₄ photocatalyst: roles of oxidative species. *Appl Catal B Environ* 221:129–139. <https://doi.org/10.1016/j.apcatb.2017.09.008>
- Zhou J, Sheng Z, Han H, Zou M, Li C (2012a) Facile synthesis of fluorescent carbon dots using watermelon peel as a carbon source. *Mater Lett* 66(1):222–224. <https://doi.org/10.1016/j.matlet.2011.08.081>
- Zhou L, Lin Y, Huang Z, Ren J, Qu X (2012b) Carbon nanodots as fluorescence probes for rapid, sensitive, and label-free detection of Hg²⁺ and biothiols in complex matrices. *Chem Commun* 48 (8):1147–1149. <https://doi.org/10.1039/C2CC16791C>
- Zhu H, Wang X, Li Y, Wang Z, Yang F, Yang X (2009) Microwave synthesis of fluorescent carbon nanoparticles with electrochemiluminescence properties. *Chem Commun* 34:5118–5120. <https://doi.org/10.1039/B907612C>
- Zhu Y, Murali S, Cai W, Li X, Suk JW, Potts JR, Ruoff RS (2010) Graphene and graphene oxide: synthesis, properties, and applications. *Adv Mater* 22(35):3906–3924. <https://doi.org/10.1002/adma.201001068>
- Zhu C, Yang S, Wang G, Mo R, He P, Sun J, Di Z, Kang Z, Yuan N, Ding J, Ding G (2015) A new mild, clean and highly efficient method for the preparation of graphene quantum dots without by-products. *J Mater Chem B* 3(34):6871–6876. <https://doi.org/10.1039/C5TB01093D>

- Zhu S, Li D, Wang D (2017) Photocatalysis: basic principles, diverse forms of implementations and emerging scientific opportunities. *Adv Energy Mater* 7(23):1700841. <https://doi.org/10.1002/aenm.201700841>
- Zong J, Zhu Y, Yang X, Shen J, Li C (2011) Synthesis of photoluminescent carbogenic dots using mesoporous silica spheres as nanoreactors. *Chem Commun* 47(2):764–766. <https://doi.org/10.1039/C0CC03092A>
- Zuo P, Lu X, Sun Z, Guo Y, He H (2016) A review on syntheses, properties, characterization and bioanalytical applications of fluorescent carbon dots. *Microchim Acta* 183(2):519–542. <https://doi.org/10.1007/s00604-015-1705-3>

Chapter 4

Photocatalytic Degradation of Azo Dyes in Water



Pooja Shandilya, Pankaj Raizada, and Pardeep Singh

Contents

| | |
|--|-----|
| 4.1 Introduction | 120 |
| 4.2 Binary Photocatalyst for Azo Dye Degradation | 125 |
| 4.3 Ternary Photocatalyst for Azo Dye Degradation | 130 |
| 4.4 Coupled Semiconductor for Azo Dye Degradation | 133 |
| 4.5 Carbon-Supported Photocatalyst for Azo Dye Degradation | 135 |
| 4.6 Others | 137 |
| 4.7 Conclusion | 139 |
| References | 140 |

Abstract Photocatalysis is an emerging method toward wastewater treatment as it needs just an appropriate amount of photocatalyst and renewable solar energy. Water pollution due to continuous dispense of hazardous industrial effluents into the water badly damages the quality of water and poses an utmost threat to the environment. Degrading industrial pollutant into non-toxic compounds by advanced oxidation method has attracted the scientific community. Degradation of a nonbiodegradable azo dyes used in textile, printing, leather, and food industries, by heterogeneous photocatalysis is utmost needed. By the virtue of excellent optical, electronic, efficient light harvesting, tunable photoluminescence, and upconversion property of carbonaceous material, its usage as photocatalytic material is more advantageous. Carbon material displayed extensive application in various fields like drug delivery, photocatalysis, optoelectronics devices, and photovoltaic.

We reviewed various binary, ternary, coupled, and carbon-supported photocatalytic systems for the removal of azo dye, as well as other reported systems adopted for azo dye removal. This book chapter concisely comprises the basic

P. Shandilya · P. Raizada · P. Singh (✉)

School of Chemistry, Faculty of Basic Sciences, Shoolini University, Solan, HP, India

Himalayan Centre for Excellence in Nanotechnology, Shoolini University, Solan, HP, India

School of Biological Sciences, Faculty of Basic Sciences, Shoolini University, Solan, HP, India

© The Editor(s) (if applicable) and The Author(s), under exclusive license to Springer Nature Switzerland AG 2021

Inamuddin et al. (eds.), *Water Pollution and Remediation: Photocatalysis*,

Environmental Chemistry for a Sustainable World 57,

https://doi.org/10.1007/978-3-030-54723-3_4

mechanism of photocatalysis, disadvantages of conventional methods of water purification, and general classification of azo dyes. Significantly, immobilizing bare metal oxide nanoparticles on the surface of certain carbonaceous support will stabilize the nanoparticles and prevent leaching of nanoparticles into the water bodies and also slow the electron–hole pair recombination. Also, the band edge position of two combining semiconductors is an important aspect for the fabrication of visible light-driven photocatalyst. The fabricated heterojunction may also utilize the special phenomena of upconversion where, the light of longer wavelength emits the light of shorter wavelength which is useful for wide band gap semiconductor to be utilized as photocatalyst. Lastly, conclusion and future perspective which opens up the area for further research to be carried out for constructing photocatalytic system that can be widely applied for various pollutants were considered and hypothesized.

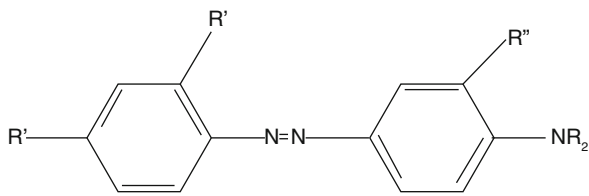
Keywords Azo dye · Heterogeneous photocatalysis · Z-scheme photocatalyst · Carbonaceous nanocomposites · Photodegradation

4.1 Introduction

The continuous dispense of hazardous organic dye into water bodies from textile, printing, food, and cosmetic industries poses an utmost threat to the environment (Singh et al. 2017, 2018; Priya et al. 2016; Raizada et al. 2017, 2018, 2019a). The effluents from the industries are major pollutant which damages the quality of water. Although physisorption, coagulation and membrane filtration are the conventional methods reported for azo dye degradation, none of them are efficient which can remove the pollutant fully from the water (Singh et al. 2013a, b; Pare et al. 2008b). Among various conventional techniques, chemical oxidation method utilizing advanced oxidation method has earned considerable attention due to the conversion of toxic pollutant into innocuous product (Kumar et al. 2019a, b; Gautam et al. 2017; Singh et al. 2019b). Heterogeneous photocatalysis has emerged as green and advanced oxidation method for the elimination of various pollutants from water bodies (Blake 2001; Sudhaik et al. 2018a; Hasija et al. 2019a; Raizada et al. 2019c).

In heterogeneous photocatalysis, metal oxide semiconductor is suspended in different phase in aqueous medium which is easy to separate from reaction medium (Hasija et al. 2019b). An ample of photocatalyst have already been reported till date and utilized in various fields; among them wastewater treatment is the exigently required field to be explored (Raizada et al. 2014a, b, 2016, 2019b; Sudhaik et al. 2018b). Water pollution is caused by many pollutants like pesticides, heavy metal ions, microbial pollution, and pollution due to azo dyes. Among these, pollution due to azo dyes is our major concern as azo dyes are nonbiodegradable due to complex structure and major constituent of industrial wastewater which continuously

Fig. 4.1 General chemical structure of azo dyes with azo (-N=N-) bond having different R' and R'' group



Where, R' = NO₂, CN (Acceptor)

R'' = OH, NHR, NR₂ (Donor)

discharge into water bodies without treatment thereby causing major threat to the environment (Jamwal et al. 2015; Pare et al. 2009a; Gautam et al. 2016; Raizada et al. 2017).

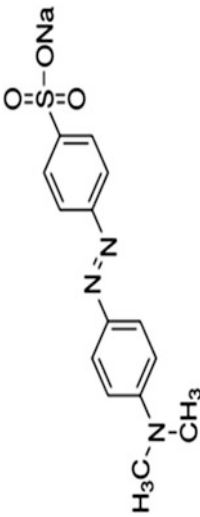
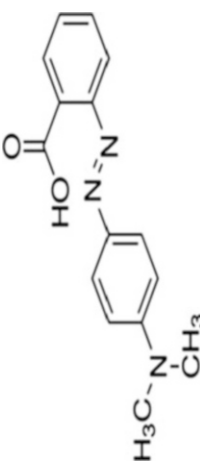
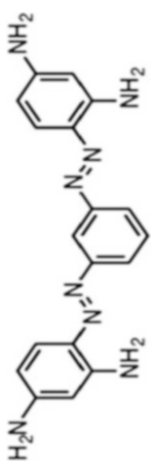
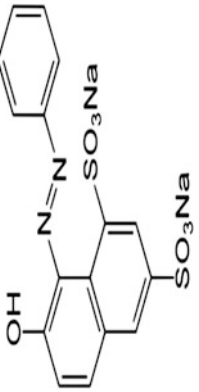
Azo dye is the most excessively used commercially dye synthesized by diazotization reaction of aromatic amine with subsequent coupling reaction between phenol and N-alkylated aromatic amine (Pare et al. 2009b). The largest group of synthetic dye containing aromatic ring structure with azo (N=N) functional group which is highly stable are called azo dyes, the basic structure of azo dyes (Fig. 4.1). Various synthetic dyes had a wide application in textile, printing, leather, and food industries. These dyes adversely affect the environment and also disturb the balanced between the ecosystems (Pare et al. 2008a). Dyes are carcinogenic in nature and harmful to the aquatic animals and also prevent penetration of light inside the water bodies and hamper photochemical activity. Some of the azo dye are listed in Table 4.1.

Overthrow, many attempts have been done to remove azo dyes through physical adsorption (Meshko et al. 2001; Amin 2009), biological method (Razo et al. 1997; Laszlo 2000; Kalme et al. 2007), photocatalytic method (Vinodgopal and Kamat 1995; Lachheb et al. 2002; Konstantinou and Albanis 2004), and degradation using zero-valent metals (Shu et al. 2007; Cao et al. 1999). These all methods have certain limitation and do not fully resolve the problem. The usage of zero-valent metal suffers rapid corrosion in water. Degradation via biological method does not have considerable efficiency and difficult to control in an aquatic environment contacting hazardous chemicals. Among these degradation methods of azo dyes considerable attention acquire by photocatalytic method as it is green method, low cost, have high degradation capability, and can be implemented on large scale (Tang et al. 2017). The process of photocatalysis primarily depends on the production of reactive oxidation species which mineralizes the pollutants through redox reactions. The major interest of the scientist is to develop a hybrid nanocomposites that are highly efficient and can be utilized in a broader area.

Photocatalysis is one of the green techniques which discples solar energy into chemical energy for sustainable energy generation (Chandel et al. 2019). Though, the basic mechanism behind the photocatalyst was very well understood and explored. Figure 4.2 depicts the mechanistic view of photocatalysis which generally involve four steps: (i) photo-generation of electron-hole pair, (ii) migration of electron from valence band to conduction band, (iii) occurrence of redox reaction

Table 4.1 Some of the common azo dye structure and characteristics

| S. No. | Common name | IUPAC name | Chemical Structure | Molecular formula | Molecular weight |
|--------|--------------------|---|---|--|------------------|
| 1 | Reactive orange 16 | Disodium;6-acetamido-4-hydroxy-3-[[4-(2 sulfonatoxyethylsulfonyl)phenyl]diazeny]naphthalene-2-sulfonate | <p style="text-align: center;">$\text{NaO}_3\text{SOCH}_2\text{CH}_2\text{CO}_2\text{S}$</p> | $\text{C}_{20}\text{H}_{17}\text{N}_3\text{Na}_2\text{O}_{11}\text{S}_3$ | 617.5 g/mol |
| 2 | Congo red | Disodium;4-amino-3-[[4-[4-(1-amino-4-sulfonatophthalen-2-yl)diazeny]phenyl]phenyl]diazeny]naphthalene-1-sulfonate | | $\text{C}_{32}\text{H}_{22}\text{N}_6\text{Na}_2\text{O}_6\text{S}_2$ | 696.7 g/mol |
| 3 | Acid orange 7 | Sodium;4-[(2-hydroxynaphthalen-1-yl)diazeny]benzenesulfonate | | $\text{C}_{16}\text{H}_{11}\text{N}_2\text{NaO}_4\text{S}$ | 350.3 g/mol |

| | | | | | |
|---|------------------|---|--|-----------------------------|-------------|
| 4 | Methyl Orange | Sodium;4-[[4-(dimethylamino)phenyl]diazenyl]benzenesulfonate |  | $C_{14}H_{14}N_3NaO_3S$ | 327.3 g/mol |
| 5 | Methyl red | 2-[[4-(dimethylamino)phenyl]diazenyl]benzoic acid |  | $C_{15}H_{15}N_3O_2$ | 269.3 g/mol |
| 6 | Bismarck brown Y | 4-[[3-[(2,4-diaminophenyl)diazenyl]phenyl]diazenyl]benzene-1,3-diamine; dihydrochloride |  | $C_{18}H_{20}Cl_2N_8$ | 419.3 g/mol |
| 7 | Orange G | Disodium;7-hydroxy-8-phenyldiazenyl)naphthalene-1,3-disulfonate |  | $C_{16}H_{10}N_2Na_2O_7S_2$ | 452.4 g/mol |

(continued)

Table 4.1 (continued)

| S. No. | Common name | IUPAC name | Chemical Structure | Molecular formula | Molecular weight |
|--------|--------------|---|--------------------|----------------------|------------------|
| 8. | Rhodamine 6B | 4-carboxy-3-[3-(dimethylamino)-6-dimethylazaniumylidenexanthene-9-yl]benzoate | | $C_{25}H_{22}N_2O_5$ | 430.5 g/mol |

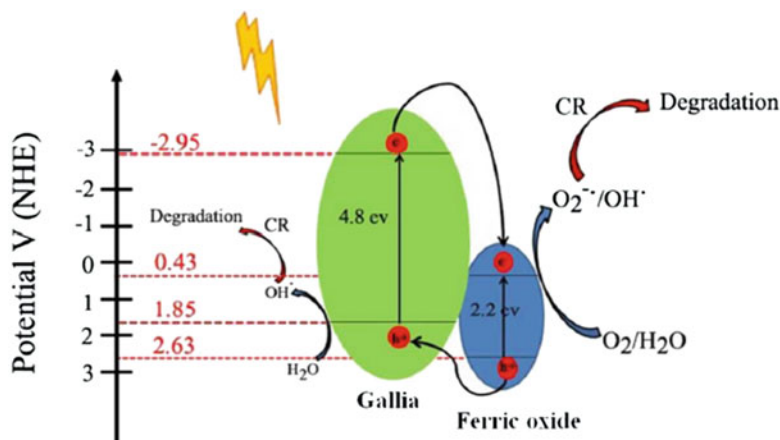


Fig. 4.2 Possible mechanism for congo red dye degradation by $\text{Fe}_2\text{O}_3\text{-Ga}_2\text{O}_3$ nanostructure under ultraviolet light irradiation, which generates reactive oxidation species like hydroxyl radical (OH^\cdot) and superoxide radical ($\text{O}_2^{\cdot-}$) that are responsible for the photodegradation of congo red dye (Reprinted with permission from Bagheri and Mahjoub (2016) copyright@2016, The Royal Society of Chemistry)

on the respective bands to generate reactive oxidation species, and (iv) recombination of electron–hole pair. Further, these generate reactive oxidation species assist in mineralization of pollutant.

Z-scheme photocatalyst is more advantageous as compared to simple binary metal oxide photocatalyst as it can efficiently harvest the solar light, separate the electron–hole pair, and conserve the reductive and oxidative ability of charge carrier (Xu et al. 2018). In Z-scheme heterojunction, electrons migrate from higher conduction band to the lower conduction band of another semiconductor. However, holes follow the reverse movement, and thus, electrons accumulate on one semiconductor for reduction, and holes accumulate on other for oxidation reaction to be carried out. Another photodegradation mechanism involves transfer of electrons from conduction band of semiconductor via metal as mediator toward the valence band of another semiconductor as shown in Fig. 4.3.

4.2 Binary Photocatalyst for Azo Dye Degradation

The photocatalysis catalyzed by metal oxide is extensively explored at laboratory scale. Some of the metal oxide photocatalyst explored till date are TiO_2 , V_2O_5 , MoO_3 , MnO_2 , Mn_3O_4 , Fe_3O_4 , RuO_2 , Co_3O_4 , Nb_2O_5 , ZrO_2 , Co_3O_4 , CuO , CdS , SiO_2 , and IrO_2 . Konstantinou and Albanis (2004) discussed effective degradation of azo dyes having different chemical groups via TiO_2 suspensions under ultraviolet visible or solar light. The kinetics of photocatalytic oxidation were explored, and Langmuir–Hinshelwood model has been followed for kinetics study (Konstantinou

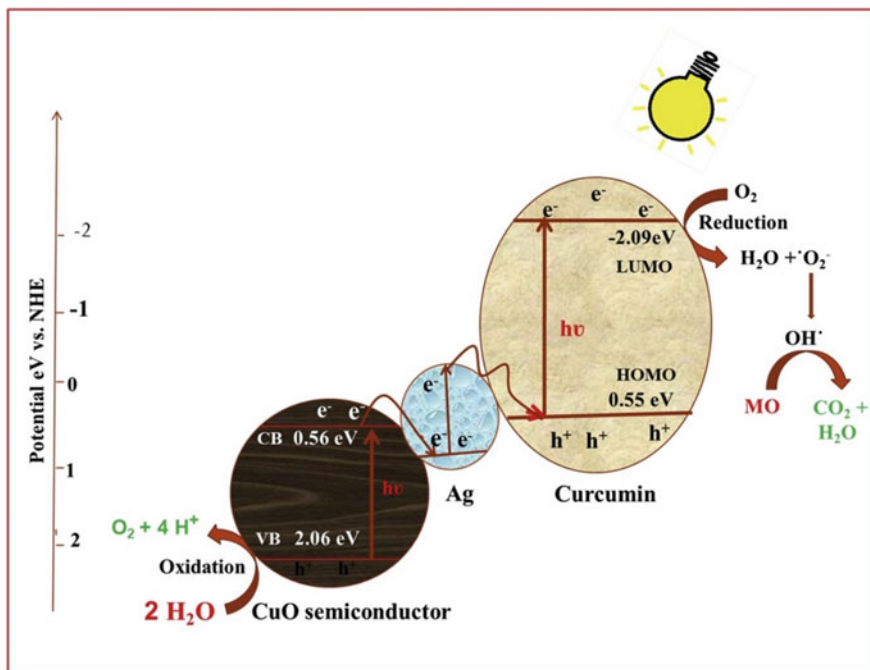


Fig. 4.3 Proposed Z-Scheme mechanism of the photocatalytic process involved in the degradation of methyl orange by curcumin-coupled CuO/Ag photocatalyst highest occupied molecular orbital (HOMO) and lowest unoccupied molecular orbital (LUMO), Here, Ag act as electron mediator and transfer conduction band electron of CuO semiconductor to valence band of curcumin, and as a result, holes in the valence band of CuO semiconductor and electrons in the conduction band of curcumin are only responsible for oxidation and reduction of methyl orange (Reprinted with permission from Kumar et al. (2019a, b) copyright@2019, Elsevier B.V. All rights reserved)

and Albanis 2004). Many factors like concentration of dye, amount of catalyst, absorption wavelength, addition of oxidants, and occurrence of humic substances or inorganic ions are responsible for altering kinetic study.

Photocatalytic degradation of azo dyes mostly depends upon observing chemical oxygen demand and decolorization of dye solution. In monoazo dyes, acid orange 7 was discussed, which is the most explored compound among azo dyes with its photodegradation ability under several parameters (Stylidi et al. 2003; Chen et al. 2001). Acid orange 7 is a targeted pollutant for oxidative removal of azo dyes, and it was specified that benzenesulfonate and naphthoquinone are the chief degradation products. For the degradation of di and triazo dyes, same conclusion was attained, and occurrence of phenol and 4-nitro-2-hydroxyphenol was inspected as intermediates (Grzechulska and Morawski 2002; Tanaka et al. 2000; Sauer et al. 2002).

The photodecomposition of azo dyes via TiO_2 modified with transition element also reported and found highly efficient (Rauf et al. 2011). On the basis of the reaction, it was discovered that molecular oxygen and other reactive species ($\text{O}_2^{\bullet-}$,

HO_2^* , H_2O_2 , OH^* and HO_2^{*-}) play significant role. These species make photodegradation processes more effective by increasing dye removal through the production of various intermediates like aromatic amines, phenolic compounds, and different organic acids. On the basis of azo dye structure, hydroxylated derivatives, aromatic amines, naphthoquinone, phenolic compounds, and several organic acids are chief intermediates formed during degradation reaction.

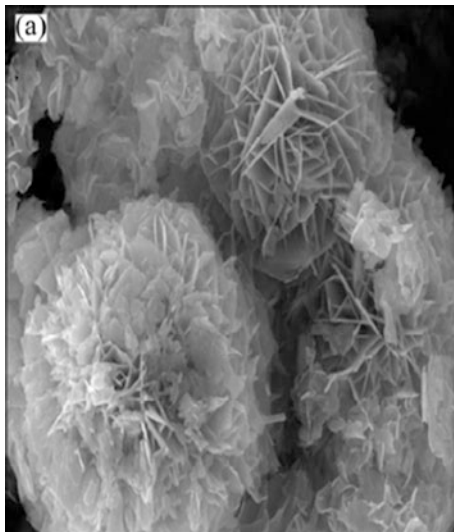
The usage of nanosized magnetic Fe_3O_4 photocatalyst via sonochemical method was also employed for degradation of azo dyes, methyl red, and congo red, respectively (Solomon et al. 2012). The synthesized photocatalyst is a novel photocatalyst due to its facile separation by the virtue of its magnetic property and good recyclability. Besides these good properties, it is cost-effective, non-toxic, and noncarcinogenic in nature. A detailed study on the degradation of azo dyes at different pH and concentrations of photocatalyst, dye, and hydrogen peroxide was revealed. The results indicate that photodegradation increases as the photocatalyst quantity increased and reached a peak value followed by substantial decreases due to enhancement in suspension opacity, diminished radiation invasion, high scattering of light, and availability of low surface area of nanoparticles due to aggregation. Due to agglomeration of photocatalyst, the photo-activated volume of suspension shortens (Konstantinou and Albanis 2004). Langmuir–Hinshelwood kinetic analysis was used to analyze the kinetics of reaction which follows pseudo-first-order reaction for the photodegradation of pollutant. The successive order of degradation is: Photo- $\text{Fe}_3\text{O}_4 > \text{Photo-H}_2\text{O}_2 > \text{Fe}_3\text{O}_4 > \text{H}_2\text{O}_2$.

Al-Anbari et al. (2016) synthesized Fe_3O_4 and used for the eradication/decolorization of red azo dye from simulated wastewater. To eliminate azo dye, various parameters like concentration, pH, photocatalyst dose, and H_2O_2 concentration have been employed, and all these features were assessed to find the optimal operation situations. Furthermore, pH, oxidation reduction potential, and electrical conductivity of solution were scrutinized to evaluate dye degradation. From the investigational findings, it was noticed that the optimal pH value for Fe_3O_4 was 6.5, and catalyst dose was 300 mg/L, respectively. Moreover, the most influential concentration of H_2O_2 was 200 mg/L for Fe_3O_4 . The co-workers have employed response surface methodology, a mathematical model which explains photodegradation process. From the results, it was concluded that Fe_3O_4 displayed approx. 85.51% degradation efficacy of reactive red dye under solar light illumination.

Manivel et al. (2015) fabricated one-dimensional molybdenum trioxide (MoO_3) nanoparticles for the degradation of azo dye via catalytic ozonation. The thermal, microwave, and sonochemical method were used to fabricate MoO_3 nanoparticles. The sonochemical synthetic route was considered as the most reliable method among all due to well dispersion of fine MoO_3 nanoparticles, and total dye removal was observed within 20 min.

Chen (2009) analyzed the degradation of reactive orange 16 one of the earliest nonbiodegradable azo dyes known since 1863. Almost 100% of dye is mineralized in 80 min by employing TiO_2 under ultraviolet light and obeys the condition of first-order reactions. The analysis of mineralized product was carried out using gas chromatography–mass spectroscopy. The fragmentation may be due to the breaking

Fig. 4.4 Scanning electron microscopy image of Bi_2S_3 microspheres indicates a flower-like morphology of photocatalyst obtained at 120°C temperature for hydrothermal reaction (Reprinted with permission from Zhao et al. in (2018) copyright@2018, The Nonferrous Metals Society of China. Published by Elsevier Ltd. All rights reserved)



of C–S, C–N, C–C, N–N bond. Lachheb et al. in (2002) employed TiO_2 nanoparticles under ultraviolet light and explored the degradation of methyl red, congo red, and crocein orange G azo dye. The photodegradation started with the evolution of di-nitrogen gas from azo group, and the aromatic ring is subsequently attacked by reactive oxidation species followed by ring cleavage followed by the evolution of CO_2 gas.

Moreover, Konstantinou and Albanis in (2004) reviewed photodegradation of azo dye using TiO_2 under visible and ultraviolet light separately and follows pseudo-first-order kinetics. The pH of solution, concentration of catalyst, and dye decide the extent of degradation of azo dyes. The various intermediates are formed during the mineralization which finally converts into aliphatic acid. Zhao et al. in (2018) prepared flower like Bi_2S_3 microsphere by urea-assisted solvothermal method at 120°C (Fig. 4.4). The photocatalytic activity was assessed against methyl orange underneath visible irradiation. Nearly 91% of methyl orange was degraded in less than 180 min. Bi_2S_3 is a narrow band gap semiconductor of 1.3 eV with high absorption range.

These binary photocatalysts were applied in suspension form for wastewater treatment, which is very difficult to recover and recycle at large scale. Moreover, being large band gap semiconductor application limits to ultra-violet region, which comprise of only 5% of solar spectrum. The major part of solar light about 45% comprise of visible region and about 50% of near infrared region. Therefore, the major concern is to construct a photocatalyst which is active under visible and infrared region (Sonu et al. 2019). While majority of research has been focused on exploring visible light active photocatalyst, only few near-infrared active semiconductor $\text{Cu}_2(\text{OH})\text{PO}_4$, BiWO_6 , and WS_2 has also been reported (Wang et al. 2013; Tian et al. 2013; Sang et al. 2015).

To construct an innovative photocatalyst which is competent of utilizing the whole solar spectrum is still challenging and extremely needed. Though, a visible light-driven photocatalyst were available for the removal of dyes, yet experiencing a challenges of high rate charge carrier recombination (Pingmuang et al. 2017; Wang et al. 2018). The rate of recombination permits only handful of charge carrier to migrate toward the surface and carry out the process of photocatalysis that retards the productivity of photocatalyst. Therefore, the better way is either immobilized the binary metal oxide on the surface as thin films support or we may use magnetic metal oxide-based nanocomposites that can be recovered easily from the system so as to maintain the quality of treated water. While using iron-based magnetic nanocomposites, a lot of iron sludge was generated which produces secondary pollutant (Sharma et al. 2019a, b).

Spinel cobalt oxide (Co_3O_4) anchored on support carbon spheres has been synthesized via precipitation deposition and wet impregnation method. The synthesized Co_3O_4 are evenly distributed on the surface of carbon spheres as justified from the transmission electron microscopy image results. The obtained photocatalyst degraded 91% methyl orange dye in 10 min of reaction time with outstanding reproducibility (Dou et al. 2016). Heterojunction has proven to be an effective strategy to enhance the photocatalytic degradation efficiency. Han and co-workers fabricated graphitic carbon nitride coupled with Co_3O_4 using an easy and economical mixing–heating of precursors melamine and $\text{Co}(\text{NO}_3)_2$. The mechanistic insight for photodegrading methyl orange dye involves $\text{O}_2^{\cdot-}$ as the key reactive oxidation species as confirmed from electron spin resonance results. With the increase in concentration of Co_3O_4 , shielding of reactive sites with a reduction in absorption of light through solution was observed. Therefore, after optimization of Co_3O_4 concentration, it was found that 0.2% of Co_3O_4 significantly leads to complete mineralization of methyl orange within 10 min of solar light radiation (Han et al. 2014).

Other than simple metal oxide, photocatalytic activity of coupled semiconductor was also keep on exploring since 1995 and till date. Xing et al. (2008) prepared a coupled heterostructure niobium pentoxide $\text{Nb}_2\text{O}_5/\text{SrNb}_2\text{O}_6$ via ball milling and annealing at 600 °C. A comparative study is executed for TiO_2 which showed 60% degradation of methyl orange dye, whereas the obtained heterostructure $\text{Nb}_2\text{O}_5/\text{SrNb}_2\text{O}_6$ resulted in 92% removal of dye within 30 min of solar irradiation (Xing et al. 2008). Photocatalytic elimination of toxic water soluble; ponceau S dye is carried out via Nb_2O_5 in suspension of carbon which acts as coadsorbent. Here, researchers have focused on the pH dependence degradation of ponceau S dye which increases a maximum to 86.2% at pH 8 (Patil et al. 2011). Ibrahim et al. fabricated nanosized ZrO_2 photocatalyst using various organic acid precursors (maleic, oxalic, citric, malic, malonic, tartaric, and succinic acids (Ibrahim et al. 2016)). The results demonstrated tremendous ability to degrade 100% orange G dye in 180 min, with $\text{O}_2^{\cdot-}$ as main reactive oxidation species (Ibrahim et al. 2016).

CuO is one of the frequently used semiconductors utilized in photocatalysis due to its easy construction, precise 1.2 eV band gap, and varied appliance (Kumar et al. 2019a, b). A recent research based on the green preparation of curcumin-coupled

CuO/Ag photocatalyst involving precipitation of spherical Ag nanoparticles over needle-shaped CuO and curcumin as the functionalization and reducing agent for aerobic eradication of methyl orange dye. The photodegradation mechanism follows Z-scheme-assisted improved electron–hole pair separation as depicted in Fig. 4.3 which involves transference of electrons from conduction band of CuO semiconductor via Ag mediator valence band of curcumin (Kumar et al. 2019a, b).

In another study, cotton-like CuO microstructures were synthesized by ultrasonic-assisted technique, which showed 95% disintegration of reactive black-5 dye under visible radiation (Rao et al. 2018). The reactive black-5 is extensively utilized in textile industry for coloring the fabrics. The continuous exposure to reactive black-5 may cause allergic or asthma problem. A possible degradation mechanism was confirmed by liquid chromatography–mass spectrometry (Fig. 4.5).

Mandal et al. (2019) fabricated an evenly dispersed Fe_2O_3 on the surface of SiO_2 via a sol–gel process involving 88% congo red dye degradation in 180 min with absorption in the range of 560 nm. SiO_2 decorated with Co core shell have been vulnerably used to degrade congo red and methyl orange. Nearly, 95% methyl orange was degraded, whereas only 82% of congo red dye at 565 nm indicating the complexity due to the presence of two ($-\text{N}=\text{N}$) which requires large concentration of synthesized photocatalyst for degradation (Zhang et al. 2016). Semiconductor quantum dots have been anchored with cadmium sulfide (CdS) photocatalyst prepared via heat quench treatment for effective removal of methyl orange dye.

Another way is to fabricate a nanoparticles with carbonaceous material as support that can help to solve its leaching problem, lower rate of recombination and make it visible light-active photocatalyst so as to achieve high efficiency for the removal of pollutant and many more. Fabrication of heterojunction depends upon the band edge position of the two combining semiconductors which also assist in upconversion photoluminescence. Heterojunction formation will help to slower down the rate of recombination as charge carrier will spent more time apart, to carry out reduction and oxidation.

4.3 Ternary Photocatalyst for Azo Dye Degradation

Wu et al. (2019) synthesized $\text{ZnO}/\text{Fe}_3\text{O}_4/\text{g}-\text{C}_3\text{N}_4$ ternary nanocomposites which is a visible light-induced and easily recoverable photocatalyst. $\text{ZnO}/\text{Fe}_3\text{O}_4/\text{g}-\text{C}_3\text{N}_4$ were employed for the degradation of monas dye and observed remarkable upgraded in photocatalytic activity of $\text{ZnO}/\text{Fe}_3\text{O}_4/\text{g}-\text{C}_3\text{N}_4$ as compared to pure graphitic carbon nitride and ZnO nanoparticle. Heterojunction of $\text{ZnO}/\text{Fe}_3\text{O}_4/\text{g}-\text{C}_3\text{N}_4$ displayed higher absorption of visible radiation and enhanced charge separation efficiency. The stability experiment exposed that $\text{ZnO}/\text{Fe}_3\text{O}_4/\text{g}-\text{C}_3\text{N}_4$ –50% nanocomposites exhibited comparatively more photodegradation activity after 5 recycles. 97.87%, 98.05%, and 83.35% degradation efficiency was observed for methyl orange, alizarin yellow R, and orange G, respectively via $\text{ZnO}/\text{Fe}_3\text{O}_4/\text{g}-\text{C}_3\text{N}_4$. High

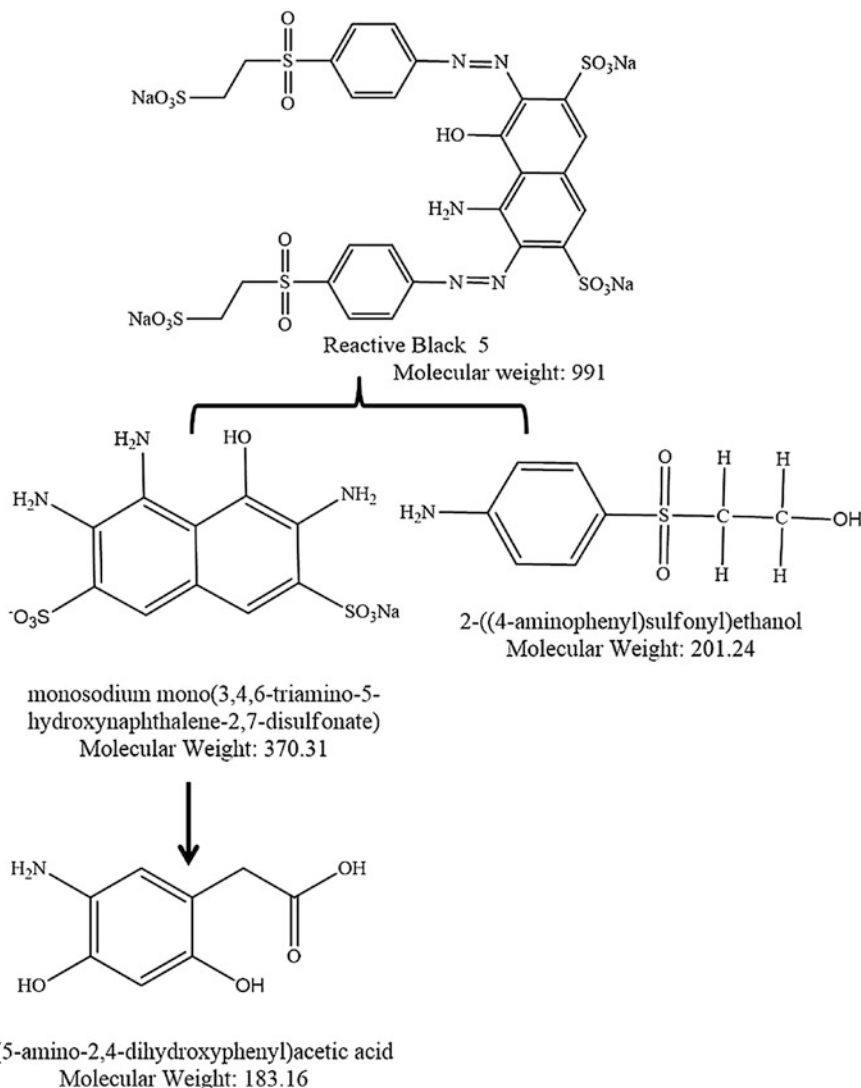


Fig. 4.5 Proposed degradation pathway of reactive black 5 into 2-(5-amino-2,4-dihydroxyphenyl)acetic acid using CuO nanosheets by photocatalytic reaction (Reprinted with permission from Rao et al. (2018) copyright@2018, Elsevier Ltd. All rights reserved)

performance owes to the absorption of number of dye molecules adsorbed on the surface of nanocomposites as well as structure of the azo dye molecule.

Moreover, the presence of Fe₃O₄ considerably enhanced the stability as well as recyclability of nanocomposites. The disintegration pathway of azo dye was mainly superoxide ion dependent. Transmission electron microscopy analysis was used for the evaluation of structure which showed typical hexagonal wurtzite structure of

pure ZnO and layered platelet-like thinner sheets having smooth morphology of g-C₃N₄ analogous to arrangement of graphene sheets (Bian et al. 2013). The transmission electron microscopy monographs of ZnO/Fe₃O₄/g-C₃N₄-50% clearly depict that ZnO and Fe₃O₄ nanoparticles were dispersed on graphitic carbon nitride nanosheets, as peak value of Fe is comparatively less which indicates the amount of ferrites is low in ZnO/Fe₃O₄/g-C₃N₄ nanocomposites.

Balu et al. (2019) synthesized α -Fe₂O₃-enriched g-C₃N₄/ZnO ternary Z-scheme nanocomposites for the acid yellow 23 photodegradation in water. The procedure involves pyrolysis followed by sol-gel synthesis of ternary photocatalyst and for confirmation various physicochemical methods were used. From photoluminescence spectra, more electron-hole pair separation in g-C₃N₄/ZnO@ α -Fe₂O₃ ternary nanocomposites was noticed compared to pristine graphitic carbon nitride, zinc oxide nanoparticles, and ZnO/ α -Fe₂O₃ (Fig. 4.6). The results also indicate the presence of feeble emission peak of ZnO at 534 nm, but incorporation with α -Fe₂O₃ leads to reduction in the peak of ZnO. Electron-hole recombination was lower for ZnO@ α -Fe₂O₃ nanocomposites than ZnO. Thus, it can be concluded from the results that the fabricated nanocomposites possessed great photodegradation ability for tartrazine due to mutual synergetic effect presented by g-C₃N₄, ZnO, and ZnO@ α -Fe₂O₃. The observed degradation efficiency of g-C₃N₄/ZnO@ α -Fe₂O₃ nanocomposites was 99.34% for tartrazine in 35 min under solar light illumination.

Further, TiO₂/FeTiO₃/WO₃ ternary nanocomposites were prepared via simple sol-gel technique for the disintegration of triazine dye reactive blue - 160 (Parvathy

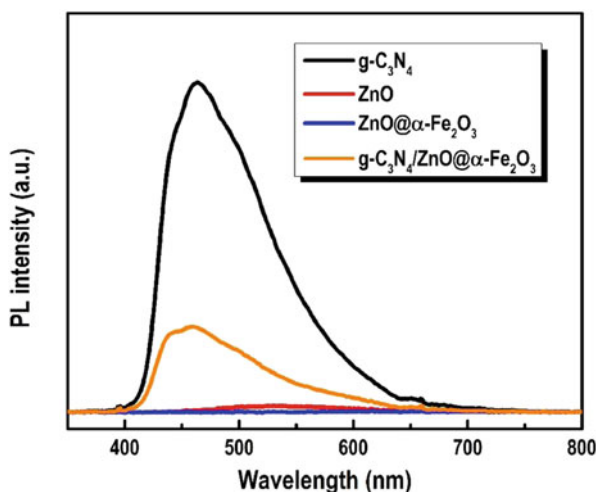


Fig. 4.6 Photoluminescence spectra of g-C₃N₄, ZnO, ZnO@ α -Fe₂O₃, and g-C₃N₄/ZnO@ α -Fe₂O₃ nanocomposites. The intensity of emission peak greatly reduced in g-C₃N₄/ZnO@ α -Fe₂O₃ which indicates significant reduction in electron-hole pair recombination, whereas rate of recombination is high for g-C₃N₄ (Reprinted with permission from Balu et al. (2019) copyright©2019, Taiwan Institute of Chemical Engineers. Published by Elsevier B.V. All rights reserved)

et al. 2019). The synthesized ternary nanocomposites (2 wt% $\text{TiO}_2/\text{FeTiO}_3/\text{WO}_3$) have verified highest photodegradation activity for reactive blue 160 with effective reusability. The $\text{TiO}_2/\text{FeTiO}_3/\text{WO}_3$ (2 wt%) nanocomposites exhibited degradation of reactive blue 160 in 120 min than bare photocatalyst. In $\text{WO}_3/\text{FeTiO}_3/\text{TiO}_2$ nanocomposites, FeTiO_3 accept electron and diminished electron–hole pair recombination and promoted degradation of dye through oxidation of holes. FeTiO_3 nanoparticles decorated on TiO_2 exhibit red shift toward visible light region owing to small band gap of FeTiO_3 (2.0 eV). Moreover, the heterojunction of WO_3 , TiO_2 , and FeTiO_3 nanoparticles generates photocurrent via transporting e^- from TiO_2 to FeTiO_3 when irradiated to solar light. Degradation results confirmed that $\text{WO}_3/\text{FeTiO}_3/\text{TiO}_2$ ternary nanocomposites exhibited more photodegradation ability than binary $\text{FeTiO}_3/\text{TiO}_2$ and WO_3/TiO_2 heterojunction at pH 3.

Recently, Hao et al. (2018) fabricated Z-scheme photocatalytic ternary system comprised of $\text{WO}_3/\text{Ag}_3\text{PO}_4/\text{Bi}_2\text{WO}_6$ via hydrothermal method. The ternary composites exhibit superior photocatalytic property for rhodamine degradation in comparison with Bi_2WO_6 and $\text{WO}_3/\text{Ag}_3\text{PO}_4$. All three WO_3 , Ag_3PO_4 , and Bi_2WO_6 with the band gap of 2.7, 2.32, and 2.75 eV, respectively, show absorption in visible region. The efficient partition of charge carrier is due to double Z-scheme electron transfer mechanism.

According to the conventional heterojunction, the electron migrates from conduction band of Bi_2WO_6 , to Ag_3PO_4 followed by WO_3 , whereas the holes transfer from valence band of WO_3 , to Ag_3PO_4 and finally toward Bi_2WO_6 . All the electron will assemble in the conduction band (0.74 eV) of WO_3 which could not reduce the oxygen to superoxide radical ($E_{\text{O}_2/\text{O}_2^-} = 0.13$ V vs. NHE), and holes assemble in valence band (1.73 eV) of Bi_2WO_6 which couldn't oxidize hydroxyl ion to hydroxyl radical ($E_{\text{OH}^-/\text{OH}^\cdot} = 1.99$ V vs. NHE) (Hao et al. 2018). These results do not support trapping experiment which showed that hydroxyl radical and superoxide radical anion were the dominant active species accountable for the azo dye degradation. The electron in the conduction band of WO_3 drifts toward valence band of Ag_3PO_4 where, electron neutralizes the holes in the valence band of Ag_3PO_4 ; thus all the electrons assembled in the conduction band of Bi_2WO_6 and holes in WO_3 valence band. Now, these electron and holes easily reduce and oxidized the oxygen and hydroxyl ion, respectively.

4.4 Coupled Semiconductor for Azo Dye Degradation

Vinodgopal and Kamat (1995) applied thin film of $\text{SnO}_2/\text{TiO}_2$ -coupled semiconductor on electrode for azo dye degradation under ultraviolet light. Coupling two semiconductors with different energy levels refines the charge separation accountable for higher efficiency. Bagheri and Mahjoub (2016) fabricated coupled nanostructures of $\text{Fe}_2\text{O}_3\text{-Ga}_2\text{O}_3$ via coprecipitation method. Among various metals, oxide-based semiconductor Ga_2O_3 is an eco-friendly material having very high band gap of 4.8 eV. The coupling of these two semiconductors inhibits the rate of

recombination and makes the charge carrier separation more facile. Here, ferric oxide with lower band gap acts as a photosensitizer for gallium oxide and assessed photocatalytic activity against congo red dye under ultraviolet light.

To explore the role of various reactive oxidation species, the effect of various scavengers has been investigated. Ammonium oxalate, AgNO_3 , tert-Butyl alcohol, and benzoquinone were used as scavengers for holes, electron, hydroxyl radical, and superoxide radical, respectively. The remarkable inhibition of congo red degradation was reported which indicates that the electron and superoxide radical play an important role in degradation. Gokul et al. (2017) reported the synthesis of $\text{CuO-TiO}_2/\text{rGO}$ photocatalyst and utilizes for the mineralization of methyl orange underneath ultraviolet light. The film carrying 40 mg of nanoparticles was sufficient to remove 3 parts per million solution of methyl orange within 13 h. Afterward five consecutive cycles, these multilayer catalysts retained its catalytic activity and stability. From photodegradation experiment, it can be concluded that the rate of degradation was increased by improving migration of electrons from TiO_2 to CuO as a function of catalyst loaded on reduced graphene oxide layer.

Fahimirad et al. (2017) synthesized $\text{La}_2\text{O}_3/\text{Al}_2\text{O}_3$ binary metal oxide nanocomposites by impregnation followed by precipitation method to degrade basic green and basic red 46 azo dyes under exposure to ultraviolet radiation. The photocatalytic efficiency of binary $\text{La}_2\text{O}_3/\text{Al}_2\text{O}_3$ nanocomposites was high than pure Al_2O_3 bare nanoparticle under the ultraviolet. The favorable parameters, pH value of 5.88, irradiation time 56.3 min, and catalyst concentration for the mineralization were 26.11 mg L^{-1} for basic green and 1.4 mg L^{-1} for basic red 46, respectively. Nearly, 100% and 87% degradation were achieved for basic green and basic red 46, respectively. The increment in photo-efficiency was achieved by reduction in energy gap of $\text{La}_2\text{O}_3/\text{Al}_2\text{O}_3$ nanocomposites against bare Al_2O_3 nanoparticle. The obtained results demonstrated that after five consecutive photocatalytic cycles, the catalytic activity of $\text{La}_2\text{O}_3/\text{Al}_2\text{O}_3$ binary photocatalyst was nearly constant.

Patil et al. (2019) designed TiO_2/WO_3 binary nanocomposites by sol-gel process using chlorosulfonic acid. The nanocomposites showed 95% degradation of congo red and methyl red dyes and azo dyes in 120 min in visible light. The degradation experiment was repeated with the same procedure for five consecutive cycles and found degradation efficiency of 90% in every repeat cycle. Thus, the synthesized TiO_2/WO_3 binary nanocomposites exhibited good reusability, stability, and recyclability during degradation process.

Further, hybrid binary metal oxide $\text{Cr}_2\text{O}_3/\text{Fe}_2\text{O}_3$ nanocomposites prepared via temperature-programmed oxidation method to produce high surface area photocatalyst (Salari 2019). Acid blue 92 were completely degraded, and a clear solution was obtained within 20 min of reaction. The magnetic separation and reusability studied for five consecutive cycles for $\text{Cr}_2\text{O}_3/\text{Fe}_2\text{O}_3$ nanocomposites were demonstrated. High recyclability of $\text{Cr}_2\text{O}_3/\text{Fe}_2\text{O}_3$ made them good contenders for wastewater treatment. Chen et al. (2015) successfully demonstrated photocatalytic ability of $\text{CuO}/\text{Co}_3\text{O}_4$ composite photocatalyst by hydrothermal process and cobalt containing solid precursor. The photostability experiment results revealed that photodegradation efficiency of 56% of original organic methylene blue

dye was obtained in case of binary metal oxide nanocomposites higher than 40% photodegradation efficiency of bare CuO nanoparticle. High photocatalytic activity of binary CuO/Co₃O₄ composite was achieved by the overlapping of band structure that displays an important role in photo carrier charge separation and transformation. CuO/Co₃O₄ binary photocatalyst was favorable for practical wastewater management because of its catalytic stability and recyclability.

4.5 Carbon-Supported Photocatalyst for Azo Dye Degradation

The carbon-supported photocatalyst had a wider range of application and can be utilized in electrochemical sensing, hydrogen production, drug delivery, water purification, and hydrogen storage and also as an antibacterial agent, as the combination of adsorption and photocatalyst offers a better alternative to decontaminate water. Thus, the adsorption capacity of nanocomposites can be enhanced by using carbonaceous material as a support which controls the size and shape of nanoparticle; it also helps to prevent the aggregation of nanoparticle (Singh et al. 2016).

Carbonaceous-based materials (carbon nanotubes, fullerenes, graphene oxide, and graphitic carbon nitride) have been widely utilized for photodegradation of azo dyes present in simulated water. Various research groups have been working on the fabrication of Z-scheme-driven g-C₃N₄/CNT/Bi₂Fe₄O₉ prepared by hydrothermal technique for efficient degradation of acid orange 7 dye. The mechanism follows a Z-scheme-driven process involving carbon nanotube as an electron mediator to reduce the electron-hole pair recombination (Di et al. 2018). Similarly, TiO₂ decorated with carbon nanotube has emerged as a potential candidate due to its property of large surface area, immense electronic properties, and high mechanical strength for photodegradation of acid orange 7 dye (Hsieh and Chen 2017). The reports on fullerenes acting as support material on mesoporous silica have been successful for photodegradation of orange G dye in the presence of ascorbic acid (Kyriakopoulos et al. 2019). Other than carbon nanotube and fullerenes, graphene oxide has also been utilized as a supporting material for MnO₂ (Saroyan et al. 2019). The GO-MnO₂ nanocomposites showed improved photoactivity against reactive black 5 azo dye. The enhanced photoactivity of the sample was ascribed by the superior contact formed between MnO₂ and graphene oxide.

Moreover, the GO-MnO₂ nanocomposites were efficient to cleave azo bonds to form NH₂ groups, and as a result, the dye gets discolored, and new products like amino naphthalene sulfonate and aromatic amines were formed. The aforementioned nanocomposites successfully discolored 98% of reactive black 5 with 20% concentration of MnO₂ in the nanohybrid. In another report, the ternary GO-TiO₂-ZnO nanocomposites were tested for its photocatalytic efficacy to remove methyl orange (Raliya et al. 2017). Besides, the photocatalytic performances of individual

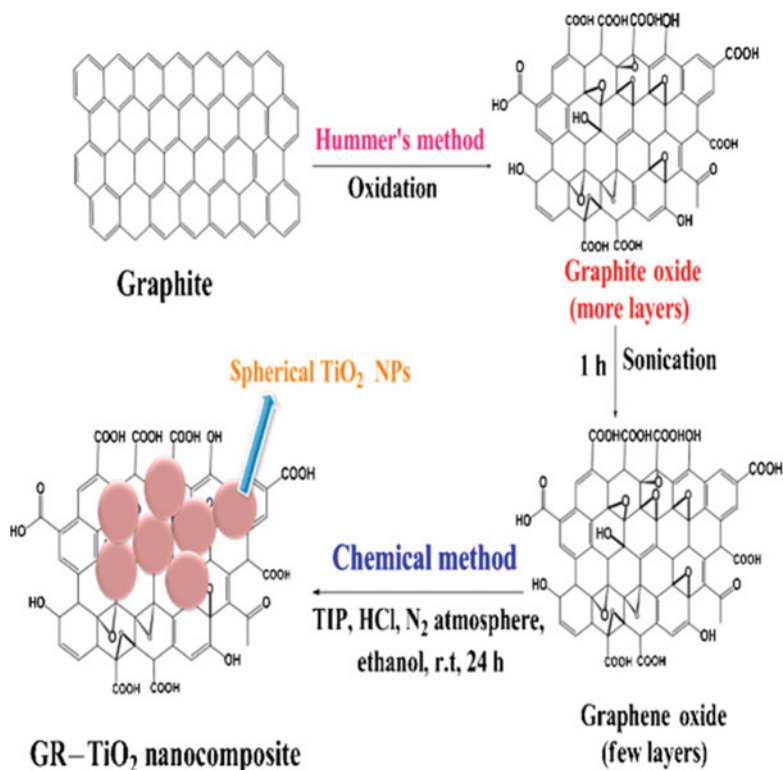


Fig. 4.7 Chemical synthetic route for the preparation of GR-TiO₂ nanocomposites where, graphite is oxidized into graphite oxide by Hummer's method followed by sonication to achieve few layered graphene oxide and finally reduction of graphene oxide into graphene and simultaneous incorporation of TiO₂ nanoparticles on graphene surface (Reprinted with permission from Posa et al. (2016) copyright@2016, Indian Academy of Sciences)

components of heterojunction were also compared with nanocomposites. The photocatalytic abilities of TiO₂, ZnO and graphene oxide were examined at lower initial concentration of methyl orange by varying the size of nanoparticles. The nanoparticles of pristine metal oxides and graphene oxide with size less than 25 nm displayed effectual photocatalytic efficiency, while the ternary nanocomposites GO-TiO₂-ZnO showed best methyl orange degradation efficiency.

Posa et al. (2016) photodegraded a non-decomposable organic azo dye using graphene/TiO₂ hybrids. Graphene was synthesized using graphite as a precursor via Hummer's method followed by oxidation and sonication of 1 h; then TiO₂ particles were then anchored over graphene oxide surface (Fig. 4.7). The nanocomposites exhibit higher efficiency as compared to bare nanoparticle toward photodegradation of acid orange 7. The hybrid structure was characterized by using various techniques.

Morales et al. (2013) prepared GO/TiO₂ via simple mixing and sonication and studied photodegradation ability against methyl orange dye. TiO₂ is the most frequently used photocatalyst utilized for water purification due to its biocompatibility and high chemical stability (Leary and Westwood 2011). As graphene a two-dimensional moiety with sp² carbon atom arranged in a honeycomb-like structure with high thermal and mechanical property (Singh et al. 2014, 2018, 2019a, b; Dutta et al. 2019a, b; Shandilya et al. 2019). The unique property of graphene makes graphene a promising material for practical application. A novel nano-graphene oxide has been prepared using graphite as a precursor via modified Hummer's method (Shandilya et al. 2018a, b).

Recently, Mathew et al. (2019) synthesized nano-graphene oxide and ZnO through sol-gel method using graphite and ZnCO₃ as precursor. The photocatalytic activity was evaluated against rhodamine 6B, and nearly 96% of azo dye were photodegraded in 3 h in the presence of nano-graphene oxide/ZnO, whereas only 66% was degraded through ZnO alone. The conversion of graphite into nano-graphene oxide was explained by powdered X-ray diffraction (Fig. 4.8). The presence of oxygen containing functionality in nano-graphene oxide was elucidated by Fourier transform infrared spectroscopy.

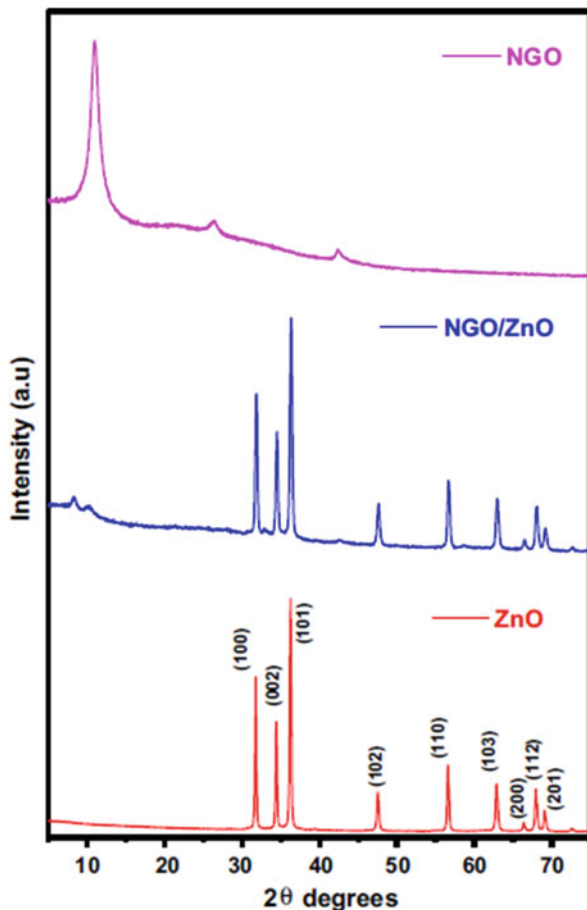
Rosu et al. (2017) prepared TiO₂-Pt/GO and TiO₂-Pt/rGO for the degradation of azo dyes in solar radiation. The degradation of various azo dyes with different structures was examined through TiO₂-Pt nanoparticles, TiO₂-Pt/GO, and TiO₂-Pt/rGO nanocomposites under sunlight. The alteration in TiO₂-Pt through graphene oxide leads to more optical absorption in visible region, and thus, increase in its photodegradation activity was observed. Results confirmed that nearly 99% of azo dyes were photodegraded, and pseudo-first-order kinetic was obtained for the reaction by using Langmuir-Hinshelwood reaction mechanism.

Other than graphene, activated carbon was also universally applied as adsorbent due to its high porosity and large specific surface area. Mahmoodi (2014) prepared activated carbon-supported TiO₂ nanoparticles for azo dye degradation. The activated carbon has been synthesized from the by-product of soya bean. The photocatalytic study was performed for the degradation of reactive red 120 and reactive red 198, respectively. The aliphatic acids like formate, acetate, and oxlate were the major compounds detected during degradation, whereas nitrate, sulfate, and chloride anions were the chief ions detected during mineralization through ultraviolet visible spectrometry and ion chromatography.

4.6 Others

Other than the above reported system, a zero-valent metal is also utilized for the degradation of various azo dyes from the polluted water. A limitation of zero-valent metal to undergo rapid corrosion can be minimized by coupling the metal atom with highly stable noble metal (Cao et al. 1999; Shu et al. 2007). But still commercializing the system is the most important part of the research for which various factors

Fig. 4.8 X-ray diffraction patterns of ZnO, NGO/ZnO, and NGO. The sharp diffraction peak indicates highly crystalline nature of ZnO, NGO/ZnO, and NGO also; the presence of characteristics peak of both ZnO and NGO in NGO/ZnO pattern represents successful fabrication of NGO (Reprinted with permission from Mathew et al. (2019) copyright@2019, King Abdulaziz City for Science and Technology)

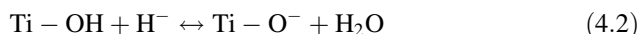
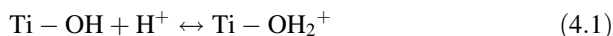


are considered, and one of the important factors is it must be cost-effective and eco-friendly. ZnIn_2S_4 , another photocatalyst, were utilized for the removal of methyl orange under visible light through adsorption and photodegradation process (Liu et al. 2017). However, no significant amount of methyl orange degradation or removal was reported. On the other side, photocatalyst is quite effective for the degradation of rhodamine B as nearly 97% of dye was degraded. High efficiency was ascribed due to the lower bond energy of $\text{C}=\text{N}$ in rhodamine B as compared to azo group in methyl orange which makes reactive oxidation species easy to break.

Petrella et al. (2014) studied the photodegradation of methyl red and methyl orange using TiO_2 immobilized on cement mortar under solar light. The immobilization of TiO_2 on cement mortar prevents the leaching of nanoparticle. The synergistic effect of TiO_2 and ultraviolet irradiation is responsible for methyl red and methyl orange degradation. The kinetics of degradation depends upon the catalyst surface thus obeys a pseudo-first-order kinetics. The initial increase in degradation

may be due to the increase rate of collision frequency between the dye molecules and generated radicals species. But, increase in dye concentration above optimal level shutters the catalyst surface from ultraviolet irradiation which hindered the activation of TiO_2 to generate radicals which considerable decline productivity of catalysts (Tang et al. 1995).

As methyl red is ionic in nature, its degradation is more as compared to nonpolar methyl orange. Also, at pH above the zero point charge (pH_{ZPC} is 6.2), TiO_2 surface is negatively charged, whereas at pH below zero point charge, its surface is positively charged (Chou and Liao 2005). The zero point charge is a state when electric charge density on the surface of catalyst is zero. Zero point charge relates the occurrence of adsorption of pollutant on the surface and can be easily understood from Eqs. (4.1) and (4.2).



Generally, the electronic structure decides absorption range, charge carrier generation, and electron–hole migration. Wang et al. (2016) synthesized La-doped BiCuSeO with layered structure of Bi and explored the photocatalytic performance against congo red, where, La doping was done to improve the band structure of BiCuSeO; however, the band gap slightly broaden after doping. With BiCuSeO 45%, 49% and 44% of congo red were photodegraded in 180 min, while after doping with La 70%, 75% and 90% congo red were degraded under ultraviolet, visible and near-infrared region, respectively.

4.7 Conclusion

Advanced oxidation process recently emerges as an important technique among various conventional methods. Carbonaceous-based materials have been widely utilized to enhance the photodegradation of azo dyes present in water due to its unique properties. The primary aim is to fabricate a photocatalyst with higher efficiency with broader absorption range, and one of the challenges is to minimize the columbic force of attraction between the opposite charges so as to inhibit the rate of recombination of charge carrier. Thus to build a visible light-driven photocatalyst which exhibits special upconversion phenomena by the virtue of which it convert longer wavelength light into shorter wavelength with high-energy light that is efficiently employed for the excitation of charge carrier from the surface of wide band gap semiconductor. Besides, many applications of carbon-supported nanocomposites have widely utilized as photocatalyst. The photocatalytic activity of nanocomposites is basically due to the generation of reactive oxidation species which oxidized the azo dye into lower aliphatic acid. This book chapter provides a basic review of various reported binary, ternary, coupled, and carbon-supported

photocatalysts utilized for the photodegradation of azo dye. Though significant effort has already been done in the field of photocatalysis, it still faces many challenges which need to be overcome before practical application. From the future prospective, certain issues need to be addressed before its practical application and more understanding of the concept behind Z-scheme, optimization of synthetic procedure for better control over size, increasing photostability of carbonaceous material or to minimize its photo-bleaching, green method to avoid chemical pollution, widen the application for other pollutant which really belongs to real world. The literature survey clearly reveals that the study was limited to certain basic pollutants like methylene blue, methyl orange, rhodamine B, and congo red. So, the complete photodegradation of azo dye by photocatalyst needs further extension to achieve 100% mineralization. Lastly, photo-efficiency and separation of charge carrier are also an important issue, as no such photocatalyst is designed yet which show high efficiency for degradation of pollutant. Despite many challenges associated, numerous opportunities are still waiting to explore endless potential of photocatalysis to be employed in various technologies.

References

- Al Anbari R, Al-Obaidy AH, Abd E (2016) Photocatalytic activity of Fe_3O_4 under solar radiation. *Mesop Environ J* 2(4):41–53. ISSN 2410-2598
- Amin NK (2009) Removal of direct blue-106 dye from aqueous solution using new activated carbons developed from pomegranate peel: adsorption equilibrium and kinetics. *J Hazard Mater* 165(1–3):52–62. <https://doi.org/10.1016/j.jhazmat.2008.09.067>
- Bagheri M, Mahjoub AR (2016) Template assisted fast photocatalytic degradation of azo dye using ferric oxide–gallia nanostructures. *RSC Adv* 6(90):87555–87563. <https://doi.org/10.1039/C6RA16317C>
- Balu S, Velmurugan S, Palanisamy S, Chen SW, Velusamy V, Yang TC, El-Shafey ESI (2019) Synthesis of $\alpha\text{-Fe}_2\text{O}_3$ decorated g- $\text{C}_3\text{N}_4/\text{ZnO}$ ternary Z-scheme photocatalyst for degradation of tartrazine dye in aqueous media. *J Taiwan Inst Chem E* 99:258–267. <https://doi.org/10.1016/j.jtice.2019.03.011>
- Bian X, Hong K, Liu L, Xu M (2013) Magnetically separable hybrid $\text{CdS-TiO}_2\text{-Fe}_3\text{O}_4$ nanomaterial; enhanced photocatalytic activity under UV and visible irradiation. *Appl Surf Sci* 280:349–353. <https://doi.org/10.1016/j.apsusc.2013.04.159>
- Blake D (2001) Bibliography of work on the heterogeneous photocatalytic removal of hazardous compounds from water and air. *Nat Renew Energ Lab NRELTP-510-31319*. <https://doi.org/10.2172/789771>
- Cao J, Wei L, Huang Q, Wang L, Han S (1999) Reducing degradation of azo dye by zero-valent iron in aqueous solution. *Chemosphere* 38(3):565–571. [https://doi.org/10.1016/S0045-6535\(98\)00201-X](https://doi.org/10.1016/S0045-6535(98)00201-X)
- Chandel N, Sharma K, Sudhaik A, Raizada P, Hosseini-Bandegharai A, Thakur VK, Singh P (2019) Magnetically separable ZnO/ZnFeO_4 and $\text{ZnO/CoFe}_2\text{O}_4$ photocatalyst supported onto nitrogen doped graphene for photocatalytic degradation of toxic dyes. *Arab J Chem* 13(2):4324–4340. <https://doi.org/10.1016/j.arabjc.2019.08.005>
- Chen CY (2009) Photocatalytic degradation of azo dye reactive orange 16 by TiO_2 . *Water Air Soil Pollut* 202(1–4):335–342. <https://doi.org/10.1007/s11270-009-9980-4>

- Chen F, Xie Y, Zhao J, Lu G (2001) Photocatalytic degradation of dyes on a magnetically separated photocatalyst under visible and UV irradiation. *Chemosphere* 44(5):1159–1168. [https://doi.org/10.1016/S0045-6535\(00\)00277-0](https://doi.org/10.1016/S0045-6535(00)00277-0)
- Chen RX, Zhu SL, Mao J, Cui ZD, Yang XJ, Liang YQ, Li ZY (2015) Synthesis of CuO/Co₃O₄ coaxial heterostructures for efficient and recycling photodegradation. *Int J Photoenerg* 2015:11. <https://doi.org/10.1155/2015/183468>
- Chou JC, Liao LP (2005) Study on pH at the point of zero charge of TiO₂ pH ion-sensitive field effect transistor made by the sputtering method. *Thin Solid Films* 476(1):157–161. <https://doi.org/10.1016/j.tsf.2004.09.061>
- Di L, Yang H, Xian T, Chen X (2018) Construction of Z-scheme g-C₃N₄/CNT/Bi₂Fe₄O₉ composites with improved simulated-sunlight photocatalytic activity for the dye degradation. *Micromachines* 9(12):613. <https://doi.org/10.3390/mi9120613>
- Dou J, Yin S, Chong JY, Zhang B, Han J, Huang Y, Xu R (2016) Carbon spheres anchored Co₃O₄ nanoclusters as an efficient catalyst for dye degradation. *Appl Cataly A Gen* 513:106–115. <https://doi.org/10.1016/j.apcata.2015.12.028>
- Dutta V, Sharma S, Raizada P, Hosseini-Bandegharai A, Gupta VK, Singh P (2019a) Review on augmentation in photocatalytic activity of CoFe₂O₄ via heterojunction formation for photocatalysis of organic pollutants in water. *J Saudi Chem Soc* 23:1119–1136. <https://doi.org/10.1016/j.jscs.2019.07.003>
- Dutta V, Singh P, Shandilya P, Sharma S, Raizada P, Saini AK, Gupta VK, Hosseini-Bandegharai A, Agarwal S, Rahmani-Sani A (2019b) Review on advances in photocatalytic water disinfection utilizing graphene and graphene derivatives-based nanocomposites. *J Environ Chem Eng* 7(3):103132. <https://doi.org/10.1016/j.jece.2019.103132>
- Fahimirad B, Asghari A, Rajabi M (2017) Photo-degradation of basic green 1 and basic red 46 dyes in their binary solution by La₂O₃-Al₂O₃ nanocomposite using first-order derivative spectra and experimental design methodology. *Spectrochim Acta A* 179:58–65. <https://doi.org/10.1016/j.saa.2017.02.022>
- Gautam S, Shandilya P, Singh VP, Raizada P, Singh P (2016) Solar photocatalytic mineralization of antibiotics using magnetically separable NiFe₂O₄ supported onto graphene sand composite and bentonite. *J Water Process Eng* 14:86–100. <https://doi.org/10.1016/j.jwpe.2016.10.008>
- Gautam S, Shandilya P, Priya B, Singh VP, Raizada P, Rai R, Valente MA, Singh P (2017) Superparamagnetic MnFe₂O₄ dispersed over graphitic carbon sand composite and bentonite as magnetically recoverable photocatalyst for antibiotic mineralization. *Sep Purif Technol* 172:498–511. <https://doi.org/10.1016/j.seppur.2016.09.006>
- Gokul P, Vinoth R, Neppolian B, Anandhakumar S (2017) Binary metal oxide nanoparticle incorporated composite multilayer thin films for sono-photocatalytic degradation of organic pollutants. *Appl Surf Sci* 418:119–127. <https://doi.org/10.1016/j.apsusc.2016.12.232>
- Grzechulska J, Morawski AW (2002) Photocatalytic decomposition of azo-dye acid black 1 in water over modified titanium dioxide. *Appl Catal B Environ* 36(1):45–51. [https://doi.org/10.1016/S0926-3373\(01\)00275-2](https://doi.org/10.1016/S0926-3373(01)00275-2)
- Han C, Ge L, Chen C, Li Y, Xiao X, Zhang Y, Guo L (2014) Novel visible light induced Co₃O₄-g-C₃N₄ heterojunction photocatalyst for efficient degradation of methyl orange. *Appl Catal B Environ* 147:546–553. <https://doi.org/10.1016/j.apcatb.2013.09.038>
- Hao H, Lu D, Zhang J (2018) Fabrication of novel double Z-scheme photocatalyst WO₃-Ag₃PO₄-Bi₂WO₆ with excellent visible photocatalytic activity. *Int J Environ Chem* 2(2):56–66. <https://doi.org/10.11648/j.ijec.20180202.15>
- Hasija V, Raizada P, Sudhaik A, Sharma K, Kumar A, Singh P, Jonnalagadda SB, Thakur VK (2019a) Recent advances in noble metal free doped graphitic carbon nitride based nanohybrids for photocatalysis of organic contaminants in water; a review. *Appl Mater Today* 15:494–524. <https://doi.org/10.1016/j.apmt.2019.04.003>
- Hasija V, Sudhaik A, Raizada P, Hosseini-Bandegharai A, Singh P (2019b) Carbon quantum dots supported AgI/ZnO/phosphorus doped graphitic carbon nitride as Z-scheme photocatalyst for efficient photodegradation of 2, 4-dinitrophenol. *Int J Environ Chem* 7(4):103272. <https://doi.org/10.1016/j.jece.2019.103272>

- Hsieh SH, Chen WJ (2017) Synthesis and characterization of TiO₂/CNT nanocomposites for azo dye degradation. *Trans Tech Publ* 909:243–248. <https://doi.org/10.4028/www.scientific.net/MSF.909.243>
- Ibrahim IM, Moustafa ME, Abdelhamid MR (2016) Effect of organic acids precursors on the morphology and size of ZrO₂ nanoparticles for photocatalytic degradation of Orange G dye from aqueous solutions. *J Mol Liq* 223:741–748. <https://doi.org/10.1016/j.molliq.2016.08.113>
- Jamwal D, Kaur G, Raizada P, Singh P, Pathak D, Thakur P (2015) Twin-tail surfactant peculiarity in superficial fabrication of semiconductor quantum dots; toward structural, optical, and electrical features. *J Phys Chem C* 119(9):5062–5073. <https://doi.org/10.1021/jp510428z>
- Kalme SD, Parshetti GK, Jadhav SU, Govindwar SP (2007) Biodegradation of benzidine based dye direct Blue-6 by *Pseudomonas desmolyticum* NCIM 2112. *Bioresour Technol* 98(7):1405–1410. <https://doi.org/10.1016/j.biortech.2006.05.023>
- Konstantinou IK, Albanis TA (2004) TiO₂-assisted photocatalytic degradation of azo dyes in aqueous solution; kinetic and mechanistic investigations; a review. *Appl Catal B Environ* 49(1):1–14. <https://doi.org/10.1016/j.apcatb.2003.11.010>
- Kumar S, Pal S, Kuntail J, Sinha I (2019a) Curcumin functionalized CuO/ag nanocomposite; efficient visible light Z-scheme photocatalyst for methyl orange degradation. *Environ Nanotechnol Monit Manag* 12:100236. <https://doi.org/10.1016/j.enmm.2019.100236>
- Kumar A, Raizada P, Singh P, Saini R, Saini A, Hosseini-Bandegharai A (2019b) Perspective and status of polymeric graphitic carbon nitride based Z-scheme photocatalytic systems for sustainable photocatalytic water purification. *Chem Eng J* 123496. <https://doi.org/10.1016/j.cej.2019.123496>
- Kyriakopoulos J, Kordouli E, Bourikas K, Kordulis C, Lycourghiotis A (2019) Decolourization of Orange-G aqueous solutions over C60/MCM-41 photocatalysts. *Appl Sci* 9(9):1958. <https://doi.org/10.3390/app9091958>
- Lachheb H, Puzenat E, Houas A, Ksibi M, Elaloui E, Guillard C, Herrmann JM (2002) Photocatalytic degradation of various types of dyes (alizarin S, Crocein Orange G, methyl red, Congo red, methylene blue) in water by UV-irradiated titania. *Appl Catal B Environ* 39(1):75–90. [https://doi.org/10.1016/S0926-3373\(02\)00078-4](https://doi.org/10.1016/S0926-3373(02)00078-4)
- Laszlo JA (2000) Regeneration of azo-dye-saturated cellulosic anion exchange resin by *Burkholderia cepacia* anaerobic dye reduction. *Environ Sci Technol* 34(1):167–172. <https://doi.org/10.1021/es990918u>
- Leary R, Westwood A (2011) Carbonaceous nanomaterials for the enhancement of TiO₂ photocatalysis. *Carbon* 49(3):741–772. <https://doi.org/10.1016/j.carbon.2010.10.010>
- Liu T, Wang L, Lu X, Fan J, Cai X, Gao B, Miao R, Wang J, Lv Y (2017) Comparative study of the photocatalytic performance for the degradation of different dyes by ZnIn₂S₄; adsorption, active species, and pathways. *RSC Adv* 7(20):12292–12300. <https://doi.org/10.1039/C7RA00199A>
- Mahmoodi NM (2014) Binary catalyst system dye degradation using photocatalysis. *Fiber Polym* 15(2):273–280. <https://doi.org/10.1007/s12221-014-0273-1>
- Mandal S, Adhikari S, Pu S, Xiaoke W, Do-Heyoung K, Patel RK (2019) Interactive Fe₂O₃/porous SiO₂ nanospheres for photocatalytic degradation of organic pollutants; kinetic and mechanistic approach. *Chemosphere* 234:596–607. <https://doi.org/10.1016/j.chemosphere.2019.06.092>
- Manivel A, Lee GJ, Chen CY, Chen JH, Ma SH, Hornig TL, Wu JJ (2015) Synthesis of MoO₃ nanoparticles for azo dye degradation by catalytic ozonation. *Mater Res Bull* 62:184–191. <https://doi.org/10.1016/j.materresbull.2014.11.016>
- Mathew S, Antony A, Kathyayini H (2019) Degradation of azo dye under visible light irradiation over nanographene oxide–zinc oxide nanocomposite as catalyst. *Appl Nanosci* 10(1):253–262. <https://doi.org/10.1007/s13204-019-01110-5>
- Meshko V, Markovska L, Mincheva M, Rodrigues AE (2001) Adsorption of basic dyes on granular activated carbon and natural zeolite. *Water Res* 35(14):3357–3366. [https://doi.org/10.1016/S0043-1354\(01\)00056-2](https://doi.org/10.1016/S0043-1354(01)00056-2)

- Morales-Torres S, Pastrana-Martínez LM, Figueiredo JL, Faria JL, Silva AM (2013) Graphene oxide-P25 photocatalyst for degradation of diphenhydramine pharmaceutical and methyl orange dye. *Appl Surf Sci* 275:361–368. <https://doi.org/10.1016/j.apsusc.2012.11.157>
- Pare B, Jonnalagadda SB, Tomar H, Singh P, Bhagwat VW (2008a) ZnO assisted photocatalytic degradation of acridine orange in aqueous solution using visible irradiation. *Desalination* 232 (1–3):80–90. <https://doi.org/10.1016/j.desal.2008.01.007>
- Pare B, Singh P, Jonnalagadda SB (2008b) Visible light induced heterogeneous advanced oxidation process to degrade pararosanilin dye in aqueous suspension of ZnO. *Indian J Chem A* 47:830–835. <https://doi.org/10.1080/19443994.2013.803342>
- Pare B, Singh P, Jonnalagadda SB (2009a) Artificial light assisted photocatalytic degradation of lissamine fast yellow dye in ZnO suspension in a slurry batch reactor. *Indian J Chem A* 48:1364–1369. <http://nopr.niscair.res.in/handle/123456789/6122>
- Pare B, Singh P, Jonnalagadda SB (2009b) Degradation and mineralization of Victoria blue B dye in a slurry photoreactor using advanced oxidation process. *J Sci Ind Res* 68:724–729. <http://nopr.niscair.res.in/handle/123456789/5300>
- Parvathy S, Saranya S, Sivakumar S (2019) TiO₂/FeO₃/WO₃ ternary composite semiconductor as efficient photocatalyst; structural designing, characterization and investigation of photocatalytic efficiency. *J Sci Technol* 7:101265. <https://doi.org/10.11131/2019/101259>
- Patil BN, Naik DB, Shrivastava VS (2011) Photocatalytic degradation of hazardous Ponceau-S dye from industrial wastewater using nanosized niobium pentoxide with carbon. *Desalination* 269 (1–3):276–283. <https://doi.org/10.1016/j.desal.2010.11.014>
- Patil SM, Deshmukh SP, More KV, Shevale VB, Mullani SB, Dhodamani AG, Delekar SD (2019) Sulfated TiO₂/WO₃ nanocomposite; An efficient photocatalyst for degradation of Congo red and methyl red dyes under visible light irradiation. *Mater Chem Phys* 225:247–255. <https://doi.org/10.1016/j.desal.2010.11.014>
- Petrella A, Boghetich G, Petrella M, Mastroilli P, Petruzzelli V, Petruzzelli D (2014) Photocatalytic degradation of azo dyes. Pilot plant investigation. *Ind Eng Chem Res* 53 (7):2566–2571. <https://doi.org/10.1021/ie403506s>
- Pingmuang K, Chen J, Kangwansupamonkon W, Wallace GG, Phanichphant S, Nattestad A (2017) Composite photocatalysts containing BiVO₄ for degradation of cationic dyes. *Sci Rep* 7 (1):8929. <https://doi.org/10.1038/s41598-017-09514-5>
- Posa VR, Annavaram V, Somala AR (2016) Fabrication of graphene–TiO₂ nanocomposite with improved photocatalytic degradation for acid orange 7 dye under solar light irradiation. *Bull Mater Sci* 39(3):759–767. <https://doi.org/10.1007/s12034-016-1215-x>
- Priya B, Shandilya P, Raizada P, Thakur P, Singh N, Singh P (2016) Photocatalytic mineralization and degradation kinetics of ampicillin and oxytetracycline antibiotics using graphene sand composite and chitosan supported BiOCl. *J Mol Catal A Chem* 423:400–413. <https://doi.org/10.1016/j.molcata.2016.07.043>
- Raizada P, Singh P, Kumar A, Sharma G, Pare B, Jonnalagadda SB, Thakur P (2014a) Solar photocatalytic activity of nano-ZnO supported on activated carbon or brick grain particles; role of adsorption in dye degradation. *Appl Catal A Gen* 486:159–169. <https://doi.org/10.1016/j.apcata.2014.08.043>
- Raizada P, Singh P, Kumar A, Pare B, Jonnalagadda SB (2014b) Zero valent iron-brick grain nanocomposite for enhanced solar-Fenton removal of malachite green. *Sep Purif Technol* 133:429–437. <https://doi.org/10.1016/j.seppur.2014.07.012>
- Raizada P, Priya B, Thakur P, Singh P (2016) Solar light induced photodegradation of oxytetracycline using Zr doped TiO₂/CaO based nanocomposite. *Indian J Chem* 55(07):803–809. <http://nopr.niscair.res.in/handle/123456789/35068>
- Raizada P, Kumari J, Shandilya P, Singh P (2017) Kinetics of photocatalytic mineralization of oxytetracycline and ampicillin using activated carbon supported ZnO/ZnWO₄. *Desalin Water Treat* 79:204–213. <https://doi.org/10.5004/dwt.2017.20831>
- Raizada P, Sudhaik A, Singh P, Shandilya P, Thakur P, Jung H (2018) Visible light assisted photodegradation of 2, 4-dinitrophenol using Ag₂CO₃ loaded phosphorus and Sulphur

- CO-doped graphitic carbon nitride nanosheets in simulated wastewater. *Arab J Chem* 13:3196–3209. <https://doi.org/10.1016/j.arabjc.2018.10.004>
- Raizada P, Sudhaik A, Singh P (2019a) Photocatalytic water decontamination using graphene and ZnO coupled photocatalyst; a review. *Mater Sci Energ Technol* 2:509–525. <https://doi.org/10.1016/j.mset.2019.04.007>
- Raizada P, Sudhaik A, Singh P, Shandilya P, Gupta VK, Hosseini-Bandegharai A, Agrawal S (2019b) Ag₃PO₄ modified phosphorus and Sulphur co-doped graphitic carbon nitride as a direct Z-scheme photocatalyst for 2, 4-dimethyl phenol degradation. *J Photoch Photobio A* 374:22–35. <https://doi.org/10.1016/j.jphotochem.2019.01.015>
- Raizada P, Sudhaik A, Singh P, Hosseini-Bandegharai A, Thakur P (2019c) Converting type II AgBr/VO into ternary Z scheme photocatalyst via coupling with phosphorus doped g-C₃N₄ for enhanced photocatalytic activity. *Sep Purif Technol* 12:115692. <https://doi.org/10.1016/j.seppur.2019.115692>
- Raliya R, Avery C, Chakrabarti S, Biswas P (2017) Photocatalytic degradation of methyl orange dye by pristine titanium dioxide, zinc oxide, and graphene oxide nanostructures and their composites under visible light irradiation. *Appl Nanosci* 7(5):253–259. <https://doi.org/10.1007/s13204-017-0565-z>
- Rao MP, Ponnusamy VK, Wu JJ, Asiri AM, Anandan S (2018) Hierarchical CuO microstructures synthesis for visible light driven photocatalytic degradation of reactive Black-5 dye. *J Environ Chem Eng* 6(5):6059–6068. <https://doi.org/10.1016/j.jece.2018.09.041>
- Rauf MA, Meetani MA, Hisaindee S (2011) An overview on the photocatalytic degradation of azo dyes in the presence of TiO₂ doped with selective transition metals. *Desalination* 276 (1–3):13–27. <https://doi.org/10.1016/j.desal.2011.03.071>
- Razo-Flores E, Luijten M, Donlon BA, Lettinga G, Field JA (1997) Complete biodegradation of the azo dye azodisalicylate under anaerobic conditions. *Environ Sci Technol* 31(7):2098–2103. <https://doi.org/10.1021/es960933o>
- Rosu MC, Coros M, Pogacean F, Magerusan L, Socaci C, Turza A, Pruneanu S (2017) Azo dyes degradation using TiO₂-Pt/graphene oxide and TiO₂-Pt/reduced graphene oxide photocatalysts under UV and natural sunlight irradiation. *Solid State Sci* 70:3–20. <https://doi.org/10.1016/j.solidstatesciences.2017.05.013>
- Salari H (2019) Kinetics and mechanism of enhanced photocatalytic activity under visible light irradiation using Cr₂O₃/Fe₂O₃ nanostructure derived from bimetallic metal organic framework. *J Environ Chem Eng* 7(3):103092. <https://doi.org/10.1016/j.jece.2019.103092>
- Sang Y, Zhao Z, Zhao M, Hao P, Leng Y, Liu H (2015) From UV to near-infrared, WS₂ nanosheet; a novel photocatalyst for full solar light spectrum photodegradation. *Adv Mater* 27(2):363–369. <https://doi.org/10.1002/adma.201403264>
- Saroyan H, Kyzas GZ, Deliyanni EA (2019) Effective dye degradation by graphene oxide supported manganese oxide. *Processes* 7(1):40. <https://doi.org/10.3390/pr7010040>
- Sauer T, Neto GC, Jose HJ, Moreira RFPM (2002) Kinetics of photocatalytic degradation of reactive dyes in a TiO₂ slurry reactor. *J Photoch Photobio A* 149(1–3):147–154. [https://doi.org/10.1016/S1010-6030\(02\)00015-1](https://doi.org/10.1016/S1010-6030(02)00015-1)
- Shandilya P, Mittal D, Soni M, Raizada P, Hosseini-Bandegharai A, Saini AK, Singh P (2018a) Fabrication of fluorine doped graphene and SmVO₄ based dispersed and adsorptive photocatalyst for abatement of phenolic compounds from water and bacterial disinfection. *J Clean Prod* 203:386–399. <https://doi.org/10.1016/j.jclepro.2018.08.271>
- Shandilya P, Mittal D, Soni M, Raizada P, Lim JH, Jeong DY, Dewedi RP, Saini AK, Singh P (2018b) Islanding of EuVO₄ on high-dispersed fluorine doped few layered graphene sheets for efficient photocatalytic mineralization of phenolic compounds and bacterial disinfection. *J Taiwan Inst Chem Eng* 93:528–542. <https://doi.org/10.1016/j.jtice.2018.08.034>
- Shandilya P, Mittal D, Sudhaik A, Soni M, Raizada P, Saini AK, Singh P (2019) GdVO₄ modified fluorine doped graphene nanosheets as dispersed photocatalyst for mitigation of phenolic compounds in aqueous environment and bacterial disinfection. *Sep Purif Technol* 210:804–816. <https://doi.org/10.1016/j.seppur.2018.08.077>
- Sharma K, Dutta V, Sharma S, Raizada P, Hosseini-Bandegharai A, Thakur P, Singh P (2019a) Recent advances in enhanced photocatalytic activity of bismuth oxyhalides for efficient

- photocatalysis of organic pollutants in water; a review. *J Ind Eng Chem* 78(25): 1–25):20. <https://doi.org/10.1016/j.jiec.2019.06.022>
- Sharma S, Dutta V, Singh P, Raizada P, Sani AR, Bandegharai AH, Thakur VK (2019b) Carbon quantum dot supported semiconductor photocatalysts for efficient degradation of organic pollutants in water; a review. *J Clean Prod* 228:755–769. <https://doi.org/10.1016/j.jclepro.2019.04.292>
- Shu HY, Chang MC, Yu HH, Chen WH (2007) Reduction of an azo dye acid black 24 solution using synthesized nanoscale zerovalent iron particles. *J Colloid Interface Sci* 314(1):89–97. <https://doi.org/10.1016/j.jcis.2007.04.071>
- Singh P, Raizada P, Pathania D, Sharma G, Sharma P (2013a) Microwave induced KOH activation of guava peel carbon as an adsorbent for Congo red dye removal from aqueous phase. *Indian J Chem Technol* 20: 305–311. <http://nopr.niscair.res.in/handle/123456789/21463>
- Singh P, Raizada P, Pathania D, Kumar A, Thakur P (2013b) Preparation of BSA-ZnWO₄ nanocomposites with enhanced adsorptional photocatalytic activity for methylene blue degradation. *Int J Photoenergy* 2013:7. <https://doi.org/10.1155/2013/726250>
- Singh P, Raizada P, Kumari S, Kumar A, Pathania D, Thakur P (2014) Solar-Fenton removal of malachite green with novel Fe⁰-activated carbon nanocomposite. *Appl Catal A Gen* 476:9–18. <https://doi.org/10.1016/j.apcata.2014.02.009>
- Singh P, Priya B, Shandilya P, Raizada P, Singh N, Pare B, Jonnalagadda SB (2016) Photocatalytic mineralization of antibiotics using 60% WO₃/BiOCl stacked to graphene sand composite and chitosan. *Arab J Chem* 12:4627–46445. <https://doi.org/10.1016/j.arabjc.2016.08.005>
- Singh P, Gautam S, Shandilya P, Priya B, Singh VP, Raizada P (2017) Graphene bentonite supported ZnFe₂O₄ as superparamagnetic photocatalyst for antibiotic degradation. *Adv Mater Lett* 8(3):229–238. <https://doi.org/10.5185/amllett.2017.1467>
- Singh P, Shandilya P, Raizada P, Sudhaik A, Rahmani-Sani A, Hosseini-Bandegharai A (2018) Review on various strategies for enhancing photocatalytic activity of graphene based nanocomposites for water purification. *Arab J Chem* 13:3498–3520. <https://doi.org/10.1016/j.arabjc.2018.12.001>
- Singh P, Raizada P, Sudhaik A, Shandilya P, Thakur P, Agarwal S, Gupta VK (2019a) Enhanced photocatalytic activity and stability of AgBr/BiOBr/graphene heterojunction for phenol degradation under visible light. *J Saudi Chem Soc* 23(5):586–599. <https://doi.org/10.1016/j.jscs.2018.10.005>
- Singh P, Sharma K, Hasija V, Sharma V, Sharma S, Raizada P, Thakur VK (2019b) Systematic review on applicability of magnetic iron oxides–integrated photocatalysts for degradation of organic pollutants in water. *Mater Today Chem* 14:100–186. <https://doi.org/10.1016/j.mtchem.2019.08.005>
- Solomon RV, Lydia IS, Merlin JP, Venuvanalingam P (2012) Enhanced photocatalytic degradation of azo dyes using nano Fe₃O₄. *J Iran Chem Soc* 9(2):101–109. <https://doi.org/10.1155/2015/797606>
- Sonu DV, Sharma S, Raizada P, Bandegharai AH, Gupta VK, Singh P (2019) Review on augmentation in photocatalytic activity of CoFe O viaheterojunction formation for photocatalysis of organic pollutants in water. *J Saudi Chem Soc* 23(8):1119–1136. <https://doi.org/10.1016/j.jscs.2019.07.003>
- Stylidi M, Kondarides DL, Verykios XE (2003) Pathways of solar light-induced photocatalytic degradation of azo dyes in aqueous TiO₂ suspensions. *Appl Catal B Environ* 40(4):271–286. [https://doi.org/10.1016/S0926-3373\(02\)00163-7](https://doi.org/10.1016/S0926-3373(02)00163-7)
- Sudhaik A, Raizada P, Shandilya P, Singh P (2018a) Magnetically recoverable graphitic carbon nitride and NiFe₂O₄ based magnetic photocatalyst for degradation of oxytetracycline antibiotic in simulated wastewater under solar light. *J Environ Chem Eng* 6(4):3874–3883. <https://doi.org/10.1016/j.jece.2018.05.039>
- Sudhaik A, Raizada P, Shandilya P, Jeong DY, Lim JH, Singh P (2018b) Review on fabrication of graphitic carbon nitride based efficient nanocomposites for photodegradation of aqueous phase organic pollutants. *J Ind Eng Chem* 67:28–51. <https://doi.org/10.1016/j.jiec.2018.07.007>

- Tanaka K, Padermpole K, Hisanaga T (2000) Photocatalytic degradation of commercial azo dyes. *Water Res* 34(1):327–333. [https://doi.org/10.1016/S0043-1354\(99\)00093-7](https://doi.org/10.1016/S0043-1354(99)00093-7)
- Tang WZ, An H (1995) Photocatalytic oxidation of commercial dyes in aqueous solutions. *Chemosphere* 31:4157–4170. [https://doi.org/10.1016/0045-6535\(95\)80015-D](https://doi.org/10.1016/0045-6535(95)80015-D)
- Tang C, Liu L, Li Y, Bian Z (2017) Aerosol spray assisted assembly of TiO₂ mesocrystals into hierarchical hollow microspheres with enhanced photocatalytic performance. *Appl Catal B Environ* 201:41–47. <https://doi.org/10.1016/j.apcatb.2016.08.006>
- Tian J, Sang Y, Yu G, Jiang H, Mu X, Liu H (2013) A Bi₂WO₆-based hybrid photocatalyst with broad spectrum photocatalytic properties under UV, visible, and near-infrared irradiation. *Adv Mater* 25(36):5075–5080. <https://doi.org/10.1002/adma.201302014>
- Vinodgopal K, Kamat PV (1995) Enhanced rates of photocatalytic degradation of an azo dye using SnO₂/TiO₂ coupled semiconductor thin films. *Environ Sci Technol* 29(3):841–845. <https://doi.org/10.1021/es00003a037>
- Wang G, Huang B, Ma X, Wang Z, Qin X, Zhang X, Dai Y, Whangbo MH (2013) Cu₂(OH)PO₄, a near-infrared-activated Photocatalyst. *Angew Chem Int Ed* 52(18):4810–4813. <https://doi.org/10.1002/anie.201301306>
- Wang H, Li S, Liu Y, Ding J, Lin YH, Xu H, Xu B, Nan CW (2016) Bi_{1-x}La_xCuSeO as new tunable full solar light active photocatalyst. *Sci Rep* 6:24620. <https://doi.org/10.1038/srep24620>
- Wang R, Zhang W, Zhu W, Yan L, Li S, Chen K, Hu N, Suo Y, Wang J (2018) Enhanced visible-light-driven photocatalytic sterilization of tungsten trioxide by surface-engineering oxygen vacancy and carbon matrix. *Chem Eng J* 348:292–300. <https://doi.org/10.1016/j.cej.2018.05.010>
- Wu Z, Chen X, Liu X, Yang X, Yang Y (2019) A ternary magnetic recyclable ZnO/Fe₃O₄/gC₃N₄ composite Photocatalyst for efficient Photodegradation of Monoazo dye. *Nanoscale Res Lett* 14(1):147. <https://doi.org/10.1186/s11671-019-2974-2>
- Xing J, Shan Z, Li K, Bian J, Lin X, Wang W, Huang F (2008) Photocatalytic activity of Nb₂O₅/SrNb₂O₆ heterojunction on the degradation of methyl orange. *J Phys Chem Solids* 69(1):3–28. <https://doi.org/10.1016/j.jpcs.2007.07.087>
- Xu Q, Zhang L, Yu J, Wageh S, Al-Ghamdi AA, Jaroniec M (2018) Direct Z-scheme photocatalysts; principles, synthesis, and applications. *Mater Today* 21(10):1042–1063. <https://doi.org/10.1016/j.mattod.2018.04.008>
- Zhang Y, Gao F, Wanjala B, Li Z, Cernigliaro G, Gu Z (2016) High efficiency reductive degradation of a wide range of azo dyes by SiO₂-Co core-shell nanoparticles. *Appl Catal B Environ* 199:504–513. <https://doi.org/10.1016/j.apcatb.2016.06.030>
- Zhao GQ, Zheng YJ, He ZG, Lu ZX, Long WANG, Li CF, Jiao FP, Deng CY (2018) Synthesis of Bi₂S₃ microsphere and its efficient photocatalytic activity under visible-light irradiation. *T Nonferr Metal Soc* 28(10):2002–2010. [https://doi.org/10.1016/S1003-6326\(18\)64844-7](https://doi.org/10.1016/S1003-6326(18)64844-7)

Chapter 5

Sonochemical Treatment of Textile Wastewater



Slimane Merouani and Oualid Hamdaoui

Contents

| | | |
|-------|---|-----|
| 5.1 | Introduction | 148 |
| 5.2 | Basic Principles of Sonochemistry and Sonochemical Treatment | 149 |
| 5.3 | Sonochemical Reactors | 152 |
| 5.3.1 | Wave and Bubbles Characteristics in Sonochemical Reactors | 152 |
| 5.3.2 | Quantification of Acoustic Power in Sonochemical Reactors | 154 |
| 5.3.3 | Quantification of Active Bubble Number in Sonochemical Reactors | 154 |
| 5.4 | Sono-oxidation of Textile Dyes | 155 |
| 5.5 | Reaction Zone and Oxidation Pathways for Textile Dyes | 166 |
| 5.5.1 | Radical Probe Technique | 166 |
| 5.5.2 | Data Fitting Using Mathematical Interfacial Models | 167 |
| 5.6 | Influence of Ultrasonic and Environmental Parameters | 169 |
| 5.6.1 | Frequency of Ultrasound | 169 |
| 5.6.2 | Ultrasonic Power | 170 |
| 5.6.3 | Liquid Temperature | 171 |
| 5.6.4 | Dissolved Gases | 172 |
| 5.6.5 | Initial Dye Concentration | 172 |
| 5.6.6 | pH | 173 |
| 5.7 | Influence of Water Matrix | 174 |
| 5.8 | Process Intensification Using Selected Additives | 176 |
| 5.8.1 | CCl ₄ | 176 |
| 5.8.2 | Iron (Fe ²⁺) | 177 |
| 5.8.3 | Persulfate (S ₂ O ₈ ²⁻) | 178 |
| 5.8.4 | Periodate (IO ₄ ⁻) | 178 |
| 5.8.5 | Nanoparticles | 179 |
| 5.9 | Conclusion | 180 |
| | References | 181 |

S. Merouani

Laboratory of Environmental Process Engineering, Department of Chemical Engineering,
Faculty of Process Engineering, Salah Boubnider Constantine 3 University, Constantine,
Algeria

O. Hamdaoui (✉)

Chemical Engineering Department, College of Engineering, King Saud University, Riyadh,
Saudi Arabia

© The Editor(s) (if applicable) and The Author(s), under exclusive license to
Springer Nature Switzerland AG 2021

Inamuddin et al. (eds.), *Water Pollution and Remediation: Photocatalysis*,
Environmental Chemistry for a Sustainable World 57,
https://doi.org/10.1007/978-3-030-54723-3_5

147

Abstract Owing to the stability and resistance to biodegradation of synthetic dyes, their elimination from industrial wastewater is a very difficult task. This problem has triggered environmental engineers and scientists to search for innovative solutions. Over the last two decades, considerable attention has been paid to the use of ultrasound as an alternative advanced oxidation process for the degradation of textile dyes in wastewater. This process offers effective destruction of contaminants via reaction with $\bullet\text{OH}$ radical or pyrolysis in different reaction zones.

In this chapter, we reviewed the major progresses in the application of ultrasound, i.e., sonochemical process, for the destruction of textile dyes in aqueous solutions: (i) principles of the sonochemical process and sonoreactors were given, (ii) the most interesting works conducted in the field were summarized together with their significant findings, (iii) the influence of sonochemical and environmental parameters on the process performance was discussed in depth, (iv) the impact of the water matrix on the sonochemical treatment of dyes was elucidated, and (v) the most recent intensification techniques of the sonochemical process were emphasized. Finally, some interesting trends and perspectives were reported together with some highlighting needs to innovation.

Keywords Industrial wastewater · Synthetic dyes · Advanced oxidation processes · Ultrasound · Sonoreactors · Hydroxyl radical · Process intensification

5.1 Introduction

Among different industrial sectors, the textile industry is one of the largest water consumers and produces about 50–100 L wastewater per kg of finished product (Arslan-Alaton et al. 2008). Estimates indicate that approximately 280,000 tons of the textile dyes are released in water basins through textile effluents (Asghar et al. 2015). These compounds are chemically stable and non-biodegradable and exist as substances that may provoke toxic and carcinogenic effects (Brown and De Vito 1993; Konstantinou and Albanis 2004). Additionally, dye effluent damages the aesthetics of receiving waters and hinders the penetration of oxygen provoking an effective perturbation of the aquatic life (Eren 2012). Therefore, the treatment of textile dyes in wastewater has received great care from the researchers.

Conventional treatment processes for textile wastewater usually involve physical and biological methods. Physical methods, i.e., precipitation, adsorption on activated carbon, coagulation–flocculation, and reverse osmosis, are mostly nondestructive and only transfer pollutants into other phases that require secondary treatment. Biological processes are in general slow, generate large amounts of sludge, and do not degrade the organic load to a suitable level (Konstantinou and Albanis 2004).

Facing this situation, advanced oxidation processes have been proposed to suppress the drawbacks of the conventional treatment techniques. These innovative

processes are based on the in situ production and use of hydroxyl radical, i.e., $\bullet\text{OH}$, as a powerful and nonselective oxidant ($E^0 = 2.8 \text{ V}$) that reacts with most organics with high rate constant, i.e., $10^6\text{--}10^9 \text{ M}^{-1} \text{ s}^{-1}$ (Stefan 2017). Advanced oxidation processes like Fenton process, electro-Fenton, UV/ H_2O_2 , UV/ozone, $\text{H}_2\text{O}_2/\text{O}_3$, and UV/ TiO_2 can mineralize partially or completely almost organic pollutants (Parsons 2004; Pignatello et al. 2006; Von Sonntag 2008).

Due to the ability of ultrasound (20–1000 kHz) to generate hydroxyl radicals, this technique has been classified as an alternative advanced oxidation process for water and wastewater treatment (Thompson and Doraiswamy 1999; Pétrier 2015). The sonochemical treatment presents several advantages like no addition of reagents, simple to handling and selective degradation depending to the nature of pollutants (Adewuyi 2001; Torres-Palma and Serna-Galvis 2018).

This chapter reviewed fundamental and application aspects of textile effluent treatment by ultrasound. The scope is restricted to efforts made in the last two decades, which one part to the literature available data and the other part on the process performance in different matrices, influencing factors and process intensification techniques. The work was then ended by a conclusion in which some interesting perspectives were highlighted.

5.2 Basic Principles of Sonochemistry and Sonochemical Treatment

Since the 1950s, it has been recognized that the passage of ultrasound in the frequency range of 20 kHz–1 MHz through aqueous solution containing solutes can produce oxidation reactions, which was called sonochemistry (Weissler et al. 1950). The simplest system evidencing the occurrence of chemical reactions is the oxidation of KI. When a solution of KI was exposed to ultrasound, the colorless solution changed to yellow, indicating the oxidation of iodide ions into triiodide ions I_3^- (Weissler et al. 1950; Hart and Henglein 1985, 1987; Gutiérrez et al. 1987). Besides, it has been well recognized that the main products of water sonolysis are hydrogen peroxide and hydrogen (Anbar and Pecht 1964; Fischer et al. 1986; Hart and Henglein 1987), while nitrite and nitrate ions can also be formed for the case of air-saturated solution (Mead et al. 1976; Hart et al. 1986).

The sonochemical effect arises from the so-called acoustic cavitation, which is described as the nucleation, growth, and collapse of transient cavities during ultrasonic irradiation of liquids (Leighton 1994; Mason and Peters 2002). The principle of this event and their subsequent chemical effects is illustrated in Fig. 5.1. The microbubbles can be either stable, oscillating about their average or equilibrium size for many acoustic cycles, or transient when they grow to a certain size in one or at most a few acoustic cycles and violently collapse during the compression part of the wave (Yasui 2011). The fast collapse of these bubbles is nearly adiabatic, yielding

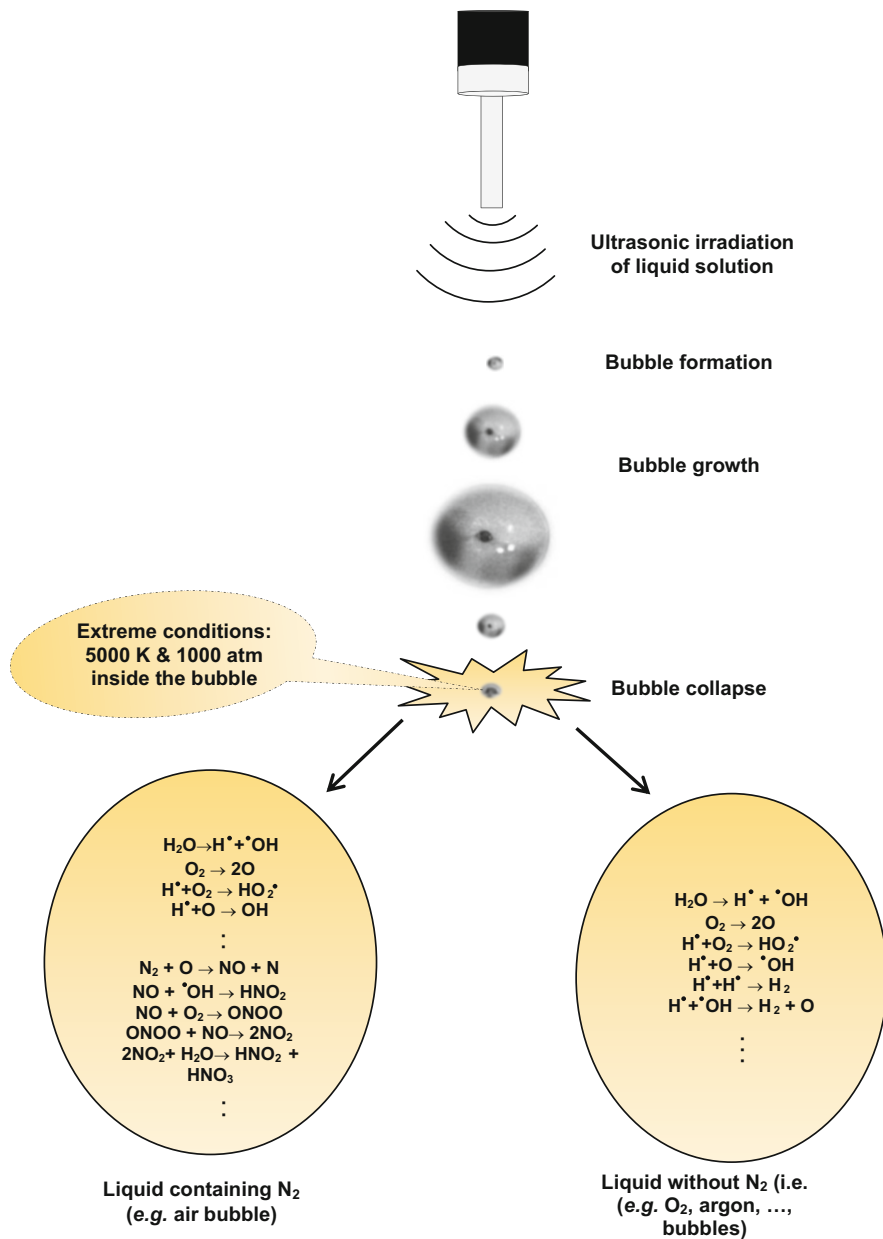


Fig. 5.1 Acoustic cavitation and water sonolysis during the sonication of aqueous solution in the absence and presence of dissolved nitrogen

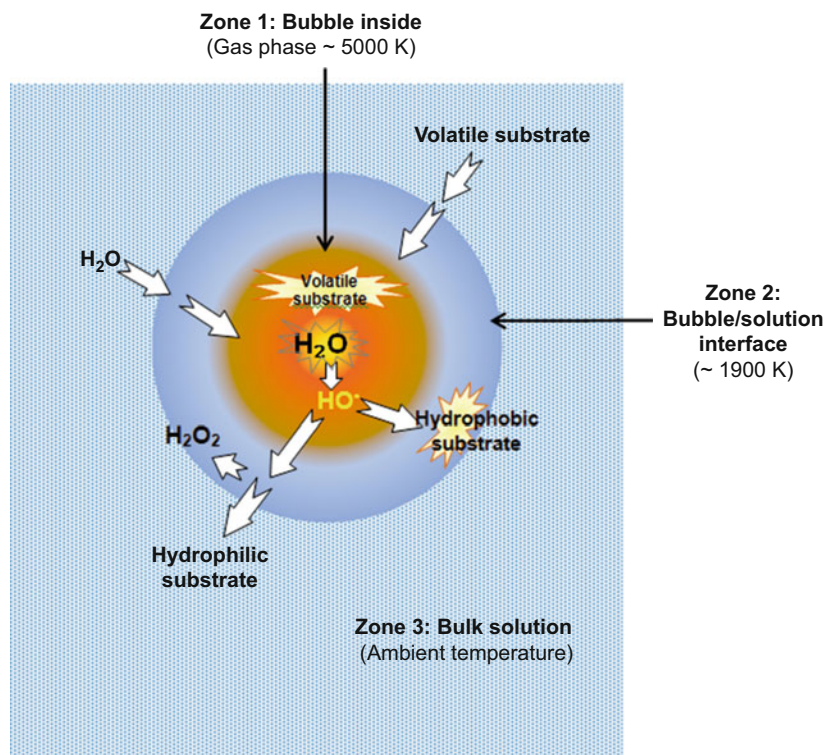


Fig. 5.2 Different reaction zones and degradation mechanisms of organic pollutants under ultrasonic treatment. Note that in the absence of aqueous substrate, $\bullet\text{OH}$ recombine at the bubble-solution interface to form H_2O_2

internal bubble temperature and pressure of ~ 5000 K and ~ 1000 atm, respectively (Merouani et al. 2014d).

Under these circumstances, water vapor molecules are decomposed into $\text{H}\bullet$ and $\text{HO}\bullet$ radicals, and with O_2 and N_2 presence, various other reactive and non-reactive entities may form (Merouani et al. 2014c). Radicals can recombine, react with the gaseous species, or diffuse out of the bubble to serve as aqueous oxidants (Adewuyi 2001). In parallel, volatile compounds, which evaporate into the bubble, can be decomposed under the high bubble temperature (P etrier and Francony 1997; Adewuyi 2001).

The sonochemical effect including reaction zones and degradation pathways is illustrated in Fig. 5.2. Sonochemistry offers three reactive zones, (i) the hot bubble interior, (ii) the bubble-solution interface, and (iii) the solution bulk, and two reaction mechanisms: (i) gas-phase pyrolytic oxidation for volatile compounds and (ii) reaction with radicals, i.e., $\text{HO}\bullet$, at the bubble-solution interface and in the liquid bulk for nonvolatile compounds (Petrier et al. 1998). It has been reported that the concentration of hydroxyl radical is higher at the liquid shell of the acoustic bubble, whereas only about 10% of radicals may reach the solution bulk (Henglein 1995; Mark et al. 1998; Tauber et al. 1999).

In addition to chemical consequence, acoustic cavitation produces several physical events such as micro-jets with speed of ~ 100 m/s, shock waves, macro- and micro-mixing (Hamdaoui 2009; Hamdaoui 2011; Hamdaoui and Naffrechoux 2007), as well as light emission, i.e., sonoluminescence (Suslick et al. 1999). SL has been recently employed to estimate the bubble temperature and pressure reached within the collapsing bubble as well as the bubble size (Lee et al. 2005; Suslick and Flannigan 2008). Temperature of ~ 5000 K and pressure of up to 1700 atm were estimated by Prof. Suslick's group through analyzing SL spectrums obtained from silicon oil and metal carbonyls (Suslick and Flannigan 2008).

5.3 Sonochemical Reactors

There are two most common types of sonochemical reactors used in sonochemical processes (Yasui et al. 2005; Torres-Palma and Serna-Galvis 2018): (i) horn-type systems, in which an immersed horn tip irradiates directly the liquid, as stated in Fig. 5.3a, and (ii) a standing wave-type systems, in which the irradiating transducer is mounted to the bottom surface of the reactor. This type includes the two common configurations of Fig. 5.3b, c: bath system with indirect sonication, in which cell containing the solution is dipped in the ultrasonic bath, and bath with direct sonication in which irradiation travels directly to the solution via a transducer fixed at the bottom of the bath, i.e., the cylindrical shape is mostly used herein. All these systems are generally equipped with heating-cooling system to control the temperature of the irradiating solution.

From the two main systems (horn and standing wave), continuous and pulsed irradiation modes are possible, even though the continuous mode is often used. Also, diverse configurations and geometries of reactors were developed (Keil and Swamy 1999). Sonochemical reactors may also be operated in continuous or batch modes (Keil and Swamy 1999; Entezari et al. 2003). Detailed information about design aspect of sonochemical reactors can be found in refs. (Keil and Swamy 1999; Gogate et al. 2003; Gogate 2008; Sutkar and Gogate 2009).

5.3.1 *Wave and Bubbles Characteristics in Sonochemical Reactors*

For an irradiation horn system, the generated wave is closely spherical, and its amplitude falloffs immediately as the liquid depth, i.e., the distance from the horn tip, increases (Yasui et al. 2005). In standing wave-type systems, the ultrasonic amplitude is much lesser than that generated in horn-type systems. Bubbles in this system gather at the location where the ultrasonic amplitude is near the critical point at which the direction of the radiation force is inversed (Yasui et al. 2005).

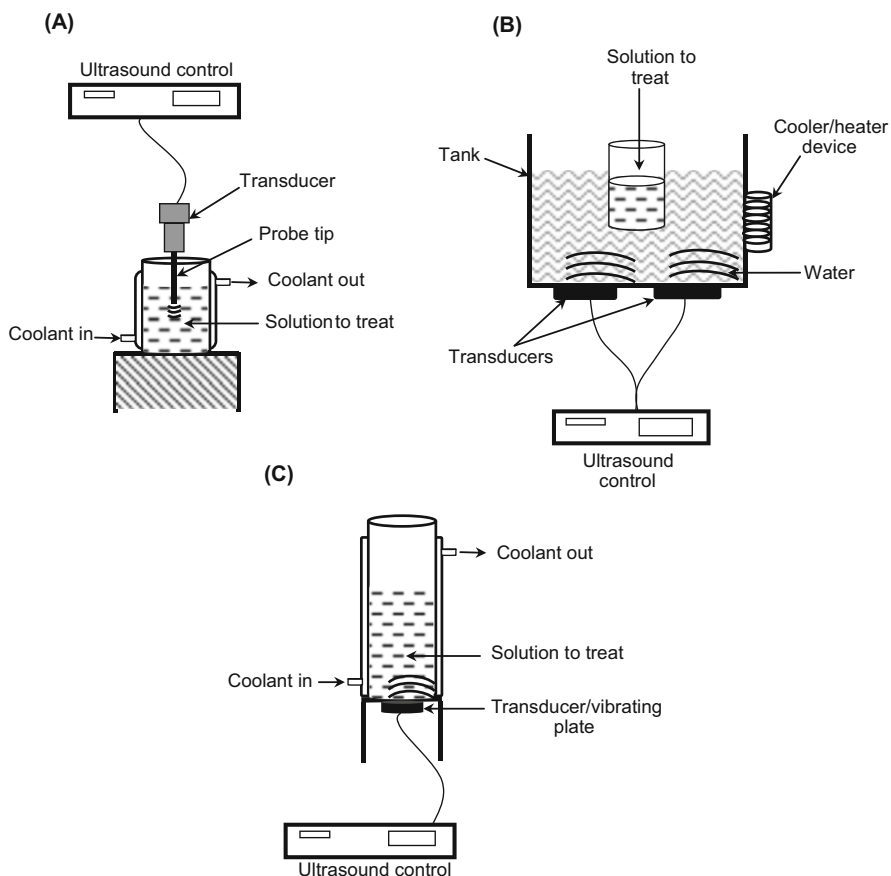


Fig. 5.3 Main types of sonochemical reactors. (a) Probe system, (b) bath system with indirect sonication, and (c) standing wave reactor with direct sonication. Reprinted with permission from (Torres-Palma and Serna-Galvis 2018)

However, in horn-tip system, cavities are concentrated near the tip where the amplitude is large (Renaudin et al. 1994). Additionally, in a horn-type sonochemical systems, bubbles are mostly of vaporous nature, whereas gaseous type of bubbles are dominant in a standing wave reactor since the bubbles density in this system is concentrated at the region where the radiation amplitude is low (Yasui et al. 2005). In general, chemiluminescence of luminol or sonochemiluminescence has been used for visualizing the reaction zones in sonochemical reactors (Renaudin et al. 1994; Pétrier et al. 2008; Son et al. 2011, 2012; Choi 2015).

5.3.2 *Quantification of Acoustic Power in Sonochemical Reactors*

In sonochemical process, the input power delivered by the ultrasonic generator will not be totally absorbed by the solution; a part will be lost by reflection at the transducer, diffraction by the solution, and other phenomena (Mason and Lorimer 2002). The absorbed part of power by the solution, mostly named as acoustic power, is responsible for all sonochemical events. Researchers have used calorimetric method for estimating the acoustic power dissipated in the solution. This latter can be estimated using the following equation (Kimura 1996; Merouani et al. 2010b):

$$P_{ac} = mC_p \frac{dT}{dt} \quad (5.1)$$

where P_{ac} is the acoustic power; dT/dt is the initial rate of solution temperature increase vs. time; C_p is the specific heat capacity of the liquid, i.e., $4.18 \text{ kJ}\cdot\text{kg}^{-1} \text{ K}^{-1}$ for water; and m is the mass of the irradiating solution. Note that during this experiment no cooling/heating operation could be used. In general, the effective energy transferred to the solution is around 30–60% of that delivered by the ultrasonic generators. Additionally, the acoustic power is volume-dependent, and an optimum solution volume was mostly reported (Merouani et al. 2010b; Son 2017).

5.3.3 *Quantification of Active Bubble Number in Sonochemical Reactors*

Active bubbles are those responsible for the chemical effect of ultrasound. Knowledge of the number of active bubbles in acoustic cavitation field is of great importance for determining of the performance of sonochemical reactors. Data on this subject is very limited, perhaps due to complexity of acoustic cavitation phenomena. Merouani et al. (2014a) have recently developed a semi-empirical model for estimating the number of active cavities in sonochemical reactors at controllable operating conditions. Equation 5.2 was obtained through carrying out material balances for $\cdot\text{OH}$, $\text{HO}_2\cdot$, and H_2O_2 in the liquid after estimating their quantities ($n_{\cdot\text{OH}}$, $n_{\text{H}_2\text{O}_2}$, and $n_{\text{HO}_2\cdot}$) released from one bubble using a single bubble sonochemistry model (Merouani et al. 2014a):

$$N = \frac{r_{\text{H}_2\text{O}_2}}{n_{\text{H}_2\text{O}_2} + 0.5(n_{\cdot\text{OH}} + n_{\text{HO}_2\cdot})} \quad (5.2)$$

The production rate of H_2O_2 , $r_{\text{H}_2\text{O}_2}$ was determined experimentally. Note that the number of bubbles N depends strongly on operational conditions of the experiment

because all parameters of Eq. 5.2 are sensitive to experimental conditions. Table 5.1 provides some estimated values of N under different experimental frequencies. Overall, it was found that billions of bubbles can be formed and increasing frequency of ultrasonication engenders a substantial increase in the number of bubbles.

5.4 Sono-oxidation of Textile Dyes

Significant amount of works on the degradation of dyes by ultrasound has been published, particularly, in the last two decades. Table 5.2 reports the most significant studies published between 2000 and 2019 for a variety of synthetic dyes. The significant results of each study were included together with experimental conditions and type of the reactor. In all these cases, consequences of using sonochemical treatment are nearly the same: dyes were effectively degraded, and at least partial mineralization was achieved.

During the treatment, the dye concentration decays exponentially with time until total bleaching, suggesting first-order reaction law. The lower TOC and COD removals under ultrasound were attributed to the formation of highly hydrophilic by-products, which have no tendency to accumulate at the reactive bubble-solution interface (Torres et al. 2007; Guzman-Duque et al. 2011; Boutamine et al. 2017; Hamdaoui and Merouani 2017b). However, these compounds may be readily biodegradable, since biodegradability analysis demonstrated that the ratio BOD_5/COD was superior than 0.4 (Guzman-Duque et al. 2011).

On the other hand, the degradation rate was strongly sensitive to the operation parameters. Generally, best degradation performances were obtained at higher levels of delivered power (or intensity), solution temperature, and lower solution pH, although strong basic pH provided higher conversion rates for some cases (Rehorek et al. 2004; Ghodbane and Hamdaoui 2009a; Merouani et al. 2010c; Dalhatou et al. 2015). Additionally, higher frequency ultrasound (higher than 100 kHz) was most effective for dye degradation than low frequencies. It seems also that there is an optimum frequency, between 200 and 800 kHz, for the degradation of textile dyes (Eren and Ince 2010; Dükkanci et al. 2012; Ferkous et al. 2015b; Rayaroth et al. 2015).

Dyes are generally highly water-soluble substrate of lower vapor pressure and Henry's law constants (Taamallah et al. 2016). They are classified as nonvolatile compounds which likely degraded via reaction with hydroxyl radicals at the exterior of the collapsing bubble (Ince and Tezcanli-Güyer 2004; Okitsu et al. 2005, 2015; Merouani et al. 2016). However, the local reaction zone at which degradation occurred may be moved between the bulk solution and the interfacial area, depending on several experimental parameters. For instance, experimental evidence showed that when the concentration of the dye is low, the bulk of the solution is the preferential reaction zone. However, the reaction zone shifts toward the bubble-solution interface by progressive increase of the initial pollutant concentration in the solution (Okitsu et al. 2005; Chiha et al. 2010; Chadi et al. 2018b).

Table 5.1 Bubble number (N) and theoretical parameters of Eq. 5.2, predicted under the experimental conditions of Pétrier and Francony (1997) and Jiang et al. (2006). Reprinted with permission from (Merouani et al. 2014a)

| Frequency (kHz) | Rate of H ₂ O ₂ production, $r_{H_2O_2}$ (μM/min) | | Single bubble yield | | | Number of bubbles N (L ⁻¹ s ⁻¹) | |
|-----------------|---|--------------|------------------------|------------------------|------------------------|--|----------------------|
| | Pétrier and Francony | Jiang et al. | n_{off} | n_{HO_2} | $n_{H_2O_2}$ | Pétrier and Francony | Jiang et al. |
| 20 | 0.7 | 1.1 | 3.09×10^{-12} | 1.04×10^{-13} | 8.95×10^{-15} | 7.2705×10^3 | 1.1425×10^4 |
| 200 | 5 | 5.2 | 3.06×10^{-14} | 1.09×10^{-15} | 8.52×10^{-17} | 5.2249×10^6 | 5.4339×10^6 |
| 500 | 2.1 | 3 | 1.80×10^{-15} | 6.49×10^{-17} | 5.19×10^{-18} | 3.7309×10^7 | 5.3299×10^7 |
| 800 | 1.4 | 2 | 7.01×10^{-16} | 2.53×10^{-17} | 2.02×10^{-18} | 6.3908×10^7 | 9.1297×10^7 |

Table 5.2 Studies utilizing ultrasound for the degradation of textile dyes

| Dye contaminant | Water matrix/ reactor type | Ultrasonic parameters/ gas atmosphere | Experimental conditions | Treatment efficiency/other results or remarks | Ref. |
|--|---|---|--|--|---|
| Azobenzene, methyl orange, o-methyl red, and p-methyl red | Deionized water (DI)/standing wave reactor (DS) | $f = 500$ kHz $P_{\text{elec}} = 50$ W air, O ₂ , and argon atmospheres | $V = 650$ mL $C_0 = 10$ µM $T = 15$ °C pH ~7 | Bleaching was completed within the first 40 min of soni- cation, whereas mineralization is attained after a longer period of time (about 30–50% reduc- tion in TOC ₀ was achieved after 300 min) The use of argon as a back- ground gas enhanced the deg- radation rate by 10% compared to air and O ₂ | Joseph et al. (1999) |
| C.I. Reactive Red 141, C.I. Reactive Black 5, C.- I. Basic Brown 4, C.I. Basic Blue 3 | Deionized water (DI)/standing wave reactor (DS) | $f = 520$ kHz $P_{\text{elec}} = 10$ –100 W Air atmosphere | $V = 300$ mL $C_0 = 20$ –40 mg/L $T = 25$ °C pH 5.5–6.5 | Reduction of more than 80% in the visible bands and about 11–92% in the 254 nm absor- bance were measured after 2 h of sonication at 100 W Significant degrees of toxicity reduction were accomplished along with color and aromatic carbon degradation | Tezcanli- Guyer and Ince (2003) |
| C.I. Reactive Yellow 15, C.- I. Reactive Red 22, C.- I. Reactive Blue 28, Remazol Dark Black N, C.I. Reactive Blue 220, and C.I. Reactive Black | Deionized water (DI)/probe | $f = 20$ kHz Intens. = 80 W/cm ² air atmosphere | $V = 50$ mL $C_0 = 10$ mg/L $T = 25$ °C pH NI | 70–96% decolorization was achieved in 7 h of sono- treatment | Vončina and Majcen-Le- Marechal (2003) |

(continued)

Table 5.2 (continued)

| Dye contaminant | Water matrix/ reactor type | Ultrasonic parameters/ gas atmosphere | Experimental conditions | Treatment efficiency/other results or remarks | Ref. |
|--|---|--|---|---|--|
| C.I. Reactive Orange 16 and C.I. acid orange 7 | Deionized water (DI)/standing wave reactor (DS) | $f = 300$ kHz $P_{elec} = 25$ W Argon atmosphere | $V = 100$ mL $C_0 = 30$ μ M $T = 20$ °C pH 3–9.5 | Removals of 90% for acid orange and 73% for Reactive Orange 16 were measured after 1 h of irradiation with destruc- tion of more than 40% of initial aromatic rings of the dyes The bleaching rates accelerated with increased acidity Decolorization of dyes was related to the size of the mole- cule and the type or position of substituents about azo bonds | Ince and Tezcanli- Güyer (2004) |
| Acid orange 5, acid orange 52, Direct Blue 71, Reactive Black 5, and Reactive Orange 16 and 107 | Deionized water (DI)/standing wave reactor (DS) | $f = 850$ kHz $P_{elec} = 60$ –120 W air atmosphere | $V = 100$ mL $C_0 = 100$ μ M $T = 30$ °C pH Ni | Ultrasound was able to remove and mineralize dyes to non-toxic end products (ace- tate, formate, oxalate, sulfate, and nitrate) First-order decay rate constants vary from 0.87 to 6.21 h^{-1} for 120 W and from 0.3 to 1.66 h^{-1} for 90 W | Rehorek et al. (2004) |
| Acid Blue 40 and methylene blue | Deionized water (DI)/bath | $f = 354.5$ kHz $P_{elec} = 35$ W Argon and air atmospheres | $V = 250$ mL $C_0 = 10$ μ M for AB40 and 3 μ M for MB $T = 25$ °C pH 9–11 | Both dyes were degraded effi- ciently, and ~80% of Acid Blue 40 was removed at only 20 min of treatment Initial decay rate of Acid Blue 40 was $k_{AB40} = 7.7 \times 10^{-9}$ M/ s, and that of methylene blue was $k = 8.1 \times 10^{-9}$ M/s under | Minero et al. (2008) |

| | | | | | |
|------------------------|--|--|--|---|-------------------------------|
| Malachite green | Deionized water (DI)/bath | $f = 35$ kHz $P_{\text{elec}} = 49$ W Air atmosphere | $V = 1000$ mL $C_0 = 2\text{--}10$ mg/L $T = 21\text{--}34$ °C Natural pH | argon saturation, but lower values were measured for air saturation | Behnajady et al. (2008) |
| Reactive brilliant red | Deionized water (DI)/probe | $f = 20$ kHz $P_{\text{elec}} = 150$ W Air atmosphere | $V = 100$ mL $C_0 = 10\text{--}100$ mg/L $T = 25\text{--}55$ °C pH 2–12 | The dye was degraded by 20 kHz ultrasound Strong acidic and basic conditions as well as lower temperature provided the best degradation performance | Wang et al. (2008) |
| Acid Blue 25 | Deionized water (DI)/probe and standing wave reactors (DS) | $f = 1700$ kHz (SW) and 22.5 kHz (probe) $P_{\text{elec}} = 17$ W Air atmosphere | $V = 100$ mL $C_0 = 10\text{--}150$ mg/L $T = 20\text{--}55$ °C pH 1–11.8 | The degradation rate of the dye increased with increasing temperature and C_0 , whereas pH 1 and 11.8 provided the best conversion yields Higher degradation rate was obtained with 1700 kHz as compared with 22.5 kHz | Ghodbane and Hamdaoui (2009a) |
| Martius yellow | Deionized water (DI)/standing wave reactor (DS) | $f = 355$ kHz $P_{\text{elec}} = 30$ W Air atmosphere | $V = 200$ mL $C_0 = 0.1$ mM $T = 20 \pm 5$ °C pH < 4 | Martius yellow was degraded after 240 min of sonication Catechol and benzoic, salicylic, and maleic acids were identified as degradation intermediates | Singla et al. (2009) |

(continued)

Table 5.2 (continued)

| Dye contaminant | Water matrix/ reactor type | Ultrasonic parameters/ gas atmosphere | Experimental conditions | Treatment efficiency/other results or remarks | Ref. |
|---|--|---|--|---|-----------------------------------|
| Rhodamine B | Deionized water (DI)/standing wave reactor (DS) | $f = 300$ kHz $P_{elec} = 20-60$ W Air atmosphere | $V = 300$ mL $C_0 = 5-50$ mg/L $T = 25-55$ °C pH 1-13 | Complete removal of the dye (5 mg/L) was achieved at 120 min with COD decrease being as ~45% Too fast degradation occurred by increasing ultrasonic power and liquid temperature The degradation rate was sig- nificantly improved at acidic and strong basic medium, as compared to neutral pH | Merouani et al. (2010c) |
| C.I. Direct Yellow 9 and C.I. Reactive Red 141 | Deionized water/ probe and standing wave reactors (DS) | $f = 20$ kHz (probe) and 577, 861, and 1145 kHz $P_{elec} = 180$ W for 20 kHz and 120 W for other frequencies Air atmosphere | $V = 100$ mL for (20 kHz) experiments and 250 mL for other frequencies $C_0 = 28.75$ µM $T = 20$ °C pH 6.6-6.9 | High frequency provided sig- nificant color decay in 30 min contact, whereas low fre- quency (20 kHz) alone was found totally ineffective for bleaching dyes 577 kHz was the optimum fre- quency for Direct Yellow 9 degradation, whereas that for Reactive Red 141 was 1145 kHz | Eren and Ince (2010) |
| Crystal violet | Deionized water/ standing wave reactor (DS) | $f = 800$ kHz $P_{elec} = 20-80$ W Argon, air, CO ₂ atmospheres | $V = 300$ mL $C_0 = 2.45-1225$ µM $T = 20$ °C pH 3-9 | The best performances were obtained at higher power (80 W) with argon as a satu- rating gas, whereas the pH had no significant effect CO ₂ suppress completely the | Guzman- Duque et al. (2011) |

| | | | | | | |
|--------------------------|---|--|--|--|---|------------------------|
| | | | | | sonochemical degradation of the dye Low TOC removal (~10%) was obtained after complete disappearance of the dye, but the degradation by-products were readily biodegradable (BOD ₅ /COD was higher than 0.4) Higher frequencies provide the best degradation yield, but the 850 kHz bath at a power of 22.07 W was the most cost-effective system for the degradation of orange II (optimum frequency) | Dükkanci et al. (2012) |
| Orange II | Deionized water/ probe and baths | $f = 20, 40, 380, 850, 1000,$ and 1176 kHz (Baths) $P_d = 11.7\text{--}22.07$ W, air atmosphere | $V = 200$ mL $C_0 = 0.14$ mM $T = 20$ °C pH 6.3 | | | |
| Coomassie Brilliant Blue | Deionized water/ standing wave reactor (DS) | $f = 200, 350, 620,$ and 1000 kHz $P_{dec} = 3.5\text{--}19.6$ W/mL Air atmosphere | $V = \text{NI}$ $C_0 = 10$ µM $T = 25$ °C pH 3–8 | | The optimum degradation performance was obtained at 350 kHz and 19.6 W/mL. At these conditions, the dye disappeared at less than 30 min The maximum degradation rate of the dye was observed under acidic pH | Rayaroth et al. (2015) |
| Malachite green | Deionized water/ standing wave reactor (DS) | $f = 300$ kHz $P_{elec} = 20\text{--}100$ W Air atmosphere | $V = 300$ L $C_0 = 5\text{--}500$ mg/L $T = 25$ °C pH 2–7 | | Ultrasound removed efficiently the dye from water, and higher degradation rates were recorded at higher power and lower solution pH Nitrate and nitrite were formed as products of water sonolysis | Moumeni et al. (2012) |

(continued)

Table 5.2 (continued)

| Dye contaminant | Water matrix/ reactor type | Ultrasonic parameters/ gas atmosphere | Experimental conditions | Treatment efficiency/other results or remarks | Ref. |
|-----------------------------------|---|--|---|--|----------------------------|
| Reactive Red 22 and methyl orange | Deionized water/ standing wave reactor (DS) | $f = 200$ kHz $P_{elec} = 200$ W Air and argon atmospheres | $V = 65$ mL $C_0 = 5.13\text{--}93.2$ μ M $T = 20$ °C pH 2 and 6.5 | Rapid disappearance of dyes was observed for lower C_0 , particularly when using argon as saturation gas The bubble/solution interface was the preferential reaction zone for dye degradation via •OH radical attack | Okitsu et al. (2005, 2015) |
| Naphthol blue black | Deionized water/ standing wave reactor (DS) | $f = 585, 860$ and 1140 kHz Intens. = 0.44–3.58 W/ cm^2 Argon, air, and N_2 atmospheres | $V = 300$ mL $C_0 = 3\text{--}120$ mg/L $T = 25$ °C pH 2–10 | More than 95% of the initial COD was achieved at 585 kHz for $C_0 = 5$ mg/L, whereas complete destruction of the dye required only 45 min The dye removal rate increased notably with increasing intensity and temperature and decreasing frequency and solution pH The degradation efficiency was much higher under Ar-saturated medium rather than air and N_2 atmospheres | Ferkous et al. (2015a, b) |
| Basic fuchsin | Deionized water/ standing wave reactor (DS) | $f = 600$ kHz $P_{elec} = 30\text{--}90$ W Air and N_2 atmospheres | $V = 300$ mL $C_0 = 1\text{--}15$ mg/L $T = 25$ °C pH 5.9 | Significant degradation was achieved (100% removal at 80 min for $C_0 = 5$ mg/L and 90% for $C_0 = 10$ mg/L) The degradation rate increased by factor of 2.8 when power | Taamallah et al. (2016) |

| | | | | | |
|---|---|--|--|---|-------------------------------|
| Cresol Red | Deionized water/ standing wave reactor (DS) | $f = 300$ kHz $P_{\text{elec}} = 20\text{--}80$ W Air atmosphere | $V = 300$ mL $C_0 = 60$ μM $T = 25$ °C pH 2–9 | increased from 30 to 90 W, whereas N_2 saturation decelerated the degradation rate Ultrasound effectively degraded the dye, and superior than 90% removal was achieved within 90 min of treatment for $C_0 = 60$ μM . Higher power and lower pH produced higher degradation rate | Fassi and Petrier (2016) |
| Rhodamine B, Acid Orange 7, and malachite green | Deionized water/ standing wave reactor (DS) | $f = 300$ kHz Intens. = 2 W/cm ² Air atmosphere | $V = 300$ mL $C_0 = 5$ mg/L $T = 25\text{--}55$ °C Natural pH (5–6) | More than 95% of the three dyes were removed after less than 60 min The removal rate increased substantially as the liquid temperature increased in the range 25–55 °C | Merouani et al. (2016) |
| Acid Orange 7 | Deionized water/ standing wave reactor (DS) | $f = 600$ kHz $P_{\text{elec}} = 40\text{--}120$ W Air atmosphere | $V = 200$ mL $C_0 = 5\text{--}30$ mg/L $T = 20$ °C pH 2–12 | 100% removal of the dye (20 mg/L) was achieved after 90 min, but only ~10% decrease in TOC_0 was obtained The treatment efficiency increased with power increase and pH decrease | Hamdaoui and Merouani (2017b) |
| Basic Red 29 | Deionized water/ standing wave reactor (DS) | $f = 300$ kHz $P_{\text{elec}} = 20\text{--}80$ W Argon, air, and N_2 atmospheres | $V = 200$ mL $C_0 = 5\text{--}200$ mg/L $T = 20$ °C pH 3–10 | 30 mg/L of the dye was completely eliminated after 120 min, but lower TOC and COD (15% and 28%) were achieved at 240 min Higher degradation rates were | Boutamine et al. (2017) |

(continued)

Table 5.2 (continued)

| Dye contaminant | Water matrix/ reactor type | Ultrasonic parameters/ gas atmosphere | Experimental conditions | Treatment efficiency/other results or remarks | Ref. |
|------------------|---|---|--|---|--|
| Brilliant Blue R | Deionized water/ standing wave reactor (DS) | $f = 300$ kHz $P_{elec} = 20-80$ W Air atmosphere | $V = 200$ mL $C_0 = 5$ mg/L $T = 25$ °C pH 2, 5.2 and 8 | associated with higher power, and the monoatomic gas (argon) showed the best deg- radiation yield 70% of the dye was eliminated after 20 min, while the com- plete degradation was achieved at 140 min The best degradation perfor- mance was attained at pH 8 and at higher ultrasonic power (80 W) | Hamdaoui and Merouani (2017a) |
| Toluidine blue | Deionized water/ standing wave reactor (DS) | $f = 1700$ kHz $P_{elec} = 17$ W Argon, air, N ₂ , and CO ₂ atmosphere | $V = 100$ mL $C_0 = 0.5-20$ mg/L $T = 20-70$ °C pH 6 | High-frequency ultrasound (1700 kHz) removed effi- ciently toluidine blue from water Argon accelerated notably the dye degradation, but CO ₂ completely suppresses the sonochemical process The effect of liquid tempera- ture was more pronounced at higher dye concentration, whereas no effect was observed for inferior than 2 mg/L | Chadi et al. (2018a, b) |

| | | | | | |
|---------------------|---|--|--|---|------------------------------|
| Naphthol blue black | Deionized water/ standing wave reactor (DS) | $f = 278$ kHz $P_{elec} = 20$ – 100 W Air atmosphere | $V = 400$ mL $C_0 = 8.1$ μ M $T = 20$ °C Natural pH | The dye removal decreased exponentially with time, and more than 95% was removed at 120 min for $C_0 = 8.1$ μ M While the degradation rate increased with power, the pH effect was dependent on the value of C_0 | Dalhatou et al. (2015, 2019) |
|---------------------|---|--|--|---|------------------------------|

Abbreviations: *DI* Deionized water, *DS* direct sonication, *NI* not indicated, C_0 initial pollutant concentration, V treated solution volume, T operating temperature, f frequency of ultrasound, P_{elec} delivered electric power, P_{ac} acoustic power, P_d power density and Intens.: acoustic intensity, *DS* direct sonication, *TOC* total organic carbon, *COD* chemical oxygen demand, *BOD₅* biochemical oxygen demand

Analysis of H_2O_2 formation versus initial dye concentration has been largely used (Guzman-Duque et al. 2011; Ferkous et al. 2015b; Boutamine et al. 2017). H_2O_2 is formed at the bubble surface via self-recombination of $\cdot\text{OH}$ (Kanthale et al. 2008; Merouani et al. 2010b). Note that H_2O_2 may also be formed via $\text{HO}_2\cdot + \text{HO}_2\cdot \rightarrow \text{H}_2\text{O}_2 + \text{O}_2$ but the rate constant of this reaction $k = 8.3 \times 10^5 \text{ M}^{-1} \text{ s}^{-1}$ is too low than that of $\cdot\text{OH} + \cdot\text{OH} \rightarrow \text{H}_2\text{O}_2$, i.e., $k = 5.5 \times 10^9 \text{ M}^{-1} \text{ s}^{-1}$ (Merouani et al. 2014a). At lower dye concentration, H_2O_2 accumulated at higher rate in the solution, but, when the initial dye concentration increased, H_2O_2 formation rate decreased progressively until reaching plateau (Ferkous et al. 2015b; Boutamine et al. 2017). These outcomes reflect that the flux of the dye molecules toward the interfacial region increased at elevated concentration provoking efficient scavenging of $\cdot\text{OH}$.

Therefore, the degradation rate of the dye will be then much higher at higher pollutant concentration. At very high concentration, the pyrolysis mechanism can also be take place as the temperature of the bubble-solution interface is too high, i.e., $\sim 1900 \text{ K}$ (Flint and Suslick 1991; Suslick et al. 1999).

5.5 Reaction Zone and Oxidation Pathways for Textile Dyes

Identification of the degradation by-products during sonolysis may give idea about the degradation mechanism and the reaction zone (Thompson and Doraiswamy 1999; Adewuyi 2001; Mason and Lorimer 2002). For example, the presence of hydroxylation products confirms the $\cdot\text{OH}$ radical pathway, whereas the formation of pyrolytic products such as methane and acetylene may reflect the pyrolysis mechanism inside the bubble (Barbier and Petrier 1996; Francony and Pétrier 1996; Pétrier and Francony 1997; Petrier et al. 1998, 2007; Pétrier 2015). However, for the case of dyes, the determination of such by products is very difficult due to the big and complex molecular structures of dyes. Other techniques for probing the reaction zone and the oxidation mechanism during the sonochemical degradation of dyes have been recently reported.

5.5.1 Radical Probe Technique

For this way, the strategy is to use radical scavengers for different regions. Alcohols were generally used for the gas-phase reactions. Alcohols are volatile compounds that easily penetrate into the bubble and degraded through a free-radical pyrolysis mechanism in which alcohols can react with $\cdot\text{OH}$ and, therefore, limit the concentration of radicals at the bubble-solution interface. Thus, alcohols trials may confirm (i) the $\cdot\text{OH}$ attack of the dye molecules at the outside of the bubble and (ii) can give evidence of the non-pyrolytic reaction of dyes in the acoustic cavity.

On the other hand, appropriate hydrophobic compounds, such as surfactant, and potassium iodide may be used for probing the interfacial region. These compounds, which are highly reactive toward $\cdot\text{OH}$, have tendency to accumulate at the bubble-solution interface and create a strong completion if the bubble-solution interface is the effective zone for degradation. Finally, more hydrophilic compounds such as sucrose, glucose, and humic acids, i.e., of high reactivity with $\cdot\text{OH}$, may be used for appreciating the contribution of bulk solution in the degradation of dyes.

Table 5.3 regroups the results of some studies that have used radical probe technique for the identification of the reaction zone and the degradation mechanism of some dyes. Overall, this method indicated that the sonochemical degradation of dyes mostly occurred at the bubble-solution interface via hydroxyl radical attack, although some radical reactions may also take place in the solution bulk.

5.5.2 Data Fitting Using Mathematical Interfacial Models

Recent progresses in sonochemistry showed that the sonolytic degradation of non-volatile compounds can be modeled by a heterogeneous kinetics models similar to that of Langmuir–Hinshelwood in photocatalysis (Okitsu et al. 2005). The first model, i.e., based on Eq. 5.3, assumes the adsorption–desorption equilibrium of the pollutant molecules at the bubble-solution interface, i.e., this region is the probable reaction zone for this model. Serpone et al. (1994) have proposed another model, i.e., based on Eq. 5.4, governing the degradation rates in both the interfacial region and the bulk of the solution:

$$r_0 = \frac{kKC_0}{1 + KC_0} \quad (5.3)$$

$$r_0 = K_b + \frac{kKC_0}{1 + KC_0} \quad (5.4)$$

In these equations, r_0 is the initial degradation rate, K_b is a constant representing the rate of degradation in the bulk liquid, K is the equilibrium constant, k is the pseudo-rate constant, and C_0 is the initial pollutant concentration.

Equations (5.3) and (5.4) perfectly fitted the degradation kinetics of various dyes under different experimental conditions, as can be consulted in refs. (Merouani et al. 2010c; Moumeni et al. 2012; Ferkous et al. 2015b; Taamallah et al. 2016; Boutamine et al. 2017; Hamdaoui and Merouani 2017b; Merouani and Hamdaoui 2017). The conclusion from all these studies was that the sonochemical degradation of dyes is predominately an interfacial event occurring via reaction with $\cdot\text{OH}$ radicals.

Table 5.3 Studies utilizing radical probe technique for the identification of the reaction zone and the oxidation pathway during ultrasonic treatment

| Dye contaminant | Conditions | Probes | Observations/ conclusions | Ref. |
|------------------|--|--|---|-------------------------------|
| Rhodamine B | $f = 300$ kHz $P_{elec} = 20\text{--}60$ W Air atmosphere $C_0 = 5$ mg/L 25 °C, natural pH | Tert-butyl alcohol (7–2500 mg/L), sucrose and glucose (0.1–5 g/L) | At high tert-butyl alcohol concentrations, the degradation was effectively quenched, but not completely The sonolytic degradation of dye slightly decreased in the presence of sucrose and glucose <i>Conclusion:</i> interfacial reactions of rhodamine B with hydroxyl radical were the main degradation mechanism | Merouani et al. (2010c) |
| Acid orange 7 | $f = 600$ kHz $P_{elec} = 120$ W Air atmosphere $C_0 = 20$ mg/L 20 °C, pH 5.3 | Tert-butyl alcohol (1–100 mM), KI (1–10 mM) and humic acid (HA: 5–40 mg/L) | Addition of 0.001 M tert-butyl alcohol considerably reduced acid orange 7 degradation and a 100-fold increase of alcohol concentration quenches, but not completely, the degradation Addition of KI resulted in a significant decrease of the dye conversion. However, HA has no significant impact on the sonolytic destruction of acid orange 7 <i>Conclusion:</i> interfacial reactions of acid orange 7 with hydroxyl radical were the main degradation mechanism | Hamdaoui and Merouani (2017b) |
| Basic fuchsin | $f = 600$ kHz $P_{elec} = 90$ W Air atmosphere $C_0 = 10$ mg/L 25 °C, natural pH | Tert-butyl alcohol (1–10 mM) | After adding 1 and 10 mg/L of alcohol, the efficiency of BF removal decreased to 10 and 3%, respectively <i>Conclusion:</i> $\bullet\text{OH}$ radical plays the major role in the oxidation of BF | Taamallah et al. (2016) |
| Brilliant Blue R | $f = 300$ kHz $P_{elec} = 80$ W Air atmosphere | 2-Propanol (1–100 mM) | The degradation of the dye was significantly reduced by the addition of 2-propanol at 1 and | Hamdaoui and Merouani (2017a) |

(continued)

Table 5.3 (continued)

| Dye contaminant | Conditions | Probes | Observations/ conclusions | Ref. |
|-----------------|--|---|--|-------------------------|
| | $C_0 = 5 \text{ mg/L}$ 25 °C, pH 5.2 | | 10 mM, whereas a 100% inhibition was obtained with 100 mM of alcohol <i>Conclusion:</i> •OH radical plays the major role in the oxidation of the dye | |
| Malachite green | $f = 300 \text{ kHz}$ $P_{\text{elec}} = 80 \text{ W}$ Air atmosphere $C_0 = 5 \text{ mg/L}$ 25 °C, pH 5.2 | Ethanol, 2-propanol, and tert-butyl alcohol (1–1000 mg/L) | The degradation rate was monotonically decreased with each alcohol addition <i>Conclusion:</i> •OH is the primary oxidant for malachite green degradation | Behnajady et al. (2008) |

Abbreviations: C_0 Initial pollutant concentration, f frequency of ultrasound, P_{elec} delivered electric power

5.6 Influence of Ultrasonic and Environmental Parameters

As briefly noticed in Sect. 5.4, the efficiency of the sonolytic process is sensitive to the various environmental and ultrasonic parameters. Ultrasonic parameters include frequency and power (or intensity), whereas the solution characteristics, i.e., pH, temperature, initial dye concentration, and dissolved gases, are the most investigated environmental factors. Although the impact of these parameters was reported in several reviews, we provide herein a new analysis approach based on the estimation of the single bubble yield and the number of collapsing bubbles in the irradiating solution.

5.6.1 Frequency of Ultrasound

Several researchers have assessed the influence of frequency in the range of 20 kHz–2 MHz on the degradation of various textile dyes. Ghodbane and Hamdaoui (2009a) have reported that for the sonochemical degradation of Acid Blue 25 at 1700 kHz, the initial degradation rate was 3.5-fold higher than that of 22.5 kHz. Ferkous et al. (2017) have tested the degradation of the azo dye naphthol blue black at 20 and 585 kHz and found that the latter frequency provoked an enhancement of 5.66-fold in the initial degradation rate. In another paper, the same authors have reported that the order of initial naphthol blue black degradation rate as well as the H_2O_2 generation rate followed the order 585 > 840 > 1140 kHz, revealing that 585 kHz is the optimum frequency for the effective degradation of the dye (Ferkous et al. 2015a).

Among 20, 577, 861, and 1145 kHz, Eren and Ince (2010) found that 577 kHz provides the best degradation efficiency of C.I. Direct Yellow 9, whereas for

C.I. Reactive Red 141, the degradation rate was null for 20 kHz and increased in the order 1145 kHz > 861 kHz > 577 kHz. Rayaroth et al. (2015) have examined the degradation of Coomassie Brilliant Blue upon 200, 350, 620, and 1000 kHz. They indicated that 350 kHz was the optimum frequency for the degradation of the dye.

In the study on sonochemical degradation of azo dye Reactive Black 5 done by Vajnhandl and Marechel (2007), 20 kHz low-frequency system and high-frequency (279 and 817 kHz) system were used. The greatest decolorization rate of Reactive Black 5 was observed at 817 kHz. In the study done by Ma et al. (2006) on the decomposition of acid orange 7, the degradation rates were higher at a frequency of 1 MHz than at a frequency of 20 kHz. In another study, degradation of rhodamine B and orange II was investigated by Inoue et al. (2006) using ultrasound at frequencies of 118, 224, 404, and 651 kHz at actual power of 28–29 W. The lower decolorization degree was achieved at the lowest frequency, for both azo dyes.

Therefore, all given works agreed with the fact that higher frequency ultrasound, i.e., more than 100 kHz, is more effective for the destruction of textile dyes. Besides, an optimal frequency in the interval 200–800 kHz is highly probable for the best degradation performance.

Recently, detailed numerical simulations of frequency effect on the single bubble yield and the number of active collapsing bubbles have been conducted by Merouani et al. (Merouani et al. 2014a, c). The authors found that the chemical bubble yield, i.e., hydroxyl radical production, decreased substantially with increasing frequency up to 1000 kHz, whereas the number of bubbles increased monotonically with increasing frequency in nearly the same range of frequency. Therefore, the existence of an optimum frequency for the sonochemical activity can be highlighted by the concurrence between the two factors; the number of bubbles controls the overall sonochemical generation of radicals when the frequency increased up to the optimum frequency, while the single bubble yield imposes its effect when the frequency continued to increase above the optimal frequency. However, it should be noted that the optimum value of frequency was dependent to other operational parameters such as power and liquid temperature, as demonstrated by Mark et al. (1998).

5.6.2 Ultrasonic Power

Most reported results agreed with the fact that the degradation of textile dyes increased with increasing ultrasonic power when operating above the cavitation threshold (Rehorek et al. 2004; Wang et al. 2008; Merouani et al. 2010c; Guzman-Duque et al. 2011; Dalhatou et al. 2015; Ferkous et al. 2015a; Rayaroth et al. 2015; Fassi and Petrier 2016; Taamallah et al. 2016; Boutamine et al. 2017; Merouani and Hamdaoui 2017). The beneficial effect of increasing power can be explained via the impact of this parameter on the single bubble yield and the number of bubbles. A computational analysis of this issue is available in refs. (Ferkous et al. 2015a; Merouani et al. 2015).

Both the cavity expansion and compression ratios increase as the acoustic power increased, allowing to increase the amount of the trapped water vapor as well as the bubble temperature at the last stage of the collapse (Merouani et al. 2014b). As a result, higher amount of free radicals could be produced at higher applied acoustic intensities leading to higher sonochemical effect within and surrounding the bubble. Besides, the number of cavitation bubbles increases when higher acoustic intensities are applied (Brotchie et al. 2009; Merouani et al. 2013; Ferkous et al. 2015a). Consequently, better sonochemical effects could be achieved with intensity increase.

5.6.3 *Liquid Temperature*

In general, an increase in the liquid temperature in the range 25–55 °C have conducted to higher degradation rate of several synthetic dyes at different sonochemical conditions (Ghodbane and Hamdaoui 2009a; Merouani et al. 2010c, 2016; Ferkous et al. 2016; Chadi et al. 2018b). These findings were accompanied with higher accumulation rates of H₂O₂ in the solution at higher liquid temperatures (Merouani et al. 2010b; Chadi et al. 2018b), meaning that higher concentration of free radicals can be generated at higher liquid temperatures.

The single bubble results showed that there exists an optimal liquid temperature (~20–30 °C) for the production of ·OH inside a single bubble (Merouani et al. 2015, 2016), but the number of active bubbles was dramatically increased with increasing liquid temperature (Merouani et al. 2016; Chadi et al. 2018b). The global production rate of ·OH radical augmented with augmenting solution temperature in the range of 25–55 °C. Based on these findings, Merouani et al. (2016) have concluded that the predominant factor that controls the effect of liquid temperature on the sonochemical degradation of dyes is the number of bubbles.

However, a new trend of the bulk liquid temperature has been lately reported by the same group: the impact of liquid temperature on the sonolytic removal of toluidine blue is sensitively dependent to the initial dye concentration. At a low dye concentration, i.e., less than 2 mg/L, the degradation rate was noted to be affected by the temperature rise in the interval of 25–70 °C. However, for higher dye concentration, the temperature rise for up to 50 °C improved significantly the degradation rate. The authors have attributed this dependence to the displacement of the reaction zone with the dye concentration. At lower dye loadings, the liquid bulk is the predominant reaction zone, and increasing the solution temperature in this case could not influence the dye removal rate as the dye molecules are always far from the interfacial region where high concentration of ·OH is suspected. However, the degradation zone may be moved progressively toward the bubble-solution interface as the dye concentration in the solution is high. In this case, higher liquid temperatures could promote the degradation rate of the dye through increasing the interfacial concentration of ·OH radicals.

5.6.4 Dissolved Gases

Argon, air, nitrogen, and sometimes CO₂ are the most used gases for studying the effect of saturation gases on the efficiency of dye removal using the sonochemical process (Joseph et al. 1999; Okitsu et al. 2005; Minero et al. 2008; Guzman-Duque et al. 2011; Ferkous et al. 2015b; Taamallah et al. 2016; Chadi et al. 2018a). Overall, the degradation rate of dyes decreased in the order Ar < air < N₂, whereas CO₂ suppress completely the degradation process (Joseph et al. 1999; Okitsu et al. 2005; Minero et al. 2008; Guzman-Duque et al. 2011; Ferkous et al. 2015b; Taamallah et al. 2016; Chadi et al. 2018a).

Dissolved gases influence the sonochemical activity via several ways: (i) more nucleation sites can be created when using a gas of high solubility, i.e., higher number of bubble could be produced in this situation, and (ii) a gas of greater polytropic index $\gamma = c_p/c_v$ and lower thermal conductivity produces higher collapsing temperatures within the bubble, and this promotes the chemical activity of the cavity. Nevertheless, Okitsu et al. (2006) have reported a new aspect of saturation gases toward the bubble temperature. Measurements of this last for different saturation gases of identical γ , and diverse thermal conductivities have given the same temperature values. The authors have concluded that the thermal conductivity has not a significant influence on the bubble temperature and the gases effect could be closely related to the number of bubbles.

Hence, the best degradation performance obtained under argon atmosphere is due to its higher γ and solubility x than other gases, i.e., $\gamma_{Ar} = 1.66$ compared to 1.4 for air and N₂ and $x_{Ar} = 2.748 \times 10^{-5}$ mol/mol compared to $x_{N_2} = 1.276 \times 10^{-5}$ mol/mol and $x_{air} = 1.524 \times 10^{-5}$ mol/mol. However, the difference in impacts of air and N₂ on the dye removal was attributed to the direct involvement of these gases in the combustion reactions inside the bubble, since the two gases have an identical γ and a marginal difference in their solubilities. Computational analysis revealed that the single bubble yield decreased as the concentration of N₂ increased in the bubble, mainly due to the huge consumption of ·OH by NO that resulted from reactions $N_2 + O \rightleftharpoons NO + N$ and $NO_2 + M \rightleftharpoons O + NO + M$ (Merouani et al. 2014c). For the case of CO₂, its effect was attributed to the too high solubility of CO₂ in water (46 times much higher than air), which could provoke a suppression of the inertial cavitation responsible for all chemical effects of ultrasound in aqueous solutions (Chadi et al. 2018a).

5.6.5 Initial Dye Concentration

In general, the concentration of synthetic dyes in textile effluents is variable. This parameter has been extensively studied by researchers (Okitsu et al. 2005, 2015; Merouani et al. 2010c; Guzman-Duque et al. 2011; Moumeni et al. 2012; Dalhatou et al. 2015; Ferkous et al. 2015b; Taamallah et al. 2016; Boutamine et al. 2017;

Hamdaoui and Merouani 2017b). All results agreed with the following behavior: when the initial concentration of pollutant is increased, the removal efficiency decreased, but the initial degradation rate increased rapidly at low dye concentration and then tends to a limit value at too high values of dye concentrations. Correspondingly, the production rate of H_2O_2 followed the inverse effect; it is higher in pure water, but it decreased progressively with increasing initial dye concentration up to reaching a minimum value.

These results were attributed to the displacement of the reaction zone with respect to the initial dye concentration (Okitsu et al. 2005, 2015; Merouani et al. 2010c; Guzman-Duque et al. 2011; Moumeni et al. 2012; Dalhatou et al. 2015; Ferkous et al. 2015b; Taamallah et al. 2016; Boutamine et al. 2017; Hamdaoui and Merouani 2017b). The bulk solution is the preferable degradation zone at lower dye concentration. Therefore, the great portion of $\cdot OH$ could recombine at the bubble interface to form H_2O_2 at higher rates, and only a lower quantity of $\cdot OH$ may reach the bulk of the solution to react with the dye molecules. Increasing the dye concentration, the reaction zone could be progressively moved to the bubble-solution interface where an elevated concentration of radicals is located. In this case, the fraction of $\cdot OH$ trapped by the dye molecules increased, leading to higher degradation rate and lower formation rate of hydrogen peroxide. At too high dye concentration, bubble surface could be completely occupied with dye molecules, and at this point any increase in dye concentration could not have any effect on the initial degradation rate (Merouani et al. 2010c; Moumeni et al. 2012).

5.6.6 pH

The solution pH of textile effluents is very variable. The solution pH can modify the physical properties of dyes and their reactivity toward the sonochemical treatment (Ince and Tezcanli-Güyer 2004; Wang et al. 2008; Ghodbane and Hamdaoui 2009a; Merouani et al. 2010c; Dalhatou et al. 2015; Ferkous et al. 2015a, b; Rayaroth et al. 2015; Taamallah et al. 2016; Fassi and Petrier 2016; Boutamine et al. 2017; Merouani and Hamdaoui 2017).

Practically, all results reported that acidic conditions favor higher degradation rate than neutral pHs ($\sim 7-8$). Researchers have attributed these findings to the less ionization state of most dyes in acidic conditions, which increases their hydrophobic character. The factor that precise the ionization state is the pK_a , which is mostly not available for synthetic dyes. However, in the majority of cases, the percentage of the ionized form of dyes increases with pH rise. Therefore, more hydrophilic forms may be present in the solution at higher pH values, thereby allowing degradation to occur in the liquid bulk where the concentration of hydroxyl radicals is low.

On the other hand, increasing pH in the basic medium have shown two possible tendencies: (i) a continuous decrease of the degradation rate (Dalhatou et al. 2015; Hamdaoui and Merouani 2017b) and (ii) a re-increase of the degradation rate (Wang et al. 2008; Ghodbane and Hamdaoui 2009a; Merouani et al. 2010c). Dalhatou et al.

(2015) attributed the re-increase of the degradation rate at strong basic conditions to the involvement of carbonate radical ($\text{CO}_3^{\cdot-}$) in the oxidation process. Under basic pH, the dissolved carbon dioxide in the solution could be converted to carbonate ions, which upon ultrasound action forms $\text{CO}_3^{\cdot-}$ radical. The advantage of this radicals, as compared to $\cdot\text{OH}$ radical, is the fact that the radical–radical recombination for $\text{CO}_3^{\cdot-}$ is less rapid than that for $\cdot\text{OH}$ (Merouani et al. 2010a). The lifetime of $\text{CO}_3^{\cdot-}$ will thus be much higher than that of $\cdot\text{OH}$.

5.7 Influence of Water Matrix

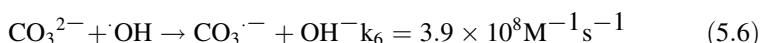
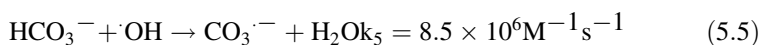
It is of practical interest to examine the performance of the sonochemical process in real environmental matrices, as the different salts may retard the ultrasonic destruction of target contaminants. Cl^- , SO_4^{2-} , and HCO_3^- ions are the common anions found in wastewater. Owing to their hydrophilic character, Cl^- and SO_4^{2-} do not interfere on the degradation of many dyes (Merouani et al. 2010c; Guzman-Duque et al. 2011; Taamallah et al. 2016), but in several cases, they can accelerate the sonolytic degradation of some dyes (Wang et al. 2008; Ghodbane and Hamdaoui 2009a; Ferkous et al. 2016).

Salts, via their potential to increase the solution ionic strength, can push hydrophilic organic substrates into the reactive interfacial region (Seymour and Gupta 1997). This event is called “salting-out effect.” Additionally, salts may diminish the bubble coalescence event, which increases the number of active bubbles (Brotchie et al. 2010). Because of these actions, salts can enhance the sonochemical degradation of dyes, i.e., as in cases of refs. (Wang et al. 2008; Ghodbane and Hamdaoui 2009a; Ferkous et al. 2016).

However, Hamdaoui and Merouani (2018) have recently reported that the salts effect may depend on the location of the dye molecules toward the bubble interface, which is controlled by several operating conditions like the dye concentration and frequency. The authors have conducted sonolytic degradation of several dyes in seawater under different sonochemical conditions and found that the seawater salts may enhance or not affect the degradation of the dyes. The degradation of basic fuchsin and acid orange 7 at 600 kHz, rhodamine B at 300, and naphthol blue black at 585 kHz was not affected by the seawater salts, but the removal rate of malachite green at 300 kHz was relatively enhanced. However, a remarked enhancement was observed for Basic Red 29 at 300 kHz and naphthol blue black at 1700 kHz. For the two last cases, the initial removal rates are 1.7 and 2 times much higher in seawater as compared to deionized water. Based on these findings, Hamdaoui and Merouani (2018) have concluded that dyes which were degraded at faster rate in seawater are more hydrophilic than those which their degradation was not affected by the seawater salts. Consequently, the salting-out effect may be benefic only for hydrophilic compounds as they will be pushed to the reactive interfacial region. Besides, the authors revealed that the frequency of ultrasound may affect the effect of salts, as

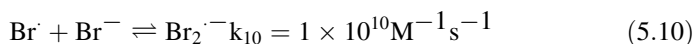
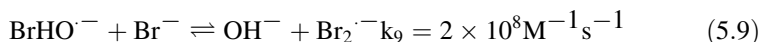
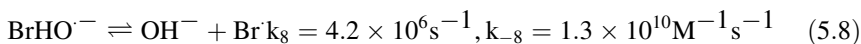
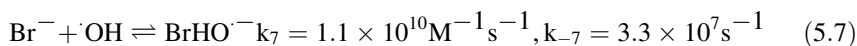
seawater induced an enhancement index of 2 for naphthol blue black at 1700 kHz against 1 for the same pollutant at 585 kHz.

Bicarbonate and carbonate showed dual trends that are related to the relative concentration of both the dye and anions (Minero et al. 2008; Merouani et al. 2010a; Guzman-Duque et al. 2011). At low concentration of the dye, the degradation rate increased with carbonate/bicarbonate concentration rise to higher level. Instead, at higher concentration of the dye, bicarbonate/carbonate ions have a competitive effect. These observations were related to the formation of $CO_3^{\cdot-}$ radical and its subsequent reaction with the dye. $CO_3^{\cdot-}$ radical is a powerful oxidant ($E^\circ = 1.78$ V) which may be formed when using ultrasound for water treatment through quenching of hydroxyl radical by HCO_3^- and CO_3^{2-} as:



Oxidation of organic compounds by carbonate radical may be more important than oxidation by hydroxyl radical. In contrast to hydroxyl radical, which reacts very rapidly with almost any organic compound, carbonate radical is very selective, and the corresponding second-order rate constants cover a range of many orders of magnitude. Carbonate radical may react by electron transfer or hydrogen transfer. At relatively high concentration of pollutant, HCO_3^-/CO_3^{2-} compete with $\cdot OH$, and a detrimental effect is observed, particularly at high ion concentrations. When the concentration of the dye is very low, the produced $CO_3^{\cdot-}$ can react with dyes with best performance than $\cdot OH$ radical because of its longer lifetime (Merouani et al. 2010a).

Moumeni and Hamdaoui (2012) have shown that bromide (Br^-) may also result in similar rate enhancement like bicarbonate/carbonate ions. The degradation of malachite green was studied at 300 kHz and 60 W for different concentrations of Br^- and MG. The ameliorating effect of bromide ions, which are augmented with augmenting Br^- concentration and decreasing MG level, was attributed to the implication of $Br_2^{\cdot-}$, formed via reactions (5.7, 5.8, 5.9 and 5.10), in the degradation route. $Br_2^{\cdot-}$ radical would be more available than hydroxyl radical for the degradation of nonvolatile substrates, both at the bubble-solution interface and in the solution bulk, as its radical-radical recombination occurring at lesser rate than that for $\cdot OH$ (Moumeni and Hamdaoui 2012):



Natural waters containing dyes and mineral anions have been efficaciously treated by sonochemical process. Comparable removals of malachite green and

rhodamine B in pure water and a mineral water was reported at 300 kHz (Merouani 2010; Moumeni and Hamdaoui 2012). On the other hand, a slightly enhancement of basic fuchsin degradation in a mineral water has been reported by Taamallah et al. (2016) at 600 kHz. The sonochemical degradation of Basic Red 29 has been investigated in mineral water, river water, and seawater and compared with that of deionized water (Boutamine et al. 2017). The degradation rate followed the order: mineral water > seawater > river water > pure water (Boutamine et al. 2017). Interestingly, the sonochemical treatment of naphthol blue black at 1700 kHz was strongly accelerated in mineral water and seawater as compared to data obtained in pure water (Ferkous et al. 2016). All these enhancements were attributed to the salting-out effect induced by the high concentration of anions in natural waters. However, Ferkous et al. (2016) have suggested that the salting-out effect is frequency dependent.

5.8 Process Intensification Using Selected Additives

In addition to carbonate/bicarbonate and bromide, other inorganic and organic substances have been recently applied as intensifying agents for the sonochemical treatment. In this section, only the most important agents have been highlighted.

5.8.1 CCl_4

The presence of CCl_4 in aqueous solutions of dyes drastically enhanced their sonochemical removal. Ghodbane and Hamdaoui (2009b) have assessed the sonochemical degradation of Acid Blue 25 in the presence of CCl_4 using a 1700 kHz ultrasonic device. The decolorization rate in the presence of 399 mg/L of CCl_4 was 106 times greater than that calculated in the absence of CCl_4 . Additionally, the addition of 399 mg/L of CCl_4 at 1700 kHz results in an 87-fold increase of the initial decolorization rate as compared with the frequency of 22.5 kHz. A similar behavior has been reported by Merouani et al. (2010c) for the sonochemical degradation of Rhodamine at 300 kHz. Gültekin et al. (2009) have reported that the degradation rate of C.I. acid orange 8 at 300 kHz and 25 W increased by factors of about 2, 3.5, and 4.66 with addition of CCl_4 at 0.5, 1, and 5 mM, respectively. Similar findings have been reported for the degradation of two azo dyes at various frequencies (Eren and Ince 2010) and for methyl orange in a 45 kHz ultrasonic cleaning bath (Okitsu et al. 2008).

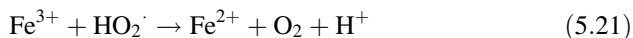
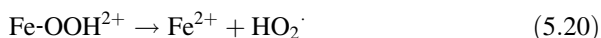
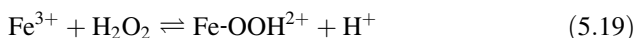
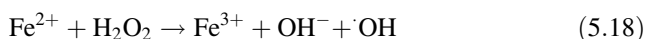
CCl_4 pyrolysis takes place inside cavitation bubbles, conducting to the release of several chlorinated oxidizing agents (Eqs. 5.11, 5.12, 5.13, 5.14, 5.15, 5.16 and 5.17) that can react efficiently with dye molecules (Okitsu et al. 2008; Ghodbane and Hamdaoui 2009b):



The main advantage of the US/ CCl_4 process is that both pollutants, the target dye and CCl_4 , could be eliminated simultaneously. However, the degradation by-products should be analyzed in depth because of the possible formation of toxic trihalomethanes in the solution.

5.8.2 Iron (Fe^{2+})

Assistance of the sonolytic treatment with Fe^{2+} at low concentration may enhance the degradation of nonvolatile compounds (Merouani et al. 2010c). The process should be operated at acidic conditions to avoid iron precipitation as hydroxide. In this system, the acoustically formed H_2O_2 can react with iron via Fenton process (Eqs. 5.18, 5.19 and 5.20) to produce an excess of hydroxyl radical in the contaminated solution (Torres et al. 2007). However, excess of iron is to be avoided because it may cause a detrimental effect through radical scavenging (Eq. 5.21):



This technique has been successfully applied for intensifying the sonochemical degradation of several dyes. The presence of Fe^{2+} in sonicated solution of Acid Blue 25 at 1700 kHz and pH 3 have resulted in 2.1-fold increase in the initial degradation rate, but lower enhancement factor of 1.7 was recorded with 50 mg/L of Fe^{2+} (Ghodbane and Hamdaoui 2009a). At 300 kHz, rate enhancements were also reported for the degradation of rhodamine B, Basic Red 29, and malachite green in the presence of low concentrations of Fe^{2+} at pH 3 (Merouani et al. 2010c; Moumeni et al. 2012; Boutamine et al. 2017). Additionally, the total organic carbon removal during Basic Red 29 treatment augmented from 2.5% to 35% after 30 min

when sonication is assisted with 15 mg/L of Fe^{2+} and from 5% to 50% after 1 h with the same iron dose (Boutamine et al. 2017). Several similar observations have been reported for different types of dyes at different sonochemical conditions (Sun et al. 2007; Wang et al. 2008; Song et al. 2009; Eren 2012; Basturk and Karatas 2014; Dükkancı et al. 2014; Verma et al. 2015).

5.8.3 Persulfate ($\text{S}_2\text{O}_8^{2-}$)

Even though persulfate can act as a direct oxidant ($E^\circ = 2.07 \text{ V}$), its reaction rates are limited for more recalcitrant contaminants (Zhang et al. 2015). The combination of persulfate with ultrasound is new tool for intensifying the sonochemical degradation of nonvolatile micropollutants in water (Neppolian et al. 2002, 2010). In this case, ultrasound can activate persulfate into sulfate radical ($\text{SO}_4^{\cdot-}$) that have an oxidation potential ($E^0 = 2.6 \text{ V}$) comparable to that of hydroxyl radical, i.e., 2.8 V (Latimer 1952). Ultrasound can activate persulfate via two main pathways: (i) reaction with the acoustically generated H^\cdot and $^\cdot\text{OH}$ radicals (Eqs. 5.22 and 5.23) and (ii) thermal decomposition at the hot bubble-solution interface (Eq. 5.24):

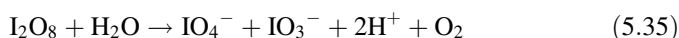
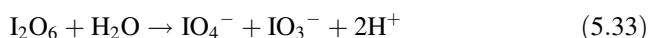
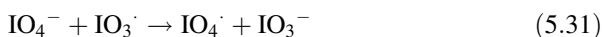
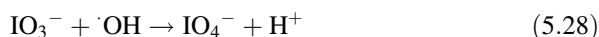
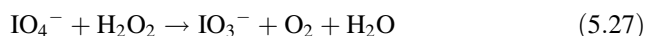


The improvement effect with ultrasound/persulfate system has been reported for several dyes (Wang et al. 2014; Rayaroth et al. 2015; Ferkous et al. 2016, 2017). A detrimental effect can also take place when operating with excess of persulfate (Ferkous et al. 2017). Additionally, the persulfate enhancement effect was strongly operating parameters-dependent (Ferkous et al. 2017).

5.8.4 Periodate (IO_4^-)

Recent work published by Hamdaoui and Merouani (2017a) showed that the periodate ions (IO_4^-) in water matrix can induce improvement of dye sonolysis. The sonochemical degradation rate of Brilliant Blue R dye was enhanced by factor of 2.4 in the presence of periodate (10 mM) under air saturation. In ultrasound/ IO_4^- system, the acoustically generated $^\cdot\text{OH}$, H^\cdot , and H_2O_2 play also a role in activating IO_4^- into a number of reactive species including $^\cdot\text{OH}$, periodyl radical (IO_4^\cdot), and iodyl radical (IO_3^\cdot) (Eqs. 5.25, 5.26, 5.27, 5.28, 5.29, 5.30, 5.31, 5.32, 5.33, 5.34 and 5.35). These entities react with organic compounds and eventually improve the degradation rates (Lee et al. 2016; Hamdaoui and Merouani 2017a). Moreover, the

positive effect of periodate was much pronounced at lower powers and higher pH (Hamdaoui and Merouani 2017a):



5.8.5 Nanoparticles

Nanoparticles such as that of TiO_2 have been used for ameliorating the degradation of organic contaminants by ultrasound. Boutamine et al. (2016) have shown that the presence of 100 mg/L of TiO_2 in ultrasound system at 300 kHz ameliorated the degradation rate of Basic Red 29 by a factor of 1.4. Similar results have been found by Balaji et al. (2011) who studied the degradation of Acid Red B at 20 kHz. The authors have reported that TiO_2 particles can facilitate the cavitation process, which enhances the number of bubble, and, thus, the concentration of free radicals in the solution would be higher. However, excess of TiO_2 should be avoided because it can alter the propagation of the sound wave in the solution, resulting in negative impact on the degradation rate (Boutamine et al. 2016). Additionally, a new branch of applied sonochemistry, called sonocatalysis, has been developed in the last decade in which several new catalysts have been synthesized and their catalytic activity under ultrasound has been demonstrated. An interesting review about sonocatalysis applied for the degradation of several textile dyes has been recently published by Chatel (2019).

5.9 Conclusion

In summary, the sonochemical treatment is a promising technique for the destruction of textile dyes in aqueous effluents. Textile dyes are nonvolatile compound that degrade mostly at the bubble-solution interface and in the solution bulk via hydroxyl radical attack. The degradation rate is affected by sonochemical parameters, i.e., frequency and power, and environmental conditions, i.e., liquid temperature, pollutant concentration, physicochemical properties of the solution, presence of salts and gases, and so forth. In this chapter, the recent researches on sonochemical treatment of the textile dyes including degradation data, influencing parameters, impact of water matrix constitutes, and process intensification techniques were presented.

Although the evident development has been attained, the sonochemical process still faces numerous challenges. More efforts may be focused on the next topics:

- (i) To better understand the effective action of the sonochemical treatment, the degradation of textile dyes should be analyzed in depth and, particularly, in terms of total organic carbon removal and by-products identification and quantification because the degradation products may be more toxic than the initial pollutant.
- (ii) Because dyes are nonvolatile, it is important to develop methods that make easy the accumulation of dyes at the reactive interfacial area of cavitation bubble. Also, novel techniques to enhance the number of inertial bubbles are researched. One recent technique for this issue is to combine ultrasound with catalysts, i.e., sonocatalysis.
- (iii) There is a requirement to improve our knowledge on the extent of sonochemical reactions in industrial-scale ultrasonic reactors. Even though much data on sonochemical degradation of textile dyes at lab scale have been accumulated, the application of this technology to large-scale operations was poorly investigated. The attenuation of the sound wave in big structures is a principal factor that affects the efficiency of the sonolytic treatment (Kerabchi et al. 2018). It is of interest to understand the characteristics of the sound field because the sound propagation in big reactors differs from those in lab-scale ones (Kerabchi et al. 2018). Thus, there are still lost links between lab-scale and industrial-scale sonochemical processes. The following topics are also required for the implementation of the sonochemical treatment for industrial use (Son 2015):
 - Reactor design including sonoreactor size/shape/material, transducer location/array, and internal structure
 - Studying of the liquid depth on the sonochemical efficiency of the process
 - Development of continuous-flow sonochemical reactors

Acknowledgments This work was supported by The Ministry of Higher Education and Scientific Research of Algeria (project No. A16N01UN250320180001) and The General Directorate of Scientific Research and Technological Development (GD-SRTD).

References

- Adeuyi YG (2001) Sonochemistry: environmental science and engineering applications. *Ind Eng Chem Res* 40:4681–4715. <https://doi.org/10.1021/ie0100961>
- Anbar M, Pecht I (1964) On the sonochemical formation of hydrogen peroxide. *J Phys Chem* 68:1959–1962. <https://doi.org/10.1021/j100784a025>
- Arslan-Alaton I, Gursoy BH, Schmidt JE (2008) Advanced oxidation of acid and reactive dyes: effect of Fenton treatment on aerobic, anoxic and anaerobic processes. *Dyes Pigments* 78:117–130. <https://doi.org/10.1016/j.dyepig.2007.11.001>
- Asghar A, Aziz A, Raman A, Mohd W, Wan A (2015) Advanced oxidation processes for in-situ production of hydrogen peroxide/hydroxyl radical for textile wastewater treatment: a review. *J Clean Prod* 87:826–838. <https://doi.org/10.1016/j.jclepro.2014.09.010>
- Balaji C, Moholkar VS, Pandit AB, Ashokkumar M (2011) Mechanistic investigations on sonophotocatalytic degradation of textile dyes with surface active solutes. *Ind Eng Chem Res* 50:11485–11494. <https://doi.org/10.1021/ie201127v>
- Barbier PF, Petrier C (1996) Study at 20 kHz and 500 kHz of the ultrasound-ozone advanced oxidation system: 4-nitrophenol degradation. *J Adv Oxid Technol* 1:154–159. <https://doi.org/10.1515/jaots-1996-0208>
- Basturk E, Karatas M (2014) Advanced oxidation of Reactive Blue 181 solution: a comparison between Fenton and Sono-Fenton process. *Ultrason Sonochem* 21:1881–1885. <https://doi.org/10.1016/j.ultsonch.2014.03.026>
- Behnajady MA, Modirshahla N, Shokri M, Vahid B (2008) Effect of operational parameters on degradation of Malachite Green by ultrasonic irradiation. *Ultrason Sonochem* 15:1009–1014. <https://doi.org/10.1016/j.ultsonch.2008.03.004>
- Boutamine Z, Hamdaoui O, Merouani S (2016) Enhanced sonolytic mineralization of basic red 29 in water by integrated ultrasound/ Fe^{2+} / TiO_2 treatment. *Res Chem Intermed* 43:1–14. <https://doi.org/10.1007/s11164-016-2724-3>
- Boutamine Z, Merouani S, Hamdaoui O (2017) Sonochemical degradation of Basic Red 29 in aqueous media. *Turkish J Chem* 41:99–115. <https://doi.org/10.3906/kim-1603-82>
- Brotchie A, Grieser F, Ashokkumar M (2009) Effect of power and frequency on bubble-size distributions in acoustic cavitation. *Phys Rev Lett* 102:1–4. <https://doi.org/10.1103/PhysRevLett.102.084302>
- Brotchie A, Statham T, Zhou M, Dharmarathne L, Grieser F, Ashokkumar M (2010) Acoustic bubble sizes, coalescence, and sonochemical activity in aqueous electrolyte solutions saturated with different gases. *Langmuir* 26:12690–12695. <https://doi.org/10.1021/la1017104>
- Brown MA, De Vito SC (1993) Predicting azo dye toxicity. *Crit Rev Environ Sci Technol* 23:249–324. <https://doi.org/10.1080/10643389309388453>
- Chadi NE, Merouani S, Hamdaoui O (2018a) Characterization and application of a 1700 kHz-acoustic cavitation field for water decontamination: a case study with toluidine blue. *Appl Water Sci* 8:160:1. <https://doi.org/10.1007/s13201-018-0809-4>
- Chadi NE, Merouani S, Hamdaoui O, Bouhelassa M (2018b) New aspect of the effect of liquid temperature on sonochemical degradation of nonvolatile organic pollutants in aqueous media. *Sep Purif Technol* 200:68–74. <https://doi.org/10.1016/j.seppur.2018.01.047>
- Chatel G (2019) Sonochemistry in nanocatalysis: the use of ultrasound from the catalyst synthesis to the catalytic reaction. *Curr Opin Green Sustain Chem* 15:1–6. <https://doi.org/10.1016/j.cogsc.2018.07.004>

- Chiha M, Merouani S, Hamdaoui O, Baup S, Gondrexon N, Pétrier C (2010) Modeling of ultrasonic degradation of non-volatile organic compounds by Langmuir-type kinetics. *Ultrason Sonochem* 17:773–782. <https://doi.org/10.1016/j.ultsonch.2010.03.007>
- Choi P (2015) Fundamental aspects of acoustic field, cavitation and sonoluminescence. In: Ashokkumar M (ed) *Handbook of ultrasonics and sonochemistry*. Springer Science+Business Media, Singapore, pp 1–29. https://doi.org/10.1007/978-981-287-470-2_2-1
- Dalhatou S, Pétrier C, Laminsi S, Baup S (2015) Sonochemical removal of naphthol blue black azo dye: influence of parameters and effect of mineral ions. *Int J Environ Sci Technol* 12:35–44. <https://doi.org/10.1007/s13762-013-0432-8>
- Dalhatou S, Laminsi S, Pétrier C, Baup S (2019) Competition in sonochemical degradation of Naphthol Blue Black: presence of an organic (nonylphenol) and a mineral (bicarbonate ions) matrix. *J Environ Chem Eng* 7:102819. <https://doi.org/10.1016/j.jece.2018.102819>
- Dükkancı M, Vinatoru M, Mason TJ (2012) Sonochemical treatment of Orange II using ultrasound at a range of frequencies and powers. *J Adv Oxid Technol* 15:277–283. <https://doi.org/10.1515/jaots-2012-0205>
- Dükkancı M, Vinatoru M, Mason TJ (2014) The sonochemical decolourisation of textile azo dye Orange II: effects of Fenton type reagents and UV light. *Ultrason Sonochem* 21:846–853. <https://doi.org/10.1016/j.ultsonch.2013.08.020>
- Entezari MH, Pétrier C, Devidal P (2003) Sonochemical degradation of phenol in water: a comparison of classical equipment with a new cylindrical reactor. *Ultrason Sonochem* 10:103–108. [https://doi.org/10.1016/S1350-4177\(02\)00136-0](https://doi.org/10.1016/S1350-4177(02)00136-0)
- Eren Z (2012) Ultrasound as a basic and auxiliary process for dye remediation: a review. *J Environ Manage* 104:127–141. <https://doi.org/10.1016/j.jenvman.2012.03.028>
- Eren Z, Ince NH (2010) Sonolytic and sonocatalytic degradation of azo dyes by low and high frequency ultrasound. *J Hazard Mater* 177:1019–1024. <https://doi.org/10.1016/j.jhazmat.2010.01.021>
- Fassi S, Pétrier C (2016) Effect of potassium monopersulfate (oxone) and operating parameters on sonochemical degradation of cationic dye in an aqueous solution. *Ultrason Sonochem* 32:343–347. <https://doi.org/10.1016/j.ultsonch.2016.03.032>
- Ferkous H, Merouani S, Hamdaoui O, Rezgui Y, Guemini M (2015a) Comprehensive experimental and numerical investigations of the effect of frequency and acoustic intensity on the sonolytic degradation of naphthol blue black in water. *Ultrason Sonochem* 26:30–39. <https://doi.org/10.1016/j.ultsonch.2015.02.004>
- Ferkous H, Hamdaoui O, Merouani S (2015b) Sonochemical degradation of naphthol blue black in water: effect of operating parameters. *Ultrason Sonochem* 26:40–47. <https://doi.org/10.1016/j.ultsonch.2015.03.013>
- Ferkous H, Merouani S, Hamdaoui O (2016) Sonolytic degradation of naphthol blue black at 1700 kHz: effects of salts, complex matrices and persulfate. *J Water Process Eng* 9:67–77. <https://doi.org/10.1016/j.str.2014.12.012>
- Ferkous H, Merouani S, Hamdaoui O, Pétrier C (2017) Persulfate-enhanced sonochemical degradation of naphthol blue black in water: evidence of sulfate radical formation. *Ultrason Sonochem* 34:580–587. <https://doi.org/10.1016/j.ultsonch.2016.06.027>
- Fischer C, Hart E, Henglein A (1986) Ultrasonic Irradiation of water in the presence of $^{18}\text{O}_2$: isotope Exchange and Isotopic Distribution of H_2O_2 . *J Phys Chem*:1954–1956. <https://doi.org/10.1021/j100400a043>
- Flint EB, Suslick KS (1991) The temperature of cavitation. *Science* (80-) 253:1397–1399. <https://doi.org/10.1126/science.253.5026.1397>
- Francony A, Pétrier C (1996) Sonochemical degradation of carbon tetrachloride in aqueous solution at two frequencies: 20 kHz and 500 kHz. *Ultrason Sonochem* 3:S77–S82. [https://doi.org/10.1016/1350-1477\(96\)00010-1](https://doi.org/10.1016/1350-1477(96)00010-1)
- Ghodbane H, Hamdaoui O (2009a) Degradation of Acid Blue 25 in aqueous media using 1700 kHz ultrasonic irradiation: ultrasound/ Fe(II) and ultrasound/ H_2O_2 combinations. *Ultrason Sonochem* 16:593–598. <https://doi.org/10.1016/j.ultsonch.2008.11.006>

- Ghodbane H, Hamdaoui O (2009b) Intensification of sonochemical decolorization of anthraquinonic dye Acid Blue 25 using carbon tetrachloride. *Ultrason Sonochem* 16:455–461. <https://doi.org/10.1016/j.ultsonch.2008.12.005>
- Gogate PR (2008) Cavitation reactors for process intensification of chemical processing applications: a critical review. *Chem Eng Process Process Intensif* 47:515–527. <https://doi.org/10.1016/j.cep.2007.09.014>
- Gogate PR, Mujumdar S, Pandit AB (2003) Large-scale sonochemical reactors for process intensification: design and experimental validation. *J Chem Technol Biotechnol* 78:685–693. <https://doi.org/10.1002/jctb.697>
- Gültekin I, Tezcanli-güyer G, Ince NH (2009) Ultrasonics Sonochemistry Sonochemical decay of C. I. Acid Orange 8: effects of CCl_4 and t-butyl alcohol. *Ultrason Sonochem* 16:577–581. <https://doi.org/10.1016/j.ultsonch.2008.12.007>
- Gutiérrez M, Henglein A, Dohrmann J (1987) H atom reactions in the sonolysis of aqueous solutions. *J Phys Chem* 91:6687–6690. <https://doi.org/10.1021/j100311a026>
- Guzman-Duque F, Pétrier C, Pulgarin C, Penuela G, Torres-Palma RA (2011) Effects of sonochemical parameters and inorganic ions during the sonochemical degradation of crystal violet in water. *Ultrason Sonochem* 18:440–446. <https://doi.org/10.1016/j.ultsonch.2010.07.019>
- Hamdaoui O, Naffrechoux E (2007) An investigation of the mechanisms of ultrasonically enhanced desorption. *AIChE J.* 53:363–373. <https://doi.org/10.1002/aic.11090>
- Hamdaoui O (2009) Removal of cadmium from aqueous medium under ultrasound assistance using olive leaves as sorbent. *Chem Eng Process* 48:1157–1166. <https://doi.org/10.1016/j.cep.2009.04.002>
- Hamdaoui O (2011) Intensification of the sorption of Rhodamine B from aqueous phase by loquat seeds using ultrasound. *Desalination* 271:279–286. <https://doi.org/10.1016/j.desal.2010.12.043>
- Hamdaoui O, Merouani S (2017a) Improvement of sonochemical degradation of brilliant blue R in water using periodate ions: implication of iodine radicals in the oxidation process. *Ultrason Sonochem* 37:344–350. <https://doi.org/10.1016/j.ultsonch.2017.01.025>
- Hamdaoui O, Merouani S (2017b) Ultrasonic destruction of acid Orange 7: effect of humic acid, surfactants and complex matrices. *Water Environ Research* 89:250–259. <https://doi.org/10.2175/106143016X14798353399539>
- Hamdaoui O, Merouani S (2018) Impact of seawater salinity on the sonochemical removal of emerging organic pollutants. *Environ Technol* in press. <https://doi.org/10.1080/09593330.2018.1564071>
- Hart EJ, Henglein A (1985) Free radical and free atom reactions in the sonolysis of aqueous iodide and formate solutions. *J Phys Chem* 89:4342–4347. <https://doi.org/10.1021/j100266a038>
- Hart EJ, Henglein A (1987) Sonochemistry of aqueous solutions: $\text{H}_2\text{-O}_2$ combustion in cavitation bubbles. *J Phys Chem* 91:3654–3656. <https://doi.org/10.1021/j100297a038>
- Hart EJ, Fischer C-H, Henglein A (1986) Isotopic exchange in the sonolysis of aqueous solutions containing nitrogen-14 and nitrogen-15 molecules. *J Phys Chem* 90:5989–5991. <https://doi.org/10.1021/j100280a104>
- Henglein A (1995) Chemical effects of continuous and pulsed ultrasound in aqueous solutions. *Ultrason Sonochem* 2:115–121. [https://doi.org/10.1016/1350-4177\(95\)00022-X](https://doi.org/10.1016/1350-4177(95)00022-X)
- Ince NH, Tezcanli-Güyer G (2004) Impacts of pH and molecular structure on ultrasonic degradation of azo dyes. *Ultrasonics* 42:591–596. <https://doi.org/10.1016/j.ultras.2004.01.097>
- Inoue M, Okada F, Sakurai A, Sakakibara M (2006) A new development of dyestuffs degradation system using ultrasound. *Ultrason Sonochem* 13:313–320. <https://doi.org/10.1016/j.ultsonch.2005.05.003>
- Jiang Y, Pétrier C, Waite TD (2006) Sonolysis of 4-chlorophenol in aqueous solution: effects of substrate concentration, aqueous temperature and ultrasonic frequency. *Ultrason Sonochem* 13:415–422. <https://doi.org/10.1016/j.ultsonch.2005.07.003>

- Joseph JM, Destaillets H, Hung H-M, Hoffmann MR (1999) The sonochemical degradation of azobenzene and related azo dyes: rate enhancements via Fenton's reactions. *J Phys Chem A* 104:301–307. <https://doi.org/10.1021/jp992354m>
- Kanthale P, Ashokkumar M, Grieser F (2008) Sonoluminescence, sonochemistry (H_2O_2 yield) and bubble dynamics: frequency and power effects. *Ultrason Sonochem* 15:143–150. <https://doi.org/10.1016/j.ultsonch.2007.03.003>
- Keil FJ, Swamy KM (1999) Reactors for sonochemical engineering-present status. *Rev Chem Eng* 15:85–155. <https://doi.org/10.1515/REVCE.1999.15.2.85>
- Kerabchi N, Merouani S, Hamdaoui O (2018) Depth effect on the inertial collapse of cavitation bubble under ultrasound: special emphasis on the role of the wave attenuation. *Ultrason Sonochem*. <https://doi.org/10.1016/j.ultsonch.2018.05.004>
- Kimura T (1996) Standardization of ultrasonic power for sonochemical reaction. *Ultrason Sonochem* 3:S157–S161. [https://doi.org/10.1016/S1350-4177\(96\)00021-1](https://doi.org/10.1016/S1350-4177(96)00021-1)
- Konstantinou IK, Albanis TA (2004) TiO_2 -assisted photocatalytic degradation of azo dyes in aqueous solution: kinetic and mechanistic investigations: a review. *Appl Catal Environ* 49:1–14. <https://doi.org/10.1016/j.apcatb.2003.11.010>
- Latimer WM (1952) Oxidation potentials. Prentice-Hall, Engewood Cliffs
- Lee J, Ashokkumar M, Kentish S, Grieser F (2005) Determination of the size distribution of sonoluminescence bubbles in a pulsed acoustic field. *J Am Chem Soc* 127:16810–16811. <https://doi.org/10.1021/ja0566432>
- Lee YC, Chen MJ, Huang CP, Kuo J, Lo SL (2016) Efficient sonochemical degradation of perfluorooctanoic acid using periodate. *Ultrason Sonochem* 31:499–505. <https://doi.org/10.1016/j.ultsonch.2016.01.030>
- Leighton TG (1994) The acoustic bubble. Academic press, London
- Ma CY, Xu JY, Liu XJ (2006) Decomposition of an azo dye in aqueous solution by combination of ultrasound and visible light. *Ultrasonics* 44:375–378. <https://doi.org/10.1016/j.ultras.2006.05.164>
- Mark G, Tauber A, Laupert R, Schuchmann HP, Schulz D, Mues A, von Sonntag C (1998) OH-radical formation by ultrasound in aqueous solution – Part II: terephthalate and Fricke dosimetry and the influence of various conditions on the sonolytic yield. *Ultrason Sonochem* 5:41–52. [https://doi.org/10.1016/S1350-4177\(98\)00012-1](https://doi.org/10.1016/S1350-4177(98)00012-1)
- Mason TJ, Dietmer P (2002) Practical Sonochemistry, 2nd edn. Woodhead Publishing, Cambridge
- Mason T, Lorimer JP (2002) Applied sonochemistry: the uses of power ultrasound in chemistry and processing. Wiley-VCH Verlag GmbH & Co. KGaA, Weinheim
- Mead EL, Sutherland RG, Verrall RE (1976) The effect of ultrasound on water in the presence of dissolved gases. *Can J Chem* 54:1114–1120. <https://doi.org/10.1139/v76-159>
- Merouani S (2010) Dégradation sonochimique de la Rhodamine B en solutions aqueuses: Effets des ions hydrogéocarbonates et carbonates et des matrices complexes. PhD thesis, Université Badj Mokhtar-Annaba, Algeria
- Merouani S, Hamdaoui O (2017) Computational and experimental sonochemistry. *Process Eng J* 1:10–18
- Merouani S, Hamdaoui O, Saoudi F, Chiha M, Pétrier C (2010a) Influence of bicarbonate and carbonate ions on sonochemical degradation of Rhodamine B in aqueous phase. *J Hazard Mater* 175:593–599. <https://doi.org/10.1016/j.jhazmat.2009.10.046>
- Merouani S, Hamdaoui O, Saoudi F, Chiha M (2010b) Influence of experimental parameters on sonochemistry dosimetries: KI oxidation, Fricke reaction and H_2O_2 production. *J Hazard Mater* 178:1007–1014. <https://doi.org/10.1016/j.jhazmat.2010.02.039>
- Merouani S, Hamdaoui O, Saoudi F, Chiha M (2010c) Sonochemical degradation of Rhodamine B in aqueous phase: effects of additives. *Chem Eng J* 158:550–557. <https://doi.org/10.1016/j.cej.2010.01.048>
- Merouani S, Hamdaoui O, Rezgui Y, Guemini M (2013) Effects of ultrasound frequency and acoustic amplitude on the size of sonochemically active bubbles-theoretical study. *Ultrason Sonochem* 20:815–819. <https://doi.org/10.1016/j.ultsonch.2012.10.015>

- Merouani S, Ferkous H, Hamdaoui O, Rezgui Y, Guemini M (2014a) A method for predicting the number of active bubbles in sonochemical reactors. *Ultrason Sonochem* 22:51–58. <https://doi.org/10.1016/j.ultsonch.2014.07.015>
- Merouani S, Hamdaoui O, Rezgui Y, Guemini M (2014b) Energy analysis during acoustic bubble oscillations: relationship between bubble energy and sonochemical parameters. *Ultrasonics* 54:227–232. <https://doi.org/10.1016/j.ultras.2013.04.014>
- Merouani S, Hamdaoui O, Rezgui Y, Guemini M (2014c) Sensitivity of free radicals production in acoustically driven bubble to the ultrasonic frequency and nature of dissolved gases. *Ultrason Sonochem* 22:41–50. <https://doi.org/10.1016/j.ultsonch.2014.07.011>
- Merouani S, Hamdaoui O, Rezgui Y, Guemini M (2014d) Theoretical estimation of the temperature and pressure within collapsing acoustical bubbles. *Ultrason Sonochem* 21:53–59. <https://doi.org/10.1016/j.ultsonch.2013.05.008>
- Merouani S, Hamdaoui O, Rezgui Y, Guemini M (2015) Computer simulation of chemical reactions occurring in collapsing acoustical bubble: dependence of free radicals production on operational conditions. *Res Chem Intermed* 41:881–897. <https://doi.org/10.1007/s11164-013-1240-y>
- Merouani S, Hamdaoui O, Boutamine Z, Rezgui Y, Guemini M (2016) Experimental and numerical investigation of the effect of liquid temperature on the sonolytic degradation of some organic dyes in water. *Ultrason Sonochem* 28:382–392. <https://doi.org/10.1016/j.ultsonch.2015.08.015>
- Minero C, Pellizzari P, Maurino V, Pelizzetti E, Vione D (2008) Enhancement of dye sonochemical degradation by some inorganic anions present in natural waters. *Appl Catal Environ* 77:308–316. <https://doi.org/10.1016/j.apcatb.2007.08.001>
- Moumeni O, Hamdaoui O (2012) Intensification of sonochemical degradation of malachite green by bromide ions. *Ultrason Sonochem* 19:404–409. <https://doi.org/10.1016/j.ultsonch.2011.08.008>
- Moumeni O, Hamdaoui O, Pétrier C (2012) Sonochemical degradation of malachite green in water. *Chem Eng Process Process Intensif* 62:47–53. <https://doi.org/10.1016/j.cep.2012.09.011>
- Neppolian B, Jung H, Choi H, Lee JH, Kang JW (2002) Sonolytic degradation of methyl tert-butyl ether: the role of coupled fenton process and persulfate ion. *Water Res* 36:4699–4708. [https://doi.org/10.1016/S0043-1354\(02\)00211-7](https://doi.org/10.1016/S0043-1354(02)00211-7)
- Neppolian B, Doronila A, Ashokkumar M (2010) Sonochemical oxidation of arsenic(III) to arsenic (V) using potassium peroxydisulfate as an oxidizing agent. *Water Res* 44:3687–3695. <https://doi.org/10.1016/j.watres.2010.04.003>
- Okitsu K, Iwasaki K, Yobiko Y, Bandow H, Nishimura R, Maeda Y (2005) Sonochemical degradation of azo dyes in aqueous solution: a new heterogeneous kinetics model taking into account the local concentration of OH radicals and azo dyes. *Ultrason Sonochem* 12:255–262. <https://doi.org/10.1016/j.ultsonch.2004.01.038>
- Okitsu K, Suzuki T, Takenaka N, Bandow H, Nishimura R, Maeda Y (2006) Acoustic multibubble cavitation in water: a new aspect of the effect of a rare gas atmosphere on bubble temperature and its relevance to sonochemistry. *J Phys Chem B* 110:20081–20084. <https://doi.org/10.1021/jp064598u>
- Okitsu K, Kawasaki K, Nanzai B, Takenaka N, Bandow H (2008) Effect of carbon tetrachloride on sonochemical decomposition of methyl orange in water. *Chemosphere* 71:36–42. <https://doi.org/10.1016/j.chemosphere.2007.10.056>
- Okitsu K, Nanzai B, Thangavadiel K (2015) Sonochemical degradation of aromatic compounds, surfactants, and dyes in aqueous solutions. In: Ashokkumar M (ed) *Handbook of ultrasonics and sonochemistry*. Springer Science+Business Media Singapore, Singapore, pp 1–28. https://doi.org/10.1007/978-981-287-470-2_57-1
- Parsons S (2004) *Advanced oxidation processes for water and wastewater treatment*. IWA Publishing, London
- Pétrier C (2015) The use of power ultrasound for water treatment. In: Gallego-Juarez JA, Graff K (eds) *Power ultrasonics: applications of high-intensity ultrasound*. Elsevier, Cambridge, pp 939–963. <https://doi.org/10.1016/B978-1-78242-028-6.00031-4>

- Pétrier C, Francony A (1997) Ultrasonic waste-water treatment: incidence of ultrasonic frequency on the rate of phenol and carbon tetrachloride degradation. *Ultrason Sonochem* 4:295–300. [https://doi.org/10.1016/S1350-4177\(97\)00036-9](https://doi.org/10.1016/S1350-4177(97)00036-9)
- Petrier C, Jiang Y, Lamy MF (1998) Ultrasound and environment: Sonochemical destruction of chloroaromatic derivatives. *Environ Sci Technol* 32:1316–1318. <https://doi.org/10.1021/es970662x>
- Pétrier C, Combet E, Mason T (2007) Oxygen-induced concurrent ultrasonic degradation of volatile and non-volatile aromatic compounds. *Ultrason Sonochem* 14:117–121. <https://doi.org/10.1016/j.ultsonch.2006.04.007>
- Pétrier C, Gondrexon N, Boldo P (2008) Ultrasons et sonochimie, *Tech l'ingénieur AF6310*, pp 1–16
- Pignatello JJ, Oliveros E, MacKay A (2006) Advanced oxidation processes for organic contaminant destruction based on the fenton reaction and related chemistry. *Crit Rev Environ Sci Technol* 36:1–84. <https://doi.org/10.1080/10643380500326564>
- Rayaroth MP, Aravind UK, Aravindakumar CT (2015) Sonochemical degradation of Coomassie Brilliant Blue: effect of frequency, power density, pH and various additives. *Chemosphere* 119:848–855. <https://doi.org/10.1016/j.chemosphere.2014.08.037>
- Rehorek A, Tauber M, Gübitz G (2004) Application of power ultrasound for azo dye degradation. *Ultrason Sonochem* 11:177–182. <https://doi.org/10.1016/j.ultsonch.2004.01.030>
- Renaudin V, Gondrexon N, Boldo P, Pétrier C, Bernis A, Gonthier Y (1994) Method for determining the chemically active zones in a high-frequency ultrasonic reactor. *Ultrason Sonochem* 1:3–7. [https://doi.org/10.1016/1350-4177\(94\)90002-7](https://doi.org/10.1016/1350-4177(94)90002-7)
- Serpone N, Terzian R, Hidaka H, Pelizzetti E (1994) Ultrasonic induced dehalogenation and oxidation of 2-, 3-, and 4-Chlorophenol in air-equilibrated aqueous media. Similarities with irradiated semiconductor particulates. *J Phys Chem* 98:2634–2640. <https://doi.org/10.1021/j100061a021>
- Seymour JD, Gupta RB (1997) Oxidation of aqueous pollutants using ultrasound: salt-induced enhancement. *Ind Eng Chem Res* 36:3453–3457. <https://doi.org/10.1021/ie970069o>
- Singla R, Grieser F, Ashokkumar M (2009) Sonochemical degradation of martius yellow dye in aqueous solution. *Ultrason Sonochem* 16:28–34. <https://doi.org/10.1016/j.ultsonch.2008.05.012>
- Son Y (2015) Advanced oxidation processes using ultrasound technology for water and wastewater treatment. In: Ashokkumar M (ed) *Handbook of Ultrasonics and Sonochemistry*. Springer Science+Business Media, Singapore, pp 1–20. https://doi.org/10.1007/978-981-287-470-2_53-1
- Son Y (2017) Simple design strategy for bath-type high-frequency sonoreactors. *Chem Eng J* 328:654–664. <https://doi.org/10.1016/j.cej.2017.07.012>
- Son Y, Lim M, Ashokkumar M, Khim J (2011) Geometric optimization of sonoreactors for the enhancement of sonochemical activity. *J Phys Chem C* 115:4096–4103. <https://doi.org/10.1021/jp110319y>
- Son Y, Lim M, Khim J, Kim L, Ashokkumar M (2012) Comparison of calorimetric energy and cavitation energy for the removal of bisphenol-A: the effects of frequency and liquid height. *Chem Eng J* 183:39–45. <https://doi.org/10.1016/j.cej.2011.12.016>
- Song YL, Li JT, Chen H (2009) Degradation of C.I. acid red 88 aqueous solution by combination of fenton's reagent and ultrasound irradiation. *J Chem Technol Biotechnol* 84:578–583. <https://doi.org/10.1002/jctb.2083>
- Stefan MI (2017) *Advanced oxidation processes for water treatment: fundamentals and applications*. IWA Publishing, London
- Sun JH, Sun SP, Sun JY, Sun RX, Qiao LP, Guo HQ, Fan MH (2007) Degradation of azo dye acid black 1 using low concentration iron of Fenton process facilitated by ultrasonic irradiation. *Ultrason Sonochem* 14:761–766. <https://doi.org/10.1016/j.ultsonch.2006.12.010>

- Suslick KS, Flannigan DJ (2008) Inside a collapsing bubble: sonoluminescence and the conditions during cavitation. *Annu Rev Phys Chem* 59:659–683. <https://doi.org/10.1146/annurev.physchem.59.032607.093739>
- Suslick KS, Didenko Y, Fang MM, Hyeon T, Kolbeck KJ, Mcnamara WB III, Mdleleni MM, Wong M, William B, Iii M, Mdleleni MM, Wong M, Trans P, Lond RS (1999) Acoustic cavitation and its chemical consequences. *Philos Trans R Soc A* 357:335–353. <https://doi.org/10.1098/rsta.1999.0330>
- Sutkar VS, Gogate PR (2009) Design aspects of sonochemical reactors: techniques for understanding cavitation activity distribution and effect of operating parameters. *Chem Eng J* 155:26–36. <https://doi.org/10.1016/j.cej.2009.07.021>
- Taamallah A, Merouani S, Hamdaoui O (2016) Sonochemical degradation of basic fuchsin in water. *Desalin Water Treat* 57:27314–27330. <https://doi.org/10.1080/19443994.2016.1168320>
- Tauber A, Mark G, Schuchmann H-P, von Sonntag C (1999) Sonolysis of tert-butyl alcohol in aqueous solution. *J Chem Soc Perkin Trans 2*(2):1129–1136. <https://doi.org/10.1039/a901085h>
- Tezcanli-Guyer G, Ince NH (2003) Degradation and toxicity reduction of textile dyestuff by ultrasound. *Ultrason Sonochem* 10:235–240. [https://doi.org/10.1016/S1350-4177\(03\)00089-0](https://doi.org/10.1016/S1350-4177(03)00089-0)
- Thompson LH, Doraiswamy LK (1999) Sonochemistry: science and engineering. *Ind Eng Chem Res*:1215–1249. <https://doi.org/10.1021/ie9804172>
- Torres RA, Petrier C, Combet E, Moulet F, Pulgarin C (2007) Bisphenol a mineralization by integrated ultrasound-UV-Iron(II) treatment. *Environ Sci Technol* 41:297–302. <https://doi.org/10.1021/es061440e>
- Torres-Palma RA, Serna-Galvis EA (2018) Sonolysis. In: Ameta SC, Ameta R (eds) *Advanced oxidation processes for wastewater treatments- emerging green chemical technology*. Elsevier Inc., pp 177–213. <https://doi.org/10.1016/B978-0-12-810499-6.0>
- Vajnhandl S, Le Marechal AM (2007) Case study of the sonochemical decolouration of textile azo dye Reactive Black 5. *J Hazard Mater* 141:329–335. <https://doi.org/10.1016/j.jhazmat.2006.07.005>
- Verma A, Kaur Hura A, Dixit D (2015) Sequential photo-Fenton and sono-photo-Fenton degradation studies of Reactive Black 5 (RB5). *Desalin Water Treat* 56:677–683. <https://doi.org/10.1080/19443994.2014.940390>
- Von Sonntag C (2008) Advanced oxidation processes: mechanistic aspects. *Water Sci Technol* 58:1015–1021. <https://doi.org/10.2166/wst.2008.467>
- Vončina DB, Majcen-Le-Marechal A (2003) Reactive dye decolorization using combined ultrasound/H₂O 2. *Dyes Pigments* 59:173–179. [https://doi.org/10.1016/S0143-7208\(03\)00101-3](https://doi.org/10.1016/S0143-7208(03)00101-3)
- Wang X, Yao Z, Wang J, Guo W, Li G (2008) Degradation of reactive brilliant red in aqueous solution by ultrasonic cavitation. *Ultrason Sonochem* 15:43–48. <https://doi.org/10.1016/j.ultsonch.2007.01.008>
- Wang X, Wang L, Li J, Qiu J, Cai C, Zhang H (2014) Degradation of Acid Orange 7 by persulfate activated with zero valent iron in the presence of ultrasonic irradiation. *Sep Purif Technol* 122:41–46. <https://doi.org/10.1016/j.seppur.2013.10.037>
- Weissler A, Cooper HW, Snyder S (1950) Chemical effect of ultrasonic waves: oxidation of potassium iodide solution by carbon tetrachloride. *J Phys Chem* 72:1769–1775. <https://doi.org/10.1021/ja01160a102>
- Yasui K (2011) Fundamentals of acoustic cavitation and sonochemistry. In: Pankaj AM (ed) *Theoretical and experimental sonochemistry involving inorganic systems*. Springer Science&Business Media, New York, pp 1–29
- Yasui K, Tuziuti T, Iida Y (2005) Dependence of the characteristics of bubbles on types of sonochemical reactors. *Ultrason Sonochem* 12:43–51. <https://doi.org/10.1016/j.ultsonch.2004.06.003>
- Zhang BT, Zhang Y, Teng Y, Fan M (2015) Sulfate radical and its application in decontamination technologies. *Crit Rev Environ Sci Technol* 45:1756–1800. <https://doi.org/10.1080/10643389.2014.970681>

Chapter 6

Degradation Mechanism of Pollutants Using Sono-hybrid Advanced Oxidation Processes



Sankar Chakma, Prachi Upadhyay, and Bablu Alawa

Contents

| | | |
|-------|--|-----|
| 6.1 | Introduction | 190 |
| 6.2 | Sonolysis | 192 |
| 6.2.1 | Influence of Initial Bubble Radius | 194 |
| 6.2.2 | Effect of Static Pressure During Sonolysis | 194 |
| 6.2.3 | Effect of Temperature on Cavitation Effect | 197 |
| 6.3 | Sono-photolysis System | 198 |
| 6.4 | Sono-Photo-Fenton Process | 200 |
| 6.5 | Sono-Photo-Fenton-Ferrioxalate System | 202 |
| 6.6 | Sono-photocatalysis System | 204 |
| 6.7 | Sono-persulfate Oxidation Process | 208 |
| 6.8 | Conclusion | 210 |
| | References | 210 |

Abstract Water is one of the essential components of our daily lives especially in agriculture, domestic care, and process industry. Though the world is covered with almost 70% of water, only 1% of water is accessible out of 2.5% freshwater. Therefore, it is very essential to recycle water to fulfill the demand of the growing population. On the other hand, many chemical process industries including textile are discharging wastewater directly to the environment without any proper treatment which causes contamination of surface water as well as groundwater including the rivers. Therefore, treatment of wastewater has become a concern of the scientific community.

This chapter also provides a brief introduction of advanced techniques for treatment of contaminated water including the synergistic effect of hybrid processes. Also, a detailed discussion on the effect of negative synergy due to simultaneous

S. Chakma (✉) · P. Upadhyay · B. Alawa
Department of Chemical Engineering, Indian Institute of Science Education and Research
Bhopal, Bhopal, Madhya Pradesh, India
e-mail: schakma@iiserb.ac.in

application of more than a single advanced technique has been presented. For effective and efficient treatment of wastewater, different hybrid techniques have been employed, and the degree of mineralization was estimated. Under the sono-hybrid technique, more than 90% of degradation was obtained within 30 min of treatment in most of the homogeneous hybrid techniques. However, the maximum total organic carbon removal of 68.4% was achieved with the sono-persulfate oxidation process.

Keywords Wastewater treatment · Degradation · Advanced oxidation processes · Fenton · Photolysis · Photocatalysis · Ferrioxalate · Sonolysis · Ultrasound · Cavitation

6.1 Introduction

The growing industrialization and urbanization is increasing the environmental sustainability issues, especially water contamination and scarcity. Water is one of the most substantial components of our daily life. But the percentage of potable water is very less though the world is covered with 70% of water. On the other hand, water discharged from various process industries such as pharmaceutical industries, chemical industries, and textile industries contain numerous toxic and hazardous recalcitrant organic molecules. These molecules are difficult to degrade using biological techniques or conventional methods such as adsorption, membrane separation, etc. which are being used in most of the wastewater treatment plants (Poyatos et al. 2010). In order to address these issues, many advanced techniques have been developed. However, advanced oxidation processes have been found to be promising techniques for effective degradation or mineralization of the toxic or hazardous molecules present in the wastewater (Andreozzi et al. 1999; Chakma and Moholkar 2015a; Bagal and Gogate 2014a). The working principle of all the advanced oxidation processes is to produce the energetic $\cdot\text{OH}$ radicals which have 2.8 eV oxidation potential. These $\cdot\text{OH}$ radicals react with the recalcitrant pollutant molecules present in the wastewater and produce complete mineralization of the recalcitrant pollutants through converting them into CO_2 , H_2O , or other inorganic compounds. Sometimes the organic molecules are difficult to degrade due to formation of chelate (Giri and Golder 2014). In that case, advanced oxidation processes at least transform them into innocuous products. On the basis of phases in the reaction system, advanced oxidation processes can be categorized into two, (i) homogeneous and (ii) heterogeneous, as shown in Fig. 6.1 (Poyatos et al. 2010). The widely used homogeneous advanced oxidation processes for wastewater treatment are Fenton reaction, photolysis, photo-ferrioxalate, ozonation, and persulfate oxidation process. The conventional heterogeneous advanced oxidation processes for wastewater treatment include photocatalysis, catalytic ozonation, and

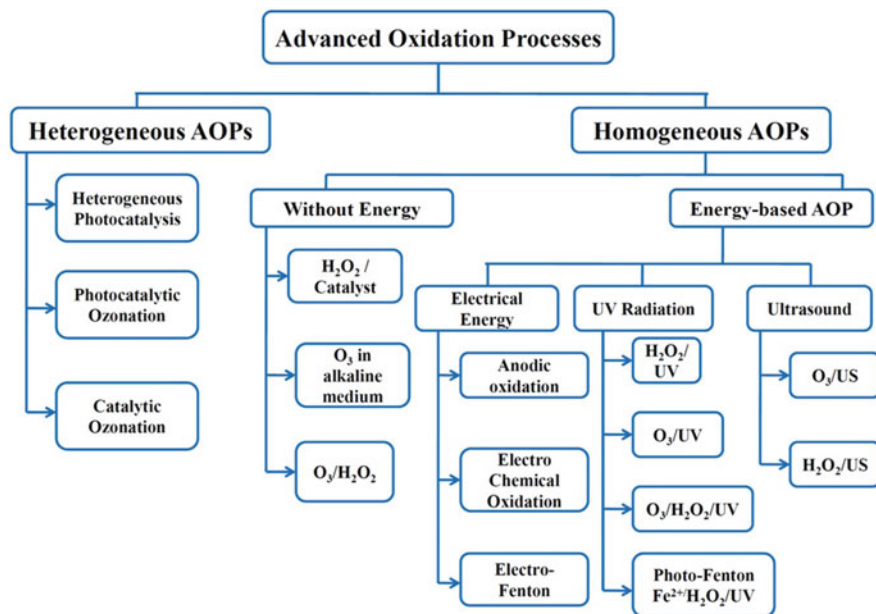


Fig. 6.1 Classification of advanced oxidation processes based on their phases and applications. Note: *AOP* advanced oxidation process, *UV* ultraviolet, *US* ultrasound. (Modified after Poyatos et al. 2010)

heterogeneous Fenton reaction – where semiconductors are used as catalysts in the reaction such as ZnO and TiO₂. To utilize the visible light, sometimes these oxides are doped with transition metals such as Fe, Au, Ag, Ni, and Mg. Recently, numerous literatures have reported the use of combined advanced oxidation processes or hybrid advanced oxidation processes for treatment of wastewater, and it has been found to be more effective for complete mineralization of organic pollutants. In these processes, two or more conventional advanced oxidation processes are applied simultaneously. The most widely used hybrid advanced oxidation techniques are photo-Fenton, photocatalysis–Fenton, photo-Fenton–ferrioxalate, ozone photolysis, and ozone microbubble system (Monteagudo et al. 2008, 2013, 2015; Katsumata et al. 2010; Kusic et al. 2011; Pang and Abdullah 2013; Nie et al. 2014; Khuntia et al. 2014; Wang et al. 2015).

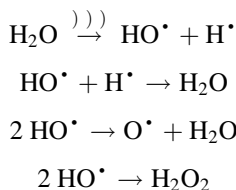
Another most effective and efficient advanced oxidation process is sonolysis process – where the wastewater is exposed to ultrasound wave irradiation. This technique is relatively new and advanced for complete mineralization of emerging pollutants' molecules from wastewater through generation of extremely energetic species during transient collapse of cavitation bubbles. Sonolysis process has been successfully implemented for degradation of a large number of toxic and recalcitrant organic pollutants (Adewuyi, 2001, 2005a, b). During the transient cavitation and at the extreme condition, several radicals are formed such as $\cdot\text{O}$, $\cdot\text{OH}$, $\text{HO}_2\cdot$, and $\text{H}\cdot$. Cavitation is the phenomenon of nucleation, growth, and implosive collapse of tiny

gas bubbles (with equilibrium size of few microns), which is driven by the pressure variation induced by the ultrasound. The implosive collapse of transient cavitation bubbles induces enormous concentrated energy which has a very diminutive, spatial, and temporal scale. During the transient collapse, a hot spot is generated, and the temperatures and pressures inside the cavitation bubble are extremely high (~5000 K and 500 bar) (Suslick 1990). The generated radicals at this extreme condition due to the dissociation of gases and solvent vapor molecules either diffuse out of the cavitation bubble (during the maximum compression or minimum radius) or get released into the bulk liquid medium as the bubble undergoes fragmentation at the point of maximum compression during radial motion. These generated radicals can induce and accelerate numerous chemical reactions in the bulk liquid medium including oxidative degradation of the organic pollutants. The coupling of sonolysis technique with other conventional advanced oxidation processes is called the sono-hybrid advanced oxidation processes. The widely used sono-hybrid advanced oxidation processes are sono-Fenton, sono-photolysis, sono-photocatalysis, sono-ferrioxalate, and sono-persulfate (Bagal and Gogate 2014a; Katsumata et al. 2010; Chakma and Moholkar 2013a, 2014, 2015a, b, c; Chakma et al. 2013, 2017; Dinesh and Chakma 2019a, b). These hybrid advanced oxidation processes are more effective and efficient for mineralization of biorecalcitrant pollutants (Entezari and Petrier 2005; Kim et al. 2015; Chakma and Moholkar 2016a; Malani et al. 2014), aniline (Chen and Huang 2015), pharmaceutical drugs (Dinesh and Chakma 2019a, b), azo and non-azo textile dyes (Chakma and Moholkar 2015c; Malani et al. 2014), plastic intermediate bisphenol A (Chakma and Moholkar 2014; Huang et al. 2012), chlorinated aromatic compounds (Peller et al. 2003), distillery wastewater (Sangave and Pandit 2006), herbicide linuron and insecticide fenitrothion (Katsumata et al. 2010, 2011), nonsteroidal anti-inflammatory drug diclofenac (Bagal and Gogate 2014b), copolymer styrene–acrylic acid (Saien et al. 2010), and cholesterol (Sun et al. 2011).

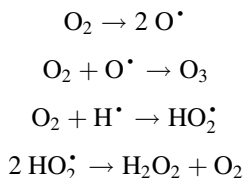
6.2 Sonolysis

Sonolysis is the application of ultrasound which induces physical and chemical effects in the medium. During sonolysis degradation, the gas and vapor molecules present in the bubbles of the liquid medium are subjected to extreme conditions generated inside the microbubbles. This results in thermal dissociation of these molecules and generation of numerous reactive chemical species including radicals as mentioned earlier. This phenomenon is directly related to the transport of vapor molecules across the bubbles' interfaces. During the growth of cavitation microbubble in radial motion, evaporation of the solvent at the interface of the bubble causes diffusion of the vapor molecules in the direction of the center of the bubble. But in the subsequent compression period, only a few vapor molecules can diffuse back at the interface of the bubble and undergo condensation. Then the “entrapped” vapor molecules undergo an extreme condition at the moment of

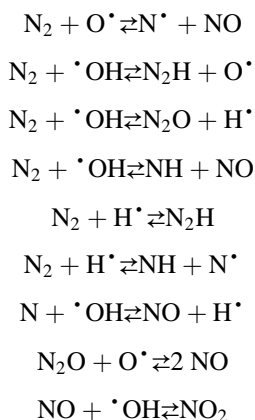
transient collapse. In sonolysis process, water is mostly considered for liquid medium, and the reactive species generated through thermal dissociation of water molecules undergo several chemical reactions as follows (Lin et al. 2008):

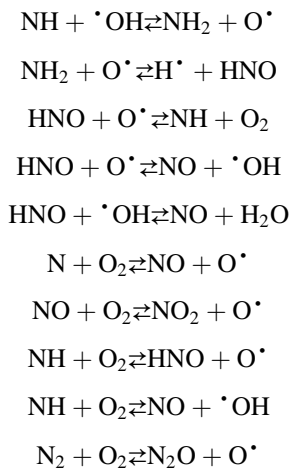


During the sonolysis process, if the liquid medium contains dissolved oxygen or the cavitation bubble contains oxygen gas (as in case of air bubbles), other parallel reactions may also occur that result in the production of other reactive or oxidizing species such as ozone (O_3) and hydrogen peroxide (H_2O_2) through the following reaction mechanism (Neppolian et al. 2002):



The air bubbles also contain nitrogen which can also give rise to numerous chemical reactions as listed below. However, some of these reactions have adverse effect on the oxidation process for degradation of pollutants as the nitrogen can also act as a scavenging agent for the generated radicals and form less reactive radicals, thus reducing the efficiency of the process (Chakma and Moholkar 2013b):





6.2.1 Influence of Initial Bubble Radius

The radius of the cavitation bubbles present in the liquid medium plays a crucial role in sonolysis method for generation of radicals. The bubble with smaller radius has higher Laplace pressure and can have a large expansion with more intense collapse during the transient collapse (Chakma and Moholkar 2013b). The cavitation dynamic model for a single bubble with initial bubble radius in the range of 5–100 μm has been investigated by Chakma and Moholkar, and the results are depicted in Table 6.1. Their results showed that the formation of $\cdot\text{OH}$ radical during the transient collapse is comparatively higher when the initial bubble radius was small, i.e., 5 μm . The results were explained as follows: the smaller diameter bubbles can experience several acoustic cycles prior to attaining the critical diameter at which moment the bubble collapses. At this point, the temperature peak reached maximum as shown in Table 6.1.

6.2.2 Effect of Static Pressure During Sonolysis

The growth of the cavitation bubbles is dependent on the applied pressure in the system. Therefore, if the microbubbles contain only vapor, the cavitation is expected to occur sufficiently because of the lowered ambient pressure when the system temperature is constant. A study of static pressure on cavitation effect has been reported by Chakma and Moholkar (Chakma and Moholkar 2013b). They have investigated five different static pressures and the results are shown in Table 6.2. The cavitation effect or the generation of radicals decreases as the system's static

Table 6.1 Effect of initial bubble radius (R_o) on physical and chemical effects of cavitation (Chakma and Moholkar 2013b)

| The conditions at the first collapse of the air bubble | | | | |
|--|--|--|--|--|
| | $R_o = 5 \mu\text{m}$ | $R_o = 25 \mu\text{m}$ | $R_o = 50 \mu\text{m}$ | $R_o = 100 \mu\text{m}$ |
| | $T_{\text{max}} = 3999 \text{ K}$ | $T_{\text{max}} = 1688 \text{ K}$ | $T_{\text{max}} = 778.5 \text{ K}$ | $T_{\text{max}} = 409 \text{ K}$ |
| | $P_{\text{max}} = 696.7 \text{ MPa}$ | $P_{\text{max}} = 30.57 \text{ MPa}$ | $P_{\text{max}} = 2.56 \text{ MPa}$ | $P_{\text{max}} = 288 \text{ kPa}$ |
| | $V_{\text{turb}} = 0.36 \text{ m/s}$ | $V_{\text{turb}} = 6.11 \text{ m/s}$ | $V_{\text{turb}} = 6.2 \text{ m/s}$ | $V_{\text{turb}} = 7.95 \text{ m/s}$ |
| | $P_{\text{AW}} = 24.04 \text{ MPa}$ | $P_{\text{AW}} = 8.80 \text{ MPa}$ | $P_{\text{AW}} = 0.63 \text{ MPa}$ | $P_{\text{AW}} = 0.27 \text{ MPa}$ |
| | $N_{\text{N}_2} = 1.28 \times 10^{10}$ | $N_{\text{N}_2} = 1.32 \times 10^{12}$ | $N_{\text{N}_2} = 1.03 \times 10^{13}$ | $N_{\text{N}_2} = 8.11 \times 10^{13}$ |
| | $N_{\text{O}_2} = 3.41 \times 10^9$ | $N_{\text{O}_2} = 3.51 \times 10^{11}$ | $N_{\text{O}_2} = 2.73 \times 10^{12}$ | $N_{\text{O}_2} = 2.16 \times 10^{13}$ |
| | $N_{\text{W}} = 2.91 \times 10^9$ | $N_{\text{W}} = 2.5 \times 10^{11}$ | $N_{\text{W}} = 9.08 \times 10^{11}$ | $N_{\text{W}} = 2.98 \times 10^{12}$ |
| Species | Equilibrium composition | | | |
| | 5 μm | 25 μm | 50 μm | 100 μm |
| N_2 | 6.26×10^{-1} | 6.86×10^{-1} | 7.38×10^{-1} | 7.68×10^{-1} |
| O_2 | 1.28×10^{-1} | 1.82×10^{-1} | 1.96×10^{-1} | 2.04×10^{-1} |
| H_2O | 1.41×10^{-2} | 1.30×10^{-1} | 6.50×10^{-2} | 2.80×10^{-2} |
| N | 1.56×10^{-5} | – | – | – |
| O | 5.95×10^{-3} | – | – | – |
| H | 2.83×10^{-4} | – | – | – |
| O_3 | 1.70×10^{-5} | – | – | – |
| H_2 | 2.53×10^{-4} | – | – | – |
| OH | 9.51×10^{-3} | 9.03×10^{-5} | – | – |
| HO_2 | 5.59×10^{-4} | 5.81×10^{-6} | – | – |
| H_2O_2 | 2.00×10^{-5} | – | – | – |
| NO | 8.47×10^{-2} | 2.58×10^{-3} | 1.49×10^{-6} | – |
| NO_2 | 1.70×10^{-3} | 1.27×10^{-4} | 2.84×10^{-6} | – |
| N_2O | 3.61×10^{-4} | 2.18×10^{-6} | – | – |
| NH | 1.70×10^{-6} | – | – | – |
| HNO | 5.95×10^{-5} | – | – | – |
| HNO_2 | 1.75×10^{-4} | 7.06×10^{-6} | – | – |

Note: N_{W} number of water molecules trapped in the bubble, N_{N_2} number of N_2 molecules in the bubble, N_{O_2} number of oxygen molecules in the cavitation bubble, P_o ambient pressure in liquid medium, P_{max} pressure peak attained inside the bubble during first collapse, P_{AW} acoustic wave pressure amplitude induced during cavitation, T cavitation bubbles' temperature, T_o ambient temperature or liquid temperature, T_{max} temperature peak attained inside the bubble during first collapse, V_{turb} average velocity of micro-turbulence in the liquid medium generated by ultrasound and cavitation (estimated at 1 mm distance from bubble center)

pressure increases, even though it may become zero in some cases. When the static pressure is high, the sonochemical effects get eradicated and drastically change in the radical generation. However, the applied static pressure should be higher or equivalent to the amplitude of acoustic pressure (Chakma and Moholkar 2013a, b, 2014). The formation of oxidizing agent such as $\cdot\text{OH}$ radical was the highest at the ambient static pressure, while the generation of $\cdot\text{OH}$ radicals was zero when the ambient pressure was 150 kPa, which is just above the acoustic pressure (P_{AW}). The highest $\cdot\text{OH}$ radical production was due to the occurrence of hot spot at which the

Table 6.2 Effect of static pressure (P_o) on sonochemical process for production of radicals and other species (Chakma and Moholkar 2013b)

| | Conditions at the first collapse of the bubble | | | |
|------------------------|--|--|--|--|
| | $P_o = 100$ kPa | $P_o = 120$ kPa | $P_o = 150$ kPa | $P_o = 200$ kPa |
| | $T_{\max} = 3999$ K | $T_{\max} = 3024$ K | $T_{\max} = 977.3$ K | $T_{\max} = 353.4$ K |
| | $P_{\max} = 696.7$ MPa | $P_{\max} = 286.3$ MPa | $P_{\max} = 4.62$ MPa | $P_{\max} = 416$ kPa |
| | $V_{\text{turb}} = 0.36$ m/s | $V_{\text{turb}} = 0.21$ m/s | $V_{\text{turb}} = 0.07$ m/s | $V_{\text{turb}} = 0.008$ m/s |
| | $P_{\text{AW}} = 24.04$ MPa | $P_{\text{AW}} = 5.43$ MPa | $P_{\text{AW}} = 120$ kPa | $P_{\text{AW}} = 2$ kPa |
| | $N_{\text{N}_2} = 1.28 \times 10^{10}$ | $N_{\text{N}_2} = 1.48 \times 10^{10}$ | $N_{\text{N}_2} = 1.78 \times 10^{10}$ | $N_{\text{N}_2} = 2.28 \times 10^{10}$ |
| | $N_{\text{O}_2} = 3.41 \times 10^9$ | $N_{\text{O}_2} = 3.95 \times 10^9$ | $N_{\text{O}_2} = 4.74 \times 10^9$ | $N_{\text{O}_2} = 6.07 \times 10^9$ |
| | $N_{\text{W}} = 2.91 \times 10^9$ | $N_{\text{W}} = 1.81 \times 10^9$ | $N_{\text{W}} = 8.86 \times 10^8$ | $N_{\text{W}} = 8.19 \times 10^{10}$ |
| Species | Equilibrium composition | | | |
| | $P_o = 100$ kPa | $P_o = 120$ kPa | $P_o = 150$ kPa | $P_o = 200$ kPa |
| N_2 | 6.26×10^{-1} | 6.99×10^{-1} | 7.60×10^{-1} | 7.68×10^{-1} |
| O_2 | 1.28×10^{-1} | 1.67×10^{-1} | 2.02×10^{-1} | 2.04×10^{-1} |
| H_2O | 1.41×10^{-2} | 7.45×10^{-2} | 3.80×10^{-2} | 2.80×10^{-2} |
| N | 1.56×10^{-5} | – | – | – |
| O | 5.95×10^{-3} | 9.35×10^{-4} | – | – |
| H | 2.83×10^{-4} | 4.09×10^{-5} | – | – |
| O_3 | 1.70×10^{-5} | 3.71×10^{-6} | – | – |
| H_2 | 2.53×10^{-4} | 1.67×10^{-4} | – | – |
| OH | 9.51×10^{-3} | 6.33×10^{-3} | – | – |
| HOO^{\cdot} | 5.59×10^{-4} | 3.60×10^{-4} | – | – |
| H_2O_2 | 2.00×10^{-5} | 2.74×10^{-5} | – | – |
| NO | 8.47×10^{-2} | 4.30×10^{-2} | 2.64×10^{-5} | – |
| NO_2 | 1.70×10^{-3} | 1.03×10^{-3} | 1.09×10^{-5} | – |
| N_2O | 3.61×10^{-4} | 1.10×10^{-4} | – | – |
| NH | 1.70×10^{-6} | – | – | – |
| HNO | 5.95×10^{-5} | 1.38×10^{-5} | – | – |
| HNO_2 | 1.75×10^{-4} | 1.40×10^{-4} | – | – |

Note: N_{W} number of water molecules trapped in the bubble, N_{N_2} number of N_2 molecules in the bubble, N_{O_2} number of oxygen molecules in the cavitation bubble, P_o ambient pressure in liquid medium, P_{\max} pressure peak attained inside the bubble during first collapse, P_{AW} acoustic wave pressure amplitude induced during cavitation, T cavitation bubbles' temperature, T_o ambient temperature or liquid temperature, T_{\max} temperature peak attained inside the bubble during first collapse, V_{turb} average velocity of micro-turbulence in the liquid medium generated by ultrasound and cavitation (estimated at 1 mm distance from bubble center)

temperature peak was 3999 K, thus water molecules dissociated and formed radicals. As the static pressure increases, the cavitation effect also reduces that results in lowest temperature peak (~313 K), leading to no production of $\cdot\text{OH}$ radicals.

6.2.3 Effect of Temperature on Cavitation Effect

The transient cavitation is directly affected by the system temperature. As the system temperature increases, the effect of cavitation is also reduced as shown in Table 6.3; thus, the formation of reactive species is also reduced which can be elucidated based on the initial diameter of the cavitation bubbles as discussed in the previous section.

Table 6.3 Summary of equilibrium composition and bubble condition at different temperatures (T_o) (Chakma and Moholkar 2013b)

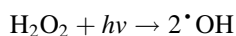
| | Properties of bubble at different temperatures | | | |
|------------------------|---|--|--|--|
| | $T = 283 \text{ K}$ | $T = 303 \text{ K}$ | $T = 323 \text{ K}$ | $T = 343 \text{ K}$ |
| | Conditions at the first collapse of cavitation bubble | | | |
| | $T_{\max} = 3989 \text{ K}$ | $T_{\max} = 3999 \text{ K}$ | $T_{\max} = 3733 \text{ K}$ | $T_{\max} = 2683 \text{ K}$ |
| | $P_{\max} = 681.5 \text{ MPa}$ | $P_{\max} = 696.7 \text{ MPa}$ | $P_{\max} = 623.9 \text{ MPa}$ | $P_{\max} = 175.3 \text{ MPa}$ |
| | $V_{\text{turb}} = 0.35 \text{ m/s}$ | $V_{\text{turb}} = 0.36 \text{ m/s}$ | $V_{\text{turb}} = 0.45 \text{ m/s}$ | $V_{\text{turb}} = 1.08 \text{ m/s}$ |
| | $P_{\text{AW}} = 24.75 \text{ MPa}$ | $P_{\text{AW}} = 24.04 \text{ MPa}$ | $P_{\text{AW}} = 21.56 \text{ MPa}$ | $P_{\text{AW}} = 4.43 \text{ MPa}$ |
| | $N_{\text{N}_2} = 1.38 \times 10^{10}$ | $N_{\text{N}_2} = 1.28 \times 10^{10}$ | $N_{\text{N}_2} = 1.21 \times 10^{10}$ | $N_{\text{N}_2} = 1.13 \times 10^{10}$ |
| | $N_{\text{O}_2} = 3.66 \times 10^9$ | $N_{\text{O}_2} = 3.41 \times 10^9$ | $N_{\text{O}_2} = 3.20 \times 10^9$ | $N_{\text{O}_2} = 3.02 \times 10^9$ |
| | $N_{\text{W}} = 7.94 \times 10^8$ | $N_{\text{W}} = 2.91 \times 10^9$ | $N_{\text{W}} = 1.23 \times 10^{10}$ | $N_{\text{W}} = 8.15 \times 10^{10}$ |
| Species | Equilibrium composition | | | |
| | 283 K | 303 K | 323 K | 343 K |
| N_2 | 7.07×10^{-1} | 6.26×10^{-1} | 4.13×10^{-1} | 1.16×10^{-1} |
| O_2 | 1.45×10^{-1} | 1.28×10^{-1} | 8.84×10^{-2} | 2.83×10^{-2} |
| H_2O | 1.63×10^{-2} | 1.41×10^{-2} | 1.21×10^{-2} | 2.80×10^{-2} |
| N | 1.72×10^{-5} | 1.56×10^{-5} | 3.84×10^{-6} | – |
| O | 6.67×10^{-3} | 5.95×10^{-3} | 2.44×10^{-3} | 5.69×10^{-5} |
| H | 3.21×10^{-4} | 2.83×10^{-4} | 1.06×10^{-4} | 2.57×10^{-6} |
| O_3 | 1.89×10^{-5} | 1.70×10^{-5} | 8.38×10^{-6} | 2.28×10^{-7} |
| H_2 | 2.91×10^{-4} | 2.53×10^{-4} | 1.30×10^{-4} | 2.29×10^{-5} |
| OH | 1.08×10^{-2} | 9.51×10^{-3} | 5.27×10^{-3} | 8.08×10^{-4} |
| HO_2 | 6.31×10^{-4} | 5.59×10^{-4} | 3.25×10^{-4} | 4.22×10^{-5} |
| H_2O_2 | 2.28×10^{-5} | 2.00×10^{-5} | 1.36×10^{-5} | 4.60×10^{-6} |
| NO | 9.51×10^{-2} | 8.47×10^{-2} | 4.72×10^{-2} | 4.57×10^{-3} |
| NO_2 | 1.90×10^{-3} | 1.70×10^{-3} | 1.04×10^{-3} | 1.11×10^{-4} |
| N_2O | 4.01×10^{-4} | 3.61×10^{-4} | 1.88×10^{-4} | 8.69×10^{-6} |
| NH | 1.89×10^{-6} | 1.70×10^{-6} | – | – |
| HNO | 6.67×10^{-5} | 5.95×10^{-5} | 2.74×10^{-5} | 9.69×10^{-7} |
| HNO_2 | 1.96×10^{-4} | 1.75×10^{-4} | 1.12×10^{-4} | 1.76×10^{-5} |

Note: N_{W} number of water molecules trapped in the bubble, N_{N_2} number of N_2 molecules in the bubble, N_{O_2} number of oxygen molecules in the cavitation bubble, P_o ambient pressure in liquid medium, P_{\max} pressure peak attained inside the bubble during first collapse, P_{AW} acoustic wave pressure amplitude induced during cavitation, T cavitation bubbles' temperature, T_o ambient temperature or liquid temperature, T_{\max} temperature peak attained inside the bubble during first collapse, V_{turb} average velocity of micro-turbulence in the liquid medium generated by ultrasound and cavitation (estimated at 1 mm distance from bubble center)

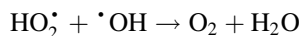
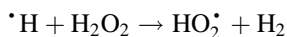
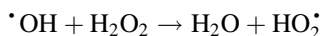
According to the phenomenon of boiling, as the temperature increases, the vapor bubble also grows. This limits the bubble's acoustic cycles, and the bubble attains the critical radius early which causes lesser cavitation effect. Therefore, to achieve the maximum cavitation effect, it is suggested to perform the experiments at lower temperature. The detailed discussion on this topic may be found at Chakma and Moholkar (2013b).

6.3 Sono-photolysis System

In the sonolysis process, the entrapped water vapor molecules in the cavitation bubble experience thermal dissociation and produce several radicals (i.e., $\cdot\text{H}$, $\cdot\text{OH}$, $\cdot\text{O}$, and $\text{HO}_2\cdot$) and other oxidizing species such as H_2O_2 and O_3 . During the transient collapse, these radicals are unconfined into the medium with the fragmentation of cavitation bubble and attack the molecules of the recalcitrant pollutants at a whopping rate constant of 10^6 – 10^9 $\text{mole}^{-1} \text{s}^{-1}$ (Andreozzi et al. 1999). However, there is also a chance of recombination due to nonuniform interaction when the concentration of pollutant molecules is comparatively less. In that case, the generated $\cdot\text{OH}$ radicals combine and produce H_2O_2 which has less oxidation potential (1.77 eV) as compared to that of $\cdot\text{OH}$ radicals (2.8 eV). Therefore, the application of UV light irradiation during the process can regenerate the $\cdot\text{OH}$ radicals through re-splitting the in situ-generated H_2O_2 as follows:



The concentration of H_2O_2 is a crucial parameter for H_2O_2 -based photolysis process. In this process, higher concentration of H_2O_2 may result in scavenging of oxidizing $\cdot\text{OH}$ radicals before it can react with the organic pollutants (Mishra and Gogate 2011; Chakma and Moholkar 2016b):



When the conventional photolysis is employed with sonolysis process, the mineralization of recalcitrant pollutants can be enhanced as shown in Fig. 6.2 (Chakma and Moholkar 2016b). During the sonolysis process, some amount of the externally added H_2O_2 is decomposed and produces $\cdot\text{OH}$ radicals, while in situ-generated H_2O_2 during sonolysis process can also undergo photodecomposition under ultraviolet light and produce additional $\cdot\text{OH}$ radicals. This process is stronger when the liquid medium contains dissolved oxygen as discussed earlier. This leads to generation of $\text{HO}_2\cdot$ and $\cdot\text{O}$ radicals as follows:

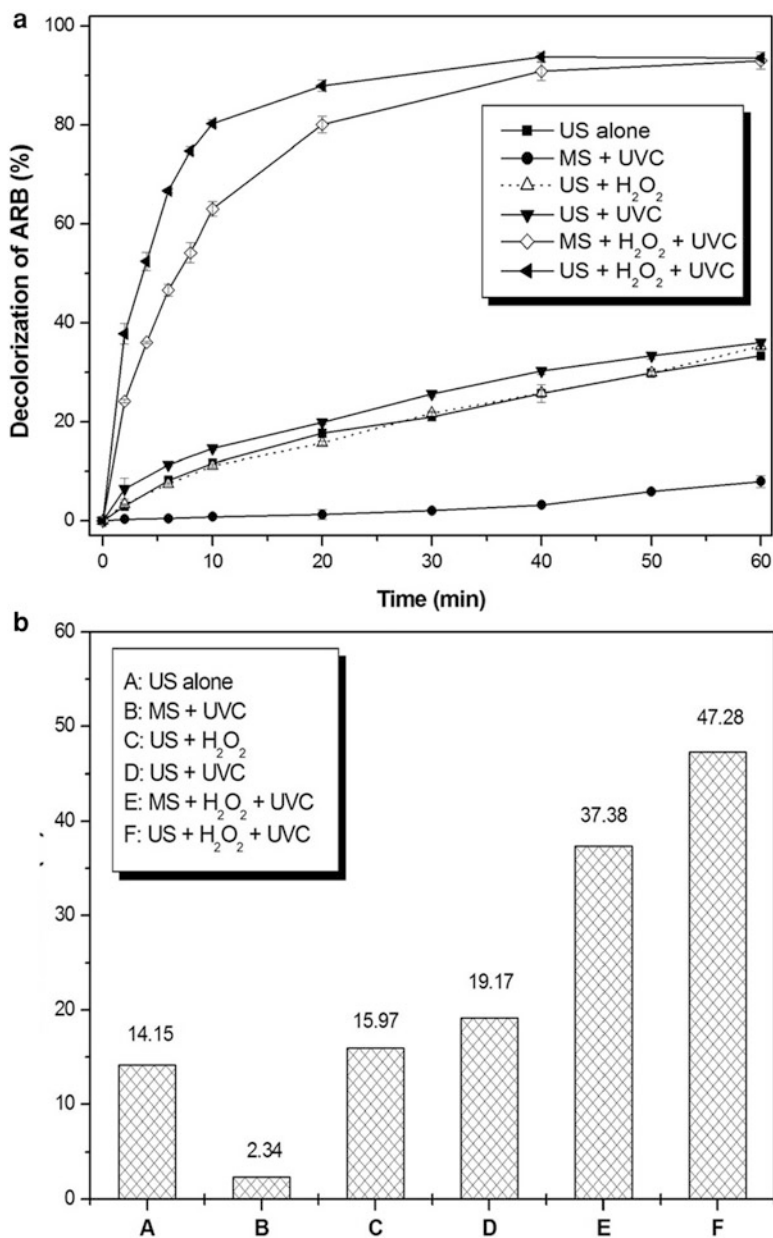
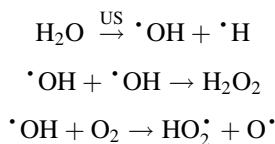
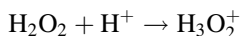


Fig. 6.2 (a) Degradation of Acid Red B and (b) total organic carbon (TOC) removal under different experimental conditions. Note: *US* ultrasound, *MS* mechanical stirring, *UVC* ultraviolet light C. (Reprinted with permission of Elsevier from Chakma and Moholkar 2016b)



Another factor that affects the sono-photolysis process is the solution pH. Under acidic medium, the H_2O_2 can react with the proton and generate oxonium ion (H_3O_2^+) through the following reaction (Daud et al. 2012):

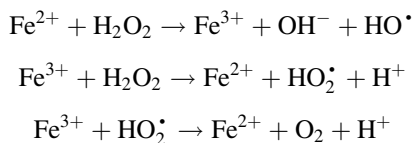


When the pH of the reaction solution is high (normally, $>pK_a$), H_2O_2 dissociates to generate HO_2^- and H^+ species (Chang et al. 2010):



6.4 Sono-Photo-Fenton Process

Fenton process is an easy and simple technique used for the production of $\cdot\text{OH}$ radicals for degradation reaction. It also does not require any expensive chemicals, specific reactors, or any specific reaction conditions for generation of $\cdot\text{OH}$ radicals. The process can be operated at atmospheric pressure and temperature. In this advanced oxidation process, the $\cdot\text{OH}$ radicals are generated by activating H_2O_2 in the presence of ferrous ion (Fe^{2+}) which is known as Fenton's reagent. The reaction mechanism for generation of $\cdot\text{OH}$ radical through the Fenton process is given below (Chakma and Moholkar 2013a, 2014):



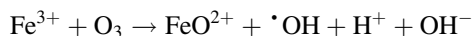
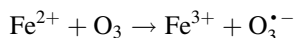
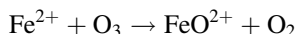
The advantage of the Fenton reaction is that it is environmental friendly and also handling of H_2O_2 is very easy. In the last few decades, numerous studies have demonstrated the Fenton reaction for degradation of enormous recalcitrant pollutants from industrial wastewater including textile dyes and pesticides (Chakma and Moholkar 2013a; Iglesias et al. 2015; Bocos et al. 2015).

In the last few years, the basic Fenton reaction has been modified for effective degradation of pollutants. The most popularly used modified Fenton processes are photo-Fenton, ozone-Fenton, H_2O_2 -ferrioxalate, and photo-Fenton-ferrioxalate

processes. In photo-Fenton reaction, the reaction mixture is exposed to light to accelerate the production of $\cdot\text{OH}$ radicals for effective degradation of toxic molecules (Katsumata et al. 2011; Giri and Golder 2014; Chakma and Moholkar 2014). During the Fenton process, the iron species make photoactive hydroxylated complex which further produces extra $\cdot\text{OH}$ radicals when exposed to ultraviolet light (Rodríguez et al. 2012; Monteagudo et al. 2013). In fact, the iron–hydroxy complexes have the ability to absorb photons within broader range of wavelength (including visible range) to produce radicals as follows:



The degradation efficiency of organic pollutants can also be increased using ozone–Fenton process, in which O_3 and Fenton reaction are applied simultaneously (Rodríguez et al. 2012). In the Fenton– O_3 process, the reaction rate depends on the concentration of O_3 . As the concentration of O_3 increases, the removal of organic pollutants not only increases due to the direct oxidation of pollutants by O_3 but also enhances the production of other radicals such as $\cdot\text{OH}$ and $\text{O}_3^{\cdot-}$ (Ziylan and Ince 2015; Rodríguez et al. 2012):



The most recent variants of Fenton reaction are sono-Fenton and sono–photo-Fenton (Segura et al. 2009; Chakma and Moholkar 2013a, 2014). In the last decade, numerous investigations have been carried out using sono-Fenton and sono–photo-Fenton processes to give effective degradation of several recalcitrant pollutants (Lin et al. 2008; Segura et al. 2009; Katsumata et al. 2011; Zhong et al. 2011; Zhao et al. 2012). In the sono-Fenton or sono–photo-Fenton process, the reaction can be initiated by the in situ H_2O_2 generated during the transient cavitation. Thus, external addition of H_2O_2 is not necessary for this system.

In this process, optimization of H_2O_2 concentration, Fe^{2+} concentration, and the solution pH is very important. Generally, the optimum pH of the Fenton process is in the range of pH 2–4 (Chakma and Moholkar 2013a, 2014). At higher pH, the Fe^{2+} ions are converted to Fe^{3+} , and the regeneration of Fe^{2+} is reduced which is one of the reagents of Fenton reaction. On the other hand, at the excess H_2O_2 concentration, it scavenges the $\cdot\text{OH}$ radicals, resulting in reduced degradation efficiency as shown in Fig. 6.3 (Chakma 2015).

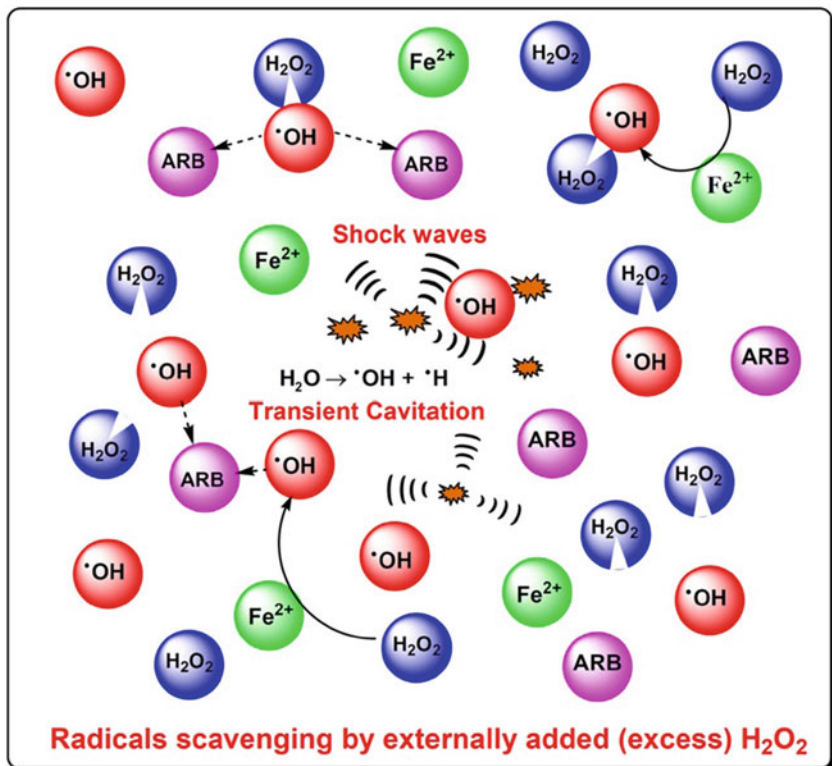
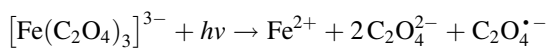
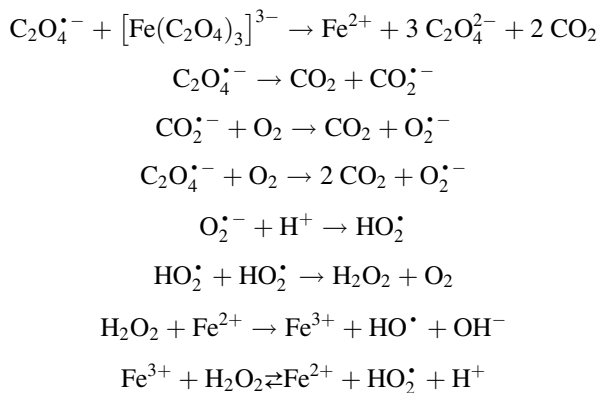


Fig. 6.3 Scavenging effect of $\cdot\text{OH}$ radicals by the externally added excess H_2O_2 during the Fenton reaction. (Reprinted with permission from Chakma 2015)

6.5 Sono-Photo-Fenton-Ferrioxalate System

In this process, the ferrioxalate complex $[\text{Fe}(\text{C}_2\text{O}_4)_3]^{3-}$ is prepared by adding iron species with oxalate salts. This complex is highly photochemically active at or near ultraviolet range (Arslan et al. 2000; Jeong and Yoon 2005; Katsumata et al. 2010; Monteagudo et al. 2013) and capable of absorbing the photons of the solar spectrum up to the wavelength range of 450 nm (Monteagudo et al. 2008). During the photoexcitation, the $[\text{Fe}(\text{C}_2\text{O}_4)_3]^{3-}$ complex undergoes a series of photochemical reactions as per the ligand-to-metal charge transfer (LMCT) reaction mechanism (Jeong and Yoon 2004; Zhou et al. 2004; Vedrenne et al. 2012) and produces $\cdot\text{OH}$, $\text{HO}_2\cdot$, and $\text{O}_2^{\cdot-}$ through the following reaction mechanism:





It is noteworthy to mention that in this process, the required H_2O_2 is produced in situ (although addition of H_2O_2 externally is also possible). It should be noted that for the production of in situ H_2O_2 , the reaction must be carried out in the air-saturated medium at pH 2–4 where $\text{C}_2\text{O}_4^{\bullet-}$ radicals react with the molecular oxygen and generate $\text{O}_2^{\bullet-}$. Then $\text{O}_2^{\bullet-}$ reacts with H^+ to form HO_2^{\bullet} which further recombine in the subsequent reactions to form H_2O_2 (Chakma et al. 2015; Chakma and Moholkar 2016c). Then, Fe^{2+} reacts with this in situ-generated H_2O_2 which results in generation of OH^{\bullet} radicals through Fenton reaction mechanism. Hence, the photo-ferrioxalate system in the presence of dissolved oxygen is a continuous process for OH^{\bullet} radical production via Fenton reaction and Fenton-like reaction. Since the production of radicals in this process is based on Fenton-like reaction, the pH of the reaction mixture has to be maintained in the range of pH 2–4 (Arslan et al. 2000; Jeong and Yoon 2004; Rodríguez et al. 2011; Zhou et al. 2013), while the ratio of iron to oxalate must be maintained at 1:3 (Arslan et al. 2000; Chakma et al. 2015; Chakma and Moholkar 2016c).

It should also be noted that the sono-photo-Fenton-ferrioxalate process consists of four individual advanced oxidation processes. Therefore, it is also possible to have some adverse effects due to the high concentration of radicals in the system as discussed earlier. Hence, it is also necessary to identify the synergy index to optimize the process for maximum degradation of recalcitrant pollutants. The synergy index can be estimated using the degradation rate constants or the total degradation obtained. Chakma and Moholkar have determined the synergy index using the following equation which is based on the rate constant (Chakma et al. 2015):

$$\text{Synergy index} = \frac{k_{\text{hybrid AOP}} - \sum k_{\text{individual AOP}}}{\sum k_{\text{individual AOP}}}$$

The results of their investigation are shown in Fig. 6.4 (Chakma et al. 2015). According to their study, the degradation depends on the combination of advanced oxidation processes. In a few cases, a negative synergy is also possible. This is due to the scavenging effect of radicals generated through different techniques, and these

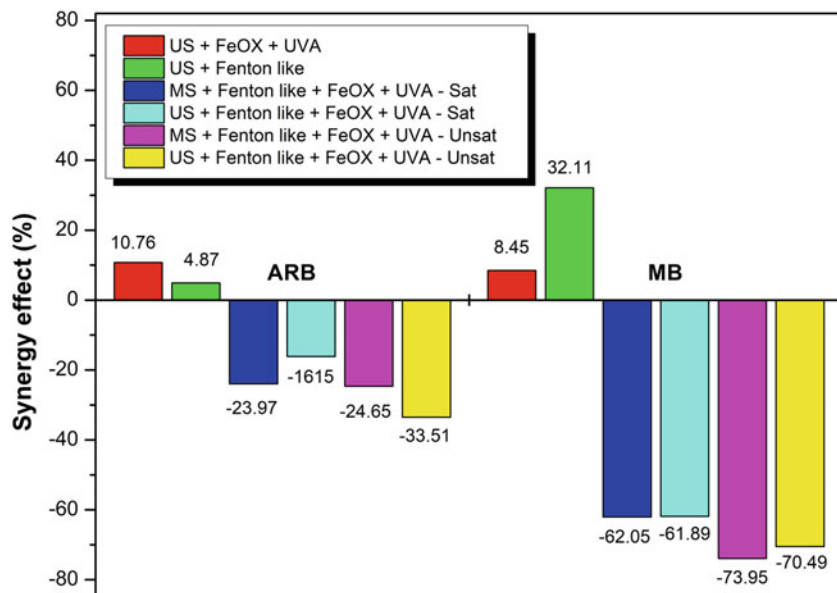


Fig. 6.4 Effect of synergism effect when hybrid advanced oxidation processes are applied for degradation of Acid Red B (azo dye) and methylene blue (non-azo dye). Note: *FeOX* ferrioxalate, *Sat.* oxygen saturated, *Unsat.* oxygen unsaturated, *US* ultrasound, *MS* mechanical stirring, *UVA* ultraviolet light A, *ARB* Acid Red B, *MB* methylene blue. (Reprinted with permission of Elsevier from Chakma et al. 2015)

radicals recombine before reacting with the pollutant molecules. As per their study, the maximum negative synergy was seen for the system sono-photo-Fenton-ferrioxalate system, a combination of four advanced oxidation processes.

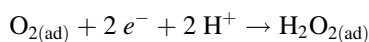
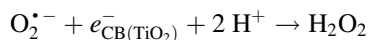
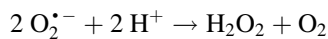
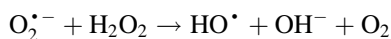
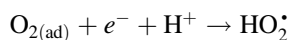
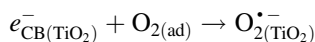
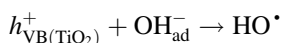
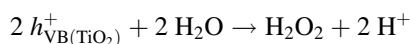
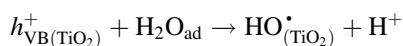
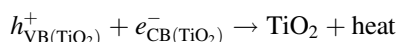
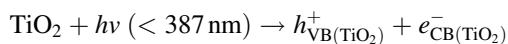
6.6 Sono-photocatalysis System

The photocatalysis process is the heterogeneous conventional advanced oxidation process used for production of free radicals. In this processes, semiconductors (e.g., TiO_2 and ZnO) are most commonly used as catalysts in the presence of O_2 as oxidizing agent (Chakma and Moholkar 2015b, c; Hu et al. 2014). This process depends on the catalysts' ability to create electron-hole ($e^- - h^+$) pairs and generate $\cdot\text{OH}$ radicals. The ZnO and TiO_2 nanoparticles are the most popular catalysts for photocatalysis reaction as they are highly stable, efficient, and more importantly inexpensive. When these catalysts are exposed to the UV light or sunlight, an electron (e^-) is promoted from valence band (VB) to the conduction band (CB), resulting in the production of a positive oxidant hole (h^+) at the VB (Adewuyi 2005b):

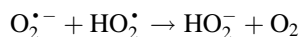
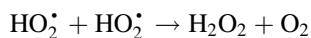
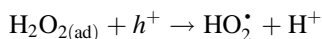
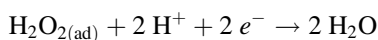
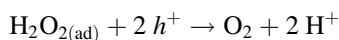


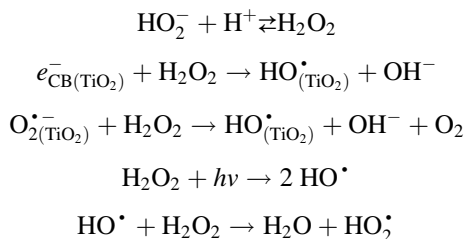
For well-illuminated reactor, the formation of electron-hole is very fast ($\sim 10^{15} \text{ s}^{-1}$) (Pareek and Adesina 2004). In the case of TiO_2 , it exists in two phases, viz., anatase and rutile phase. The band gap energy for anatase phase is $\sim 3.2 \text{ eV}$, while for rutile phase is $\sim 3.0 \text{ eV}$. The anatase phase normally exhibits superior photocatalytic activity than the rutile phase. Also, a large surface area is observed for the anatase phase of TiO_2 that helps to absorb greater extent of radicals. The reaction mechanism for radical generation using TiO_2 is given below (Adewuyi 2005a, b).

(a) Photocatalysis in the presence of TiO_2 and O_2 :

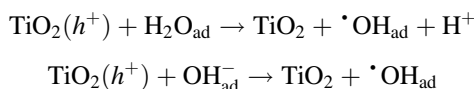


(b) TiO_2 - H_2O_2 (in situ generated during sonolysis) system:

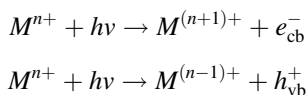




The electrons from the above equations may also help in generating $\text{O}_2^{\bullet-}$ in the presence of dissolved oxygen, and the holes (h^+) react with the adsorbed water molecules on the metal oxide surface and generate $^\bullet\text{OH}$ radicals:



Similar to every advanced oxidation process, photocatalysis process also has some advantage and disadvantage. The demerit of the process is that most of the photocatalysts are not photoactive in visible light. In the recent studies, it has been reported that doping of transition metals or rare-earth elements can increase the photoactivity in the range of visible light. For efficient treatment of wastewater using the solar light energy, the band gap energy has to be reduced to increase the visible light absorption range so that the electron can be transferred easily from CB to VB under visible light. To reduce the band gap energy, transition metals such as Fe, Ag, Ni, Au, Mg, and Co (Chakma and Moholkar 2015b; Zaleska 2008; Kudo and Miseki 2009; Yao et al. 2010; Etacheri et al. 2012; Ng et al. 2012); rare-earth elements such as Ce, Er, and Yb (Shirsath et al. 2013; Reszczyńska et al. 2015); and in some cases nonmetals such as N, S, and F (Qin et al. 2011; Zhu et al. 2013; Asiri et al. 2014) are being used to increase the absorption of photons. When the transition metal ions are integrated into semiconductors' lattice, the impurity energy levels in the semiconductors' band gap are induced as follows (Ni et al. 2007):



where M is the metal, M^{n+} is the metal ion dopant, e_{cb}^- is the conduction band electron, and h_{vb}^+ is the hole at the valence band. The electron-hole ($e^- - h^+$) transfer between the photocatalyst and the metal ions (M^{n+}) alters the ($e^- - h^+$) recombination as shown below:

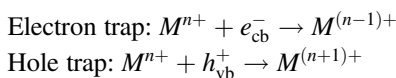


Table 6.4 Degradation summary of methylene blue and Acid Red B using pure and Fe-doped ZnO (Chakma and Moholkar 2015b)

| Experimental category | Methylene blue (non-azo dye) | | | |
|-----------------------|------------------------------|-----------------------------|---|-----------------------------|
| Sonolysis (US) | 7.14 ± 0.48 | | $k \text{ (s}^{-1}\text{)} = 2.17 \times 10^{-5}$ | |
| | ZnO | | Fe-doped ZnO | |
| | $\eta\%$ | $k \text{ (s}^{-1}\text{)}$ | $\eta\%$ | $k \text{ (s}^{-1}\text{)}$ |
| MS + UV | 41.15 ± 1.05 | 2.48×10^{-4} | 69.23 ± 2.43 | 4.14×10^{-4} |
| US + saturated | 47.93 ± 0.79 | 5.42×10^{-4} | 55.46 ± 0.63 | 6.86×10^{-4} |
| US + unsaturated | 43.45 ± 0.50 | 4.20×10^{-4} | 54.31 ± 0.98 | 5.78×10^{-4} |
| US + UV + saturated | 53.28 ± 0.07 | 6.39×10^{-4} | 67.55 ± 0.28 | 9.07×10^{-4} |
| US + UV + unsaturated | 53.38 ± 3.83 | 3.19×10^{-4} | 71.50 ± 1.65 | 8.13×10^{-4} |
| | Acid Red B (azo dye) | | | |
| Sonolysis (US) | 16.36 ± 1.48 | | $k \text{ (s}^{-1}\text{)} = 4.34 \times 10^{-5}$ | |
| | ZnO | | Fe-doped ZnO | |
| | $\eta\%$ | $k \text{ (s}^{-1}\text{)}$ | $\eta\%$ | $k \text{ (s}^{-1}\text{)}$ |
| MS + UV | 63.45 ± 1.91 | 6.28×10^{-4} | 74.3 ± 1.06 | 8.49×10^{-4} |
| US + saturated | 50.21 ± 1.01 | 3.49×10^{-4} | 58.52 ± 0.23 | 7.24×10^{-4} |
| US + unsaturated | 43.12 ± 1.20 | 1.21×10^{-4} | 52.42 ± 0.30 | 6.13×10^{-4} |
| US + UV + saturated | 80.98 ± 1.02 | 9.22×10^{-4} | 74.75 ± 0.64 | 1.13×10^{-3} |
| US + UV + unsaturated | 73.32 ± 1.39 | 6.05×10^{-4} | 74.13 ± 2.90 | 8.70×10^{-4} |

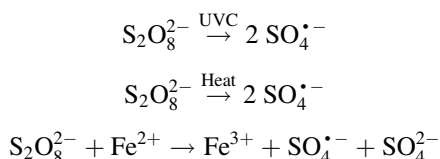
Note: k pseudo-first-order kinetic constant (s^{-1}), *MS* mechanical stirring, *US* ultrasound, *UV* ultraviolet light, η degradation efficiency (%)

The energy level of $M^{n+}/M^{(n-1)+}$ is less negative as compared with CB energy level of the native photocatalyst; but the energy level of $M^{n+}/M^{(n+1)+}$ is slightly positive as compared with the VB energy level of the native photocatalyst.

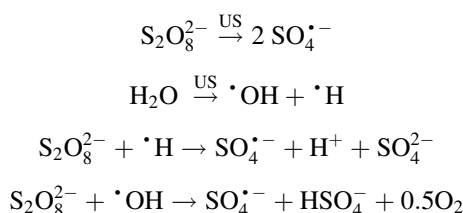
In order to explain in details about the advantage of doping and application of ultrasound in photocatalysis process, the degradation results of methylene blue and Acid Red B is presented in Table 6.4 (Chakma and Moholkar 2015b). The results revealed that doping of Fe- into ZnO increased the methylene blue degradation from 41.15% to 69.23% under conventional photocatalysis process, while integration of sonolysis process into the conventional photocatalysis methods increased the methylene blue degradation up to 53.28% which is an ~29.5% enhancement compared to the conventional technique. A similar trend was also seen for Acid Red B dye degradation. As discussed earlier, dissolved oxygen plays an important role in the treatment of wastewater for generation of free radicals which is a direct evidence in the degradation of Acid Red B under saturated and unsaturated medium. However, this effect is not significant for degradation of methylene blue – which essentially indicates that dissolved oxygen plays an essential role for degradation of complex molecules such as azo dye, Acid Red B.

6.7 Sono-persulfate Oxidation Process

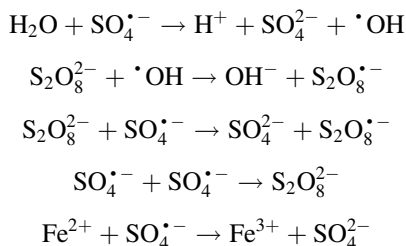
Persulfate oxidation process is another advanced oxidation process for degrading the recalcitrant pollutants effectively. In this process, metal persulfate generates sulfate radical anion ($\text{SO}_4^{\bullet-}$) which has oxidation potential of 2.6 eV (Zou et al. 2014). This radical can degrade a large variety of organic molecules. To generate $\text{SO}_4^{\bullet-}$ radical anions, the persulfate anion ($\text{S}_2\text{O}_8^{2-}$) can be activated using ultraviolet light (254 nm), heat, and metal ions such as Fe^{2+} (Monteagudo et al. 2015; Wang et al. 2015):



Recently, the new method of persulfate activation is sonolysis. When persulfate is added to the solution during the sonolysis process, the persulfate anions get activated at the interfacial region of the cavitation bubble due to the generation of hot spot during transient collapse. On the other hand, persulfate can also be activated through $\cdot\text{OH}$ and $\cdot\text{H}$ radicals which are produced from the cavitation. The generation of sulfate radical anion ($\text{SO}_4^{\bullet-}$) through sonolysis process is given below (Wang et al. 2015; Roshani and veLeitner 2011; Kusic et al. 2011; Chakma et al. 2017):



Apart from the above reaction, there are few reactions which can also occur during persulfate oxidation process as follows:



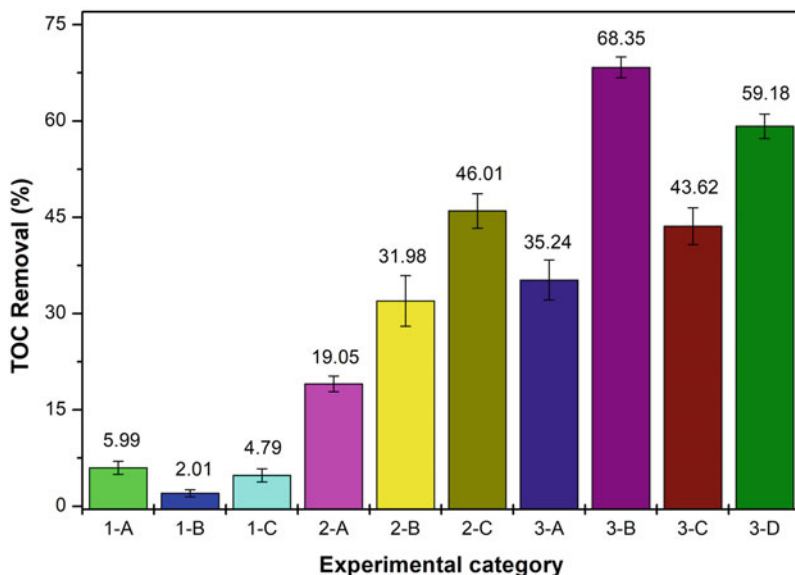


Fig. 6.5 Total organic carbon (TOC) removal during degradation of Acid Red B dye using different experimental conditions. Note: *US* ultrasound, *MS* mechanical stirring, 1A, *US* alone (or sonolysis); 1B, [*MS* + *UV*], 1C: [*MS* + *PS*]; 2A, [*US* + *PS*]; 2B, [*MS* + *PS* + Fe^{2+}]; 2C, [*MS* + *PS* + *UV*]; 3A, [*US* + *PS* + Fe^{2+}]; 3B, [*US* + *PS* + *UV*]; 3C, [*MS* + *PS* + Fe^{2+} + *UV*]; 3D, [*US* + *PS* + Fe^{2+} + *UV*]. *US* ultrasound, *MS* mechanical stirring, *PS* persulfate, *UV* ultraviolet. (Reprinted with permission of Elsevier from Chakma et al. 2017)

However, there is also a loss of oxidation potential due to either recombination of $\text{SO}_4^{\bullet-}$ or scavenging of $\text{SO}_4^{\bullet-}$ by ferrous ions (Fe^{2+}) as shown in the last two reactions.

Chakma et al. have investigated sono-hybrid persulfate oxidation mechanism for mineralization of textile dyes under different experimental conditions (Chakma et al. 2017). According to their studies, the binary activation method (*US* + *UV*) was found to be the effective hybrid advanced oxidation process for degradation of Acid Red B, an azo dye, as shown in Fig. 6.5 (Chakma et al. 2017). On the other hand, when the persulfate was activated using three activators (*US* + *UV* + Fe^{2+}), the TOC removal was reduced as compared to the process where the persulfate was activated using *US* + *UV*. This could be due to the scavenging effect of free radicals by the Fe^{2+} ions.

6.8 Conclusion

In this chapter, the different sono-hybrid techniques such as sono-photolysis, sono-Fenton, sono-photo-Fenton, sono-photo-ferrioxalate, sono-photocatalysis, and sono-persulfate have been discussed in detail for the treatment of wastewater. Fenton, Fenton-like, and hydrogen peroxide-based photolysis processes are dependent on the solution pH, while sonolysis, sonocatalysis, photocatalysis, and persulfate processes are independent of the solution pH. Moreover, the concentration of hydrogen peroxide, Fe^{2+} ions, and pH of the reaction must be optimized to achieve the maximum mineralization. With the addition of catalyst nanoparticle during sonolysis process, the degradation efficiency increases which could be attributed to the more nucleation sites that help in the formation of cavitation bubbles on the catalyst's surface. The hybrid advanced oxidation processes are not always beneficial for the wastewater treatment as they also have a few disadvantages. In the hybrid processes, if the generation of $\cdot\text{OH}$ radicals is comparatively large or the oxidant concentration is in excess in the reaction mixture, the mineralization efficiency drastically reduces as the radicals are either recombined or scavenged by the oxidants. Therefore, the selection of the right combination of advanced oxidation processes is very important for efficient wastewater treatment.

References

- Adeyuyi Y (2001) Sonochemistry: environmental science and engineering applications. *Ind Eng Chem Res* 40:4681–4715. <https://doi.org/10.1021/ie010096l>
- Adeyuyi Y (2005a) Sonochemistry in environmental remediation-1: combinative and hybrid sono-photochemical oxidation processes for the treatment of pollutants in water. *Environ Sci Technol* 39:3409–3420. <https://doi.org/10.1021/es049138y>
- Adeyuyi Y (2005b) Sonochemistry in environmental remediation-2: heterogeneous sono-photocatalytic oxidation processes for the treatment of pollutants in water. *Environ Sci Technol* 39:8557–8570. <https://doi.org/10.1021/es0509127>
- Andreozzi R, Caprio V, Insola A, Marotta R (1999) Advanced oxidation processes (AOP) for water purification and recovery. *Catal Today* 53:51–59. [https://doi.org/10.1016/S0920-5861\(99\)00102-9](https://doi.org/10.1016/S0920-5861(99)00102-9)
- Arslan I, Balcioglu IA, Bahnemann DW (2000) Advanced chemical oxidation of reactive dyes in simulated dyehouse effluents by ferrioxalate-Fenton/UV-A and TiO_2 /UV-A processes. *Dyes Pigments* 47:207–218. [https://doi.org/10.1016/S0143-7208\(00\)00082-6](https://doi.org/10.1016/S0143-7208(00)00082-6)
- Asiri AM, Al-Amoudi MS, Bazaid SA, Adam AA, Alamry KA, Anandan S (2014) Enhanced visible light photodegradation of water pollutants over N-, S-doped titanium dioxide and n-titanium dioxide in the presence of inorganic anions. *J Saudi Chem Soc* 18:155–163. <https://doi.org/10.1016/j.jscs.2011.06.008>
- Bagal MV, Gogate PR (2014a) Wastewater treatment using hybrid treatment schemes based on cavitation and Fenton chemistry: a review. *Ultrason Sonochem* 21:1–14. <https://doi.org/10.1016/j.ultsonch.2013.07.009>
- Bagal MV, Gogate PR (2014b) Degradation of diclofenac sodium using combined processes based on hydrodynamic cavitation and heterogeneous photocatalysis. *Ultrason Sonochem* 21:1035–1043. <https://doi.org/10.1016/j.ultsonch.2013.10.020>

- Bocos E, Fernández-Costas C, Pazos M, Sanromán MA (2015) Removal of PAHs and pesticides from polluted soils by enhanced electrokinetic-Fenton treatment. *Chemosphere* 125:168–174. <https://doi.org/10.1016/j.chemosphere.2014.12.049>
- Chakma S (2015) Mechanistic investigations in hybrid advanced oxidation processes for degradation of recalcitrant pollutants. Ph.D dissertation, IIT Guwahati
- Chakma S, Moholkar VS (2013a) Physical mechanism of sono-Fenton process. *AIChE J* 59:4303–4313. <https://doi.org/10.1002/aic.14150>
- Chakma S, Moholkar VS (2013b) Numerical simulation and investigation of system parameters of sonochemical process. *Chin J Eng* 1–14. <https://doi.org/10.1155/2013/362682>
- Chakma S, Moholkar VS (2014) Investigations in synergism of hybrid advanced oxidation processes with combinations of sonolysis + Fenton process + UV for degradation of bisphenol-A. *Ind Eng Chem Res* 53:6855–6865. <https://doi.org/10.1021/ie500474f>
- Chakma S, Moholkar VS (2015a) Intensification of wastewater treatment using sono-hybrid processes: an overview of mechanistic synergism. *Indian Chem Eng* 1–23. <https://doi.org/10.1080/00194506.2015.1026948>
- Chakma S, Moholkar VS (2015b) Investigation in mechanistic issues of sonocatalysis and sonophotocatalysis using pure and doped photocatalysts. *Ultrason Sonochem* 22:287–299. <https://doi.org/10.1016/j.ultsonch.2014.06.008>
- Chakma S, Moholkar VS (2015c) Sonochemical synthesis of mesoporous $ZrFe_2O_5$ and its application for degradation of recalcitrant pollutants. *RSC Adv* 5:53529–53542. <https://doi.org/10.1039/C5RA06148B>
- Chakma S, Moholkar VS (2016a) Investigations in sono-enzymatic degradation of ibuprofen. *Ultrason Sonochem* 29:485–494. <https://doi.org/10.1016/j.ultsonch.2015.11.002>
- Chakma S, Moholkar VS (2016b) Mechanistic analysis of sono-photolysis degradation of carmoisine. *J Ind Eng Chem* 33:276–287. <https://doi.org/10.1016/j.jiec.2015.10.015>
- Chakma S, Moholkar VS (2016c) Mechanistic analysis of hybrid sono-photo-ferrioxalate system for decolorization of azo dye. *J Taiwan Inst Chem Eng* 60:469–478. <https://doi.org/10.1016/j.jtice.2015.11.009>
- Chakma S, Bhasarkar JB, Moholkar VS (2013) Preparation, characterization and application of sonochemically doped Fe^{3+} into ZnO nanoparticles. *Int J Res Eng Tech* 2:177–183. <https://doi.org/10.15623/ijret.2013.0208030>
- Chakma S, Das L, Moholkar VS (2015) Dye decolorization with hybrid advanced oxidation processes comprising sonolysis/Fenton-like/photo-ferrioxalate systems: a mechanistic investigation. *Sep Purif Technol* 156:596–607. <https://doi.org/10.1016/j.seppur.2015.10.055>
- Chakma S, Praneeth S, Moholkar VS (2017) Mechanistic investigations in sono-hybrid (ultrasound/ Fe^{2+} /UVC) techniques of persulfate activation for degradation of azorubine. *Ultrason Sonochem* 38:652–663. <https://doi.org/10.1016/j.ultsonch.2016.08.015>
- Chang M-W, Chung C-C, Chern J-M, Chen T-S (2010) Dye decomposition kinetics by UV/ H_2O_2 : initial rate analysis by effective kinetic modelling methodology. *Chem Eng Sci* 65:135–140. <https://doi.org/10.1016/j.ces.2009.01.056>
- Chen W-S, Huang C-P (2015) Mineralization of aniline in aqueous solution by electro-activated persulfate oxidation enhanced with ultrasound. *Chem Eng J* 266:279–288. <https://doi.org/10.1016/j.cej.2014.12.100>
- Daud NK, Akpan UG, Hameed BH (2012) Decolorization of Sunzol Black DN conc. in aqueous solution by Fenton oxidation process: effect of system parameters and kinetic study. *Desalin Water Treat* 37:1–7. <https://doi.org/10.1080/19443994.2012.661246>
- Dinesh GK, Chakma S (2019a) Mechanistic investigation in degradation mechanism of 5-fluorouracil using graphitic carbon nitride. *Ultrason Sonochem* 50:311–321. <https://doi.org/10.1016/j.ultsonch.2018.09.032>
- Dinesh GK, Chakma S (2019b) Degradation kinetic study of cholesterol lowering statin drug using sono-hybrid techniques initiated by metal-free polymeric catalyst. *J Taiwan Inst Chem Eng* 100:95–104. <https://doi.org/10.1016/j.jtice.2019.04.009>

- Entezari MH, Petrier C (2005) A combination of ultrasound and oxidative enzyme: sono-enzyme degradation of phenols in a mixture. *Ultrason Sonochem* 12:283–288. <https://doi.org/10.1016/j.ultsonch.2004.01.040>
- Etacheri V, Roshan R, Kumar V (2012) Mg-doped ZnO nanoparticles for efficient sunlight-driven photocatalysis. *ACS Appl Mater Interfaces* 4:2717–2725. <https://doi.org/10.1021/am300359h>
- Giri AS, Golder AK (2014) Chloramphenicol degradation in Fenton and photo-Fenton: formation of Fe²⁺-chloramphenicol chelate and reaction pathways. *Ind Eng Chem Res* 53:16196–16203. <https://doi.org/10.1021/ie501508d>
- Hu B, Wu C, Zhang Z, Wang L (2014) Sonophotocatalytic degradation of trichloroacetic acid in aqueous solution. *Ceram Int* 40:7015–7021. <https://doi.org/10.1016/j.ceramint.2013.12.029>
- Huang R, Fang Z, Yan X, Cheng W (2012) Heterogeneous sono-Fenton catalytic degradation of bisphenol A by Fe₃O₄ magnetic nanoparticles under neutral condition. *Chem Eng J* 197:242–249. <https://doi.org/10.1016/j.cej.2012.05.035>
- Iglesias O, Fernández de Dios MA, Tavares T, Sanromán MA, Pazos M (2015) Heterogeneous electro-Fenton treatment: preparation, characterization and performance in groundwater pesticide removal. *J Ind Eng Chem* 27:276–282. <https://doi.org/10.1016/j.jiec.2014.12.044>
- Jeong J, Yoon J (2004) Dual roles of CO₂^{•-} for degrading synthetic organic chemicals in the photo/ferrioxalate system. *Water Res* 38:3531–3540. <https://doi.org/10.1016/j.watres.2004.05.016>
- Jeong J, Yoon J (2005) pH effect on [•]OH radical production in photo/ferrioxalate system. *Water Res* 39:2893–2900. <https://doi.org/10.1016/j.watres.2005.05.014>
- Katsumata H, Okada T, Kaneco S, Suzuki T, Ohta K (2010) Degradation of fenitrothion by ultrasound/ferrioxalate/UV system. *Ultrason Sonochem* 17:200–206. <https://doi.org/10.1016/j.ultsonch.2009.06.011>
- Katsumata H, Kobayashi T, Kaneco S, Suzuki T, Ohta K (2011) Degradation of linuron by ultrasound combined with photo-Fenton treatment. *Chem Eng J* 166:468–473. <https://doi.org/10.1016/j.cej.2010.10.073>
- Khuntia S, Majumder SK, Ghosh P (2014) Oxidation of As(III) to As(V) using ozone microbubbles. *Chemosphere* 97:120–124. <https://doi.org/10.1016/j.chemosphere.2013.10.046>
- Kim K, Cho E, Thokchom B, Cui M, Jang M, Khim J (2015) Synergistic sonoelectrochemical removal of substituted phenols: implications of ultrasonic parameters and physicochemical properties. *Ultrason Sonochem* 24:172–177. <https://doi.org/10.1016/j.ultsonch.2014.11.004>
- Kudo A, Miseki Y (2009) Heterogeneous photocatalyst materials for water splitting. *Chem Soc Rev* 253–278. <https://doi.org/10.1039/B800489G>
- Kusic H, Peternel I, Ukcic S, Koprivanac N, Bolanca T, Papic S, Bozic AL (2011) Modeling of iron activated persulfate oxidation treating reactive azo dye in water matrix. *Chem Eng J* 172:109–121. <https://doi.org/10.1016/j.cej.2011.05.076>
- Lin J-J, Zhao X-S, Liu D, Yu Z-G, Zhang Y, Xu H (2008) The decoloration and mineralization of azo dye C.I. Acid Red 14 by sonochemical process: rate improvement via Fenton's reactions. *J Hazard Mater* 157:541–546. <https://doi.org/10.1016/j.jhazmat.2008.01.050>
- Malani RS, Khanna S, Chakma S, Moholkar VS (2014) Mechanistic insight into sono-enzymatic degradation of organic pollutants with kinetic and thermodynamic analysis. *Ultrason Sonochem* 21:1400–1406. <https://doi.org/10.1016/j.ultsonch.2014.01.028>
- Mishra KP, Gogate PR (2011) Intensification of sonophotocatalytic degradation of p-nitrophenol at pilot scale capacity. *Ultrason Sonochem* 18:739–744. <https://doi.org/10.1016/j.ultsonch.2010.11.004>
- Monteagudo JM, Durán A, López-Almodóvar C (2008) Homogeneous ferrioxalate-assisted solar photo-Fenton degradation of Orange II aqueous solutions. *Appl Catal B Environ* 83:46–55. <https://doi.org/10.1016/j.apcatb.2008.02.002>
- Monteagudo JM, Durán A, Culebradas R, San Martín I, Carnicer A (2013) Optimization of pharmaceutical wastewater treatment by solar/ferrioxalate photo-catalysis. *J Environ Manag* 128:210–219. <https://doi.org/10.1016/j.jenvman.2013.05.013>

- Monteagudo JM, Durán A, González R, Expósito AJ (2015) In situ chemical oxidation of carbamazepine solutions using persulfate simultaneously activated by heat energy, UV light, Fe^{2+} ions, and H_2O_2 . *Appl Catal B Environ* 176–177:120–129. <https://doi.org/10.1016/j.apcatb.2015.03.055>
- Neppolian B, Jung H, Choi H, Lee JH, Kang J-W (2002) Sonolytic degradation of methyl tert-butyl ether: the role of coupled Fenton process and persulphate ion. *Water Res* 36:4699–4708. [https://doi.org/10.1016/S0043-1354\(02\)00211-7](https://doi.org/10.1016/S0043-1354(02)00211-7)
- Ng CM, Chen PC, Sivakumar M (2012) Hydrothermal crystallization of titania on silver nucleation sites for the synthesis of visible light nano-photocatalysts-enhanced photoactivity using Rhodamine 6G. *Appl Catal A Gen* 433–434:75–80. <https://doi.org/10.1016/j.apcata.2012.05.004>
- Ni M, Leung MKH, Leung DYC, Sumathy K (2007) A review and recent developments in photocatalytic water-splitting using TiO_2 for hydrogen production. *Renew Sustain Energ Rev* 11:401–425. <https://doi.org/10.1016/j.rser.2005.01.00>
- Nie M, Yang Y, Zhang Z, Yan C, Wang X, Li H, Dong W (2014) Degradation of chloramphenicol by thermally activated persulfate in aqueous solution. *Chem Eng J* 246:373–382. <https://doi.org/10.1016/j.cej.2014.02.047>
- Pang YL, Abdullah AZ (2013) Fe^{3+} doped TiO_2 nanotubes for combined adsorption–sonocatalytic degradation of real textile wastewater. *Appl Catal B Environ* 129:473–481. <https://doi.org/10.1016/j.apcatb.2012.09.051>
- Pareek VK, Adesina AA (2004) Light intensity distribution in a photocatalytic reactor using finite volume. *AICHE J* 50:1273–1288. <https://doi.org/10.1002/aic.10107>
- Peller J, Wiest O, Kamat PV (2003) Synergy of combining sonolysis and photocatalysis in the degradation and mineralization of chlorinated aromatic compounds. *Environ Sci Technol* 37:1926–1932. <https://doi.org/10.1021/es0261630>
- Poyatos JM, Munio MM, Almecija MC, Torres JC, Hontoria E, Osorio F (2010) Advanced oxidation processes for wastewater treatment: state of the art. *Water Air Soil Pollut* 205:187–204. <https://doi.org/10.1007/s11270-009-0065-1>
- Qin H, Li W, Xia Y, He T (2011) Photocatalytic activity of heterostructures based on ZnO and N–doped ZnO. *ACS Appl Mater Interfaces* 3:3152–3156. <https://doi.org/10.1021/am200655h>
- Reszczyńska J, Grzyb T, Sobczak JW, Lisowski W, Gazda M, Ohtani B, Zaleska A (2015) Visible light activity of rare earth metal doped (Er^{3+} , Yb^{3+} or $\text{Er}^{3+}/\text{Yb}^{3+}$) titania photocatalysts. *Appl Catal B Environ* 163:40–49. <https://doi.org/10.1016/j.apcatb.2014.07.010>
- Rodríguez EM, Fernández G, Álvarez PM, Hernández R, Beltrán FJ (2011) Photocatalytic degradation of organics in water in the presence of iron oxides: effects of pH and light source. *Appl Catal B Environ* 102:572–583. <https://doi.org/10.1016/j.apcatb.2010.12.041>
- Rodríguez EM, Fernández G, Alvarez PM, Beltrán FJ (2012) TiO_2 and Fe (III) photocatalytic ozonation processes of a mixture of emergent contaminants of water. *Water Res* 46:152–166. <https://doi.org/10.1016/j.watres.2011.10.038>
- Roshani B, velLeitner NK (2011) The influence of persulfate addition for the degradation of micropollutants by ionizing radiation. *Chem Eng J* 168:784–789. <https://doi.org/10.1016/j.cej.2010.12.023>
- Saien J, Delavari H, Solymani AR (2010) Sono-assisted photocatalytic degradation of styrene-acrylic acid copolymer in aqueous media with nanotitania particles and kinetic studies. *J Hazard Mater* 177:1031–1038. <https://doi.org/10.1016/j.jhazmat.2010.01.024>
- Sangave PC, Pandit AB (2006) Ultrasound and enzyme assisted biodegradation of distillery wastewater. *J Environ Manag* 80:36–46. <https://doi.org/10.1016/j.jenvman.2005.08.010>
- Segura Y, Molina R, Martínez F, Melero JA (2009) Integrated heterogeneous sono–photo Fenton processes for the degradation of phenolic aqueous solutions. *Ultrason Sonochem* 16:417–424. <https://doi.org/10.1016/j.ultsonch.2008.10.004>
- Shirsath SR, Pinjari DV, Gogate PR, Sonawane SH, Pandit AB (2013) Ultrasound assisted synthesis of doped TiO_2 nano–particles: characterization and comparison of effectiveness for photocatalytic oxidation of dyestuff effluent. *Ultrason Sonochem* 20:277–286. <https://doi.org/10.1016/j.ultsonch.2012.05.015>

- Sun Y, Yang H, Zhong X, Zhang L, Wang W (2011) Ultrasound-assisted enzymatic degradation of cholesterol in egg yolk. *Innov Food Sci Emerg Technol* 12:505–508. <https://doi.org/10.1016/j.ifset.2011.07.012>
- Suslick KS (1990) Sonochemistry. *Science* 247:1439–1445. <https://doi.org/10.1126/science.247.4949.1439>
- Vedrenne M, Vasquez-Medrano R, Prato-Garcia D, Frontana-Uribe BA, Hernandez-Esparza M, de Andrés JM (2012) A ferrous oxalate mediated photo-Fenton system: toward an increased biodegradability of indigo dyed wastewaters. *J Hazard Mater* 243:292–301. <https://doi.org/10.1016/j.jhazmat.2012.10.032>
- Wang S, Zhou N, Wu S, Zhang Q, Yang Z (2015) Modeling the oxidation kinetics of sono-activated persulfate's process on the degradation of humic acid. *Ultrason Sonochem* 23:128–134. <https://doi.org/10.1016/j.ultsonch.2014.10.026>
- Yao Z, Jia F, Tian S, Li CX, Jiang Z, Bai X (2010) Microporous Ni-doped TiO₂ film photocatalyst by plasma electrolytic oxidation. *ACS Appl Mater Int* 2:2617–2622. <https://doi.org/10.1021/am100450h>
- Zaleska A (2008) Doped-TiO₂: a review. *Recent Pat Eng* 2:157–164. <https://doi.org/10.2174/187221208786306289>
- Zhao D, Ding C, Wu C, Xu X (2012) Kinetics of ultrasound-enhanced oxidation of p-nitrophenol by fenton's reagent. *Energy Procedia* 16:146–152. <https://doi.org/10.1016/j.egypro.2012.01.025>
- Zhong X, Royer S, Zhang H, Huang Q, Xiang L, Valange S, Barrault J (2011) Mesoporous silica iron-doped as stable and efficient heterogeneous catalyst for the degradation of C.I. Acid Orange 7 using sono-photo-Fenton process. *Sep Purif Technol* 80:163–171. <https://doi.org/10.1016/j.seppur.2011.04.024>
- Zhou D, Wu F, Deng N, Xiang W (2004) Photooxidation of bisphenol A (BPA) in water in the presence of ferric and carboxylate salts. *Water Res* 38:4107–4116. <https://doi.org/10.1016/j.watres.2004.07.021>
- Zhou T, Wu X, Zhang Y, Li J, Lim T-T (2013) Synergistic catalytic degradation of antibiotic sulfamethazine in a heterogeneous sonophotolytic goethite/oxalate Fenton-like system. *Appl Catal B Environ* 136–137:294–301. <https://doi.org/10.1016/j.apcatb.2013.02.004>
- Zhu LP, Wang LL, Bing NC, Huang C, Wang LJ, Liao GH (2013) Porous fluorine-doped γ -Fe₂O₃ hollow spheres: synthesis, growth mechanism, and their application in photocatalysis. *ACS Appl Mater Int* 5:12478–12487. <https://doi.org/10.1021/am403720r>
- Ziylan A, Ince NH (2015) Catalytic ozonation of ibuprofen with ultrasound and Fe-based catalysts. *Catal Today* 240:2–8. <https://doi.org/10.1016/j.cattod.2014.03.002>
- Zou X, Zhou T, Mao J, Wu X (2014) Synergistic degradation of antibiotic sulfadiazine in a heterogeneous ultrasound-enhanced Fe⁰/persulfate Fenton-like system. *Chem Eng J* 257:36–44. <https://doi.org/10.1016/j.cej.2014.07.048>

Chapter 7

Photocatalytic Nanomaterials for Bacterial Disinfection



Teklit Gebregiorgis Ambaye, Mentore Vaccari, and Eric D. van Hullebusch

Contents

| | | |
|-------|--|-----|
| 7.1 | Introduction | 216 |
| 7.2 | Nanostructured Materials for Water Disinfection | 219 |
| 7.2.1 | Zero-Dimensional Nanostructures | 219 |
| 7.2.2 | One-Dimensional Nanostructures | 220 |
| 7.2.3 | Two-Dimensional Nanostructured Materials | 223 |
| 7.3 | Natural Minerals as Photocatalysts for Water Disinfection | 226 |
| 7.4 | Mechanisms of the Photocatalytic Disinfection of Bacteria | 227 |
| 7.5 | The Effect of the Water Matrix on the Disinfection Process | 228 |
| 7.5.1 | Factors Affecting Water Mix Property on the Water Disinfection Process | 228 |
| 7.6 | Supported Catalysts for Water/Wastewater Disinfection | 229 |
| 7.6.1 | Electrocoagulation | 230 |
| 7.6.2 | Direct Oxidation | 232 |
| 7.6.3 | Indirect Electro-oxidation | 232 |
| 7.7 | Future Perspectives | 233 |
| 7.8 | Conclusions | 234 |
| | References | 235 |

T. G. Ambaye (✉)

Department of Civil, Environmental, Architectural Engineering and Mathematics, University of Brescia, Brescia, Italy

Department of Chemistry, Mekelle University, Mekelle, Ethiopia

e-mail: t.ambaye@unibs.it

M. Vaccari

Department of Civil, Environmental, Architectural Engineering and Mathematics, University of Brescia, Brescia, Italy

e-mail: mentore.vaccari@unibs.it

E. D. van Hullebusch

Université de Paris, Institut de Physique du Globe de Paris, CNRS, Paris, France

e-mail: vanhullebusch@ipgp.fr

© The Editor(s) (if applicable) and The Author(s), under exclusive license to Springer Nature Switzerland AG 2021

215

Inamuddin et al. (eds.), *Water Pollution and Remediation: Photocatalysis*, Environmental Chemistry for a Sustainable World 57, https://doi.org/10.1007/978-3-030-54723-3_7

Abstract With rapidly growing urbanization and industrialization in developing countries around the world, a large volume of wastewater is produced by industries that contain waterborne diseases, and photocatalysis is confirmed as a promising technology for water disinfection. Nevertheless, specific photocatalysts are required with the ability to produce high amounts of diffusible reactive species with a long lifetime, such as H_2O_2 . The latter has been considered as the main obstacle that restricts its efficiency for water disinfection process. Indeed, nanostructured materials having a definite morphology have a large surface area and size enhances higher photocatalytic oxidation separation. This makes it possible to accomplish better efficiency in the water disinfection process that has now attracted more attention from policymakers and scientists to develop novel photocatalysts. This review discusses recent applications of low-dimensional nanostructured photocatalysts and their preparation, characterization, and efficiency for the removal of pathogenic microorganisms. It also highlights the reacting mechanism of the photogenerated reactive oxygen species and supported catalysis for the disinfection of pathogenic microorganisms, and the effect of the chemical characteristics of the water matrix barrier is reviewed comprehensively. Finally, the recent development of low-dimensional nanostructured photocatalysts for water disinfection and its challenges and perspectives in the future are discussed. This review suggests that the in-depth study of the electrochemical cell using boron-doped electrodes such as its characterization is extremely promising for the disinfection of bacterial cells with the utilization of natural minerals and genetic technologies.

Keywords Supported photocatalysis · Solar light · Nanomaterials · Photocatalysis · Disinfection · Advanced oxidation processes

7.1 Introduction

Currently, it is worldwide recognized that water is a crucial natural resource and accessibility to safe drinking water is getting more attention, particularly in rural areas of developing countries (Montgomery and Elimelech 2007). However, with rapidly growing urbanization and industrialization in developing countries, the pressure on water resources is drastically increasing. For instance, according to the World Health Organization (WHO 2012), about 884 million people in the developing countries have inadequate access to clean water and depend on contaminated freshwater which leads to different waterborne transmitted diseases like hepatitis and cholera. This contributes to about 80% of diseases in developing countries (Montgomery and Elimelech 2007; Supply and Programme 2014). Moreover, these pathogenic microbes can also lead to various mortal diseases like typhoid fever, pneumonia, and tuberculosis. Besides, according to the WHO (2012), about 1.5 million deaths were reported due to diarrheal diseases triggered by these pathogenic

microbes (Tsydenova et al. 2015). These statistics indicated that water pollution by numerous pollutants becomes an alarming issue worldwide. Therefore, developing sustainable or low-cost alternative pathways for disinfecting pathogenic microorganisms has attracted more attention from policymakers and scientists (Wang et al. 2017c). Different conventional water disinfection methods like ozonation, chlorination, and ultraviolet disinfection were believed to be efficient ways for water disinfection. Yet, these methods have not been widely applied to water disinfection due to cost and disposal issues (Foster et al. 2011).

Moreover, these disinfection methods have their own merits and demerits to treat wastewater. Among the chemical methods, advanced oxidation processes are of sufficient interest in disinfection process for the effective oxidation of a wide variety of organic and inorganic pollutants due to the generation of dominant reactive oxygen species, such as the hydroxyl radical, H_2O_2 , and superoxide radical (Nieuwenhuijsen et al. 2000). Among these methods, top priority goes to semiconductor-assisted photocatalytic disinfection process, which can use sunlight (Huang et al. 2005). The application of photocatalysis for water disinfection of *Lactobacillus acidophilus*, *Saccharomyces cerevisiae*, and *Escherichia coli* was applied for the first time in 1985 by Matsunaga et al. (1985a). After that, more researches have been carried out in the development of the photocatalytic disinfection process. According to Christensen et al. (2003) and Gong et al. (2011), three pathogenic microorganisms, namely, *Pseudomonas aeruginosa*, *Candida albicans*, and *Enterococcus faecium*, using solar/ultraviolet radiation were effectively inhibited by using titanium as a photocatalyst. Similar results were reported for the disinfection of *Staphylococcus aureus* (Makoday et al. 2015), *Streptococcus mutants* (Kühn et al. 2003), *Salmonella choleraesuis*, *Vibrio parahaemolyticus*, and *Listeria monocytogenes* (Melián et al. 2000). Figure 7.1 shows the photocatalytic bacterial disinfection mechanism involving reactive oxygen species (Maness et al. 1999; Rahmawati et al. 2010; Spuhler et al. 2010; Dunlop et al. 2011). Recently, Liu et al. (2017) investigated the effective photocatalytic TiO_2 disinfection of *Cryptosporidium* and *Giardia* that are resistant to chlorination.

Recently some researches are carried out using TiO_2 as photocatalyst for the disinfection of microbes because of having a large bandgap structure, surface defects, electronic structure, and microstructure by different methods like developing TiO_2 photocatalysts with metal oxides, sulfides, nitrides, and oxynitrides (Castaneda et al. 2019; Munawar et al. 2020; Cantarella et al. 2018; Zhou et al. 2018; Huang et al. 2017). Other researchers went to the preparation of non- TiO_2 photocatalysts showing fast bacterial disinfection or organic pollutant degradation from wastewater effluents (Gong et al. 2011; Zhang et al. 2014, 2018; Liu et al. 2018; Yang et al. 2016a, b; Zhou et al. 2014). More recently, research has been focused on dye sensitization, noble metal deposition, and ion doping (Asahi et al. 2001; Chandran et al. 2014; Chen et al. 2016; Mikolajczyk et al. 2016; Umezawa and Janotti 2016; Vaiano et al. 2016; Wang et al. 2017c; Yu et al. 2005; Zhang et al. 2016a; Zhao et al. 2016; Li et al. 2017). However, these photocatalytic systems differed in their photogenerated reactive species leading to the disinfection process. A recent study by Wang et al. (2011b) reported that H_2O_2 -reactive species are more

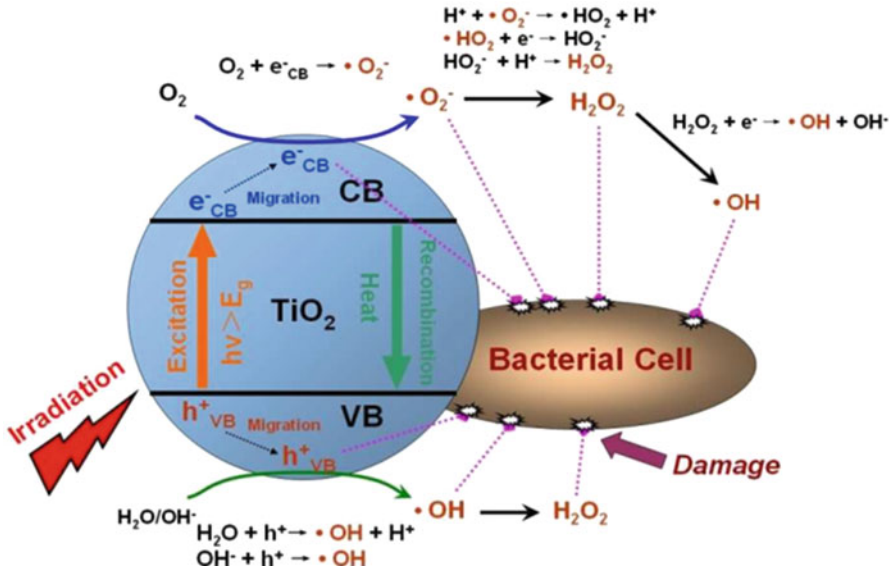


Fig. 7.1 Photocatalytic disinfection with TiO_2 irradiated by ultraviolet light. (Modified from Wang et al. (2013b))

effective in the disinfection process than hydroxyl radical and superoxide anion radicals due to the high span time to damage the outer membrane and cell wall of the pathogenic microbes because the existence of the pathogenic microbes depends on these organelles. Furthermore, the relationship between the gap energy with the configuration (i.e., heterojunction and intra-gap states) as well as the microstructure is a crucial factor in increasing the performance of the photocatalytic materials. However, nanostructured photocatalytic materials such as zero-dimensional, one-dimensional, and two-dimensional coupled with ultrafine particle materials have been reported to show high efficiency to select the preferred reactive species than the bulk materials. This is depending upon the design and the morphology of the nanostructured materials (Gao et al. 2007; Kong et al. 2010; Lu et al. 2008; Naveenraj et al. 2015; Zhang et al. 2006, 2018). Consequently, understanding the application of nanostructured photocatalytic materials in water disinfection and water purification gets increasing attention in the scientific community, even if there is a lack of published results dealing with the use of nanostructured as photocatalytic material.

The objective of this book chapter is to review the progress of photocatalytic nanomaterials for water disinfection under both ultraviolet and visible light irradiations. The assessment of the current status of the preparation, characterization, design, and application of highly efficient photocatalytic nanomaterials such as zero-dimensional, one-dimensional, and two-dimensional as well as supported catalysts for water disinfection and the challenges and perspectives for further

improvements are discussed. Also, the importance of the use of direct sunlight irradiation for the photocatalytic water disinfection and its scale-up is discussed.

7.2 Nanostructured Materials for Water Disinfection

The nanostructured materials coupled with fine particles with a definite morphology lead to large surface area and size, enhance the spectral absorption toward visible wavelengths, and improve the photocatalytic oxidation of organic pollutants and pathogens by reducing the photogenerated charge recombination. These nanostructured materials can be classified into three types: zero-dimensional, one-dimensional, and two-dimensional materials. However, their efficiency for the disinfection process depends on the preparation protocols allowing different light absorption edges (ultraviolet and visible light) (Wang et al. 2017c).

7.2.1 Zero-Dimensional Nanostructures

Zero-dimensional nanostructure materials are characterized by a large surface area populated by numerous active sites. Surface-dependent photocatalysts are getting more attention from researchers working on water disinfection and remediation (Lee and Jang 2014; Li et al. 2014).

According to Li et al. (2008a, b), four pathogenic microorganisms, namely, MS2 bacteriophage, poliovirus 1, herpes simplex virus, and hepatitis B virus, were adequately disinfected by using nano-sized titanium oxide as a photocatalyst under solar/UV radiation. Wei et al. (1994) have reported that the disinfection process depends on the used light and the size of the TiO₂ particles. ZnO was found to behave similarly to TiO₂ for the water disinfection process (Alikhani et al. 2012). Barnes et al. (2013) investigated both TiO₂ and ZnO efficiencies in the disinfection process of *E. coli* and *B. subtilis*. This study showed that TiO₂ nanoparticles generated more reactive oxygen species than ZnO nanoparticles. However, ZnO nanoparticles were more toxic to pathogenic microbes like *E. coli* and *B. subtilis* even in the dark.

Li et al. (2014) explain that having small particle size does not mean to have higher efficiency because the reduction in the number of hole layers makes the generated reactive species to closely conjugate to each other and leads to decrease the efficiency of the disinfection process, and this explains why the type of migration is related to surface properties and morphology of the nanoparticle material (Lee and Jang 2014; Li et al. 2014). Thus, more research shall be carried out in the future in modifying, designing, and constructing between the surface properties and morphology of the nanocomposite material to ease the separation of reactive species as well as increase the disinfection process (Lee and Jang 2014).

Muñoz-Batista et al. (2016) studied the disinfection of *E. coli* 1337-H irradiated under ultraviolet and visible light and synthesized CeO₂-TiO₂ composite photocatalytic material. These authors reported high disinfection capacity for the composite material mixed with 0.025CeTi and 0.05CeTi concentrations while increasing the concentration of CeO₂ to 25% leads to a decrease in the disinfection compared to pure titanium oxide. This shows that the disinfection process of titanium oxide depends upon the light irradiation as well as the ratio of the composite material. However, titanium oxide only shows a high disinfection process, whereas CeO₂ shows no disinfection process. Similar results are also reported in several recent studies (Aslan et al. 2014; Hassan et al. 2016; Jeong and Guyot-Sionnest 2016; Li et al. 2016b; Roushani et al. 2015; Shi et al. 2015; Xie et al. 2015; Zhou et al. 2011, 2012).

In general, composite nanoparticles show a higher disinfection process than bulk photocatalytic material (Wang et al. 2017a, b, c); however, optimizing the ratio component of the composite material is necessary to increase the activity of the disinfection process.

7.2.2 One-Dimensional Nanostructures

After discovering carbon nanotubes in 1935, significant research efforts have been dedicated to studying the one-dimensional nanostructures. These structures can be obtained by combining different nanostructures such as nanoribbons, nanobelts, nanotubes, nanowires, and nanorods. These structures present unique physical properties and promising disinfection applications than bulk material as it was reported (Iijima 1991; Liang et al. 2010; Liu et al. 2012a).

The main advantages of one-dimensional nanostructures are (i) their ability to improve the process charge separation, (ii) their high surface area and pore volume, and (iii) their high absorbance compared to bulk materials used for disinfection (Shankar et al. 2009; Tang et al. 2011; Weng et al. 2014). Among the reported one-dimensional nanostructures, great attention was given toward nanorods and nanowires.

Nanorods

One-dimensional material can be prepared with TiO₂ and ZnO using various approaches such as flame spray pyrolysis, electrodeposition, and hydrothermal process (Hassan et al. 2012; Karunakaran et al. 2012; Sapkota et al. 2011). Bai et al. (2013) reported on the preparation of 1 μm nanorods prepared by the calcination of TiO₂ in different superficial, no hydrothermal approaches. These authors showed that high surface area and pore volume nanorods prepared at 400 °C (TiO₂-400) could disinfect bacteria and degrade organic pollutants. Moreover, by increasing the preparation temperature from 400 to 900 °C, these TiO₂ nanorods led to the failure of its structure. However, they showed a high degradation capacity for

organic pollutants as well as a high disinfection activity. This activity was attributed to the higher light adsorption (Bai et al. 2013; Hamadian et al. 2010).

Sanchez et al. (2014) also reported that nanorods could be prepared from the calcination of ZnO at 350 °C using spray pyrolysis solution in a water–ethanol mixture grown on substrate fluorine-doped tin oxide. These nanorods showed different disinfection mechanisms toward *E. coli* cells. The structure of the nanorods of ZnO changed by modifying the ratio of the ethanol–water mixture, which controls the evaporation of the solvent due to the fall in imposing the substrate under ultraviolet and visible light irradiation. The same results were also reported by other researchers (Alarcón et al. 2011; Sanchez et al. 2014, 2015). The ZnO and TiO₂ nanorods showed similar bacterial disinfection under visible light (Basnet et al. 2013). Recently, Bi-based nanorods were prepared using monoclinic bismuth tetraoxide (m-Bi₂O₄) by hydrothermal process. These nanorods showed high bacterial disinfection as well as fast disintegration of organic pollutants under visible light irradiation than CdS and Bi₂O₃. This finding encouraged many studies on Bi₂O₄ nanorods under visible light irradiation. Bi₂O₄ nanorods were reported to be highly active and non-toxic and show stable photocatalytic performance (Wang et al. 2015a).

Nanowires

Nanowires are another one-dimensional nanomaterial type with a diameter of 20–100 nm which displays high-performance photocatalytic activity for water disinfection. For instance, Zhang et al. (2008) reported that organic contaminants, such as foulants, were effectively removed under ultraviolet radiation. Titanium nanowires prepared by hydrothermal synthesis–filtration method showed high anti-fouling property (Zhang et al. 2008). The use of these photoactive materials and their performance opens the opportunity for their application in the water disinfection process. Liu et al. (2016) fabricated iron oxide nanowires (Bac-FeO_xNWs) produced by bacteria (*Mariprofundus ferrooxydans*) as photocatalytic material which displays photocatalytic disinfection properties (Wang et al. 2016). These nanowires displayed excellent reusability with no significant loss of activity even after six cycles. These nanowires are naturally produced, inexpensive, highly active, stable, and magnetic and have the potential to be used for broad applications including water disinfection.

Recently, efforts have been made on combining TiO₂ nanowire/nanofiber membrane with other materials such as Ag to form Ag/TiO₂ nanofiber membrane as photocatalytic material for bacterial disinfection (Chong et al. 2010; Janpetch et al. 2015; Jin et al. 2007; Liu et al. 2012b). This combination has been shown to render active surface sites exposed to bacteria and organic pollutants as well as the loading of Ag nanoparticles facilitated the photogenerated e⁻/h⁺ separation concomitant with the inherent antibacterial properties of Ag nanoparticles, making the combination as an excellent photocatalyst material for water disinfection. Similar to nanowire photocatalyst, nanobelts have been reported to exhibit bacterial inactivation activity. However, the high exposed surface area in the nanobelt crystals makes these

nanostructures highly efficient for photocatalytic water disinfection. For instance, Wu et al. (2010) reported that TiO₂ nanobelts prepared by the hydrothermal method and having {101} surface area show high photocatalytic oxidation activity for bacteria cells due to the lower e⁻/h⁺ recombination compared to TiO₂ nanospheres. Moreover, combining TiO₂ nanobelts with noble metal cocatalysts such as Au/TiO₂ nanobelts and Ag₂O/TiO₂ nanobelts further enhanced the bacterial disinfection process in water (Guo et al. 2015; Jin et al. 2013). In addition to this nanobelt, materials based on β-AgVO₃ prepared by superficial hydrothermal method showed a high photocatalytic activity under low-energy fluorescent light irradiation for the disinfection of *E. coli* (Ren et al. 2010).

Nanotubes

In addition to the aforementioned one-dimensional nanostructure, nanotubes exhibit hollow structure. This configuration enhances the electron transfer and reduces the photogenerated charge recombination, making them an excellent choice for water disinfection than bulk materials.

Wang et al. (2014) compared the photocatalytic activity of nanotube-based graphitic C₃N₄ with pure graphitic C₃N₄ and P25-TiO₂ under visible light disinfection. This study showed that the nanotube-based graphitic C₃N₄ material has better disinfection performance than pure graphitic C₃N₄ and P25-TiO₂. This observed activity was attributed to the high surface area and the active site of nanotube-based graphitic C₃N₄ photocatalytic material. Yang et al. (2016a, b) also reported that TiO₂-based nanotubes showed high photocatalytic activity for bacterial cell disinfection such as *Actinobacillus actinomycetemcomitans* and *Staphylococcus aureus* under ultraviolet irradiation. Moreover, to increase the efficiency of nanotubes for bacterial disinfection, Nie et al. (2014) prepared TiO₂ nanotubular photo-anode by applying external photoelectrocatalysis for the disinfection of *E. coli* K-12 and its mutant *E. coli* BW25113. The result shows that the photoelectrocatalysis TiO₂ nanotubular material has high efficiency in removing the bacterial cells and the mutant reacted faster than with pure bulk photocatalytic TiO₂ nanotube. The photocatalytic activity of nanotubular TiO₂ can be enhanced when applying an external force leading to reduced recombination of the photogenerated charges. However, both the photoelectrocatalysis and photocatalytic treatments showed moderate activities toward the mutant of *E. coli* BW25113 compared to the parental bacteria *E. coli* K-12 cell. This difference was attributed to the genotype differences (Wang et al. 2014).

In conclusion, one-dimensional nanostructure with different combinations of nanobelts, nanorods, and nanowires has high performance in water disinfection due to the superior-oriented charge transfer properties, large specific surface area, and more active sites that attracted more attention in fabricated cost-efficient photocatalysts material for water disinfection. However, there is a difference in the characteristics and performance efficiency of photocatalytic material of nanobelts, nanorods, and nanowires in their status of exposed facets, surface atomic

arrangement, and oxygen vacancies, so more research must be carried out in the future in optimizing the main parameters to produce one-dimensional nanostructure with different combinations of nanobelts, nanorods, and nanowires to increase photocatalytic activity for water disinfection process.

7.2.3 Two-Dimensional Nanostructured Materials

Currently, two-dimensional photocatalytic materials in the water disinfection process get more attention because they have a specific surface area and specific thickness. At the same time, it balances the drawback of the photocatalytic process compared with zero-dimensional, one-dimensional, and bulk photocatalytic material due to having these properties. In the last decade, more research are carried out to use two-dimensional novel nanomaterial such as graphene, metal oxides such as TiO_2 and WO_3 nanosheets, graphitic carbon nitride, transition metal dichalcogenides, metal oxyhalides (e.g., BiOB and BiOI), and metallates (e.g., Bi_2WO_4 and Bi_2MoO_6) as novel photocatalyst material in water disinfection process has been published (Carlson et al. 2016; Liu et al. 2014; Miao et al. 2016; Pan et al. 2008; Sajjan et al. 2016; Shi et al. 2014; Wang et al. 2012; Yang et al. 2016b; Zhang et al. 2016b, 2016c), though most of the research on water disinfection investigated metal oxyhalides, graphite carbon nitride, and graphene nanosheets of two-dimensional nanomaterials as photocatalytic material. For this reason some research shows that using metal oxyhalides such as BiOBr nanosheets as photocatalyst showed promising result in removing organic contaminants under visible light (Ye et al. 2014; Zhang et al. 2014).

According to Wu et al. (2015), in their research to disinfect microorganism such as *E. coli* using BiOBr nanosheets as a photocatalytic material produced by hydrothermal condition having a specific surface of {001} and {010} nanosheets as a shows that the nanosheets with surface {001} can remove the bacteria cells to about 10^7 CFU mL^{-1} under visible light within 2 h. In contrast, the nanosheets with {010} surface take about 6 h for the same removal efficiency. This can be due to the arrangement of nanosheets with surface {001} perpendicular to the direction of the electric field. Moreover, they claimed that the removal of bacterial cells was depended upon the surface of nanosheets and their atomic arrangement.

This opens an avenue for the production of self-doped and exogenously doped nanosheets of BiOBr with a high percentage of {001} facets as photocatalytic material for the disinfection process under visible light (Wu et al. 2016a, b, 2017). For example, Wu et al. (2016a, b) fabricated nanosheets with {001} facets for removal of bacteria using self-doped B-BiOBr before treatment shows that total removal of the bacteria happened within 30 min under visible light. This approach involves the enhancement of light absorption, charge separation, and total removal of bacteria with the use of B-BiOBr as photocatalyst material, followed by hydrothermal treatment allowing the oxidation of BiOBr to Bi^{5+} for complete removal of bacteria in disinfection process in UV irradiation (An et al. 1996). However, posttreated B-BiOBr with NaOH under Xenon lamp has led to the oxidation of the

photocatalyst material to Bi_2O_4 showing complete removal of the bacterial cells in 15 min under visible light irradiation. The undecorated BiOBr nanosheets showed removal of 10^4 CFU mL^{-1} bacterial cells within 20 min under the same light due to doped Bi^{5+} acting as electron traps to narrow the bandgap and to enhance the separation of the photogenerated charges leading to increase the efficiency of the water disinfection process (Wu et al. 2016a). The same result was also reported by Wang et al. (2011b). In general, the use of BiO_x nanosheets as photocatalyst material shows a new alternative and methods in the synthesis of two-dimensional heterojunctions for water disinfection.

Another two-dimensional material that shows multiple advantages in the water disinfection process with lamellar structure is the graphitic carbon nitride as a visible light photocatalyst (Ong et al. 2016). Recent publications have provided evidence of graphitic carbon nitride as a photocatalyst for water disinfection due to the various morphologies, high stability, broad light response spectrum up to 460 nm, and simple fabrication methods. This gives carbon nitride high feasibility in the water disinfection process (Deng et al. 2017; Gu et al. 2017; Jiang et al. 2018; Lam et al. 2016; Li et al. 2016c, 2017; Masih et al. 2017; Ong et al. 2016; Song et al. 2016; Wang et al. 2017a; Wei et al. 2017). However, due to the low surface area and high recombination rate, it may affect the disinfection process of the pure carbon nitride (Lam et al. 2016). In this regard, metal or element doping, specific morphology design, and integration with other components can play a significant role in overcoming the limitations of pure carbon nitride for the water disinfection process. For instance, according to Huang et al. (2014) in their research to compare porous structured graphitic carbon nitride and modified graphitic carbon nitride by adding elemental silica template using polymerization method with pure graphitic carbon nitride shows that the porous structured graphitic carbon nitride has higher *E. coli* disinfection efficiency than the pure material. This was attributed to the generation of more active sites in the porous material. Moreover, they showed that during the designing and fabrication of the porous material, it is difficult to remove the templated silica after treatment. This opens the possibility to synthesize porous graphitic carbon nitride nanosheets without a template using thermal etching and hydrothermal treatment. Their results showed that the synthesis of porous graphitic carbon nitride nanosheets has removed bacterial cells under visible light within 4 h, whereas the pure graphitic carbon nitride has removed only 71% of the bacterial cells within the same time frame. This is due to the large surface area, more active sites, efficient charge separation, and higher reactive species production leading to enhanced disinfection process of the porous graphitic carbon nitride nanosheets compared to pure graphitic carbon nitride (Wang et al. 2017a).

Significant research efforts have been devoted to improving the water disinfection process by pure graphitic carbon nitride-based materials (g- C_3N_4). Combining graphitic carbon nitride with different photocatalytic materials such as Bi_2MoO_6 /graphitic carbon nitride, Ag/graphitic carbon nitride, graphene/graphitic carbon nitride, and TiO_2 /graphitic carbon nitride using simple adsorption–deposition method led to construct composite materials that have more adsorption sites and

larger lateral size (Li et al. 2015; Liu et al. 2016; Ma et al. 2016; Munoz-Batista et al. 2016).

Silver ion (Ag^+) has high charge transfer in the visible light as well as it is toxic to bacteria cells. For this reason, the combination of Ag with g- C_3N_4 has led to heterojunction of the photocatalytic materials showing higher efficiency for water disinfection (Bosetti et al. 2002; Chou et al. 2005; Deng et al. 2017; Li et al. 2017; Ma et al. 2016). However, large-scale applications must consider the reusability of Ag-based photocatalysts for water disinfection because the release of silver may affect human health. At the same time, this can lead to photoconversion which further affects the Ag disinfection property (Deng et al. 2017; Li et al. 2017).

Another interesting method for exploitation g- C_3N_4 is to combine it with other materials like graphene oxide/ TiO_2 /Ag and graphene. The use of graphene and its derivatives as photocatalytic materials enhances the charge separation and responds to both ultraviolet and visible light irradiations (Sun et al. 2017). Liu et al. (2016) reported that the hybrid graphene oxide/g- C_3N_4 photocatalytic material showed higher efficiency than pure g- C_3N_4 in the disinfection of *E. coli* cells. Wang et al. (2013a) also reported similar trends on this approach, and they confirmed the use of hybrid graphene oxide/g- C_3N_4 as photocatalytic material in large-scale application leads to high photostability, low leakage of elements, and having consistent performance in the disinfection over several runs.

Even if titanium dioxide as photocatalytic material shows high performance in the disinfection process under ultraviolet region (Fagan et al. 2016; Matsunaga et al. 1985b; Reddy et al. 2017; Wei et al. 1994), the combination of TiO_2 with g- C_3N_4 could lead to high-performance photocatalytic material for water disinfection process (Gu et al. 2017; Ong 2017; Song et al. 2016; Wei et al. 2017). Recent publications have provided evidence of hybrid TiO_2 -g- C_3N_4 composite photocatalytic material for microorganism removal. Li et al. (2015) proposed in their research to remove *E. coli* from wastewater using hybrid TiO_2 -graphitic carbon nitride photocatalytic material produced by hydrothermal-calcination approach. Their results show that the hybrid composite photocatalytic material removed *E. coli* within 180 min under visible light. This activity is fast compared with pure TiO_2 and pure graphitic carbon nitride. They attributed this activity to the high charge transfer efficiency by the hybrid TiO_2 -graphitic carbon nitride composite. Pure graphitic carbon nitride showed less photocatalytic disinfection kinetics with about 6 log reduction of bacterial cells within 300 min under visible light irradiation.

However, the heterostructure photocatalyst material has low oxidation potential in the decomposition of a pharmaceutical compound such as acyclovir (Li et al. 2016a). This opens a new research area for the development Z-scheme heterojunctions of photocatalytic materials using heterojunction-based graphitic carbon nitride material that has high oxidation and reduction ability towards graphitic carbon nitride (Jiang et al. 2018; Zhou et al. 2014).

According to Xia et al. (2017), hybrid photocatalytic material combining g- C_3N_4 with Bi_2O_4 using the Z-scheme photocatalytic mechanism for *E. coli* disinfection was prepared. Z-scheme involves a two-step photoexcitation (ref). The results show that the Z-photocatalytic scheme material (monoclinic m- Bi_2O_4 /g- C_3N_4) shows

higher bacteria removal efficiency compared to pure g-C₃N₄ and m-Bi₂O₄. This is due to the direct generation of H₂O₂, and the reduction of O₂ by the m-Bi₂O₄-graphitic carbon nitride (Xia et al. 2017). Similar results were also reported by Wang et al. (2017b).

In general, combining graphitic carbon nitride with other materials such as Ag and Bi showed high charge diffusion pathway, enhanced separation of photogenerated charges, and high reactive oxygen species generation. Therefore, it would be useful to find the proper posttreatment and method for the recovery of the photocatalytic material. This will be a critical factor in the future to apply these materials on a large scale under visible light for water/wastewater disinfection.

7.3 Natural Minerals as Photocatalysts for Water Disinfection

Currently, nanostructured materials are a promising technology for water disinfection. Therefore, more efforts are taking place in design and material synthesis for large-scale applications. However, it is required to build different procedures for the fabrication and manufacturing of these materials taking into consideration energy consumption. This is aligned with the so-called water–energy nexus.

Minerals which are found naturally in the form of solid substance that is molded through biogeochemical processes present distinct properties and chemical composition. These minerals represent a promising method for the disinfection process that can be applied on a large scale. Peng et al. (2017) studied the feasibility of using natural minerals such as natural magenetic sphalerite in large scale for disinfection process in their research, and they developed batch cylindrical reactor of 5 L with a plastic stirrer and a magnetic field generator to hold the natural minerals. They showed that it thoroughly disinfected *E. coli*, *S. aureus*, *M. barkeri*, and *B. subtilis* within three rotations in 120 min under sunlight irradiation. In addition to this, the authors claimed that after water disinfection, they could recycle natural minerals as cost-effective photocatalyst. However, the disinfection ability decreased over time due to the decomposition of the bacterial cells and the accumulations of the biomass on the mineral active sites.

Recent publications have provided evidence for natural minerals such as natural magnetic sphalerite (NMS) as outstanding composites for water disinfection and organic compound degradation in practical application (Chen et al. 2011, 2013; Li et al. 2008b, 2009; Xia et al. 2013). However, when compared with fabricated nanostructured materials, NMS has a lower disinfection activity. This could be due to its large size and reduced specific surface areas. To increase their efficiency for bacterial disinfection and to enhance their stability, some researchers proposed the modification of natural minerals such as pyrrhotite using thermal calcination (Xia et al. 2015a). This opens the opportunity for the complete disinfection of bacteria cell at a low cost with the potential application at large scale.

7.4 Mechanisms of the Photocatalytic Disinfection of Bacteria

In general, the photocatalytic bacterial disinfection involves (1) the generation of electron/hole pairs by the excitation of the semiconductor, (2) the reaction of the pathogenic microbes with the photogenerated reactive oxygen species generated at the surface of the photocatalyst, and (3) the penetration of toxic ions inside the bacterial cells leading to the disturbance of their enzymatic and replication machinery. At this level, it is crucial to understand the mechanisms involved in the disinfection process when operating any nanostructured photocatalytic material (Wang et al. 2011b, 2015b). Wang et al. (2015a, b) developed a mechanism for the generation of reactive oxygen species and their contributions for the disinfection of bacterial cells and the degradation of organic pollutants by integrating semipermeable membrane (preventing the direct contact between bacterial cells and semiconductor photocatalytic material) using appropriate scavengers under visible light. They showed that high degradation of the organic pollutants and disinfection of the bacterial cells were due to the toxic property of scavengers. Besides, they claimed that more research must be carried out in the future to optimize the concentration of scavengers during the disinfection process to prevent the toxicity of the bacteria cells. Recent publications have provided evidence for other antioxidant enzymes like superoxide dismutase and catalase (Leung et al. 2008), which are essential for bacteria cells to face the toxicity. However, recent research by Sun et al. (2014) reported that the disinfection of the bacterial cell is due to H_2O_2 generated by the photolytic material rather than the antioxidant enzyme. This research shows that the different photocatalytic systems differed in their reactive species generated during the disinfection process and depend upon the gene of the bacterial cell.

In general, the role of reactive species is to make oxidative stress on the cell membrane by attacking its integrity. The genetic material of the microorganisms such as DNA and nucleic acids will also be targeted leading to cell death. Some studies showed that photocatalytic disinfection mechanisms differ with the used semiconductor producing different reactive oxygen species (An et al. 2017; Xia et al. 2015b).

Currently, recent research carried out on the genetic technology of the bacterial cells and its single-gene knockout mutants for a better understanding of the disinfection process using advanced molecular technologies. For example, Sun et al. (2017) in their research to study investigated the photoelectrocatalytic inactivation mechanism of bacteria using parental *E. coli* BW25113 and its isogenic mutants deficient in catalase HPI (katG-1, JW3914-1) as well as using deficient superoxide dismutase Mn-SOD (sodA-1, JW3879-1). shows that the mutants experienced damages earlier and at higher levels, confirming the essential roles of catalase and superoxide dismutase (SOD) in the bacterial photoelectrocatalytic resistance. Similar results were also reported by An et al. (2016) and Huang et al. (2015), who claimed that due to the complexity of the organism, the disinfection of different pathogenic microbe favors different photocatalytic materials and mechanisms. Moreover, the

inactivation of specific target cells and parental cells favors the production of different reactive species. This research opens an era for further research in the water disinfection process by integrating genetic technology and cytobiology. Reddy et al. (2017) showed that the interaction between the photocatalytic material and the pathogenic microorganisms leading to the generation of reactive species is profoundly affected by the water matrix property such as oxygen content, pH, and ionic strength.

7.5 The Effect of the Water Matrix on the Disinfection Process

Other than the essential characteristics of disinfection materials, the performance of photocatalyst materials can be inhibited by the environmental parameters (Smith and Rodrigues 2015). Some microorganisms are sensitive to a specific type of catalyst (metal oxides, ceramic materials, graphene), not for others, but are more sensitive to the ionic composition of reaction media (Li et al. 2016a; Marugán et al. 2010). Moreover, similar results were also reported by Huang et al. (2017), who investigated the interaction between the photocatalytic material and the pathogenic microorganisms and showed that the generation of reactive species was profoundly affected by the water matrix property such as oxygen and ionic content.

7.5.1 Factors Affecting Water Mix Property on the Water Disinfection Process

The pH of the Solution

One of the most critical factors reported as affecting the water disinfection process is the pH of the reaction media. The changes in the pH value can lead to a change in the charge of the photocatalytic material surface in direct relation with the microbial cell wall membrane. Jia et al. (2016) in their research to disinfect bacteria using $\text{TiO}_2\text{-Bi}_2\text{WO}_6$ showed that high disinfection was found in acidic media. This result is an inconsistency with the results reported by Liang et al. (2015). However, Deng et al. (2017) investigated that increasing the pH of solution leads to enhancing the disinfection process as well as the oxidation of the photocatalytic $g\text{-C}_3\text{N}_4\text{-AgBr}$ leading to generate more hydroxyl radicals and favors the conditions for cell disinfection. This leads to include the effect of pH during the experimental study of adsorption bacteria and oxidation of the photocatalytic material to disinfect microorganisms from wastewater.

Oxygen Content in the Water

The adsorption of bacteria on the surface of a photocatalytic material can also be affected by the content of oxygen in the media. Deng et al. (2017) investigated the generation of reactive species from the photocatalytic material with the intracellular respiration. They showed that bacteria were profoundly affected by the absence of oxygen. Low oxygen levels not only hindered the generation of reactive oxygen species, but the microorganism respiration was also affected (Deng et al. 2017).

Ionic Strength in Water

Another aspect that affects the performance of the photocatalytic disinfection process is the existence of anions, such as SO_4^{2-} , NO_3^- , and Cl^- , in the water solution. Liang et al. (2017) proposed to disinfect bacterial cells using $\text{Bi}_2\text{MoO}_6\text{-AgI}$ as photocatalytic materials. They showed that the bacterial inactivation was significantly affected by the existence of common ions in the solution. This increases the repulsion forces between the anions of the nanomaterials with bacterial cell walls leading to a decrease in the disinfection process (Liang et al. 2017). Hu et al. (2003) showed that the existence of anions in the solution enhanced the generation of reactive species inactivating the bacterial cells. However, in another study, Liang et al. (2017) investigated the resistance of phosphate ions in a solution and showed a decline in the rate of disinfection when compared to chloride ion, which can act as an electron donor to generate reactive species. Marugán et al. (2010) also reported the same result. Having a small concentration of phosphate ions in the photocatalyst materials led to a decrease in the disinfection process (Marugán et al. 2010).

In general, to have effective disinfection of bacterial cells, a full understanding of the effect of the chemical characteristics of the water matrix is needed. However, there is a massive difference in the water matrix characteristics and performance efficiency and generation of reactive species so that more research must be carried out shortly. Optimizing the chemical characteristics of the water matrix can increase the generation of reactive species and the bacterial disinfection on the surface of nanomaterial to apply on a large scale.

7.6 Supported Catalysts for Water/Wastewater Disinfection

Currently, our world faces problems related to the removal of hazardous substances and disinfection of pathogens from wastewater and remediation of pollutants in the groundwater and surface water to prevent the expansion of waterborne diseases that affect public health. Hence, to solve this problem, different oxidation processes such as biological, chemical, and physical methods are applied. However, the presence of

solid particles and toxic pollutant leads to partial mineralization of water contaminants, shielding the viruses and bacteria from being decomposed by the disinfectants (Blume and Neis 2004).

In recent years, different catalytic technologies have been proposed for the disinfection of microbes and removal of organic pollutants using catalyst material generating such as hydroxyl radicals, superoxide radicals and hydroperoxyl and combine oxidation of irradiation, an electron with H_2O_2 , O_3 at standard temperature and pressure. However, when compared each reactive species with a synergistic effect to increase the efficiency of mineralization and to disinfect pathogenic microorganism shows that the synergistic effect of reactive species has high efficiency in mineralization of organic pollutants and decreasing the effect of shielding of suspended particles to disinfect pathogenic microorganism using catalytic technologies which predominantly include photocatalysis, electrochemical catalysis, photoelectrochemical catalysis, catalytic ozonation, and so on. This opens for the new chapter in water and wastewater treatment.

One of the catalytic technologies used for the disinfection of pathogenic microorganism and removal of toxic pollutants from wastewater treatment is using an external electric current is electrochemical process and classified in to electrocoagulation methods and electro-oxidation systems and produce disinfection through direct oxidation in which the inactivation occurred on the surface of the electrode using reactive oxygen species of from hydroxyl radicals, hydrogen peroxide and ozone, or the electric field effect whereas indirect oxidation the inactivation depends upon the generation of oxidants such as chlorine and persulfate species and when compared with the conventional methods such as physical, chemical and biological process, electrochemical process can give the following essential beneficiaries (i) it is simple operation, (ii) no addition of chemicals, (iii) it can easily optimize the process (Barrera-Díaz et al. 2003). In the following section, the electrochemical disinfection methods to disinfect wastewater are discussed.

7.6.1 Electrocoagulation

Electrocoagulation is a process in which the waste water treated using energy, direct electric current in particular, to produce metal ions in the anode (iron and aluminum). It is and currently it attracts high attention in waste water treatment due to its simple method to operate as well as it has, high efficiency in complete disinfection of pathogenic microorganisms and removal of various ions and organic matters when compared with other physicochemical methods (Nasrullah et al. 2017, Daida 2005; Kim et al. 2002). Moreover, when compared with other physicochemical methods, it has the following advantages: simple equipment, easy to operate, low chemical addition, rapid sedimentation of electrogenerated flocs, and smaller amount of sludge production (Nasrullah et al. 2017; Ramesh et al. 2007; Ghernaout et al. 2008).

Ghernaout et al. (2008) explained the principle behind of electrochemical coagulation cell has three stages. That is the first stage there is. forming of coagulants in the anode due to electrical oxidation secondly mineralization and emulsion of breaking of pollutants and suspended particles through the mechanism of adsorption, electrical double-layer compression, enmeshment in a precipitate and inter-particle bridging and charge neutralization, finally in the last stage the mineralized a particles and bacteria, fecal coliforms can form floc.

Over all mechanism of the electrocoagulation of wastewater using catalysis of Fe and Al metals for the production of $\text{Fe}(\text{OH})_2$ and $\text{Al}(\text{OH})_3$, which are insoluble chemical species as shown in the following equation (Gonzalez et al. 2019):

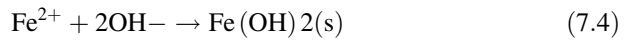
Reaction in the anode:



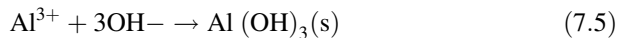
Or



Reaction in the cathode



Or



Ahmed et al. (2012) in their research to disinfect bacteria using coagulation techniques as pretreatment using an aluminum electrode in the anode shows that the pretreatment can decrease the number of bacteria from 2500 to 2 MPN/100 mL, when compared with the ultrafiltration method due to the electric field inside the electrochemical cell, is harmful to bacteria cells and affects the permeability of the cell membrane. In another study by Ghernaout et al. (2008) in their study to inactivate *Escherichia coli* bacteria of surface water using electrocoagulation methods as disinfection using aluminum electrode in the anode shows that it can remove about 97.3% of the *Escherichia coli* bacteria because of the neutralize the surface Zeta potential of the colloidal matter and microorganisms by the liberated metal ion of Al in the aqueous solution neutralize the surface Zeta potential of the colloidal matter and microorganisms. In summary, coagulation is a promising technique for waster disinfection; however, more research must be carried out in the future to apply it on a large scale.

7.6.2 *Direct Oxidation*

Direct oxidation is a process in which the organic pollutants can be removed when it reaches the electrode surface and then the oxidation will take place on the surface and finally return to the bulk of the solution (Barrera-díaz et al. 2014). Moreover, they added that the movement of the pollutant to the electrode surface depends upon the mass transfer activity such as migration, convection, and diffusion.

In this process, the degradation of the pollutant and the disinfection of the microorganism depend upon the production of hydrogen and hydrogen peroxide bubbles in the cathode and the intensity of the current applied, that is, if the concentration of the bubbles is low, it enhanced the formation of hydrogen peroxide, and this leads to the electro-disinfection of the wastewater. Furthermore, this hydrogen peroxide can react with the organic pollutants in the wastewater in the cathode to form hydroxyl radicals (Lakshmi and Vasudevan 2013). However, their efficiency to degrade phenol in the electron-Fenton process shows the generation of hydrogen peroxide in the cathode is indirect electro-oxidation because they are generated by the reduction dissolved oxygen in the solution and it will depend upon the nature of the electrode such as polyacrylonitrile-based carbon fiber brush (Xia et al. 2015).

Llanos et al. (2014) reported that their research treating urban wastewater using electro-disinfection combined with the electro-coagulation process in which boron-doped diamond is used as anode and stainless steel as the cathode and having perforated iron plate as a bipolar electrode shows that they have the efficiency to remove bacteria to about 99% from the solution. Recent study by Ghasemian et al. (2017) to disinfect wastewater which has bacteria-laden water using electrodes of antimony-doped tin-tungsten oxide shows that they disinfect the *E.coli* bacteria entirely because of the electrodes containing high oxygen potential. This leads to the production of hydroxyl radicals and oxidation of the pollutants present in the wastewater. In general, using boron-doped diamond as an electrode to generate oxygen potential in the disinfection of bacteria as well as complete mineralization of organic pollutants when compared with other electrodes such as SnO_2 and PbO_2 because it has high oxygen evolution potential (Panizza and Cerisola 2009).

7.6.3 *Indirect Electro-oxidation*

This is another method of electro-oxidation in which it can disinfect or degrade the wastewater using strong oxidants of disinfection agents such as carbonates, sulfates, and chlorides which lead to the generation of free chlorine on the surface of the electrode of anode; however, the generation of the free chlorine will depend upon the applied current, duration of time, and pH of the solution. Moreover, it can also degrade and disinfect the wastewater using oxidants such as ozone, peroxides, and hydroxyl radicals that can be directly generated from the wastewater (Polcaro et al. 2007).

For example, in the recent research by La Motta et al. (2017), in their research in the treatment of municipal water using electro-disinfection method by the generation of free chlorine which concentration of 1500 mg/l and IrO₂ electrodes shows that this indirect electro-oxidation process can remove *E. Coli* to about 99%. Moreover, they claimed that using free chlorine might lead to the formation of another hazardous material such as organic- chlorinated species which can persist in degrading and staying a long time in the environment. To overcome the above problem, a new research methodology developed by Ahmadi and Wu (2017) showing that using other oxidants such as C₂O₆₂⁻, S₂O₈₂⁻, and P₂O₈₄ which are electrochemically formed using PbO₂ and boron-doped diamond electrodes can altogether remove the organic pollutant with no formation of organochlorinated species. However, its application in water disinfection is limited due to the type of oxidants added to disinfect the bacteria, for example, according to Qi et al. (2018), adding activated persulfate to generate oxidant can remove *E. coli* O157: H7 and *Listeria monocytogenes* completely in 120 s. However, in another study by Xing et al. (2018), using phosphate for the generation of oxidants can remove *Mycobacterium avium*, *Aeromonas* spp., *Pseudomonas aeruginosa*, *Hartmannella vermiformis*, and *Mycobacterium* spp. and resistance to *Klebsiella pneumoniae*, so more research must be carried out in the future to solve its limitation to apply on a large scale.

In general, from all electrochemical disinfection approaches, direct electro-oxidation using boron-doped electrodes showed high efficiency in electrochemical water treatments due to its excellent properties such as very low capacitance, extreme electrochemical stability, and high charge diffusion pathway, enhanced separation of photogenerated charges, and high oxygen potential for generation of oxidants. Therefore, it would be useful to find the proper posttreatment and method of recovery of the electrochemical material electrode. This will be a critical factor in the future to apply these materials on a large scale under visible light for water/wastewater disinfection.

7.7 Future Perspectives

Nanostructured materials as photocatalyst have a great significance in the field of water disinfection of bacterial cell and wastewater treatment of organic pollutants. However, the study on the specific morphology and reactor design of nanostructure material as a photocatalyst is extremely promising for the disinfection of bacterial cells with the utilization of green technology and genetic technology but its application at large scale is still on the initial stage. Therefore, the following research areas should be carried out in the future:

1. Most of the previous studies on water disinfection using photocatalyst are under visible light and ultraviolet irradiation. However, recent studies show that integrating visible light and ultraviolet irradiation as photocatalyst material is highly efficient for the disinfection process because it accounts 44% sunlight spectrum

so that more research could be carried out on the fabrication of near-infrared light and full spectrum of sunlight.

2. Fabrication of nanomaterials using various approaches like liquid–solid solution, reverse microemulsion route, and hot-injection pyrolysis by adding organic surfactants, ligands, and chemicals may provide a new way of controlling and monitoring the growth process and crystal nucleation effects (Lin et al. 2015; Manna et al. 2000; Wang et al. 2011a) for the synthesis of a nanomaterial as photocatalyst for the disinfection process needs further investigation in the future.
3. Nanomaterials that are chemically prepared as a photocatalyst for the disinfection process show high efficiency; however, its application is restricted due to the requirement of complicated procedure for fabrication, high cost, and production in small quantity. While using chemical minerals, which are found naturally in large size and low cost, is a promising technology as photocatalyst material for the disinfection process, however, due its large particle size, it hinders its application for water disinfection process. Therefore, reducing the size of natural minerals to small size (nanoscale) followed by calcination to improve crystallinity for the fabrication of composite material for the disinfection process needs further investigation in the future.
4. The photocatalytic system differed in the reactive species produced for the disinfection bacterial cells. Due to some microorganisms resistant to the reactive species so that more research needs in the future by integrating nanostructured imposing gene technology with nanostructured material as a photocatalyst to select typical microorganisms with tremendous efficiency.

In general, more research and efforts are devoted to the past in the development of photocatalytic water disinfection. To realize the goal of scaling up the nanomaterials as photocatalyst for water disinfection process, the future research should focus on the photostability, reactor design, immobilization photocatalyst, optimization of disinfection parameters and method of separating the photocatalytic material, reusability, and water matrix as well as electrochemical disinfection using boron-doped electrodes, its capacitance, and electrochemical stability. Thus, a critical factor in better usage of a nanomaterial as photocatalyst in the water disinfection process will be the development of new sustainable photocatalytic material via solar irradiation pathways by using naturally occurring nanostructured materials and chemically synthesized material.

7.8 Conclusions

The above review showed that solar-driven nanostructured material as photocatalyst material has broad prospects in the field of water disinfection for typical pathogenic microbes and degradation of organic pollutants of industrial wastewater. This chapter discussed the recent progress regarding the use of nanostructured material (i.e., 0D, 1D, and 2D) for water disinfection systems under visible light irradiation

because these nanostructured materials have a large surface area, high separation of reactive species efficiency, and more active site compared to other photocatalytic material. However, due to the requirements of the different procedures involved in nanostructured material fabrication and high-energy consumption, several obstacles should be overcome before applying such disinfection processes to a large scale. The use of supported catalysts for water/wastewater disinfection approaches also showed high efficiency in electrochemical water treatments due to its excellent properties such as very low capacitance, extreme electrochemical stability, and high charge diffusion pathway, enhanced separation of photogenerated charges, and high oxygen potential for generation of oxidants. Finally, the review suggests that with the in-depth study of the specific morphology and reactor design, nanostructure material as a photocatalyst is extremely promising for the disinfection of bacterial cells with the utilization of natural minerals and genetic engineering technology.

Conflict of Interest The authors declare that they have no conflict of interest.

References

- Ahmed AAA, Talib ZA, bin Hussein MZ, Zakaria A (2012) Improvement of the crystallinity and photocatalytic property of zinc oxide as calcination product of Zn–Al layered double hydroxide. *Journal of alloys and compounds* 539:154–160
- Ahmadi A, Wu T (2017) Inactivation of *E. coli* using a novel TiO₂ nanotube electrode. *Environ Sci Water Res Technol* 3(3):534–545
- Alarcón J, Ponce S, Paraguay-Delgado F, Rodríguez J (2011) Effect of γ -irradiation on the growth of ZnO nanorod films for photocatalytic disinfection of contaminated water. *J Colloid Interface Sci* 364(1):49–55. <https://doi.org/10.1016/j.jcis.2011.08.025>
- Alikhani M-Y et al (2012) Photocatalytic removal of *Escherichia coli* from aquatic solutions using synthesized ZnO nanoparticles: a kinetic study. *Water Sci Technol* 67(3):557–563. <https://doi.org/10.2166/wst.2012.593>
- An H, Qian Y, Gu X, Tang WZ (1996) Biological treatment of dye wastewaters using an anaerobic-oxic system. *Chemosphere* 33(12):2533–2542. [https://doi.org/10.1016/S0045-6535\(96\)00349-9](https://doi.org/10.1016/S0045-6535(96)00349-9)
- An T, Sun H, Li G, Zhao H, Wong PK (2016) Differences in photoelectrocatalytic inactivation processes between *E. coli* and its isogenic single gene knockoff mutants: destruction of membrane framework or associated proteins? *Appl Catal B Environ* 188:360–366. <https://doi.org/10.1016/j.apcatb.2016.02.014>
- An T, Zhao H, Wong PK (2017) *Advances in photocatalytic disinfection*. Springer, Berlin/Heidelberg. <https://link.springer.com/book/10.1007%2F978-3-662-53496-0>
- Asahi R, Morikawa T, Ohwaki T, Aoki K, Taga Y (2001) Visible-light photocatalysis in nitrogen-doped titanium oxides. *Science* 293(5528):269–271. <https://doi.org/10.1126/science.1061051>
- Aslan E et al (2014) Photocatalytic hydrogen evolution by oleic acid-capped CdS, CdSe, and CdS_{0.75}Se_{0.25} alloy nanocrystals. *ChemPhysChem* 15(13):2668–2671. <https://doi.org/10.1002/cphc.201402229>
- Bai H, Liu Z, Liu L, Sun DD (2013) Large-scale production of hierarchical TiO₂ Nanorod spheres for photocatalytic elimination of contaminants and killing Bacteria. *Chem Eur J* 19(9):3061–3070. <https://doi.org/10.1002/chem.201204013>
- Barnes RJ, Molina R, Xu J, Dobson PJ, Thompson IP (2013) Comparison of TiO₂ and ZnO nanoparticles for photocatalytic degradation of methylene blue and the correlated inactivation

- of gram-positive and gram-negative bacteria. *J Nanopart Res* 15(2):1432. <https://doi.org/10.1007/s11051-013-1432-9>
- Barrera-Díaz C, Urena-Núñez F, Campos E, Palomar-Pardavé M, Romero-Romo M (2003) A combined electrochemical-irradiation treatment of highly colored and polluted industrial wastewater. *Radiat Phys Chem* 67(5):657–663. [https://doi.org/10.1016/S0969-806X\(02\)00497-8](https://doi.org/10.1016/S0969-806X(02)00497-8)
- Barrera-Díaz CE, Roa-Morales G, Hernández PB, Fernández-Marchante CM, Rodrigo MA (2014) Enhanced electrocoagulation: New approaches to improve the electrochemical process. *Journal of Electrochemical Science and Engineering* 4(4):285–296
- Basnet P, Larsen GK, Jadeja RP, Hung Y-C, Zhao Y (2013) α -Fe₂O₃ nanocolumns and nanorods fabricated by electron beam evaporation for visible light photocatalytic and antimicrobial applications. *ACS Appl Mater Interfaces* 5(6):2085–2095. <https://doi.org/10.1021/am303017c>
- Blume T, Neis U (2004) Improved wastewater disinfection by ultrasonic pre-treatment. *Ultrason Sonochem* 11(5):333–336. [https://doi.org/10.1016/S1350-4177\(03\)00156-1](https://doi.org/10.1016/S1350-4177(03)00156-1)
- Bosetti M, Massè A, Tobin E, Cannas M (2002) Silver coated materials for external fixation devices: in vitro biocompatibility and genotoxicity. *Biomaterials* 23(3):887–892. [https://doi.org/10.1016/s0142-9612\(01\)00198-3](https://doi.org/10.1016/s0142-9612(01)00198-3)
- Cantarella M, Di Mauro A, Gulino A, Spitaleri L, Nicotra G, Privitera V, Impellizzeri G (2018) Selective photodegradation of paracetamol by molecularly imprinted ZnO nanonuts. *Applied Catalysis B: Environmental* 238:509–517
- Carlson K, Elliott C, Walker S, Misra M, Mohanty S (2016) An effective, point-of-use water disinfection device using immobilized black TiO₂ nanotubes as an electrocatalyst. *J Electrochem Soc* 163(6):H395–H401. <https://doi.org/10.1149/2.0651606jes>
- Castañeda-Juárez M, Martínez-Miranda V, Almazán-Sánchez PT, Linares-Hernández I, Santoyo-Tepole F, Vázquez-Mejía G (2019) Synthesis of TiO₂ catalysts doped with Cu, Fe, and Fe/Cu supported on clinoptilolite zeolite by an electrochemical-thermal method for the degradation of diclofenac by heterogeneous photocatalysis. *Journal of Photochemistry and Photobiology A: Chemistry* 380:111834
- Chandran P, Kumari P, Khan SS (2014) Photocatalytic activation of CdS NPs under visible light for environmental cleanup and disinfection. *Sol Energy* 105:542–547. <https://doi.org/10.1016/j.solener.2014.04.028>
- Chen Y et al (2011) Naturally occurring sphalerite as a novel cost-effective photocatalyst for bacterial disinfection under visible light. *Environ Sci Technol* 45(13):5689–5695. <https://doi.org/10.1021/es200778p>
- Chen Y et al (2013) Comparative study of visible-light-driven photocatalytic inactivation of two different wastewater bacteria by natural sphalerite. *Chem Eng J* 234:43–48. <https://doi.org/10.1016/j.cej.2013.08.106>
- Chen F et al (2016) Photo-reduction of bromate in drinking water by metallic Ag and reduced graphene oxide (RGO) jointly modified BiVO₄ under visible light irradiation. *Water Res* 101:555–563. <https://doi.org/10.1016/j.watres.2016.06.006>
- Chong MN, Jin B, Zhu H, Saint C (2010) Bacterial inactivation kinetics, regrowth and synergistic competition in a photocatalytic disinfection system using anatase titanate nanofiber catalyst. *J Photochem Photobiol A Chem* 214(1):1–9. <https://doi.org/10.1016/j.jphotochem.2010.05.018>
- Chou WL, Yu DG, Yang MC (2005) The preparation and characterization of silver-loading cellulose acetate hollow fiber membrane for water treatment. *Polym Adv Technol* 16(8):600–607. <https://doi.org/10.1002/pat.630>
- Christensen P, Curtis T, Egerton T, Kosa S, Tinlin J (2003) Photoelectrocatalytic and photocatalytic disinfection of *E. coli* suspensions by titanium dioxide. *Appl Catal B Environ* 41(4):371–386. [https://doi.org/10.1016/S0926-3373\(02\)00172-8](https://doi.org/10.1016/S0926-3373(02)00172-8)
- Daida P (2005) Removal of arsenic from water by electrocoagulation using Al – Al, Fe – Fe electrode pair systems and characterization of by-product. *UMI Microform* 1–68. <https://doi.org/10.1016/j.jhazmat.2005.11.108>

- Deng J, Liang J, Li M, Tong M (2017) Enhanced visible-light-driven photocatalytic bacteria disinfection by g-C₃N₄-AgBr. *Colloids Surf B Biointerfaces* 152:49–57. <https://doi.org/10.1016/j.colsurfb.2017.01.003>
- Dunlop P, Ciavola M, Rizzo L, Byrne J (2011) Inactivation and injury assessment of *Escherichia coli* during solar and photocatalytic disinfection in LDPE bags. *Chemosphere* 85(7):1160–1166. <https://doi.org/10.1016/j.chemosphere.2011.09.006>
- Fagan R, McCormack DE, Dionysiou DD, Pillai SC (2016) A review of solar and visible light active TiO₂ photocatalysis for treating bacteria, cyanotoxins, and contaminants of emerging concern. *Mater Sci Semicond Process* 42:2–14. <https://doi.org/10.1016/j.mssp.2015.07.052>
- Foster HA, Ditta IB, Varghese S, Steele A (2011) Photocatalytic disinfection using titanium dioxide: spectrum and mechanism of antimicrobial activity. *Appl Microbiol Biotechnol* 90(6):1847–1868. <https://doi.org/10.1007/s00253-011-3213-7>
- Gao F et al (2007) Visible-light photocatalytic properties of weak magnetic BiFeO₃ nanoparticles. *Adv Mater* 19(19):2889–2892. <https://doi.org/10.1002/adma.200602377>
- Ghasemian S, Asadishad B, Omanovic S, Tufenkji N (2017) Electrochemical disinfection of bacteria-laden water using antimony-doped tin-tungsten-oxide electrodes. *Water Res* 126:299–307. <https://doi.org/10.1016/j.watres.2017.09.029>
- Ghernaout D, Badis A, Kellil A, Ghernaout B (2008) Application of electrocoagulation in *Escherichia coli* culture and two surface waters. *Desalination* 219:118–125. <https://doi.org/10.1016/j.desal.2007.05.010>
- Gong AS, Lanzl CA, Cwiertny DM, Walker SL (2011) Lack of influence of extracellular polymeric substances (EPS) level on hydroxyl radical-mediated disinfection of *Escherichia coli*. *Environ Sci Technol* 46(1):241–249. <https://doi.org/10.1021/es202541r>
- Gonzalez-Rivas N, Reyes-Pérez H, Barrera-Díaz CE (2019) Recent advances in water and wastewater electrodisinfection. *ChemElectroChem* 6(7):1978–1983. <https://doi.org/10.1002/celec.201801746>
- Gu W et al (2017) Face-to-face interfacial assembly of ultrathin g-C₃N₄ and Anatase TiO₂ Nanosheets for enhanced solar photocatalytic activity. *ACS Appl Mater Interfaces* 9(34):28674–28684. <https://doi.org/10.1021/acsami.7b10010>
- Guo L, Shan C, Liang J, Ni J, Tong M (2015) Bactericidal mechanisms of Au@ TNBs under visible light irradiation. *Colloids Surf B: Biointerfaces* 128:211–218. <https://doi.org/10.1016/j.colsurfb.2015.01.013>
- Hamadani M, Reisi-Vanani A, Majedi A (2010) Synthesis, characterization, and effect of calcination temperature on phase transformation and photocatalytic activity of Cu, S-codoped TiO₂ nanoparticles. *Appl Surf Sci* 256(6):1837–1844. <https://doi.org/10.1016/j.apsusc.2009.10.016>
- Hassan MS et al (2012) Fabrication, characterization and antibacterial effect of novel electrospun TiO₂ nanorods on a panel of pathogenic bacteria. *J Biomed Nanotechnol* 8(3):394–404. <https://www.ncbi.nlm.nih.gov/pubmed/22764408>
- Hassan MS et al (2016) The influence of synthesis method on size and toxicity of CeO₂ quantum dots: potential in the environmental remediation. *Ceram Int* 42(1):576–582. <https://doi.org/10.1016/j.ceramint.2015.08.149>
- Hu C, Jimmy CY, Hao Z, Wong P (2003) Effects of acidity and inorganic ions on the photocatalytic degradation of different azo dyes. *Appl Catal B Environ* 46(1):35–47. [https://doi.org/10.1016/S0926-3373\(03\)00139-5](https://doi.org/10.1016/S0926-3373(03)00139-5)
- Huang W-J, Fang G-C, Wang C-C (2005) The determination and fate of disinfection by-products from ozonation of polluted raw water. *Sci Total Environ* 345(1–3):261–272. <https://doi.org/10.1016/j.scitotenv.2004.10.019>
- Huang J, Ho W, Wang X (2014) Metal-free disinfection effects induced by graphitic carbon nitride polymers under visible light illumination. *Chem Commun* 50(33):4338–4340. <https://doi.org/10.1039/C3CC48374F>

- Huang G et al (2015) Dual roles of capsular extracellular polymeric substances in photocatalytic inactivation of *Escherichiacoli*: comparison of *E. coli* BW25113 and isogenic mutants. *Appl Environ Microbiol* 81(15):5174–5183. <https://doi.org/10.1128/AEM.00775-15>
- Huang G et al (2017) Probing the intracellular matters released from the photocatalytic inactivation of bacteria using fractionation procedure and excitation-emission-matrix fluorescence. *Water Res* 110:270–280. <https://doi.org/10.1016/j.watres.2016.12.032>
- Iijima S (1991) Helical microtubules of graphitic carbon. *Nature* 354(6348):56. <https://doi.org/10.1038/354056a0>
- Janpetch N, Vanichvattanadecha C, Rujiravanit R (2015) Photocatalytic disinfection of water by bacterial cellulose/N–F co-doped TiO₂ under fluorescent light. *Cellulose* 22(5):3321–3335. <https://doi.org/10.1007/s10570-015-0721-0>
- Jeong KS, Guyot-Sionnest P (2016) Mid-infrared photoluminescence of CdS and CdSe colloidal quantum dots. *ACS Nano* 10(2):2225–2231. <https://doi.org/10.1021/acsnano.5b06882>
- Jia Y, Zhan S, Ma S, Zhou Q (2016) Fabrication of TiO₂–Bi₂WO₆ nanosheet for enhanced solar photocatalytic disinfection of *E. coli*: insights on the mechanism. *ACS Appl Mater Interfaces* 8(11):6841–6851. <https://doi.org/10.1021/acsami.6b00004>
- Jiang L et al (2018) Construction of an all-solid-state Z-scheme photocatalyst based on graphite carbon nitride and its enhancement to catalytic activity. *Environ Sci Nano* 5(3):599–615. <https://doi.org/10.1039/C7EN01031A>
- Jin M et al (2007) Light-stimulated composition conversion in TiO₂-based nanofibers. *J Phys Chem C* 111(2):658–665. <https://doi.org/10.1021/jp065590n>
- Jin Y et al (2013) Bactericidal mechanisms of Ag₂O/TNBs under both dark and light conditions. *Water Res* 47(5):1837–1847. <https://doi.org/10.1016/j.watres.2013.01.003>
- Karunakaran C, Vijayabalan A, Manikandan G (2012) Photocatalytic and bactericidal activities of hydrothermally synthesized nanocrystalline Cd-doped ZnO. *Superlattice Microst* 51(3):443–453. <http://adsabs.harvard.edu/abs/2012SuMi...51..443K>
- Kim TK, Perk's SEB, Kim S (2002) Decolorization of disperse and reactive dyes by continuous electrocoagulation process. *Desalination* 150:165–175. [https://doi.org/10.1016/S0011-9164\(02\)00941-4](https://doi.org/10.1016/S0011-9164(02)00941-4)
- Kong H, Song J, Jang J (2010) Photocatalytic antibacterial capabilities of TiO₂–biocidal polymer nanocomposites synthesized by a surface-initiated photopolymerization. *Environ Sci Technol* 44(14):5672–5676. <https://doi.org/10.1021/es1010779>
- Kühn KP et al (2003) Disinfection of surfaces by photocatalytic oxidation with titanium dioxide and UVA light. *Chemosphere* 53(1):71–77. [https://doi.org/10.1016/S0045-6535\(03\)00362-X](https://doi.org/10.1016/S0045-6535(03)00362-X)
- La Motta EJ, Rincón GJ, De Grau LE, Jovanovich KD (2017) Field testing of a small-scale continuous-flow wastewater electrodisinfection unit using direct current. *J Environ Eng* 144(1):04017090. <https://doi.org/10.1061/%28ASCE%29EE.1943-7870.0001303>
- Lakshmi J, Vasudevan S (2013) Graphene—a promising material for removal of perchlorate (ClO₄[−]) from water. *Environ Sci Pollut Res* 20(8):5114–5124. <https://doi.org/10.1007/s11356-013-1499-y>
- Lam S-M, Sin J-C, Mohamed AR (2016) A review on photocatalytic application of g-C₃N₄/semiconductor (CNS) nanocomposites towards the erasure of dyeing wastewater. *Mater Sci Semicond Process* 47:62–84. <https://doi.org/10.1016/j.mssp.2016.02.019>
- Lee JS, Jang J (2014) Hetero-structured semiconductor nanomaterials for photocatalytic applications. *J Ind Eng Chem* 20(2):363–371. <https://doi.org/10.1016/j.jiec.2013.11.050>
- Leung T, Chan C, Hu C, Yu J, Wong P (2008) Photocatalytic disinfection of marine bacteria using fluorescent light. *Water Res* 42(19):4827–4837. <https://doi.org/10.1016/j.watres.2008.08.031>
- Li Q et al (2008a) Antimicrobial nanomaterials for water disinfection and microbial control: potential applications and implications. *Water Res* 42(18):4591–4602. <https://doi.org/10.1016/j.watres.2008.08.015>
- Li Y, Lu A, Wang C, Wu X (2008b) Characterization of natural sphalerite as a novel visible-light-driven photocatalyst. *Sol Energy Mater Sol Cells* 92(8):953–959. <https://doi.org/10.1016/j.solmat.2008.02.023>

- LI Y, Lu A, WANG C (2009) Semiconducting mineralogical characteristics of natural Sphalerite gestating visible-light photocatalysis. *Acta Geol Sin Engl Ed* 83(3):633–639. <https://doi.org/10.1111/j.1755-6724.2009.00053.x>
- Llano B, Hidalgo MC, Rios LA, Navio JA (2014) Effect of the type of acid used in the synthesis of titania–silica mixed oxides on their photocatalytic properties. *Applied Catalysis B: Environmental* 150:389–395
- Li L, Salvador PA, Rohrer GS (2014) Photocatalysts with internal electric fields. *Nanoscale* 6(1):24–42. <https://doi.org/10.1039/C3NR03998F>
- Li G et al (2015) Enhanced visible-light-driven photocatalytic inactivation of *Escherichia coli* using g-C₃N₄/TiO₂ hybrid photocatalyst synthesized using a hydrothermal-calcination approach. *Water Res* 86:17–24. <https://doi.org/10.1016/j.watres.2015.05.053>
- Li G, Nie X, Gao Y, An T (2016a) Can environmental pharmaceuticals be photocatalytically degraded and completely mineralized in water using g-C₃N₄/TiO₂ under visible light irradiation? – Implications of persistent toxic intermediates. *Appl Catal B Environ* 180:726–732. <https://doi.org/10.1016/j.apcatb.2015.07.014>
- Li X, Wang J, Men Y, Bian Z (2016b) TiO₂ meso crystal with exposed (001) facets and CdS quantum dots as an active visible photocatalyst for selective oxidation reactions. *Appl Catal B Environ* 187:115–121. <https://doi.org/10.1016/j.apcatb.2016.01.034>
- Li Y et al (2016c) Visible-light-driven photocatalytic inactivation of MS2 by metal-free g-C₃N₄: virucidal performance and mechanism. *Water Res* 106:249–258. <https://doi.org/10.1016/j.watres.2016.10.009>
- Li Y et al (2017) Efficient water disinfection with Ag₂WO₄-doped mesoporous g-C₃N₄ under visible light. *J Hazard Mater* 338:33–46. <https://doi.org/10.1016/j.jhazmat.2017.05.011>
- Liang HW, Liu S, Yu SH (2010) Controlled synthesis of one-dimensional inorganic nanostructures using pre-existing one-dimensional nanostructures as templates. *Adv Mater* 22(35):3925–3937. <https://doi.org/10.1002/adma.200904391>
- Liang J, Shan C, Zhang X, Tong M (2015) Bactericidal mechanism of BiOI–AgI under visible light irradiation. *Chem Eng J* 279:277–285. <https://doi.org/10.1016/j.cej.2015.05.024>
- Liang J, Liu F, Deng J, Li M, Tong M (2017) Efficient bacterial inactivation with Z-scheme AgI/Bi₂MoO₆ under visible light irradiation. *Water Res* 123:632–641. <https://doi.org/10.1016/j.watres.2017.06.060>
- Lin C-H et al (2015) Formation of hollow silica nanospheres by reverse microemulsion. *Nanoscale* 7(21):9614–9626. <https://doi.org/10.1039/c5nr01395j>
- Liu J-W, Liang H-W, Yu S-H (2012a) Macroscopic-scale assembled nanowire thin films and their functionalities. *Chem Rev* 112(8):4770–4799. <https://doi.org/10.1021/cr200347w>
- Liu L, Liu Z, Bai H, Sun DD (2012b) Concurrent filtration and solar photocatalytic disinfection/ degradation using high-performance Ag/TiO₂ nanofiber membrane. *Water Res* 46(4):1101–1112. <https://doi.org/10.1016/j.watres.2011.12.009>
- Liu Q et al (2014) Single-crystalline, ultrathin ZnGa₂O₄ nanosheet scaffolds to promote photocatalytic activity in CO₂ reduction into methane. *ACS Appl Mater Interfaces* 6(4):2356–2361. <https://doi.org/10.1021/am404572g>
- Liu Q, Guo Y, Chen Z, Zhang Z, Fang X (2016) Constructing a novel ternary Fe (III)/graphene/g-C₃N₄ composite photocatalyst with enhanced visible-light-driven photocatalytic activity via interfacial charge transfer effect. *Appl Catal B Environ* 183:231–241. <https://doi.org/10.1016/j.apcatb.2015.10.054>
- Liu B et al (2017) Visible-light-driven TiO₂/Ag₃PO₄ heterostructures with enhanced antifungal activity against agricultural pathogenic fungi *Fusarium graminearum* and mechanism insight. *Environ Sci Nano* 4(1):255–264. <https://doi.org/10.1039/C6EN00415F>
- Liu Y, Zeng X, Hu X, Hu J, Zhang X (2018) Two-dimensional nanomaterials for photocatalytic water disinfection: recent progress and future challenges. *J Chem Technol Biotechnol* 94(1):22–37. <https://doi.org/10.1002/jctb.5779>

- Lu F, Cai W, Zhang Y (2008) ZnO hierarchical micro/nano architectures: solvothermal synthesis and structurally enhanced photocatalytic performance. *Adv Funct Mater* 18(7):1047–1056. <https://doi.org/10.1002/adfm.200700973>
- Ma S, Zhan S, Jia Y, Shi Q, Zhou Q (2016) Enhanced disinfection application of Ag-modified g-C₃N₄ composite under visible light. *Appl Catal B Environ* 186:77–87. <https://doi.org/10.1016/j.apcatb.2015.12.051>
- Makoday N, Saprykina M, Soboleva N, Savluk O, Goncharuk V (2015) Inactivation of *Candida Albicans* in the UV/TiO₂/Fe³⁺ system. *J Water Chem Technol* 37(3):140–144. <https://doi.org/10.3103/S1063455X15030078>
- Maness P-C et al (1999) Bactericidal activity of photocatalytic TiO₂ reaction: toward an understanding of its killing mechanism. *Appl Environ Microbiol* 65(9):4094–4098. 10473421
- Manna L, Scher EC, Alivisatos AP (2000) Synthesis of soluble and processable rod-, arrow-, teardrop-, and tetrapod-shaped CdSe nanocrystals. *J Am Chem Soc* 122(51):12700–12706. <https://doi.org/10.1021/ja003055+>
- Marugán J, van Grieken R, Pablos C, Sordo C (2010) Analogies and differences between photocatalytic oxidation of chemicals and photocatalytic inactivation of microorganisms. *Water research* 44(3):789–796
- Masih D, Ma Y, Rohani S (2017) Graphitic C₃N₄ based noble-metal-free photocatalyst systems: a review. *Appl Catal B Environ* 206:556–588. <https://doi.org/10.1016/j.apcatb.2017.01.061>
- Matsunaga T, Tomoda R, Nakajima T, Wake H (1985a) Photoelectrochemical sterilization of microbial cells by semiconductor powders. *FEMS Microbiol Lett* 29(1–2):211–214. <https://doi.org/10.1111/j.1574-6968.1985.tb00864.x>
- Matsunaga T, Tomoda R, Nakajima T, Wake H (1985b) Photoelectrochemical sterilization of microbial cells by semiconductor powders. *FEMS Microbiol Lett* 29(1–2):211–214. <https://doi.org/10.1111/j.1574-6968.1985.tb00864.x>
- Melián JH et al (2000) The photocatalytic disinfection of urban wastewaters. *Chemosphere* 41(3):323–327. [https://doi.org/10.1016/S0045-6535\(99\)00502-0](https://doi.org/10.1016/S0045-6535(99)00502-0)
- Miao G et al (2016) Visible-light-induced photocatalytic oxidative desulfurization using BiVO₄/C₃N₄@ SiO₂ with air/cumene hydroperoxide under ambient conditions. *Appl Catal B Environ* 192:72–79
- Mikolajczyk A et al (2016) A combined experimental and computational approach to developing efficient photocatalysts based on Au/Pd–TiO₂ nanoparticles. *Environ Sci Nano* 3(6):1425–1435. <https://doi.org/10.1039/C6EN00232C>
- Montgomery MA, Elimelech M (2007) Water and sanitation in developing countries: including health in the equation. ACS Publications. <https://doi.org/10.1021/es072435t>
- Munoz-Batista MJ, Fontelles-Carceller O, Ferrer M, Fernández-García M, Kubacka A (2016) Disinfection capability of Ag/g-C₃N₄ composite photocatalysts under UV and visible light illumination. *Appl Catal B Environ* 183:86–95. <https://doi.org/10.1016/j.apcatb.2015.10.024>
- Munawar T, Yasmeeen S, Hussain F, Mahmood K, Hussain A, Asghar M, Iqbal F (2020) Synthesis of novel heterostructured ZnO-CdO-CuO nanocomposite: Characterization and enhanced sunlight driven photocatalytic activity. *Materials Chemistry and Physics*:122983
- Nasrullah M, Singh L, Mohamad Z, Norsita S, Krishnan S, Wahida N, Zularisam AW (2017) Treatment of palm oil mill effluent by electrocoagulation with the presence of hydrogen peroxide as an oxidizing agent and polialuminum chloride as coagulant-aid. *Water Resour Ind* 17:7–10. <https://doi.org/10.1016/j.wri.2016.11.001>
- Naveenraj S, Lee G-J, Anandan S, Wu JJ (2015) Nanosized tantalum based materials—synthesis and applications. *Mater Res Bull* 67:20–46. <https://doi.org/10.1016/j.materresbull.2015.02.060>
- Nie X et al (2014) Comparative study on the photoelectrocatalytic inactivation of *Escherichia coli* K-12 and its mutant *Escherichia coli* BW25113 using TiO₂ nanotubes as a photoanode. *Appl Catal B Environ* 147:562–570. <https://doi.org/10.1016/j.apcatb.2013.09.037>
- Nieuwenhuijsen MJ, Toledano MB, Eaton NE, Fawell J, Elliott P (2000) Chlorination disinfection byproducts in water and their association with adverse reproductive outcomes: a review. *Occup Environ Med* 57(2):73–85. <https://doi.org/10.1136/oem.57.2.73>

- Ong W-J (2017) 2D/2D graphitic carbon nitride (g-C₃N₄) heterojunction nanocomposites for photocatalysis: why does face-to-face interface matter? *Front Mater* 4:11. <https://doi.org/10.3389/fmats.2017.00011>
- Ong W-J, Tan L-L, Ng YH, Yong S-T, Chai S-P (2016) Graphitic carbon nitride (g-C₃N₄)-based photocatalysts for artificial photosynthesis and environmental remediation: are we a step closer to achieving sustainability. *Chem Rev* 116(12):7159–7329. <https://doi.org/10.1021/acs.chemrev.6b00075>
- Pan B et al (2008) Effects of carbon nanotubes on photoluminescence properties of quantum dots. *J Phys Chem C* 112(4):939–944. <https://doi.org/10.1021/jp068920c>
- Panizza M, Cerisola G (2009) Direct and mediated anodic oxidation of organic pollutants. *Chem Rev* 109(12):6541–6569. <https://doi.org/10.1021/cr9001319>
- Peng X et al (2017) Bacterial disinfection in a sunlight/visible-light-driven photocatalytic reactor by recyclable natural magnetic sphalerite. *Chemosphere* 166:521–527. <https://doi.org/10.1016/j.chemosphere.2016.09.090>
- Polcaro AM, Vacca A, Mascia M, Palmas S, Pompei R, Laconi S (2007) Characterization of a stirred tank electrochemical cell for water disinfection processes. *Electrochim Acta* 52 (7):2595–2602. <https://doi.org/10.1016/j.electacta.2006.09.015>
- Qi H, Huang Q, Hung YC (2018) Efficacy of activated persulfate in inactivating *Escherichia coli* O157: H7 and *Listeria monocytogenes*. *Int J Food Microbiol* 284:40–47. <https://doi.org/10.1016/j.ijfoodmicro.2018.06.021>
- Rahmawati F, Kusumaningsih T, Hapsari AM, Hastuti A (2010) Ag and Cu loaded on TiO₂/graphite as a catalyst for *Escherichia coli*-contaminated water disinfection. *Chem Pap* 64 (5):557–565. <https://doi.org/10.2478/s11696-010-0036-4>
- Ramesh RB, Bhadrinarayana NS, Meera SBKM, Anantharaman N (2007) Treatment of tannery wastewater by electrocoagulation. *J Univ Chem Technol Metall* 42(2):201–220. [https://doi.org/10.1016/S1001-0742\(07\)60230-7](https://doi.org/10.1016/S1001-0742(07)60230-7)
- Reddy PVL, Kavitha B, Reddy PAK, Kim K-H (2017) TiO₂-based photocatalytic disinfection of microbes in aqueous media: a review. *Environ Res* 154:296–303. <https://doi.org/10.1016/j.envres.2017.01.018>
- Ren J et al (2010) Photocatalytic activity of silver vanadate with a one-dimensional structure under fluorescent light. *J Hazard Mater* 183(1–3):950–953. <https://doi.org/10.1016/j.jhazmat.2010.07.108>
- Roushani M, Mavaei M, Rajabi HR (2015) Graphene quantum dots as novel and green nanomaterials for the visible-light-driven photocatalytic degradation of cationic dye. *J Mol Catal A Chem* 409:102–109. <https://doi.org/10.1016/j.molcata.2015.08.011>
- Sajan CP, Wageh S, Al-Ghamdi AA, Yu J, Cao S (2016) TiO₂ nanosheets with exposed {001} facets for photocatalytic applications. *Nano Res* 9(1):3–27. <https://doi.org/10.1007/s12274-015-0919-3>
- Sanchez L et al (2014) Influence of pyrolytic seeds on ZnO nanorod growth onto rigid substrates for photocatalytic abatement of *Escherichia coli* in water. *Water Sci Technol Water Supply* 14 (6):1087–1094. <https://doi.org/10.2166/ws.2014.068>
- Sanchez L et al (2015) Synthesis and characterization of ZnO nanorod films on PET for photocatalytic disinfection of water. *J Adv Oxid Technol* 18(2):246–252. <https://doi.org/10.1515/jaots-2015-0210>
- Sapkota A, Anceno AJ, Baruah S, Shipin OV, Dutta J (2011) Zinc oxide nanorod mediated visible light photoinactivation of model microbes in water. *Nanotechnology* 22(21):215703. <https://doi.org/10.1088/0957-4484/22/21/215703>
- Shankar K et al (2009) Recent advances in the use of TiO₂ nanotube and nanowire arrays for oxidative photoelectrochemistry. *J Phys Chem C* 113(16):6327–6359. <https://doi.org/10.1021/jp809385x>
- Shi H et al (2014) Visible-light-driven photocatalytic inactivation of *E. coli* by Ag/AgX-CNTs (X = Cl, Br, I) plasmonic photocatalysts: bacterial performance and deactivation mechanism. *Appl Catal B Environ* 158:301–307. <https://doi.org/10.1016/j.apcatb.2014.04.033>

- Shi J-W et al (2015) CdS quantum dots modified N-doped titania plates for the photocatalytic mineralization of diclofenac in water under visible light irradiation. *J Mol Catal A Chem* 399:79–85. <https://doi.org/10.1016/j.molcata.2015.01.030>
- Smith SC, Rodrigues DF (2015) Carbon-based nanomaterials for removal of chemical and biological contaminants from water: a review of mechanisms and applications. *Carbon* 91:122–143. <https://doi.org/10.1016/j.carbon.2015.04.043>
- Song X, Hu Y, Zheng M, Wei C (2016) Solvent-free in situ synthesis of g-C₃N₄/0 0 1 TiO₂ composite with enhanced UV-and visible-light photocatalytic activity for NO oxidation. *Appl Catal B Environ* 182:587–597. <https://doi.org/10.1016/j.apcatb.2015.10.007>
- Spuhler D, Rengifo-Herrera JA, Pulgarin C (2010) The effect of Fe²⁺, Fe³⁺, H₂O₂, and the photo-Fenton reagent at near-neutral pH on the solar disinfection (SODIS) at low temperatures of water containing *Escherichia coli* K12. *Appl Catal B Environ* 96(1–2):126–141. <https://doi.org/10.1016/j.apcatb.2010.02.010>
- Sun H et al (2014) A systematic approach to an in-depth understanding of photoelectrocatalytic bacterial inactivation mechanisms by tracking the decomposed building blocks. *Environ Sci Technol* 48(16):9412–9419. <https://doi.org/10.1021/es502471h>
- Sun L et al (2017) Antibacterial activity of graphene oxide/g-C₃N₄ composite through photocatalytic disinfection under visible light. *ACS Sustain Chem Eng* 5(10):8693–8701. <https://doi.org/10.1021/acssuschemeng.7b01431>
- Supply WUJW, Programme SM (2014) Progress on drinking water and sanitation: 2014 update. World Health Organization. https://www.who.int/water_sanitation_health/publications/2014/jmp-report/en/
- Tang Z-R, Li F, Zhang Y, Fu X, Xu Y-J (2011) Composites of titanate nanotube and carbon nanotube as photocatalyst with high mineralization ratio for gas-phase degradation of volatile aromatic pollutants. *J Phys Chem C* 115(16):7880–7886. <https://doi.org/10.1021/jp1115838>
- Tsydenova O, Batoev V, Batoeva A (2015) Solar-enhanced advanced oxidation processes for water treatment: simultaneous removal of pathogens and chemical pollutants. *Int J Environ Res Public Health* 12(8):9542–9561. <https://doi.org/10.3390/ijerph120809542>
- Umezawa N, Janotti A (2016) Controlling the electronic structures of perovskite oxynitrides and their solid solutions for photocatalysis. *ChemSusChem* 9(9):1027–1031. <https://doi.org/10.1002/cssc.201600040>
- Vaiano V et al (2016) Photocatalytic removal of patent blue V dye on Au-TiO₂ and Pt-TiO₂ catalysts. *Appl Catal B Environ* 188:134–146. <https://doi.org/10.1016/j.apcatb.2016.02.001>
- Wang G, Peng Q, Li Y (2011a) Lanthanide-doped nanocrystals: synthesis, optical-magnetic properties, and applications. *Acc Chem Res* 44(5):322–332. <https://doi.org/10.1021/ar100129p>
- Wang W et al (2011b) Comparative study of visible-light-driven photocatalytic mechanisms of dye decolorization and bacterial disinfection by B–Ni-codoped TiO₂ microspheres: the role of different reactive species. *Appl Catal B Environ* 108:108–116. <https://doi.org/10.1016/j.apcatb.2011.08.015>
- Wang W et al (2012) Visible-light-driven photocatalytic inactivation of *E. coli* K-12 by bismuth vanadate nanotubes: bactericidal performance and mechanism. *Environ Sci Technol* 46(8):4599–4606. <https://doi.org/10.1021/es2042977>
- Wang W, Yu JC, Xia D, Wong PK, Li Y (2013a) Graphene and g-C₃N₄ nanosheets cowrapped elemental α-sulfur as a novel metal-free heterojunction photocatalyst for bacterial inactivation under visible-light. *Environ Sci Technol* 47(15):8724–8732. <https://doi.org/10.1021/es4013504>
- Wang WJ, Yu JC, Wong PK (2013b) Photocatalysts for solar-induced water disinfection: new developments and opportunities, materials science forum. *Trans Tech Publ*:63–89. <https://doi.org/10.4028/www.scientific.net/MSF.734.63>
- Wang S et al (2014) Controllable synthesis of nanotube-type graphitic C₃N₄ and their visible-light photocatalytic and fluorescent properties. *J Mater Chem A* 2(9):2885–2890. <https://doi.org/10.1039/C3TA14576J>

- Wang W et al (2015a) Monoclinic dibismuth tetraoxide: a new visible-light-driven photocatalyst for environmental remediation. *Appl Catal B Environ* 176:444–453. <https://doi.org/10.1016/j.apcatb.2015.04.026>
- Wang W, Huang G, Jimmy CY, Wong PK (2015b) Advances in photocatalytic disinfection of bacteria: development of photocatalysts and mechanisms. *J Environ Sci* 34:232–247. <https://doi.org/10.1016/j.jes.2015.05.003>
- Wang L et al (2016) Iron oxide nanowires from bacteria biofilm as an efficient visible-light magnetic photocatalyst. *ACS Appl Mater Interfaces* 8(31):20110–20119. <https://doi.org/10.1021/acsami.6b06486>
- Wang K, Zhang G, Li J, Li Y, Wu X (2017a) 0D/2D Z-scheme heterojunctions of bismuth tantalate quantum dots/ultrathin g-C₃N₄ nanosheets for highly efficient visible-light photocatalytic degradation of antibiotics. *ACS Appl Mater Interfaces* 9(50):43704–43715. <https://doi.org/10.1021/acsami.7b14275>
- Wang W et al (2017b) Earth-abundant Ni₂P/g-C₃N₄ lamellar nanohybrids for enhanced photocatalytic hydrogen evolution and bacterial inactivation under visible light irradiation. *Appl Catal B Environ* 217:570–580. <https://doi.org/10.1016/j.apcatb.2017.06.027>
- Wang W et al (2017c) Photocatalytic nanomaterials for solar-driven bacterial inactivation: recent progress and challenges. *Environ Sci Nano* 4(4):782–799. <https://doi.org/10.1039/C7EN00063D>
- Wei C et al (1994) Bactericidal activity of TiO₂ photocatalyst in aqueous media: toward a solar-assisted water disinfection system. *Environ Sci Technol* 28(5):934–938. <https://doi.org/10.1021/es00054a027>
- Wei H et al (2017) Mesoporous TiO₂/g-C₃N₄ microspheres with enhanced visible-light photocatalytic activity. *J Phys Chem C* 121(40):22114–22122. <https://doi.org/10.1021/acs.jpcc.7b06493>
- Weng B, Liu S, Tang Z-R, Xu Y-J (2014) One-dimensional nanostructure-based materials for versatile photocatalytic applications. *RSC Adv* 4(25):12685–12700. <https://doi.org/10.1039/C3RA47910B>
- WHO/UNICEF (2012) Progress on drinking water and sanitation. Monitoring Programme update, WHO report, pp 1–58. https://www.who.int/water_sanitation_health/publications/jmp_report-2012/en/
- Wu N et al (2010) Shape-enhanced photocatalytic activity of single-crystalline anatase TiO₂ (101) nanobelts. *J Am Chem Soc* 132(19):6679–6685. <https://doi.org/10.1021/ja909456f>
- Wu D et al (2015) Visible-light-driven BiOBr nanosheets for highly facet-dependent photocatalytic inactivation of *Escherichia coli*. *J Mater Chem A* 3(29):15148–15155. <https://doi.org/10.1039/C5TA02757H>
- Wu D et al (2016a) Alkali-induced in situ fabrication of Bi₂O₄-decorated BiOBr nanosheets with excellent photocatalytic performance. *J Phys Chem C* 120(14):7715–7727. <https://doi.org/10.1021/acs.jpcc.6b02365>
- Wu D et al (2016b) Boron-doped BiOBr nanosheets with enhanced photocatalytic inactivation of *Escherichia coli*. *Appl Catal B Environ* 192:35–45. <https://doi.org/10.1016/j.apcatb.2016.03.046>
- Wu D et al (2017) Influence of photoinduced Bi-related self-doping on the photocatalytic activity of BiOBr nanosheets. *Appl Surf Sci* 391:516–524. <https://doi.org/10.1016/j.apsusc.2016.05.144>
- Xia D et al (2013) A recyclable mineral catalyst for visible-light-driven photocatalytic inactivation of bacteria: natural magnetic sphalerite. *Environ Sci Technol* 47(19):11166–11173. <https://doi.org/10.1021/es402170b>
- Xia G, Lu Y, Xu H (2015) Electrogeneration of hydrogen peroxide for electro-Fenton via oxygen reduction using polyacrylonitrile-based carbon fiber brush cathode. *Electrochim Acta* 158:390–396. <https://doi.org/10.1016/j.electacta.2015.01.102>
- Xia D et al (2015a) Visible-light-driven inactivation of *Escherichia coli* K-12 over thermal treated natural pyrrhotite. *Appl Catal B Environ* 176:749–756. <https://doi.org/10.1016/j.apcatb.2015.04.024>

- Xia D et al (2015b) Red phosphorus: an earth-abundant elemental photocatalyst for “green” bacterial inactivation under visible light. *Environ Sci Technol* 49(10):6264–6273. <https://doi.org/10.1021/acs.est.5b00531>
- Xia D et al (2017) Enhanced photocatalytic inactivation of *Escherichia coli* by a novel Z-scheme g-C₃N₄/m-Bi₂O₄ hybrid photocatalyst under visible light: the role of reactive oxygen species. *Appl Catal B Environ* 214:23–33. <https://doi.org/10.1016/j.apcatb.2017.05.035>
- Xie Z et al (2015) Enhanced photoelectrochemical and photocatalytic performance of TiO₂ nanorod arrays/CdS quantum dots by coating TiO₂ through atomic layer deposition. *Nano Energy* 11:400–408. <https://doi.org/10.1016/j.nanoen.2014.11.024>
- Xing X, Wang H, Hu C, Liu L (2018) Effects of phosphate-enhanced ozone/biofiltration on the formation of disinfection byproducts and the occurrence of opportunistic pathogens in drinking water distribution systems. *Water Res* 139:168–176. <https://doi.org/10.1016/j.watres.2018.03.073>
- Yang H, Mei S, Zhao L, Zhang Y (2016a) Effects of ultraviolet irradiation on the antibacterial activity of TiO₂ nanotubes. *Nanosci Nanotechnol Lett* 8(6):498–504. <https://doi.org/10.1166/nl.2016.2135>
- Yang X et al (2016b) Facile fabrication of acidified g-C₃N₄/g-C₃N₄ hybrids with enhanced photocatalysis performance under visible light irradiation. *Appl Catal B Environ* 193:22–35. <https://doi.org/10.1016/j.apcatb.2016.03.060>
- Ye L, Su Y, Jin X, Xie H, Zhang C (2014) Recent advances in BiOX (X= Cl, Br and I) photocatalysts: synthesis, modification, facet effects, and mechanisms. *Environ Sci Nano* 1(2):90–112. <https://doi.org/10.1039/C3EN00098B>
- Yu J, Xiong J, Cheng B, Liu S (2005) Fabrication and characterization of Ag–TiO₂ multiphase nanocomposite thin films with enhanced photocatalytic activity. *Appl Catal B Environ* 60(3–4):211–221. <https://doi.org/10.1016/j.apcatb.2005.03.009>
- Zhang L, Chen D, Jiao X (2006) Monoclinic structured BiVO₄ nanosheets: hydrothermal preparation, formation mechanism, and coloristic and photocatalytic properties. *J Phys Chem B* 110(6):2668–2673. <https://doi.org/10.1021/jp056367d>
- Zhang X, Du AJ, Lee P, Sun DD, Leckie JO (2008) TiO₂ nanowire membrane for concurrent filtration and photocatalytic oxidation of humic acid in water. *J Membr Sci* 313(1–2):44–51. <https://doi.org/10.1016/j.memsci.2007.12.045>
- Zhang H, Yang Y, Zhou Z, Zhao Y, Liu L (2014) Enhanced photocatalytic properties in BiOBr nanosheets with dominantly exposed (102) facets. *J Phys Chem C* 118(26):14662–14669. <https://doi.org/10.1021/jp5035079>
- Zhang Q et al (2016a) The dependence of photocatalytic activity on the selective and nonselective deposition of noble metal cocatalysts on the facets of rutile TiO₂. *J Catal* 337:36–44. <https://doi.org/10.1016/j.jcat.2016.01.001>
- Zhang Q, Luo M, Sun Y-P, Liu Y, Cao A (2016b) Efficient Z-scheme photocatalyst from the simultaneous decoration of In₂S₃ nanosheets and WO₃ nanorods on graphene sheets. *Nanotechnology* 27(28):285602. <https://doi.org/10.1088/0957-4484/27/28/285602>
- Zhang Z, Jiang D, Li D, He M, Chen M (2016c) Construction of SnNb₂O₆ nanosheet/g-C₃N₄ nanosheet two-dimensional heterostructures with improved photocatalytic activity: synergistic effect and mechanism insight. *Appl Catal B Environ* 183:113–123. <https://doi.org/10.1016/j.apcatb.2015.10.022>
- Zhang L, Shi Y, Wang L, Hu C (2018) AgBr-wrapped Ag chelated on nitrogen-doped reduced graphene oxide for water purification under visible light. *Appl Catal B Environ* 220:118–125. <https://doi.org/10.1016/j.apcatb.2017.08.038>
- Zhao Z et al (2016) Noble metal-free Bi nanoparticles supported on TiO₂ with plasmon-enhanced visible light photocatalytic air purification. *Environ Sci Nano* 3(6):1306–1317. <https://doi.org/10.1039/C6EN00341A>
- Zhou Q, Fu M-L, Yuan B-L, Cui H-J, Shi J-W (2011) Assembly, characterization, and photocatalytic activities of TiO₂ nanotubes/CdS quantum dots nanocomposites. *J Nanopart Res* 13(12):6661–6672. <https://doi.org/10.1007/s11051-011-0573-y>

- Zhou P, Yu J, Jaroniec M (2014) All-solid-state Z-scheme photocatalytic systems. *Adv Mater* 26 (29):4920–4935. <https://doi.org/10.1002/adma.201400288>
- Zhuo S, Shao M, Lee S-T (2012) Upconversion and downconversion fluorescent graphene quantum dots: ultrasonic preparation and photocatalysis. *ACS Nano* 6(2):1059–1064. <https://doi.org/10.1021/nn2040395>
- Zhu Z, Cai H, Sun DW (2018) Titanium dioxide (TiO₂) photocatalysis technology for nonthermal inactivation of microorganisms in foods. *Trends in Food Science & Technology* 75:23–35

Chapter 8

Role of Membranes in Wastewater Treatment



Ashish Kapoor, Sivasamy Balasubramanian, Edward Kavitha, Elangovan Poonguzhali, and Sivaraman Prabhakar

Contents

| | | |
|-------|--|-----|
| 8.1 | Introduction | 249 |
| 8.2 | Membranes and Membrane Configuration | 250 |
| 8.2.1 | Membrane Preparation | 250 |
| 8.2.2 | Membrane Configuration | 252 |
| 8.3 | Membrane Processes | 255 |
| 8.3.1 | Principle of Membrane Separation | 255 |
| 8.3.2 | Pressure-Driven Membrane Processes | 256 |
| 8.3.3 | Electro-membrane Processes | 257 |
| 8.3.4 | Other Membrane Processes | 259 |
| 8.4 | Application of Membrane Processes in Water Treatment | 261 |
| 8.4.1 | Pressure-Driven Processes | 262 |
| 8.4.2 | Electro-membrane Process Applications | 266 |
| 8.4.3 | Membrane Distillation | 267 |
| 8.4.4 | Ultrafiltration | 268 |
| 8.4.5 | Membrane Contactors | 269 |
| 8.4.6 | Forward Osmosis | 272 |
| 8.4.7 | Diffusion Dialysis | 272 |
| 8.4.8 | Synergism of Different Membrane Processes in Water Treatment | 273 |
| 8.4.9 | Membrane Processes for Point-of-Use Applications | 275 |
| 8.5 | Future Outlook and Prospects | 275 |
| | References | 276 |

Abstract Demand for water is on the rise as population and human activities increase including industries and agriculture. Freshwater resources have a skewed distribution besides being inadequate to meet the demands. Even though actual water consumed by humans and their activities is much less, large quantum of water is used for peripheral activities and discharged into the environment as wastewater. Hence, to meet the demand for water and to protect the environment, wastewater

A. Kapoor · S. Balasubramanian · E. Kavitha · E. Poonguzhali · S. Prabhakar (✉)
Department of Chemical Engineering, SRM Institute of Science and Technology,
Kattankulathur, Tamil Nadu, India

treatment is necessary. Conventional methods of treatment are cumbersome requiring large footprints, use of chemicals, and subsequent management of sludge generated.

Membrane is a barrier which helps in the preferential transport of some species under a potential gradient, be it mechanical, chemical, or electrical. Membranes can be made from different materials, in different forms, and with different morphologies. Membranes can be porous or nonporous, charged or neutral, and solid or liquid. Because of its flexibility, a variety of membrane processes has been developed and is being used to mitigate many industrial challenges. Membrane processes used in wastewater treatment are ambient temperature processes with no phase change and are rate-governed. The chemical requirements are significantly less compared to conventional processes leading to less sludge production.

An overview of different membrane processes motivated by pressure, concentration, and thermal and electrical gradients is discussed in the context of mitigating water stress situations. The technologies discussed include desalination, water recovery, and recycle and removal of toxic contaminants from wastewater streams including the latest developments in application areas. Utility of membrane contactors in improving the performance of the conventional separation processes is highlighted through membrane solvent extraction, supported liquid membranes, and membrane bioreactors. The potential applications of forward osmosis in water treatment are also indicated.

The roles of electrically driven membrane processes such as electrodialysis, bipolar membrane-based electrodialysis, electrodialysis reversal, and electro-deionization in water treatment are explained along with its limitations and challenges. The role of membranes in providing safe drinking water at the point of use has also been highlighted.

The prospects of combining two or more membrane processes like nanofiltration, reverse osmosis, and electrodialysis in water and wastewater treatment are highlighted. With increasing environmental consciousness and the need to recover value from waste, the concept of decentralization of wastewater treatment is proposed wherein the source of waste is isolated, as membrane processes can operate on any scale.

In the future, environmental protection is going to become a critical concern, and the best strategy is to recover everything in the wastewater stream as value toward realizing the concept of "Waste is unutilized Wealth." The best way to achieve this is by isolating the individual wastewater streams as produced and treating them at the source without mixing with other waste streams. In this context, membrane processes have varieties and are economically viable for different capacities. Since the various streams are isolated, both the product and retentate streams can be recycled, thus leading not only to recovering value but also zero discharge to the environment. This chapter aims at providing necessary background knowledge to select a suitable scheme for the treatment of the specific wastewater including point-of-use devices and value recovery.

Keywords Membrane · Porous · Nonporous · Pressure-driven · Thermal gradient · Electrically driven · Reverse osmosis · Ultrafiltration · Nanofiltration · Forward osmosis · Size enhanced ultrafiltration · Electrodialysis · Liquid membrane · Hybrid membrane processes · Water recovery and recycle · Wastewater treatment · Membrane bioreactors · Membrane solvent extraction · Value recovery · Point-of-use device

8.1 Introduction

In the current scenario, water has become a scarce commodity compared to its free availability as a natural resource. The transformation is basically triggered by increase in population and the consequent growth in industries, agriculture, and lifestyle conveniences. Further, the supplies have dwindled due to a variety of reasons including climate change resulting in skewed rainfall pattern, inefficient use of water, pollution, overexploitation of groundwater, etc. This calls for an approach whereby demand is decreased and supply is increased. Demand can be reduced by improving water use efficiency, economizing specific consumption on various products and activities, quality use linkages, and recovery and reuse of water from spent streams. Supply augmentation can be achieved by improving the collection and storage efficiencies of natural resources including rain harvesting, linking the different sources of water to guard against avoidable overflows, and using desalination technologies in coastal areas.

Water being a universal solvent carries along with a variety of chemical species, essential minerals, and toxic components both in dissolved and suspended states. It is necessary that humans get safe water and the industries get water as per their requirement. Since most of the sources are contaminated physically, chemically, and biologically, water treatment is necessary. The contaminants of natural water can be either geo-genic or anthropogenic in origin. The former depends on the local geology, while the latter depends on human activities surrounding the water source. Conventional method of water treatment is primarily *point-of-source* treatment requiring chemicals and large footprint area. The treatment process is also quite sensitive to operating parameters such as pH, efficiency of mixing, and dosage of chemicals and generates significant amount of sludge for disposal.

The early 1980s witnessed the induction of large-scale commercial desalination plants based on reverse osmosis, and the subsequent phenomenal growth of membrane desalination over the conventional thermal processes has triggered the development of membrane applications in other areas of water treatment. The entire water treatment scenario has changed consequently with reference to time, efforts, and costs for both domestic and industrial uses. Since the late 1990s, a variety of membrane processes have been developed to suit different streams of water requiring much less footprint area and chemical requirement. These membrane processes

operate on different energy gradients leading to separation of pure water (Schrotter et al. 2010); specific removal of contaminants such as heavy metals (Qudais and Moussa 2004), dyes (Karisma et al. 2017), and microorganisms; production of sterile and safe drinking water both as *point-of-use* and *point-of-source* devices; and splitting of salts to produce parent acid and base (Reig et al. 2016). Membrane processes, using *porous membranes*, operate on physical or physicochemical mechanisms and are mostly rate-governed ambient temperature operation without phase change. Being modular in nature capacity addition is simple, and the economics is not sensitive to capacity.

8.2 Membranes and Membrane Configuration

Membranes can be understood as physical barriers which can selectively allow permeation of particular species, under an appropriate gradient, when in contact with a solution. The separation mechanism can be physical, physicochemical, or chemical in nature independently or severally. The membrane materials can be natural or synthetic products, organic or inorganic. The commercial membrane processes use mostly organic membranes made up of synthetic polymer materials and operate under pressure, concentration, or electrical potential gradient.

8.2.1 Membrane Preparation

Membranes can be in any state, solid, liquid, or gas. As of now, the gaseous membranes are not known, while the liquid membranes are used in small scale, high value separations (K. K. Bhatluri et al. 2014). All the commercial membranes used otherwise are solid matrices. Depending on the mechanism of separation, the membranes used can be porous or nonporous.

Membranes can be prepared using different techniques involving *phase inversion*, *stretching*, *sintering*, *track etching*, and *electrospinning* (Zare and Kargari 2018). *Phase inversion* technique involves the dissolution of the polymer in a solvent and precipitating the same by the release of the solvent from the matrix. Any of the techniques such as evaporation-induced phase separation, non-solvent-induced phase separation, vapor-induced phase separation, and thermally induced phase separation (Ulbricht 2006) can be used depending on the nature of solvent. In evaporation-induced phase separation, the polymer is dissolved in a volatile solvent and cast as a film. The solvent is then allowed to evaporate under controlled conditions. The solvent is withdrawn from the cast sheet by immersing it in a non-solvent medium in the case of non-solvent-induced phase separation. In vapor-induced phase separation, non-solvent vapor is kept in contact with the cast film, allowing the solvent to saturate the non-solvent present in the vapor phase and enabling precipitation of the membrane. The thermal energy enables evaporation of

the solvent, leading to the formation of membranes in thermally induced phase separation. Among these techniques, non-solvent-induced phase separation and thermally induced phase separation are mostly used for the production of commercial membranes (Liu et al. 2011; Lalia et al. 2013). In *stretching*, the polymer is heated above the melting point and then extruded into a thin film, which is subsequently stretched to form a porous matrix (Sadeghi et al. 2007). This technique does not need any solvent. In *sintering*, the polymer powder is pressed into a thin film and is sintered at a temperature just below the melting point. *Electrospinning* is a developing technology which produces nano-fibers (Ray et al. 2016) under the application of an electric field. *Track-etched* membranes are prepared by bombarding a thin nonporous film with accelerated heavy ions, followed by etching (Apel 2001).

Membranes used in water treatment are required to exhibit good solute rejection and water-flux characteristics. Accordingly, the membranes should have less resistance for water flow without compromise on the strength of the membrane to withstand the operating conditions. Reverse osmosis and nanofiltration membranes by design have pores less than 2 nm and have to withstand operating pressures ranging from 20 to 70 bars. In order to achieve these properties, membranes are prepared in a two-step process. First, a porous support layer is prepared by phase inversion, and then a very thin active layer is formed on its surface by in situ polymerization of two reactive monomers (Petersen 1993).

Phase inversion techniques allow the preparation of porous membranes with different ranges of pore-size distribution by varying the dope composition, the casting conditions, and the posttreatment of the membranes. The average pore size can be controlled by the variation of size and quantum of *pore-inducing additives* in the membrane dope solution. The pore formation in the phase inversion technique is a stochastic process, and hence, there would be a distribution of pore sizes, which is assumed to follow *normal distribution*. On the other hand, stretching leads to somewhat uniform pore size. Track etching gives nearly uniform pore size, but the pore density would be very low, and the cost is very high. Charged membranes are nonporous and prepared using resins mixed with some binding materials and cast into films (Drioli and Giorno 2010).

Depending on the chemicals used and conditions of casting, membranes can be prepared with hydrophilic or hydrophobic characteristics. The membrane processes relevant to water treatment are pressure-driven ultrafiltration, nanofiltration and reverse osmosis, concentration-driven forward osmosis and diffusion dialysis, thermally driven membrane distillation and electrically driven electrodialysis, electro-deionization, and bipolar membrane electrodialysis. Capacitive deionization is also an electrically driven desalination technique but without the use of membranes and is not to be discussed further.

Membranes used in pressure-driven membrane processes are on the hydrophilic side. Reverse osmosis and nanofiltration membranes operate at high pressures and are asymmetric in nature to reduce the resistance for water flow. Electrodialysis and bipolar membrane use nonporous charged membranes and remove ions from solution. Forward osmosis and diffusion dialysis are passive processes using neutral

porous and nonporous charged membrane, respectively. Membrane distillation is the process where the hydrophobic membranes are used for the recovery of water.

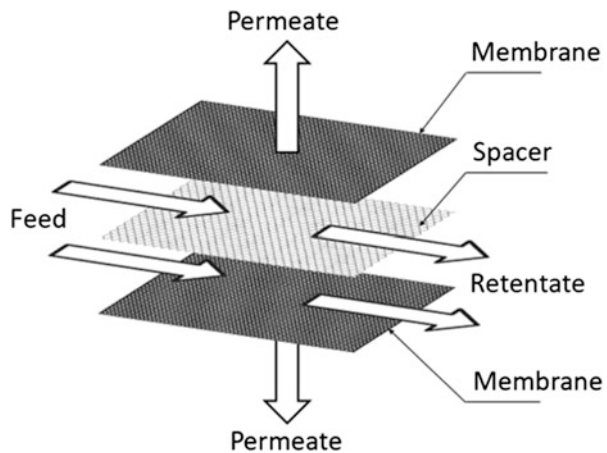
Membrane contactors are a class of membrane products, which are used to carry out conventional separation techniques by providing large interfacial contact area without the bother of mixing the contacting phases. These are porous inert membrane matrices with potential application in the removal of pollutants from water. Membrane bioreactor, which is extensively used in the treatment of wastewater, is a contactor between the microorganisms and waste stream. Further applications include membrane solvent extraction, gas absorption, etc.

8.2.2 Membrane Configuration

The commercial membranes are prepared as either flat sheets or cylindrical ones with different diameters. The membranes so prepared are configured in different geometries such as plate and frame, spiral, tubular, and hollow fiber. Each of these configurations has their unique characteristics and suited for certain environment. A *membrane element* describes the membrane housed in a particular configuration with inlet and outlets as a single unit. These membrane elements can be connected in series to assemble a *membrane module*. For large capacity plants, the modules can be connected in series or in parallel depending on the design objectives. Selection of a configuration depends on the compactness, hydrodynamic characteristics, ease of cleaning and maintenance, and economics. Plate and frame and spiral elements are prepared from flat sheets, while tubular and hollow fiber elements are based on cylindrical membranes.

Plate and Frame Flat sheets are used directly in a plate and frame configuration (Fig. 8.1). Membranes supported by nonwoven fabric are placed on either side of the pressure plate and sealed to the plate with gaskets, glue, o-rings, etc., with the active

Fig. 8.1 Plate and frame module concept. Water permeating the membrane is transported to the channels provided on the plates to the collection tube. (Modified from Mulder 1996)



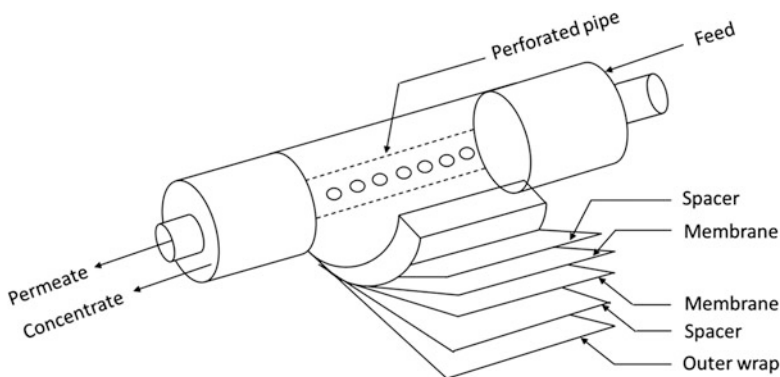


Fig. 8.2 Spiral element configuration. Assembly of membranes and feed spacer wound over a perforated central pipe is illustrated

surface of the membrane facing the plate surface. The pores provided by design in the plate allow the feed to be in contact with the membrane. The water permeating the membrane is transported via the nonwoven fabric to the channels provided on the plates and then to the collection tube. Many such plates assembled one over the other constitute a membrane module. The end plates would have only one membrane and a blinder plate. For example, a 50-plate configuration can hold 98 membrane sheets with the outer side of the end plates sealed. The sheets can be of any shape, circular, square, or hexagonal, depending on the pressure plate configuration (Pal 2017).

Spiral Element Alternately, a pair of long flat sheets can be made into an envelope with active surface membrane facing out and sealing three sides leaving one of the sides (breadth) open. Through the open side, a nonwoven fabric is inserted into the envelope covering the entire area. Many such envelopes are made. After inserting the feed spacer between the envelopes, the envelopes are wound over a porous central tube. The wound envelope is secured by using adhesive tape or fiber-reinforced plastic. The spiral element (Fig. 8.2) so prepared can be inserted in a pressure vessel.

Tubular Element The membranes are cast in a tubular form, inserted into porous support tubes, and assembled similar to a shell and tube heat exchanger (Fig. 8.3). The inner diameter of the tubes can vary from 6 mm to 18 mm normally.

Hollow Fibers Hollow fibers can be prepared by any of the three techniques, namely, wet, dry, or melt spinning (Vandekar 2015), even though wet spinning is the most used technique. The dope containing the polymer, solvent, and additive is extruded into the non-solvent where the precipitation of the polymer occurs. The inner diameter of the membranes may vary from 0.5 mm to 1.5 mm and the outer diameters from 0.7 mm to 2.00 mm. After extruding, the fibers are bundled and sealed together on both the ends with an adhesive (without affecting the flow channels) and inserted into a pressure vessel (Fig. 8.4).

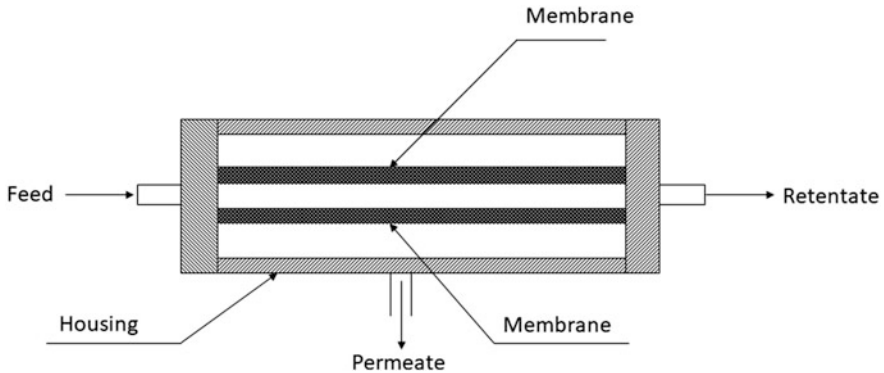


Fig. 8.3 Tubular element configuration. Tubular membranes are inserted into porous support tubes and assembled in shell and tube manner

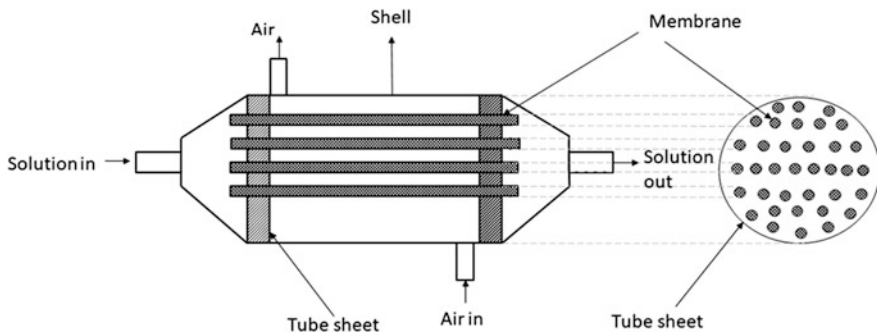


Fig. 8.4 Hollow fiber element. Hollow fiber elements are bundled and sealed together on each end of the module, making arrangements for inlets and outlets for shell and tube sides. (Modified from Mulder 1996)

The membranes can be made with different pore-size ranges normally designated in terms of molecular weight cutoff. Hollow fiber-based membrane elements with fiber dimensions around 100–150 microns were used for reverse osmosis applications. The use of hollow fine fiber for reverse osmosis is almost discontinued due to operational and maintenance problems. After the unsatisfactory performance of polyamide-based hollow fiber elements, cellulose triacetate membrane-based hollow fine fibers were assessed at some field reverse osmosis plants, but further progress is not reported. However, hollow fine fiber configuration is the most popular for many ultrafiltration applications. Comparative characteristics of the membrane module configurations can be found in Table 8.1.

Table 8.1 Comparison of membrane module configurations

| | Tubular | Plate and frame | Spiral | Hollow fiber | Characteristics |
|-------------------------------|---------------|--|---|---|---|
| Compactness (packing density) | Least compact | Better than tubular | Fairly compact but less than hollow fiber | Maximum compact | Relates to foot print area requirement |
| Flow regime | Turbulent | Promoted turbulence | Turbulent promoters | Laminar | The more the turbulence, the less will be the fouling tendency |
| Fouling tendency | Least | Less | High | Very high | |
| Cleaning and maintenance | Easy | Easy but slightly cumbersome | Difficult | Very difficult | Individual membranes can be removed in tubular and plate and frame. In spiral and hollow fiber, whole element requires to be replaced |
| Application areas | Food industry | Food industry/ships for drinking water | Desalination/wastewater treatment | Pretreatment for desalination As membrane contactors | Desalination – mostly spiral Filtration – hollow fiber Food industry – tubular/plate and frame |

Bhattacharjee et al. (2017) and Belfort (1988)

8.3 Membrane Processes

The membrane processes can be divided into two categories: passive and active. Passive processes do not require external energy for carrying out the separation, while the active processes require an external source of energy to bring out the separation. Passive processes include forward osmosis, diffusion dialysis, hemodialysis, membrane solvent extraction, supported liquid membranes, etc., while the active processes include reverse osmosis, electrodialysis, ultrafiltration, nanofiltration, and membrane distillation. Membrane is a barrier, and its surface controls the separation excepting in cases where the separation is diffusion controlled like membrane solvent extraction (in such cases, membrane provides a large interfacial contact area to enhance the separation).

8.3.1 Principle of Membrane Separation

One can visualize the membrane separation as described in the diagram (Fig. 8.5).

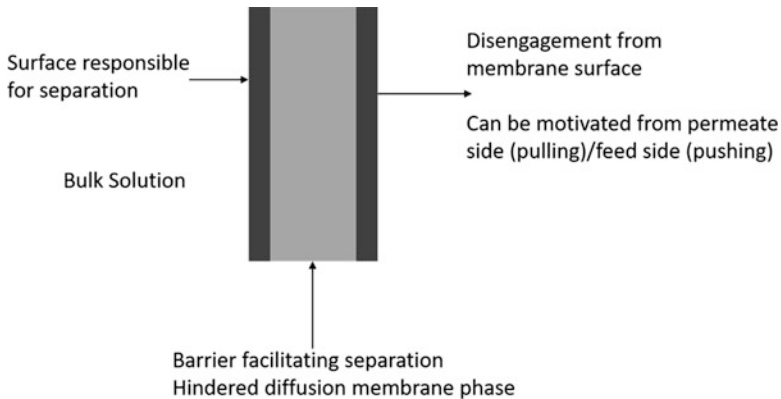


Fig. 8.5 Principle of membrane separation. Membrane serves as a barrier and facilitates separation of desired components

From the bulk, the species present in the solution reach the active surface of the membrane (either by diffusion or forced convection), where the separation occurs because of the specific property of the membrane. The species which is not allowed to pass through accumulates on the boundary surface or diffuses back to the bulk. The species permeating through the membrane flows through the capillary pores (in case of porous membrane) or diffuse through the membrane (in case of nonporous membrane) and gets disengaged from the other side of the membrane. The force for disengagement can be a pulling force like application of vacuum on the permeate side or lower concentration of the permeating species. Alternately, it can be a pushing force like hydrostatic pressure or higher vapor pressure (induced by thermal energy) on the feed side. The preferential separation at the membrane surface can be physical (size exclusion), physicochemical like sorption, chemical (ion exchange), or dissolution (chemical affinity) in the matrix.

The membrane processes are normally classified based on the driving force under which the separation occurs such as pressure-driven, concentration-driven, thermally driven, and electrically driven. Pressure-driven processes which include reverse osmosis, nanofiltration, ultrafiltration, and microfiltration are the ones mostly used in water treatment. Recent developments in forward osmosis and membrane distillation are slowly becoming tools for water treatment.

8.3.2 Pressure-Driven Membrane Processes

The membranes used in pressure-driven processes are almost neutral membranes. Reverse osmosis and nanofiltration have pore sizes less than 2 nm and 1 nm, respectively, and the interaction between the species and membranes plays a role in the separation process. Reverse osmosis membranes have a surface which has a

balance of hydrophilic and hydrophobic character so that water alone can be preferentially sorbed onto its surface, and under the application of external pressure greater than the osmotic pressure. The sorbed water flows through the capillaries, thus effecting the separation of water from solution. Nanofiltration membranes are also similar to reverse osmosis membranes except that the pore sizes are slightly larger. These membranes may have slight positive or negative charge depending on the type of chemical treatment (Teixeira et al. 2005). In both the processes, hydrostatic pressure in excess of osmotic pressure of the boundary layer has to be applied for the removal of water from the solution. Since nanofiltration allows the permeation of monovalent solutes, the product water will have significant osmotic pressure compared to reverse osmosis permeate which is nearly pure. In view of this, for the same values of total dissolved solids (containing a mixture of ionic solutes), nanofiltration would require less applied pressure compared to reverse osmosis. When macromolecules like dyes are to be separated from a given solution, nanofiltration would be a better choice, as it would allow the solutes to permeate through the membrane retaining macromolecules. Both in reverse osmosis and nanofiltration, as the process proceeds, the feed solution becomes more and more concentrated resulting in rise of osmotic pressure and becomes susceptible for scaling, consequently limiting the percent separation (percent recovery). The inability to achieve total separation is one of the major limitations of nanofiltration and reverse osmosis.

Ultrafiltration whose pores are larger than nanofiltration operates based on size exclusion mechanism. The attractive features of the process are the flexibility to operate both in dead-end and cross flow mode and the backwash possibility. Unlike reverse osmosis and nanofiltration, osmotic pressure has no significant impact on the performance of ultrafiltration membranes affording the operation at very low pressures in the range of 1–5 bar. Table 8.2 presents the comparative aspects of pressure-driven membrane processes.

8.3.3 *Electro-membrane Processes*

Electro-membrane processes are performed under electrical potential gradient, where ions migrate from the solution toward the corresponding electrodes. Depending on the arrangement of the membranes, desired separation can be achieved. The processes include electrodialysis, electrodialysis reversal, electro-deionization, and electrodialysis with bipolar membrane.

Electrodialysis In electrodialysis (Campione et al. 2018), a number of pairs of cation and anion exchange membranes (cell pair) are arranged alternately in between two electrodes. Feed solution containing ionic solutes are fed parallelly between each pair of membranes (Fig. 8.6). When connected to power source, the ions (cations and anions) start moving in opposite direction toward their respective electrodes. During the migration, the cations pass through cationic membranes and

Table 8.2 Comparison of pressure-driven membrane processes

| Description | Microfiltration | Ultrafiltration | Nanofiltration | Reverse osmosis |
|--------------------------|---|--|---|--|
| Membrane characteristics | Porous | Porous marginally asymmetric | Porous with marginal surface charge | Porous |
| Pore-size range | >0.1 μm | 2 nm and 0.05 μm | 1–2 nm | 0.1–1.0 nm |
| Mechanism | Size (solid/liquid separation) | Size exclusion | Physicochemical + size exclusion | Physicochemical mechanism |
| Operating pressure | 0.5–2 bar | 1 and 10 bar | 5–20 bar | 7–80 bar (pressure > osmotic pressure) |
| Application areas | Industrial filtration systems | Sterilization of water, removal of colloids, microorganisms, etc. pretreatment for reverse osmosis | Water softening, separation of macromolecules from solutions | Desalination. Recovery and recycle of water |
| Process characteristics | Colloids and dissolved solids cannot be separated | Backwashing is possible, tolerant to chlorine. Also used as membrane contactors | Requires less pressure. Separation of multivalent contaminants possible. Constrained by recovery limitation | Constrained by recovery limitation. Disposal of membranes might be a problem in future |

Van der Bruggen et al. (2003)

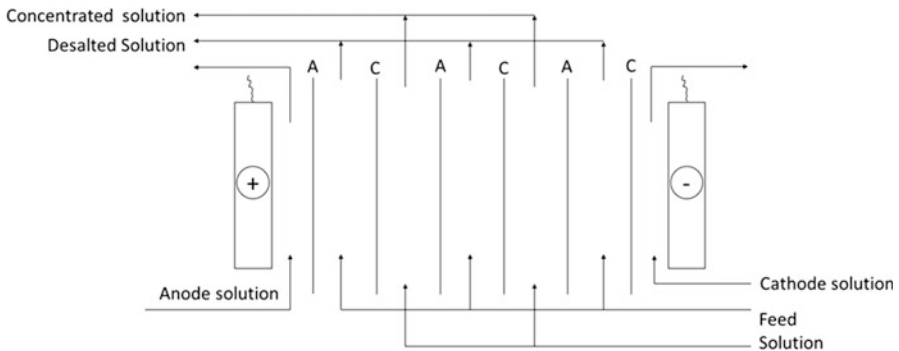


Fig. 8.6 Electrodialysis. Several pairs of cation and anion exchange membranes are arranged in alternate fashion between cathode and anode

are stopped by anionic membranes, and similarly, anions are stopped by cationic membranes since the direction of migration is fixed by the polarity of the electrodes. This results in the feed solution getting split into two streams (one dilute stream and

another concentrate stream) in alternate compartments. The diluent is the desalinated solution.

Electro-deionization This process is the modified version of electrodialysis (Nagel 2005) wherein ion exchange resins are filled in each compartment. The process is applicable to very low-salinity water (much less than 50 ppm). Upon application of the electrical potential, ions migrate and saturate the resins of alternate compartments. As the ionic concentration reduces, water splitting occurs leading to the migration of hydrogen and hydroxyl ions which regenerate the resins, thus avoiding the need for acid and alkali. This process is useful only at very low concentrations. Hence, it is used as a polishing step for the preparation of ultrapure water from reverse osmosis product.

Electrodialysis with Bipolar Membrane This is another modified version of electrodialysis where a bipolar membrane (anion and cation membrane joined together) is inserted between two pairs (each pair having one anion exchange and one cation exchange) of membranes, and as a result, the dissolved salt is converted to parent acid and base from the solution (Oztekin and Yazicigil 2007). Further studies have indicated the possibility of fractionation of the ionic species (Reig et al. 2016). These processes are still in the development stage particularly with reference to the membranes whose stability under the process conditions is a challenge.

8.3.4 Other Membrane Processes

Concentration-Driven Processes

Forward Osmosis All the concentration-driven processes are passive in nature. In forward osmosis, water flows through the membrane from the feed solution toward the draw solute motivated by the osmotic pressure difference through the semipermeable membrane. The draw solution gets diluted, but the ultimate osmotic pressure of the draw solution is always greater than the feed solution. A second step separation is required to get pure water as shown in Fig. 8.7.

Selection of draw solute, which can be separated by a simple process, is critical to the performance.

The challenges are the development of membranes with a good flux and a suitable draw solute from which water could be recovered. Recent development of aquaporin (Ma et al. 2012) membrane with a water channel to transport water is expected to trigger practical applications in many areas including wastewater treatment.

Diffusion Dialysis Diffusion dialysis describes the movement of ionic species through a charged membrane. The membrane can be anionic or cationic. Unlike electrodialysis, where both cationic and anionic membranes are used, diffusion dialysis requires only one of the two membranes. When an anion membrane is

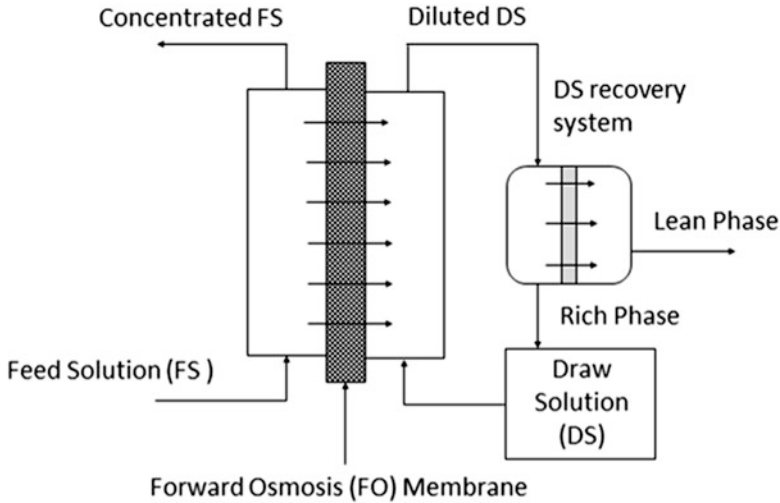


Fig. 8.7 Forward osmosis. Water flows from the feed solution toward the draw solute due to osmotic pressure difference through the semipermeable membrane. (Modified from Luo et al. 2014)

interfaced between the acid solution along with its metal salts (say hydrochloric acid) and water, chloride ions would diffuse through the anionic membrane. Hydrogen ions as well as metal ions would also tend to pass through the membrane to maintain *Donnan criteria* of electroneutrality (Luo et al. 2011). Since the mobility of hydrogen ions is higher compared to metal ions, hydrogen ions move faster, thus enabling the separation of acid from its solution. Based on the same philosophy, bases can also be separated from its salt solutions.

Thermally Driven Processes

Membrane distillation is a thermally driven membrane process which uses hydrophobic membranes (Fig. 8.8). When a hot stream of water is circulated through the membrane, the water vapor passes through the membrane pores and gets condensed on the permeate side by any of the techniques such as direct contact with a *cold water* stream, application of vacuum, air gap condensation, or sweep gas process (Wang and Chung 2015). This is a low-flux process with an ability to use waste heat. Liquid water which does not wet the membrane cannot permeate through the hydrophobic membrane up to a particular pressure commonly known as liquid entry pressure, whereas water vapor, which does not exhibit hydrophilicity, passes through the membrane. The critical points of concern are the maintenance of feed pressure less than the liquid entry pressure with reference to the membrane, the low flux, and the ease of recovering water. As the vapor produced is indirectly related to temperature, the possibility of increasing the flux is low unless some external source of thermal energy is provided.

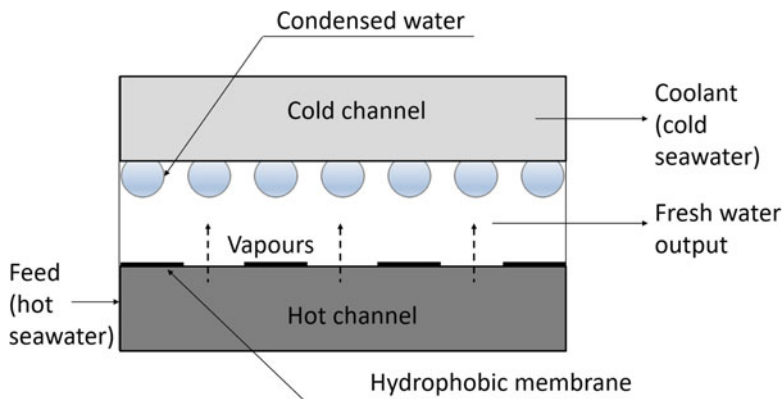


Fig. 8.8 Concept of membrane distillation. Thermally driven separation process allows vapors to pass through porous hydrophobic membrane that condense on the permeate side

Membrane Contactors

Membrane contactors are porous membrane devices mostly in the ultrafiltration range which provide interfacial contact between two phases to facilitate mass transfer. The driving force is concentration difference or chemical affinity. Membrane contactors provide very high contact area depending on the membrane configuration. Normally, hollow fiber/capillary membranes are used which offer about one to two orders of higher contact area per unit volume compared to conventional systems. As the two phases are separated by the membrane, problems related to intermixing of phases such as flooding and emulsification do not arise. Moreover, the choice of contacting fluids is not restricted by physical properties of the fluid such as density. The processes are less energy-intensive and mostly rate-governed and do not depend on the physical properties of the contacting phases. The limitations include additional mass transfer resistance and transmembrane pressure. Being compact and adaptable to different capacity operations, these contactors have potential use in replacing or supporting the conventional unit operations such as membrane bioreactors, liquid–liquid extraction, and gaseous separation (Drioli et al. 2011).

8.4 Application of Membrane Processes in Water Treatment

Membrane process made its foray into water treatment as reverse osmosis technology for desalination of brackish seawater. With the phenomenal success, the applications of reverse osmosis were extended to effluent streams for water recovery and recycle. Further innovations in membranes led to the development of membrane

distillation, forward osmosis, and nanofiltration which are impacting desalination, wastewater treatment, and other separation processes. Development of ultrafiltration initially as a pretreatment for reverse osmosis systems has found more utility as membrane bioreactors for the secondary treatment of wastewater and many other applications in the production of safe drinking water and sterile water. These membranes can be used as membrane contactors for carrying out conventional unit operations such as membrane solvent extraction, gas separation, and crystallization. Charged membranes have been demonstrated for processes such as electro-deionization and electrodialysis with bipolar membrane besides electrodialysis which are more environment-friendly and are capable of not only treating wastewater but also recovering value. The membranes available today separate either water or a few solutes from its solution. Consequently, all these processes have a role to play in the water treatment.

8.4.1 Pressure-Driven Processes

Applications of Reverse Osmosis

Desalination Reverse osmosis application for seawater desalination has recorded a tremendous growth with the developments of membranes (Yang et al. 2018), energy recovery devices (Kadai and Bosleman 2018), and rugged pretreatment systems. A state-of-the-art review published (Qasim et al. 2019) recently recounts the various developments taken place over the last few decades. The present specific energy consumption for seawater desalination is reported to be around 2.5–4 kWh/m³ (Voutchkov 2018; Karabelas et al. 2018). The advent of ultrafiltration membranes as a pretreatment system has contributed to the improved design with higher specific recoveries for the membrane element. Even though desalination systems can be designed using any of the four configurations, spiral configuration is extensively used in large-scale installations. Hollow fiber configuration was used in the initial period but later discontinued due to practical problems with reference to maintenance. Even though the first demonstrated reverse osmosis plant was in tubular configuration, it is not the preferred configuration in many applications being the least compact configuration. Plate and frame modules are used for small-capacity desalination systems particularly for seawater desalination in ships where constraints of space, head room, and inventory-carrying capacity exist.

A membrane element is the basic unit which can be assembled in series. A number of spiral membrane elements (not more than seven) assembled in a pressure vessel is called a module. When feedwater flows through the module, two streams emerge: one concentrated stream and the other permeate stream normally designated as “product.” The performance parameters are solute rejection, recovery, product water (permeate) flux, and module pressure drop. Solute rejection is defined as the fraction of the solutes, which is retained in the feed side (concentrate) and is mathematically represented as follows:

Solute rejection = (feed concentration – permeate concentration)/feed concentration and is more often expressed as percent.

Recovery refers to the fraction of water from the feed recovered as desalinated water, and it is mathematically represented by:

Recovery = product (permeate) rate/feed rate. It is also expressed as percent.

Product (permeate) water flux is defined as the water produced per unit area per unit time. Since the membrane area is fixed in an element and hence in a module, sometimes the flux is reported as cubic meters/element.

Module pressure drop indicates the extent of scaling/fouling. Initially, the pressure drop would be minimum but increases with time. Cleaning of the membrane modules would reduce the pressure drop.

Seawater Reverse Osmosis Desalination Reverse osmosis systems consist of a number of modules in parallel depending on the capacity. Each module consists of a number of elements in series contained in a pressure vessel. The membrane elements prepared by different manufacturers have varying internal arrangements with unique hydrodynamic characteristics. Each of them provides software for designing a reverse osmosis system for desalination. Within the design constraints with reference to feed flow rates, concentrate flow rates, and applied pressure, system design is evolved for a targeted capacity and product water quality subject to the fouling/scaling characteristics of the available feed. The number of elements in series governs the recovery (ratio of feed to product rate), while the number of modules in parallel corresponds to the capacity of the plant. In order to work within the membrane element specifications and to have higher recoveries, one may design a second reverse osmosis stage, where the reject from different modules in the first stage is redistributed to a lesser number of modules in the second stage. Depending on the initial pressure, a booster pump may be used for the second stage if required. Similarly, to improve the product quality of first stage, the *permeate* may be processed through one more reverse osmosis system under low pressures, popularly designated as “pass.” The objectives of the design would be to produce product water of a certain quality and quantity at minimum cost or energy consumption. The restraining factor would be the input quality of feed seawater, the scaling potential, and the rigor of pretreatment system. Final evolved design would specify the operating pressure, feed flow rate, arrangement of modules, and expected quality. This has to be supplemented by the specifications of high-pressure pump and the compatible energy recovery system, feed pretreatment, membrane cleaning, and posttreatment system.

A typical seawater reverse osmosis plant consists of the subsystems: intake; pretreatment system consisting of particulate filters, chemical dosing; high pressure pump, and energy recovery; reverse osmosis system; posttreatment; and cleaning systems as shown in Fig. 8.9.

The reverse osmosis performance deteriorates following the slow degradation of the membranes and thus has a life, warranting periodic replacement. The degradation leads to high permeate salinity. By the adoption of two-pass system, it is possible to

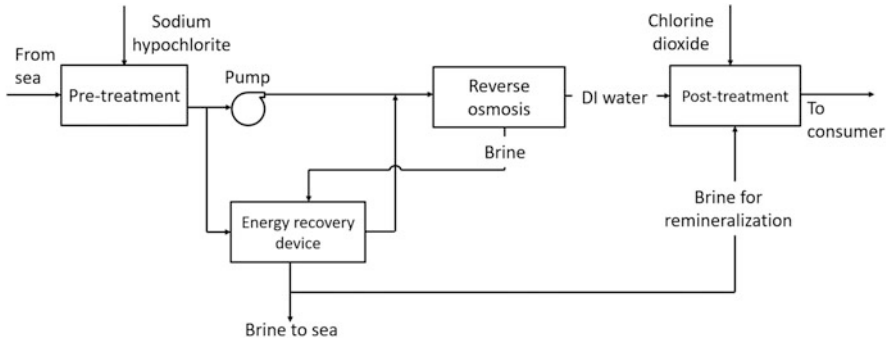


Fig. 8.9 Seawater reverse osmosis desalination plant block diagram. Key components including intake, pretreatment system, chemical dosing, high pressure pump and energy recovery, reverse osmosis system, posttreatment, and cleaning system are represented

achieve consistently high purity levels, wherein permeate from the first pass becomes the feed to the second pass. The concentrated reject water is dispersed into the sea with a diffuser to prevent any sort of salinity shocks to organisms of the sea. Since the process requires strict control of physical, biological, and chemical parameters, operator efficiency plays an important role.

Brackish Water Desalination Brackish water desalination is the viable alternative for remote areas having brackish water as the only source of water. With the dissolved contents being much lower compared to seawater, these plants can be operated at much lower operating pressures. The process is similar to seawater reverse osmosis, but parameters of design and operation are different.

Capacities of brackish water plants are far less compared to seawater desalination plants due to nonavailability of adequate raw water. The composition of the brackish water may vary from source to source, particularly with respect to hardness and trace metals. The raw water may be nearly free of suspended matter and microorganisms. Accordingly, the pretreatment system may be relatively less complicated. Most of the brackish water plants particularly small-capacity plants are located in rural or remote areas, may not operate round the clock, and hence may require protection measures to prevent faster deterioration of the membranes. The reject disposal is a big challenge, as it would find its way to the groundwater resulting in the increase of salinity over time, over and above the increase in salinity in the normal course due to constant withdrawal. Therefore, the design should be directed toward conserving the water resources with dual quality usage. Further, the design should be flexible with a provision for reject recycle so that one can deliver constant quality of product water albeit at different recoveries (Prabhakar et al. 1989; Sarkar et al. 2008). Depending on the salinity of the feed, the withdrawal amount of groundwater may vary, but the plant would operate at constant output quality and capacity. Further, the flexibility would lead to conservation of groundwater to the extent possible.

Water Recovery and Recycle

Reclamation and reuse of water have become quite popular with the advent of membrane technologies because of its cost-effectiveness. Reverse osmosis has been used for the reclamation of water from effluents (Shang et al. 2011). Integrated use of reverse osmosis along with ultrafiltration and microfiltration is common for the tertiary treatment of municipal wastewater to augment water sources as exemplified by 270 MLD plant at the Orange County Water District in Southern California and many other plants in Singapore (Wong 2012). Similar systems have been used in petrochemical industries such as China American Petrochemical Company for recovering 9000 m³/day at Taiwan and 26,000 m³/d zero liquid discharge system at PEMEX refinery in Minatitlan, Veracruz, Mexico. Recovery of water from sewage has been in practice in India since the late 19280s, and a number of reverse plants have been established. Currently most of the industries and small residential communities in water stress regions are recovering water for recycle. Virtually all industrial effluent streams including leather (Cassano et al. 1999), paper (Zhang et al. 2009), and textiles (Bottino et al. 2001) can be treated with membrane processes to reclaim water for reuse through reverse osmosis. In all these processes, reclamation of water for reuse is obtained through reverse osmosis, while other membrane processes could be used as a pretreatment or in some cases recovery of valuables.

Reverse osmosis plant follows the primary and secondary treatment in all the effluent treatment systems. One may have to ensure that during the postsecondary treatment, neither chlorine nor microorganisms enter the reverse osmosis system by appropriate treatment. Since the dissolved solid contents are likely to be less, mostly below 3000 ppm, one can achieve high recoveries of about 70–80%. The product water can be further polished or posttreated to suit the end-use quality requirements. Reverse osmosis has been used for the concentration of aqueous radioactive effluents to reduce the volume for further treatment. When cellulose acetate membranes were used, reverse osmosis gave a poor rejection of nitrate species as the concentration increased. This factor was exploited in isolating uranyl species from ammonium nitrate solution (Prabhakar et al. 1992, 1994, 1996).

In general, the role of reverse osmosis process in wastewater treatment is to recover water and concentrate the contaminants to a small volume for further treatment. The *recovery* is limited by the scaling threat and the osmotic pressure of the concentrating feed due to the continuous removal of water through the membrane. The concentrated streams would contain all the contaminants and salts, and their disposal would be a challenge environmentally. For zero liquid discharge, one more unit operation such as evaporator or crystallizers may have to be used. As the water demand and value are in the ascending trend, it is imperative to recover water from any spent stream and in that reverse osmosis has a major role to play.

Applications of Nanofiltration

Nanofiltration is slowly emerging as an alternative to reverse osmosis in some applications and as supplementary technology in some other cases. The nanofiltration membrane elements are available in many average pore sizes designated as NF40, NF90, etc., indicating the approximate solute rejection of sodium chloride. Minor charge on the surface of the membrane coupled with higher pore sizes relative to reverse osmosis enables the separation of monovalent species resulting in the concentration of macromolecules. Because of the passage of some solutes, the effective operating pressure is less due to the net osmotic pressure being lower. Consequently, larger molecules and multivalent ionic species can be separated through nanofiltration, like dyes, as well as uranyl species from the solution. Nanofiltration has potential applications (Astro chemicals and Bio Technologies 2019) in many areas including water softening and removal of natural organic materials. Experimental investigations on using reverse osmosis and nanofiltration (Abid et al. 2012) for the dye removal indicated that nanofiltration system can provide permeate water, meeting the environmental standards by a big margin at 50% electric power relative to reverse osmosis membranes due to reduction in operating pressure. A number of studies have also confirmed the utility of separation of dyes and intermediates (Kelewou et al. 2015; Zhu et al. 2013) using nanofiltration. Review of existing processes for dye removal found that membrane processes have high potential (Ahmad et al. 2015) and require some of the challenges like fouling and sludge production that need to be addressed. Nanofiltration finds use in the separation of low-molecular-weight species from the bulk solution as indicated by studies, where the separation of ammonium nitrate could be achieved from uranyl nitrate (Prabhakar et al. 1996; Zhongwei et al. 2017).

8.4.2 *Electro-membrane Process Applications*

Electrodialysis process was used for desalination particularly for brackish water desalination in the late 1980s and early 1990s. The following are the limitations of electrodialysis:

1. It is difficult to produce high purity water because of the inherent electrical resistance of water.
2. Polarization near the membrane surface decreases the efficiency of the system leading to increase in power consumption. In addition, power consumption also increases with the concentration of the feed, as more ions have to be transported through the membrane.
3. The efficiency of electrodialysis decreases in the presence of bivalent salts such as calcium, sulfate, magnesium, etc.
4. As on date, no practical energy recovery system is available even though some attempts are made to recover energy using the concept of reverse electrodialysis.

Electrodialysis system can be operated in batch mode for small-scale applications or continuously for large industrial applications. Earliest applications of electrodialysis systems were in brackish desalination. Electrodialysis units have been deployed for desalination up to 15,000 ppm salinity (Burn et al. 2015) with multiple stages. For brackish water desalination up to 3000 ppm feed salinity, electrodialysis can achieve about 80% recovery. Efforts to extend to seawater desalination could not be successful because of very high specific power consumption. Improvements to overcome the challenge through electrodialysis reversal also did not yield desired results due to practical difficulties. Recent innovation of reverse electrodialysis (Mei and Tang 2018) for recovering energy has shown positive results. Perhaps, in the future with further developments, electrodialysis could become a viable alternative for seawater desalination (Galama et al. 2014).

The major challenge of electrodialysis is the power consumption and concentration polarization, both of which increase with concentration of the feed. The challenges were addressed by electrodialysis reversal to some extent, where the polarity of the electrodes was frequently altered. Even though the issues were addressed to some extent, the product water purity was affected due the frequent change of “dilute” and “concentrate” compartments. Moreover, because of the inherent poor conductivity of water, one has to contend with higher salinities of product compared to reverse osmosis. In view of this, electrodialysis is not a preferred alternative for desalination or water treatment applications. Electrodeionization is a minor modification of electrodialysis and is restricted to very low salinity levels. Apart from desalination, electrodialysis has been studied extensively for industrial wastewater treatment for the recovery of chromium (Nataraj et al. 2007), cadmium (Marder et al. 2003), and nickel (Scarazzato et al. 2018) from plating industry effluents and acid mine drainage for recovering water (Cardoso et al. 2013) and to concentrate and recover nutrients from waste streams (Zhang et al. 2013).

8.4.3 Membrane Distillation

Membrane distillation has been demonstrated for its performance in desalination of seawater (Camacho et al. 2013) in a number of studies. The process involves initially the formation of vapor and subsequently its transfer through the membrane. The transfer medium (membrane) and water vapor both are hydrophobic in nature, and the product can be highly pure for an ideal membrane. Since the membrane has pore-size distribution, some contamination is inevitable in condensed water. For large-scale sustainable deployment, the challenges of low-flux and low liquid entry pressure of the membranes have to be addressed.

Apart from desalination, direct contact membrane distillation has been utilized for the recovery of water from pharmaceutical wastewater and radioactive wastewater (Wang and Chung 2015). Studies were conducted to recover water in the crystallization process using membrane distillation crystallization (Chan et al. 2005; Ji et al.

2010). This concept could be quite useful for the recovery of salts and water from the blowdown of thermal desalination plant. One of the potential applications of the membrane distillation in water treatment besides recovering water is to reduce the temperature of return cooling water being disposed into the environment (Jansen et al. 2007). Membrane distillation can be coupled with renewable energy (Blanco Gálvez et al. 2009), particularly solar, for the concentration of solutions including wastewater (Walton et al. 2004). Membrane distillation can be used for de-moisturization of wet steam as moisture can get condensed on the retentate side while dry steam can be sent for appropriate use. Condensation assisted by membrane represents a new source of water (Drioli et al. 2015).

8.4.4 Ultrafiltration

Ultrafiltration membranes were commercially developed later than reverse osmosis membranes. The applications have encompassed many areas including wastewater treatment and water purification. Being a low-pressure technique, the energy consumption is low compared to other pressure-driven processes, and the virtue of ultrafilters is its amenability for backwashing and possibility of dead-end operation mode, which provides nearly 100% recovery of the fluid or solids. The nominal pore size of ultrafilters may be in the range of about 20 nm to 0.1 microns. Commercially ultrafiltration systems are available in different ranges of pore sizes, specified in terms of molecular weight cutoff from 5 kilo Dalton to 1.2 lakh kilo Dalton. Size exclusion is the basic philosophy of separation, and osmotic pressure is normally not a limitation to the process. As the filtration proceeds, the pressure drop across the membrane, i.e., transmembrane pressure drop, would increase leading to reduction in flux. The flux can be nearly restored by backwashing, i.e., by allowing the water to flow from product to feed side for about a minute. The commercially operating system has a backwash cycle for about 1–2 min, for every 40–50 min of service cycle. Most of the seawater reverse osmosis desalination plants use ultrafiltration for the pretreatment as it gives high-quality treated water. After many pilot studies between 1995 and 2005, ultrafiltration has been installed as pretreatment system in many large-scale seawater reverse osmosis plants (Busch et al. 2009).

Size-enhanced ultrafiltration is a technique whereby the size of the desired species is enhanced and separated through ultrafiltration. This method is limited to small concentration of solutes present in bulk solution such as the presence of very small amounts of heavy metal species. Increase in size can be due to complexation, coprecipitation, and adsorption. Because of the size, these species are retained by the ultrafiltration membranes. The advantages of this technique include:

1. Isolation and removal of trace metal species in the presence of bulk component based on size exclusion principle.
2. The process is not limited by osmotic pressure constraints as in reverse osmosis and nanofiltration.

3. Since the concentration of the heavy metal species are so low, the consumption of additives would be very small,
4. Ultrafiltration is backwashable, and hence the complex can be recovered as such in a backwash cycle.
5. Further, most of the complexation or adsorption processes are sensitive to pH. Hence, after size enhancement and separation of heavy ions, the size enhancement can be reversed by altering pH or other conditions, enabling the separation and recovery of metal ion species as well as the complex for reuse.

Removal of copper, nickel, and chromium has been extensively studied using a variety of complexing agents such as polyethylenimine (Sarkar et al. 2013; Kadioglu et al. 2010), carboxymethyl cellulose (Kavitha et al. 2018), and chitosan derivative (Kavitha et al. 2019). The removal of cesium and strontium, the radioactive contaminants of nuclear waste from the supernatant solution (after cesium was co-precipitated along with copper ferrocyanide and strontium as phosphate), indicated that *size-enhanced ultrafiltration* can be used as a last mile separation process (Rao et al. 2000) because of the fact that even the original waste, before precipitation, would contain less than a ppm even though the radioactivity would be high.

8.4.5 Membrane Contactors

Unlike other membrane processes which are driven by external energy for the separation, membrane contactors do not need external energy for membrane role in the separation process. It enables the conventional techniques of separation in somewhat convenient manner with reference to environment, capacity, and resource requirements. Membrane contactors are porous barriers. The contactors can exhibit different functions: *filters* for the removal of colloids/suspended matter, *interphase contactor* in liquid–liquid extraction, *absorber* for gaseous separation, *barrier* in membrane bioreactors, and immobilizer of solvent in supported liquid membrane. Membrane bioreactors, solvent extraction, gas absorption, and gaseous separation are some of the examples where membrane contactors have been used. With reference to water treatment, membrane bioreactors play a very critical role both in the industrial and domestic wastewater treatments. Membrane solvent extraction is a developing process which can help in recovering the organics or heavy metal species from effluents.

Membrane Bioreactor

A membrane bioreactor combines the activated sludge process with a membrane separation process. The membrane process could be either microfiltration or ultrafiltration. The membrane acts as a barrier filter which enables it to hold the microorganisms and allow the transport of nutrients, oxygen, and degradation products

through the pores. The operational range of membrane bioreactors is much higher compared to conventional activated sludge process. The solid retention time for membrane bioreactor can be up to a month compared to about a few days for conventional processes. Membrane bioreactors can operate at high suspended loads usually known as mixed liquor suspended solids unlike conventional systems. The configuration of the membranes in membrane bioreactor can be flat sheet, tubular, or hollow fiber, depending on the design constraints. Ceramic membranes with multiple tubes can also be used. There are two ways by which membrane bioreactors can be deployed, namely, wet (submerged or immersed) installation and dry side stream (outside the activation tank). In wet installation, membrane module is directly submerged into the activation tank, while in dry installation, membrane module is installed outside the tank. Aeration is done for wet installation from the bottom toward the membrane, while for the side-stream design, air is injected along with wastewater. Both of them have their merits and demerits (Dohare and Trivedi 2014). Side-stream installation requires higher power but can be easily cleaned and can handle variations in the feed conditions. On the other hand, the power consumption is less for submerged membrane bioreactor, but cleaning in the membrane is difficult and time-consuming (Gupta et al. 2008). Nowadays more installation follows side-stream installation. The advantages of membrane bioreactor include low footprint area, low hydraulic retention time, and high solid retention time besides high-quality treated water. Membrane bioreactors have been used in the treatment of many industrial effluents having high organic loading such as in food and beverage, petroleum, pharmaceutical, pulp and paper, textiles (Dohare and Trivedi 2014; Mutamim et al. 2012), and municipal wastes. The major challenges include fouling, membrane life, energy consumption, and the overall cost of treatment, particularly due to limited membrane life and energy consumption.

Solvent Extraction Using Membranes

There are two types of membrane contactors used for liquid–liquid extraction, namely, supported liquid membranes and membrane solvent extraction.

Supported Liquid Membrane

Supported liquid membrane technique provides for simultaneous extraction and stripping, less inventory of solvent, and high selectivity. Hollow fiber ultrafiltration membranes are the preferred configuration as it offers high interfacial surface area. In supported liquid membrane, a solvent is immobilized within the pores of the membrane. The feed and the strip solutions are passed through either side of the membranes (tube/shell), and the contact between them is established by the solvent immobilized in the pores. The species, which is being separated, gets transported through the solvent, diffuses through it, and gets stripped by the strip solution. The advantage of this process is its high selectivity and the possibility of uphill transport.

Reviews (Parhi 2013; Dzygiel and Wieczorek 2010) on the supported liquid membrane indicate a variety of laboratory studies including the separation of radioisotopes such as plutonium, cesium-137, europium-154, and ruthenium-106. The liquid–liquid extraction with supported liquid membrane has been shown to have a good potential by a number of studies related to the extraction of metal ions in hydrometallurgical separations as well as from wastewater (Zhang et al. 2010; Ren et al. 2010). Recoveries of copper and uranium from sulfate leach liquors, uranium from wet phosphoric acid, and zinc from the waste liquors were demonstrated on pilot scale (Smith et al. 2014). Many solvents have been used including chelating or acidic extractants for the extraction of various metal ions such as copper, zinc, cobalt, nickel, iron, manganese, and molybdenum (VI). Extractants such as Alamine-336, Aliquat-336, and Alamine-304 based on amines have been used for molybdenum, chromium, and vanadium in the chloride solutions and crown ethers for alkali or alkaline earth metals (Padwal et al. 2018). In spite of all the potentialities including high selectivity, supported liquid membrane is not a commercially viable proposition because of the instability of the immobilized solvent which acts as a membrane and its high cost.

Membrane Solvent Extraction

In membrane solvent extraction, the feed and the solvent are independently circulated through the hollow fiber membrane element, one through the shell side and the other through tube side, depending on the design. Mass transfer occurs between the two streams in contact across the membrane pores. Unlike supported liquid membrane, extraction and stripping are carried out in two independent steps. However, when two sets of membrane elements are assembled together in a loop such that the extracting solvent passes through both the units, extraction and stripping occur continuously. The first unit extracts the species from the feed, while in the second unit, stripping takes place, thus enabling the simultaneous extraction and stripping resulting in the recycling of solvent and recovery of the species (Hemmati et al. 2015).

A number of investigations have been reported on the wastewater treatment for the removal and recovery of contaminants such as acetic acid (Sofiya et al. 2019), phenol (Shen et al. 2009), metal ions such as plutonium (Gupta et al. 2005), and cadmium (Fouad and Bart 2007). The advantage of using membranes includes large interfacial contact area without mixing of the phases and freedom to choose the solvent without density considerations. As the two phases are distinct, the flow rates can be varied independently, and problems of flooding and emulsification do not arise.

8.4.6 Forward Osmosis

Forward osmosis is gaining importance as a technology for desalination, concentration of solutions, and energy recovery. Its advantage emanates from being a passive process in nature (not requiring any external source of energy) as the separation is driven osmotic pressure differential between the draw solution and the feed. The challenges to realize the potential require a membrane with good water flux, a less reverse solute transport, and above all a convenient and cost-effective means of recovering pure water from the diluted osmotic sink. No doubt, the literature is replete with novel membranes such as cellulose triacetate (Ong et al. 2015), thin film composite (Ren and McCutcheon 2014), thin film nanofiltration (Ma et al. 2013), biomimetic (Fane and Tang 2012), and draw solute ranging from inorganic solutes, phase change material, low-molecular-weight organic solutes, and volatile solute or dissolved gas solutions (Lutchmiah et al. 2014). Since forward osmosis desalination is a two-step process, many combinations are being investigated using thermal and mechanical energy. Basically, the present methods adopted for forward osmosis desalination includes the combination of forward osmosis and reverse osmosis (Cath et al. 2010), forward osmosis–nanofiltration (Kim et al. 2018), forward osmosis–distillation (McCutcheon et al. 2006), and forward osmosis–phase change material (Kim et al. 2016). Apart from these, *aquaporin-incorporated vesicles* exhibit excellent water permeability and high salt rejection, owing to the superior intrinsic characteristics of the *aquaporin*'s as water channels (Li et al. 2017). Double-skinned forward osmosis membranes have also been proposed (Song et al. 2015a).

Forward osmosis as a standalone desalination option is not practical because of the nonavailability suitable draw solute which can be easily regenerated to recover the product water. Forward osmosis has more potential in wastewater treatment (Lutchmiah et al. 2014) as it can be used for the concentration of the waste. Besides, the water that is removed can be recovered by secondary processes such as reverse osmosis/nanofiltration. Alternately, fertilizers can be used as draw solute so that the resulting dilute solution can be directly used in the field. Similarly, if pretreated seawater is used as a draw solution for wastewater, the seawater would get diluted, thereby savings in energy cost for seawater desalination (Akther et al. 2015).

8.4.7 Diffusion Dialysis

Because of the low flux, the applications of diffusion dialysis have been limited to the recovery of acids and alkalis from the discharges from steel production, metal-refining, electroplating, cation exchange resin regeneration, nonferrous metal smelting, aluminum etching, and tungsten ore smelting (Jeong et al. 2005). An excellent review by Luo et al. (2011) indicate that many acid recovery systems installed in different industries have made profits suggesting diffusion dialysis is

adaptable to industries in a profitable manner even though the process is slow and is limited to acid/base recovery.

8.4.8 Synergism of Different Membrane Processes in Water Treatment

Each membrane process has its unique advantages and challenges. The pressure-driven membrane processes, ultrafiltration, nanofiltration, and reverse osmosis, have complementary characteristics. The processes, in pairs or sometimes all together, are used in water treatment applications. The process sequence ultrafiltration–nanofiltration–reverse osmosis may have to be maintained to get the synergism. In fact, ultrafiltration is a standard pretreatment for reverse osmosis in most instances. Ultrafiltration–reverse osmosis and ultrafiltration–nanofiltration–reverse osmosis are combinations which can provide fractionation of the solute species besides recovery of water. Since the operating pressure increases along the sequence, booster pumps are necessary between each membrane operation.

The advantages of using hyphenated membrane systems include satisfactory pretreatment through ultrafiltration to improve the sustainability of the nanofiltration or reverse osmosis systems. The use of nanofiltration in combination with reverse osmosis has the following advantages:

- (a) The operating pressure can be reduced because of the poor rejection of monovalent species by nanofiltration and the consequent reduction in net osmotic pressure.
- (b) Reverse osmosis can operate at lower pressures due to less concentration of nanofiltration permeate leading to better recovery and better quality of the product (Helal 2009).
- (c) Since the reject of reverse osmosis plant would be having mostly monovalent solutes and less in concentration corresponding to the seawater feed, it can be blended with feed to bring down the salinity and hence obtain higher recovery (Song et al. 2015b).
- (d) The intangible advantage of nanofiltration–reverse osmosis could possibly be less fouling and less maintenance requirements because of slight charge on nanofiltration membrane surface.

Ahunbay (2019) has indicated that by a combination of reverse osmosis and nanofiltration in a multistage configuration, the specific energy consumption can be brought lower than single-stage seawater desalination system. However, one may have to assess the specific energy consumption of seawater reverse osmosis versus nanofiltration–reverse osmosis system, as the energy recovery component would be less for nanofiltration–reverse osmosis system. For example, in seawater desalination, the combination of nanofiltration and reverse osmosis can lead to recovery of value. The concentrate of reverse osmosis would be rich in sodium chloride with

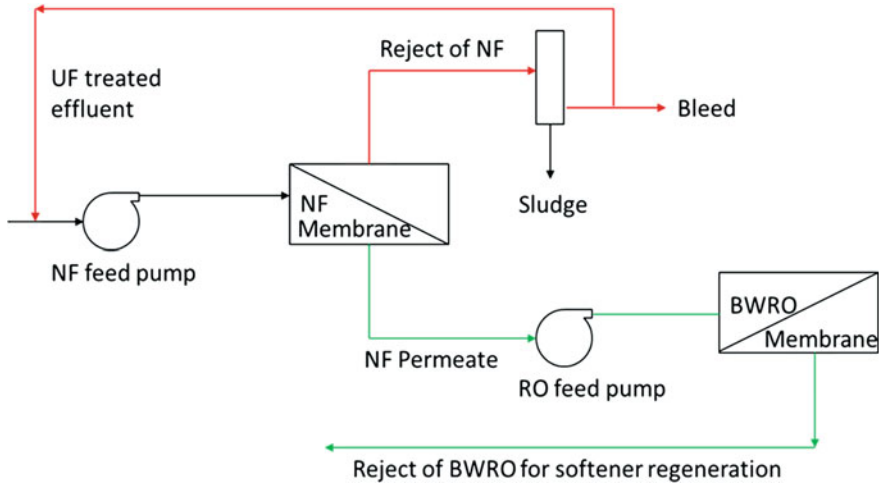


Fig. 8.10 Nanofiltration–reverse osmosis hybrid system for the treatment of mine effluents. Such configuration is useful for the separation of sulfates, chlorides, etc. along with the recovery of water for recycle. (Modified from Sarkar et al. 2011)

relatively less concentration of multivalent solutes and can serve as a feed to electrolytic production of sodium hydroxide at higher efficiencies. Ramaswami et al. (2018) have investigated the removal of water from landfill leachates using nanofiltration–reverse osmosis as well as reverse osmosis–nanofiltration combinations and concluded that nanofiltration–reverse osmosis is advantageous and energy-efficient over reverse osmosis–nanofiltration. Sarkar et al. (2011) have demonstrated that a combination of nanofiltration and reverse osmosis can lead to the separation of sulfates and chlorides, besides recovering water for recycle. The concentrated reverse osmosis stream containing concentrated sodium chloride can be used for the regeneration of the softener being used in the process, as shown in Fig. 8.10. The separation was possible, because of the fact that calcium sulfate requires significant induction period to form the precipitate at reasonable supersaturation level. In wastewater treatment, nanofiltration–reverse osmosis sequence helps in the recovery of nutrients besides water (van Voorthuizen et al. 2005). The use of reverse osmosis–electrodialysis has been suggested for crystallizers (Tanaka et al. 2003). In wastewater treatment and desalination, forward osmosis has a major role to play, and the combination of forward osmosis and reverse osmosis has the potential to reduce energy consumption as percent recovery can be increased provided a wastewater stream is available. A combination of diffusion dialysis and reverse osmosis can recover acid and water from acidic effluents. Removal of organic contaminants and recovery of water can be achieved by using a combination of membrane solvent extraction and reverse osmosis.

8.4.9 Membrane Processes for Point-of-Use Applications

Reverse osmosis water purification systems are easily available in the market across most of the countries which can be fixed in individual apartments for providing point-of-use safe water. Only concern in such plants is the very low recovery which results in wastage of water. Ultrafiltration is used as a final treatment step for the production of ultrapure water for electronic, pharmaceutical, and potable water applications. In places where salinity levels are acceptable, ultrafiltration membranes can be used for obtaining safe water without microbial contaminants. Further ultrafiltration-assisted devices have been developed (Bindal et al. 2011) for the remediation of groundwater contaminants such as arsenic, fluoride, iron, and so on.

8.5 Future Outlook and Prospects

As the society moves toward environmental conservation, membrane processes have more important role to play, particularly in recovering and recycling every component present in the waste stream. Most of waste streams contain value materials but normally not recoverable at an acceptable cost and effort. The availability of a variety of membrane processes and membranes offers plenty of opportunities to realize *wealth from waste*.

The general practice in waste management is to mix all the spent streams (effluents) and treat them as a single batch. Naturally, the whole system becomes complex and complicated, and other than water not much is recoverable.

Membrane processes are modular in nature and the capacity is flexible. Accordingly, small-capacity units can be installed without the requirement of much foot print. In this context, it is possible to decentralize the water treatment operation both in industries and residences. Spent streams emanating from different processes can be isolated and processed which will be easier, and many times value can be recovered. Consequently, each stream will have only one type of contaminant which can be easily separated. The contaminant may be a valuable raw material or product or an intermediate. This is possible even in domestic waste where gray water can be isolated from black water. Water can be recovered from gray water using ultrafiltration and reverse osmosis, while the black water can be bioprocessed to generate energy.

Forward osmosis being a passive process can be used to link the *wastewater-resource* loop. This would help in recovering water from waste without using energy. Membrane distillation also has a bright prospect if it could be used for recovering water from return cooling water of industries or power plants. If the cooling circuit uses less water, the temperature of the cooling water would be higher to provide better yield of a desalinated water which could be a win-win situation. Recovery of values particularly heavy metal species such as in mine discharges and electroplating industries through size-enhanced ultrafiltration looks promising after recovery of acid through diffusion dialysis. It is expected the membranes would have a larger role to play in water treatment in the years to come.

References

- Abid MF, Zablouk MA, Abid-Alameer AM (2012) Experimental study of dye removal from industrial wastewater by membrane technologies of reverse osmosis and nanofiltration. *Iran J Environ Health Sci Eng* 9(1):17. <https://doi.org/10.1186/1735-2746-9-17>
- Ahmad A, Mohd-Setapar SH, Chuo SC, Khatoon A, Wani WA, Kumard R, Rafatullahe M (2015) Recent advances in new generation dye removal technologies: novel search of approaches to reprocess waste water. *RSC Adv* 5(39):30801–30818. <https://doi.org/10.1039/C4RA16959J>
- Ahunbay MG (2019) Achieving high water recovery at low pressure in reverse osmosis processes for seawater desalination. *Desalination* 465(1):58–68. <https://doi.org/10.1016/j.desal.2019.04.023>
- Akther N, Sodiq A, Giwa A, Daer S, Arafat HA, Hasan SW (2015) Recent advancements in forward osmosis desalination: a review. *Chem Eng J* 281:502–522. <https://doi.org/10.1016/j.cej.2015.05.080>
- Apel P (2001) Track-etching technique in membrane technology. *Radiat Meas* 34:559–566. [https://doi.org/10.1016/S1350-4487\(01\)00228-1](https://doi.org/10.1016/S1350-4487(01)00228-1)
- Astro chemicals and Bio Technologies (2019). <https://www.austrowatertech.com/services/nanofiltration-wastewater-treatment/>
- Belfort G (1988) Membrane modules: comparison of different configurations using fluid mechanics. *J Membr Sci* 35(3):245–270
- Bhatluri KK, Manna MS, Saha P, Ghosal AK (2014) Supported liquid membrane based Simultaneous separation of cadmium and Lead from wastewater. *J Membr Sci* 459:256–263. <https://doi.org/10.1016/j.memsci.2014.02.019>
- Bhattacharjee C, Saxena VK, Dutta S (2017) Fruit juice processing using membrane technology: a review. *Innovative Food Sci Emerg Technol* 43:136–153
- Bindal RC, Prabhakar S, Tewari PK (2011) Ultrafiltration membrane technology for water purification and effluent treatment: BARC Newsletter Founder's Day Special Issue October 128. <http://www.barc.gov.in/publications/nl/2011/pdf/DAE%20EA/Paper%2025.pdf>
- Blanco Gálvez J, García-Rodríguez L, Martín-Mateos I (2009) Seawater desalination by an innovative solar-powered membrane distillation system: the MEDESOL project. *Desalination* 246:567–576. <https://doi.org/10.1016/j.desal.2008.12.005>
- Bottino K, Capannelli G, Tocchi G (2001) (Dipartimento di Chimica e Chimanda Industriale, University of Genova, Geneva, Italy), and M. Marcucci and G. Ciardelli (Tecnossile Srl, Prato, Italy): Membrane separation processes tackle textile waste-water treatment: Membrane Technology No. 130, pp 9–11. [https://doi.org/10.1016/S0958-2118\(01\)80128-2](https://doi.org/10.1016/S0958-2118(01)80128-2)
- Burn S, Hoang M, Zarzo D, Olewniak F, Campos E, Bolto B, Barron O (2015) Desalination techniques-a review of the opportunities for desalination in agriculture. *Desalination* 364:2–16. <https://doi.org/10.1016/j.desal.2015.01.041>
- Busch M, Chu R, Kolbe U, Meng Q-Q, Li S-J (2009) Integrated ultrafiltration and reverse osmosis membrane system for seawater desalination – 1000 days field experience with Dow™ UF and Filmtec™ Technology in the Wangtan Datang Power Plant. *Desalin Water Treat* (10):1–20. <https://doi.org/10.5004/dwt.2009.702>
- Camacho LM, Dumée L, Zhang J, De Li J, Duke M, Gomez J et al (2013) Advances in membrane distillation for water desalination and purification applications. *Water (Switzerland)* 5:94–196. <https://doi.org/10.3390/w5010094>
- Campione L, Gurreri M, Ciofalo G, Micale A, Tamburini AC (2018) Electrodialysis for water desalination: a critical assessment of recent developments on process fundamentals, models and applications. *Desalination* 434:121–160. <https://doi.org/10.1016/j.desal.2017.12.044>
- Cardoso D, Stéphano L, Antônio M, Rodrigues S, Moura A, Alberto J, Tenório S (2013) Water recovery from acid mine drainage by electrodialysis. *Miner Eng* 40:82–89. <https://doi.org/10.1016/j.mineng.2012.08.005>

- Cassano A, Molinari R, Drioli E (1999) Saving of water and chemicals in tanning industry by membrane processes. *Water Sci Technol* 40(4–5). [https://doi.org/10.1016/S0273-1223\(99\)00528-4](https://doi.org/10.1016/S0273-1223(99)00528-4)
- Cath TY, Hancock NT, Lundin CD, Hoppe-Jones C, Drewes JE (2010) A multi-barrier osmotic dilution process for simultaneous desalination and purification of impaired water. *J Membr Sci* 362:417–426. <https://doi.org/10.1016/j.memsci.2010.06.056>
- Chan MT, Fane AG, Matheickal JT, Sheikholeslami R (2005) Membrane distillation crystallization of concentrated salts – flux and crystal formation. *J Membr Sci* 257:144–155. <https://doi.org/10.1016/j.memsci.2004.09.051>
- Dohare D, Trivedi R (2014) A review on membrane bioreactors: an emerging technology for industrial wastewater treatment. *Int J Emerg Technol Adv Eng* 4(12):226–236
- Drioli E, Giorno L (ed) (2010) *Comprehensive membrane science and engineering*. Elsevier. ISBN 978-0-08-093250-7
- Drioli E, Cirsucoli A, Curcio E (2011) *Membranes contactors: fundamentals, applications and potentialities*, Membrane science and technology series, vol 11. Elsevier, Amsterdam, 516 pages Hardcover ISBN: 9780444522030 eBook ISBN: 9780080457017
- Drioli E, Ali A, Macedonio F (2015) Membrane distillation: recent developments and perspectives. *Desalination* 356:56–84. <https://doi.org/10.1016/j.desal.2014.10.028>
- Dzygiel P, Wiczorek P (2010) Chapter 3: Supported liquid membrane and their modifications: definition, classifications, theory, stability, applications and perspectives. In: Kislik V (ed) *Liquid membranes principles and applications in chemical separations and wastewater treatment*, 1st edn. Elsevier, Amsterdam, pp 73–140. <https://doi.org/10.1016/B978-0-444-53218-3.00003-9>
- Fane AG, Tang CY (2012) Synthesis of robust and high-performance aquaporin-based biomimetic membranes by interfacial polymerization-membrane preparation and RO performance characterization. *J Membr Sci* 423–424:422–428. <https://doi.org/10.1016/j.memsci.2012.08.039>
- Fouad EA, Bart H-J (2007) Separation of zinc by a non-dispersion solvent extraction process in a hollow fiber contactor. *Solvent Extr Ion Exch* 25(6):857–877. <https://doi.org/10.1080/07366290701634610>
- Galama AH, Saakes M, Bruning H, Rijnaarts HHM, Post JW (2014) Seawater pre desalination with electro dialysis. *Desalination* 342:61–69. <https://doi.org/10.1016/j.desal.2013.07.012>
- Gupta SK, Rathore N, Sonawane JV, Pabby AK (2005) Application of hollow fiber contactor in nondispersive solvent extraction of Pu(IV) by TBP. *Sep Sci Technol* 40(9):1911–1926. <https://doi.org/10.1081/SS-200064546>
- Gupta N, Jana N, Majumder CB (2008) Submerged membrane bioreactor system for municipal wastewater treatment process: an overview. *Indian J Chem Technol* 15:604–608
- Helal AM (2009) Hybridization — a new trend in desalination. *Desalin Water Treat* 3:120–135. <https://doi.org/10.5004/dwt.2009.263>
- Hemmati M, Nazari N, Hemmati A, Shirazian S (2015) Phenol removal from wastewater by means of nanoporous membrane contactors. *J Ind Eng Chem* 21:1410–1416. <https://doi.org/10.1016/j.jiec.2014.06.015>
- Jansen AE, Assink JW, Hanemaaijer JH, Van Medevoort J (2007) Membrane distillation – producing high quality water from saline streams by deploying waste heat. https://www.tno.nl/media/1509/membrane_distillation.pdf
- Jeong JK, Kim MS, Kim BS (2005) Recovery of H₂SO₄ from waste acid solution by a diffusion dialysis method. *J Hazard Mater* 124:230–235. <https://doi.org/10.1016/j.jhazmat.2005.05.005>
- Ji X, Curcio E, Al Obaidani S, Di Profio G, Fontananova E, Drioli E (2010) Membrane distillation-crystallization of seawater reverse osmosis brines. *Sep Purif Technol* 71:76–82. <https://doi.org/10.1016/j.seppur.2009.11.004>
- Kadai E, Bosleman R (2018) Energy recovery devices in membrane desalination processes. In: *Renewable energy powered desalination handbook*. Butterworth-Heinemann, pp 415–444. <https://doi.org/10.1016/B978-0-12-815244-7.00011-8>

- Kadioglu SI, Yilmaz L, Aydogan N, Onder Ozbelge H (2010) Removal of heavy metals from multicomponent metal mixtures by polymer enhanced ultrafiltration: effects of pH, ionic strength and conformational changes in polymer structure. *Sep Sci Technol* 45 (10):1363–1373. <https://doi.org/10.1080/01496391003674274>
- Karabelas AJ, Koutsou CP, Kostoglou M, Sioutopoulos DC (2018) Analysis of specific energy consumption in reverse osmosis desalination processes. *Desalination* 431:15–21. <https://doi.org/10.1016/j.desal.2017.04.006>
- Karisma D, Febrianto G, Mangindaan D (2017) Removal of dyes from textile wastewater by using nanofiltration polyetherimide membrane. *IOP Conf Ser Earth Environ Sci* 109:012012. <https://doi.org/10.1088/1755-1315/109/1/012012>
- Kavitha E, Prabhakar S, Rajesh MP (2018) Removal and recovery of heavy metals from aqueous solution using β -cyclodextrin polymer and optimization of complexation conditions. *Desalin Water Treat* 122:219–230. <https://doi.org/10.5004/dwt.2018.22783>
- Kavitha E, Sowmya A, Prabhakar S, Jain P, Surya R, Rajesh MP (2019) Removal and recovery of heavy metals through size enhanced ultrafiltration using chitosan derivatives and optimization with response surface modeling. *Int J Biol Macromol* 132:278–288. <https://doi.org/10.1016/j.ijbiomac.2019.03.128>
- Kelewou H, Lhassani A, Merzouki M, Drogui P (2015) Removal of textile-based dyes by nanofiltration: study of physicochemical parameters' effect on the retention by experimental designs methodology. *Desalin Water Treat* 54(6):1735–1746. <https://doi.org/10.1080/19443994.2014.890132>
- Kim J-J, Kang H, Choi Y-S, Yu YA, Lee J-C (2016) Thermo-responsive oligomeric poly (tetrabutylphosphonium styrenesulfonate)s as draw solutes for forward osmosis (FO) applications. *Desalination* 381:84–94. <https://doi.org/10.1016/j.desal.2015.11.013>
- Kim JE, Phuntsho S, Chekli L, Choi JY, Shon HK (2018) Environmental and economic assessment of hybrid FO-RO/NF system with selected inorganic draw solutes for the treatment of mine impaired water. *Desalination* 429:96–104. <https://doi.org/10.1016/j.desal.2017.12.016>
- Lalia BS, Kochkodan V, Hashaikher R, Hilal N (2013) A review on membrane fabrication: structure, properties and performance relationship. *Desalination* 326:77–95. <https://doi.org/10.1016/j.desal.2013.06.016>
- Li X, Loh CH, Wang R, Widjajanti W, Torres J (2017) Fabrication of a robust high performance FO membrane by optimizing substrate structure and incorporating aquaporin into selective layer. *J Membr Sci* 525:257–268. <https://doi.org/10.1016/j.memsci.2016.10.051>
- Liu F, Hashim NA, Liu Y, Abed MM, Li K (2011) Progress in the production and modification of PVDF membranes. *J Membr Sci* 375(1):1–27. <https://doi.org/10.1016/j.memsci.2011.03.014>
- Luo J, Wu C, Xu T, Wu Y (2011) Diffusion dialysis-concept, principle and applications. *J Membr Sci* 366(1–2):1–16. <https://doi.org/10.1016/j.memsci.2010.10.028>
- Luo H, Wang Q, Zhang TC, Tao T, Zhou A, Chen L, Bie X (2014) A review on the recovery methods of draw solutes in forward osmosis. *J Water Process Eng* 4:212–223
- Lutchmiah K, Verliefe ARD, Roest K, Cornelissen ER (2014) Forward osmosis for application in wastewater treatment: a review. *Water Res* 58:179–197. <https://doi.org/10.1016/j.watres.2014.03.045>
- Ma H, Burger C, Hsiao BS, Chu B (2012) Highly permeable polymer membranes containing directed channels for water purification. *ACS Macro Lett* 1:723–726
- Ma N, Wei J, Qi S, Zhao Y, Gao Y, Tang CY (2013) Nanocomposite substrates for controlling internal concentration polarization in forward osmosis membranes. *J Membr Sci* 441:54–62. <https://doi.org/10.1016/j.memsci.2013.04.004>
- Marder L, Sulzbach GO, Bernardes AM, Ferreira JZ (2003) Removal of cadmium and cyanide from aqueous solutions through electro dialysis. *J Braz Chem Soc* 14:610–615. <https://doi.org/10.1590/S0103-50532003000400018>
- McCutcheon JR, McGinnis RL, Elimelech M (2006) Desalination by ammonia–carbon dioxide forward osmosis: influence of draw and feed solution concentrations on process performance. *J Membr Sci* 278(1–2):114–123. <https://doi.org/10.1016/j.memsci.2005.10.048>

- Mei Y, Tang CY (2018) Recent developments and future perspectives of reverse electrodialysis technology: a review. *Desalination* 425:156–174. <https://doi.org/10.1016/j.desal.2017.10.021>
- Mulder M (1996) Basic principles of membrane technology, 2nd edn, Kluwer Academic Press. ISBN-13: 978-0-7923-4248-9. <https://doi.org/10.1007/978-94-009-1766-8>
- Mutamim NSA, Noor ZZ, Hassan MAA, Olsson G (2012) Application of membrane bioreactor technology in treating high strength industrial wastewater: a performance review. *Desalination* 305:1–11. <https://doi.org/10.1016/j.desal.2012.07.033>
- Nagel R (2005) Electrodeionisation (EDI) for make-up water treatment in power plant applications. *VGB Powertech Int* 85:112–117. ISSN 1435-3199; TRN: DE05GA039
- Nataraj SK, Hosamani KM, Aminabhavi TM (2007) Potential application of an electrodialysis pilot plant containing ion-exchange membranes in chromium removal. *Desalination* 217:181–190. <https://doi.org/10.1016/j.desal.2007.02.012>
- Ong RC, Chung T-S, de Wit JS, Helmer BJ (2015) Novel cellulose ester substrates for high performance flat-sheet thin-film composite (TFC) forward osmosis (FO) membranes. *J Membr Sci* 473:63–71. <https://doi.org/10.1016/j.memsci.2014.08.046>
- Oztekin Y, Yazicigil Z (2007) Recovery of acids from salt forms of sodium using cation-exchange membranes. *Desalination* 212(1–3):62–69
- Padwal N, Prakash SS, Thakkar S, Deshpande T (2018) Supported liquid membrane technology: advances and review of its applications. *Indian J Adv Chem Sci* 6(3):118–129. <https://doi.org/10.22607/IJACS.2018.603004>
- Pal P (2017) Chapter 5 – water treatment by membrane-separation technology: industrial water treatment process technology, pp 173–242. <https://doi.org/10.1016/B978-0-12-810391-3.000059>
- Parhi PK (2013) Supported liquid membrane principle and its practices: a short review. *J Chem*, Article ID 618236, 11 pages. <https://doi.org/10.1155/2013/618236>
- Petersen RJ (1993) Composite reverse osmosis and nanofiltration membranes. *J Membr Sci* 83:81. [https://doi.org/10.1016/0376-7388\(93\)80014-O](https://doi.org/10.1016/0376-7388(93)80014-O)
- Prabhakar S, Misra BM, Ramani MPS (1989) Management and feasibility of reverse osmosis schemes for rural water supply in India. *Desalination* 73:37–46. [https://doi.org/10.1016/0011-9164\(89\)87003-1](https://doi.org/10.1016/0011-9164(89)87003-1)
- Prabhakar S, Panicker ST, Misra BM, Ramani MPS (1992) Studies on the reverse osmosis treatment of uranyl nitrate solution. *Sep Sci Technol* 27(3):349–359. <https://doi.org/10.1080/01496399208018885>
- Prabhakar S, Misra BM, Roy SB, Meghal AM, Mukherjee TK (1994) Reverse osmosis separation of radio-contaminants from ammonium diuranate effluents. *Sep Sci Technol* 29(8):1001–1010. <https://doi.org/10.1080/01496399408005613>
- Prabhakar S, Balasubramanian C, Hanra MS, Misra BM, Roy SB, Meghal AM, Mukherjee TK (1996) Performance evaluation of reverse osmosis (RO) and nanofiltration (NF) membranes for the decontamination of ammonium Di-uranate effluents. *Sep Sci Technol* 31(4):533–544. <https://doi.org/10.1080/01496399608002215>
- Qasim M, Badrelzaman M, Darwish NN, Darwish NA, Hilal N (2019) Reverse osmosis desalination: a state-of-the-art review. *Desalination* 459:59–104. <https://doi.org/10.1016/j.desal.2019.02.008>
- Qudais HA, Moussa H (2004) Removal of heavy metals from wastewater by membrane processes: a comparative study. *Desalination* 164(2):105–110. [https://doi.org/10.1016/S0011-9164\(04\)00169-9](https://doi.org/10.1016/S0011-9164(04)00169-9)
- Ramaswami S, Behrendt J, Otterpohl R (2018) Comparison of NF-RO and RO-NF for the treatment of mature landfill leachates: a guide for landfill operators. *Membranes* 8(2):17. <https://doi.org/10.3390/membranes8020017>
- Rao SVS, Paul B, Lal KB, Narasimhan SV, Ahmed J (2000) Effective removal of cesium and strontium from radioactive wastes using chemical treatment followed by ultra filtration. *J Radioanal Nucl Chem* 246(2):413–418. <https://doi.org/10.1023/A:1006771918337>

- Ray SS, Chen SS, Li CW, Nguyen NC, Nguyen HT (2016) A comprehensive review: electrospinning technique for fabrication and surface modification of membranes for water treatment application. *RSC Adv* 6(88):85495–85514. <https://doi.org/10.1039/C6RA14952A>
- Reig M, Valderrama C, Gibert O, Cortina JL (2016) Electrodialysis and bipolar membrane electro dialysis combination for industrial process brines treatment: Monovalent-divalent ions separation and acid and base production. *Desalination* 399(1):88–95. <https://doi.org/10.1016/j.desal.2016.08.010>
- Ren J, McCutcheon JR (2014) A new commercial thin film composite membrane for forward osmosis. *Desalination* 343:187–193. <https://doi.org/10.1016/j.desal.2013.11.026>
- Ren Z, Zhang W, Meng H, Liu J, Wang S (2010) Extraction separation of Cu(II) and Co(II) from sulfuric solutions by hollow fiber renewal liquid membrane. *J Membr Sci* 365(1–2):260–268. <https://doi.org/10.1016/j.memsci.2010.09.017>
- Sadeghi F, Aji A, Carreau PJ (2007) Analysis of microporous membranes obtained from polypropylene films by stretching. *J Membr Sci* 292:62–71. <https://doi.org/10.1016/j.memsci.2007.01.023>
- Sarkar P, Goswami D, Prabhakar S, Tewari PK (2008) Optimized design of a reverse osmosis system with a recycle. *Desalination* 230(1):128–139. <https://doi.org/10.1016/j.desal.2007.11.021>
- Sarkar P, Tiwari S, Prabhakar S, Tewari PK (2011) Recovery of water from saturated solutions by membrane processes. *Desalin Water Treat* 36(1–3):65–74. <https://doi.org/10.5004/dwt.2011.1968>
- Sarkar P, Goswami D, Prabhakar S, Tewari PK (2013) Mathematical model for the removal of trace metal by complexation-ultrafiltration. *Desalin Water Treat* 51(22–24):4435–4446. <https://doi.org/10.1080/19443994.2013.770117>
- Scarazzato T, Panossian Z, Tenório JAS, Pérez-Herranz V, Espinosa DCR (2018) Water reclamation and chemicals recovery from a novel cyanide-free copper plating bath using electro dialysis membrane process. *Desalination* 436:114–124. <https://doi.org/10.1016/j.desal.2018.01.005>
- Schrotter JC, Rapenne S, Leparç J, Remize PJ, Casas S (2010) Current and emerging developments in desalination with reverse osmosis membrane systems. In: Drioli E, Georno L (eds) *Comprehensive membrane science and engineering*, vol 2, pp 35–65. <https://doi.org/10.3390/membranes8030060>
- Shang R, Van den Broek W, Heijman SGJ, Van Agtmaal S, Rietveld LC (October 2011) Wastewater reuse through RO: a case study of four RO plants producing industrial water. *Desalin Water Treat* 34:408–415. <https://doi.org/10.5004/dwt.2011.2895>
- Shen SF, Smith KH, Cook S, Kentish SE, Perera JM, Bowser T, Stevens GW (2009) Phenol recovery with tributyl phosphate in a hollow fiber membrane contactor: experimental and model analysis in two separate hollow fiber membrane modules in co-current mode using 10% (v/v) TBP/ Shellsol2046. *Sep Purif Technol* 69:48–56. <https://doi.org/10.1016/j.seppur.2009.06.024>
- Smith EL, Abbott AP, Ryder KS (2014) Deep eutectic solvents (DESs) and their applications. *Chem Rev* 114(21):11060–11082. <https://doi.org/10.1021/cr300162p>
- Sofiya K, Poonguzhali E, Kapoor A, Delfino P, Prabhakar S (2019) Separation of carboxylic acids from aqueous solutions using hollow fiber membrane contactors. *J Membr Sci Res* 5:233–239. <https://doi.org/10.22079/JMSR.2018.88804.1199>
- Song X, Wang L, Tang CY, Wang Z, Gao C (2015a) Fabrication of carbon nanotubes incorporated double-skinned thin film nanocomposite membranes for enhanced separation performance and antifouling capability in forward osmosis process. *Desalination* 369:1–9. <https://doi.org/10.1016/j.desal.2015.04.020>
- Song Y, Gao X, Li T, Gao C, Zhou J (2015b) Improvement of overall water recovery by increasing RNF with recirculation in a NF–RO integrated membrane process for seawater desalination. *Desalination* 361:95–104. <https://doi.org/10.1016/j.desal.2015.01.023>
- Tanaka Y, Ehara R, Itoi S, Goto T (2003) Ion-exchange membrane electro dialytic salt production using brine discharged from a reverse osmosis seawater desalination plant. *J Membr Sci* 222:71–86. [https://doi.org/10.1016/S0376-7388\(03\)00217-5](https://doi.org/10.1016/S0376-7388(03)00217-5)

- Teixeira MR, Rosa MJ, Nyström M (2005) The role of membrane charge on nanofiltration performance. *J Membr Sci* 265(1–2):160–166. <https://doi.org/10.1016/j.memsci.2005.04.046>
- Ulbricht M (2006) Advanced functional polymer membranes. *Polymer* 47(7):2217–2262. <https://doi.org/10.1016/j.polymer.2006.01.084>
- Van der Bruggen B, Vandecasteele C, Van Gestel T, Doyen W, Leysen R (2003) A review of pressure-driven membrane processes in wastewater treatment and drinking water production. *Environ Prog* 22(1):46–56
- van Voorthuizen EM, Zwijnenburg A, Wessling M (2005) Nutrient removal by NF and RO membranes in a decentralized sanitation system. *Water Res* 39(15):3657–3667. <https://doi.org/10.1016/j.watres.2005.06.005>
- Vandekar VD (2015) Manufacturing of hollow fiber membrane. *Int J Sci Res (IJSR)* 4(9) https://www.ijsr.net/archive/v4i9/v4i9_02.php
- Voutchkov N (2018) Energy use for membrane seawater desalination – current status and trends. *Desalination* 431:2–14. <https://doi.org/10.1016/j.desal.2017.10.033>
- Walton J, Lu H, Turner C, Solis S, Hein H (2004) Solar and waste heat desalination by membrane distillation. Denver. <https://www.usbr.gov/research/dwpr/reportpdfs/report081.pdf>
- Wang P, Chung T-S (2015) Recent advances in membrane distillation processes: membrane development, configuration design and application exploring. *J Membr Sci* 474:39–56. <https://doi.org/10.1016/j.memsci.2014.09.016>
- Wong JM (2012, May). www.waterworld.com/home/article/16211563/water-reuse-for-petroleum-oil-product-processing-industries
- Yang Z, Ma X-H, Chuyang YT (2018) Recent development of novel membranes for desalination. *Desalination* 434:37–59. <https://doi.org/10.1016/j.desal.2017.11.046>
- Zare S, Kargari A (2018) Emerging technologies for sustainable desalination handbook. Elsevier. ISBN 978-0-12-815818-0. <https://doi.org/10.1016/C2017-0-03562-0>
- Zhang Y, Ma C, Ye F, Kong Y, Li H (2009) The treatment of wastewater of paper mill with integrated membrane process. *Desalination* 236:349–356. <https://doi.org/10.1016/j.desal.2007.10.086>
- Zhang W, Cui C, Hao Z (2010) Transport study of Cu(II) through hollow fiber supported liquid membrane. *Chin J Chem Eng* 18(1):48–54. [https://doi.org/10.1016/S1004-9541\(08\)60322-5](https://doi.org/10.1016/S1004-9541(08)60322-5)
- Zhang Y, Desmidt E, Van Looveren A, Pinoy L, Meesschaert B, Van Der Bruggen B (2013) Phosphate separation and recovery from wastewater by novel electrodialysis. *Environ Sci Technol* 47(11):5888–5895
- Zhongwei Y, Runci W, Taihong Y, Weifang Z (2017) The removal of uranium from simulated ammonium diuranate filtrate by nanofiltration. 25th International conference on nuclear engineering volume 7: fuel cycle, decontamination and decommissioning, radiation protection, shielding, and waste management; mitigation strategies for beyond design basis Shanghai, China, July 2–6, 2017 Paper No. ICONE25-67899, pp V007T10A042; 5 pages ISBN: 978-0-7918-5785-4. <https://doi.org/10.1115/ICONE25-67899>
- Zhu X, Zheng Y, Chen Z, Chen Q, Gao B, Yu S (2013) Removal of reactive dye from textile effluent through submerged filtration using hollow fiber composite nanofiltration membrane. *Desalin Water Treat* 51(31–33):6101–6109. <https://doi.org/10.1080/19443994.2013.770225>

Chapter 9

Nanomaterials for the Photoremediation of Pollutants



Mohammad Chahkandi and Mahboobeh Zargazi

Contents

| | | |
|-------|---|-----|
| 9.1 | Introduction | 284 |
| 9.1.1 | General Views of Photocatalytic Remediation | 284 |
| 9.1.2 | Photo-Effective Nanostructures | 286 |
| 9.2 | Principles of Photocatalytic Progress | 286 |
| 9.2.1 | Sunlight Interactions | 286 |
| 9.2.2 | Mechanistic View | 287 |
| 9.2.3 | Thermodynamic | 290 |
| 9.2.4 | Kinetics of Catalytic Reactions | 290 |
| 9.3 | The Mechanistic Aspects of Visible/Sunlight Photoactivity | 292 |
| 9.3.1 | Heterogeneous Coupling | 294 |
| 9.3.2 | Z-Scheme | 297 |
| 9.3.3 | p–n Junction Materials | 300 |
| 9.3.4 | Ion-Exchangeable Semiconductors | 301 |
| 9.3.5 | Photocatalytic Compounds Kind | 304 |
| 9.4 | Future Remarks and Limitations | 307 |
| 9.5 | Conclusions | 308 |
| | References | 309 |

Abstract The restricted global fear within contaminated ecosystem has been motivated the impress works to employ the photocatalytic degradation of organic pollutants and pesticides. Generally, stability and water solubility of pesticides cause high impacts on environment due to high resistance in ecosystem. Heterogeneous nano-photocatalyst can be introduced as one of the most appealing technologies bearing great remediation performance because of the high surface area and intense correlated activity. The heterogeneous catalytic nanomaterials have been operated to

M. Chahkandi (✉)

Department of Chemistry, Hakim Sabzevari University, Sabzevar, Iran
e-mail: m.chahkandi@hsu.ac.ir

M. Zargazi

Department of Chemistry, Faculty of Science, Ferdowsi University of Mashhad, Mashhad, Iran

© The Editor(s) (if applicable) and The Author(s), under exclusive license to Springer Nature Switzerland AG 2021

283

Inamuddin et al. (eds.), *Water Pollution and Remediation: Photocatalysis*, Environmental Chemistry for a Sustainable World 57, https://doi.org/10.1007/978-3-030-54723-3_9

harvest, turn, and supply clean and renewable sunlight energy. It can be performed through entire water splitting and CO production to provide green-sustainable solar fuels alongside of wide ranges of environmental aspects. We reviewed in the presented chapter focusing on the application of effective nanomaterials in environmental remediation about industrial and agricultural effluents. For years TiO₂ photocatalyst has been largely utilized but includes restricted activity just in UV spectrum due to wide band gap. Therefore, it is crucial to development of new effective visible light-sensitive photocatalysts with lower band gap that can be activated by a notable percentage of the solar irradiations. Herein, we try to discuss the basic science drives for performance improving of visible/solar light photocatalysts. First, the corresponding principles which include of thermodynamics, kinetics, and recombination rate are followed. The second section reviews the new effective reported visible-activated photocatalytic compounds considering with proposed photoexcitation mechanisms and reducing the charges recombination. Finally, the main challenges and future prospects for better handling of photocatalytic technology were briefly discussed.

Keywords Nano-photocatalyst · Photocatalytic mechanism · UV-activated · Visible-activated · Semiconductor

9.1 Introduction

9.1.1 *General Views of Photocatalytic Remediation*

During the past centuries, increasing human energy demands have been resolved by fossil combustion-based sources such as oil, coal, and natural gases. The used sources caused different overproductions with known and unknown impacts on environment. Awareness about some other mineral fuel energies like nuclear source are insufficient from waste access and defect of technology points of view (Da Rosa 2012). However, the main adverse effects of mineral fuels on air, water, and soil can be regarded as global warming or impact on climate. Therefore, economic and population growing global societies have urgently asked for new, renewable, inexpensive, and easy affordable clean energy sources (Nuraje et al. 2012; Da Rosa 2012; Asmatulu 2015). The clean energy sources can be mainly achieved from natural sunlight, tides, wind, rain, biomass, and other sources without damaging the earth. The greatest and clean sun energy source has huge magnitude releasing near to 105 terawatts versus world's current energy requirement of 12 terawatts, 0.01% of total amount. Nanotechnology as ongoing technology can suggest approaches to degrading production charges, improving efficiency, and stashing energy, healthy environmental remediation, and so on (Asmatulu et al. 2010, 2011; Luque and Balu 2013; Nuraje et al. 2013). Obviously, industrialization have picked up greenhouse gas emission and particulate dust pollutants, continued over

Table 9.1 Advances oxidation processes for environmental remediation

| Type of degradation technology | Example | References |
|--------------------------------|---|--|
| Non-photochemical degradation | Sonochemical | Ghows and Entezari (2013) |
| | Electrochemical | Li et al. (2007) |
| | Fenton method (Fenton, electro-Fenton, Sono-Fenton) | Homem and Santos (2011) and Zhang et al. (2019) |
| | H ₂ O ₂ oxidation | Bokare and Choi (2014) |
| | Supercritical water oxidation | Yao et al. (2018) |
| | Solvated electron reduction | Yu et al. (2018) |
| | Enzymatic treatment | Ahmed et al. (2017) |
| | Ozonation | Yang et al. (2018) |
| | O ₃ /H ₂ O ₂ O ₃ /Catalyst | |
| Photochemical degradation | O ₃ /UV | Homem and Santos (2011) |
| | O ₃ /UV/H ₂ O ₂ | Rivera-Utrilla et al. (2013) |
| | Photo-Fenton, Photo- Fenton-electro, photo-Sono-Fenton | Barrera-Salgado et al. (2016) and Zhao et al. (2017) |
| | Photo-activated catalytic oxidation by UV/Visible | Chen et al. (2016) and Opoku et al. (2017) |

the decades. Alternative route can be addressed by nanomaterials with photocatalytic degradation ability of greenhouse gases and other emission pollutants (Taherzadeh et al. 2013).

Environmental remediation can be performed by different methodologies, and that one of the widely used is chemical degradation. It can be achieved by different methods such as (1) photocatalytic, (2) Fenton method, (3) ozone/UV radiation/H₂O₂ oxidation, (4) sonochemical, (5) electrochemical, (6) supercritical water oxidation, (7) solvated electron reduction, (8) enzymatic treatment, and (9) the electron beam irradiation (Table 9.1) (Andreozzi et al. 1996, 1999; Jayaweera 2003; Gogate and Pandit 2004a, b; Babuponnusami and Muthukumar 2014). UV light and ozone alone have disinfection applications. The combined O₃/UV/H₂O₂ method progresses through oxidation/photolysis reactions, and generation of free hydroxyl radicals can highly degrade the organic pollutants. However, the secondary treatment for complete neutralization of pollutants should be executed through advanced oxidation processes. Advanced oxidation processes are achieved by complete mineralization of matters to H₂O and CO₂ through in fold of strong vibrant hydroxyl and superoxide radicals. Some of the most prevalent advanced oxidation processing technologies are listed in Table 9.1. One of the effective photodegradation reactions can be progressed using nano-semiconductor and solvated O₂ gas to form the promoter radicals. The principles of photocatalysis process of titania substrates were investigated based on “Honda–Fujishima effect” relating to photoinduced water splitting (Fujishima et al. 2008). Heterogeneous photocatalysts introduce efficient advanced oxidation processes within abatement of chemical pollutions. Advanced oxidation processes are associated with advantages of visible/white light-sensitive

photocatalysts having wide range of absorption spectra from UV to visible wavelengths (Herrmann 1995).

9.1.2 Photo-Effective Nanostructures

The binary and ternary metal oxides are initial photoactive particles used in photocatalytic structural devices such as solar cell, photoremediation, and water splitting. In order of environmental concerns, green, easygoing, and safe-producing methods of nanomaterials are fruitful. The desired techniques should include low temperature and high progress rate, with lowered hazardous agents or by-products. For example, one of the best photocatalysts, TiO_2 , is generally synthesized by polymerizable complex approach, sol-gel reaction, and solid-state progress. However, the two first ones offer applicable performance than the last one because of providing small crystallite and particle size and controllable particle shape (Nuraje et al. 2012). Pure TiO_2 photocatalysts have not enough power to hydrogen production through water splitting. Therefore, some modification is needed such as loaded Pt or other metal ions to approach band gap of 3.2 eV or lower activated under UV light (Nuraje et al. 2012; Luque and Balu 2013; Asmatulu 2015). Despite above, ZrO_2 having high 5.0 eV band gap as an UV photocatalyst can split water without assisting of any co-catalyst. Photo-UV catalytic ability of ZrO_2 decreased by loading co-catalysts such as Pt, Au, and RuO_2 . In the next sections, the base interaction of photon and photocatalysts, the mechanism, and thermodynamic aspects have been discussed. In the following, different kinds of UV-visible-activated catalysts have been investigated, in details.

9.2 Principles of Photocatalytic Progress

9.2.1 Sunlight Interactions

Green photo-induced nanostructures are considered due to its applicability for sustained energy generation and environmental remediation strategies through interactions with infinite sunlight irradiations. Nanoscale structures with great ratio of surface area to volume resulted in highly increase of sunlight interactions compared to bulk format of materials. Nanostructures can be suggested as ideal entrant for a broad diversity of environmental issues grounded on photocatalysis and photosynthesis (Frank et al. 2004; Kay et al. 2006; Verma et al. 2011; Spinelli et al. 2012; Beard et al. 2014; Yeo et al. 2014). Among whole releasing sun energy, only a few small portion is absorbed by the earth. Therefore, the important photosynthesis reactions are proceedings that can influence on human life as cultivation and forestry. Sunlight as continuous light spectrum includes from high wavelengths of radio to low ones of X, and gamma ray ranges in $1-10^{-13}$ m of wavelength

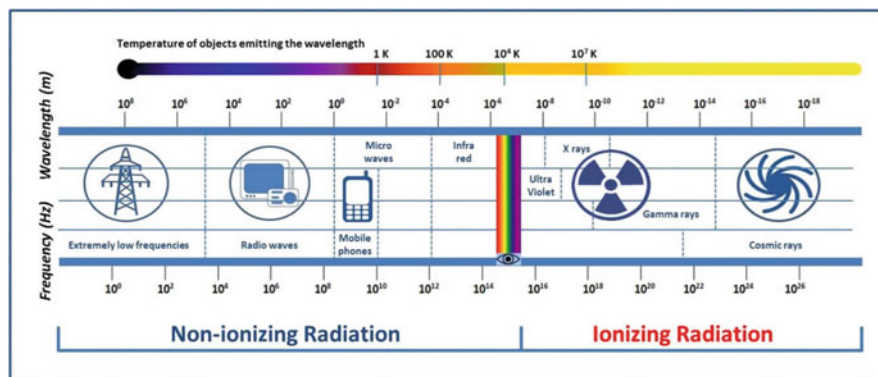


Fig. 9.1 Spectrum of electromagnetic waves. Sunlight as continuous light spectrum includes from high wavelengths of radio to low ones of X, and gamma rays range in $1\text{--}10^{-13}$ m of wavelength. (Saliev et al. 2019)

(Fig. 9.1). The small division of visible wavelengths from violet to red lights is considered in interaction of photocatalyst and visible light.

Actually, the passed sunlight from atmosphere of the earth interacts with photoactive materials in three ways: reflection, scattering, and absorption. Reflection specified as the fraction of reflected energy calls the reflectivity, R :

$$R = \frac{n_1 - n_2}{n_1 + n_2} \quad (9.1)$$

where n_1 and n_2 are refractive indices of two interface sides of the materials. Refractive index is explained as the ratio of light speed in vacuum against material. Scattering is defined as light orientation changing in randomly manner during the interaction to media that is divided to elastic and inelastic scattering kinds. Absorption happens when energy value of the light adapts the transition energy of the electrons of materials. In clear expression, absorption by an isolated material-bearing electronic density leads to the charge transition of the valence band across the band gap to the conduction band (Neil and Ashcroft 2016). For every transferred electron to conduction band, an unoccupied hole in valence band generates a pair known as e^-h^+ . It must be rephrased that absorption as the basic step of photocatalytic process is necessary for often applications of solar energy (Fig. 9.2).

9.2.2 Mechanistic View

There are 5-main steps involving the heterogeneous photocatalyst occurred from bulk of media toward to the final yield include of surface adsorption, photodegradation reactions, and desorption of conclusive products over the surface to the bulk media (see Fig. 9.3).

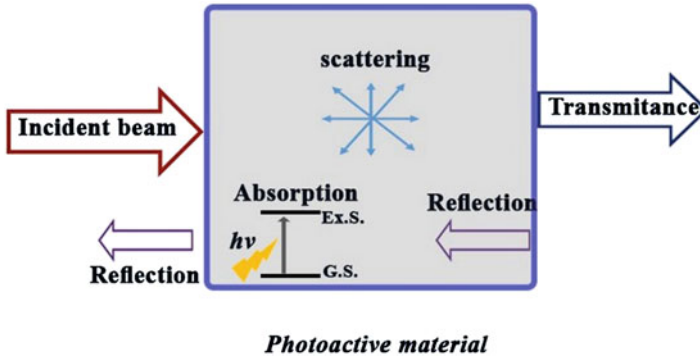


Fig. 9.2 Three ways of interaction of light with the material including reflection, scattering, and absorption. Ex. S. and G. S. represent excitation and ground states, respectively

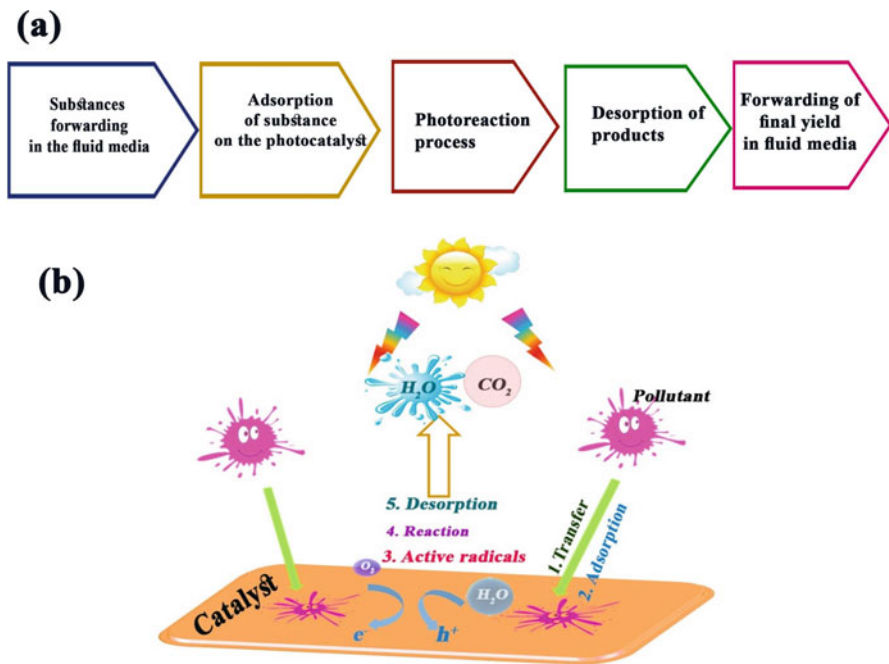


Fig. 9.3 Five possible main steps for interaction of light to the bulk of media and surface of the heterogeneous photocatalyst include surface adsorption, photodegradation reactions, and desorption of conclusive products over the surface to the bulk media

The basic photocatalytic reactions can be explained with six equations (see Fig. 9.4). The absorption of higher-energy photons versus the energy level of photocatalyst band gap is an essential primer step. Equation 9.2: Photon absorption leads to transfer of valence band electrons to conduction band and creation of hole

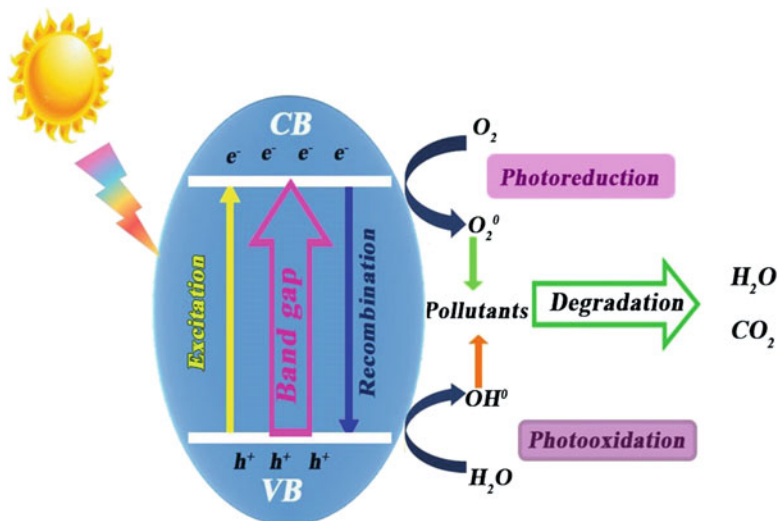
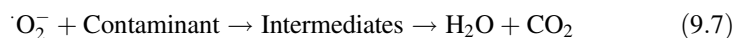
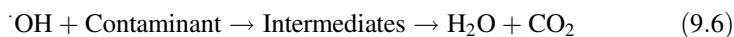
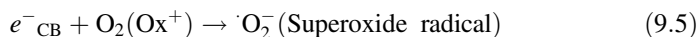
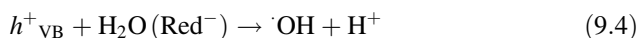


Fig. 9.4 The basic photocatalytic reactions can be explained with six equations: absorption of higher energy photons; transfer of valence band electrons to conduction band; recombination of existing electrons and holes and liberation of heat energy; reaction of produced electrons and involved oxidants; and reaction of holes and reductants. CB and VB stand for conductive band and valence band, respectively

over the valence band. Equation 9.3: The recombination of existing electrons and holes and liberation of energy in heat form is possible. Equations 9.4 and 9.5: Probable reaction of produced electrons and involved oxidants and also reaction of holes and reductants, to build vibrant radicals. Equations 9.6 and 9.7: The following shows degradation of pollution substances to mineralized carbon dioxide and water:



9.2.3 Thermodynamic

The efficiency of catalytic process can be measured by two numeric and energetic methods. The numeric method needs to “inherent quantum efficiency; \emptyset ” definition which means the products value ratio, based on primer photoreaction rate, and to value absorbed photons by system. In practical, in heterogeneous photocatalytic system, a mathematical term named “apparent quantum efficiency; ξ ” is described as the ratio of reaction rate to the intensity of monochromatic light for concentration of i species C_i :

$$\xi_{C_i} = \pm(d[C_i]/dt)_0 / (d[h\nu]_{\text{int}}/dt) \quad (9.8)$$

where $\pm(d[C_i]/dt)_0$ is change of initial rate of species concentration and $(d[h\nu]_{\text{int}}/dt)$ is change of incident photo rate (Hoffmann et al. 1995).

Efficiency of energy conversion, ϵ , can be evaluated by ξ product to the changes ratio of Gibb’s free energy to effective photon energy, E_p (Ohtani 2010):

$$\epsilon = \xi \cdot (\Delta G/E_p) \quad (9.9)$$

The accurate value of recombination rate of hole and electron cannot be measured by the inherent quantum efficiency.

9.2.4 Kinetics of Catalytic Reactions

The reaction rate of general form of Eqs. 9.6 and 9.7 as $A + B \rightarrow C + D$ is given by:

$$r = -dC_A/dt = k C_A C_B \quad (9.10)$$

where C_A , conduction band, and k are concentrations of A , B , and constant of reaction rate, respectively.

As illustrated in Fig. 9.3, heterogeneous photocatalytic process includes adsorption–desorption and reaction over the surface. It can be supposed that adsorption and desorption of reactants over the surface of catalyst is rapid. However, photocatalytic reaction is obviously the slowest step considered as the rate-determining step generally followed by Langmuir–Hinshelwood or L–H model. It should be formulated as:

$$r = -d[\text{Red}]/dt = -d[\text{Ox}]/dt = k\theta_{\text{Red}}\theta_{\text{Ox}} \quad (9.11)$$

where θ_{Red} means fraction of adsorbed reductant over the catalyst surface and θ_{Ox} means fraction of adsorbed oxidant over the catalyst surface.

Moreover, θ_i can be defined based on K_i , adsorption constant:

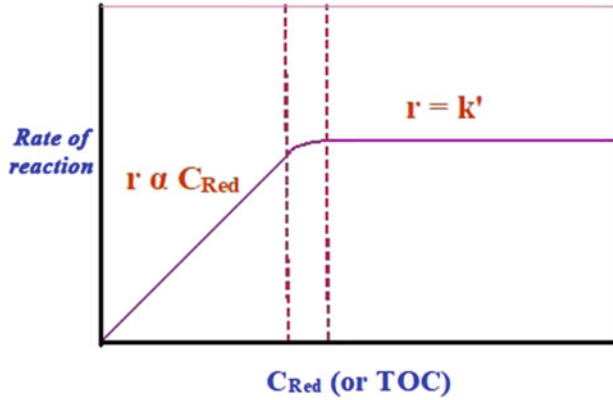


Fig. 9.5 The degradation rates at low concentrations of reductant conforms to first-order kinetics while independent at higher concentrations. C_{Red} stands for concentration of reduction

$$\theta_i = K_i C_i / (K_i C_i + 1) \tag{9.12}$$

Combination of Eqs. (9.11) and (9.12) can be rephrased as:

$$r = k K_{Red} C_{Red} K_{Ox} C_{Ox} / (K_{Red} C_{Red} + 1) (K_{Ox} C_{Ox} + 1) \tag{9.13}$$

Actually, K_i value which is experimentally determined in dark means no photocatalytic reaction. Some simple approximations can reduce the complexity form of Eq. (9.13). The oxidant can be considered as a pure liquid, so $\theta_{Ox} = 1$; or as a fluid solution, based on Henry’s law, $\theta_{Ox} = \text{constant}$. Therefore:

$$r = k' \theta_{Red} = k' K_{Red} C_{Red} / (K_{Red} C_{Red} + 1) \tag{9.14}$$

If $C_{Red} = C_{Red, \max}$, so $\theta_{Red} = 1$ and $r = k'$.

In contrast, if $C_{Red} \ll C_{Red, \max}$, so $\theta_{Red} = K_{Red} C_{Red}$ and $r = k' K_{Red} C_{Red} = K_{\text{apparent}} C_{Red}$ (9.15)

Therefore, the degradation rates at low concentrations of reductant conform to first-order kinetics while independent at higher concentrations (Fig. 9.5).

For overall rate estimation as complementary consideration, photomineralization rate of produced intermediates through Eqs. (9.6) and (9.7) can be stated based on total organic carbon; TOC or chemical oxygen demand; COD values (Minero et al. 1996; Malato et al. 2009):

$$r_{TOC,0} = \beta_1 [TOC] / (\beta_2 + \beta_3 [TOC]) \tag{9.16}$$

that $[TOC]_0$ is considered as the prime content of TOC at zero time, $t = 0$.

9.3 The Mechanistic Aspects of Visible/Sunlight Photoactivity

As aforementioned notes, a semiconductor photocatalyst absorbs the energetic photons that lead to the generation of electron–hole pairs with electron photoexcitation through heavy valence band to empty conduction band. As we know, very quick recombination of the generated electron–hole give rise to energy destruction and diminishing of quantum efficiency. Accordingly, novel-improving mechanisms for spare recombination are constantly pursued. The key issue for spare recombination is to stretch the photo-absorption region along with separation performance of electron–hole pairs. Producing of heterojunction kind of crystalline semiconductors is proposed as an operational solution. The effectiveness of a semiconductor within photocatalytic behavior crucially belongs to the energy alignment of the band gap. Interfaces of semiconductor heterojunction can be categorized into three types: straddling gap, type I; staggered gap, type II; and broken gap, type III (Fig. 9.6a). The great improvement can be achieved by conversion of traditional type II into direct Z- and S-schemes. S-scheme is built up as a combination of two n-type semiconductor photocatalysts. (Di et al. 2017; Low et al. 2017; Zhu et al. 2017; Fu et al. 2018, 2019; Tan et al. 2018; Li et al. 2019e) (Fig. 9.6b).

The effective developed photocatalysts can be categorized in four main classes: metal oxides (Zhu et al. 2017; Tan et al. 2018; Li et al. 2019e), sulfides (Tada et al. 2011; Zhang et al. 2012, 2016; Bai et al. 2013; Wei et al. 2018b), valuable metal semiconductors (Miao et al. 2013; Cai et al. 2017; Li et al. 2018a; Zhang et al. 2018b), and non-metallic semiconductors (Feng et al. 2018; Wu et al. 2018; Zheng et al. 2018; Qi et al. 2019; Reddy et al. 2019; Wang et al. 2019b). However, each photocatalyst has some disutility such as heavy metal or harmful leaching pollution, expensive, high thermal treatment, and low stability within catalytic reactions. Wang et al. (2008) reported that an applicable synthesized organic conjugated photocatalyst, named graphite carbon nitride (g-C₃N₄), has the capability of visible light absorption with band gap = 2.7 eV and $\lambda > 420$ nm for water splitting. g-C₃N₄ has various advantages such as easy preparation route, high stability, low cost, and visible frequencies sensitivity (Nayak et al. 2015; Jiang et al. 2018a; Li et al. 2019d; Xu et al. 2019b; Zhu et al. 2019). Therefore, recently huge attentions have been grown for preparation of pure g-C₃N₄ (Ma et al. 2018; Wang et al. 2018; Zhao et al. 2018), elemental loading modification (Wang et al. 2017; Bellardita et al. 2018; Da Silva et al. 2018; Deng et al. 2018; Shanker et al. 2018), heterogeneous composites (Tian et al. 2013; Zhou et al. 2014; Ran et al. 2018a), and diverse morphology preparation (Yang et al. 2015; Yu et al. 2016; Shakeel et al. 2019). The notable issue has many defects which exist with pure bulk g-C₃N₄ including small specific surface area (Sun and Liang 2017; Jiang et al. 2018b), low performance in solar irradiation ranges due to low absorption of wavelengths longer than 460 nm (Ye et al. 2015; Naseri et al. 2017; Shen et al. 2018; Zhang et al. 2018a), difficult film forming, and rapid electron–hole recombination (Hao et al. 2018; Jin et al. 2018; Shi et al. 2018) (see Fig. 9.7). Therefore, new composite compounds with specific morphology can

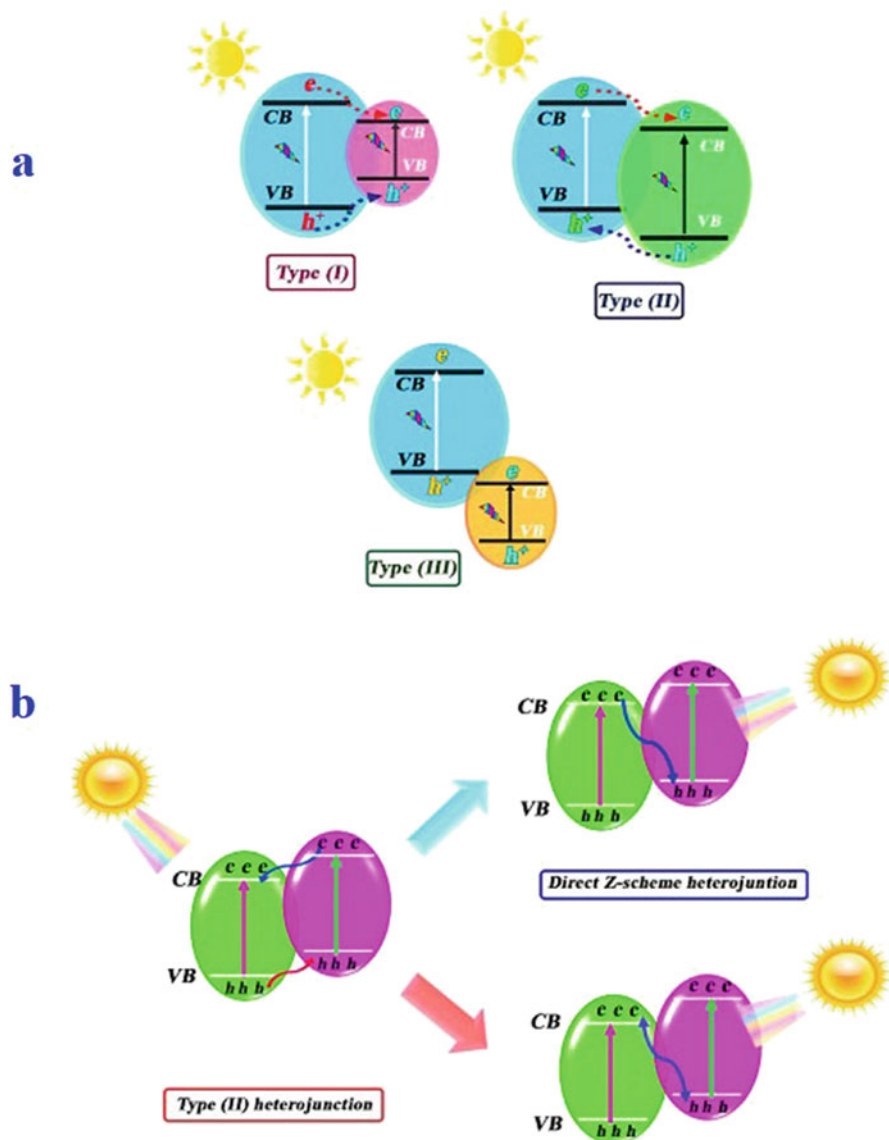


Fig. 9.6 (a) Three categories of interfaces of semiconductor heterojunction: straddling gap, type I; staggered gap, type II; and broken gap, type III. (b) The great improvement by conversion of traditional type II into direct Z- and S-schemes. CB and VB stand for conductive band and valence band, respectively

enhance photocatalytic efficiency (Li et al. 2015b, 2017c; Ong et al. 2016) using improved synthetic methods (Che et al. 2017; Li et al. 2017b), design of electrical structure (Ran et al. 2018b; Wei et al. 2018a; Wu et al. 2019), and nanostructure

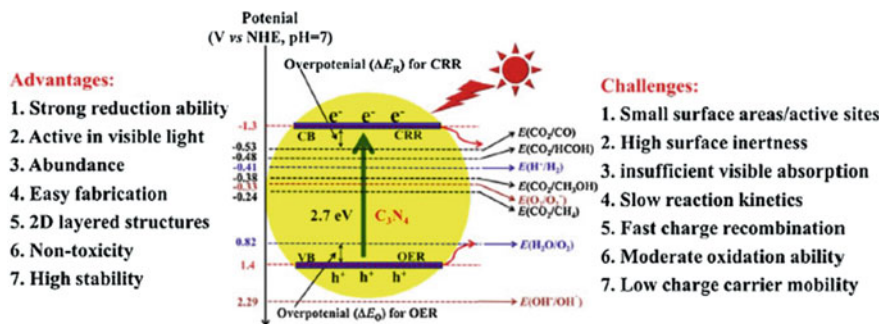


Fig. 9.7 The band gap influencing for redox potential of the appropriate reactions of g-C₃N₄ band edges at pH = 7. (Reprinted with permission of Elsevier from Wen et al. 2017)

manipulation (Dong et al. 2017; Ma et al. 2017; Li et al. 2018b). However, increasing researches about new composite materials of g-C₃N₄ highlight the potentially photocatalytic ability (Li et al. 2019c).

9.3.1 Heterogeneous Coupling

In order to inhibit recombination of formed electron and hole, achieving different surfaces of composited catalyst can be an approach. Therefore, heterostructured catalysts having various potentials of conduction bands and valence bands can be prepared. Through coupling construction, the excited electrons of conduction band having higher energy can move to the coupled catalyst conduction band. Analogously, electrons of valence band state of photocatalyst having higher potential should be excited to the valence band state of the coupled catalyst with lower-energy state (see Fig. 9.8). The progress is equivalent to the hole transferring of valence band with lower potential to the valence band of coupled one having higher potential state. Therefore, recombination rate will be reduced with transferring of generated electron–hole pairs to different surfaces of new coupled photocatalysts, resulting in improving photocatalytic efficiency.

UV-Activated Catalysts

Binary Metal Oxides

The binary metal oxides have mainly metal ions with d^0 configuration, which valence band and conduction band are combined of O 2p orbitals and d metal ones. The general examples are bimetallic TiO₂, Nb₂O₅, ZrO₂, Ta₂O₅, and WO₃, the anatase phase of the first one with lower band gap energy of 3.2 eV, determined as water splitting photocatalyst under UV irradiation. In order of effective photon

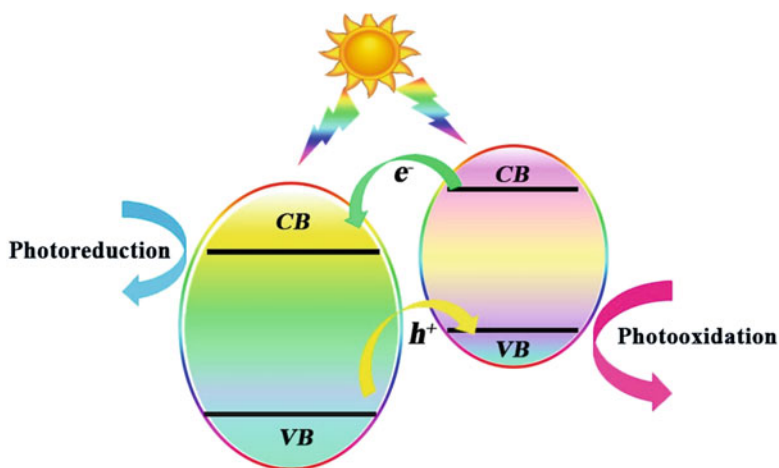


Fig. 9.8 Heterogeneous coupling leads to transfer of photo-prepared electrons and holes between surfaces of coupled photocatalysts and thus inhibition of recombination. CB and VB stand for conductive band and valence band, respectively

absorption of UV range, the band energy gap of photocatalyst should be lower than the UV energy light. The metal oxide having lesser energy of band gap must be reconstructed using cocystal additives for proper water molecules splitting. TiO_2 with particles loading of Pt, RuO_2 , NaOH, and Na_2CO_3 into photo-cocystal TiO_2/Pt raises the water splitting activity (Duonghong et al. 1981; Akihiko et al. 1987). Moreover, coupling of TiO_2 with some second semiconductors of metal oxides such as SnO_2 , Ag_xO , and ZrO_2 improves the photocatalytic efficiency. Therefore, the useful formed of heterostructures have higher photocatalytic ability of hydrogen production from an aqueous media including electron donors (Park and Kang 2007; Yuan et al. 2009). Metal oxides based on Nb like Nb_2O_5 with band gap = 3.4 eV can improved photocatalytic hydrogen evolution through coupling of Pt (Chen et al. 2007). The photoactivated splitting efficiency of water by the metal oxides of Ga_2O_3 with band gap = 4.6 eV and CeO_2 with d^{10} electronic configuration of metal ions is highly enhanced when coupled with Zn, Sr, Cr, Ta, Ba, Ca, and RuO_2 (Yanagida et al. 2004; Kadowaki et al. 2007).

Ternary Metal Oxides

Ternary metal oxide based on Ti with interlayered additives of TiO_2 shows efficient splitting reaction of water under UV light. The titanates with layered structures such as $\text{K}_2\text{Ti}_4\text{O}_9$, $\text{Na}_2\text{Ti}_3\text{O}_7$, and $\text{K}_2\text{Ti}_2\text{O}_5$ have enough photoactivity to hydrogen production via splitting reaction of water (Shibata et al. 1987). LaTiO_3 incorporated with NO- and Ba-doped in the presence of additive of alkaline hydroxide show permanent increasing of photocatalytic water splitting (Kim et al. 2005a). SrTiO_3

photocatalytic ability may be improved by some suitable metal cation coupling, such as La and Ga (Qin et al. 2007). Also, perovskite crystallite structure of CaTiO_3 with band gap = 3.5 eV doped with Zr shows higher photocatalytic performance under UV light (Sun et al. 2007). $\text{K}_4\text{Nb}_6\text{O}_{17}$ with layered structure show excellent photosplitting of water in an aqueous methanolic solution. The structure modified with cocatalysts of NiO, Au, Pt, and Cs perform increased photocatalytic activity for H_2 production (Sayama et al. 1998). Tantalate metal oxides like LiTaO_3 with band gap = 4.7 eV, KTaO_3 with band gap = 3.6 eV, and perovskite NaTaO_3 with band gap = 4.0 eV have high water splitting yields that mainly depend on band angles of Ta–O–Ta. Opening the angles near to 180° caused more easily transportation of electron–hole pairs and much reduction of the band gap. Some of W- and Mo-based heterogeneous materials show photoactive performance of water splitting just under UV light such as PbWO_4 with band gap = 3.9 eV and PbMoO_4 with band gap = 3.31 eV (Akihiko et al. 1990).

Visible Light-Activated Catalysts

The pure metal oxide usually bears some disadvantages of great resistivity and fast recombination pace of photo-produced charges. For example, WO_3 , Bi_2WO_6 , Bi_2MoO_6 , and $\alpha\text{-Fe}_2\text{O}_3$ have band gaps 2.8, 2.8, 2.7, and 2.2 eV, respectively, because positions of low conduction band do not have photoactivity about H_2 evolution (Aroutiounian et al. 2002; Ingler et al. 2004; Satsangi et al. 2008). Therefore, recent investigations try to improve the photoconductivity and low recombination rate of charges. One route is metal or non-metal doping to engineer the band gap energy. The electron donor species with higher levels of band gap than valence band of original photocatalyst, or electron acceptor ones with lower levels of band gap than original conduction band, provide wide ranges of band gap of metal oxides with visible light photoactivity. Coupling of TiO_2 with Pt^{4+} and Ag^+ increases the photocatalytic performance underneath both visible and UV irradiations (Kim et al. 2005b; Rengaraj and Li 2006). Pt^{4+} and Ag^+ metal ions participating in visible light absorption resulted in reducing of recombination rate. Using dye for sensitizing of metal oxides caused in reduction of wide band gap is another approaching method within improving the visible light sensitivity of water splitting. The process progresses with shift of excited electron of HOMO to LUMO of dye molecule and next transferring to conduction band of original photocatalysts. TiO_2 loaded with dye and $\text{K}_4\text{Nb}_6\text{O}_{17}$ show enhanced capability of H_2 evolution. Moreover, numerous coordination compounds Co(II), Zn(II), Pt(II), and Cr(II) with polypyridine, phthalocyanine, alizarine, and metalloporphyrins perform photocatalytic efficiency within H_2 generation (Shimidzu et al. 1985). A new heptazine-based porous organic polymer named POP–HE show intense visible light catalytic activity of oxidative conversion of benzyl alcohol to benzaldehyde. The researchers claimed that POP–HE compound has higher photocatalytic efficiency than graphite carbon nitride (Xu et al. 2019a). Another new research shows that anchoring of Pd nanoparticles to TiO_2 can permanently improve the

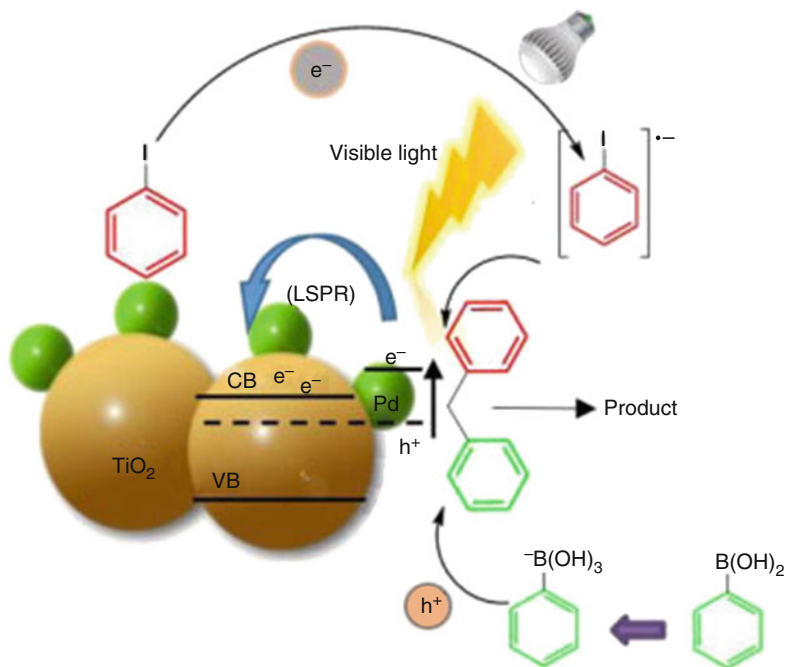


Fig. 9.9 Proposed mechanism of charge separation in Pd/TiO₂ compounds led to enhancement of Suzuki–Miyaura coupling reaction. LSPR represents localized surface plasmon resonance. (Reprinted with permission of Elsevier from Koohgard and Hosseini-Sarvari 2018)

photocatalytic activity of TiO₂ heterogeneous coupled catalyst within Suzuki–Miyaura coupling reaction. The applied synthetic method was resulted in reducing of recombination rate of hole–electron through the shown mechanism in Fig. 9.9 (Koohgard and Hosseini-Sarvari 2018). Li et al. introduced an effective coupled photocatalyst of BiVO₄/Ag₂O with low band gap prepared with impregnation–evaporation technique. BiVO₄/Ag₂O has shown higher photodegradation rate within methyl orange in comparison with pure BiVO₄ as a p–n heterojunction type (Li et al. 2015a). Also another p–n heterojunction semiconductor with BiVO₄ coupled with Cu₂O showed more photocatalytic degradation of methylene blue and colorless organic pollutant of phenol than BiVO₄ (Wang et al. 2013). The discussed and some more of visible light photocatalysts have been listed in Table 9.2.

9.3.2 Z-Scheme

Despite that many pure or couple metal oxides show suitable photocatalytic performance especially water splitting under irradiation of UV or visible light, some weaknesses diminish the quality of process:

Table 9.2 Photocatalysts coupled heterogeneously and the related usage

| No. | Photocatalyst | Usage | References |
|-----|---|-------------------------------|--------------------------------------|
| 1. | TiO ₂ /Pt/RuO ₂ | Water splitting/Rhodamine B | Duonghong et al. (1981) |
| 2. | TiO ₂ /Ag _x O | Hydrogen evolution | Park and Kang (2007) |
| 3. | Nb ₂ O ₅ /Pt | Hydrogen production | Chen et al. (2007) |
| 4. | POP-HE | Benzyl alcohol oxidation | Xu et al. (2019a) |
| 5. | TiO ₂ /Pd | Suzuki-Miyaura coupling | Koohgard and Hosseini-Sarvari (2018) |
| 6. | BiVO ₄ /Ag ₂ O | Methyl Orange | Li et al. (2015a) |
| 7. | g-C ₃ N ₄ / BiOCl _x Br _{1-x} | Rhodamine B and Rhodamine 640 | Shi et al. (2014) |
| 8. | Bi ₅ O ₇ I/Bi ₂ O ₃ | Malachite Green | Cheng and Kang (2015) |

- (a) A low percentage of light absorption up to the photocatalysts band gap
 (b) Returned reaction of water formation

Beyond three interface kinds of heterojunction semiconductors, only type II bears acceptable photocatalytic activity. The conversion of type II with a direct Z-scheme mechanism can more increase the efficiency and suggests the solution for the abovementioned disadvantages. The system includes two photocatalysts coupled through redox charges carrying. The mentioned system is a biomimetic mechanism occurred in the photosynthesis reactions for transferring of the photo-induced electron of H₂O to nicotinamide adenine dinucleotide phosphate. The formed couple of heterojunction includes several photocatalysts species as the relevant redox potentials of the generated charges are held at higher capacity. Therefore, a recombination reaction of a small amount of electron–hole pairs causes them to be sacrifice that makes the excited charges with higher energies leave behind (see Fig. 9.10). The interesting mechanism provides the capability for visible photons with relatively low energies to promote an efficient degradation process. Since Z-scheme mechanism donates the mentioned benefits to a single photocatalyst having wide band gap, the respected studies have been greatly increased. Some of them are summarized in Table 9.3. One of notable study reports Pt-loaded in ZrO₂–TaON and Pt-loaded in WO₃ that demonstrate permanent photocatalytic H₂ generation from water with high apparent quantum yield at 420 nm. ZrO₂ extends the lifetime of the photogenerated charges and inhibition of the recombination because of modification of TaON n-type semiconductor (Maeda et al. 2010). A modified silver chromate with graphene oxide as binary Ag₂CrO₄–GO photocatalyst has shown notable degradation of methylene blue and phenol under visible light (Xu et al. 2015). The energy levels of conduction band and valence band for single Ag₂CrO₄ and graphene oxide were measured ca. 0.47 V and 2.27 V vs. NHE and ca. –0.75 V and 1.75 V vs. NHE, respectively. The photogenerated electrons of the conduction band of silver chromate combine with cavities of valence band from graphene oxide resulted in leaving of conduction band electrons of graphene oxide with higher potential and more negatively potential than the –0.28 V as potential value of O₂^{*}/O₂. In some recent studies, the effective Z-scheme heterojunctions

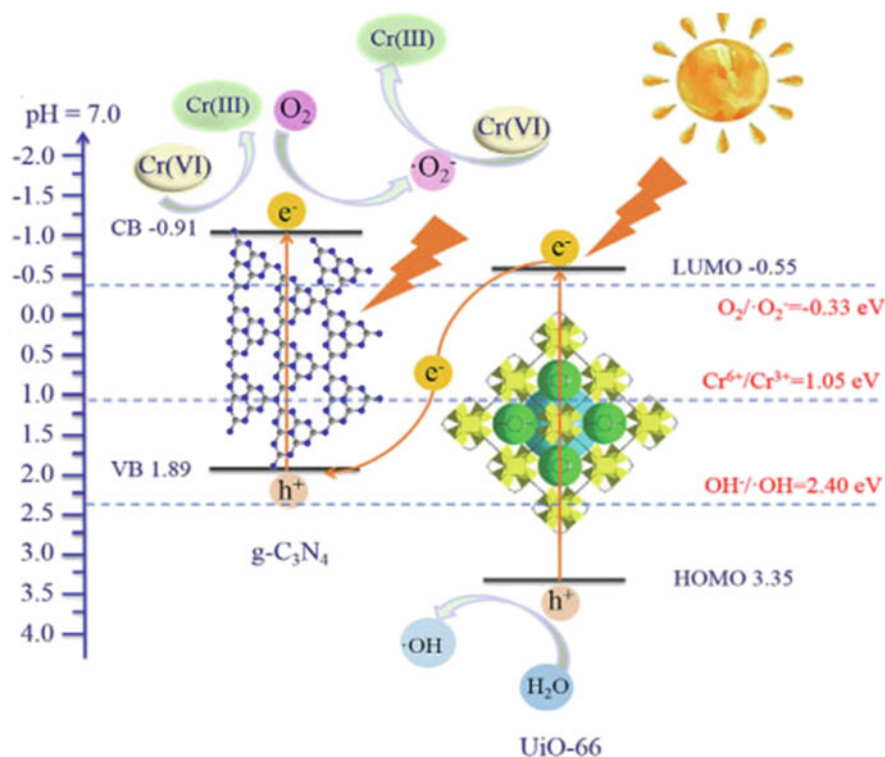


Fig. 9.10 A mechanistic view of photocatalytic Cr(VI) reduction mechanism of g-C₃N₄/UiO-66. HOMO energy of UiO-66 which is smaller than OH⁻/[·]OH pairs caused to form [·]OH with oxidation of OH⁻ or H₂O. CB and VB stand for conductive band and valence band, respectively. (Reprinted with permission of Elsevier from Yi et al. 2019)

within visible light photocatalytic performance have been prepared by loading of cuprous oxide, graphite carbon nitride, bismuth oxide, cadmium sulfite, and metal organic frameworks (Li et al. 2019a; Yi et al. 2019; Hu et al. 2020; Wang et al. 2020; Xu et al. 2020). A new interesting one is a heterojunction of g-C₃N₄/UiO-66 (BG_xU_y) prepared by 3D UiO-66 and 2D g-C₃N₄ sheets through ball milling method. The superior improvement of Cr(VI) reduction upon white light irradiation was shown in comparison with both of single contents. Yi et al. (Yi et al. 2019) reported a facile fabrication of 2D/3D Z-scheme g-C₃N₄/UiO-66 heterojunction with enhanced photocatalytic Cr(VI) reduction performance under white light (see Fig. 9.10).

Table 9.3 Photocatalysts of Z-scheme modified and their summarized reaction

| Sr. No. | Photocatalyst | Usage | References |
|---------|---|--|---------------------|
| 1. | Pt-loaded WO ₃ & Pt-loaded ZrO ₂ /TaON | Water splitting | Maeda et al. (2010) |
| 2. | Ag ₂ CrO ₄ -GO | Methylene Blue and Phenol | Xu et al. (2015) |
| 3. | Cu ₂ O/Bi ₂ MoO ₆ | Decontamination of Sulfadiazine and Ni(II) | Xu et al. (2020) |
| 4. | CdS/polyimide (PI) | Hydrogen evolution | Hu et al. (2020) |
| 5. | α -Fe ₂ O ₃ /d-C ₃ N ₄ and α -Fe ₂ O ₃ /g-C ₃ N ₄ | Tetracycline | Wang et al. (2020) |
| 6. | BiOBr/Bi ₁₂ O ₁₇ Br ₂ | Resorcinol degradation and NO removal | Li et al. (2019a) |
| 7. | Tungsten trioxide/polyimide (PWO/PI) | Imidacloprid | Meng et al. (2018) |
| 8. | Er ³⁺ :Y ₃ A ₁₅ O ₁₂ @NiGa ₂ O ₄ -MWCNTs-WO ₃ | Methylene Blue and Hydrogen evolution | Tang et al. (2019) |

9.3.3 p–n Junction Materials

Other improved photocatalysts as dual semiconductors reported in literature are heterojunctions of two p-type and n-type semiconductors. The considered photocatalysts including trivalent and pentavalent additives, respectively, resulted in electron–hole generation in the electronic states of semiconductor (Beydoun et al. 2000; Spasiano et al. 2013). The designed p–n junctions of photocatalysts allow the charge transfer between two semiconductor contents through the direct contact. The structure provides the advantage of separation of charge carriers along with reduction of electron–hole pair recombination. The charge transfer mechanism in a general p–n junction type is illustrated in Fig. 9.11. Through the connection of two types of p–n semiconductors, a small content of electron from n-type is transferred to p-type. Therefore, the resulted hole in interfacial establishes an inner electric field where the n-type extends the positive charge and vice versa for p-type. The formed inner electric field prohibits to flux of the remaining hole and electron into the related negative and positive fields. Therefore, the effective charge separation and reduced recombination rate can be achieved.

The position of valence band of g-C₃N₄ as 1.89 eV vs. NHE is more in comparison with OH⁻/^{*}OH standard potential with 2.40 eV vs. NHE, so photo-excited holes on g-C₃N₄ will not respond with OH⁻/H₂O to form ^{*}OH. It can be rephrased that HOMO energy of UiO-66 with 3.35 eV vs. NHE is smaller than OH⁻/^{*}OH pairs with 2.40 eV vs. NHE, caused to form ^{*}OH with oxidation of OH⁻ or H₂O.

Lee et al. (Kim et al. 2017; Chae et al. 2019) introduced some p–n junction having photocatalytic behavior or usable in diodes/solar cells with semiconductor combination, viz., p-poly(3-hexylthiophene)/n-ZnO and p-Co₃O₄/n-ZnO. For the first one

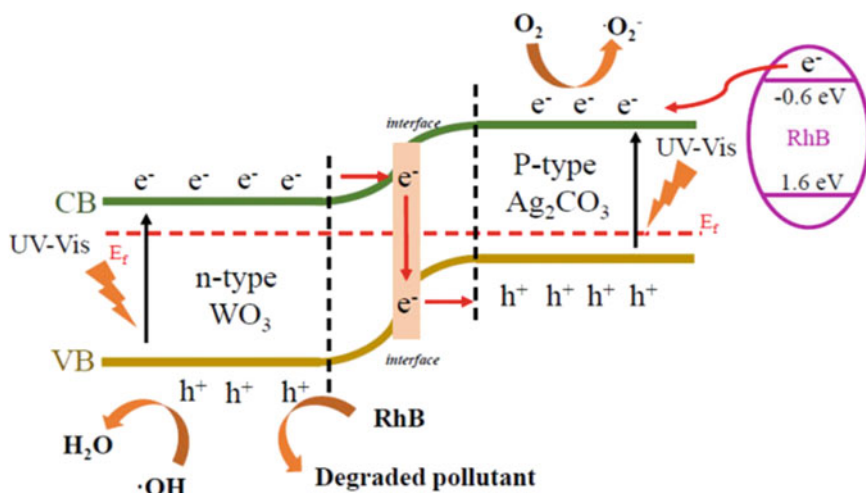


Fig. 9.11 Photoexcited electron–hole separation in n–p heterojunction $\text{WO}_3\text{-Ag}_2\text{CO}_3$ at photocatalytic degradation process of Rhodamine B. CB and VB stand for conductive band and valence band, respectively. RhB stands for Rhodamine B. (Reprinted with permission of Elsevier from Gao et al. 2019)

Table 9.4 *p-n* heterojunction photocatalysts and the summarized usage

| Number | Photocatalyst | Usage | References |
|--------|--|----------------------------|------------------------|
| 1. | $\text{TiO}_2/\text{Cu(II)}$ | Production of Benzaldehyde | Spasiano et al. (2013) |
| 2. | $\text{TiO}_2/\text{Fe}_3\text{O}_4$ | Photodissolution | Beydoun et al. (2000) |
| 3. | $p\text{-WO}_3/n\text{-Ag}_2\text{CO}_3$ | Rhodamine B | Gao et al. (2019) |
| 4. | $p\text{-P3HT}/n\text{-ZnO}$ | Rhodamine 6G | Chae et al. (2019) |
| 5. | $p\text{-Co}_3\text{O}_4/n\text{-ZnO}$ | Light-Emitting Diode | Kim et al. (2017) |

through self-grown organic content over ZnO surface, the hybrid *p-n* junction was prepared. It shows the catalysis activity for Rhodamine 6G degradation (Chae et al. 2019) and the next one prepared from aqueous media at low temperature and growing of ZnO over Co_3O_4 having light-emitting diode property (Kim et al. 2017). Some of more recent introduced *p-n* heterojunction photocatalyst are collected in Table 9.4.

9.3.4 Ion-Exchangeable Semiconductors

The wide range of ion-exchangeable compounds with layered structures can be classified into oxides and hydroxides. The ion-exchangeable compounds bear zigzag lepidocrocite sheet type intercalated with counter ions of hydrates protons arrive with high capability of solar energy utilization. As above discussed, adequate

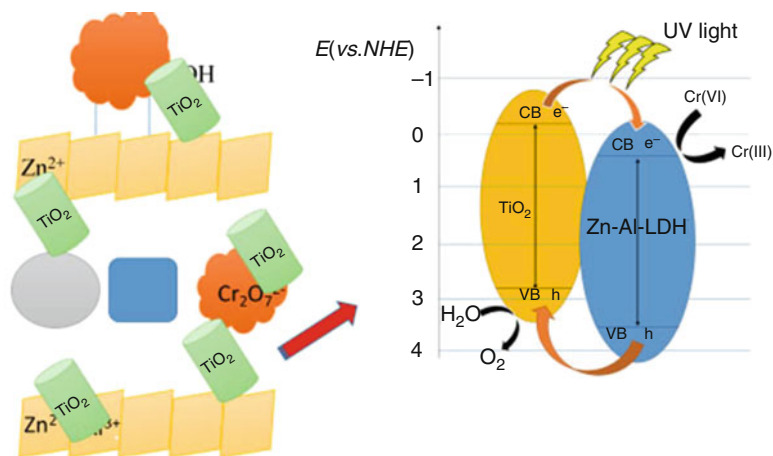


Fig. 9.12 Photocatalytic reduction of Cr(VI) using Zn-Al-layered double hydroxide and TiO₂ composites. CB and VB stand for conductive band and valence band, respectively. (Reprinted with permission of Elsevier from Yang et al. 2019)

separation of electron–hole with low recombination rate is a key involving factor of performance of photo-remediation, water splitting, and general photocatalytic applications. An advanced method to gain the purpose of adequate separation of electron–hole is structural manipulation of layered materials with interstitial inserting of heteroatoms to engineering charge transfer procedure (Zong et al. 2011; Gao et al. 2013; Xiong et al. 2016; Cui et al. 2017; Li et al. 2017a; Cao et al. 2018). Further alternative structure is two-dimensional layered double hydroxide having general formula of $[M_{1-x}^{2+}M_x^{3+}(\text{OH})_2]^{x+}(\text{A}^{n-1})_{x/n} \cdot m\text{H}_2\text{O}$. The negatively charged A anion is accommodated betwixt of positive-charged M layers of two various divalent and trivalent metal ions (Chen et al. 2019; Jo et al. 2019; Li et al. 2019b; Wang et al. 2019a; Yang et al. 2019). Generally, the main applicable researching fields on ion-exchangeable materials can be highlighted as dye degradation, removal of toxic gaseous like NO, toluene, and so on, water splitting, light-emitting diode, solar cell, Cr(VI) reduction, CO₂ transformation to carbonic fuel like methane, and so on (Zong et al. 2011; Gao et al. 2013; Xiong et al. 2016; Cui et al. 2017; Lee et al. 2017; Li et al. 2017a, 2018c, 2019b; Cao et al. 2018; Chen et al. 2019; Yang et al. 2019; Jo et al. 2019; Wang et al. 2019a). The reported ion-exchangeable layered sheets having negatively charged particles intercalated between layers with positive charge have different species like carbonate/Zn, ZnNi and ZnCu hydroxides, carbonated/Bi₂WO₆, TiO₂/polyvinyl alcohol, alkaline metal ions/carbon nitride, NO₃⁻/g-C₃N₄, and so on. As obviously illustrated in Fig. 9.12, the titania nanoparticles were uniformly intercalated in the layered double hydroxide of Zn–Al. The combination of TiO₂/Zn–Al–layered double hydroxide is the main reason for enhancing performance of transformation of photogenerated electron–hole and separation for reduction of Cr(VI) (Yang et al. 2019).

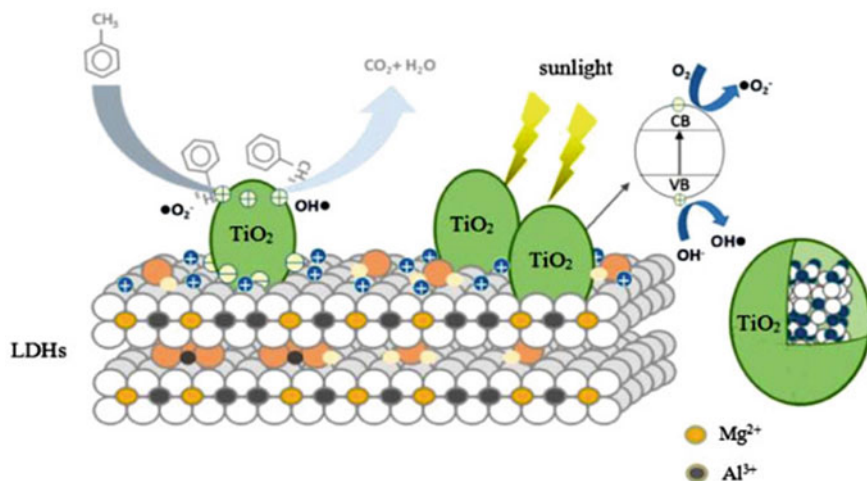


Fig. 9.13 A proposed photocatalytic mechanism of $\text{TiO}_2@$ layered double hydroxide under simulated sunlight. CB and VB stand for conductive band and valence band, respectively. LDH represent layered double hydroxide. (Reprinted with permission of Elsevier from Wang et al. 2019a)

Lee et al. (Lee et al. 2017) claimed to fabrication of sandwich structures bear transparent pliable light-emitting diodes with capable usage in wearable electronic instruments with transparent textiles. Lee et al. (Lee et al. 2017) used electrospinning method to intercalating light-emitting diodes of $\text{ZnO}@$ graphene quantum dots in transparent nanofiber textile to safeguard QLED devices versus the degradation. Lee et al. (Lee et al. 2017) attended the obtained results can inspire new-generation methods of wearable electronic cloths and so on.

Moreover, Wang et al. (2019a) reported a new synthesized $\text{TiO}_2@$ layered double hydroxide having permanent photocatalytic degradation of gaseous toluene under true sunlight irradiation. Actually, TiO_2 was formed through hydrolyzation of tetrabutyl titanate over initially designed MgAl -layered double hydroxide substrate. Large surface area of designed substrate, acceptable separation of generated hole and electron charges, and existence of necessity amount of OH^\bullet and $^\bullet\text{O}_2^-$ radicals are the main reasons of highly observed photocatalytic efficiency. For more information see proposed mechanism in Fig. 9.13.

Along with photodegradation of organic pollutants like dyes, the ion-exchangeable intercalated and layered double hydroxides show the ability for hydrogen and oxygen generation and energy production. Some of the interested recently reported results have been listed in Table 9.5.

Table 9.5 Ion-exchangeable photocatalysts having layered structure and their summarized applications

| Number | Photocatalyst | Application | References |
|--------|---|-------------------------------------|----------------------------|
| 1. | Li/g-C ₃ N ₄ | Rhodamine B | Zhang et al. (2019) |
| 2. | PbS-CdS/Ti ₆ O ₁₃ | Reactive Black 5 | Sehati and Entezari (2017) |
| 3. | g-C ₃ N ₄ NT/rGO | Rhodamine B | Wei et al. (2019) |
| 4. | RGO@ZnAlTi-LDO | Cr(VI) reduction | Ye et al. (2019) |
| 5. | Nd/CoAL LDH | Acid Red 14/Ciprofloxacin/Ibuprofen | Khodam et al. (2018) |
| 6. | CoNiSe ₂ LDH | Hydrogen evolution | Yang et al. (2019b) |
| 7. | NiFeSP/Nickel Foam | Hydrogen evolution | Xue and Sun (2019) |
| 8. | CoOx/ZnS@CdS/Ni | Hydrogen production | Xin et al. (2018) |

9.3.5 Photocatalytic Compounds Kind

Numerous photocatalysts have prepared and examined the activity toward environmental purification. Many of them show high performance under UV irradiation. Finally, there have been continual tries to development and improvement of visible light photocatalytic efficiency. The related efforts necessitate more studies of physicochemical properties of powerful photocatalysts.

TiO₂ as one of known powerful photocatalyst can be modified to achieve higher than promising results of photocatalytic activity. The sophistication include loading of TiO₂ with carbon, fullerene, graphite, activated carbon, different forms of grapheme oxide, nanosheets, single-walled carbon nanotubes, multiple-walled carbon nanotube, and so on (Wu et al. 2010; Cong et al. 2011; Meng and Oh 2012; Mohammadi and Sabbaghi 2014; Rong et al. 2015). However, some alternative modifications have been attended on the incorporation of metallic and nonmetallic elements (such as S, I, N, La, and Fe) in related structure (Li et al. 2011; Collazzo et al. 2012; Niu et al. 2013). Loaded TiO₂ over MWCNT using a modified sol-gel technique was shown better activity of TiO₂/MCNT composite within photodegradation of Reactive Black 5 dye in comparison with function of single TiO₂ (Hamid et al. 2014). Except modifications of titania, the photocatalysts can be widely classified as oxides, oxyhalides, and sulfides of metals and non-metals. In addition, their combinations and composite compounds have been investigated on different substrates. Actually, the catalytic performances of modified titania compounds for contaminant photodegradation for irradiation of UV-visible-solar light were examined. Table 9.6 was subdivided with numerous recent reported photocatalysts having high efficient performance.

Table 9.6 Routine classification of effective visible/solar light photocatalysts

| Number | Class | Photocatalyst | Irradiation | Dye/pollutant | Light time | Destruction | References |
|--------|--|--|--------------------|--------------------------------|------------|--|------------------------------|
| 1. | Bi_2S_3 | Bi_2S_3 coated on Stainless steel mesh | Natural sunlight | Cr (VI)/Rhodamine B | 60 min | Photodegradation of single mode of 10 ppm Cr(VI) and binary mixture of 10 ppm Cr(VI) and 5 ppm RhB | Chahkandi and Zargazi (2019) |
| 2. | BiFeO_3 | Coated on SS mesh | Natural sunlight | Phenol | 30 min | | Zargazi and Entezari (2019a) |
| 3. | Bi_2WO_6 | Coated on SS mesh | Natural sunlight | 4-Nitrophenol/ chlorophenol | 140 min | | Zargazi and Entezari (2019b) |
| 4. | Bi_2WO_6 | Flower like powder | Natural sunlight | Rhodamine B/Methylene Blue | 30 min | | Zargazi and Entezari (2018) |
| 5. | $\text{g-C}_3\text{N}_4$ | Heptazine-based $\text{g-C}_3\text{N}_4$ | Natural sunlight | Water splitting | – | High efficient visible light photocatalyst of C_6N_7 monolayer for water splitting | Liu et al. (2019) |
| 6. | BiOC | $\text{Ag@Ag}_2\text{O/BiOC}$ | 150 W xenon | Rhodamine B | 120 min | Heterojunction of $\text{Ag@Ag}_2\text{O/BiOC}$ as efficient photodegradation of 10 ppm RhB | Zhao et al. (2019) |
| 7. | BiOBr | p-n junction of $\text{Bi}_4\text{Tl}_3\text{O}_{12/\text{BiOBr}}$ | $\lambda > 400$ nm | Ciprofloxacin/ tetracycline | 180 min | p-n junction of $\text{Bi}_4\text{Tl}_3\text{O}_{12/\text{BiOBr}}$ as photodegradation of 20 ppm CIP/TC | Shen et al. (2019) |
| 8. | $\text{BaTa}_2\text{O}_6/\text{Ir,L a}/\text{SrTiO}_3/\text{Ir}$ | Z-scheme BaTa_2O_6 and SrTiO_3 doped with Ir and La | 300 W Xe lamp | Water splitting | – | Z-scheme $\text{BaTa}_2\text{O}_6/\text{Ir,L a}/\text{SrTiO}_3/\text{Ir}$ as effective for H_2 and O_2 evolution | Kudo et al. (2019) |

(continued)

Table 9.6 (continued)

| Number | Class | Photocatalyst | Irradiation | Dye/pollutant | Light time | Destruction | References |
|--------|--------------------------------------|--|---|------------------------------------|------------|--|-------------------------|
| 9. | Fluorescein | Fluorescein | 10 W blue LED lamp | Synthesis of benzimidazoles | | Benzimidazoles synthesis from aromatic aldehydes and o-phenylenediamines | Li et al. (2019f) |
| 10. | FeOCPc | FeOCPc@Ni | Sunlight lamp (220 V, 8 W, white light LED) | Methyl orange and p-nitrophenol | 30 min | Degradation of 97.91% and 97.99% of MO and PNP by (FeOCPc@Ni) | Ma et al. (2019) |
| 11. | RGO | Silver doped RGO | 350–370 nm | Oxidative coupling of benzylamines | 12 h | Plasmonic photocatalyst of silver for benzylamines coupling | Kumar et al. (2019) |
| 12. | Amine functionalised ZnCr LDH–MCM-41 | Au/Pd alloy on an amine functionalised ZnCr LDH–MCM-41 | 300 wt xenon lamp | One-pot imine synthesis | 45 min | Au/Pd bimetallic alloy loaded amine (APTES) functionalised LDH (Layered double hydroxide)–MCM-41 composite for imine synthesis | Sahoo et al. (2019) |
| 13. | MOF | Pt/[Zn2(BODIPY)(BPDC)2]·H2O | 420 nm | Hydrogen production | – | Visible photocatalyst of pillared-paddlewheel type metal-organic framework decorated with Pt nanoparticles for efficient H2 generation | Yang et al. (2019a) |
| 14. | BVO4 | Z-scheme ZnRh2O4/Au/BiVO4 | Xenon lamp $\lambda > 400$ nm | Liberation of H2 and O2 | – | Hierarchical structure of efficient photocatalyst of ZnRh2O4/Au/BiVO4 for production of H2 and O2 | Takashima et al. (2019) |

9.4 Future Remarks and Limitations

During the twentieth century and for future enhancing outlook, one of the main universal fears should be environmental remediation aspects. The required energy for remediation and environmental have close dependence about numerous issues having interplaying effects. The ultimate goal of green remediation for minimizing the greenhouse gas emissions needs most spending efforts. The well-known different nanomaterials have been introduced to achieve detection and elimination of pathogens. The respected nanomaterials can act through applicable routes with high sensitivity, lower cost, in-line and real-time detection, lower turnaround times, and more throughput and transportability in environmental purification. Among them, nanomaterials of metal oxide and metal especially chemical-functionalized ones can be utilized for removal of aqueous and aerial organic pollutants. Further improvements have to be exerted in selective and complete photocatalytic remediation through degradation of contaminants to non-toxic products to changing of pH and concentration of chemical staffs and cost optimization. TiO_2 has been considered one of the most effective ones because of its stability and some other advantages. However, several efforts have been and are being followed to decrease the major failure of TiO_2 to enhance usage in a huge area of solar light for more asked applications. The original importance of sophistication of proper band gap and chemistry of surface/interface addressed the required researches. The appropriate studies are (i) usage of metals–non-metals having general suitable characters as semiconductor, surface plasmon resonance, and so on, (ii) introduction of novel composite compounds; (iii) study of the effect of dopants–additives–sensitizers; (iv) finding the catalytic mechanism; (v) production of thin films of photocatalysts within titania, alumina, stainless steel, and molecular sieves; (vi) enhancing the effective surface area of photocatalyst; (vii) development of more sensitive photocatalyst in natural sunlight against of fictional light; and (viii) applying of diverse synthesis methods such as hydrothermal, co-precipitation, electrochemical, sol–gel, and so on. Another important challenge regarded to designing of appropriate photoreactor and the commercial concerns. Despite the great contents of mercantile contaminants needing remedy, the running conditions of technology should not be enough. However, at first an effective multiphasic impact of pollutant, oxygen, solar light, and photocatalyst is required. In order to commercialize of scale implementation for reliable scale-up, the specification of eminent factors and simulation of a reliable rate declaration are necessary. Investigations are still pursuing to improve quantum yield and maximize the impact of substances and photons regarding fluctuations in solar irradiation. Nonetheless, designing of photoreactors are followed according to alternative and approximate kinetic statements. Main designs of a photoreactor are performed for concentrating collector–reactor, compound parabolic collector–reactor, and non-concentrating collector one (Blanco et al. 2009; Braham and Harris 2009; Spasiano et al. 2015). Of the related more routine designs, compound parabolic collector–reactor includes more advantages about utilizing both of beam and reactive components and is resulted as the most modern

and applicable design (Tanveer and Tezcanli Guyer 2013). However, even the perfected design involved with some process limitations include (i) more effective performance for oxidative process like dyes with low concentration, (ii) sensitivity to mutability in solar intensity, (iii) complete contact of catalyst and effluent and then asking for separation of catalyst and treated effluent, and (iv) far from of headed commercialization. Resolving the last case along with commercial livability needs a facile, cost-effective, sustainable, and safety operation. To achieve the respected goals and minimize the pertinent limitations, it seems employing of proper UV-visible light photocatalysts is promised.

9.5 Conclusions

One can state that the best technique and material for pesticide removing can be chosen according to all involved parameters such as pH, temperature, quantity of contaminated environments, kind of matrix, and solubility of pesticides. The applied physicochemical process of pesticides remediation is permanently based on the forms of usage energy to degradation of the related pollutants, along with photolysis, ultrasound, and the other alternative methods. For purpose of pesticides remediation, metal oxide photocatalysts like TiO_2 using Fenton reactions joined to light, electric current, and ultrasound can highly extend the destruction of pesticides especially in aqueous phase. However, the current study was furnished the fundamental issues of the photocatalytic process. The most important ones contents are appropriate mechanism, thermodynamics, kinetics and recombination of reaction, suggested mechanism of an active photocatalyst, and the impact of effective factors on photocatalytic performance. Typical heterogeneous photocatalysis progresses by generation of electron–hole pairs commenced through band gap agitation of particle of a semiconductor. Adsorption of a photon with required potential equal or greater than band gap as the initial necessity of photocatalytic reactions resulted in electron transition from valence band to conduction band. Desired thermodynamically catalytic process can be evaluated based on intrinsic, apparent, and official quantum yield and efficiency of conversion. Conclusive measurement of total carbon content of the contaminants in terms of TOC or COD can be used to quantity determination of the photoreaction rate in a pseudo-L–H model. Since visible light active photocatalysts have small band gap energy, arresting of charge recombination is needful. The main mechanisms of effectual excitation and charge pair separation have been noted and discussed with clear examples. The governed parameters influencing on photocatalytic activity have been studied at length, completed with accounted results in literature. The parameters are (i) intrinsic photocatalyst type related to contents and band structure, (ii) irradiation energy effect on the number of generated electron–hole pairs, (iii) kind and character of pollutants having different functional groups, (iv) scattering and blockage of adventure light that can restrict the amount of loaded catalyst into the system, (v) pH of media and substrate, and (vi) value and property of dopant in composited catalyst–substrate influenced on surface

chemistry. However, a plenary path across for achieving optimized factors should be figured out. For applicable scale-up of photocatalysis process, an impact face of the photocatalyst and contaminant/goal, irradiation light, and O₂ should be provided. Finally, the most attended conclusions can be derived from the presented review chapter as:

1. Effective photocatalysis using natural sunlight energy and without any new generated footprint can decolorized/degrade the industrial effluent including paints and/or organics.
2. Manipulation of a photocatalyst band gap by hetero-coupling with the purpose of extending of absorption of visible region of spectrum.
3. Investigation of effective parameters can be useful to improve the photocatalytic performance.

Acknowledgments MCH highly appreciates for the financial support by the Hakim Sabzevari University, Sabzevar, Iran.

References

- Ahmed I, Iqbal HMN, Dhama K (2017) Enzyme-based biodegradation of hazardous pollutants – an overview. *JEBAS* 5(4):402–411
- Akihiko K, Kazunari D, Ken-ichi M, Onishi T (1987) Photocatalytic activities of TiO₂ loaded with NiO. *Chem Phys Lett* 133:517–519
- Akihiko K, Steinberg M, Bard AJ et al (1990) Photoactivity of ternary lead-group IVB oxides for hydrogen and oxygen evolution. *Catal Lett* 5:61–66
- Andreozzi R, Caprio V, Ermellino I et al (1996) Ozone solubility in phosphate-buffered aqueous solutions: effect of temperature, tert-butyl alcohol, and pH. *Ind Eng Chem Res* 35:1467–1471
- Andreozzi R, Caprio V, Insola A, Marotta R (1999) Advanced oxidation processes (AOP) for water purification and recovery. *Catal Today* 53:51–59. [https://doi.org/10.1016/S0920-5861\(99\)00102-9](https://doi.org/10.1016/S0920-5861(99)00102-9)
- Aroutiounian VM, Arakelyan VM, Shahnazaryan GE et al (2002) Investigation of ceramic Fe₂O₃ (Ta) photoelectrodes for solar energy photoelectrochemical converters. *Int J Hydrog Energy* 27:33–38. [https://doi.org/10.1016/S0360-3199\(01\)00085-4](https://doi.org/10.1016/S0360-3199(01)00085-4)
- Asmatulu R (2015) Photo-active metal oxide nanomaterials for water splitting. *Sci Lett J* 169
- Asmatulu R, Haynes H, Shinde M et al (2010) Magnetic characterizations of sol-gel-produced Mn-doped ZnO. *J Nanomater* 2010:80–83. <https://doi.org/10.1155/2010/715282>
- Asmatulu R, Ceylan M, Nuraje N (2011) Study of superhydrophobic electrospun nanocomposite fibers for energy systems. *Langmuir* 27:504–507. <https://doi.org/10.1021/la103661c>
- Babuponnusami A, Muthukumar K (2014) A review on Fenton and improvements to the Fenton process for wastewater treatment. *J Environ Chem Eng* 2:557–572. <https://doi.org/10.1016/j.jece.2013.10.011>
- Bai X, Wang L, Zong R, Zhu Y (2013) Photocatalytic activity enhanced via g-C₃N₄ nanoplates to nanorods. *J Phys Chem C* 117:9952–9961. <https://doi.org/10.1021/jp402062d>
- Barrera-Salgado KE, Ramírez-Robledo G, Álvarez-Gallegos A, Pineda-Arellano CA, Sierra-Espinosa FZ, Hernández-Pérez JA, Silva-Martínez S (2016) Fenton process coupled to ultrasound and UV light irradiation for the oxidation of a model pollutant. *J Chem* 2016:1–7
- Beard MC, Luther JM, Nozik AJ (2014) The promise and challenge of nanostructured solar cells. *Nat Nanotechnol* 9:951–954. <https://doi.org/10.1038/nnano.2014.292>

- Bellardita M, García-López EI, Marcì G et al (2018) Selective photocatalytic oxidation of aromatic alcohols in water by using P-doped g-C₃N₄. *Appl Catal B Environ* 220:222–233. <https://doi.org/10.1016/j.apcatb.2017.08.033>
- Beydoun D, Amal R, Low GKC, McEvoy S (2000) Novel photocatalyst: titania-coated magnetite. Activity and photodissolution. *J Phys Chem B* 104:4387–4396
- Blanco J, Malato S, Fernández-Ibañez P et al (2009) Review of feasible solar energy applications to water processes. *Renew Sust Energ Rev* 13:1437–1445. <https://doi.org/10.1016/j.rser.2008.08.016>
- Bokare AD, Choi W (2014) Review of iron-free Fenton-like systems for activating H₂O₂ in advanced oxidation processes. *J Hazard Mater* 275:121–135
- Braham RJ, Harris AT (2009) Review of major design and scale-up considerations for solar photocatalytic reactors. *Ind Eng Chem Res* 48:8890–8905. <https://doi.org/10.1021/ie900859z>
- Cai J, Wu X, Li S, Zheng F (2017) Controllable location of Au nanoparticles as cocatalyst onto TiO₂@CeO₂ nanocomposite hollow spheres for enhancing photocatalytic activity. *Appl Catal B Environ* 201:12–21. <https://doi.org/10.1016/j.apcatb.2016.08.003>
- Cao S, Li H, Tong T et al (2018) Single-atom engineering of directional charge transfer channels and active sites for photocatalytic hydrogen evolution. *Adv Funct Mater* 1802169:1–9. <https://doi.org/10.1002/adfm.201802169>
- Chae S, Yu J, Oh JY, Lee T (2019) Hybrid poly (3-hexylthiophene) (P₃HT) nanomesh/ZnO nanorod p-n junction visible photocatalyst for efficient indoor air purification. *Appl Surf Sci* 496:143641. <https://doi.org/10.1016/j.apsusc.2019.143641>
- Chahkandi M, Zargazi M (2019) Novel method of square wave voltammetry for deposition of Bi₂S₃ thin film: photocatalytic reduction of hexavalent Cr in single and binary mixtures. *J Hazard Mater* 380:120879
- Cheng L, Kang Y (2015) Bi₅O₇I/Bi₂O₃ composite photocatalyst with enhanced visible light photocatalytic activity. *Catal Commun* 72:16–19
- Che W, Cheng W, Yao T et al (2017) Fast photoelectron transfer in (Cring)-C₃N₄ plane heterostructural nanosheets for overall water splitting. *J Am Chem Soc* 139:3021–3026. <https://doi.org/10.1021/jacs.6b11878>
- Chen X, Yu T, Fan X et al (2007) Enhanced activity of mesoporous Nb₂O₅ for photocatalytic hydrogen production. *Appl Surf Sci* 253:8500–8506. <https://doi.org/10.1016/j.apsusc.2007.04.035>
- Chen L, He J, Liu Y, Chen P, Au C-T, Yin S-F (2016) Recent advances in bismuth-containing photocatalysts with heterojunctions. *Chin J Catal* 37(6):780–791
- Chen C, Zeng H, Yi M et al (2019) In-situ growth of Ag₃PO₄ on calcined Zn-Al layered double hydroxides for enhanced photocatalytic degradation of tetracycline under simulated solar light irradiation and toxicity assessment. *Appl Catal B Environ*:47–54. <https://doi.org/10.1016/j.apcatb.2019.03.083>
- Collazzo GC, Foletto EL, Jahn SL, Villetti MA (2012) Degradation of direct black 38 dye under visible light and sunlight irradiation by N-doped anatase TiO₂ as photocatalyst. *J Environ Manag* 98:107–111. <https://doi.org/10.1016/j.jenvman.2011.12.029>
- Cong Y, Li X, Qin Y et al (2011) Carbon-doped TiO₂ coating on multiwalled carbon nanotubes with higher visible light photocatalytic activity. *Appl Catal B Environ* 107:128–134. <https://doi.org/10.1016/j.apcatb.2011.07.005>
- Cui W, Li J, Cen W et al (2017) Steering the interlayer energy barrier and charge flow via bioriented transportation channels in g-C₃N₄: enhanced photocatalysis and reaction mechanism. *J Catal* 352:351–360. <https://doi.org/10.1016/j.jcat.2017.05.017>
- Da Rosa AV (2012) Fundamentals of renewable energy processes, 3rd edn. Academic, New York
- Da Silva ES, Moura NMM, Coutinho A et al (2018) β-Cyclodextrin as a precursor to holey C-doped g-C₃N₄ nanosheets for photocatalytic hydrogen generation. *ChemSusChem* 11:2639–2639. <https://doi.org/10.1002/cssc.201801789>
- Deng Y, Tang L, Feng C et al (2018) Construction of plasmonic Ag modified phosphorous-doped ultrathin g-C₃N₄ nanosheets/BiVO₄ photocatalyst with enhanced visible-near-infrared response

- ability for ciprofloxacin degradation. *J Hazard Mater* 344:758–769. <https://doi.org/10.1016/j.jhazmat.2017.11.027>
- Di T, Zhu B, Cheng B et al (2017) A direct Z-scheme g-C₃N₄/SnS₂ photocatalyst with superior visible-light CO₂ reduction performance. *J Catal* 352:532–541. <https://doi.org/10.1016/j.jcat.2017.06.006>
- Dong B, Li M, Chen S et al (2017) Formation of g-C₃N₄@Ni(OH)₂ honeycomb nanostructure and asymmetric supercapacitor with high energy and power density. *ACS Appl Mater Interfaces* 9:17890–17896. <https://doi.org/10.1021/acsami.7b02693>
- Duonghong D, Borgarello E, Grätzel M (1981) Dynamics of light-induced water cleavage in colloidal systems. *J Am Chem Soc* 103:4685–4690. <https://doi.org/10.1021/ja00406a004>
- Feng R, Lei W, Sui X et al (2018) Anchoring black phosphorus quantum dots on molybdenum disulfide nanosheets: a 0D/2D nanohybrid with enhanced visible- and NIR -light photoactivity. *Appl Catal B Environ* 238:444–453. <https://doi.org/10.1016/j.apcatb.2018.07.052>
- Frank AJ, Kopidakis N, Van De Lagemaat J (2004) Electrons in nanostructured TiO₂ solar cells: transport, recombination and photovoltaic properties. *Coord Chem Rev* 248:1165–1179. <https://doi.org/10.1016/j.ccr.2004.03.015>
- Fu J, Yu J, Jiang C, Cheng B (2018) g-C₃N₄-based heterostructured photocatalysts. *Adv Energy Mater* 8:1–31. <https://doi.org/10.1002/aenm.201701503>
- Fu J, Xu Q, Low J et al (2019) Ultrathin 2D/2D WO₃/g-C₃N₄ step-scheme H₂-production photocatalyst. *Appl Catal B Environ*:556–565. <https://doi.org/10.1016/j.apcatb.2018.11.011>
- Fujishima A, Zhang X, Tryk DA (2008) TiO₂ photocatalysis and related surface phenomena. *Surf Sci Rep* 63:515–582. <https://doi.org/10.1016/j.surfrep.2008.10.001>
- Gao H, Yan S, Wang J et al (2013) Towards efficient solar hydrogen production by intercalated carbon nitride photocatalyst. *Phys Chem Chem Phys* 15:18077–18084. <https://doi.org/10.1039/c3cp53774a>
- Gao M, You L, Guo L, Li T (2019) Fabrication of a novel polyhedron-like WO₃/Ag₂CO₃ p-n junction photocatalyst with highly enhanced photocatalytic activity. *J Photochem Photobiol A Chem* 374:206–217. <https://doi.org/10.1016/j.jphotochem.2019.01.022>
- Ghows N, Entezari MH (2013) Kinetic investigation on sono-degradation of reactive black 5 with core-shell nanocrystal. *Ultrason Sonochem* 20(1):386–394
- Gogate PR, Pandit AB (2004a) A review of imperative technologies for wastewater treatment I: oxidation technologies at ambient conditions. *Adv Environ Res* 8:501–551. [https://doi.org/10.1016/S1093-0191\(03\)00032-7](https://doi.org/10.1016/S1093-0191(03)00032-7)
- Gogate PR, Pandit AB (2004b) A review of imperative technologies for wastewater treatment II: hybrid methods. *Adv Environ Res* 8:553–597. [https://doi.org/10.1016/S1093-0191\(03\)00031-5](https://doi.org/10.1016/S1093-0191(03)00031-5)
- Hamid SBA, Tan TL, Lai CW, Samsudin EM (2014) Multiwalled carbon nanotube/TiO₂ nanocomposite as a highly active photocatalyst for photodegradation of Reactive Black 5 dye. *Chin J Catal* 35:2014–2019. [https://doi.org/10.1016/S1872-2067\(14\)60210-2](https://doi.org/10.1016/S1872-2067(14)60210-2)
- Hao X, Zhou J, Cui Z et al (2018) Zn-vacancy mediated electron-hole separation in ZnS/g-C₃N₄ heterojunction for efficient visible-light photocatalytic hydrogen production. *Appl Catal B Environ* 229:41–51. <https://doi.org/10.1016/j.apcatb.2018.02.006>
- Herrmann JM (1995) Heterogeneous photocatalysis: an emerging discipline involving multiphase systems. *Catal Today* 24:157–164. [https://doi.org/10.1016/0920-5861\(95\)00005-Z](https://doi.org/10.1016/0920-5861(95)00005-Z)
- Hoffmann MR, Martin ST, Choi W, Bahnemann DW (1995) Environmental applications of semiconductor photocatalysis. *Chem Rev* 95:69–96. <https://doi.org/10.1021/cr00033a004>
- Homem V, Santos L (2011) Degradation and removal methods of antibiotics from aqueous matrices – a review. *J Environ Manag* 92(10):2304–2347
- Hu Y, Hao X, Cui Z et al (2020) Enhanced photocarrier separation in conjugated polymer engineered CdS for direct Z-scheme photocatalytic hydrogen evolution. *Appl Catal B Environ* 260:118131. <https://doi.org/10.1016/j.apcatb.2019.118131>
- Inglar WB, Baltrus JP, Khan SUM (2004) Photoresponse of p-type zinc-doped iron(III) oxide thin films. *J Am Chem Soc* 126:10238–10239. <https://doi.org/10.1021/ja048461y>

- Jayaweera I (2003) Chemical degradation methods for wastes and pollutants, Environmental science and pollution control series. CRC Press, Boca Raton, pp 121–163
- Jiang L, Yuan X, Zeng G et al (2018a) A facile band alignment of polymeric carbon nitride isotype heterojunctions for enhanced photocatalytic tetracycline degradation. *Environ Sci Nano* 5:2604–2617. <https://doi.org/10.1039/C8EN00807H>
- Jiang L, Yuan X, Zeng G et al (2018b) Metal-free efficient photocatalyst for stable visible-light photocatalytic degradation of refractory pollutant. *Appl Catal B Environ* 221:715–725. <https://doi.org/10.1016/j.apcatb.2017.09.059>
- Jin H, Bu Y, Li J et al (2018) Strong graphene 3D assemblies with high elastic recovery and hardness. *Adv Mater* 30:1–8. <https://doi.org/10.1002/adma.201707424>
- Jo W-K, Kumar S, Tonda S (2019) N-doped C dot/CoAl-layered double hydroxide/g-C₃N₄ hybrid composites for efficient and selective solar-driven conversion of CO₂ into CH₄. *Compos Part B Eng* 176:107212. <https://doi.org/10.1016/j.compositesb.2019.107212>
- Kadowaki H, Saito N, Nishiyama H, Inoue Y (2007) RuO₂-loaded Sr²⁺-doped CeO₂ with d⁰ electronic configuration as a new photocatalyst for overall water splitting. *Chem Lett* 36:440–441. <https://doi.org/10.1246/cl.2007.440>
- Kay A, Cesar I, Grätzel M (2006) New benchmark for water photooxidation by nanostructured α -Fe₂O₃ films. *J Am Chem Soc* 128:15714–15721. <https://doi.org/10.1021/ja064380i>
- Khodam F, Amani-Ghadim HR, Aber S, Amani-Ghadim AR, Ahadzadeh I (2018) Neodymium doped mixed metal oxide derived from CoAl-layered double hydroxide: considerable enhancement in visible light photocatalytic activity. *J Ind Eng Chem* 68:311–324
- Kim J, Hwang DW, Kim HG et al (2005a) Highly efficient overall water splitting through optimization of preparation and operation conditions of layered perovskite photocatalysts. *Top Catal* 35:295–303. <https://doi.org/10.1007/s11244-005-3837-x>
- Kim S, Hwang S, Choi W (2005b) Visible light active platinum-ion-doped TiO₂ photocatalyst. *J Phys Chem B* 109:24260–24267
- Kim JW, Lee SJ, Biswas P et al (2017) Solution-processed n-ZnO nanorod/p-Co₃O₄ nanoplate heterojunction light-emitting diode. *Appl Surf Sci* 406:192–198. <https://doi.org/10.1016/j.apsusc.2017.02.129>
- Koohgard M, Hosseini-Sarvari M (2018) Enhancement of Suzuki–Miyaura coupling reaction by photocatalytic palladium nanoparticles anchored to TiO₂ under visible light irradiation. *Catal Commun* 111:10–15. <https://doi.org/10.1016/j.catcom.2018.03.026>
- Kudo A, Yoshino S, Tsuchiya T, Udagawa Y, Takahashi Y, Yamaguchi M, Ogasawara I, Matsumoto H, Iwase A (2019) Z-scheme photocatalyst systems employing Rh- and Ir-doped metal oxide materials for water splitting under visible light irradiation. *Faraday Discuss* 215:313–328
- Kumar A, Sadanandhan AM, Jain SL (2019) Silver doped reduced graphene oxide as a promising plasmonic photocatalyst for oxidative coupling of benzylamines under visible light irradiation. *New J Chem* 43(23):9116–9122
- Lee KS, Shim J, Park M et al (2017) Transparent nanofiber textiles with intercalated ZnO@graphene QD LEDs for wearable electronics. *Compos Part B Eng* 130:70–75. <https://doi.org/10.1016/j.compositesb.2017.07.046>
- Li J, Zhang X, Ai Z, Jia F, Zhang L, Lin J (2007) Efficient visible light degradation of rhodamine B by a photo-electrochemical process based on a Bi WO nanoplate film electrode. *J Phys Chem C* 111(18):6832–6836
- Li L, Zhuang H, Bu D (2011) Characterization and activity of visible-light-driven TiO₂ photocatalyst codoped with lanthanum and iodine. *Appl Surf Sci* 257:9221–9225. <https://doi.org/10.1016/j.apsusc.2011.06.007>
- Li J, Cui M, Guo Z et al (2015a) Preparation of p-n junction BiVO₄/Ag₂O heterogeneous nanostructures with enhanced visible-light photocatalytic activity. *Mater Lett* 151:75–78. <https://doi.org/10.1016/j.matlet.2015.03.078>
- Li X, Yu J, Low J et al (2015b) Engineering heterogeneous semiconductors for solar water splitting. *J Mater Chem A* 3:2485–2534. <https://doi.org/10.1039/c4ta04461d>

- Li J, Cui W, Sun Y et al (2017a) Directional electron delivery: via a vertical channel between g-C₃N₄ layers promotes photocatalytic efficiency. *J Mater Chem A* 5:9358–9364. <https://doi.org/10.1039/c7ta02183f>
- Li X, Zhang H, Huang J et al (2017b) Folded nano-porous graphene-like carbon nitride with significantly improved visible-light photocatalytic activity for dye degradation. *Ceram Int* 43:15785–15792. <https://doi.org/10.1016/j.ceramint.2017.08.144>
- Li Y, Li YL, Sa B, Ahuja R (2017c) Review of two-dimensional materials for photocatalytic water splitting from a theoretical perspective. *Cat Sci Technol* 7:545–559. <https://doi.org/10.1039/c6cy02178f>
- Li S, Cai J, Wu X et al (2018a) TiO₂@Pt@CeO₂ nanocomposite as a bifunctional catalyst for enhancing photo-reduction of Cr (VI) and photo-oxidation of benzyl alcohol. *J Hazard Mater* 346:52–61. <https://doi.org/10.1016/j.jhazmat.2017.12.001>
- Li Y, Ho W, Lv K et al (2018b) Carbon vacancy-induced enhancement of the visible light-driven photocatalytic oxidation of NO over g-C₃N₄ nanosheets. *Appl Surf Sci* 430:380–389. <https://doi.org/10.1016/j.apsusc.2017.06.054>
- Li Z, Ma Q, Li Y et al (2018c) Flexible woven metal wires supported nanosheets and nanoparticles double-layered nitrogen-doped zinc stannate toward enhanced solar energy utilization. *Ceram Int* 44:905–914. <https://doi.org/10.1016/j.ceramint.2017.10.021>
- Li R, Xie F, Liu J et al (2019a) Room-temperature hydrolysis fabrication of BiOBr/Bi₁₂O₁₇Br₂ Z-scheme photocatalyst with enhanced resorcinol degradation and NO removal activity. *Chemosphere* 235:767–775. <https://doi.org/10.1016/j.chemosphere.2019.06.231>
- Li S, Wang L, Li YD et al (2019b) Novel photocatalyst incorporating Ni-Co layered double hydroxides with P-doped CdS for enhancing photocatalytic activity towards hydrogen evolution. *Appl Catal B Environ* 254:145–155. <https://doi.org/10.1016/j.apcatb.2019.05.001>
- Li X, Xiong J, Gao X et al (2019c) Recent advances in 3D g-C₃N₄ composite photocatalysts for photocatalytic water splitting, degradation of pollutants and CO₂ reduction. *J Alloys Compd* 802:196–209. <https://doi.org/10.1016/j.jallcom.2019.06.185>
- Li X, Xiong J, Huang J et al (2019d) Novel g-C₃N₄/h⁺ZnTiO₃-a⁺/TiO₂ direct Z-scheme heterojunction with significantly enhanced visible-light photocatalytic activity. *J Alloys Compd* 774:768–778. <https://doi.org/10.1016/j.jallcom.2018.10.034>
- Li X, Xiong J, Xu Y et al (2019e) Defect-assisted surface modification enhances the visible light photocatalytic performance of g-C₃N₄@C-TiO₂ direct Z-scheme heterojunctions. *Chin J Catal* 40:424–433. [https://doi.org/10.1016/S1872-2067\(18\)63183-3](https://doi.org/10.1016/S1872-2067(18)63183-3)
- Li Z, Song H, Guo R, Zuo M, Hou C, Sun S, He X, Sun Z, Chu W (2019f) Visible-light-induced condensation cyclization to synthesize benzimidazoles using fluorescein as a photocatalyst. *Green Chem* 21(13):3602–3605
- Liu B, Xu B, Li S, Du J, Liu Z, Zhong W (2019) Heptazine-based porous graphitic carbon nitride: a visible-light driven photocatalyst for water splitting. *J Mater Chem A* 7(36):20799–20805
- Low J, Yu J, Jaroniec M et al (2017) Heterojunction photocatalysts. *Adv Mater* 29:1–20. <https://doi.org/10.1002/adma.201601694>
- Lluque R, Balu AM (2013) Producing fuels and fine chemicals from biomass using nanomaterials. In: *Producing fuels and fine chemicals from biomass using nanomaterials*. SCITUS Academics LLC, New York, pp 1–315
- Ma L, Fan H, Fu K et al (2017) Protonation of graphitic carbon nitride (g-C₃N₄) for an electrostatically self-assembling carbon@g-C₃N₄ core-shell nanostructure toward high hydrogen evolution. *ACS Sustain Chem Eng* 5:7093–7103. <https://doi.org/10.1021/acssuschemeng.7b01312>
- Ma L, Wang G, Jiang C et al (2018) Synthesis of core-shell TiO₂@g-C₃N₄ hollow microspheres for efficient photocatalytic degradation of rhodamine B under visible light. *Appl Surf Sci* 430:263–272. <https://doi.org/10.1016/j.apsusc.2017.07.282>
- Ma X, Luo M, Yan L, Tang N, Li J (2019) Preparation of a magnetically recyclable visible-light-driven photocatalyst based on phthalocyanine and its visible light catalytic degradation of methyl orange and -nitrophenol. *New J Chem* 43(24):9589–9595

- Maeda K, Higashi M, Lu D, Abe R, Domen K (2010) Efficient nonsacrificial water splitting through two-step photoexcitation by visible light using a modified Oxynitride as a hydrogen evolution Photocatalyst. *J Am Chem Soc* 132(16):5858–5868
- Malato S, Fernández-Ibáñez P, Maldonado MI et al (2009) Decontamination and disinfection of water by solar photocatalysis: recent overview and trends. *Catal Today* 147:1–59. <https://doi.org/10.1016/j.cattod.2009.06.018>
- Meng Z, Oh W (2012) Photodegradation of organic dye by CoS₂ and carbon (C₆₀, graphene, CNT)/TiO₂ composite sensitizer. *Chin J Catal* 33:1495–1501. [https://doi.org/10.1016/S1872-2067\(11\)60429-4](https://doi.org/10.1016/S1872-2067(11)60429-4)
- Meng P, Heng H, Sun Y, Liu X (2018) In situ polymerization synthesis of Z-scheme tungsten trioxide/polyimide photocatalyst with enhanced visible-light photocatalytic activity. *Appl Surf Sci* 428:1130–1140
- Miao Y, Pan G, Huo Y, Li H (2013) Aerosol-spraying preparation of Bi₂MoO₆: a visible photocatalyst in hollow microspheres with a porous outer shell and enhanced activity. *Dyes Pigments* 99:382–389. <https://doi.org/10.1016/j.dyepig.2013.05.005>
- Minero C, Pelizzetti E, Malato S, Blanco J (1996) Large solar plant photocatalytic water decontamination: effect of operational parameters. *Solar Energy* 56:421–428
- Mohammadi M, Sabbaghi S (2014) Photo-catalytic degradation of 2,4-DCP wastewater using MWCNT/TiO₂ nano-composite activated by UV and solar light. *Environ Nanotechnol Monit Manag* 1–2:24–29. <https://doi.org/10.1016/j.enmm.2014.09.002>
- Naseri A, Samadi M, Pourjavadi A et al (2017) Graphitic carbon nitride (g-C₃N₄)-based photocatalysts for solar hydrogen generation: recent advances and future development directions. *J Mater Chem A* 5:23406–23433. <https://doi.org/10.1039/c7ta05131j>
- Nayak S, Mohapatra L, Parida K (2015) Visible light-driven novel g-C₃N₄/NiFe-LDH composite photocatalyst with enhanced photocatalytic activity towards water oxidation and reduction reaction. *J Mater Chem A* 3:18622–18635. <https://doi.org/10.1039/c5ta05002b>
- Neil W, Ashcroft NDM (2016) Solid state physics. In: Facial plastic and reconstructive surgery. Thieme, New York, p 848
- Niu Y, Xing M, Zhang J, Tian B (2013) Visible light activated sulfur and iron co-doped TiO₂ photocatalyst for the photocatalytic degradation of phenol. *Catal Today* 201:159–166. <https://doi.org/10.1016/j.cattod.2012.04.035>
- Nuraje N, Asmatulu R, Kudaibergenov S (2012) Metal oxide-based functional materials for solar energy conversion: a review. *Curr Inorg Chem* 2:124–146. <https://doi.org/10.2174/1877944111202020124>
- Nuraje N, Khan WS, Lei Y et al (2013) Superhydrophobic electrospun nanofibers. *J Mater Chem A* 1:1929–1946. <https://doi.org/10.1039/c2ta00189f>
- Ohtani B (2010) Photocatalysis A to Z-what we know and what we do not know in a scientific sense. *J Photochem Photobiol C: Photochem Rev* 11:157–178. <https://doi.org/10.1016/j.jphotochemrev.2011.02.001>
- Ong WJ, Tan LL, Ng YH et al (2016) Graphitic carbon nitride (g-C₃N₄)-based photocatalysts for artificial photosynthesis and environmental remediation: are we a step closer to achieving sustainability? *Chem Rev* 116:7159–7329. <https://doi.org/10.1021/acs.chemrev.6b00075>
- Opoku F, Govender KK, van Sittert CGCE, Govender PP (2017) Recent progress in the development of semiconductor-based photocatalyst materials for applications in photocatalytic water splitting and degradation of pollutants. *Adv Sustain Syst* 1(7):1700006
- Park JW, Kang M (2007) Synthesis and characterization of Ag_xO, and hydrogen production from methanol photodecomposition over the mixture of Ag_xO and TiO₂. *Int J Hydrog Energy* 32:4840–4846. <https://doi.org/10.1016/j.ijhydene.2007.07.045>
- Qi K, Xie Y, Wang R et al (2019) Electroless plating Ni-P cocatalyst decorated g-C₃N₄ with enhanced photocatalytic water splitting for H₂ generation. *Appl Surf Sci* 466:847–853. <https://doi.org/10.1016/j.apsusc.2018.10.037>
- Qin Y, Wang G, Wang Y (2007) Study on the photocatalytic property of La-doped CoO/SrTiO₃ for water decomposition to hydrogen. *Catal Commun* 8:926–930. <https://doi.org/10.1016/j.catcom.2006.11.025>

- Ran J, Guo W, Wang H et al (2018a) Metal-free 2D/2D phosphorene/g-C₃N₄ van der waals heterojunction for highly enhanced visible-light photocatalytic H₂ production. *Adv Mater* 30:2–7. <https://doi.org/10.1002/adma.201800128>
- Ran M, Li J, Cui W et al (2018b) Efficient and stable photocatalytic NO removal on C self-doped g-C₃N₄: electronic structure and reaction mechanism. *Cat Sci Technol* 8:3387–3394. <https://doi.org/10.1039/c8cy00887f>
- Reddy DA, Kim EH, Gopannagari M et al (2019) Few layered black phosphorus/MoS₂ nanohybrid: a promising co-catalyst for solar driven hydrogen evolution. *Appl Catal B Environ* 241:491–498. <https://doi.org/10.1016/j.apcatb.2018.09.055>
- Rengaraj S, Li XZ (2006) Enhanced photocatalytic activity of TiO₂ by doping with Ag for degradation of 2,4,6-trichlorophenol in aqueous suspension. *J Mol Catal A Chem* 243:60–67. <https://doi.org/10.1016/j.molcata.2005.08.010>
- Rivera-Utrilla J, Sánchez-Polo M, Ferro-García MÁ, Prados-Joya G, Ocampo-Pérez R (2013) Pharmaceuticals as emerging contaminants and their removal from water: a review. *Chemosphere* 93(7):1268–1287
- Rong X, Qiu F, Zhang C et al (2015) Preparation, characterization and photocatalytic application of TiO₂-graphene photocatalyst under visible light irradiation. *Ceram Int* 41:2502–2511. <https://doi.org/10.1016/j.ceramint.2014.10.072>
- Sahoo DP, Patnaik S, Rath D, Mohapatra P, Mohanty A, Parida K (2019) Influence of Au/Pd alloy on an amine functionalised ZnCr LDH–MCM-41 nanocomposite: a visible light sensitive photocatalyst towards one-pot imine synthesis. *Cat Sci Technol* 9(10):2493–2513
- Saliev T, Begimbetova D, Masoud AR, Matkarimov B (2019) Biological effects of non-ionizing electromagnetic fields: two sides of a coin. *Prog Biophys Mol Biol* 141:25–36. <https://doi.org/10.1016/j.pbiomolbio.2018.07.009>
- Satsangi VR, Kumari S, Singh AP et al (2008) Nanostructured hematite for photoelectrochemical generation of hydrogen. *Int J Hydrog Energy* 33:312–318. <https://doi.org/10.1016/j.ijhydene.2007.07.034>
- Sayama K, Yase K, Arakawa H, Asakura K, Tanaka A, Domen K (1998) Photocatalytic activity and reaction mechanism of Pt-intercalated K₄Nb₆O₁₇ catalyst on the water splitting in carbonate salt aqueous solution. *J Photochem Photobiol A Chem* 114:125–135
- Sehati S, Entezari MH (2017) High visible light intercalated nanophotocatalyst (PbS-CdS/Ti6O13) synthesized by ultrasound: photocatalytic activity, photocorrosion resistance and degradation mechanism. *Sep Purif Technol* 174:482–492
- Shakeel M, Arif M, Yasin G et al (2019) Layered by layered Ni-Mn-LDH/g-C₃N₄ nanohybrid for multi-purpose photo/electrocatalysis: morphology controlled strategy for effective charge carriers separation. *Appl Catal B Environ* 242:485–498. <https://doi.org/10.1016/j.apcatb.2018.10.005>
- Shanker GS, Bhosale R, Ogale S, Nag A (2018) 2D nanocomposite of g-C₃N₄ and TiN embedded N-doped graphene for photoelectrochemical reduction of water using sunlight. *Adv Mater Interfaces* 5:1–8. <https://doi.org/10.1002/admi.201801488>
- Shen R, Xie J, Zhang H et al (2018) Enhanced solar fuel H₂ generation over g-C₃N₄ nanosheet photocatalysts by the synergetic effect of noble metal-free Co₂P cocatalyst and the environmental phosphorylation strategy. *ACS Sustain Chem Eng* 6:816–826. <https://doi.org/10.1021/acsschemeng.7b03169>
- Shen G, Pu Y, Sun R, Shi Y, Cui Y, Jing P (2019) Enhanced visible light photocatalytic performance of a novel heterostructured Bi Ti O/BiOBr photocatalyst. *New J Chem* 43(33):12932–12940
- Shi S, Gondal MA, Rashid SG, Qi Q, Al-Saadi AA, Yamani ZH, Sui Y, Xu Q, Shen K (2014) Synthesis of g-C₃N₄/BiOCl_xBr_{1-x} hybrid photocatalysts and the photoactivity enhancement driven by visible light. *Colloids Surf A Physicochem Eng Asp* 461:202–211
- Shi X, Fujitsuka M, Kim S, Majima T (2018) Faster electron injection and more active sites for efficient photocatalytic H₂ evolution in g-C₃N₄/MoS₂ hybrid. *Small* 14:1–9. <https://doi.org/10.1002/sml.201703277>

- Shibata M, Kudo KA, Tanaka A et al (1987) Photocatalytic activities of layered titanium compounds and their derivatives for H₂ evolution from aqueous methanol solution. *Chem Lett*:1017–1018
- Shimidzu T, Iyoda T, Koide Y (1985) An advanced visible- light- induced water reduction with Dye-sensitized semiconductor powder catalyst. *J Am Chem Soc* 107:35–41
- Spasiano D, Del Pilar Prieto Rodriguez L, Olleros JC et al (2013) TiO₂/Cu(II) photocatalytic production of benzaldehyde from benzyl alcohol in solar pilot plant reactor. *Appl Catal B Environ* 136–137:56–63. <https://doi.org/10.1016/j.apcatb.2013.01.055>
- Spasiano D, Marotta R, Malato S et al (2015) Solar photocatalysis: materials, reactors, some commercial, and pre-industrialized applications. A comprehensive approach. *Appl Catal B Environ* 170–171:90–123. <https://doi.org/10.1016/j.apcatb.2014.12.050>
- Spinelli P, Ferry E, Van De Groep J et al (2012) Plasmonic light trapping in thin-film Si solar cells. *J Opt* 14. <https://doi.org/10.1088/2040-8978/14/2/024002>
- Sun S, Liang S (2017) Recent advances in functional mesoporous graphitic carbon nitride (mp g-C₃N₄) polymers Shaodong. *Nanoscale*:1–33. <https://doi.org/10.1039/b000000x>
- Sun W, Zhang S, Wang C et al (2007) Enhanced photocatalytic hydrogen evolution over CaTi_{1-x}Zr_xO₃ composites synthesized by polymerized complex method. *Catal Lett* 119:148–153. <https://doi.org/10.1007/s10562-007-9212-8>
- Tada H, Jin Q, Nishijima H et al (2011) Titanium(IV) dioxide surface-modified with iron oxide as a visible light photocatalyst. *Angew Chemie Int Ed* 50:3501–3505. <https://doi.org/10.1002/anie.201007869>
- Tahezadeh MJ, Lennartsson PR, Teichert O, Nordholm H (2013) Bioethanol production processes. In: *Biofuels production*, Wiley, Hoboken, pp 211–253
- Takashima T, Moriyama N, Fujishiro Y, Osaki J, Takeuchi S, Ohtani B, Irie H (2019) Visible-light-induced water splitting on a hierarchically constructed Z-scheme photocatalyst composed of zinc rhodium oxide and bismuth vanadate. *J Mater Chem A* 7(17):10372–10378
- Tan B, Ye X, Li Y et al (2018) Defective anatase TiO_{2-x} mesocrystal growth in situ on g-C₃N₄ nanosheets: construction of 3D/2D Z-scheme heterostructures for highly efficient visible-light photocatalysis. *Chem A Eur J* 24:13311–13321. <https://doi.org/10.1002/chem.201802366>
- Tang L, Wang J, Liu X, Shu X, Zhang Z, Wang J (2019) Fabrication of Z-scheme photocatalyst, Er³⁺:Y₃Al₅O₁₂@NiGa₂O₄-MWCNTs-WO₃, and visible-light photocatalytic activity for degradation of organic pollutant with simultaneous hydrogen evolution. *Renew Energy* 138:474–488
- Tanveer M, Tezcanli Guyer G (2013) Solar assisted photo degradation of wastewater by compound parabolic collectors: review of design and operational parameters. *Renew Sust Energy Rev* 24:534–543. <https://doi.org/10.1016/j.rser.2013.03.053>
- Tian Y, Chang B, Lu J et al (2013) Hydrothermal synthesis of graphitic carbon nitride-Bi₂WO₆ heterojunctions with enhanced visible light photocatalytic activities. *ACS Appl Mater Interfaces* 5:7079–7085. <https://doi.org/10.1021/am4013819>
- Verma LK, Sakhuja M, Son J et al (2011) Self-cleaning and antireflective packaging glass for solar modules. *Renew Energy* 36:2489–2493. <https://doi.org/10.1016/j.renene.2011.02.017>
- Wang X, Maeda K, Thomas A, Takanabe K, Xin G, Carlsson JM, Domen K, Antonietti M (2008) A metal-free polymeric photocatalyst for hydrogen production from water under visible light. *Nat Mater* 8:76–80. <https://doi.org/10.1038/NMAT2317>
- Wang W, Huang X, Wu S et al (2013) Preparation of p-n junction Cu₂O/BiVO₄ heterogeneous nanostructures with enhanced visible-light photocatalytic activity. *Appl Catal B Environ* 134–135:293–301. <https://doi.org/10.1016/j.apcatb.2013.01.013>
- Wang Y, Wang H, Chen F et al (2017) Facile synthesis of oxygen doped carbon nitride hollow microsphere for photocatalysis. *Appl Catal B Environ* 206:417–425. <https://doi.org/10.1016/j.apcatb.2017.01.041>
- Wang W, Li G, An T et al (2018) Photocatalytic hydrogen evolution and bacterial inactivation utilizing sonochemical-synthesized g-C₃N₄/red phosphorus hybrid nanosheets as a wide-spectral-responsive photocatalyst: the role of type I band alignment. *Appl Catal B Environ* 238:126–135. <https://doi.org/10.1016/j.apcatb.2018.07.004>

- Wang L, Gao X, Cheng Y et al (2019a) TiO₂@MgAl-layered double hydroxide with enhanced photocatalytic activity towards degradation of gaseous toluene. *J Photochem Photobiol A Chem* 369:44–53. <https://doi.org/10.1016/j.jphotochem.2018.10.004>
- Wang X, Xiang Y, Zhou B et al (2019b) Enhanced photocatalytic performance of Ag/TiO₂ nanohybrid sensitized by black phosphorus nanosheets in visible and near-infrared light. *J Colloid Interface Sci* 534:1–11. <https://doi.org/10.1016/j.jcis.2018.09.013>
- Wang S, Teng Z, Xu Y et al (2020) Defect as the essential factor in engineering carbon-nitride-based visible-light-driven Z-scheme photocatalyst. *Appl Catal B Environ* 260:118145. <https://doi.org/10.1016/j.apcatb.2019.118145>
- Wei F, Liu Y, Zhao H et al (2018a) Oxygen self-doped g-C₃N₄ with tunable electronic band structure for unprecedentedly enhanced photocatalytic performance. *Nanoscale* 10:4515–4522. <https://doi.org/10.1039/c7nr09660g>
- Wei H, McMaster WA, Tan JZY et al (2018b) Tricomponent brookite/anatase TiO₂/g-C₃N₄ heterojunction in mesoporous hollow microspheres for enhanced visible-light photocatalysis. *J Mater Chem A* 6:7236–7245. <https://doi.org/10.1039/c8ta00386f>
- Wei Y, Zhu Y, Jiang Y (2019) Photocatalytic self-cleaning carbon nitride nanotube intercalated reduced graphene oxide membranes for enhanced water purification. *Chem Eng J* 356:915–925
- Wen J, Xie J, Chen X, Li X (2017) A review on g-C₃N₄-based photocatalysts. *Appl Surf Sci* 391:72–123
- Wu Y, Zhang J, Xiao L, Chen F (2010) Properties of carbon and iron modified TiO₂ photocatalyst synthesized at low temperature and photodegradation of acid orange 7 under visible light. *Appl Surf Sci* 256:4260–4268. <https://doi.org/10.1016/j.apsusc.2010.02.012>
- Wu J, Huang S, Jin Z et al (2018) Black phosphorus: an efficient co-catalyst for charge separation and enhanced photocatalytic hydrogen evolution. *J Mater Sci* 53:16557–16566. <https://doi.org/10.1007/s10853-018-2830-2>
- Wu H-Z, Liu J, Li L-L, Wang Z, Zhong Q-H, Bandaru S, Lau WM (2019) Exploring the formation and electronic structure properties of the g-C₃N₄ nanoribbon with density functional theory. *J Phys Condens Matter* 30:22
- Xin Y, Huang Y, Lin K, Yu Y, Zhang B (2018) Self-template synthesis of double-layered porous nanotubes with spatially separated photoredox surfaces for efficient photocatalytic hydrogen production. *Sci Bull* 63(10):601–608
- Xiong T, Cen W, Zhang Y, Dong F (2016) Bridging the g-C₃N₄ interlayers for enhanced photocatalysis. *ACS Catal*. <https://doi.org/10.1021/acscatal.5b02922>
- Xue Y, Sun M (2019) Engineering hierarchical NiFe-layered double hydroxides derived phosphosulfide for high-efficiency hydrogen evolving electrocatalysis. *Int J Hydrog Energy* 44(31):16378–16386
- Xu D, Cheng B, Cao S, Yu J (2015) Enhanced photocatalytic activity and stability of Z-scheme Ag₂CrO₄-GO composite photocatalysts for organic pollutant degradation. *Appl Catal B Environ* 164:380–388. <https://doi.org/10.1016/j.apcatb.2014.09.051>
- Xu C, Qian L, Lin J et al (2019a) Heptazine-based porous polymer for selective CO₂ sorption and visible light photocatalytic oxidation of benzyl alcohol. *Microporous Mesoporous Mater*:9–14. <https://doi.org/10.1016/j.micromeso.2019.03.011>
- Xu J, Fujitsuka M, Kim S et al (2019b) Unprecedented effect of CO₂ calcination atmosphere on photocatalytic H₂ production activity from water using g-C₃N₄ synthesized from triazole polymerization. *Appl Catal B Environ* 241:141–148. <https://doi.org/10.1016/j.apcatb.2018.09.023>
- Xu X, Meng L, Dai Y et al (2020) Bi spheres SPR-coupled Cu₂O/Bi₂MoO₆ with hollow spheres forming Z-scheme Cu₂O/Bi/Bi₂MoO₆ heterostructure for simultaneous photocatalytic decontamination of sulfadiazine and Ni(II). *J Hazard Mater* 381:120953. <https://doi.org/10.1016/j.jhazmat.2019.120953>
- Yanagida T, Sakata Y, Imamura H (2004) Photocatalytic decomposition of H₂O into H₂ and O₂ over Ga₂O₃ loaded with NiO. *Chem Lett* 33:726–727. <https://doi.org/10.1246/cl.2004.726>

- Yang X, Chen Z, Xu J et al (2015) Tuning the morphology of g-C₃N₄ for improvement of Z-scheme photocatalytic water oxidation. *ACS Appl Mater Interfaces* 7:15285–15293. <https://doi.org/10.1021/acsami.5b02649>
- Yang T, Peng J, Zheng Y, He X, Hou Y, Wu L, Fu X (2018) Enhanced photocatalytic ozonation degradation of organic pollutants by ZnO modified TiO₂ nanocomposites. *Appl Catal B Environ* 221:223–234
- Yang Y, Yan L, Li J et al (2019a) Synergistic adsorption and photocatalytic reduction of Cr (VI) using Zn-Al-layered double hydroxide and TiO₂ composites. *Appl Surf Sci* 492:487–496. <https://doi.org/10.1016/j.apsusc.2019.06.229>
- Yang H, Wang J, Ma J, Yang H, Zhang J, Lv K, Wen L, Peng T (2019b) A novel BODIPY-based MOF photocatalyst for efficient visible-light-driven hydrogen evolution. *J Mater Chem A* 7(17):10439–10445
- Yao G, Chen Z, Chen Q, Li D, Xie Z, Zhou Y, Xiong X, Xu Y (2018) Behaviors of organic and heavy metallic pollutants during supercritical water oxidation of oil-based drill cuttings. *Water Air Soil Pollut* 229(3)
- Ye C, Li JX, Li ZJ et al (2015) Enhanced driving force and charge separation efficiency of protonated g-C₃N₄ for photocatalytic O₂ evolution. *ACS Catal* 5:6973–6979. <https://doi.org/10.1021/acscatal.5b02185>
- Ye J, Liu J, Huang Z, Wu S, Dai X, Zhang L, Cui L (2019) Effect of reduced graphene oxide doping on photocatalytic reduction of Cr(VI) and photocatalytic oxidation of tetracycline by ZnAlTi layered double oxides under visible light. *Chemosphere* 227:505–513
- Yeo CI, Kang EK, Lee SK, Song YM, Lee YT, Song YM, Lee YT (2014) Efficiency enhancement of III–V triple-junction solar cell using nanostructured bifunctional coverglass with enhanced transmittance and self-cleaning property. *IEEE Photon J* 6:1–9. <https://doi.org/10.1109/JPHOT.2014.2319100>
- Yi XH, Ma SQ, Du XD et al (2019) The facile fabrication of 2D/3D Z-scheme g-C₃N₄/UiO-66 heterojunction with enhanced photocatalytic Cr(VI) reduction performance under white light. *Chem Eng J*:375. <https://doi.org/10.1016/j.cej.2019.121944>
- Yu H, Shang L, Bian T et al (2016) Nitrogen-doped porous carbon nanosheets templated from g-C₃N₄ as metal-free electrocatalysts for efficient oxygen reduction reaction. *Adv Mater*:5080–5086. <https://doi.org/10.1002/adma.201600398>
- Yu K, Li X, Chen L, Fang J, Chen H, Li Q, Chi N, Ma J (2018) Mechanism and efficiency of contaminant reduction by hydrated electron in the sulfite/iodide/UV process. *Water Res* 129:357–364
- Yuan Q, Liu Y, Le Li L et al (2009) Highly ordered mesoporous titania-zirconia photocatalyst for applications in degradation of rhodamine-B and hydrogen evolution. *Microporous Mesoporous Mater* 124:169–178. <https://doi.org/10.1016/j.micromeso.2009.05.006>
- Zargazi M, Entezari MH (2018) BFO thin film on the stainless steel mesh by anodic EPD: a visible light photocatalyst for degradation of Rhodamin B. *J Photochem Photobiol A Chem* 365:185–198
- Zargazi M, Entezari MH (2019a) Sonochemical versus hydrothermal synthesis of bismuth tungstate nanostructures: photocatalytic, sonocatalytic and sonophotocatalytic activities. *Ultrason Sonochem* 51:1–11
- Zargazi M, Entezari MH (2019b) Anodic electrophoretic deposition of Bi₂WO₆ thin film: high photocatalytic activity for degradation of a binary mixture. *Appl Catal B Environ* 242:507–517
- Zhang YC, Li J, Xu HY (2012) One-step in situ solvothermal synthesis of SnS₂/TiO₂ nanocomposites with high performance in visible light-driven photocatalytic reduction of aqueous Cr(VI). *Appl Catal B Environ* 123–124:18–26. <https://doi.org/10.1016/j.apcatb.2012.04.018>
- Zhang AY, Wang WK, Pei DN, Yu HQ (2016) Degradation of refractory pollutants under solar light irradiation by a robust and self-protected ZnO/CdS/TiO₂ hybrid photocatalyst. *Water Res* 92:78–86. <https://doi.org/10.1016/j.watres.2016.01.045>

- Zhang J, Qian H, Liu W et al (2018a) The construction of the heterostructural Bi₂O₃/g-C₃N₄ composites with an enhanced photocatalytic activity. *Nano* 13:1–9. <https://doi.org/10.1142/S1793292018500637>
- Zhang L, Zhang Y, Huang S et al (2018b) Co₃O₄/Ni-based MOFs on carbon cloth for flexible alkaline battery-supercapacitor hybrid devices and near-infrared photocatalytic hydrogen evolution. *Electrochim Acta* 281:189–197. <https://doi.org/10.1016/j.electacta.2018.05.162>
- Zhang W, Zhang Z, Choi SH, Yang W (2019) Facile enhancement of photocatalytic efficiency of g-C₃N₄ by Li-intercalation. *Catal Today* 321–322:67–73
- Zhao H, Chen Y, Peng Q, Wang Q, Zhao G (2017) Catalytic activity of MOF(2Fe/Co)/carbon aerogel for improving H₂O₂ and OH generation in solar photo–electro–Fenton process. *Appl Catal B Environ* 203:127–137
- Zhao S, Zhang Y, Zhou Y et al (2018) Facile one-step synthesis of hollow mesoporous g-C₃N₄ spheres with ultrathin nanosheets for photoredox water splitting. *Carbon N Y* 126:247–256. <https://doi.org/10.1016/j.carbon.2017.10.033>
- Zhao H, Liu X, Dong Y, Li H, Song R, Xia Y, Wang H (2019) A novel visible-light-driven ternary Ag@Ag₂O/BiOCl Z-scheme photocatalyst with enhanced removal efficiency of RhB. *New J Chem* 43(35):13929–13937
- Zheng Y, Yu Z, Ou H et al (2018) Black phosphorus and polymeric carbon nitride heterostructure for photoinduced molecular oxygen activation. *Adv Funct Mater* 28:1–9. <https://doi.org/10.1002/adfm.201705407>
- Zhou S, Liu Y, Li J et al (2014) Facile in situ synthesis of graphitic carbon nitride (g-C₃N₄)-N-TiO₂ heterojunction as an efficient photocatalyst for the selective photoreduction of CO₂ to CO. *Appl Catal B Environ* 158–159:20–29. <https://doi.org/10.1016/j.apcatb.2014.03.037>
- Zhu B, Xia P, Li Y et al (2017) Fabrication and photocatalytic activity enhanced mechanism of direct Z-scheme g-C₃N₄/Ag₂WO₄ photocatalyst. *Appl Surf Sci* 391:175–183. <https://doi.org/10.1016/j.apsusc.2016.07.104>
- Zhu Y, Wang T, Xu T et al (2019) Size effect of Pt co-catalyst on photocatalytic efficiency of g-C₃N₄ for hydrogen evolution. *Appl Surf Sci* 464:36–42. <https://doi.org/10.1016/j.apsusc.2018.09.061>
- Zong X, Sun C, Chen Z et al (2011) Nitrogen doping in ion-exchangeable layered tantalate towards visible-light induced water oxidation. *Chem Commun* 47:6293–6295. <https://doi.org/10.1039/c0cc05440b>

Chapter 10

Bismuth-Based Compounds as Visible Light Photocatalyst for Remediation and Water Splitting



Mahboobeh Zargazi and Mohammad Chahkandi

Contents

| | | |
|--------|------------------------------------|-----|
| 10.1 | Introduction | 322 |
| 10.2 | Photocatalyst Semiconductors | 323 |
| 10.2.1 | Bi–compounds | 324 |
| 10.2.2 | Modification of Bi–compounds | 334 |
| 10.3 | Application | 343 |
| 10.3.1 | Water Remediation | 343 |
| 10.3.2 | Water Splitting | 345 |
| 10.4 | Conclusions and Prospects | 347 |
| | References | 349 |

Abstract Enhancing demand for environmental protection has become an urgent need more than ever. For this purpose, water the most known indispensable essences for survivorship of aboveground organisms should be specifically considered. Today, quality of water as dominant source influence of the animate systems has been endangered by various harmful contamination levels. Accordingly, rescuing approaches and cleaning compounds in safe manner demanding for improvement of the quality of potable and industrial utilizing waters are daily pursued. Different materials of bismuth having layered structures, hybridized orbitals, low band gap, and band positions can be attended because of significant ability of water remediation. At this book chapter, we reviewed the photocatalytic efficiency of Bi–compounds, the heterojunction and Z–scheme composites of them, and the synthesization method. Heterojunction or Z–scheme combinations led to obtain high separation photogenerated electrons–hole and reduction of the recombination rate. Furthermore, type II of heterojunction and Z–scheme connections with other

M. Zargazi (✉)

Department of Chemistry, Faculty of Science, Ferdowsi University of Mashhad, Mashhad, Iran

M. Chahkandi (✉)

Department of Chemistry, Hakim Sabzevari University, Sabzevar, Iran

e-mail: m.chahkandi@hsu.ac.ir

Bi- or non-Bi compounds was applied as an effective solution to enhance photocatalytic performance. The major points are related to the activity about (1) water remediation and (2) photoelectrochemical water splitting. The presented review tries to demonstrate the high potential of Bi-compounds and Bi-composites for water remediation and hydrogen and oxygen production through redox reactions of water activated by solar light irradiation, respectively.

Keywords Bi-compounds · Photocatalyst · Water splitting · Remediation · Heterojunction · Morphology

10.1 Introduction

Worldwide problem of harmful pollutants has been known as the most challenging issue in view of environmental hygiene, health of human, and living organisms on earth (Schwarzenbach et al. 2010; Mahlambi et al. 2015). Human and living organisms need pure and healthy water and air for surviving. Hence, useful technology of photocatalysis process was done in versatile arena like elimination of organic pollutants and produce sustainable energy (Aziz and Sopyan 2010; Patil et al. 2015; Kumar 2017). Photocatalyst process started under light irradiation as excitation source for produce active oxidant species on the surface catalyst for proceeding pollutant degradation. Nowadays, attention of researchers for gaining high degradation efficiency with cost-effective has been drawn to use available, non-expensive, and renewable energies such as light source of natural sunlight. It is well clear that sunlight as most available global source could be applied for photocatalysis process. Sunlight spectrum composed of three regions: UV – region about 5%, visible – region about 53%, and infrared region about 42%. The percentage of sunlight constituents can answer to photocatalysts necessity to get light energies and electron stimulation and move them up from conduction band to valence band (Fig. 10.1). From this view, photocatalysts can be categorized to UV-activated and visible light-activated photocatalysts. UV photocatalysts are composed from the semiconductors with wide band gaps more than 3 eV such as ZrO_2 , TiO_2 , and ZnO but visible ones own lower band gaps between 2 and 3 eV (Akueus 2012; Alahiane et al. 2014; Reddy et al. 2018). Today, researchers have been focused on the synthesise of visible light photocatalysts to benefit from optimal using of main region of natural sunlight. For this matter, we tried to introduce and describe Bi-compounds as visible light photocatalyst within remediation and splitting of water.

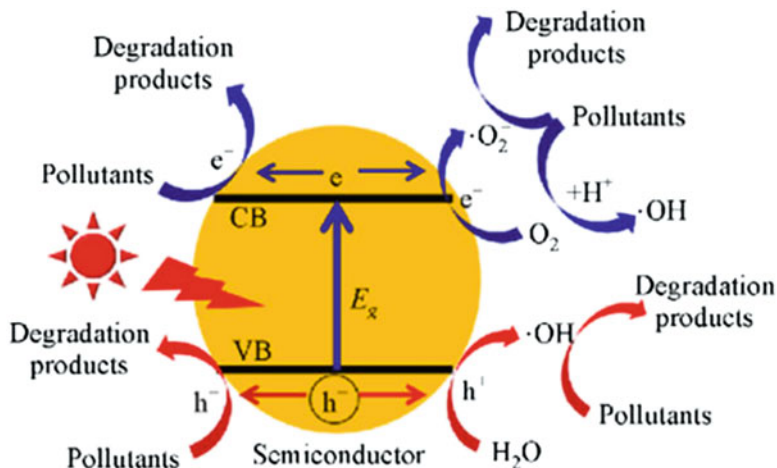


Fig. 10.1 Mechanism of photocatalytic degradation of pollutants over the semiconductor surface. (Reprinted with permission of Springer from Li et al. 2018)

10.2 Photocatalyst Semiconductors

A good photocatalyst should have special properties including (a) sensitive to light, (b) activation under visible or UV light, (c) biological and chemical inert, (d) stable under light without photocorrosion phenomena, (e) affordable, and (f) environmentally safety. To achieve this purpose, vast ranges of semiconductors have been used in photocatalysis process. Effective photocatalysts should produce capability of active radicals (OH^\bullet , O_2^\bullet) for oxidation of pollutants which shown in Fig. 10.1. Redox potential of photogenerated valence band holes is positive as enough value ($\text{H}_2\text{O}/\text{OH}^\bullet = 2.23 \text{ eV}$) to react with adsorbed water molecules to generate hydroxyl radicals. Position of conduction band is sufficient negative for reduction of adsorbed oxygen molecules to produce superoxide radicals. Figure 10.2 shows the various semiconductors including of oxide metals such as TiO_2 , ZnO , CuO , SnO_2 , WO_3 , MnO_2 , Bi_2O_3 , and Fe_2O_3 ; chalcogenide metals such as ZnS , MoS_2 , WS_2 , Bi_2S_3 , and FeS ; non-metallic such as GO, g-C $_3$ N $_4$, and rGO; and mixed metals such as Cu-TiO $_2$ and Bi-TiO $_2$ (Opoku et al. 2017). There are different proposed processes to enhance the photocatalytic efficiency, such as preparation of the composites through the elemental modification, heterojunctions with the other semiconductors, and doping with the other elements. Ag and Au metals form could produce plasmonic electrons acting as electron donor for plasmonic nanocomposites (Myung et al. 2014; Alarfaj 2016). Photocatalysts could be interacted with other narrow band gap semiconductors in order to obtain effective heterojunction. Heterojunction helped transferring of charged species between two semiconductors which led to reduce recombination rate of photogenerated electron–hole. Band positions of semiconductors have a key effect at various heterojunctions (Wang

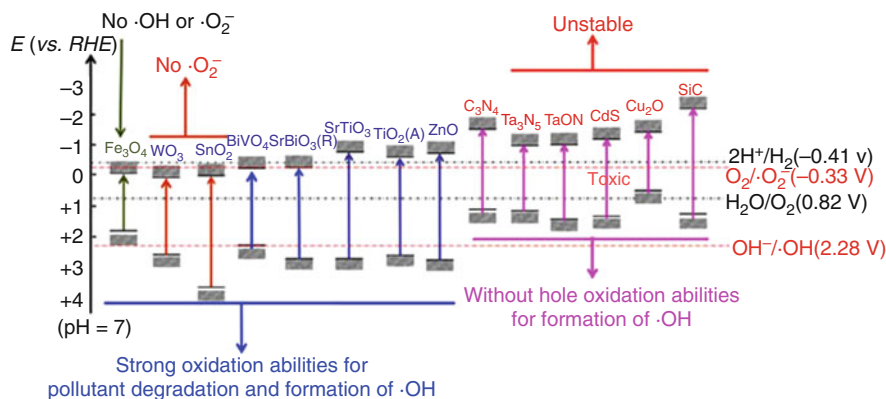


Fig. 10.2 Positions of conduction and valence bands and potentials of typical semiconductors for environmental purifications and capability of them in generation of reactive oxygen species. (Reprinted with permission of Springer from Li et al. 2018)

et al. 2014; Ge et al. 2019). Photocatalysts were used in two forms of powder and film within degradation reactions with some advantages and disadvantages for each of them.

10.2.1 Bi-compounds

Bi-compounds considered as bold visible light-active photocatalysts and have recently drawn rapidly great attention from photocatalyst researchers. Bi^{3+} shows remarkable stability in the different compounds such as Bi_2S_3 (Jin and He 2017), Bi_2WO_6 (Chen et al. 2010), BiFeO_3 (Ponraj et al. 2017), BiVO_4 (Yin et al. 2010b), $\text{Bi}_4\text{Ti}_3\text{O}_{12}$ (Buscaglia et al. 2011), BiPO_4 (Li et al. 2011), $\text{Bi}_2\text{O}_2\text{CO}_3$ (Huang et al. 2015b), and BiOX ($X = \text{Cl}, \text{Br}, \text{I}$) (Zhang et al. 2008) highly noticed owing to the respected tight band gap, high stability, cost-effective, and environment friendly. Almost all of them have layered structure and sheet like from the view of shape. Although Bi^{5+} -compounds, such as KBiO_3 and NaBiO_3 , can also be activated by visible light, Bi^{5+} -compounds are less considered due to the instability of Bi^{5+} ions. In Bi^{3+} compounds, hybridization of O 2p and Bi 6s orbitals leads to move valence bands to upward states which favor for photocatalytic applications. It can be highlighted that high mobility predicted for photo-induced charge carriers on the Bi-compounds surface due to dispersion of 6s orbitals of bismuth. On the other hand, Bi-compounds have band gaps <3.0 eV that indicate the high activity in visible region. Bi-photocatalysts have interesting capabilities within the environmental issues for removing the organic pollutants such of azo dyes (Zhang et al. 2007; Qin et al. 2012), redox treatments of toxic gases such as NO and CO_2 (Ai et al. 2011a; Jin and He 2017), photoactivated water splitting for H_2 and O_2 evolution reaction. A diverse scientific studies about photocatalytic performance of

Bi-compounds and many other reviewing literature about the photocatalyst field were done (Zhao et al. 2014; Meng and Zhang 2016; He et al. 2018). The present review focused on the photocatalytic activity of various Bi-compounds.

Bi₂X₃

Bi₂X₃ (X = O, S, Se, Te) compounds including Bi and other elements of group VI are generally named bismuth chalcogenides with nomenclature of Bi₂O₃, Bi₂S₃, Bi₂Se₃, and Bi₂T₃. Bi₂O₃, based on the phase structures has different band gap values in the range of 2.1–2.8 eV, causing for consideration as a durable photoactivated by the white light. Bi₂O₃ formed from different polymorph phases which include α , β , δ , γ , and ω with crystal network of monoclinic, tetragonal, body-centered cubic, face-centered cubic, and triclinic, respectively. Various Bi₂O₃ known phases have low stability which lead to quick interphase conversion through switching of the temperature condition. Bi₂O₃ nanostructures have remarkable physicochemical characters such as band gap having low energy, dielectric permittivity, ion conductivity, and photoconductivity which the highlighted properties make Bi₂O₃ as a stable visible light photocatalytic candidates within water splitting and remediation of organic pollutants. Recently, controlled synthetization of Bi₂O₃ with specified morphology and certain phase has become a hotspot for photocatalysis researchers. For instance, uniform hierarchical bismuth oxide structures were synthesized and demonstrated excellent visible light activity about degradation of rhodamine B (Zhou et al. 2009). Monoclinic phase of Bi₂O₃ was prepared via calcination of hydrothermal production from (BiO)₂CO₃ precursor and indicated excellent photoactivated degradation of NO gas and formaldehyde via visible light radiance (Ai et al. 2011b). Bi₂S₃ was exhibited as a wonderful light-harvesting photocatalyst because of having tight band gap \sim 1.7 eV and excited in visible and near-IR regions. Bi₂S₃ nanocatalysts have been synthesized in a variety of dimensions of one-directional, e.g., rode in Fig. (10.3a), two-dimensional, e.g., sheet in Fig. 10.3b, and three-dimensional, e.g., urchin-like in Fig. 10.3c by standard

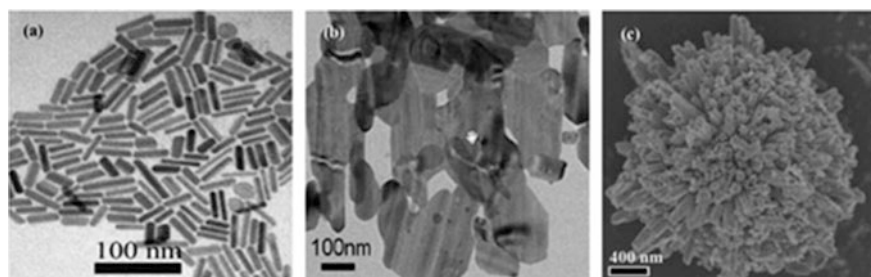


Fig. 10.3 Transmittance electron microscopy images of (a) nanorods, (b) nanosheets, and (c) scanning electron microscopy image of nanospheres of Bi₂S₃. (Reprinted with permission of Springer from Meng and Zhang 2016)

oxygen-free, hot injection, and solvothermal methods, respectively (Wu et al. 2010; Zhang et al. 2011). The photogenerated holes on the Bi_2S_3 semiconductor have efficient energy about 1.62 eV for oxidation of adsorbed water molecules to produce high oxidants such as OH^\bullet for degradation of dye contaminants (Zhang et al. 2011). Wu et al. (2010) reported that Bi_2S_3 nanodots and nanorods were synthesized by hot injection method. Uniform Bi_2S_3 nanodots show high photocatalytic degradation for rhodamine B due to the presence of high surface area.

Bi_2Se_3 semiconductor with the layered structure is composed from several monolayers with 0.96 nm thickness that bonded around z -axis with the following configuration Se-Bi-Se-Bi-Se (Sun et al. 2012). Bi_2Se_3 has great potential in photoelectrochemical, optical, and thermoelectrically devices and photocatalysis applications owing to the small band gap and high mobility of charge species (Sun et al. 2012). Bismuth telluride (Bi_2Te_3) also has very narrow band gap about 0.15 eV with trigonal structure and high melting point. Bi_2Te_3 applied in thermoelectric generators and refrigeration due to the thermoelectric properties at 25 °C (Teweldebrhan et al. 2010). Big problem for Bi_2Se_3 and Bi_2Te_3 arrived from the great probability of recombination rate of photogenerated electron–hole pairs that deprives them of the eventual photocatalytic activity.

BiOX

Bismuth oxyhalides represented by BiOX ($X = \text{Cl}, \text{Br}, \text{I}$) can be considered as the most famous bismuth compounds due to appropriate optical properties and high applications in environment treatment. BiOX s have layered structures similar to other Bi-compounds which characterized by segments of Bi_2O_2 interleaved by double segments of halogens. Layered structures suggested promising large space for polarizing orbitals and created dipoles which could lead to separate charge carriers (Lei et al. 2009).

Density functional theory calculation method simulated electrical structures of Bi-oxyhalides (Huang and Zhu 2008). Both the valence band and conduction band of BiOX composed of X $n\text{p}$ ($n = 2-5$ for $X = \text{F}, \text{Cl}, \text{Br},$ and I , respectively), O 2p , and Bi 6p orbitals. The observed band gaps based on computations have resulted as 2.79 eV, 2.34 eV, 1.99, and 1.38 eV for BiOF , BiOCl , BiOBr , and BiOI , respectively (Zhang et al. 2008; Su et al. 2010). Results exhibited that heavy halogen has smaller band gap. So, BiOF as photocatalyst could be excited by UV light, while BiOI activated by visible and near-IR light. It can be stated that BiOBr and BiOCl are repeatedly applied because of the desired amounts of band gaps. The conduction band orbital density isosurfaces are illustrated in Fig. 10.4 for BiOX with the involving of Bi 5d states.

BiOCl is a UV-sensitive photocatalyst with experimental band gap with range of 3.1–3.5 eV and computational calculated band gap of 2.8 eV (Zhang et al. 2006, 2016; Lei et al. 2009). Excited- BiOCl indicated eminent photocatalytic efficiency for pollutant elimination. For instance, Zhang et al. (2006) synthesized durable BiOCl nanoplates via simple hydrolysis method which shown high efficiency about photodegradation of methyl orange activated by UV light. BiOCl nanosheets with

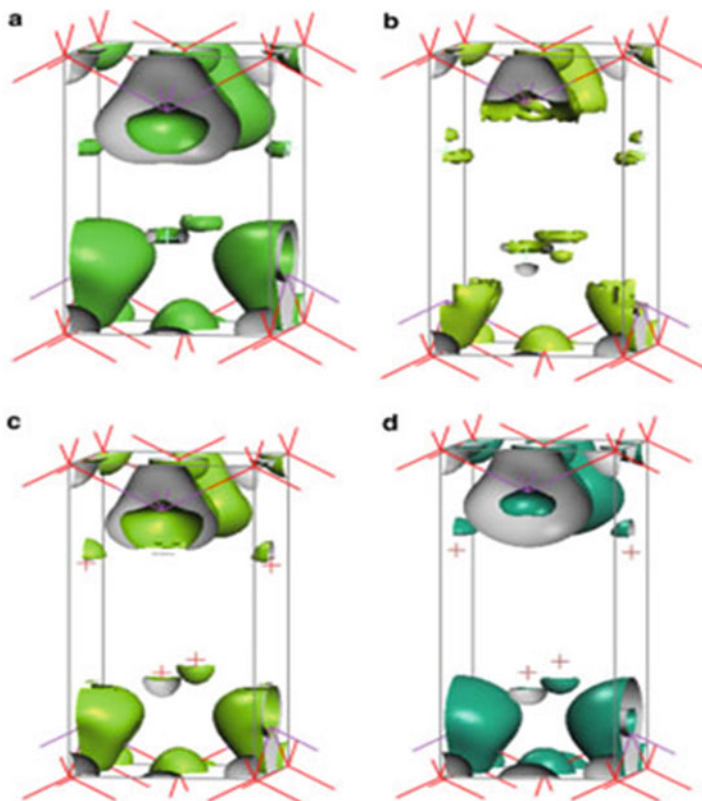


Fig. 10.4 The conduction band orbital density isosurfaces of BiOX (a) X = F, (b) X = Cl, (c) X = Br, and (d) X = I with the adoption of Bi 5d states. (Reprinted with permission of Elsevier from Huang and Zhu 2008)

{100} facet could exhibit high photocatalytic activity due to produce oxygen vacancies under UV illumination. In order to make optimum usage of solar energy, there is a remarkable tendency for evaluation of photocatalytic activity of BiOCl under visible light irradiation. If BiOCl coupled with some dyes which have intrinsic physicochemical properties could have visible light activity. For example, Xiong et al. (2011) reported that synthesis of square-like BiOCl nanoplates by hydrothermal method, which has [Cl–Bi–O–Bi–Cl] layered structure and demonstrated high photocatalyst performance for rhodamine B compared to commercial TiO₂ (P25). In this work, diffraction reflectance UV spectroscopy studies for BiOCl nanoplates reported a wide band gap 2.9 eV, so photosensitization process overcome on the photocatalytic process for rhodamine B degradation. At other work, Ye et al. (2012) fabricated marvelous BiOCl with oxygen vacancies under Ar purging, which exhibited 20 times photocatalytic activity than conventional BiOCl for photodegradation of rhodamine B induced via visible light. Porous BiOCl nanosheets also demonstrated photosensitized removal of rhodamine B. Also,

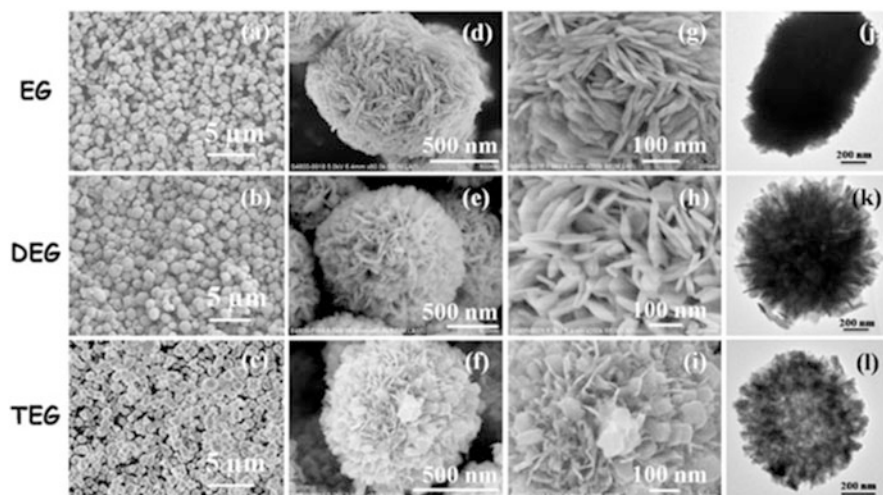


Fig. 10.5 Scanning electron microscopy images (a–i) and transmission electron microscopy images (j–l) of BiOCl nanostructures synthesized via solvothermal method in the presence of polyols: ethylene glycol, diethylene glycol, and triethylene glycol. EG, DEG, and TEG stand for ethylene glycol, diethylene glycol, and triethylene glycol, respectively. (Reprinted with permission of Elsevier from Xiong et al. 2013)

three-dimensional hierarchical BiOCl nanoplates having remarkable photocatalysis efficiency have been successfully prepared. For example, solvothermal with polyol mediator technique was applied for synthesis of specific morphologies BiOCl hierarchical nanostructures. Hierarchical BiOCl (see Fig. 10.5) showed high photoremediation of rhodamine B activated by visible light compared with nanosheets or nanoplates of BiOCl and P25 (Xiong et al. 2013). Unlike BiOCl, BiOBr were introduced as visible light-sensitive semiconductor with inherently appropriate band gap for utilization of sunlight and suggested as a powerful catalyst about photodegradation of organic pollutants under white light illumination. Recently, considerable researches have been done to evaluate photocatalytic activity of BiOBr in environmental treatment and photocatalytic water splitting fields. Lamellar and plate-based BiOBr structures were prepared that showed great photocatalyst performance for pollutant degradation (Shang et al. 2009).

BiOBr nanosheets used for photoreduction of Cr(VI) induced by visible light and the reusability indicated high efficiency for reduction process. Researchers have also attracted to synthesize three-dimensional hierarchical BiOBr to enhance the photocatalytic properties which has more advantages in comparison with one-dimensional or two-dimensional structures (Shi et al. 2013). BiOBr with mesoporous structure showed higher visible light photocatalytic efficiency for harmful tetrabromobisphenol A compared to commercial TiO₂. High ranges of pollutants such as dyes, e.g., rhodamine B, methyl orange, methylene blue, and organic, e.g., phenol and toluene have been proposed as mannequin pollutants to exhibit the photocatalyst activity of BiOBr compounds under visible light irradiation

(Zhao et al. 2014). Among BiOX compounds, BiOI has narrowest band gap besides highest utilization of solar source. BiOI is a semiconductor with intrinsic rapid recombination of charge carriers singly, so BiOI cannot show acceptable photocatalytic performance. Therefore, a lot of strategies were proposed for combination/synthetization of BiOI with other semiconductors to improve the related photocatalytic activity.

Bi₂MO₆

Bi₂MO₆ are known as the famous triplet oxygen – bismuth compounds with Aurivillius¹ structure depicted by $(\text{Bi}_2\text{O}_2)^{2+}(\text{A}_{n-1}\text{B}_n\text{O}_{3n+1})^{2-}$ (A = Ba, Bi, Pb, so on., B = Ti, Nb, W, Mo, so on.) which has intercalated structures with sheets of perovskite-bearing octahedral $(\text{A}_{n-1}\text{B}_n\text{O}_{3n+1})^{2-}$ sandwiched array between $(\text{Bi}_2\text{O}_2)^{2+}$ layers. Until now, a variety of bismuth Aurivillius oxides containing bismuth tungstate, bismuth molybdate, and bismuth subcarbonate have been fabricated, which has excellent potential for photocatalysis usages such as water treatment and photocatalytic water splitting (Zhao et al. 2014; Meng and Zhang 2016).

Bismuth tungstate (Bi₂WO₆) is known as one of the easiest structures of the Aurivillius group ($n = 1$) having a layered standing with WO₆ sheets. The perovskite block in Bi₂WO₆ composited of 2D array of WO₆ octahedral linked corner, with thick octahedral layer. Bi₂WO₆ has great potential for oxygen evolution reaction within hydrolysis and oxidation of toxic pollutants under white light. Zhang et al. (2007) reported that various morphologies of Bi₂WO₆ nano and microstructures, including flower-, tire-, and spiral-like shapes, showed excellent solar light photo-activated catalytic efficiency for remediation of rhodamine B that could be related to the presented morphology, size, and structure. Furthermore, the pH value of the solution contained of pollutant also defines the photocatalytic performance of photocatalyst. Zhu et al. (2016) proved the pH effect of initial solution on the photocatalysis performance of nanosheets Bi₂WO₆ for degradation of rhodamine B which could be related to mode and adsorption–desorption of rhodamine B on the semiconductor surface. Bi₂WO₆ also exhibited high performance for air treatment and water splitting applications (Larson and Zhao 2016). Yu et al. suggested that well-crystalized bismuth tungstate with high surface area which could perform photocatalytic degradation of formaldehyde gas in air (Yu et al. 2005).

Bi₂MoO₆ is also another layered member of Aurivillius compounds which has recently drawn enormous scientific attentions due to the photocatalytic properties within hydrolysis and photooxidation of contaminants. The layered structure Bi₂MoO₆ is synthesized via refluxing method which exhibited high photocatalytic efficiency for oxygen liberation from an aqueous solution of AgNO₃ induced by solar light (Shimodaira et al. 2006). The obtained results suggested that

¹Aurivillius phases are a form of perovskite built by alternating layers of $[\text{Bi}_2\text{O}_2]^{2+}$ and pseudo-perovskite blocks.

photocatalytic activity attributed to crystallinity and high rate of charge transfer in layered structure Bi_2MoO_6 . Zhang et al. (Huang et al. 2018) suggested that nanosheets and microrods of Bi_2MoO_6 were selectively synthesized via change of pH of precursor solution in hydrothermal method and demonstrated efficient visible light photocatalytic degradation of methylene blue. Bi_2MoO_6 has been synthesized via solid state and solvothermal or hydrothermal methods similar to Bi_2WO_6 (Yin et al. 2010a; Zhang et al. 2010). Comparison studies for synthesis method of Bi_2MoO_6 showed that smaller size, large surface area, and efficient photocatalytic performance obtained from samples which fabricated via hydrothermal and solvothermal methods not solid-state reaction. Furthermore, microwave method was also applied to synthesize of Bi_2MoO_6 in short time with good photocatalytic performance (Xie et al. 2008). Different work, thin film of Bi_2MoO_6 (200 nm thickness) fabricated via thermal evaporation deposition process (see Fig. 10.6) which showed high visible light-responsive photocatalyst property for rhodamine B degradation (Cuéllar et al. 2011).

Bismuth titanate, also one important member of Aurivillius oxide family, introduced by a variety of compositions and showed high visible light-sensitive or UV-sensitive photocatalytic for pollutants. Sillenite $\text{Bi}_{12}\text{TiO}_{20}$ nanowires (Hou et al. 2009) and perovskite $\text{Bi}_4\text{Ti}_3\text{O}_{12}$ (Li et al. 2016) demonstrated high photocatalytic efficiency for methyl orange under light (<400 nm). Cubic phase – Bismuth titanates ($\text{Bi}_{12}\text{TiO}_{20}$) with a variety of morphological structures such as flower-looking like, belt-looking like, and tetrahedral-looking-like shapes prepared by easy approach showed in Fig. 10.7, which exhibited high photocatalytic degradation performance for methylene orange and *p*-nitrophenol (Guo et al. 2013).

BiVO₄

Bismuth vanadate (BiVO_4) is known as the most versatile member of Bi–compounds which has three crystallite phases: tetragonal zircon, monoclinic, and tetragonal scheelite structures. BiVO_4 with monoclinic crystalline phase became white light photoactivated because of low required energy band gap about 2.4 eV compared to other phases. Hence, BiVO_4 with high adsorption in visible light region and narrow band gap was considered as new materials for photocatalytic applications and other related researches. Due to special physicochemical features of BiVO_4 such as Ferro elasticity and theoretical band gap about 2.047 eV obtained from density functional theory method, it has been considered as photocatalytic activity, recently (Wang et al. 2019a). Multi shell hollow spheres of BiVO_4 synthesized via carbonate template under thermal conditions are depicted in Fig. 10.8. Hollow shapers bear great photo-induced performance within elimination of methylene blue under solar light. Figure 10.9 also confirmed the claimed morphology for BiVO_4 with scanning electron microscopy and transmittance electron microscopy images (Zong et al. 2017).

Recently, variety ranges of BiVO_4 structures have been synthesized and applied in photocatalytic performances such as elimination of pollutants and H_2 or O_2

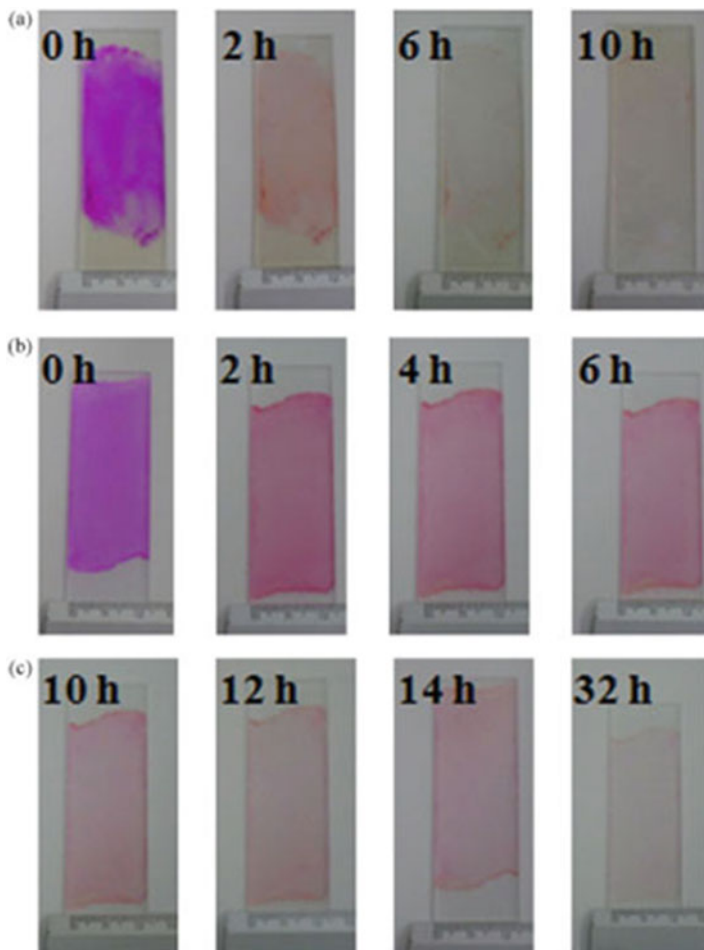


Fig. 10.6 Evaluation of color changing of adsorbed rhodamine B on the Bi_2MoO_6 thin film at different interval time (a) and an experiment done on the bare glass (b and c). (Reprinted with permission of Elsevier from Cuéllar et al. 2011)

liberation from water splitting process (Wang et al. 2019b). Hollow microspheres of BiVO_4 showed considerable solar light photocatalysis efficiency for remediation of rhodamine B and 2-propanol (Sun et al. 2013a). At 1998, Kudo's team reported a great candidate with high potential for photocatalytic water splitting named BiVO_4 for the first time (Huang et al. 2017). Years later, Kudo et al. demonstrated photoactivated efficiency of bismuth vanadate for O_2 liberation from AgNO_3 solution under visible light (Kudo et al. 1999).

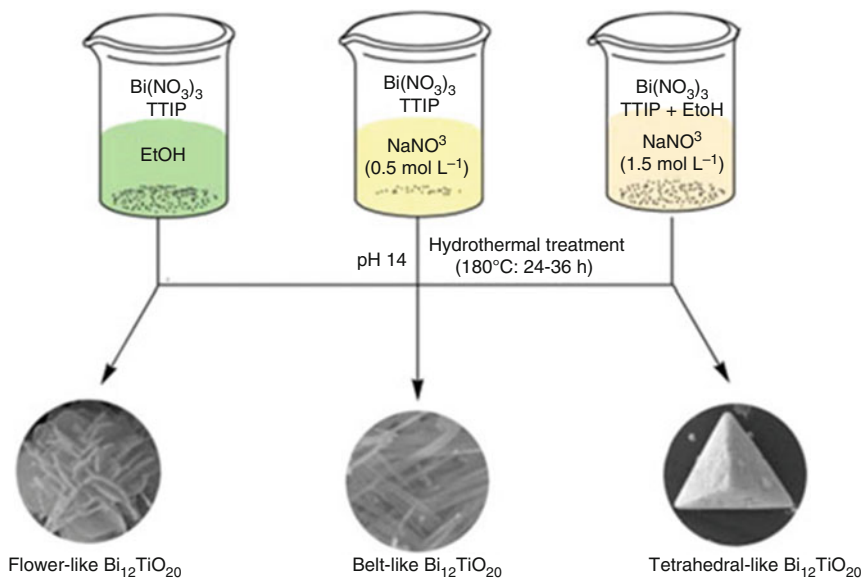


Fig. 10.7 Schematic for fabrication of different morphology for $\text{Bi}_{12}\text{TiO}_{20}$ by hydrothermal approach. TTIP rephrases for $\text{Ti}(\text{OC}_3\text{H}_7)_4$. (Reprinted with permission of Royal Society of Chemistry from Guo et al. 2013)

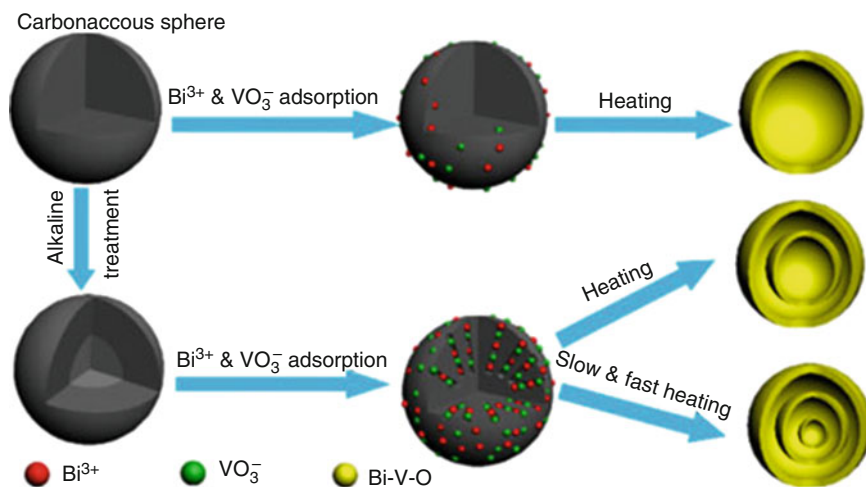


Fig. 10.8 Schematic depicts the fabrication approach of hollow spheres BiVO_4 . (Reprinted with permission of Elsevier from Zong et al. 2017)

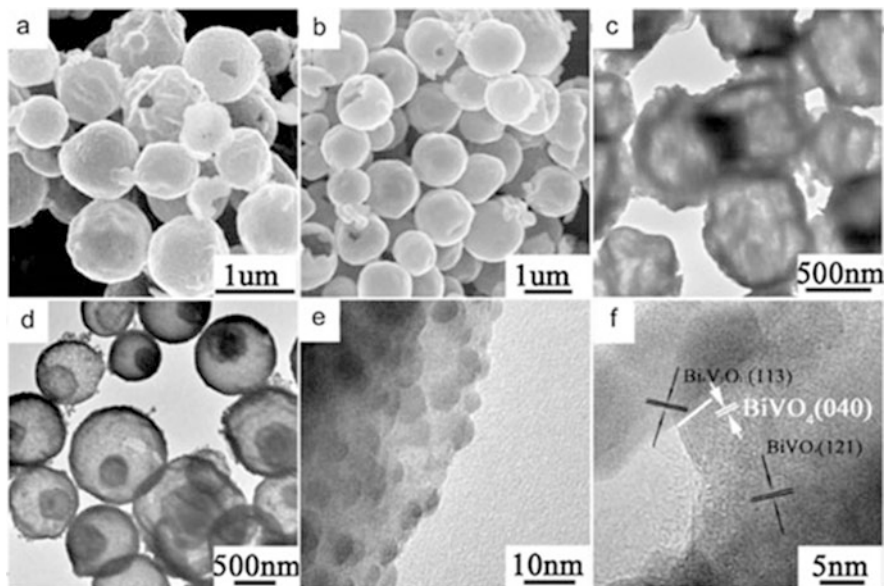


Fig. 10.9 (a) Scanning electron microscopy image of Bi-V-O single-shell hollow spheres, (b) scanning electron microscopy image of Bi-V-O double-shell hollow spheres, (c) transmission electron microscopy image of Bi-V-O single-shell hollow spheres, (d) transmission electron microscopy image of Bi-V-O double-shell hollow spheres, (e) transmission electron microscopy image of an individual Bi-V-O double-shell hollow spheres, (f) high-resolution transmission electron microscopy image of an individual Bi-V-O double-shell hollow spheres. (Reprinted with permission of Elsevier from Zong et al. 2017)

BiFeO₃

BiFeO₃ compound shows simultaneous multiferroic and magnetoelectric behaviors at ambient conditions that led to widely employing of BiFeO₃ in the arena of nonvolatile memory, spintronic, sensors, and piezoelectric apparatus (Lam et al. 2017; Ponraj et al. 2017). BiFeO₃ photocatalyst having rhombohedral disordered perovskite is a new kind of reliable solar light-activated photocatalyst within the organic pollutant remediation because of its small band gap and great chemical stability. Last year, BiFeO₃ attracted considerable attention in photocatalytic environmental applications (particular degradation dye pollutants such as methylene blue and rhodamine B due to its weak ferromagnetic feature led to recycling from treated solution (Ponraj et al. 2017). Optical band gap of BiFeO₃ reported between 2.2 and 2.8 eV in literatures. Mesoporous BiFeO₃ hollow sphere was synthesized and used for degradation of rhodamine B and 4-chlorophenol under 500 W Xe-lamp irradiation (Gao et al. 2015). Soltani et al. (Soltani and Entezari 2013a) demonstrated that reactive black 5 bears three main UV/visible peaks at wavelengths of 620, 312, and 254 nm. The generation of some new intermediates such as sulfone, sulfonate, and amine groups prepared in the UV/visible regions is the reason for observation of

three main peaks. The residual of small organic intermediates can explain the changing of color solution as well as the decrease of pH.

10.2.2 Modification of Bi-compounds

Although Bi-compounds were introduced as visible light-responsive photocatalysts in water treatment, some compounds such as BiFeO₃ and BiOXs have weak adsorption ability which led to poor performance for photocatalytic degradation of pollutants. Relatively poor efficiency can attribute to (i) high recombination rate of electron-hole in bulk or surface, (ii) positions of conduction band or valence band related to O₂ reduction or H₂O oxidation, respectively, and (iii) small surface area for photocatalytic process. So far, many researches were devised for resolving the problematic issues such as morphology modifications, doping, and heterojunctions (Chen et al. 2016a) with other semiconductors and generation of vacancies over the surface. Applying the solutions, either the recombination rate or light harvesting can be effectively decreased or increased, respectively, which led to high performance. For more clearance, follow the more detailed discussion below.

Morphology Control

The chemophysical properties of semiconductors could be changed by main structural factors, size, morphology, and defects, respectively. Subsequently, photocatalytic properties of catalysts can improve by the structural parameters. In this section, we are focused on morphology control of Bi-compounds and investigated photocatalytic performance. Morphology studies were shown improved photocatalytic efficiency because of produce low-dimensional or hierarchical structures, which could create reactive sites, high rate of mass transfer, and more harvesting amount of visible light. In the following, some more innovative producing techniques of low-dimensional and hierarchical structures of Bi-compounds were discussed.

Bi-compounds with Low-Dimensional Structure

Nanomaterials have multifarious dimensions which could be classified to four categories: zero-dimension such as nanoparticles, one-dimension such as nanorods and nanowires, two-dimension such as nanoplates or nanosheets, and three-dimension such as nanospheres or nanoflowers (Jeevanandam et al. 2018). At the recent years, Bi-compounds were synthesized by control of synthesization parameters to obtain special size including nanoparticles, nanobelts, and nanoflowers for photocatalytic applications. Soltani et al. (Soltani and Entezari 2013b, c) reported that BiFeO₃ nanoparticles synthesized via ultrasound with narrow size distribution

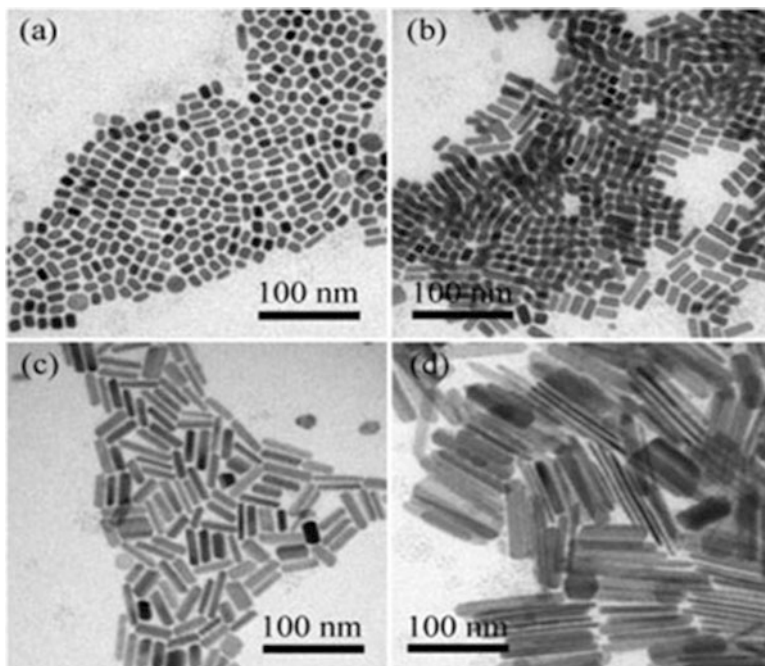


Fig. 10.10 Transmittance electron microscopy images of synthesized Bi_2S_3 nanostructures with various concentrations of Bi (a) 1:0.5, (b) 1:1, (c) 1:1.5, and (d) 1:1.7. (Zong et al. 2017). (Modified)

as visible light photocatalyst which exhibited higher photocatalytic performance for methylene blue and rhodamine B compared to BiFeO_3 synthesized by sol-gel method. Nanodots, nanorods, and nanosheets of Bi_2S_3 nanostructures synthesized and used for degradation of rhodamine B, methylene blue, and methyl orange which results pointed to photocatalytic activity depends to dimension (see Fig. 10.10) (Wu et al. 2010).

The properties of size and porosity of snow-like Bi_2WO_6 particles depicted in Fig. 10.11 resulted in high white light photoactivated performance for degradation of rhodamine B (Zhuo et al. 2013). Spherical Bi_2WO_6 nanoparticles were fabricated via hydrothermal route with average size 85 nm bear great photoactivity for elimination of rhodamine B under solar light (Wang et al. 2015). Bi_2WO_6 with nanoplate two-dimensional structure with 30 nm length size exhibited high performance for photoactivated remediation of aquatic solution of rhodamine B under solar light which could be related to small particle size and high surface area (Zhang and Zhu 2005). Another work reported the hydrothermal preparation of nanoplate $\text{Bi}_2\text{WO}_{6-x}$ with high surface oxygen vacancy with 2.1 times higher photocatalytic degradation of 2–4-dichlorophenol than pristine Bi_2WO_6 (Lv et al. 2016). High photocatalytic performance can attribute to high surface oxygen vacancy states.

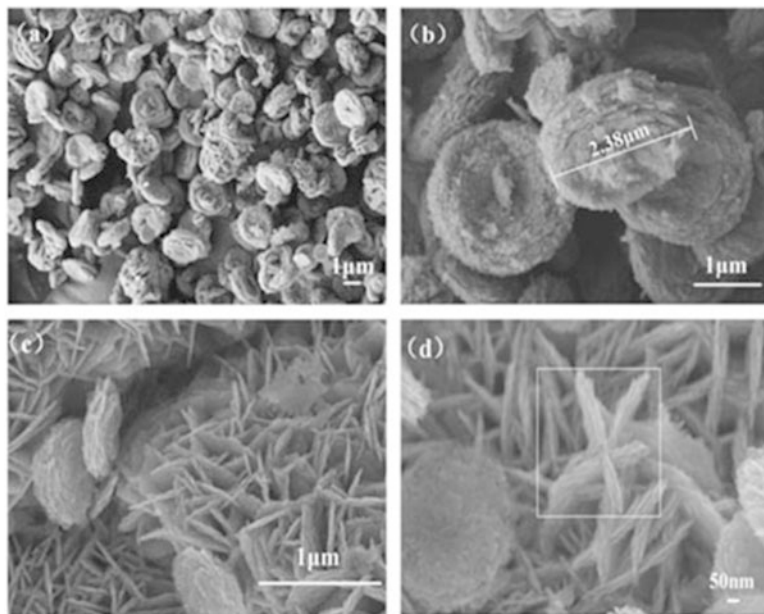


Fig. 10.11 Scanning electron microscopy images of Bi_2WO_6 with different morphologies synthesized at $\text{pH} = 1$ and $\text{pH} = 5$. (Reprinted with permission of Elsevier from Zhuo et al. 2013)

One-dimensional Bi_2MoO_6 nanosheets were fabricated via electrospinning which demonstrated remarkable photocatalytic efficiency within remediation of rhodamine B and methylene blue under simulated visible light (Sun et al. 2013b).

Hierarchical Bi-compounds

Hierarchical structures can be highlighted as ordered architectures assembled from low-dimensional building blocks, such as nanofibers, nanorods, nanoribbons, nanosheets, and nanoplates. Recently, great attention has been attracted to hierarchical assemblies due to the proper electronic, optical properties, layered structure, and catalytic efficiency which has bold difference with low-dimensional sub-component (Luo et al. 2019; Song et al. 2019). Herein, the synthesis of hierarchical Bi-compounds has attracted more efforts from the view of specific morphologies to gain high photocatalytic performance. The hierarchical Bi_2WO_6 hollow tubes demonstrated high photo-induced catalytic efficiency for elimination of rhodamine B under simulated visible light, which was related to Bi_2WO_6 structure, tight band gap, and gross surface area (Yafei et al. 2013). Zargazi et al. indicated the high simultaneous photocatalytic and sonophotocatalytic performances of Bi_2WO_6 nanoflowers for binary mixture (methylene blue and rhodamine B) synthesized by ultrasonic-assisted hydrothermal which attributed effect of morphology in

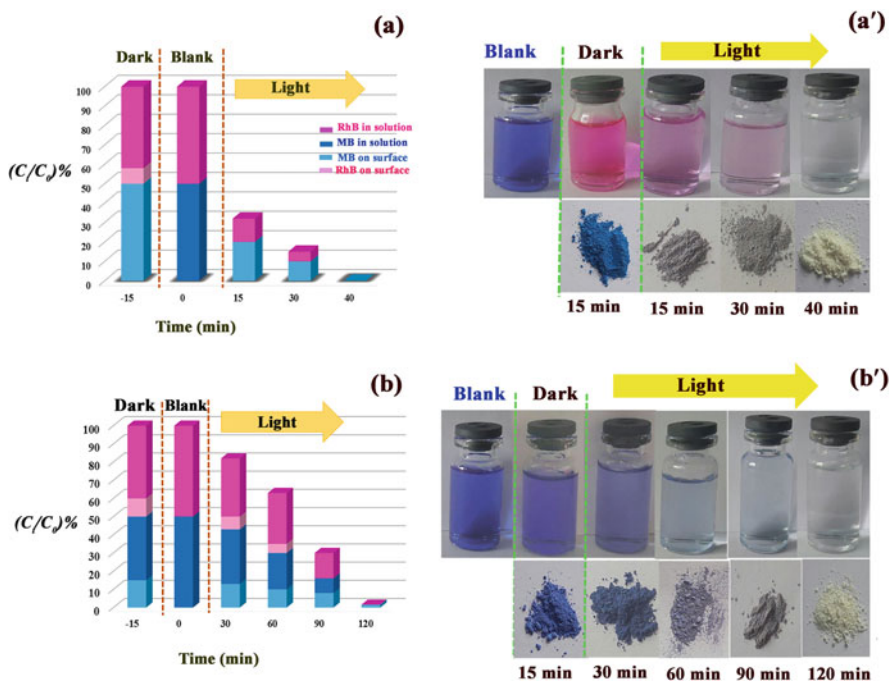


Fig. 10.12 Adsorption behaviors (dark) and sonophotocatalytic (light and US) degradation of rhodamine B/methylene B: Sono-BWO sample (a and a'), Hydro-BWO sample (b and b'). (Reprinted with permission of Elsevier from Zargazi and Entezari 2019c)

adsorption of pollutants from binary mixtures (Zargazi and Entezari 2019c). Both dyes were decomposed on the catalyst surface and bulk solution by sonophotocatalytic process which is observed in Fig. 10.12. Hierarchical flowerlike Bi_2MoO_6 crystals synthesized by simple hydrothermal method show permanent photo-induced reduction of CO_2 into methanol and ethanol (Dai et al. 2016). Morphology of Bi_2MoO_6 flower showed high influence in separation of photogenerated electron-hole and adsorption of light. Sharma et al. reported the preparation of Bi_2S_3 nanoflowers which exhibited the high photocatalytic degradation of two different binary mixtures of rhodamine B and methylene blue and 4-nitrophenol and 4-chlorophenol from suspension (Sharma and Khare 2018). Novel nanoflower structures of BiOCl with small band gap about 2.87 eV but huge average size about 1.5 μm were routinely prepared at 25 $^\circ\text{C}$ using the L-Lysine template. The interesting structure indicated high photocatalytic remediation of rhodamine B under solar light. The observed perfect photocatalytic performance can be appropriated to phase purity, high exposure of $\{110\}$ planes, thin nano-petals structure, tight band gap, and the relatively large surface area.

Nano Bi Films

Recently, nano thin films of Bi–compounds attracted great attentions due to special applications in multiple fields such as water splitting, solar cell, and remediation environmental (Patil et al. 2015; Lee and Ebong 2017). Generally, powder compounds have serious problems including recollection and reusing, agglomeration effect, and respiration problems for human. To resolve problem's powders, immobilized films introduced as new solution for photocatalytic applications. Until now, Bi–films prepared by various methods such as chemical bath deposition (Gao et al. 2011), liquid phase deposition (Song et al. 2004), spin coating (Tyagi et al. 2015), sol–gel (Zargazi and Entezari 2019a), chemical vapor deposition (Brack et al. 2015), electrochemical deposition (Chahkandi and Zargazi 2019), electrophoretic deposition (Zargazi and Entezari 2019b), and so on.

Using the abovementioned methods, Bi–thin films deposited on conductive and non-conductive substrate were applied for degradation of various pollutants. For instance, Bi_2WO_6 deposited over the surface of stainless steel mesh using the anodic electrophoretic method and applied for remediation of binary mixture of 4–nitrophenol and 4–chlorophenol (Zargazi and Entezari 2019b). High photocatalytic degradation for film could be attributed to the effect of film thickness and substrate in separation of electron–hole. Alfaifi et al. reported the preparation of Bi_2WO_6 electrodes with nanoplates and Bucky ball-shaped microsphere morphologies by aerosol-assisted chemical vapor deposition which was applied for degradation of methylene blue and rhodamine B (Alfaifi and Bayahia 2019). Alfaifi and Bayahia suggested the energetic and interfacial features of Bi_2WO_6 film to increase solar energy and photocatalytic activity of film. BiFeO_3 film also deposited on the same substrate by anodic electrophoretic deposition method which exhibited high photocatalytic efficiency for decomposition of rhodamine B dye (Zargazi and Entezari 2018). BiFeO_3 film demonstrated higher photocatalytic degradation than BiFeO_3 powder due to substrate effect in decreasing of recombination rate of photo-induced charge pairs. At another work, forestlike BiFeO_3 films are fabricated by using cathodic electrophoretic deposition on the stainless steel mesh which indicated high photocatalytic performance for phenol compounds. Forestlike morphology of BiFeO_3 film depicts in Fig. 10.13 shows key effect in harvesting and multi-scattering of visible light which led to high degradation efficiency (Zargazi and Entezari 2019a). Venkatesan et al. (2018) shown the preparation of stable monoclinic – BiVO_4 film by radio frequency – sputtering on the fluoride tin oxide and the degradation application of rhodamine 6G. Photocatalytic reduction of Cr hexavalent is conducted by Bi_2S_3 films in single and binary mixtures. Chahkandi et al. reported the novel deposition square wave voltammetry method of Bi_2S_3 film on the stainless steel mesh which exhibited high reduction rate for conversion toxic Cr(VI) to non-toxic Cr(III) (Chahkandi and Zargazi 2019).

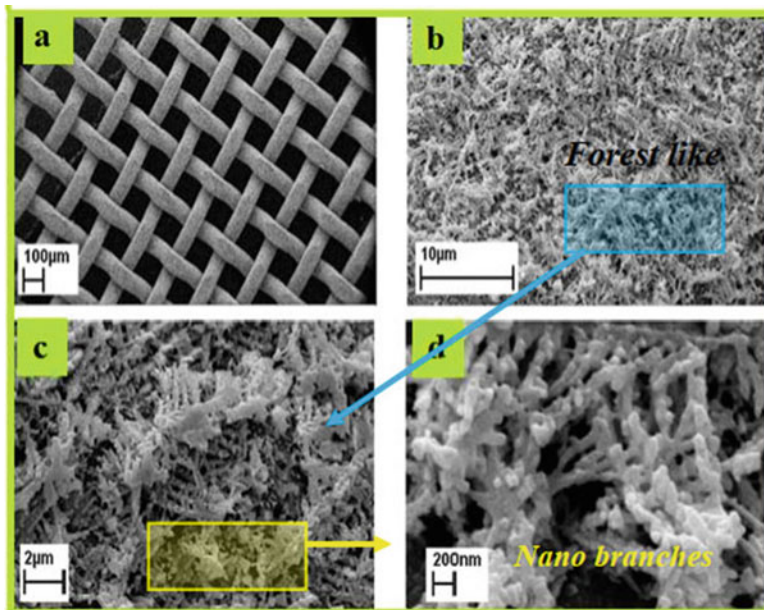


Fig. 10.13 BiFO₃ film coated on substrate (stainless steel mesh) (a), BiFO₃ film on wire surface (b), treelike structure (c) and nanobranches of BiFO₃ (d). (Reprinted with permission of Elsevier from Zargazi and Entezari 2019a)

Heterojunction

Over the past decades, designing of heterojunctions was introduced as a best route to reduce the recombination rate of electron–hole produced under light irradiation (Wang et al. 2014; Huang et al. 2015a). The Bi-based photocatalysts, with an appropriate band gap, have capability to produce electrons under solar light. However, the excited electron and holes potentially recombined very fast together. From this view, heterojunction construction can have a great role in enhancing photocatalytic efficiencies of Bi-based photocatalysts. Bi-based heterojunctions include conventional and Z–scheme heterojunctions. Among the conventional heterojunctions, the type II junction is the most usual one, while in Z–scheme type, the newly merged direct Z–scheme heterojunction appears to be the most effective junction structure used for exploring the capacity of photo-generated carriers (Wang et al. 2014; Low et al. 2017). Figure 10.14 depicted schematics for heterojunctions (Type II) and Z–scheme heterojunction.

Binary Bi are heterojunctions with two kinds of Bi–compounds, and also Binary Bi compounds can produce heterojunctions with non-Bi–compound.

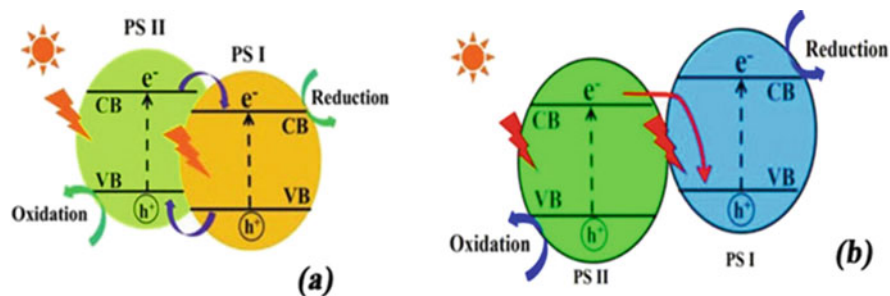


Fig. 10.14 Charge separation of (a) heterojunction (Type II) and (b) direct Z-scheme heterojunction. CB, VB, and PS stand for conductive band, valence band, and photocatalyst semiconductors, respectively. (Modified)

Type II: Conventional Heterojunction

In comparison with the ternary types of heterojunctions, the second junction type is the most suitable one. Bi-compounds and semiconductors with small band gap formed heterojunction (type II) as conduction band and valence band levels of semiconductors should be lower than the Bi-compound portion. For example, Fan et al. (2016) fabricated a binary Bi-compounds $\text{Bi}_2\text{MoO}_6\text{-BiOI}$ heterojunction (Fig. 10.15a, b) by anion exchange method which exhibited high photocatalytic degradation efficiency for rhodamine B in comparison with BiOI or Bi_2MoO_6 alone (Fig. 10.15c). Optimal molar ratio of Mo/I is 50% made heterojunction (Type II) between two components having highest efficiency under white light (Fig. 10.15d). It is notable that three matched Bi-compounds can be combined together to produce a ternary heterojunction such as $\text{Bi}_2\text{S}_3/\text{Bi}_2\text{O}_3/\text{MoS}_2$ (Ke et al. 2017). Improved photocatalytic activity of $\text{Bi}_2\text{S}_3/\text{Bi}_2\text{O}_3/\text{MoS}_2$ ternary Bi-compounds can be attributed to enhancing of light adsorption and high separation of electron-hole by double heterojunction (Type II) (Fig. 10.16). Moreover, some other heterojunctions with low band gap semiconductors such as non-Bi-compounds were performed for improving photocatalytic degradation of different pollutants.

For instance, $g\text{-C}_3\text{N}_4$ compounds could be coupled with Bi_2WO_6 , BiVO_4 , Bi_2S_3 , Bi_2O_3 , and Bi_2MoO_6 which exhibited improved photocatalytic properties in degradation of pollutants. Numerous synthesis strategies for heterojunctions (Type II) have been introduced, and most of Bi-based heterojunctions led to improve photocatalytic efficiency (Table 10.1).

Direct Z-Scheme Heterojunctions

Yu et al. (2013) introduced a direct Z-scheme heterojunction to clarify the improvement of photocatalytic property of a $\text{TiO}_2/g\text{-C}_3\text{N}_4$ composite. The reported type of Z-scheme heterojunction does not need electron medium unlike other Z-scheme heterojunctions such as liquid phase. Built-in electric field between the interface of

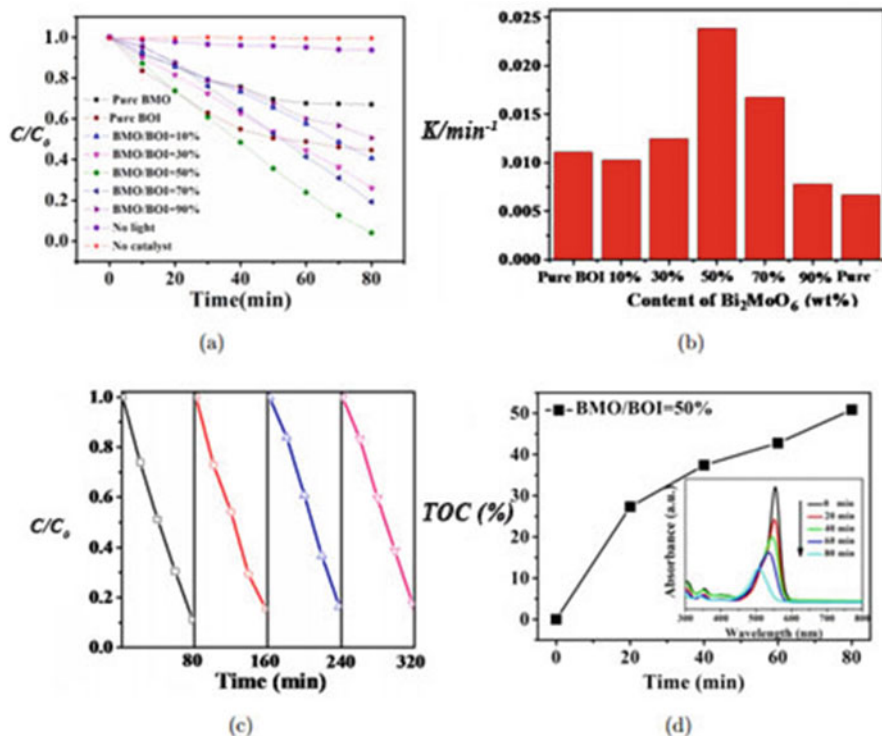


Fig. 10.15 (a) Photocatalytic degradation of rhodamine B. (b) The rate constants for Rhodamine B degradation on BOI, Bi_2Mo_6 , and $\text{Bi}_2\text{Mo}_6/\text{BOI}$ composites. (c) Recycling. (d) Total organic carbon changes for photocatalytic degradation of rhodamine B by using $\text{Bi}_2\text{Mo}_6/\text{BOI} = 50\%$ as photocatalyst. (Reprinted with permission of World Scientific from Fan et al. 2016)

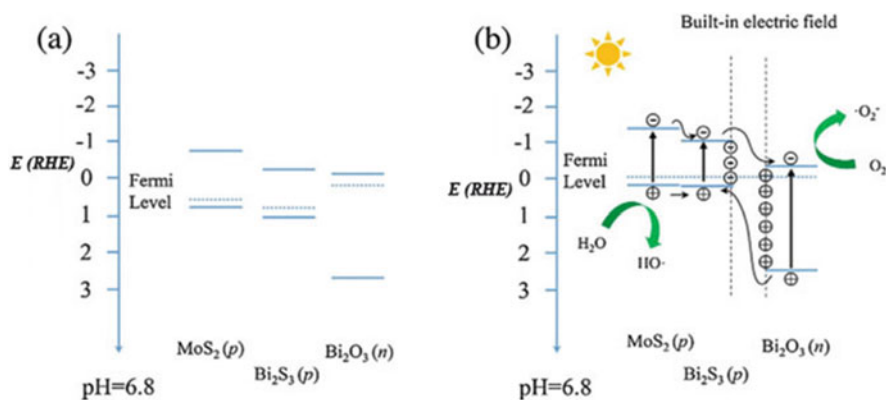


Fig. 10.16 Diagram for (a) energy band of Bi_2O_3 , MoS_2 , and Bi_2S_3 and (b) the formation of the three-phase p-n heterojunction and the possible charge separation. (Reprinted with permission of Elsevier from Ke et al. 2017)

Table 10.1 Some heterojunctions of Bi-based with Bi and non-Bi semiconductors

| Bi-base | Second element | Method | Application | References |
|----------------------------------|--|---------------------|---------------------------|-------------------------|
| <i>Bi-Binary heterojunctions</i> | | | | |
| Bi ₂ O ₃ | BiVO ₄ | Alkaline etching | RhB ^a | Han et al. (2013) |
| Bi ₂ S ₃ | Bi ₂ WO ₆ | Anion exchange | RhB | Yan et al. (2017) |
| Bi ₂ S ₃ | BiOCl | Solvothermal | SA ^b | Mi et al. (2017) |
| Bi ₂ MoO ₆ | BiOI | Ion exchange | RhB | Fan et al. (2016) |
| BiOI | BiVO ₄ | Precipitation | MO ^c | Ni et al. (2018) |
| BiOI | Bi ₂ MoO ₆ | Precipitation | BPA ^d | Yan et al. (2015) |
| BiOCl | BiVO ₄ | Co-precipitation | RhB | Gomez et al. (2018) |
| BiOCl | Bi ₁₂ O ₁₇ C ₁₂ | Hydrothermal | MO | Hao et al. (2017) |
| <i>Non-Bi heterojunctions</i> | | | | |
| Bi ₂ O ₃ | FeVO ₄ | Calcination | Malachite green | Liu and Kang (2016) |
| Bi ₂ O ₃ | g-C ₃ N ₄ | Self-assembly | RhB | Dang et al. (2015) |
| Bi ₂ S ₃ | ZnS | Cation exchange | MB ^e | Xiong et al. (2011) |
| BiFeO ₃ | g-C ₃ N ₄ | Hydrothermal | Guaiacol | An et al. (2016) |
| BiFeO ₃ | CuO | Hydrothermal | MO | Niu et al. (2015) |
| BiVO ₄ | g-C ₃ N ₄ | Ultrasonic assembly | CO ₂ reduction | Huang (2015) |
| BiVO ₄ | CeO ₂ | Co-precipitation | MB/MO | Wetchakun et al. (2012) |
| Bi ₂ WO ₆ | TiO ₂ | Hydrothermal | RhB, MO | Xu et al. (2018) |
| Bi ₂ MoO ₆ | g-C ₃ N ₄ | Solvothermal | Phenol | Li et al. (2014) |
| Bi ₂ MoO ₆ | AgBr | Precipitation | RhB | Jonjana et al. (2016) |
| BiOCl | g-C ₃ N ₄ | Solvothermal | RhB | Song et al. (2017) |
| BiOCl | CuS | Hydrothermal | RhB | Wang et al. (2015) |
| BiOI | TiO ₂ | Impregnation | MO | Wang et al. (2016) |

^aRhodamine B, ^bSalicylic acid, ^cMethyl orange, ^dBisphenol A, ^eMethyl orange

two semiconductors (I, II) acted as cite for charge transfer. The Z-scheme heterojunction has the same structure to a conventional heterojunction (type II), while charge transfer is different for two heterojunctions (Fig. 10.14b). In a Z-scheme heterojunction, charge transferring occurred by the built-in field at the interface of two semiconductors, while spatial separation conducted in heterojunction (type II). Cost-effective and high redox ability are the most prominent features for direct Z-scheme heterojunction. Numerous Bi-based Z-scheme heterojunctions have been fabricated and suggested. For example, BiOBr/g-C₃N₄ direct Z-scheme heterojunction was prepared via simple reflux method. The resulted BiOBr/g-C₃N₄ indicated more photocatalytic efficiency for remediation of rhodamine B, levofloxacin in comparison with BiOBr, or g-C₃N₄ alone. Meanwhile, BiVO₄ and Ag₃VO₄ composited together under hydrothermal treatment to form direct Z-scheme. The obtained composite has high photocatalytic activity for degradation and reduction of bisphenol and Cr(VI), respectively (Jing et al. 2019). Ternary Z-scheme heterojunctions synthesized for Bi-based compounds such as Bi₂WO₆/g-C₃N₄/rGO show enhanced efficiency by transferring of electrons

Table 10.2 Some of synthesized Z-scheme heterojunctions for Bi-based materials

| Bi-Base | Other element | Method | Application | References |
|----------------------------------|---|-----------------------------|------------------------------------|---------------------|
| <i>Double Z-scheme</i> | | | | |
| Bi ₂ O ₃ | g-C ₃ N ₄ | In situ calcination | MB | Liu et al. (2018) |
| Bi ₂ WO ₆ | MoS ₂ | Hydrothermal | RhB | Wang et al. (2017) |
| Bi ₂ MoO ₆ | BiOBr | Solvothermal | MB | Hu et al. (2018) |
| BiVO ₄ | Ag ₃ VO ₄ | Hydrothermal | Cr(VI), Bisphenol | Jing et al. (2019) |
| BiOI | g-C ₃ N ₄ | Hydrothermal/stirring | MB | Zhang et al. (2018) |
| BiOBr | g-C ₃ N ₄ | Reflux | RhB, levofloxacin | Shi et al. (2013) |
| BiOCl | g-C ₃ N ₄ | Chemical bath deposition | RhB | Bai et al. (2014) |
| <i>Ternary Z-scheme</i> | | | | |
| Bi ₂ WO ₆ | g-C ₃ N ₄ /rGO | Hydrothermal | 2,4,6Trichlorophenol | Ma et al. (2016) |
| Bi ₂ MoO ₆ | Ag/Ag ₃ PO ₄ | In situ-precipitation | RhB | Lin et al. (2015) |
| BiVO ₄ | ZnIn ₂ S ₄ /g-C ₃ N ₄ | Wet-impregnation | CR ^a , MTN ^b | Zhu et al. (2019) |
| BiOI | UIO-66/g-C ₃ N ₄ | In situ, solvo-hydrothermal | RhB, TC ^c | Liang et al. (2018) |
| BiOCl | CQD-SnNb ₂ O ₆ | Hydrothermal | Benzocaine | Jiang et al. (2019) |
| BiOBr | r-GO/g-C ₃ N ₄ | Solvothermal | RhB, phenol | Bao and Chen (2018) |

^aCongo red, ^bMetronidazole, ^cTetracycline

between double Z-scheme heterojunctions. Some of Z-scheme heterojunctions including Bi-compounds are summarized in Table 10.2.

10.3 Application

10.3.1 Water Remediation

According to previous section, the function of Bi-based photocatalysts through water remediation was extended. Bi-based nanocomposites, plasmonic composites, and carbon-based are the most famous composites which are applied for degradation of pollutants existed in water [134–167]. Existed pollutants include dyes, pharmaceutical, phenolic compounds, and toxic heavy metals. Table 10.3 shown some of Bi-compounds and composites in two forms of powder and film which applied for degradation of pollutants.

Table 10.3 Some of Bi–based photocatalysts in powder and film forms used for water remediation

| Bi-based | Method | Performance | References |
|----------------------------------|-------------------------------|--------------------------------------|------------------------------------|
| <i>Bi-based powder</i> | | | |
| Bi ₂ O ₃ | Solid-state | RhB | Oudghiri-Hassani et al. (2015) |
| Bi ₂ S ₃ | Hydrothermal | RhB, 1.5 h | Jia et al. (2016) |
| | Hot injection | RhB, 2 h | Wu et al. (2010) |
| | Hydrothermal | RhB/MB, 2 h | Sharma and Khare (2018) |
| BiFeO ₃ | Sonochemistry | MB | Soltani and Entezari (2013a, b, c) |
| | Sonochemistry | RhB | Soltani and Entezari (2013c) |
| | Hydrothermal | MO, 3 h | Niu et al. (2015) |
| Bi ₂ WO ₆ | Sonochemistry | MB/RhB | Zargazi and Entezari (2019c) |
| | CTAB-hydrothermal | RhB, 1 h | Yuxue Zhou (2017) |
| Bi ₂ MoO ₆ | Co-precipitation | MB, 6 h | Guo et al. (2018b) |
| | Solvothermal | RhB, 20 min | Li et al. (2013) |
| | Hydrothermal | RhB, 3 h | Phuruangrat et al. (2013) |
| BiVO ₄ | Microwave | MB, 5 h | Intaphong et al. (2016) |
| | Hydrothermal | RhB, 2 h | Ran et al. (2015) |
| | Solid phase | Cr, 30%, 2 h | Li et al. (2019) |
| | Thermal decomposition | MB, 105 min | Sivakumar et al. (2015) |
| BiOCl | Precipitation, calcination | RhB, 100 min | Xiong et al. (2011) |
| | Hydrolysis | MO, 9 h | Zhang et al. (2006) |
| BiOBr | Solvothermal | RhB, 2 h | Feng et al. (2015) |
| | Solvothermal | Acid Gallic | Mera et al. (2018) |
| BiOI | Soft chemical | MO, 3 h | Wang et al. (2011) |
| | Chemical bath deposition | RhB, Cr (VI) | Lv et al. (2018) |
| <i>Bi-based film</i> | | | |
| Bi ₂ O ₃ | Spray pyrolysis | MO, 3 h | Barrera-Mota et al. (2015) |
| | Sol-gel | RhB, 3.5 h | Weidong et al. (2007) |
| | EPD ^a | RB, 2 h | Guo et al. (2015) |
| Bi ₂ S ₃ | Hydrothermal | MB, 4 h | Tang et al. (2016) |
| | Electrodeposition | RhB/Cr, 1.5 h | Chahkandi and Zargazi (2019) |
| BiFeO ₃ | EPD | RhB | Zargazi and Entezari (2018) |
| | Sol-EPD | Phenol | Zargazi and Entezari (2019a) |
| Bi ₂ WO ₆ | EPD | 4-NP ^b /4-CP ^c | Zargazi and Entezari (2019b) |
| | Spin coating | MB, 5 h | Zhang et al. (2009) |
| Bi ₂ MoO ₆ | Thermal evaporation | RhB, 10 h | Cuellar et al. (2011) |
| | Reactive Magnetron deposition | RhB (80%), MB (60%), 1 h | Ratova et al. (2016) |
| | Dip-coating | ... | Man (2007) |

(continued)

Table 10.3 (continued)

| Bi-based | Method | Performance | References |
|-------------------|-------------------------|-------------|--------------------------|
| BiVO ₄ | Sputtering | Rh6G, 4 h | Venkatesan et al. (2018) |
| | Spray pyrolysis | RhB, 3 h | Ravidhas et al. (2018) |
| | Pulsed laser deposition | ... | Jeong et al. (2016) |
| BiOCl | Dip-coating | RhB, 10 h | Liang et al. (2013) |
| | Sol-gel | RhB, 90 min | Wu et al. (2011) |
| | Alcoholysis-coating | MO, 150 min | Xiaoxia et al. (2012) |
| BiOI | Sol-gel | BPA, 2 h | Zhang et al. (2019) |
| | Dip-hydrothermal | RhB, 2 h | Wang et al. (2017) |
| BiOBr | Solvothermal | RhB, 3 h | Huo et al. (2015) |
| | Alcoholysis-coating | MO, 2.5 h | Li et al. (2014) |

^aElectrophoretic deposition, ^b4-Nitrophenol, ^c4-chlorophenol

10.3.2 Water Splitting

Energy frugality in the near future will be a major challenge around the world. Scientists are focused on researches providing clean and sustainable energy sources to decrease probability of complete disappear the unrenewable energies and to manage the pollutants. Burning of hydrogen in the presence of oxygen is not emitted any contaminants. Hence, hydrogen can be considered as a promising renewable fuel which is applied in vehicles, aircrafts, and electrical devices. Water splitting is a promising way to produce H₂. Different techniques for water splitting have been applied such as photoelectrochemical systems (Chen et al. 2016b), photocatalytic (Ni et al. 2007), photobiological (Poudyal et al. 2015), and thermal decomposition (Lapicque 1983). Among them, photoelectrochemical and photocatalytic water splitting are known as simplest, cost-effective, and efficient methods for hydrogen production which mechanism of H₂ production depicted in Fig. 10.17 (Abe 2011).

Photoelectrochemical water splitting manners are categorized in three types which are depicted in Fig. 10.18. The solar light is considered as effective source by Z-scheme compared to the conversional process. Therefore, the hydrogen evolution occurred under proton reduction by electrons of conduction band and oxygen evolution take place by holes of valence band. It can be concluded that the water hydrolysis progressed through the event of cyclic redox pair. Figure 10.18a, b shows n- and p-type semiconductors involved in water splitting. Figure 10.18c illustrates the combination of two various photo electrodes, as oxidation and reduction reactions can be simultaneously done and can more effectively employ solar energy. Over the surface of nanomaterials having high ratio of surface to volume, the charge carriers are generated because of the reduced size with high surface area, different shapes, and controlled morphology. Therefore, nanomaterials can be applied in water splitting process established at the nanomaterials surface. Many researches demonstrate the 50–90% increment in the efficiency of photoelectrochemical water splitting.

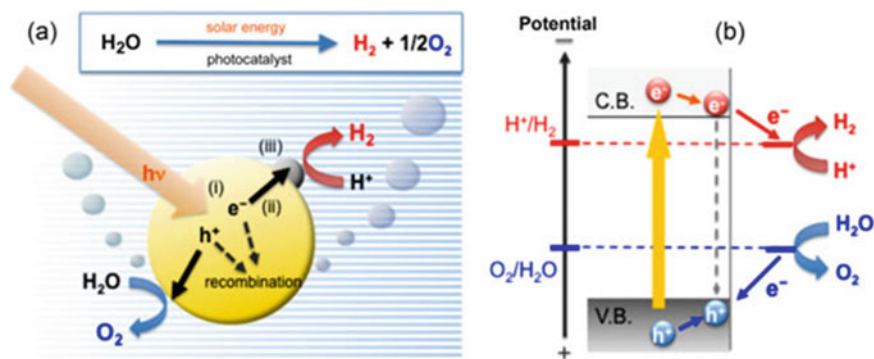


Fig. 10.17 (a) Mechanism of water splitting over semiconductor photocatalyst and (b) levels of conduction and valence bands for photocatalyst with overall water splitting efficiency. C.B. and V.B. stand for conductive band and valence band, respectively. (Reprinted with permission of Elsevier from Abe 2011)

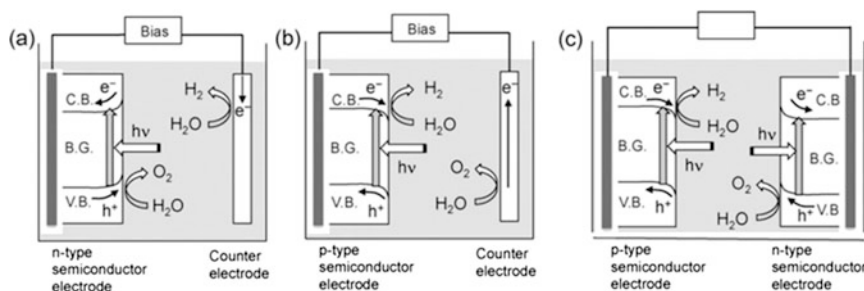


Fig. 10.18 Photoelectrochemical water splitting systems using n-type semiconductor (a), p-type semiconductor (b), and tandem system (c). C.B., V.B., and B.G. stand for conductive band, valence band, and band gap, respectively. (Reprinted with permission of Elsevier from Abe 2011)

The structural and electronic features of applied photo-anodes/cathodes in nanomaterials are the main factors affecting the photoelectrochemical water splitting mechanism. Various visible light materials were applied in photoelectrochemical water splitting as photo-electrodes. Recently, Bi-based materials have been widely used in the manufacturing of photo-electrodes in visible light materials systems. For instance, $BiFeO_3$ photo-anodes were synthesized by using dual-source low-pressure chemical vapor deposition and used in photocatalytic and photoelectrochemical water splitting induced by solar light. Results of incident photon-to-electron conversion efficiency suggested 23% efficiency for photoelectrochemical water splitting activated by light illumination (400 nm) (Moniz et al. 2015). Another work has reported high efficient nanoporous Bi_2WO_6 photo-anodes which synthesized by facile drop-casting method (Dong et al. 2017). The Bi_2WO_6 photo-electrode showed highly significant efficiency for photoelectrochemical water splitting which exhibited photocurrent almost ten times higher than traditional photo-electrodes.

Some of Bi-based compounds and nanocomposites synthesized by various methods and applied in photoelectrochemical and photocatalytic water splitting are reported in Table. 10.4.

10.4 Conclusions and Prospects

Some of special properties of Bi-based semiconductors, such as narrow band gap, layered structures, and controllable morphologies, have attracted more attentions from researchers in photocatalyst field. Almost all of Bi-based photocatalysts type and the catalytic applications have been discussed in this chapter. According to some challenges about Bi-based photocatalytic compounds, noted as fast recombination rate of electrons–hole and low light adsorption and practical approaches suggested to defeat the related challenges. Furthermore, main accomplished works until now have been summarized within morphology control and heterojunctions. However, probable problems for using Bi-based semiconductors can be disappeared, but further studies are still needed to improve the related progresses. Future works could be focused on below issues:

1. Until now, significant applications of Bi–nanomaterials can be highlighted as destruction of organic polluters and bacteria of wastewater and purification of air through denitration. Preparation of Z–scheme structures can be nominated as an applicable method for increasing the H₂ generation via photoactivated water splitting under solar light. Further works try to develop advanced Bi–nanomaterials to improve the applicable arena such as photocatalytic synthetization of organic compounds and photoactivated reduction for elimination of heavy metals.
2. Pragmatic applications of photocatalysts based on bismuth compounds are rarely storied. Designing the new applicable photocatalytic reactor can permanently precipitate the scale-up process. It can represent the potential industrialization capability of the advanced Bi–nanomaterial. Moreover, establishing of experiments by a solar simulator instead of a bulb shows the more reality of solar-activated photocatalysis performance of mentioned compounds.
3. The applicable fields along with further advancements can be propagated through consolidation of different useful techniques such as electrochemistry, membrane technique, and biotechnology. Despite many of bismuth-based semiconductors establish remarkable photoactivity efficiency induced by solar/visible light, they are far from full-fledged commercialization of the advanced nanomaterial. The perfect promised and interesting properties of Bi-based compounds can gift a bright future within environmental aspects and renewable energy sources.

Table 10.4 Some of Bi-compounds applied for water splitting

| Bi-Based | Sort | Method | Performance | References |
|--|------------|--|--|--------------------------|
| Bi ₂ WO ₆ | Electrode | Angle deposition | 4.3 $\mu\text{A cm}^{-2}$ | Larson and Zhao (2016) |
| N-Bi ₂ WO ₆ | Electrode | Drop-casting | 120 $\mu\text{A cm}^{-2}$ (1.23 V) | Dong et al. (2017) |
| P-Bi ₂ WO ₆ | Electrode | Drop casting | 500 $\mu\text{A cm}^{-2}$ (1V) | Dong et al. (2017) |
| Bi ₂ WO ₆ - Cu ₃ P | Suspension | Ball milling | 9 μmolg^{-1} (H ₂) | Rauf et al. (2018) |
| In ₂ O ₃ / Bi ₂ WO ₆ | Electrode | Chemical bath deposition | 1.0 mA cm^{-2} (0.7 V) | Joshi (2015) |
| Bi ₂ MoO ₆ / TiO ₂ | Electrode | ... | 0.668 mmolh ⁻¹ g ⁻¹ (O ₂) | Wo et al. (2013) |
| BiVO ₄ | Electrode | Solvothermal | 8 $\mu\text{A cm}^{-2}$ (0.5 V) | Rani et al. (2019) |
| BiVO ₄ | Suspension | Solid-liquid state reaction | 210 μmolh^{-1} (O ₂) | Iwase et al. (2016) |
| Cu ₂ O/ BiVO ₄ | Electrode | Electrodeposition | 2.34 mA cm^{-2} (1.23 V) | Kim et al. (2018a) |
| TiO ₂ /BiVO ₄ | Electrode | Chemical bath deposition | 0.8 mA cm^{-2} (1.23 V) | Cheng et al. (2016) |
| Co-Pi/ CuWO ₄ / BiVO ₄ | Electrode | Drop casting | 2.25 mA cm^{-2} (1.23 V) | Peng et al. (2018) |
| ZnIn ₂ S ₄ / RGO/BiVO ₄ | Suspension | Hydrothermal | 180 μmolg^{-1} (H ₂) | Zhu et al. (2019) |
| β -Bi ₂ O ₃ | Electrode | Spray deposition | 0.97 mA cm^{-2} (0.5 V) | Kim et al. (2018b) |
| Pt-Bi ₂ O ₃ | Electrode | Aerosol-assisted chemical vapor deposition | 3.1 $\mu\text{molg}^{-1}\text{h}^{-1}$ (H ₂) | Moniz et al. (2012) |
| Pt-Bi ₂ O ₃ / RuO ₂ | Suspension | Sonochemical hydrolysis | 14.5 $\mu\text{molg}^{-1}\text{h}^{-1}$ (H ₂) | Hsieh et al. (2013) |
| Bi ₂ O ₃ /WO ₃ | Electrode | Hydrothermal | 0.85 $\mu\text{A cm}^{-2}$ | Khan et al. (2016) |
| Bi ₂ O ₃ /Bi ₂ S ₃ / MoS ₂ | Electrode | Hydrothermal | 529.1 $\mu\text{molh}^{-1}\text{g}^{-1}$ (O ₂) | Ke et al. (2017) |
| Bi ₂ O ₃ /TiO ₂ - xN _x | Suspension | Soft chemical rout | 198.4 μmolh^{-1} (H ₂) | Naik et al. (2011) |
| Bi ₂ O ₃ / Bi ₂ WO ₆ | Electrode | Pulse electrodeposition | 35 $\mu\text{A cm}^{-2}$ | Ying et al. (2018) |
| BiOCl | Suspension | Ionic liquid method | 10.5 $\mu\text{A cm}^{-2}$ | Stephenson et al. (2018) |
| BiOCl | Electrode | Chemical Vapor Deposition | ... | Stephenson et al. (2018) |
| Bi-BiOCl | Electrode | In-situ photoelectroreduce | 2.4 μmolh^{-1} (H ₂) | Fan et al. (2017) |

(continued)

Table 10.4 (continued)

| Bi-Based | Sort | Method | Performance | References |
|-------------------------------------|------------|---|--|-------------------------|
| BiOX (X = Cl, Br, I) | Electrode | Aerosol-assisted chemical vapour deposition | 10.5 $\mu\text{A cm}^{-2}$ (1.23 V) | Gomez et al. (2018) |
| Zn-BiOBr | Electrode | Doctor-blade | 9.5 μmolh^{-1} (H_2) | Guo et al. (2018a) |
| Cu ₂ S-BiOBr | Suspension | Precipitation | 717 μmolg^{-1} (H_2) | Paquin et al. (2015) |
| Bi ₄ NbO ₈ Cl | Suspension | Solid state reaction | 30 μmolh^{-1} (O_2) | Fujito et al. (2016) |

Acknowledgments MCH and MZ thankfully appreciate the financial support by the Hakim Sabzevari University and Ferdowsi University of Mashhad, Iran.

References

- Abe R (2011) Recent progress on photocatalytic and photoelectrochemical water splitting under visible light irradiation. *J Photochem Photobiol C Photochem Rev* 11:179–209. <https://doi.org/10.1016/j.jphotochemrev.2011.02.003>
- Ai Z, Ho W, Lee S (2011a) Efficient visible light photocatalytic removal of NO with BiOBr-graphene nanocomposites. *J Phys Chem C* 115:25330–25337. <https://doi.org/10.1021/jp206808g>
- Ai Z, Huang Y, Lee S, Zhang L (2011b) Monoclinic α -Bi₂O₃ photocatalyst for efficient removal of gaseous NO and HCHO under visible light irradiation. *J Alloys Compd* 509:2044–2049. <https://doi.org/10.1016/j.jallcom.2010.10.132>
- Akueus F (2012) Electrodeposited zn/zn photocatalysts for the degradation of benzene-toluene-xylene mixture in aqueous phase fotomangkin zn/zn electroendapan bagi degradasi campuran benzena-toluena-xilena. *Malay J Anal Sci* 16:277–282
- Alahiane S, Qourzal S, Ouardi ME et al (2014) Factors influencing the photocatalytic degradation of reactive Yellow 145 by TiO₂-coated non-woven fibres. *Am J Anal Chem* 5:445–454. <https://doi.org/10.4236/ajac.2014.58053>
- Alarfaj E (2016) Investigation of Ag-TiO₂ nanostructures photocatalytic properties prepared by modified dip coating method. *Philos Mag* 96:1386–1398. <https://doi.org/10.1080/14786435.2016.1163432>
- Alfaifi BY, Bayahia H (2019) Highly efficient nanostructured Bi₂WO₆ thin film electrodes for photoelectrochemical and environment remediation. *Nanomaterials* 9:755
- Aziz RA, Sopyan I (2010) Recent progress on development of TiO₂ thin film photocatalysts for pollutant removal. *Recent Patents Mater Sci* 2:88–111. <https://doi.org/10.2174/1874465610902020088>
- Bai Y, Wang P-Q, Liu J-Y, Liu X-J (2014) Enhanced photocatalytic performance of direct Z-scheme BiOCl-g-C₃N₄ photocatalysts. *RSC Adv* 4(37):19456
- Bao Y, Chen K (2018) Novel Z-scheme BiOBr/reduced graphene oxide/protonated g-C₃N₄ photocatalyst: synthesis, characterization, visible light photocatalytic activity and mechanism. *Appl Surf Sci* 437:51–61

- Barrera-Mota K, Bizarro M, Castellino M et al (2015) Spray deposited β - Bi_2O_3 nanostructured films with visible photocatalytic activity for solar water treatment. *Photochem Photobiol Sci* 14:1110–1119. <https://doi.org/10.1039/c4pp00367e>
- Brack P, Sagu JS, Peiris TAN et al (2015) Aerosol-assisted CVD of bismuth vanadate thin films and their photoelectrochemical properties. *Chem Vap Depos* 21:41–45. <https://doi.org/10.1002/cvde.201407142>
- Buscaglia MT, Sennour M, Buscaglia V et al (2011) Formation of $\text{Bi}_4\text{Ti}_3\text{O}_{12}$ one-dimensional structures by solid-state reactive diffusion. From core-shell templates to nanorods and nanotubes. *Cryst Growth Des* 11:1394–1401. <https://doi.org/10.1021/cg101697r>
- Chahkandi M, Zargazi M (2019) Novel method of square wave voltammetry for deposition of Bi_2S_3 thin film: photocatalytic reduction of hexavalent Cr in single and binary mixtures. *J Hazard Mater* 380:120879. <https://doi.org/10.1016/j.jhazmat.2019.120879>
- Chen Z, Qian L, Zhu J et al (2010) Controlled synthesis of hierarchical Bi_2WO_6 microspheres with improved visible-light-driven photocatalytic activity. *CrystEngComm* 12:2100. <https://doi.org/10.1039/b921228k>
- Chen L, He J, Liu Y et al (2016a) Recent advances in bismuth – containing photocatalysts with heterojunctions. *Chin J Catal* 37:780–791. [https://doi.org/10.1016/S1872-2067\(15\)61061-0](https://doi.org/10.1016/S1872-2067(15)61061-0)
- Chen X, Zhang Z, Chi L, Nair AK (2016b) Recent advances in visible-light-driven photoelectrochemical water splitting: catalyst nanostructures and reaction systems. *Nano-Micro Lett* 8:1–12. <https://doi.org/10.1007/s40820-015-0063-3>
- Cheng BY, Yang JS, Cho HW, Wu JJ (2016) Fabrication of an efficient BiVO_4 - TiO_2 heterojunction photoanode for photoelectrochemical water oxidation. *ACS Appl Mater Interfaces* 8:20032–20039. <https://doi.org/10.1021/acsami.6b05489>
- Cuéllar EL, Martínez-De La Cruz A, Rodríguez KHL, Méndez UO (2011) Preparation of γ - Bi_2MoO_6 thin films by thermal evaporation deposition and characterization for photocatalytic applications. *Catal Today*, In, pp 140–145
- Dai W, Yu J, Xu H et al (2016) Synthesis of hierarchical flower-like Bi_2MoO_6 microspheres as efficient photocatalyst for photoreduction of CO_2 into solar fuels under. *CrystEngComm*. <https://doi.org/10.1039/C6CE00248J>
- Dang X, Zhang X, Chen Y, Dong X, Wang G, Ma C, Zhang X, Ma H, Xue M (2015) Preparation of β - Bi_2O_3 /g-C $_3\text{N}_4$ nanosheet p–n junction for enhanced photocatalytic ability under visible light illumination. *J Nanopart Res* 17(2)
- Dong G, Zhang Y, Wang W et al (2016) Facile fabrication of nanoporous Bi_2WO_6 photoanodes for efficient solar water splitting. *Energ Technol* 5:1912–1918. <https://doi.org/10.1002/ente.201700138>
- Fan L, Wei B, Xu L et al (2016) Ion exchange synthesis of $\text{Bi}_2\text{MoO}_6/\text{BiOI}$ heterojunctions for photocatalytic degradation and photoelectrochemical water splitting. *Nano* 11:1–10. <https://doi.org/10.1142/S1793292016500958>
- Fan W, Li C, Bai H et al (2017) An in situ photoelectroreduction approach to fabricate Bi/BiOCl heterostructure photocathodes: understanding the role of Bi metal for solar water splitting. *J Mater Chem A* 5:4894–4903. <https://doi.org/10.1039/c6ta11059b>
- Feng H, Wang L, Mitchell DRG (2015) Modulation of photocatalytic properties by strain in 2d BiOBr nanosheets. *ACS Appl Mater Interfaces* 7:27592–27596
- Fujito H, Kunioku H, Kato D et al (2016) Layered perovskite oxychloride $\text{Bi}_4\text{NbO}_8\text{Cl}$: a stable visible light responsive photocatalyst for water splitting. *J Am Chem Soc* 138(7):2082–2085
- Gao C, Shen H, Sun L, Shen Z (2011) Chemical bath deposition of Bi_2S_3 films by a novel deposition system. *Appl Surf Sci* 257:7529–7533. <https://doi.org/10.1016/j.apsusc.2011.03.080>
- Gao T, Chen Z, Huang Q et al (2015) A review: preparation of bismuth ferrite nanoparticles and its applications in visible-light induced photocatalyses. *Rev Adv Mater Sci* 40:97–109
- Ge J, Zhang Y, Heo YJ, Park SJ (2019) Advanced design and synthesis of composite photocatalysts for the remediation of wastewater: a review. *Catalysts* 9(2):122
- Gomez JJ, Arnaiz B, Cacioppo M et al (2018) Nitrogen-doped carbon nanodots for bioimaging and delivery of paclitaxel. *J Mater Chem B* 6:1–10. <https://doi.org/10.1039/x0xx00000x>

- Guo W, Zhang S, Guo Y et al (2013) Template-free and morphology-controlled hydrothermal growth of single-crystalline $\text{Bi}_{12}\text{TiO}_{20}$ with excellent simulated sunlight photocatalytic activity. *RSC Adv* 3:4008–4017. <https://doi.org/10.1039/c3ra22592e>
- Guo X, Li X, Lai C et al (2015) Cathodic electrophoretic deposition of bismuth oxide (Bi_2O_3) coatings and their photocatalytic activities. *Appl Surf Sci* 331:455–462. <https://doi.org/10.1016/j.apsusc.2015.01.034>
- Guo AJ, Liao X, Lee M, Hyett G (2018a) Experimental and DFT insights of the Zn-doping effects on the visible-light photocatalytic water splitting and dye decomposition over Zn-doped BiOBr photocatalyst. *Appl Catal B Environ*. <https://doi.org/10.1016/j.apcatb.2018.09.089>
- Guo J, Shi L, Zhao J et al (2018b) Enhanced visible-light photocatalytic activity of Bi_2MoO_6 nanoplates with heterogeneous $\text{Bi}_2\text{MoO}_{6-x}$ @ Bi_2MoO_6 core-shell structure. *Appl Catal B Environ* 224:692–704. <https://doi.org/10.1016/j.apcatb.2017.11.030>
- Han M, Sun T, Tan PY, Chen X, Tan OK, Tse MS (2013) M-BiVO₄@ γ -Bi₂O₃ core-shell p-n heterogeneous nanostructure for enhanced visible-light photocatalytic performance. *RSC Adv* 3(47):24964
- Hao L, Huang H, Guo Y, Du X, Zhang Y (2017) Bismuth oxychloride homogeneous phase junction BiOCl/Bi₂O₃ with unselectively efficient photocatalytic activity and mechanism insight. *Appl Surf Sci* 420:303–312
- He R, Xu D, Cheng B et al (2018) Review on nanoscale Bi-based photocatalysts. *Nanoscale Horiz* 3:464–504
- Hou J, Qu Y, Krsmanovic D et al (2009) Solution-phase synthesis of single-crystalline $\text{Bi}_{12}\text{TiO}_{20}$ nanowires with photocatalytic properties. *Chem Commun*:3937–3939. <https://doi.org/10.1039/b906290d>
- Hsieh SH, Lee GJ, Davies SH et al (2013) Synthesis of Cr_2O_3 and Pt doped $\text{RuO}_2/\text{Bi}_2\text{O}_3$ photocatalysts for hydrogen production from water splitting. *Am J Environ Eng* 3:115–120. <https://doi.org/10.5923/j.ajee.20130303.01>
- Hu T, Yang Y, Dai K, Zhang J, Liang C (2018) A novel Z-scheme $\text{Bi}_2\text{MoO}_6/\text{BiOBr}$ photocatalyst for enhanced photocatalytic activity under visible light irradiation. *Appl Surf Sci* 456:473–481
- Huang WL, Zhu Q (2008) Electronic structures of relaxed BiOX (X = F, Cl, Br, I) photocatalysts. *Comput Mater Sci* 43:1101–1108. <https://doi.org/10.1016/j.commatsci.2008.03.005>
- Huang Yan, Fu Min, He Tao (2015) 31 (6):1145-1152
- Huang H, Han X, Li X et al (2015a) Fabrication of multiple heterojunctions with tunable visible-light-active photocatalytic reactivity in BiOBr-BiOI full-range composites based on microstructure modulation and band structures. *ACS Appl Mater Interfaces* 7:482–492. <https://doi.org/10.1021/am5065409>
- Huang H, Li X, Wang J et al (2015b) Anionic group self-doping as a promising strategy: band-gap engineering and multi-functional applications of high-performance CO_3^{2-} -doped $\text{Bi}_2\text{O}_2\text{CO}_3$. *ACS Catal* 5:4094–4103. <https://doi.org/10.1021/acscatal.5b00444>
- Huang CK, Wu T, Huang CW et al (2017) Enhanced photocatalytic performance of BiVO_4 in aqueous AgNO_3 solution under visible light irradiation. *Appl Surf Sci* 399:10–19. <https://doi.org/10.1016/j.apsusc.2016.12.038>
- Huang Y, Lin Y, Tong Y (2018) Ultrathin Bi_2MoO_6 nanosheets for photocatalysis: performance enhancement by atomic interfacial engineering. *Energy Technol Environ Sci* 3:1–7. <https://doi.org/10.1002/sltc.201800908>
- Huo Y, Hou R, Chen X et al (2015) BiOBr visible-light photocatalytic films in a rotating disk reactor for the degradation of organics. *J Mater Chem A* 3:14801–14808. <https://doi.org/10.1039/c5ta03279b>
- Intaphong P, Phuruangrat A, Pookmanee P (2016) Synthesis and characterization of BiVO_4 photocatalyst by microwave method. *Integr Ferroelectr* 175:51–58. <https://doi.org/10.1080/10584587.2016.1200910>
- Iwase A, Kato H, Kudo A (2016) A simple preparation method of visible-light-driven BiVO_4 starting materials Bi_2O_3 and photocatalysts from oxide activities. *J Sol Energy Eng* 132:1–5. <https://doi.org/10.1115/1.4001172>

- Jeevanandam J, Barhoum A, Chan YS et al (2018) Review on nanoparticles and nanostructured materials: history, sources, toxicity and regulations. *Beilstein J Nanotechnol* 9:1050–1074. <https://doi.org/10.3762/bjnano.9.98>
- Jeong SY, Choi KS, Shin H et al (2016) Enhanced photocatalytic performance depending on morphology of bismuth vanadate thin film synthesized by pulsed laser deposition. *ACS Appl Mater Interfaces*. <https://doi.org/10.1021/acsami.6b15034>
- Jia T, Wang X, Long F et al (2016) Facile synthesis, characterization, and visible-light photocatalytic activities of 3D hierarchical Bi₂S₃ architectures assembled by nanoplatelets. *Crystals*:6. <https://doi.org/10.3390/cryst6110140>
- Jiang R, Lu G, Yan Z, Wu D, Zhou R, Bao X (2019) Insights into a CQD-SnNb₂O₆/BiOCl Z-scheme system for the degradation of benzocaine: influence factors, intermediate toxicity and photocatalytic mechanism. *Chem Eng J* 374:79–90
- Jin J, He T (2017) Facile synthesis of Bi₂S₃ nanoribbons for photocatalytic reduction of CO₂ into CH₃OH. *Appl Surf Sci* 394:364–370. <https://doi.org/10.1016/j.apsusc.2016.10.118>
- Jing L, Lili Z, Benlin D, Jiming X (2019) A novel Z-scheme Ag₃VO₄/BiVO₄ heterojunction photocatalyst: study on the excellent photocatalytic performance and photocatalytic mechanism. *Appl Catal B Environ*. <https://doi.org/10.1016/j.apcatb.2019.01.001>
- Jonjana S, Phuruangrat A, Thongtem T, Thongtem S (2016) Synthesis, analysis and photocatalysis of AgBr/Bi₂MoO₆ nanocomposites. *Mater Lett* 172:11–14
- Joshi B (2015) Heterojunction photoanodes for solar water splitting using chemical-bath-deposited In₂O₃ micro-cubes and electro-sprayed Bi₂WO₆ textured nanopillars. *RSC Adv* 5:85323–85328. <https://doi.org/10.1039/C5RA16833C>
- Ke J, Liu J, Sun H et al (2017) Facile assembly of Bi₂O₃/Bi₂S₃/MoS₂ n-p heterojunction with layered n -Bi₂O₃ and p -MoS₂ for enhanced photocatalytic water oxidation and pollutant degradation. *Appl Catal B Environ* 200:47–55. <https://doi.org/10.1016/j.apcatb.2016.06.071>
- Khan I, Abdalla A, Qurashi A (2016) Synthesis of hierarchical WO₃ and Bi₂O₃/WO₃ nanocomposite for solar-driven water splitting applications. *Int J Hydrog Energy*:1–9. <https://doi.org/10.1016/j.ijhydene.2016.11.105>
- Kim H, Bae S, Jeon D, Ryu J (2018a) Fully solution-processable Cu₂O-BiVO₄ photoelectrochemical cells for bias-free solar water splitting. *Green Chem* 20:3732–3742. <https://doi.org/10.1039/c8gc00681d>
- Kim M, Joshi B, Samuel E et al (2018b) Highly nanotextured b -Bi₂O₃ pillars by electrostatic spray deposition as photoanodes for solar water splitting. *J Alloys Compd* 764:881–889. <https://doi.org/10.1016/j.jallcom.2018.06.047>
- Kudo A, Omori K, Kato H (1999) A novel aqueous process for preparation of crystal form-controlled and highly crystalline BiVO₄ powder from layered vanadates at room temperature and its photocatalytic and photophysical properties. *J Am Chem Soc* 121:11459–11467. <https://doi.org/10.1021/ja992541y>
- Kumar A (2017) A review on the factors affecting the photocatalytic degradation of hazardous materials. *Mater Sci Eng Int J* 1:1–10. <https://doi.org/10.15406/mseij.2017.01.00018>
- Lam SM, Sin JC, Mohamed AR (2017) A newly emerging visible light-responsive BiFeO₃ perovskite for photocatalytic applications: a mini review. *Mater Res Bull* 90:15–30
- Lapicque F (1983) Production of hydrogen by direct thermal decomposition of water. *Int J Hydrog Energy* 8:675–679
- Larson S, Zhao Y (2016) Tuning the composition of Bi_xW₃O nanorods towards zero bias PEC water splitting. *Nanotechnology* 27:1–12. <https://doi.org/10.1088/0957-4484/27/25/255401>
- Lee TD, Ebong AU (2017) A review of thin film solar cell technologies and challenges. *Renew Sust Energy Rev* 70:1286–1297. <https://doi.org/10.1016/j.rser.2016.12.028>
- Lei Y, Wang G, Song S et al (2009) Synthesis, characterization and assembly of BiOCl nanostructure and their photocatalytic properties. *CrystEngComm* 11:1857–1862. <https://doi.org/10.1039/b909013b>

- Li G, Ding Y, Zhang Y et al (2011) Microwave synthesis of BiPO₄ nanostructures and their morphology-dependent photocatalytic performances. *J Colloid Interface Sci* 363:497–503. <https://doi.org/10.1016/j.jcis.2011.07.090>
- Li Z, Chen X, Xue Z (2013) Bi₂MoO₆ microstructures: controllable synthesis, growth mechanism, and visible-light-driven photocatalytic activities. *CrystEngComm* 15:498–508. <https://doi.org/10.1039/c2ce26260f>
- Li R, Fan C, Zhang X et al (2014) Preparation of BiOBr thin films with micro-nano-structure and their photocatalytic applications. *Thin Solid Films*. <https://doi.org/10.1016/j.tsf.2014.04.077>
- Li L, Ma Z, Bi F et al (2016) Sol-gel preparation and properties of Bi₄Ti₃O₁₂ photocatalyst supported on micrometer-sized quartz spheres. *J Adv Oxid Technol* 19:310–316. <https://doi.org/10.1515/jaots-2016-0215>
- Li X, Xie J, Jiang C et al (2018) Review on design and evaluation of environmental photocatalysts. *Front Environ Sci Eng* 12:1–32
- Li J, Chen Y, Chen C, Wang S (2019) Solid-phase synthesis of visible-light-driven BiVO₄ photocatalyst and photocatalytic reduction of aqueous Cr (VI). *Bull Chem React Eng Catal* 14:336–344. <https://doi.org/10.9767/bcrec.14.2.3182.336-344>
- Liang Y, Guo C, Cao S et al (2013) A high quality BiOCl film with petal-like hierarchical structures and its visible-light photocatalytic property. *J Nanosci Nanotechnol* 13:919–923. <https://doi.org/10.1166/jnn.2013.5972>
- Liang Q, Cui S, Jin J, Liu C, Xu S, Yao C, Li Z (2018) Fabrication of BiOI@UIO-66(NH₂)@g-C₃N₄ ternary Z-scheme heterojunction with enhanced visible-light photocatalytic activity. *Appl Surf Sci* 456:899–907
- Lin X, Hou J, Jiang S, Lin Z, Wang M, Che G (2015) A Z-scheme visible-light-driven Ag/Ag PO/Bi MoO photocatalyst: synthesis and enhanced photocatalytic activity. *RSC Adv* 5(127):104815–104821
- Liu X, Kang Y (2016) Synthesis and high visible-light activity of novel Bi₂O₃/FeVO₄ heterojunction photocatalyst. *Mater Lett* 164:229–231
- Liu S, Chen J, Xu D, Zhang X, Shen M (2018) Enhanced photocatalytic activity of direct Z-scheme BiO/g-C₃N composites via facile one-step fabrication. *J Mater Res* 33(10):1391–1400
- Low J, Yu J, Jaroniec M et al (2017) Heterojunction photocatalysts. *Adv Mater* 29:1–20. <https://doi.org/10.1002/adma.201601694>
- Luo B, Kim A, Smith JW et al (2019) Hierarchical self-assembly of 3D lattices from polydisperse anisometric colloids. *Nat Commun*:1–9. <https://doi.org/10.1038/s41467-019-09787-6>
- Lv Y, Yao W, Zong R, Zhu Y (2016) Fabrication of wide-range-visible photocatalyst Bi₂WO_{6-x} nanoplates via surface oxygen vacancies. *Sci Rep* 6:1–9. <https://doi.org/10.1038/srep19347>
- Lv Y, Li P, Che Y et al (2018) Facile Preparation and Characterization of Nanostructured BiOI microspheres with certain adsorption-photocatalytic properties. *Mater Res* 21
- Ma D, Wu J, Gao M, Xin Y, Ma T, Sun Y (2016) Fabrication of Z-scheme g-C₃N₄/RGO/Bi₂WO₆ photocatalyst with enhanced visible-light photocatalytic activity. *Chem Eng J* 290:136–146
- Mahlambi MM, Ngila CJ, Mamba BB (2015) Recent developments in environmental photocatalytic degradation of organic pollutants: the case of titanium dioxide nanoparticles – a review. *J Nanomater* 2015:1–29. <https://doi.org/10.1155/2015/790173>
- Man Y (2007) Preparation and photoelectrochemical properties of Bi₂MoO₆ films. *Acta Physico-Chimica Sinica* 23:1671–1676
- Meng X, Zhang Z (2016) Bismuth-based photocatalytic semiconductors: introduction, challenges and possible approaches. *J Mol Catal A Chem* 423:533–549
- Mera AC, Rodríguez CA, Valdés H et al (2018) Solvothermal synthesis and photocatalytic activity of BiOBr microspheres with hierarchical morphologies. *Acta Chimica Slovenica* 65:429–437. <https://doi.org/10.17344/acsi.2018.4181>
- Mi Y, Li H, Zhang Y, Zhang R, Hou W (2017) One-pot synthesis of belt-like Bi₂S₃/BiOCl hierarchical composites with enhanced visible light photocatalytic activity. *Appl Surf Sci* 423:1062–1071

- Moniz SJA, Bhachu D, Blackman CS et al (2012) A novel route to Pt – Bi₂O₃ composite thin films and their application in photo-reduction of water. *Inorganica Chim Acta* 380:328–335. <https://doi.org/10.1016/j.ica.2011.09.029>
- Moniz SJA, Blackman CS, Southern P et al (2015) Visible-light driven water splitting over BiFeO₃ photoanodes grown via the LPCVD reaction of [Bi(OtBu)₃] and [Fe(OtBu)₃]₂ and enhanced with a surface nickel oxygen evolution catalyst. *Nanoscale* 7:16343–16353. <https://doi.org/10.1039/c5nr04804d>
- Myung N, Lee W, Lee C et al (2014) Synthesis of Au-BiVO₄ nanocomposite through anodic electrodeposition followed by galvanic replacement and its application to the photocatalytic decomposition of methyl orange. *ChemPhysChem* 15:2052–2057. <https://doi.org/10.1002/cphc.201402032>
- Naik B, Martha S, Parida KM (2011) Facile fabrication of Bi₂O₃/TiO_{2-x}N_x nanocomposites for excellent visible light driven photocatalytic hydrogen evolution. *Int J Hydrog Energy* 36:2794–2802. <https://doi.org/10.1016/j.ijhydene.2010.11.104>
- Ni M, Leung MKH, Leung DYC, Sumathy K (2007) A review and recent developments in photocatalytic water-splitting using TiO₂ for hydrogen production. *Renew Sust Energ Rev* 11:401–425. <https://doi.org/10.1016/j.rser.2005.01.009>
- Ni S, Zhou T, Zhang H, Cao Y, Yang P (2018) BiOI/BiVO two-dimensional Heteronanostructures for visible-light photocatalytic degradation of rhodamine B. *ACS Applied Nano Materials* 1(9):5128–5141
- Niu F, Chen Z, Qin L (2015) Hydrothermal synthesis of BiFeO₃ nanoparticles for visible light photocatalytic applications. *J Nanosci Nanotechnol* 15(12):9693–9698. <https://doi.org/10.1166/jnn.2015.10682>
- Opoku F, Govender KK, van Sittert CGCE, Govender PP (2017) Recent progress in the development of semiconductor-based photocatalyst materials for applications in photocatalytic water splitting and degradation of pollutants. *Adv Sustain Syst* 1:1700006. <https://doi.org/10.1002/adsu.201700006>
- Oudghiri-Hassani H, Rakass S, Al Wadaani FT et al (2015) Synthesis, characterization and photocatalytic activity of α-Bi₂O₃ nanoparticles. *J Taibah Univ Sci* 9:508–512. <https://doi.org/10.1016/j.jtusci.2015.01.009>
- Paquin F, Rivnay J, Salleo A et al (2015) Multi-phase semicrystalline microstructures drive exciton dissociation in neat plastic semiconductors. *J Mater Chem C* 3:10715–10722. <https://doi.org/10.1039/b000000x>
- Patil M, Shaikh S, Ganesh I (2015) Recent advances on TiO₂ thin film based photocatalytic applications – a review. *Curr Nanosci* 11:271–285. <https://doi.org/10.2174/1573413711666150212235054>
- Peng B, Xia M, Li C et al (2018) Network structured CuWO₄/BiVO₄/Co-Pi nanocomposite for solar water splitting. *Catalysts*:1–9. <https://doi.org/10.3390/catal8120663>
- Phruangrat A, Jitrou P, Dumrongrojthanath P et al (2013) Hydrothermal synthesis and characterization of Bi₂MoO₆ nanoplates and their photocatalytic activities. *J Nanomater* 2013. <https://doi.org/10.1155/2013/789705>
- Ponraj C, Vinitha G, Daniel J (2017) A review on the visible light active BiFeO₃ nanostructures as suitable photocatalyst in the degradation of different textile dyes. *Environ Nanotechnol Monit Manag* 7:110–120
- Poudyal RS, Koirala AR, Masukawa H, Inoue K (2015) Hydrogen production using photobiological methods. *Compend Hydrog Energy*:289–317. <https://doi.org/10.1016/B978-1-78242-361-4.00010-8>
- Qin F, Li G, Wang R et al (2012) Template-free fabrication of Bi₂O₃ and (BiO)₂CO₃ nanotubes and their application in water treatment. *Chem A Eur J* 18:16491–16497. <https://doi.org/10.1002/chem.201201989>
- Ran R, McEvoy JG, Zhang Z (2015) Synthesis and optimization of visible light active BiVO₄ photocatalysts for the degradation of RhB. *Int J Photoenergy* 2015. <https://doi.org/10.1155/2015/612857>

- Rani BJ, Praveenkumar M, Ravichandran S et al (2019) BiVO₄ nanostructures for photoelectrochemical (PEC) solar water splitting applications. *J Nanosci Nanotechnol* 19:7427–7435. <https://doi.org/10.1166/jnn.2019.16642>
- Ratova M, Kelly P, West G et al (2016) Deposition of visible light active photocatalytic bismuth molybdate thin films by reactive magnetron sputtering. *Materials (Basel)* 9:67–80. <https://doi.org/10.3390/ma9020067>
- Rauf A, Ma M, Kim S et al (2018) Mediator- and co-catalyst-free direct Z-scheme composites of Bi₂WO₆-Cu₃P for solar-water splitting. *Nanoscale* 10:3026–3036. <https://doi.org/10.1039/c7nr07952d>
- Ravidhas C, Arivukarasan D, Venkatesh R et al (2018) Substrate temperature induced (040) growth facets of nebulizer sprayed BiVO₄ thin films for effective photodegradation of rhodamine B. *1700257:1–11*. <https://doi.org/10.1002/crat.201700257>
- Reddy CV, Babu B, Reddy IN, Shim J (2018) Synthesis and characterization of pure tetragonal ZrO₂ nanoparticles with enhanced photocatalytic activity. *Ceram Int* 44:6940–6948. <https://doi.org/10.1016/j.ceramint.2018.01.123>
- Schwarzenbach RP, Egli T, Hofstetter TB et al (2010) Global water pollution and human health. *Annu Rev Environ Resour* 35:109–136. <https://doi.org/10.1146/annurev-environ-100809-125342>
- Shang M, Wang W, Zhang L (2009) Preparation of BiOBr lamellar structure with high photocatalytic activity by CTAB as Br source and template. *J Hazard Mater* 167:803–809. <https://doi.org/10.1016/j.jhazmat.2009.01.053>
- Sharma S, Khare N (2018) Hierarchical Bi₂S₃ nanoflowers: a novel photocatalyst for enhanced photocatalytic degradation of binary mixture of rhodamine B and methylene blue dyes and degradation of mixture of p-nitrophenol and p-chlorophenol. *Adv Powder Technol* 29:3336–3347. <https://doi.org/10.1016/j.apt.2018.09.012>
- Shi X, Chen X, Chen X et al (2013) PVP assisted hydrothermal synthesis of BiOBr hierarchical nanostructures and high photocatalytic capacity. *Chem Eng J* 222:120–127. <https://doi.org/10.1016/j.cej.2013.02.034>
- Shimodaira Y, Kato H, Kobayashi H, Kudo A (2006) Photophysical properties and photocatalytic activities of bismuth molybdates under visible light irradiation. *J Phys Chem B* 110:17790–17797. <https://doi.org/10.1021/jp0622482>
- Sivakumar V, Suresh R, Giribabu K (2015) BiVO₄ nanoparticles: preparation, characterization and photocatalytic activity. *Cogent Chem* 133:1–10. <https://doi.org/10.1080/23312009.2015.1074647>
- Soltani T, Entezari MH (2013a) Solar photocatalytic degradation of RB5 by ferrite bismuth nanoparticles synthesized via ultrasound. *Ultrason Sonochem* 20:1245–1253. <https://doi.org/10.1016/j.ultsonch.2013.01.012>
- Soltani T, Entezari MH (2013b) Sono-synthesis of bismuth ferrite nanoparticles with high photocatalytic activity in degradation of Rhodamine B under solar light irradiation. *Chem Eng J* 223:145–154. <https://doi.org/10.1016/j.cej.2013.02.124>
- Soltani T, Entezari MH (2013c) Photolysis and photocatalysis of methylene blue by ferrite bismuth nanoparticles under sunlight irradiation. *J Mol Catal A Chem* 377:197–203. <https://doi.org/10.1016/j.molcata.2013.05.004>
- Song DW, Shen W-N, Dunn B et al (2004) Thermal conductivity of nanoporous bismuth thin films. *Appl Phys Lett* 84:1883–1885. <https://doi.org/10.1063/1.1682679>
- Song L, Pang Y, Zheng Y, Ge L (2017) Hydrothermal synthesis of novel g-C₃N₄/BiOCl heterostructure nanodiscs for efficient visible light photodegradation of rhodamine B. *Applied Physics A* 123(8)
- Song G, Li J, Yuan Y et al (2019) Large-area 3D hierarchical superstructures assembled from colloidal nanoparticles. *Small* 15:1–8. <https://doi.org/10.1002/sml.201805308>
- Stephenson J, Celorrio V, Tiwari D et al (2018) Photoelectrochemical properties of BiOCl microplatelets. *J Electroanal Chem* 819:171–177. <https://doi.org/10.1016/j.jelechem.2017.10.024>

- Su W, Wang J, Huang Y et al (2010) Synthesis and catalytic performances of a novel photocatalyst BiOF. *Scr Mater* 62:345–348. <https://doi.org/10.1016/j.scriptamat.2009.10.039>
- Sun Y, Cheng H, Gao S et al (2012) Atomically thick bismuth selenide freestanding single layers achieving enhanced thermoelectric energy harvesting. *J Am Chem Soc* 134:20294–20297. <https://doi.org/10.1021/ja3102049>
- Sun J, Chen G, Wu J et al (2013a) Environmental bismuth vanadate hollow spheres: bubble template synthesis and enhanced photocatalytic properties for photodegradation. *Appl Catal B Environ* 132–133:304–314. <https://doi.org/10.1016/j.apcatb.2012.12.002>
- Sun Y, Wang W, Sun S, Zhang L (2013b) A general synthesis strategy for one-dimensional Bi_2MO_6 ($M = \text{Mo}, \text{W}$) photocatalysts using an electrospinning method. *CrystEngComm* 15:7959–7964. <https://doi.org/10.1039/c3ce41347k>
- Tang C, Zhang Y, Su J et al (2016) Synthesis and photocatalytic properties of vertically aligned Bi_2S_3 platelets. *Solid State Sci* 51:24–29. <https://doi.org/10.1016/j.solidstatesciences.2015.11.004>
- Teweldebrhan D, Goyal V, Balandin AA (2010) Exfoliation and characterization of bismuth telluride atomic quintuples and quasi-two-dimensional crystals. *Nano Lett* 10:1209–1218. <https://doi.org/10.1021/nl903590b>
- Tyagi M, Chatterjee R, Sharma P (2015) Structural, optical and ferroelectric behavior of pure BiFeO_3 thin films synthesized by the sol–gel method. *J Mater Sci Mater Electron* 26:1987–1992. <https://doi.org/10.1007/s10854-014-2639-y>
- Venkatesan R, Velumani S, Ordon K et al (2018) Nanostructured bismuth vanadate (BiVO_4) thin films for efficient visible light photocatalysis. *Mater Chem Phys* 205:325–333. <https://doi.org/10.1016/j.matchemphys.2017.11.004>
- Wang Y, Deng K, Zhang L (2011) Visible light photocatalysis of BiOI and its photocatalytic activity enhancement by in situ ionic liquid modification. *J Phys Chem C* 115:14300–14308. <https://doi.org/10.1021/jp2042069>
- Wang H, Zhang L, Chen Z et al (2014) Semiconductor heterojunction photocatalysts: design, construction, and photocatalytic. *Chem Soc Rev* 43:5234–5244. <https://doi.org/10.1039/c4cs00126e>
- Wang B, Yang H, Xian T et al (2015) Synthesis of spherical Bi_2WO_6 nanoparticles by a hydrothermal route and their photocatalytic properties. *J Nanomater* 2015. <https://doi.org/10.1155/2015/146327>
- Wang K, Shao C, Li X, Miao F, Lu N, Liu Y (2016) Heterojunctions of p- BiOI Nanosheets/n- TiO_2 nanofibers: preparation and enhanced visible-light photocatalytic activity. *Materials* 9(2):90
- Wang Y, Long Y, Zhang D (2017) Facile in situ growth of high strong BiOI network films on metal wire meshes with photocatalytic activity. *ACS Sustain Chem Eng*. <https://doi.org/10.1021/acssuschemeng.6b02810>
- Wang L, Liu J, Song W et al (2019a) Experimental and DFT insights of BiVO_4 as an effective photocatalytic catalyst for N_2O decomposition. *Chem Eng J* 366:504–513. <https://doi.org/10.1016/j.cej.2019.02.038>
- Wang Z, Huang X, Wang X (2019b) Recent progresses in the design of BiVO_4 -based photocatalysts for efficient solar water splitting. *Catal Today*. <https://doi.org/10.1016/j.cattod.2019.01.067>
- Weidong H, Wei Q, Xiaohong W et al (2007) The photocatalytic properties of bismuth oxide films prepared through the sol–gel method. *Thin Solid Films* 515:5362–5365. <https://doi.org/10.1016/j.tsf.2007.01.031>
- Wetchakun N, Chaiwichain S, Inceesungvorn B, Pingmuang K, Phanichphant S, Minett AI, Chen J (2012) BiVO_4/CeO nanocomposites with high visible-light-induced photocatalytic activity. *ACS Appl Mater Interfaces* 4(7):3718–3723
- Wo B, Powers T, Haifeng C, Ting YAN (2013) Hydrothermal synthesis and photocatalytic properties of nano $\text{Bi}_2\text{WO}_6/\text{TiO}_2$ powers. *Key Eng Mater*:473–476. <https://doi.org/10.4028/www.scientific.net/KEM.531-532.473>

- Wu T, Zhou X, Zhang H, Zhong X (2010) Bi₂S₃ nanostructures: a new photocatalyst. *Nano Res* 3:379–386. <https://doi.org/10.1007/s12274-010-1042-0>
- Wu S, Wang C, Cui Y et al (2011) BiOCl nano/microstructures on substrates: synthesis and photocatalytic properties. *Mater Lett* 65(9):1344–1347
- Xiaoxia LIU, Caimei FAN, Yunfang W et al (2012) Low temperature preparation of flower-like BiOCl film and its photocatalytic activity. *Sci China Chem* 55:2438–2444. <https://doi.org/10.1007/s11426-012-4549-2>
- Xie H, Shen D, Wang X, Shen G (2008) Microwave hydrothermal synthesis and visible-light photocatalytic activity of γ -Bi₂MoO₆ nanoplates. *Mater Chem Phys* 110:332–336. <https://doi.org/10.1016/j.matchemphys.2008.02.008>
- Xiong J, Cheng G, Li G et al (2011) Well-crystallized square-like 2D BiOCl nanoplates: mannitol-assisted hydrothermal synthesis and improved visible-light-driven photocatalytic performance. *RSC Adv* 1:1542–1553. <https://doi.org/10.1039/c1ra00335f>
- Xiong J, Cheng G, Qin F et al (2013) Tunable BiOCl hierarchical nanostructures for high-efficient photocatalysis under visible light irradiation. *Chem Eng J* 220:228–236. <https://doi.org/10.1016/j.cej.2013.01.033>
- Xu P, Shen X, Luo L, Shi Z, Liu Z, Chen Z, Zhu M, Zhang L (2018) Preparation of TiO₂/Bi₂WO₆ nanostructured heterojunctions on carbon fibers as a weaveable visible-light photocatalyst/ photoelectrode. *Environ Sci Nano* 5(2):327–337
- Yafei H, Zhang Y, Wang Y (2013) One-dimensional hierarchical Bi₂WO₆ hollow tubes with porous walls: synthesis and photocatalytic property. *CrystEngComm* 15:4124. <https://doi.org/10.1039/C3CE40237A>
- Yan T, Sun M, Liu H, Wu T, Liu X, Yan Q, Xu W, Du B (2015) Fabrication of hierarchical BiOI/Bi₂MoO₆ heterojunction for degradation of bisphenol a and dye under visible light irradiation. *J Alloys Compd* 634:223–231
- Yan L, Wang Y, Shen H, Zhang Y, Li J, Wang D (2017) Photocatalytic activity of Bi₂WO₆/Bi₂S₃ heterojunctions: the facilitation of exposed facets of Bi₂WO₆ substrate. *Appl Surf Sci* 393:496–503
- Ye L, Deng K, Xu F et al (2012) Increasing visible-light absorption for photocatalysis with black BiOCl. *Phys Chem Chem Phys* 14:82–85. <https://doi.org/10.1039/c1cp22876e>
- Yin W, Wang W, Sun S (2010a) Photocatalytic degradation of phenol over cage-like Bi₂MoO₆ hollow spheres under visible-light irradiation. *Catal Commun* 11:647–650. <https://doi.org/10.1016/j.catcom.2010.01.014>
- Yin W, Wang W, Zhou L et al (2010b) CTAB-assisted synthesis of monoclinic BiVO₄ photocatalyst and its highly efficient degradation of organic dye under visible-light irradiation. *J Hazard Mater* 173:194–199. <https://doi.org/10.1016/j.jhazmat.2009.08.068>
- Ying H, Chen W, Wen X et al (2018) Oxygen-deficient bismuth tungstate and bismuth oxide composite photoanode with improved photostability. *Sci Bull*:990. <https://doi.org/10.1016/j.scib.2018.06.012>
- Yu J, Xiong J, Cheng B et al (2005) Hydrothermal preparation and visible-light photocatalytic activity of Bi₂WO₆ powders. *J Solid State Chem* 178:1968–1972. <https://doi.org/10.1016/j.jssc.2005.04.003>
- Yu J, Wang S, Low J, Xiao W (2013) Enhanced photocatalytic performance of direct Z-scheme g-C₃N₄-TiO₂ photocatalysts for the decomposition of formaldehyde in air. *Phys Chem Chem Phys* 15:16883–16890. <https://doi.org/10.1039/c3cp53131g>
- Yuxue Zhou PL (2017) CTAB-assisted fabrication of Bi₂WO₆ thin nanoplates with high adsorption and enhanced visible light-driven photocatalytic performance. *Mol Artic*. <https://doi.org/10.3390/molecules22050859>
- Zargazi M, Entezari MH (2018) BFO thin film on the stainless steel mesh by anodic EPD: a visible light photocatalyst for degradation of Rhodamine B. *J Photochem Photobiol A Chem* 365:185–198. <https://doi.org/10.1016/j.jphotochem.2018.07.042>
- Zargazi M, Entezari MH (2019a) A novel synthesis of forest like BiFeO₃ thin film: photoelectrochemical studies and its application as a photocatalyst for phenol degradation. *Appl Surf Sci* 483:793–802. <https://doi.org/10.1016/j.apsusc.2019.03.347>

- Zargazi M, Entezari MH (2019b) Anodic electrophoretic deposition of Bi_2WO_6 thin film: high photocatalytic activity for degradation of a binary mixture. *Appl Catal B Environ* 242:507–517. <https://doi.org/10.1016/j.apcatb.2018.09.093>
- Zargazi M, Entezari MH (2019c) Sonochemical versus hydrothermal synthesis of bismuth tungstate nanostructures: photocatalytic, sonocatalytic and sonophotocatalytic activities. *Ultrason Sonochem* 51:1–11. <https://doi.org/10.1016/j.ultsonch.2018.10.010>
- Zhang C, Zhu Y (2005) Synthesis of square Bi_2WO_6 nanoplates as high-activity visible-light-driven photocatalysts. *Chem Mater* 17:3537–3545. <https://doi.org/10.1021/cm0501517>
- Zhang K, Liu C, Huang F et al (2006) Study of the electronic structure and photocatalytic activity of the BiOCl photocatalyst. *Appl Catal B Environ* 68:125–129. <https://doi.org/10.1016/j.apcatb.2006.08.002>
- Zhang L, Wang W, Zhou L, Xu H (2007) Bi_2WO_6 nano- and microstructures: shape control and associated visible-light-driven photocatalytic activities. *Small* 3:1618–1625. <https://doi.org/10.1002/sml.200700043>
- Zhang X, Ai Z, Jia F, Zhang L (2008) Generalized one-pot synthesis, characterization, and photocatalytic activity of hierarchical BiOX ($X = \text{Cl}, \text{Br}, \text{I}$) nanoplate microspheres. *J Phys Chem C* 112:747–753. <https://doi.org/10.1021/jp077471t>
- Zhang BLW, Wang YJ, Cheng HY et al (2009) Synthesis of porous Bi_2WO_6 thin films as efficient visible-light-active photocatalysts. *Adv Mater* 21:1286–1290. <https://doi.org/10.1002/adma.200801354>
- Zhang L, Xu T, Zhao X, Zhu Y (2010) Controllable synthesis of Bi_2MoO_6 and effect of morphology and variation in local structure on photocatalytic activities. *Appl Catal B Environ* 98:138–146. <https://doi.org/10.1016/j.apcatb.2010.05.022>
- Zhang H, Huang J, Zhou X, Zhong X (2011) Single-crystal Bi_2S_3 nanosheets growing via attachment-recrystallization of nanorods. *Inorg Chem* 50:7729–7734. <https://doi.org/10.1021/ic201332n>
- Zhang D, Chen L, Xiao C et al (2016) Facile synthesis of high {001} facets dominated BiOCl nanosheets and their selective dye-sensitized photocatalytic activity induced by visible light. *J Nanomater* 2016. <https://doi.org/10.1155/2016/5697672>
- Zhang J, Fu J, Wang Z, Cheng B, Dai K, Ho W (2018) Direct Z-scheme porous g-C $_3\text{N}_4$ / BiOI heterojunction for enhanced visible-light photocatalytic activity. *J Alloys Compd* 766:841–850
- Zhang Y, Shan G, Dong F et al (2019) Glass fiber supported BiOI thin-film fixed-bed photocatalytic reactor for water decontamination under solar light irradiation. *J Environ Sci*:1–10. <https://doi.org/10.1016/j.jes.2019.01.004>
- Zhao H, Tian F, Wang R, Chen R (2014) A review on bismuth-related nanomaterials for photocatalysis. *Rev Adv Sci Eng* 3:3–27. <https://doi.org/10.1166/rase.2014.1050>
- Zhou L, Wang W, Xu H et al (2009) Bi_2O_3 hierarchical nanostructures: controllable synthesis, growth mechanism, and their application in photocatalysis. *Chem A Eur J* 15:1776–1782. <https://doi.org/10.1002/chem.200801234>
- Zhou Y, Meng X, Tong L et al (2016) Template-free fabrication of Bi_2WO_6 hierarchical hollow microspheres with visible-light-driven photocatalytic activity. *Energies* 9:764–775. <https://doi.org/10.3390/en9100764>
- Zhu R, Tian F, Yang R et al (2019) Z Scheme system $\text{ZnIn}_2\text{S}_4/\text{RGO}/\text{BiVO}_4$ for hydrogen generation from water splitting and simultaneous degradation of organic pollutants under visible light. *Renew Energy*. <https://doi.org/10.1016/j.renene.2019.02.049>
- Zhuo Y, Huang J, Cao L et al (2013) Photocatalytic activity of snow-like Bi_2WO_6 microcrystalline for decomposition of Rhodamine B under natural sunlight irradiation. *Mater Lett* 90:107–110. <https://doi.org/10.1016/j.matlet.2012.09.009>
- Zong L, Cui P, Qin F et al (2017) Heterostructured bismuth vanadate multi-shell hollow spheres with high visible-light-driven photocatalytic activity. *Mater Res Bull* 86:44–50. <https://doi.org/10.1016/j.materresbull.2016.09.031>

Chapter 11

Solar Photocatalytic Treatment of Tannery Effluents



Alok Tripathi and Sheeba Narayanan

Contents

| | | |
|-------|---|-----|
| 11.1 | Introduction | 360 |
| 11.2 | Advantages and Limitations of Solar Energy | 361 |
| | 11.2.1 Advantages | 361 |
| | 11.2.2 Limitations | 361 |
| 11.3 | Solar Energy Application in Wastewater Treatment | 362 |
| 11.4 | Nature of Tannery Effluent | 362 |
| 11.5 | Treatment Methodology for Tannery Wastewater | 366 |
| | 11.5.1 Primary Treatment | 366 |
| | 11.5.2 Treatment Ponds/Constructed Wetlands | 367 |
| | 11.5.3 Biological Treatment | 367 |
| 11.6 | Modern Technologies for Tannery Wastewater Treatment | 369 |
| | 11.6.1 Membrane-Based Technologies | 369 |
| | 11.6.2 Membrane Bioreactors | 369 |
| | 11.6.3 Anaerobic Ammonium Oxidation | 370 |
| | 11.6.4 Advanced Oxidation Processes | 370 |
| 11.7 | Solar Photocatalysis Process | 371 |
| | 11.7.1 Key Steps of Pollutant Degradation During Solar Photocatalysis | 374 |
| | 11.7.2 Transformation of Contaminants | 374 |
| 11.8 | Factors Affecting Solar Photocatalysis | 376 |
| | 11.8.1 Solar Irradiance | 376 |
| | 11.8.2 Oxygen Concentration | 376 |
| | 11.8.3 Potential of Hydrogen | 376 |
| | 11.8.4 Temperature | 377 |
| | 11.8.5 Catalysis Load | 377 |
| 11.9 | Photocatalytic Reactors | 378 |
| | 11.9.1 Non-concentrating Collectors | 378 |
| | 11.9.2 Parabolic Trough Collectors | 379 |
| | 11.9.3 Compound Parabolic Collectors | 380 |
| 11.10 | Conclusion | 381 |
| | References | 382 |

A. Tripathi · S. Narayanan (✉)

Department of Chemical Engineering, National Institute of Technology, Tiruchirappalli, India
e-mail: sheeba@nitt.edu

Abstract Leather industries have a predominant place in the economic growth of various countries and have been a substantial contributor to export and employment potential. However, due to environmental impacts and water consumption, they are categorized as red-category industries, and as a result of the complex nature of their wastewater, currently available water treatment technologies are still inefficient to meet the standard discharge limits set by various pollution control authorities. This situation demands the need to introduce green technologies to decrease the pollutant load, and in recent years enormous research and progress has been observed in solar energy utilization, which has shown a great potential and has been extensively implemented for the removal of organic and inorganic compounds from industrial wastewater.

This chapter contributes the basic knowledge of tannery wastewater, and various treatment approaches along with the description of geometrical concept of photocatalytic reactors. The chapter provides an overview and application of solar photocatalysis in wastewater treatment. Various factors such as solar irradiance, oxygen concentration, potential of hydrogen production, temperature and catalysis load which affects solar photocatalysis have been explained in detail.

Keywords Leather industries · Environmental impact · Green technologies · Pollutant load · Tannery wastewater · Solar photocatalysis · Photocatalytic reactor

11.1 Introduction

In the context of increased energy demand, and the rapid depletion of conventional energy resources, attention has been focused towards the development of long-term permanent energy sources. The development of unique solar-powered technologies is considered as a key solution to fulfil the worldwide energy demand since the use of solar energy has been known to mankind and nature from a long time in terms of food production and heat utilization. Another vision of solar research is related with the diminishing worldwide carbon emission which is a significant social and environmental issue worldwide (Kabir et al. 2018). Approximately 4×10^6 exajoules of solar energy that reaches the earth annually can be easily harvestable. Efficient technologies are readily available to harvest and properly utilize this energy, solar energy has a potential to fulfil the worldwide energy demand (Blaschke et al. 2013).

Research over the past few decades made possible to harvest solar energy to generate mechanical and electrical power, but the utilization of solar energy in the field of wastewater treatment is limited and gaining the interest of researchers from the last two decades to develop clean, efficient and economic approaches.

11.2 Advantages and Limitations of Solar Energy

Solar energy is an ultimate source which can deliver secure self-governed energy. Such an ability is tremendously imperative for people as well as for the social and economic growth of the nation. However, solar energy is considered as a generous and consistent segment for electricity production in many developed and developing countries besides the various constraints and benefits related to solar energy utilization.

11.2.1 Advantages

Solar energy is a sustainable non-polluting, virtuous and consistent energy source, which is never going to deplete. The utilization of solar energy will not discharge volatile organic compounds and toxic gases into the atmosphere. Approximately 25% of anthropogenic greenhouse gases emissions is due to the power plants (Jerez et al. 2015). Thus, the replacement of fossil fuel-based power sources with solar-based energy will inevitably be advantageous to accomplish sustainable development. In addition, there is massive water consumption due to fossil fuel-driven power plants, which is a critical issue for droughts and heat affected areas. At the same time, the power generation from solar power plants doesn't require any water source to operate (Kabir et al. 2018).

Furthermore, to enhance the energy generation capacity, additional modules can also be added in the course of time. Over the years an increase in the efficiency of solar-powered technologies has been observed along with reduced capital and operating cost. All these points highlight the adaptability of solar-powered technologies over existing conventional technologies (Kabir et al. 2018).

11.2.2 Limitations

The high initial capital investment is a major disadvantage for solar-based technology, and the extended payback time with a limited revenue decreases the estimation of credits for such frameworks. On the other hand, less efficiency (10–20%) of domestic solar panels is another deficiency for the development of solar technology. However, there is an availability of more efficient solar panels (>20%) but at more expensive rates (Kabir et al. 2018).

The large space required by solar-based accessories such as batteries and inverters is another concern. Furthermore, a short lifespan of the batteries and their disposal are the other side effects regarding this system. Other variables related to such systems is the scarcity of skilled workforce to meet the demands for the establishment, support and assessment of solar powered systems. Another inadequacy is the

day-to-day and area-to-area variation of solar light intensity (Kabir et al. 2018). Therefore this is not authentic for an area with unsustainable climate or atmospheric conditions.

11.3 Solar Energy Application in Wastewater Treatment

From the last few decades, the mechanism of solar energy utilization along with the combination of heterogeneous catalysis to treat wastewater has gained considerable attraction for many researchers; such process is known as photocatalysis which is a kind of advanced oxidation processes.

Numerous reports have been published conferring the various application and mechanism of photocatalysis with a favourable laboratory and pilot-plant-based studies, and most of these studies have discussed the detailed, complex reaction mechanisms of photodegradation of many organic and inorganic pollutant present in wastewater (Ollis and Turchi 1990; Kisch and Twardzik 1991; Künne et al. 1993; Vidal et al. 1994; Herrmann 1995; Serpone 1995; Serpone et al. 1996; Peral et al. 1997; Kemeny et al. 2000; Botta et al. 2002; Ustinovich et al. 2005; Doll and Frimmel 2005; Gonçalves et al. 2005; Augugliaro et al. 2006; Sirtori et al. 2006; Guo and Hu 2007; Bayarri et al. 2007; Palmisano et al. 2007; Robert 2007; Sadik et al. 2007; Fujishima et al. 2007; Kiliç and Çinar 2008; Lair et al. 2008; Rodrigues et al. 2008; Chen et al. 2008; Du et al. 2008; Augugliaro and Palmisano 2010; Kisch 2010; Shan et al. 2010; Bickley 2010; Khataee et al. 2011; Valencia et al. 2011; Wang et al. 2011b; Xiong et al. 2011). Hence, these studies support the possibility of complete degradation of pollutant through solar photocatalysis.

11.4 Nature of Tannery Effluent

Extensive volume of water and pollutants, which has an adverse effect on the environment, is released during the tanning operations. Table 11.1 (Dixit et al. 2015) illustrates the details of the wastewater and characteristics of pollutants generated throughout the various tanning process.

Mostly the tannery wastewater is of dark brown in colour, possessing a strong odour with a large chemical oxygen demand, biochemical oxygen demand, total dissolved solids, chrome and a phenolic compound which has an adverse effect on the environment (Kusturica et al. 2015). Even after conventional treatment processes, there is a difficulty to remove them, and approximately 90% of total tannery pollution results from traditional tanning and pre-tanning processes. These processes cause an increment of chemical oxygen demand, sulphates, chlorides and total dissolved solids with a variation in potential of hydrogen (Dixit et al. 2015). The usage of lime with sodium sulphite in the liming process contributes to 92%

Table 11.1 Volume of wastewater generated during various tanning processes (Dixit et al. 2015)

| Process | Pollutant load kg/ton of hide | | | | | | | | | |
|----------------|------------------------------------|------------------------|---------------------------|----------|--------------------|-------------------------|------------------|-----------|-----------|--|
| | Waste water generated (kilolitres) | Chemical oxygen demand | Biochemical oxygen demand | Chromium | Ammonical nitrogen | Total Kjeldahl nitrogen | Suspended solids | Sulphates | Chlorides | |
| Soaking | 9.0–12.0 | 22–33 | 7–11 | – | 0.1–0.2 | 1–2 | 11–17 | 1–2 | 85–113 | |
| Liming | 4.0–6.0 | 79–122 | 28–45 | – | 0.4–0.5 | 6–8 | 53–97 | 1–2 | 5–15 | |
| Delimiting | 1.5–2.0 | 13–20 | 5–9 | – | 2.6–3.9 | 3–5 | 8–12 | 10–26 | 2–4 | |
| Chrome tanning | 1.0–2.0 | 7–11 | 2–4 | 2–5 | 0.6–0.9 | 0.6–0.9 | 5–10 | 30–55 | 40–60 | |
| Post tanning | 1.0–1.5 | 24–40 | 8–15 | 1–2 | 0.3–0.5 | 1–2 | 6–11 | 10–25 | 5–10 | |
| Finishing | 1.0–2.0 | 0–5 | 0–2 | – | – | – | 0–2 | – | – | |

suspended solids, 75% chemical oxygen demand and 84% biochemical oxygen demand to tannery wastewater (Dixit et al. 2015).

Furthermore, in the course of tanning operation, a number of chemicals such as tanning agents (organic and inorganic), dyes, acids, salts, and sulphonated oils were applied to mutate animal skins into a persistent product. This makes leather withstand against thermal, chemical and microbial degradation, and due to the non-biodegradability of tanned leather, management of sludge produced from tanneries is a challenging task (Lofrano et al. 2008). In addition to that, the implementation of such chemicals and their low biodegradability makes the effluent a severe environmental and technological threat (Schrank et al. 2004).

The pre-tanning operations such as liming delimiting are marked as alkaline in nature as they impart high organic and sulphide contents, while the existence of a high concentration of chromium, ammonium, sulphate and chloride salts in tanning operations makes the effluent highly acidic with a high chemical oxygen demand value (Saxena et al. 2016).

The existence of various toxic chemicals, for example, formaldehyde, resins, chlorophenols, oils, chrome, phthalates and detergents categorized the tannery wastewater as a substantial contributor of pollutants (Lofrano et al. 2013). The poisoning potential of chemicals utilized during numerous tanning operations is summarized in Table 11.2 (Saxena et al. 2016).

The partially treated tannery wastewater is of dark brown colour and is a prime cause of harmful effects in water and soil; in addition to that, tannery wastewater restricts sunlight insertion to water bodies resulting in a reduced photosynthetic activity and thus causing a deleterious effect to aquatic system (Saxena et al. 2016). Furthermore, the exhaustion of dissolved oxygen in water promotes anaerobic conditions causing a rotten smell through water (Rai et al. 2005; Verma et al. 2008). Tannery wastewater restraint the nitrification process with the formation of foam on the water surface, and the high organic and inorganic pollutant content leads to the growth of an extensive range of pathogenic bacteria in water bodies (Saxena et al. 2016).

Chandra et al. studied tannery wastewater collected from common effluent treatment plant, with respect to seedling growth and seed germination on mung bean, and they found that there was a presence of bacterial communities along with various organic pollutants (Chandra et al. 2011).

The practice to discharge tannery wastewater (directly or indirectly) to rivers and canals and their use in irrigation leads to a severe toxic effect on the plant, animals and human (Saxena et al. 2016). Despite that, hexavalent chromium modulates the structure of microbes present in soil and diminishes their growth to inhibit bioremediation process, and its input in food chain prompts ulceration, nasal irritation, lung carcinoma and skin irritation in human being (Saxena et al. 2016).

Improper discharge of high salt content of tannery wastewater results in relevant soil pollution; the presence of high sulphide in tannery wastewater creates inadequacy of micronutrients present in soil (Raj et al. 2014). The removal of azo dyes present in tannery wastewater is one of the difficult tasks as they are complex and xenobiotic in nature, and their discharge to water bodies gives rise to eye and skin

Table 11.2 Poisoning potential of chemicals used in the tanning process (Saxena et al. 2016)

| Chemical | Use | Lethal dose in rats, oral (milligrams/kg) | Intent organs |
|----------------------------------|---|---|---|
| Lead chromate | Fastening agent and material surfacing | 1000 | Liver, lung, issues and reproductive system |
| Anthracene | Additive in tanning | 16,000 | Liver and kidney |
| Arsenic | Used in the finishing process | 763 | Liver, lung, kidney, skin and lymphatic system |
| Pentachlorophenol | Preservative | 2000 | Liver, kidney, skin, eyes, nose, blood, respiratory tract, immune and reproductive system |
| Methyl isothiazolinone | Biocide | 1800 | Skin and eyes |
| Short chain chlorinated paraffin | Oiling agent used for smoothness | 3090 | Liver, kidney and thyroid |
| Cobalt dichloride | Used in dyeing and finishing | 80 | Lung, liver, kidney, skin and heart |
| Benzyl butyl phthalate | Used in micro-porous artificial coating | 2330 | Eyes, lung, liver and reproductive system |
| Formaldehyde | Used in finishing | 100 | Eyes and lungs |
| Nonylphenol | Used in finishing | 1475 | Eyes, lungs, skin, kidney, blood and central nervous system |
| Di-butyl phthalate | Used in artificial leather production | 7499 | Gastrointestinal tract, lungs and eyes |
| 2-Ethylhexyl phthalate | Used in artificial leather production | 30,000 | Liver |
| Chromium | Tanning agent | 3250 | Kidney, central nervous system and hematopoietic system |
| Azo dyes | Used for dyeing | 3418 | Liver and blood |
| Hexachlorobenzene | Applied as a preservative for raw hide and skin | 10,000 | Reproductive system |

irritation, aesthetic, dermatitis and respiratory problems (Saratale et al. 2010; Gang et al. 2011). Hence there is a need for appropriate treatment of tannery wastewater before discharge to the environment.

11.5 Treatment Methodology for Tannery Wastewater

11.5.1 Primary Treatment

Primary treatment includes coagulation, flocculation and sedimentation process and is focused on the separation of colloidal particles (Fig. 11.1).

In the coagulation process, a coagulant (like iron chloride, iron sulphate, aluminium and sulphate) is applied with rapid mixing to neutralize the negative charges contained in the wastewater within a short contact time. However, the concentration and effectiveness depend on potential of hydrogen and nature of wastewater (Song et al. 2004). During flocculation, the applied flocculent increases the size and density of flocs and allows them to stick together to accumulate. While in sedimentation, the flocs are removed by solid-liquid separation (Song et al. 2004).

The next stage of treatment is adsorption (Fig. 11.2), which is generally used to separate metals, usually chromium (Fabbricino et al. 2013). This is a solid-fluid operation where the sedimented water is allowed to contact with adsorbent, and the certain pollutant present in the water gets adsorbed on the surface of adsorbent, and the treated water is discharged to next stage (Faust and Aly 2013).

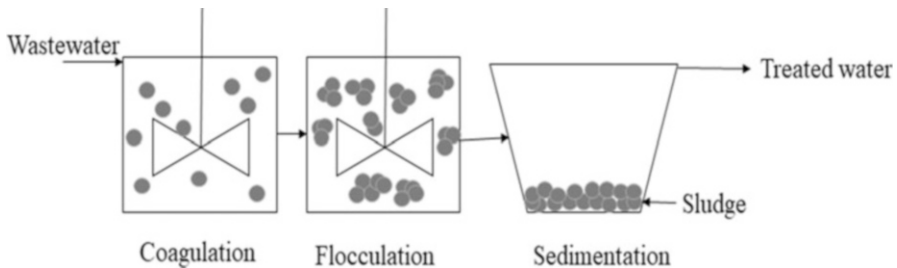
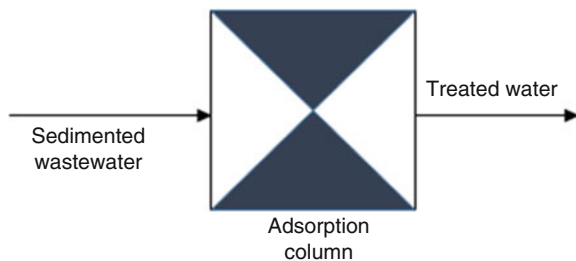


Fig. 11.1 Separation of colloidal particles through coagulation, flocculation and sedimentation process. (Modified after Song et al. 2004)

Fig. 11.2 Separation of toxic metals present in wastewater through solid-fluid operation in a packed adsorption column. (Modified after Faust and Aly 2013)



11.5.2 Treatment Ponds/Constructed Wetlands

The utilization of these systems has been expanded and effectively implemented to expel various contaminants from wastewaters. They are a man-made environmentally friendly system intended for the dismissal of pollutants from industrial and municipal wastewater (Mant et al. 2006). Their functioning depends on various parameters such as type of soil, nature of wastewater, microorganisms and plants. Hence, there is a need to develop a categorized microbial populations to treat wastewater (Calheiros et al. 2007).

The findings of Calheiros et al. indicates the development of *P. australis* and *T. latifolia* in constructed wetlands under 0.3 and 0.6 m/day hydraulic load leads to a chemical oxygen demand reduction 41–73%, and 41–58% biochemical oxygen demand in tannery wastewater (Calheiros et al. 2007). In a study conducted by Mant et al. for chrome removal, *P. purpureum* and removes 97–99.6% chrome, while *B. decumbens* removes 78.1% and 68.5% within 24 h (Mant et al. 2006). The establishment of two plant species, i.e., *Arundo donax* and *Sarcocornia fruticosa*, in constructed wetland to treat tannery wastewater results in 51 and 80% chemical oxygen demand and 53 and 90% biochemical oxygen demand reduction (Calheiros et al. 2012).

The integrated treatment pond system can be employed to treat tannery wastewater on pilot scale and a combination of maturation pond, and the secondary facultative pond was also an efficient approach for tannery wastewater treatment (Tadesse et al. 2004).

11.5.3 Biological Treatment

Biological treatment includes the decomposition of waste by aerobic or anaerobic processes to form innocuous solids. Usually activated sludge process, as shown in Fig. 11.3, is used for aerobic treatment, which has a fast decomposition rate in

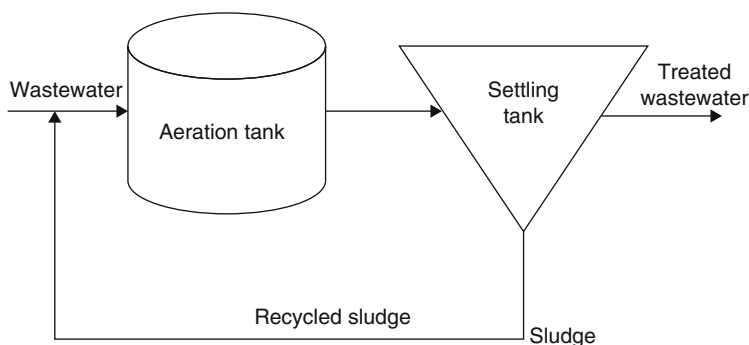


Fig. 11.3 Layout of an activated sludge process including aeration tank where air is injected in mixed liquor and settling tank to allow the biological flocs to settle. (Modified after Ram et al. 1999)

Table 11.3 Various microorganisms used in activated sludge process for tannery wastewater treatment

| Microorganisms | Chrome reduction (%) | Chemical oxygen demand reduction (%) | Biochemical oxygen demand reduction (%) | References |
|---|----------------------|--------------------------------------|---|------------------------------|
| Bacterial strain | 87 | – | – | Shakoori et al. (2000) |
| <i>Hirsutella</i> sp. | 70 | – | – | Srivastava and Thakur (2006) |
| <i>A. thiooxidans</i> | 99.7 | – | – | Yuan-Shan et al. (2007) |
| <i>Acinetobacter</i> sp. | 90 | – | – | Srivastava et al. (2007) |
| <i>S. condensate</i> and <i>R. hieroglyphicum</i> | >75 | – | – | Onyancha et al. (2008) |
| <i>Trichoderma</i> sp. | 97.93 | – | – | Vankar and Bajpai (2008) |
| <i>E. coli</i> | 68.3 | 90 | 90 | Noorjahan (2014) |
| <i>Brachymonas denitrificans</i> | 88.5 | 98.3 | – | Kim et al. (2014) |

conjunction with the generation of enormous amount of sludge. Table 11.3 indicates the various microorganisms used in this technique to treat tannery wastewater.

Due to the saline nature of tannery wastewater, there is a limited adaption of conventional cultures, and the variation in ionic strength results in cell disruption, which sometimes leads to a failure in the biological treatment process. Likewise, the existence of inadequately degraded tannins, chromium and toxic materials restrains the biological treatment by inhibiting the growth of heterotrophs and bacteria (Schrank et al. 2004). Hence, to conquer this issue, many researchers suggested the use of sequencing batch reactor to treat tannery wastewater (Ram et al. 1999; Cooman et al. 2003; Rameshraj and Suresh 2011; Lofrano et al. 2013).

Another problem in aerobic biological treatment of tannery wastewater is the temperature variation which affects the efficiency of process in terms of organic carbon and nitrogen removal, as there was 60% nitrogen removal efficiency reported in 21 °C to 35 °C temperature range (Görgün et al. 2007; Insel et al. 2008).

Owing to low energy consumption in comparison to aerobic treatment, anaerobic processes are one of the good options to treat tannery wastewater, but the absence of electron acceptor during sulphate reduction leads to form sulphide, and the high content of protein in effluent slows down the hydrolysis kinetics. Further, to reduce high chemical oxygen demand, there is a need of aerobic treatment (Mannucci et al. 2010, 2014).

11.6 Modern Technologies for Tannery Wastewater Treatment

As discussed in the previous sections after the conventional treatment process, the complete pollutant removal is still a major task. Hence, there is a need for the implementation of new modern techniques; some of them are discussed below.

11.6.1 Membrane-Based Technologies

Membrane technology has several advantages over conventional processes, which includes the high quality of treated water, effective removal of organic micro-pollutants, reduced sludge production and better process consistency. These techniques employ permeable membranes for separation and purification of industrial wastewater. Due to their continuous cost reduction and extended applications, their utilization to treat tannery wastewater is getting importance (Ranganathan and Kabadgi 2011). For the treatment of tannery wastewater, this technique provides many cost-effective benefits such as the recovery of chrome (Ranganathan and Kabadgi 2011), reduction of load in degreasing (Wang et al. 2011a), removal of salt during biological treatment and the reuse of water in many other processes (Scholz and Lucas 2003).

De Gisi et al. suggested that the reverse osmosis can be used as a post-treatment process after the biological treatment with an objective to reuse tannery wastewater and hence to reduce the freshwater consumption. In their study, the treatment was carried out through a plane reverse osmosis membrane which has reduced chemical oxygen demand along with the generation of high-grade permeate and enabled the reuse of water in the production cycle (De Gisi et al. 2009).

Scholz and Lucas used membrane technology to retrieve chemicals from tanning and deliming process and to reuse saline stream. The implementation of membrane filter results in the recovery of 90% treated liquors, and the obtained permeate out of the various process was confined with a high concentration of chemicals which were reused in the tanning processes (Scholz and Lucas 2003).

11.6.2 Membrane Bioreactors

This is a combined technology comprising membrane and bioreactor and has been developed as an alternative to the conventional activated sludge process. The advantages of this system include less space requirement, no need for secondary clarifiers, shorter hydraulic retention times, less sludge production and high removal of pollutants (Iorhemen et al. 2016).

Keerthi et al. have reported 90 and 93% of reduction in chemical oxygen demand and colour in tannery wastewater through hybrid membrane bioreactor (Keerthi et al. 2013). However, the severe fouling due to the plugging of several pollutants is the main disadvantage of this process, but extensive research is in process to overcome this issue, such as the integration of membrane bioreactors with another treatment process will reduce the fouling and mineralize majority of the pollutants (Fazal et al. 2015).

11.6.3 Anaerobic Ammonium Oxidation

This process is also known as anammox technology, used to separate nitrogen from wastewater, and compared to conventional nitrification and denitrification processes anammox process consumes low energy, with high efficiency (Ali and Okabe 2015). In the presence of nitrogen dioxide as an electron acceptor, this process transforms ammonium cation to dinitrogen and produces 90% less sludge in comparison to conventional nitrification and denitrification. This is a two-step process: in the first step, oxidation of ammonium cation to nitrogen dioxide happens, and in the second stage, ammonium cation oxidizes with nitrogen dioxide to form dinitrogen; afterwards, the process was introduced to single-stage reactor (Ali and Okabe 2015).

The anammox methodology was implemented by Anjali and Sabumon to remove ammonia from tannery wastewater, which saved 90% of operational cost in sludge discharge, and ingests 100% less organic carbon and 50% less oxygen (Anjali and Sabumon 2014). Hence, for the industries having effluent of high ammonia concentration, anammox oxidation could be a good economic approach (Ali and Okabe 2015).

11.6.4 Advanced Oxidation Processes

The drawbacks of conventional treatment technologies encouraged the scientific community to develop novel approaches towards efficient removal of contaminants from wastewater generated through various industries. To this context, advanced oxidation processes can fill the gap between the treatability limit of conventional process and rigorously increasing limit of environmental regulations (Dewil et al. 2017).

Usually, advanced oxidation processes are applied after secondary treatment of wastewater, and hence they are considered as tertiary treatment techniques (Audenaert et al. 2011). Advanced oxidation processes are the inclusion of heterogeneous and homogeneous photocatalysis, ozonation, ultrasonication, electrochemical processes, Fenton process and wet oxidation processes (Dewil et al. 2017). The main benefit of these processes is the effective degradation of pollutant without

generation of secondary waste, and maximum pollutants get transformed to water, carbon dioxide and salts during mineralization (Saxena et al. 2016).

The general objective of advanced oxidation processes to treat tannery wastewater is to lessen the contamination load to such a degree that they might be restored to the water reservoirs or reused during the other operations. Table 11.4 highlights the various advanced oxidation processes applied over tannery wastewater.

As shown in above table, there are few studies which implements solar energy as photocatalysis to treat tannery wastewater, and in the context to current environmental scenario, the use of solar energy in terms of photocatalysis could play a key role to treat groundwater, drinking water and industrial wastewater. However, solar photocatalysis technique has been used for water splitting to produce hydrogen and degradation of toxic elements, dyes and chemicals (Shimura and Yoshida 2011). Hence, the treatment of tannery wastewater through solar photocatalysis could be an economic and cost-effective approach.

11.7 Solar Photocatalysis Process

The solar photocatalysis process involves the use of solar energy to excite a semiconductor catalyst also known as a photocatalyst, and the electronic structure of a photocatalyst (consists of a valence band and conduction band) can act as a sensitizer for the light-driven redox reaction. If a surface reaction has more positive oxidation potential in comparison to valence band potential, then there will be no oxidation; similarly if a surface reaction has more negative reduction potential compared to conduction band, then reduction will not take place, which denotes the absence of hydroxyl and superoxide radicals (Simonsen 2014). Hence, the position of conduction and valence band potential plays an important role in solar photocatalysis. If a photocatalyst is exposed through light having a wavelength equal or larger than its band gap energy, an electron will be excited to the conduction band leaving a positive hole in the valence band, and these electron and hole initiate reduction and oxidation process. Furthermore, the electron and hole tend to recombine very rapidly; if an appropriate surface defect or scavenger restricts this recombination rate, then there will be an efficient photocatalytic effect to mineralize organic impurities present in wastewater. In addition, the oxygen present in the atmosphere leads to produce superoxide ions which are a dominant oxidant (Spasiano et al. 2015).

The fundamentals of this technique are well established, and the characteristics of solar photocatalysis which make the applicability to treat industrial effluent are followed (Malato et al. 2009):

1. The process takes place at ambient condition.
2. Complete oxidation of polluting substance into carbon dioxide and other inorganic species.

Table 11.4 Various advanced oxidation processes employed for tannery wastewater treatment

| Type of tannery wastewater | Advanced oxidation process applied | Pollutant reduction | References |
|---|--|---|---|
| Raw tannery wastewater | Fenton reagent | 70% reduction in chemical oxygen demand | Lins et al. (2003) |
| Coagulated/flocculated tannery wastewater | Photocatalysis (ultraviolet rays/titanium dioxide) | 6% reduction in chemical oxygen demand, 15% reduction in biochemical oxygen demand removal and 11% total organic carbon | Schrank et al. (2004) |
| Biological treated tannery wastewater | Ozone | 30% reduction in chemical oxygen demand | Serdar Dogruel M.D., Esra Ates Genceli (2004) |
| Coagulated tannery wastewater | Fenton reagent | 80% reduction in chemical oxygen demand | Schrank et al. (2005) |
| Coagulated tannery wastewater | Ultraviolet rays/hydrogen peroxide | 60% reduction in chemical oxygen demand | Sauer et al. (2006) |
| Raw tannery wastewater | Electrochemical process | 70% reduction in chemical oxygen demand | Kurt et al. (2007) |
| Equalized tannery wastewater | Electrochemical process | 83.9% phenol degradation 40.5% total organic carbon reduction | Costa et al. (2008) |
| Chromium-containing tannery wastewater | Electrocoagulation | 95% of chromium removal | Kongjao et al. (2008) |
| Equalized tannery wastewater | Electrochemical process | 51–56% reduction in chemical oxygen demand 30–700% total suspended solids reduction | Espinoza-Quifones et al. (2009) |
| Raw tannery wastewater | Ozone | 60% reduction in chemical oxygen demand | Preethi et al. (2009) |
| Pre-treated tannery wastewater | Ozone | 85% reduction in chemical oxygen demand | Schrank et al. (2009) |
| Synthetic tannery wastewater | Electrochemical | 89% reduction in chemical oxygen demand | Sundarapandiyar et al. (2010) |

(continued)

Table 11.4 (continued)

| Type of tannery wastewater | Advanced oxidation process applied | Pollutant reduction | References |
|--|--|--|--------------------------------|
| Biological treated tannery wastewater | Ozone | 97% reduction in chemical oxygen demand | Di Iaconi et al. (2010) |
| | | 91% total Kjeldahl nitrogen reduction | |
| | | 96% total suspended solids reduction | |
| | | 98% surfactant reduction 96% colour reduction | |
| Pre-alkalized tannery wastewater | Ozone | 30–70% reduction in chemical oxygen demand | Houshyar et al. (2012) |
| Equalized tannery wastewater | Photo-Fenton | 90% reduction in chemical oxygen demand | Módenes et al. (2012) |
| | | 50% total suspended solids reduction | |
| Coagulated tannery wastewater | Coagulation + hydrogen peroxide/ultraviolet rays + electro-oxidation | 97.5% reduction in chemical oxygen demand | Naumczyk and Kucharska (2017) |
| Common effluent treatment plant of tannery | Coagulation + aeration + ozone | 80–90% reduction in chemical oxygen demand | Sivagami et al. (2018) |
| Pre-treated tannery wastewater | Ultraviolet rays/titanium dioxide | 93.06% phenol reduction | Tripathi and Narayanan (2018) |
| | | 85.62% reduction in chemical oxygen demand | |
| | | 80.23% colour reduction | |
| Pre-treated tannery wastewater | Solar photocatalysis | 84.22% phenol reduction | Tripathi and Narayanan (2019a) |
| Pre-treated tannery wastewater | Solar photocatalysis | 89.06% phenol reduction | Tripathi and Narayanan (2019b) |

3. The essential oxygen for the reaction can be directly obtained from the atmosphere.
4. The catalyst can be attached to different types of inert matrices.
5. The energy for the photo-excitation of the catalyst can be obtained from the sun.

The capability of this process to completely mineralize organic pollutants to carbon dioxide, water and inorganic ions, applicability at ambient conditions, and the absence of fouling differentiate solar photocatalysis with other conventional techniques of wastewater treatment (Mamba and Mishra 2016).

11.7.1 Key Steps of Pollutant Degradation During Solar Photocatalysis

The solar photocatalysis, as shown Fig. 11.4, is very complex and may involve a lot of possible reaction mechanism for pollutant degradation. Still there is a general concurrence to summarize solar photocatalysis in five key steps:

1. The dissemination of organic pollutants from bulk solution to the surface of the photocatalyst.
2. Photoexcitation of catalyst along with the adsorption of the organic pollutant.
3. Degradation of pollutant through oxidizing species.
4. Detachment of degraded products from photocatalyst surface.
5. The degradation products diffuse from the photocatalyst interface into the bulk solution.

11.7.2 Transformation of Contaminants

Mineralizing and eliminating organic compound present in wastewater is the primary objective of solar photocatalysis; so far for s-triazine herbicides, complete mineralization has been observed with a final product named as cyanuric acid which is non-toxic in nature. Today there is a need to pay attention towards the solar photocatalytic degradation of contaminants emerging from various industrial sources which have adverse effect on health and on the environment; many of them are still unknown and are in the focus of research (Petrović et al. 2003).

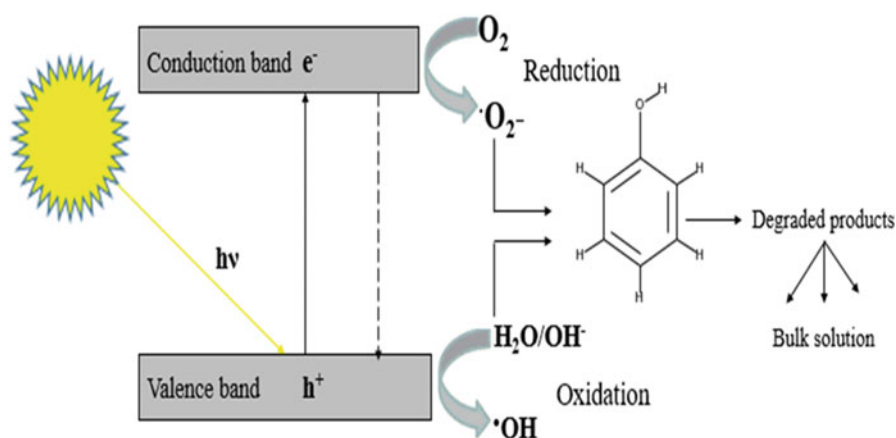


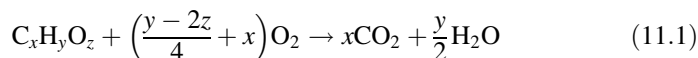
Fig. 11.4 Photocatalyst is exposed to light having a wavelength equal or larger than its band gap energy, leading to excitation of an electron and leaving a hole in valence band; these electrons and holes initiate reduction and oxidation process. (Modified after Spasiano et al. 2015)

The mineralization of nitrogen-containing compounds leads to form ammonium cation and nitrate, these ammonium cation are relatively consistent, and their proportionality is influenced by irradiation time and oxidation phase of organic nitrogen. For the amine compounds, the primary product exists in the form of ammonium cation, and the invasions of hydrogen-containing species on the amino group govern the formation of ammonium cation. Hence at the end of experiments, the amount of nitrogen-containing ions existing in the solution are much lesser than expected from stoichiometry, implying the adsorption of nitrogen-containing species on the surface of photocatalyst (Calza et al. 2005).

The generation of nitrogen in azo compounds can be represented by similar procedures which are accountable for ammonium cation formation and comprises of an exemplary case of decontamination reaction involving total innocuous nitrogen as a concluding product (Konstantinou and Albanis 2004). In the case of photo-Fenton treatment of phosphates, more iron is necessary, and at potential of hydrogen below 4, the phosphate ions stay adsorbed on the surface of photocatalyst (Malato et al. 2009).

The photo-induced hydroxide radicals attack on sulphur-containing atom present in wastewater to mineralize as sulphate ion; in most of the cases during the final stage of photoreaction, stoichiometric formation was observed when organic intermediates remained present in effluent solution (Malato et al. 2009). The strong adsorption of sulphate ion on photocatalyst surface could inhibit the reaction rate and forms non-stoichiometric sulphate ions. The presence of sulphate ion, chloride ion and phosphate ion in concentration > 1 milli-molar can reduce the reaction rate because of adsorption on the photo-activated reaction sites (Malato et al. 2009).

Industrial wastewater treatment is one of the major advantageous applications of solar photocatalysis, and there is always a need to assess the probable pollutant for optimized operations (Malato et al. 2007a). Generally, the compounds which have been degraded by solar photocatalysis comprise of dyes, aliphatic alcohols, alkanes, carboxylic acids, polymers, aromatics, alkenes, pesticides, surfactants, alkanes and herbicides. Equation 11.1 represents a general mechanism of organic pollutant degradation (Malato et al. 2009):



From an analytical point of view, determination of degraded products and the intermediate compounds is a most challenging task due to not selective nature of hydroxyl radicals. There are following types of degradation products (Malato et al. 2009):

1. Hydroxylated and de-halogenated products
2. Derived products of alkali chain oxidation
3. Products from aromatic contaminants
4. Isomerization and cyclization products
5. Decarboxylation products

The determination of these complex reaction mechanism is very difficult, and their estimation is restricted to identifying the dissipation of primary pollutant, in combination with a reduced total organic carbon. Therefore, the oxidation rate and kinetic of the process are usually evaluated (Malato et al. 2009).

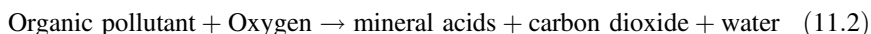
11.8 Factors Affecting Solar Photocatalysis

11.8.1 Solar Irradiance

In case of solar photocatalysis, the reaction rate increases with increase in solar irradiance, and beyond a certain point, the rate of reaction depends as the square of the solar irradiance which is due to higher recombination rate of electron-hole pair. Furthermore, at high solar irradiance, the effect is negligible, and the rate remains constant. Such condition appears due to the deficiency of electron scavengers or excess of products conquering the catalyst surface which implies the lesser contact of catalyst with the effluent (Silva et al. 2007; Spasiano et al. 2015).

11.8.2 Oxygen Concentration

The degradation of organic pollutant present in wastewater can be summarized by Eq. 11.2 which concludes that in the absence of oxygen, there is no photodegradation.



The availability of oxygen in water not only serves as an electron acceptor but also leads to the formation of oxidative species (Malato et al. 2009).

11.8.3 Potential of Hydrogen

Usually, solar photocatalysis indicates a strong potential of hydrogen dependency, and with the variation in potential of hydrogen, the valence and conduction band edges of a photocatalyst move by 0.059 per unit potential of hydrogen, which makes electrons of valence band more effective, and holes of conduction band less effective (Hoffmann et al. 1995). Another notable characteristic of solar photocatalysis generally not taken into consideration during water decontamination is the formation of intermediate compounds which may respond divergently depending on potential of hydrogen.

Furthermore, potential of hydrogen also affects the surface charge of a photocatalyst which could affect the efficiency of photocatalysis process (Spasiano et al. 2015). Hence, potential of hydrogen is one of the most important parameters which must be considered during the study of any photocatalytic process.

11.8.4 Temperature

Due to the photonic activation, the photocatalysis systems do not require heating and can be operated at ambient conditions. Many studies concludes that at temperature below 0 °C, the rate-limiting step is controlled by the final product desorption, and at this point the apparent activation energy increases (Malato et al. 2009; Nan et al. 2010). While at temperature above 80 °C the exothermic adsorption of reactants becomes rate-limiting step, the apparent activation energy becomes negative. Furthermore, at higher temperature, recombination of electron-hole pairs increases and demonizes the adsorption of organic compounds onto the photocatalyst surface (Malato et al. 2009; Nan et al. 2010).

In addition, the solubility of oxygen decreases with increased temperature and affects the photocatalytic kinetics. Hence for the photocatalysis system, 20 and 80 °C temperature range is considered as optimum (Malato et al. 2009; Nan et al. 2010).

11.8.5 Catalysis Load

Catalysis load and solar photocatalytic reactor diameter are interconnected reactor design parameters. In the case of slurry reactors, the rate of reaction is proportional to the load of catalyst, but after a specific dose due to particle agglomeration and poor penetration of sunlight, the photocatalytic activity decreases (Assano and Alfano 1998; Silva et al. 2007). Hence optimization of the photocatalyst dose for a better efficiency is required; various reports conclude that 25–50 mm must be the ideal diameter of a solar photocatalytic slurry reactor. Lesser than this range may result in operating pressure loss (Dillert et al. 1999; Guillard et al. 1999).

In immobilized photocatalytic reactor system, the film thickness plays an important role which depends on photocatalyst deposition technique, optical and physical properties of the material used and the nature of light wavelength. When the film thickness is very low (<1 μm), the photons will absorb on the photocatalyst surface, whereas the thick film gives rise to an unreactive “dark zone” (Chen et al. 2000; Camera-Roda and Santarelli 2007).

11.9 Photocatalytic Reactors

For the detoxification of pollutant, the sun provides UV flux $20\text{--}30\text{ Wm}^{-2}$ in the range of $300\text{--}400\text{ nm}$ with $0.2\text{--}0.3\text{ mol photons m}^2\text{ h}^{-1}$, which suggests the use of sun as an economical source of sensible light, and a photocatalytic reactor is a device which brings photons and pollutant in contact with the photocatalyst (Bahnmann 2004). These reactors are different from chemical reactors in terms of geometry and operating parameters; the primary objective of these reactors is to transmit sufficient light to initiate the reaction mechanism. Figure 11.5 highlights the design concept of these photocatalytic reactor systems. In these systems, temperature doesn't play an important role; hence no insulation is required. The solar photocatalytic reactors can be classified as:

1. Non-concentrating collectors
2. Parabolic trough collectors
3. Compound parabolic collectors

11.9.1 Non-concentrating Collectors

They are also known as an inclined plane collector, over which the fluid flows and interacts with the photocatalyst immobilized on the surface (Fig. 11.6). This reactor is capable of utilizing both direct and diffuse radiations from the sun. Due to simplicity and low capital cost, non-concentrating collectors have been proved an impressive choice for small-scale functions, especially in the areas having an infeasible wastewater treatment plants. Though these reactors demand large area in comparison to other reactors, but they have been successfully implemented for agro-industrial, organic pollutants and bio-refractory wastewater treatment (Spasiano et al. 2015).

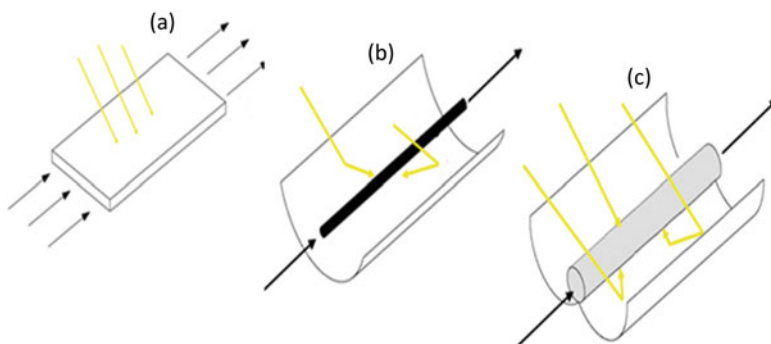


Fig. 11.5 Geometrical concept in terms of incident solar radiations for (a) non-concentrating collectors, (b) parabolic trough collectors and (c) compound parabolic collectors. (Modified after Malato et al. 2009)

Fig. 11.6 Interaction of fluid over photocatalyst immobilized surface of non-concentrating collector reactor operated in continuous recycle mode. (Modified after Bahnemann 2004)

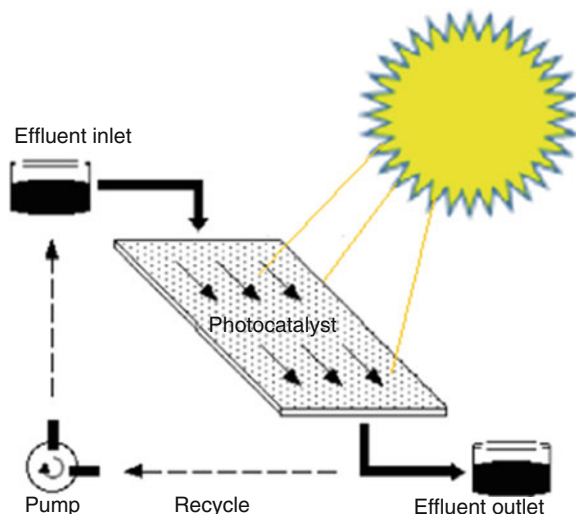
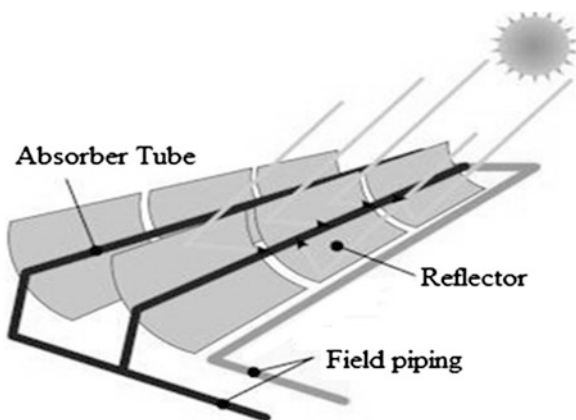


Fig. 11.7 Parabolic trough collectors composed of a parabolic trough-shaped concentrator that reflects direct solar radiation onto a receiver or absorber tube located in the focal line of the parabola. (Modified after Spasiano et al. 2015)



This reactor immobilized with titanium dioxide, and having a 50 m² of exposed area with a combination of two bioreactors, was installed in Tunisian textile mill to decolorize water (Spasiano et al. 2015) and has also been used for transformation of 1,1-dicarbonitrile through dicyano tetramethyl benzene as the electron acceptor (Will et al. 2004).

11.9.2 Parabolic Trough Collectors

The design of parabolic trough collectors (Fig. 11.7) is inspired from thermal energy application derived from the sun. Parabolic trough collector contains a reflective

parabolic surface used to concentrate the transparent tube through solar radiations by which the fluid flows.

For maximum efficiency, the platform of the collector is controlled by two motors in an azimuth and elevation tracking system to keep the aperture of parabolic trough collector in perpendicular to the solar radiation (Fernández-García et al. 2010). With regard to photocatalytic applications, the concentration factor of parabolic trough collectors reactor lies from 5 to 35 suns; the concentration factor is the ratio of collector's aperture area and absorber area (Alfano et al. 2000). This system sustains turbulent flow with well-organized uniforming, and the closed system of the tube prevents the vapourization of volatile compounds during experiments.

In this reactor system, photocatalyst is usually suspended in a fluid, and the main disadvantage of this system is the dependency on the direct radiation beams which makes them impractical during cloudy days; in addition, their tracking system contributes extra capital and operating cost (Fernández-García et al. 2010). The parabolic trough collectors were used to treat wastewater containing heavy metals and chlorinated solvents (Spasiano et al. 2015), for the production of 5-hydroxy-1,4-naphthoquinone (Oelgemöller et al. 2006), for heterocyclization of ethyne (Jung et al. 2005), acylation reaction of naphthoquinones and quinones (Schiel et al. 2001).

11.9.3 Compound Parabolic Collectors

They are immobile collectors having parabolic reflective surface around to a cylindrical reactor tube as shown in Fig. 11.8; compound parabolic collector is an intercross of parabolic trough collector and non-concentrating collector reactors (Islam et al. 2015). Their geometry is capable of capturing both direct and diffuse radiations

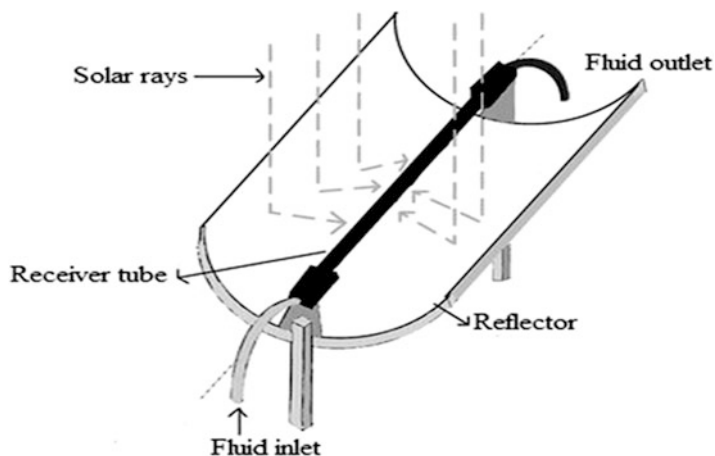


Fig. 11.8 Heating of working fluid in receiver tube using solar radiation falling on reflector of a compound parabolic collectors. (Modified after Islam et al. 2015)

Table 11.5 Advantages and disadvantages of photocatalytic reactors (Spasiano et al. 2015)

| Non-concentrating collectors | | Parabolic trough collectors | | Compound parabolic collectors | |
|---|-----------------------------|-----------------------------|----------------------|-------------------------------|----------------------------|
| Advantages | disadvantages | Advantages | disadvantages | Advantages | disadvantages |
| High optical efficiency | Large reactor area required | Small reactor volume | Required tracking | Small reactor volume | Reasonable capital cost |
| Simple design | Pressure limitations | High flow rate | Utilize direct beams | High flow rate | Reasonable heat generation |
| Utilization of direct and diffuse beams | Poor mass transfer | Improved mass transfer | Optical losses | Good mass transfer | Complex to scale up |
| Low cost | Laminar flow | Low catalyst load | Overheating | Turbulent flow | |
| No heating | Reactant evaporation | Small area required | Low efficiency | Low catalyst load | |

from the sun, and the extent of sunlight absorbed by a compound parabolic collectors is far better than parabolic trough collectors. Hence they can be used on overcast days without the use of solar tracking systems which substantially reduces system complexity with cost (Malato et al. 1997).

The pilot-scale compound parabolic collectors, have demonstrated photocatalytic removal of biorecalcitrant compounds (Sarria et al. 2003; Malato et al. 2007b), chlorophenols (Gernjak et al. 2003), bacteria (Fernández et al. 2005), pesticides (Oller et al. 2006), chlorinated solvents (Blanco-Galvez et al. 2007), dyes (Malato et al. 1997) and pathogenic organisms (Sarria et al. 2003; Malato et al. 2007b). They have also been used for urban and olive mill wastewater treatment (Gernjak et al. 2004; Kositz et al. 2004) and the treatment of sanitary landfill leachate (Silva et al. 2013).

The advantages and disadvantages of these reactors are described in Table 11.5.

11.10 Conclusion

Among all the industrial wastewater, tannery wastewater is very complex in nature and a significant source of environmental pollution; the conventional wastewater treatment methods are not efficient to meet the standards. Hence to achieve cost-effective high-efficiency treatment, advanced oxidation processes in various combinations have been used as a pre- or post-treatment method. In recent years, solar photocatalysis, a kind of an advanced oxidation process, has gained the attention of researchers worldwide; the utilization of natural sunlight as the leading factor is a unique approach compared to other advanced oxidation processes. However, as the number of pollutants and their concentration increases, this process becomes more complicated and results in low photo-efficiency and slow kinetics along with an

unpredicted mechanism (Nan et al. 2010). Furthermore, the reliability on the natural light source is another factor which needs to be resolved through the integration of various solar collecting technologies for an efficient outcome (Malato et al. 2009).

Hence to promote solar photocatalytic wastewater treatment technology in the near future, few technical barriers still need to be overcome:

- Development of high photo-efficient catalyst for extensive solar spectrum utilization.
- For cost-effective pollutant separations, catalyst immobilization approach needs to develop.
- Coupling of solar photocatalysis with other treatment techniques.
- Inadequate experimental data and prolonged dependability on solar energy.
- Lack of techno-economic study.
- The effective and efficient design of the photocatalytic reactor.

The photocatalytic reactor design is a major challenge for the scale-up of the solar photocatalytic process. In addition, based on process requirement, optimization of photoreactor must consider into account, as the continuous light exposure to the reactor leads to a rapid and efficient pollutant degradation.

Another issue with the solar photocatalysis process, which is needed to be addressed, is the environmental impact assessment and life cycle analysis studies. Finally, for wide industrial application, solar photocatalysis has to be developed as a sustainable, robust and cost-effective approach.

References

- Ali M, Okabe S (2015) Anammox-based technologies for nitrogen removal: advances in process start-up and remaining issues. *Chemosphere* 141:144–153. <https://doi.org/10.1016/j.chemosphere.2015.06.094>
- Anjali G, Sabumon PC (2014) Bioresource technology unprecedented development of anammox in presence of organic carbon using seed biomass from a tannery Common Effluent Treatment Plant (CETP). *Bioresour Technol* 153:30–38. <https://doi.org/10.1016/j.biortech.2013.11.061>
- Assano AE, Alfano OM (1998) Reaction engineering of heterogeneous photocatalytic reactors. *Z Phys Chem* 1:237–252. <https://doi.org/10.1524/zpch.1998.1.1.237>
- Audenaert WTM, Vermeersch Y, Van Hulle SWH et al (2011) Application of a mechanistic UV/hydrogen peroxide model at full-scale: sensitivity analysis, calibration and performance evaluation. *Chem Eng J* 171:113–126. <https://doi.org/10.1016/j.cej.2011.03.071>
- Augugliaro V, Palmisano L (2010) Green oxidation of alcohols to carbonyl compounds by heterogeneous photocatalysis. *ChemSusChem* 3:1135–1138. <https://doi.org/10.1002/cssc.201000156>
- Augugliaro V, Litter M, Palmisano L, Soria J (2006) The combination of heterogeneous photocatalysis with chemical and physical operations: a tool for improving the photoprocess performance. *J Photochem Photobiol C: Photochem Rev* 7:127–144. <https://doi.org/10.1016/j.jphotochemrev.2006.12.001>
- Bahnemann D (2004) Photocatalytic water treatment: solar energy applications. *Sol Energy* 77:445–459. <https://doi.org/10.1016/j.solener.2004.03.031>

- Bayarri B, Abellán MN, Giménez J, Esplugas S (2007) Study of the wavelength effect in the photolysis and heterogeneous photocatalysis. *Catal Today* 129:231–239. <https://doi.org/10.1016/j.cattod.2007.08.006>
- Bickley RI (2010) Heterogeneous photocatalysis at liquid-solid interfaces. Oxidative dehydrogenation of propan-2-ol as a method of assessing photocatalytic activity. *J Photochem Photobiol A Chem* 216:256–260. <https://doi.org/10.1016/j.jphotochem.2010.06.037>
- Blanco-Galvez J, Fernández-Ibáñez P, Malato-Rodríguez S (2007) Solar photocatalytic detoxification and disinfection of water: recent overview. *J Sol Energy Eng* 129:4. <https://doi.org/10.1115/1.2390948>
- Blaschke T, Biberacher M, Gadocha S, Schardinger I (2013) “Energy landscapes”: meeting energy demands and human aspirations. *Biomass Bioenergy* 55:3–16. <https://doi.org/10.1016/j.biombioe.2012.11.022>
- Botta SG, Rodríguez DJ, Leyva AG, Litter MI (2002) Features of the transformation of HgII by heterogeneous photocatalysis over TiO₂. *Catal Today* 76:247–258. [https://doi.org/10.1016/S0920-5861\(02\)00223-7](https://doi.org/10.1016/S0920-5861(02)00223-7)
- Calheiros CSC, Rangel AOSS, Castro PML (2007) Constructed wetland systems vegetated with different plants applied to the treatment of tannery wastewater. *Water Res* 41:1790–1798. <https://doi.org/10.1016/j.watres.2007.01.012>
- Calheiros CSC, Quitério PVB, Silva G et al (2012) Use of constructed wetland systems with Arundo and Sarcocornia for polishing high salinity tannery wastewater. *J Environ Manag* 95:66–71. <https://doi.org/10.1016/j.jenvman.2011.10.003>
- Calza P, Pelizzetti E, Minero C (2005) The fate of organic nitrogen in photocatalysis: an overview. *J Appl Electrochem* 35:665–673. <https://doi.org/10.1007/s10800-005-1626-7>
- Camera-Roda G, Santarelli F (2007) Optimization of the thickness of a photocatalytic film on the basis of the effectiveness factor. *Catal Today* 129:161–168. <https://doi.org/10.1016/j.cattod.2007.06.062>
- Chandra R, Bharagava RN, Kapley A, Purohit HJ (2011) Bacterial diversity, organic pollutants and their metabolites in two aeration lagoons of common effluent treatment plant (CETP) during the degradation and detoxification of tannery wastewater. *Bioresour Technol* 102:2333–2341. <https://doi.org/10.1016/j.biortech.2010.10.087>
- Chen D, Li F, Ray AK (2000) Effect of mass transfer and catalyst layer thickness on photocatalytic reaction. *AICHE J* 46:1034–1045. <https://doi.org/10.1002/aic.690460515>
- Chen D, Sivakumar M, Ray AK (2008) Heterogeneous photocatalysis in environmental remediation. *Dev Chem Eng Miner Process* 8:505–550. <https://doi.org/10.1002/apj.5500080507>
- Cooman K, Gajardo M, Nieto J et al (2003) Tannery wastewater characterization and toxicity effects on *Daphnia* spp. *Environ Toxicol* 18:45–51. <https://doi.org/10.1002/tox.10094>
- Costa CR, Botta CMR, Espindola ELG, Olivi P (2008) Electrochemical treatment of tannery wastewater using DSA electrodes. *J Hazard Mater* 153:616–627. <https://doi.org/10.1016/j.jhazmat.2007.09.005>
- De Gisi S, Galasso M, De Feo G (2009) Treatment of tannery wastewater through the combination of a conventional activated sludge process and reverse osmosis with a plane membrane. *Desalination* 249:337–342. <https://doi.org/10.1016/j.desal.2009.03.014>
- Dewil R, Mantzavinos D, Poullos I, Rodrigo MA (2017) New perspectives for advanced oxidation processes. *J Environ Manag* 195:93–99. <https://doi.org/10.1016/j.jenvman.2017.04.010>
- Di Iaconi C, Del Moro G, De Sanctis M, Rossetti S (2010) A chemically enhanced biological process for lowering operative costs and solid residues of industrial recalcitrant wastewater treatment. *Water Res* 44:3635–3644. <https://doi.org/10.1016/j.watres.2010.04.017>
- Dillert R, Cassano AE, Goslich R, Bahnemann D (1999) Large scale studies in solar catalytic wastewater treatment. *Catal Today* 54:267–282. [https://doi.org/10.1016/S0920-5861\(99\)00188-1](https://doi.org/10.1016/S0920-5861(99)00188-1)
- Dixit S, Yadav A, Dwivedi PD, Das M (2015) Toxic hazards of leather industry and technologies to combat threat: a review. *J Clean Prod* 87:39–49. <https://doi.org/10.1016/j.jclepro.2014.10.017>

- Doll TE, Frimmel FH (2005) Removal of selected persistent organic pollutants by heterogeneous photocatalysis in water. *Catal Today* 101:195–202. <https://doi.org/10.1016/j.cattod.2005.03.005>
- Du P, Carneiro JT, Moulijn JA, Mul G (2008) A novel photocatalytic monolith reactor for multiphase heterogeneous photocatalysis. *Appl Catal A Gen* 334:119–128. <https://doi.org/10.1016/j.apcata.2007.09.045>
- Espinoza-Quiñones FR, Fornari MMT, Módenes AN et al (2009) Pollutant removal from tannery effluent by electrocoagulation. *Chem Eng J* 151:59–65. <https://doi.org/10.1016/j.cej.2009.01.043>
- Fabbricino M, Naviglio B, Tortora G, d'Antonio L (2013) An environmental friendly cycle for Cr (III) removal and recovery from tannery wastewater. *J Environ Manag* 117:1–6. <https://doi.org/10.1016/j.jenvman.2012.12.012>
- Faust SD, Aly OM (2013) Removal of inorganic compounds. In: Adsorption processes for water treatment. Elsevier Science, Cambridge, pp 287–328
- Fazal S, Zhang B, Zhong Z et al (2015) Industrial wastewater treatment by using MBR (membrane bioreactor) review study. *J Environ Prot (Irvine, CA)* 6:584–598. <https://doi.org/10.4236/jep.2015.66053>
- Fernández P, Blanco J, Sichel C, Malato S (2005) Water disinfection by solar photocatalysis using compound parabolic collectors. *Catal Today* 101:345–352. <https://doi.org/10.1016/j.cattod.2005.03.062>
- Fernández-García A, Zarza E, Valenzuela L, Pérez M (2010) Parabolic-trough solar collectors and their applications. *Renew Sust Energ Rev* 14:1695–1721. <https://doi.org/10.1016/j.rser.2010.03.012>
- Fujishima A, Zhang X, Tryk DA (2007) Heterogeneous photocatalysis: from water photolysis to applications in environmental cleanup. *Int J Hydrog Energy* 32:2664–2672. <https://doi.org/10.1016/j.ijhydene.2006.09.009>
- Gang C, Man H, Liang C, Hui Chen D (2011) A batch decolorization and kinetic study of Reactive Black 5 by a bacterial strain *Enterobacter* sp. GY-1. *Int Biodeterior Biodegradation* 65:790–796
- Gernjak W, Krutzler T, Glaser A et al (2003) Photo-Fenton treatment of water containing natural phenolic pollutants. *Chemosphere* 50:71–78. [https://doi.org/10.1016/S0045-6535\(02\)00403-4](https://doi.org/10.1016/S0045-6535(02)00403-4)
- Gernjak W, Maldonado ML, Malato S et al (2004) Pilot-plant treatment of olive mill wastewater (OMW) by solar TiO₂ photocatalysis and solar photo-Fenton. *Sol Energy* 77:567–572. <https://doi.org/10.1016/j.solener.2004.03.030>
- Gonçalves MST, Pinto EMS, Nkeonye P, Oliveira-Campos AMF (2005) Degradation of C.I. Reactive Orange 4 and its simulated dyebath wastewater by heterogeneous photocatalysis. *Dyes Pigments* 64:135–139. <https://doi.org/10.1016/j.dyepig.2004.05.004>
- Görgün E, Insel G, Artan N, Orhon D (2007) Model evaluation of temperature dependency for carbon and nitrogen removal in a full-scale activated sludge plant treating leather-tanning wastewater. *J Environ Sci Health* 42:747–756. <https://doi.org/10.1080/10934520701304427>
- Guillard C, Disdier J, Herrmann JM et al (1999) Comparison of various titania samples of industrial origin in the solar photocatalytic detoxification of water containing 4-chlorophenol. *Catal Today* 54:217–228. [https://doi.org/10.1016/S0920-5861\(99\)00184-4](https://doi.org/10.1016/S0920-5861(99)00184-4)
- Guo Y, Hu C (2007) Heterogeneous photocatalysis by solid polyoxometalates. *J Mol Catal A Chem* 262:136–148. <https://doi.org/10.1016/j.molcata.2006.08.039>
- Herrmann JM (1995) Heterogeneous photocatalysis: an emerging discipline involving multiphase systems. *Catal Today* 24:157–164. [https://doi.org/10.1016/0920-5861\(95\)00005-Z](https://doi.org/10.1016/0920-5861(95)00005-Z)
- Hoffmann MR, Martin ST, Choi W, Bahnemann DW (1995) Environmental applications of semiconductor. *Photocatalysis*:69–96
- Houshyar Z, Khoshfetrat AB, Fatehifar E (2012) Influence of ozonation process on characteristics of pre-alkalized tannery effluents. *Chem Eng J* 191:59–65. <https://doi.org/10.1016/j.cej.2012.02.053>

- Insel HG, Görgün E, Artan N, Orhon D (2008) Model based optimization of nitrogen removal in a full scale activated sludge plant. *Environ Eng Sci* 26:471–480. <https://doi.org/10.1089/ees.2007.0272>
- Iorhemen OT, Hamza RA, Tay JH (2016) Membrane bioreactor (Mbr) technology for wastewater treatment and reclamation: membrane fouling. *Membranes (Basel)* 6:13–16. <https://doi.org/10.3390/membranes6020033>
- Islam MK, Hasanuzzaman M, Rahim NA (2015) Modelling and analysis of the effect of different parameters on a parabolic-trough concentrating solar system. *RSC Adv* 5:36540–36546. <https://doi.org/10.1039/c4ra12919a>
- Jerez S, Tobin I, Vautard R et al (2015) The impact of climate change on photovoltaic power generation in Europe. *Nat Commun*. <https://doi.org/10.1038/ncomms10014>
- Jung C, Funken KH, Ortner J (2005) PROPHIS: parabolic trough-facility for organic photochemical syntheses in sunlight. *Photochem Photobiol Sci* 4:409–411. <https://doi.org/10.1039/b500294j>
- Kabir E, Kumar P, Kumar S et al (2018) Solar energy: potential and future prospects. *Renew Sust Energ Rev* 82:894–900. <https://doi.org/10.1016/j.rser.2017.09.094>
- Keerthi SV, Mahalakshmi M, Balasubramanian N (2013) Development of hybrid membrane bioreactor for tannery effluent treatment. *Desalination* 309:231–236. <https://doi.org/10.1016/j.desal.2012.10.014>
- Kemeny N, Huang Y, Cohen AM (2000) Erratum: Hepatic arterial infusion of chemotherapy after resection of hepatic metastases from colorectal cancer (*N Engl J Med* (December 30, 1999) 341:2039–2048). *N Engl J Med* 342:1524. [https://doi.org/10.1016/0920-5861\(93\)80003-J](https://doi.org/10.1016/0920-5861(93)80003-J)
- Khataee AR, Zarei M, Ordikhani-Seyedlar R (2011) Heterogeneous photocatalysis of a dye solution using supported TiO₂ nanoparticles combined with homogeneous photoelectrochemical process: molecular degradation products. *J Mol Catal A Chem* 338:84–91. <https://doi.org/10.1016/j.molcata.2011.01.028>
- Kiliç M, Çınar Z (2008) Hydroxyl radical reactions with 4-chlorophenol as a model for heterogeneous photocatalysis. *J Mol Struct THEOCHEM* 851:263–270. <https://doi.org/10.1016/j.theochem.2007.11.022>
- Kim IS, Ekpeghere KI, Ha SY et al (2014) Full-scale biological treatment of tannery wastewater using the novel microbial consortium BM-S-1. *J Environ Sci Health* 49:355–364. <https://doi.org/10.1080/10934529.2014.846707>
- Kisch H (2010) On the problem of comparing rates or apparent quantum yields in heterogeneous photocatalysis. *Angew Chemie Int Ed* 49:9588–9589. <https://doi.org/10.1002/anie.201002653>
- Kisch H, Twardzik G (1991) Zinc sulfide catalyzed photoreduction of carbon dioxide. *Chem Ber*:1161–1162
- Kongjao S, Damronglerd S, Hunsom M (2008) Simultaneous removal of organic and inorganic pollutants in tannery wastewater using electrocoagulation technique. *Korean J Chem Eng* 25:703–709. <https://doi.org/10.1007/s11814-008-0115-1>
- Konstantinou IK, Albanis TA (2004) TiO₂-assisted photocatalytic degradation of azo dyes in aqueous solution: kinetic and mechanistic investigations: a review. *Appl Catal B Environ* 49:1–14. <https://doi.org/10.1016/j.apcatb.2003.11.010>
- Kositzi M, Poullos I, Malato S et al (2004) Solar photocatalytic treatment of synthetic municipal wastewater. *Water Res* 38:1147–1154. <https://doi.org/10.1016/j.watres.2003.11.024>
- Künne R, Twardzik G, Emig G, Kisch H (1993) Heterogeneous photocatalysis XI. Zinc sulphide catalysed dehydrodimerization of dihydropyrans and cyclohexene. *J Photochem Photobiol A Chem* 76:209–215. [https://doi.org/10.1016/1010-6030\(93\)80137-X](https://doi.org/10.1016/1010-6030(93)80137-X)
- Kurt U, Apaydin O, Gonullu MT (2007) Reduction of COD in wastewater from an organized tannery industrial region by Electro-Fenton process. *J Hazard Mater* 143:33–40. <https://doi.org/10.1016/j.jhazmat.2006.08.065>
- Kusturica M, Tomas A, Sabo A (2015) Disposal of unused drugs: knowledge and behaviour among people around the world. *Rev Environ Contam Toxicol* 240:77. <https://doi.org/10.1007/398>

- Lair A, Ferronato C, Chovelon JM, Herrmann JM (2008) Naphthalene degradation in water by heterogeneous photocatalysis: an investigation of the influence of inorganic anions. *J Photochem Photobiol A Chem* 193:193–203. <https://doi.org/10.1016/j.jphotochem.2007.06.025>
- Lins T, Dantas P, José HJ et al (2003) Fenton and Photo-Fenton oxidation of tannery wastewater. *Acta Sci Technol* 25:91–95
- Lofrano G, Aydin E, Russo F et al (2008) Characterization, fluxes and toxicity of leather tanning bath chemicals in a large tanning district area (IT). *Water Air Soil Pollut Focus* 8:529–542. <https://doi.org/10.1007/s11267-008-9177-7>
- Lofrano G, Meriç S, Zengin GE, Orhon D (2013) Chemical and biological treatment technologies for leather tannery chemicals and wastewaters: a review. *Sci Total Environ* 461–462:265–281. <https://doi.org/10.1016/j.scitotenv.2013.05.004>
- Malato S, Blanco J, Richter C et al (1997) Low-concentration CPC collectors for photocatalytic water detoxification: comparison with a medium concentrating solar collector. *Water Sci Technol* 35:157–164. [https://doi.org/10.1016/S0273-1223\(97\)00021-8](https://doi.org/10.1016/S0273-1223(97)00021-8)
- Malato S, Blanco J, Alarcón DC et al (2007a) Photocatalytic decontamination and disinfection of water with solar collectors. *Catal Today* 122:137–149. <https://doi.org/10.1016/j.cattod.2007.01.034>
- Malato S, Blanco J, Maldonado MI et al (2007b) Coupling solar photo-Fenton and biotreatment at industrial scale: main results of a demonstration plant. *J Hazard Mater* 146:440–446. <https://doi.org/10.1016/j.jhazmat.2007.04.084>
- Malato S, Fernández-Ibez P, Maldonado MI et al (2009) Decontamination and disinfection of water by solar photocatalysis: recent overview and trends. *Catal Today* 147:1–59. <https://doi.org/10.1016/j.cattod.2009.06.018>
- Mamba G, Mishra AK (2016) Graphitic carbon nitride (g-C₃N₄) nanocomposites: a new and exciting generation of visible light driven photocatalysts for environmental pollution remediation. *Appl Catal B Environ* 198:347–377. <https://doi.org/10.1016/j.apcatb.2016.05.052>
- Mannucci A, Munz G, Mori G, Lubello C (2010) Anaerobic treatment of vegetable tannery wastewaters: a review. *Desalination* 264:1–8
- Mannucci A, Munz G, Mori G, Lubello C (2014) Factors affecting biological sulphate reduction in tannery wastewater treatment. *Environ Eng Manag J* 13:1005–1012. <https://doi.org/10.30638/eemj.2014.104>
- Mant C, Costa S, Williams J, Tambourgi E (2006) Phytoremediation of chromium by model constructed wetland. *Bioresour Technol* 97:1767–1772. <https://doi.org/10.1016/j.biortech.2005.09.010>
- Módenes AN, Espinoza-Quñones FR, Borba FH, Manenti DR (2012) Performance evaluation of an integrated photo-Fenton – electrocoagulation process applied to pollutant removal from tannery effluent in batch system. *Chem Eng J* 197:1–9. <https://doi.org/10.1016/j.cej.2012.05.015>
- Nan M, Jin B, Chow CWK, Saint C (2010) Recent developments in photocatalytic water treatment technology: a review. *Water Res* 44:2997–3027. <https://doi.org/10.1016/j.watres.2010.02.039>
- Naumczyk JH, Kucharska MA (2017) Electrochemical treatment of tannery wastewater – Raw, coagulated, and pretreated by AOPs. *J Environ Sci Health* 52:649–664. <https://doi.org/10.1080/10934529.2017.1297140>
- Noorjahan CM (2014) Physicochemical characteristics, identification of bacteria and biodegradation of industrial effluent. *Indian J Appl Res* 4:678–682. <https://doi.org/10.15373/2249555x/august2014/178>
- Oelgemöller M, Healy N, De Oliveira L et al (2006) Green photochemistry: solar-chemical synthesis of Juglone with medium concentrated sunlight. *Green Chem* 8:831–834. <https://doi.org/10.1039/b605906f>
- Oller I, Gernjak W, Maldonado MI et al (2006) Solar photocatalytic degradation of some hazardous water-soluble pesticides at pilot-plant scale. *J Hazard Mater* 138:507–517. <https://doi.org/10.1016/j.jhazmat.2006.05.075>

- Ollis DF, Turchi C (1990) Heterogeneous photocatalysis for water purification: contaminant mineralization kinetics and elementary reactor analysis. *Environ Prog* 9:229–234. <https://doi.org/10.1002/ep.670090417>
- Onyancha D, Mavura W, Catherine Ngila J et al (2008) Studies of chromium removal from tannery wastewaters by algae biosorbents, *Spirogyra condensata* and *Rhizoclonium hieroglyphicum*. *J Hazard Mater* 158:605–614
- Palmisano G, Addamo M, Augugliaro V et al (2007) Selectivity of hydroxyl radical in the partial oxidation of aromatic compounds in heterogeneous photocatalysis. *Catal Today* 122:118–127. <https://doi.org/10.1016/j.cattod.2007.01.026>
- Peral J, Domènech X, Ollis DF (1997) Heterogeneous photocatalysis for purification, decontamination and deodorization of air. *J Chem Technol Biotechnol* 70:117–140. [https://doi.org/10.1002/\(SICI\)1097-4660\(199710\)70:2<117::AID-JCTB746>3.0.CO;2-F](https://doi.org/10.1002/(SICI)1097-4660(199710)70:2<117::AID-JCTB746>3.0.CO;2-F)
- Petrović M, Gonzalez S, Barceló D (2003) Analysis and removal of emerging contaminants in wastewater and drinking water. *TrAC Trends Anal Chem* 22:685–696. [https://doi.org/10.1016/S0165-9936\(03\)01105-1](https://doi.org/10.1016/S0165-9936(03)01105-1)
- Preethi V, Parama Kalyani KS, Iyappan K et al (2009) Ozonation of tannery effluent for removal of cod and color. *J Hazard Mater* 166:150–154. <https://doi.org/10.1016/j.jhazmat.2008.11.035>
- Rai UN, Dwivedi S, Tripathi RD et al (2005) Algal biomass: an economical method for removal of chromium from tannery effluent. *Bull Environ Contam Toxicol* 75:297–303. <https://doi.org/10.1007/s00128-005-0752-6>
- Raj A, Kumar S, Haq I, Kumar M (2014) Detection of tannery effluents induced DNA damage in mung bean by use of random amplified polymorphic DNA markers. *ISRN Biotechnol* 2014:1–8. <https://doi.org/10.1155/2014/727623>
- Ram B, Bajpai PK, Parwana HK (1999) Kinetics of chrome-tannery effluent treatment by the activated-sludge system. *Process Biochem* 35:255–265. [https://doi.org/10.1016/S0032-9592\(99\)00062-X](https://doi.org/10.1016/S0032-9592(99)00062-X)
- Rameshraj D, Suresh S (2011) Treatment of tannery wastewater by various oxidation and combined processes. *Int J Environ Res* 5:349–360
- Ranganathan K, Kabadgi SD (2011) Studies on feasibility of reverse osmosis (membrane) technology for treatment of tannery wastewater. *J Environ Prot (Irvine, CA)* 2:37–46. <https://doi.org/10.4236/jep.2011.21004>
- Robert D (2007) Photosensitization of TiO₂ by MxOy and MxSy nanoparticles for heterogeneous photocatalysis applications. *Catal Today* 122:20–26. <https://doi.org/10.1016/j.cattod.2007.01.060>
- Rodrigues AC, Boroski M, Shimada NS et al (2008) Treatment of paper pulp and paper mill wastewater by coagulation-flocculation followed by heterogeneous photocatalysis. *J Photochem Photobiol A Chem* 194:1–10. <https://doi.org/10.1016/j.jphotochem.2007.07.007>
- Sadik WA, Nashed AW, El-Demerdash AGM (2007) Photodecolourization of ponceau 4R by heterogeneous photocatalysis. *J Photochem Photobiol A Chem* 189:135–140. <https://doi.org/10.1016/j.jphotochem.2007.01.025>
- Saratale RG, Saratale GD, Chang JS, Govindwar SP (2010) Decolorization and biodegradation of reactive dyes and dye wastewater by a developed bacterial consortium. *Biodegradation* 21:999–1015. <https://doi.org/10.1007/s10532-010-9360-1>
- Sarria V, Kenfack S, Guillod O, Pulgarin C (2003) An innovative coupled solar-biological system at field pilot scale for the treatment of biorecalcitrant pollutants. *J Photochem Photobiol A Chem* 159:89–99. [https://doi.org/10.1016/S1010-6030\(03\)00105-9](https://doi.org/10.1016/S1010-6030(03)00105-9)
- Sauer TP, Casaril L, Oberziner ALB et al (2006) Advanced oxidation processes applied to tannery wastewater containing Direct Black 38-Elimination and degradation kinetics. *J Hazard Mater* 135:274–279. <https://doi.org/10.1016/j.jhazmat.2005.11.063>
- Saxena G, Chandra R, Bharagava RN (2016) Environmental pollution, toxicity profile and treatment approaches for tannery wastewater and its chemical pollutants. In: *Reviews of environmental contamination and toxicology*. Springer, Cham, pp 31–69
- Schiel C, Oelgemöller M, Ortner J, Mattay J (2001) Green photochemistry: the solar-chemical “Photo-Friedel-Crafts acylation” of quinones. *Green Chem* 3:224–228. <https://doi.org/10.1039/b106425h>

- Scholz W, Lucas M (2003) Techno-economic evaluation of membrane filtration for the recovery and re-use of tanning chemicals. *Water Res* 37:1859–1867. [https://doi.org/10.1016/S0043-1354\(02\)00560-2](https://doi.org/10.1016/S0043-1354(02)00560-2)
- Schrank SG, José HJ, Moreira RFP, Schröder HF (2004) Elucidation of the behavior of tannery wastewater under advanced oxidation conditions. *Chemosphere* 56:411–423. <https://doi.org/10.1016/j.chemosphere.2004.04.012>
- Schrank SG, José HJ, Moreira RFP, Schröder HF (2005) Applicability of Fenton and H₂O₂/UV reactions in the treatment of tannery wastewaters. *Chemosphere* 60:644–655. <https://doi.org/10.1016/j.chemosphere.2005.01.033>
- Schrank SG, Bieling U, Jos HJ et al (2009) Generation of endocrine disruptor compounds during ozone treatment of tannery wastewater confirmed by biological effect analysis and substance specific analysis. *Water Sci Technol* 59:31–38. <https://doi.org/10.2166/wst.2009.762>
- Dogruel S, Ates Genceli E (2004) Ozonation of non biodegradable organics in tannery wastewater. *J Environ Sci Health Part A* 39:1705–1715
- Serpone N (1995) Brief introductory remarks on heterogeneous photocatalysis. *Sol Energy Mater Sol Cells* 38:369–379. [https://doi.org/10.1016/0927-0248\(94\)00230-4](https://doi.org/10.1016/0927-0248(94)00230-4)
- Serpone N, Sauvé G, Koch R et al (1996) Standardization protocol of process efficiencies and activation parameters in heterogeneous photocatalysis: relative photonic efficiencies ζ_r . *J Photochem Photobiol A Chem* 94:191–203. [https://doi.org/10.1016/1010-6030\(95\)04223-7](https://doi.org/10.1016/1010-6030(95)04223-7)
- Shakoori AR, Makhdoom M, Haq RU (2000) Hexavalent chromium reduction by a dichromate-resistant gram-positive bacterium isolated from effluents of tanneries. *Appl Microbiol Biotechnol* 53:348–351
- Shan AY, Ghazi TIM, Rashid SA (2010) Immobilisation of titanium dioxide onto supporting materials in heterogeneous photocatalysis: a review. *Appl Catal A Gen* 389:1–8. <https://doi.org/10.1016/j.apcata.2010.08.053>
- Shimura K, Yoshida H (2011) Heterogeneous photocatalytic hydrogen production from water and biomass derivatives. *Energy Environ Sci* 4:2467. <https://doi.org/10.1039/c1ee01120k>
- Silva AMT, Nouli E, Xekoukoulotakis NP, Mantzavinos D (2007) Effect of key operating parameters on phenols degradation during H₂O₂-assisted TiO₂ photocatalytic treatment of simulated and actual olive mill wastewaters. *Appl Catal B Environ* 73:11–22. <https://doi.org/10.1016/j.apcatb.2006.12.007>
- Silva TFCV, Silva MEF, Cristina Cunha-Queda A et al (2013) Sanitary landfill leachate treatment using combined solar photo-Fenton and biological oxidation processes at pre-industrial scale. *Chem Eng J* 228:850–866. <https://doi.org/10.1016/j.cej.2013.05.060>
- Simonsen ME (2014) Heterogeneous photocatalysis. *Chem Adv Environ Purif Process Water Fundam Appl*:135–170. <https://doi.org/10.1016/B978-0-444-53178-0.00004-3>
- Sirtori C, Altwater PK, Freitas AMD, Peralta-Zamora PG (2006) Degradation of aqueous solutions of camphor by heterogeneous photocatalysis. *J Hazard Mater* 129:110–115. <https://doi.org/10.1016/j.jhazmat.2005.08.017>
- Sivagami K, Sakthivel KP, Nambi IM (2018) Advanced oxidation processes for the treatment of tannery wastewater. *J Environ Chem Eng* 6:3656–3663. <https://doi.org/10.1016/j.jece.2017.06.004>
- Song Z, Williams CJ, Edyvean RGJ (2004) Treatment of tannery wastewater by chemical coagulation. *Desalination* 164:249–259
- Spasiano D, Marotta R, Malato S et al (2015) Solar photocatalysis: materials, reactors, some commercial, and pre-industrialized applications. A comprehensive approach. *Appl Catal B Environ* 170–171:90–123. <https://doi.org/10.1016/j.apcatb.2014.12.050>
- Srivastava S, Thakur IS (2006) Isolation and process parameter optimization of *Aspergillus* sp. for removal of chromium from tannery effluent. *Bioresour Technol* 97:1167–1173
- Srivastava S, Ahmad A, Thakur IS (2007) Removal of chromium and pentachlorophenol from tannery effluents. *Bioresour Technol* 98:1128–1132

- Sundarapandiyan S, Chandrasekar R, Ramanaiah B et al (2010) Electrochemical oxidation and reuse of tannery saline wastewater. *J Hazard Mater* 180:197–203. <https://doi.org/10.1016/j.jhazmat.2010.04.013>
- Tadesse I, Green FB, Puhakka JA (2004) Seasonal and diurnal variations of temperature, pH and dissolved oxygen in advanced integrated wastewater pond system® treating tannery effluent. *Water Res* 38:645–654. <https://doi.org/10.1016/j.watres.2003.10.006>
- Tripathi A, Narayanan S (2018) Impact of TiO₂ and TiO₂/g-C₃N₄ nanocomposite to treat industrial wastewater. *Environ Nanotechnol Monit Manag* 10:280–291. <https://doi.org/10.1016/j.enmm.2018.07.010>
- Tripathi A, Narayanan S (2019a) Skeletal tailoring of two-dimensional π -conjugated polymer (g-C₃N₄) through sodium salt for solar-light driven photocatalysis. *J Photochem Photobiol A Chem* 373:1–11. <https://doi.org/10.1016/j.jphotochem.2018.12.031>
- Tripathi A, Narayanan S (2019b) Potassium doped graphitic carbon nitride with extended optical absorbance for solar light driven photocatalysis. *Appl Surf Sci* 479:1–11. <https://doi.org/10.1016/j.apsusc.2019.01.265>
- Ustinovich EA, Shchukin DG, Sviridov DV (2005) Heterogeneous photocatalysis in titania-stabilized perfluorocarbon-in-water emulsions: urea photosynthesis and chloroform photodegradation. *J Photochem Photobiol A Chem* 175:249–252. <https://doi.org/10.1016/j.jphotochem.2005.04.037>
- Valencia S, Cataño F, Rios L et al (2011) A new kinetic model for heterogeneous photocatalysis with titanium dioxide: case of non-specific adsorption considering back reaction. *Appl Catal B Environ* 104:300–304. <https://doi.org/10.1016/j.apcatb.2011.03.015>
- Vankar P, Bajpai D (2008) Phyto-remediation of chrome-VI of tannery effluent by *Trichoderma* species. *Desalination* 222:255–262
- Verma T, Rameke PW, Garg SK (2008) Quality assessment of treated tannery wastewater with special emphasis on pathogenic *E. coli* detection through serotyping. *Environ Monit Assess* 145:243–249. <https://doi.org/10.1007/s10661-007-0033-4>
- Vidal A, Herrero J, Romero M et al (1994) Heterogeneous photocatalysis: degradation of ethylbenzene in TiO₂ aqueous suspensions. *J Photochem Photobiol A Chem* 79:213–219. [https://doi.org/10.1016/1010-6030\(93\)03763-7](https://doi.org/10.1016/1010-6030(93)03763-7)
- Wang H, Wang Y, Zhou L (2011a) Purification and recycling of tannery degreasing wastewater by ultrafiltration with polyimide membrane. In: International conference on Remote Sensing, Environment and Transportation Engineering, Nanjing
- Wang Z, Ma W, Chen C et al (2011b) Probing paramagnetic species in titania-based heterogeneous photocatalysis by electron spin resonance (ESR) spectroscopy – a mini review. *Chem Eng J* 170:353–362. <https://doi.org/10.1016/j.cej.2010.12.002>
- Will IBS, Moraes JEF, Teixeira ACSC et al (2004) Photo-Fenton degradation of wastewater containing organic compounds in solar reactors. *Sep Purif Technol* 34:51–57. [https://doi.org/10.1016/S1383-5866\(03\)00174-6](https://doi.org/10.1016/S1383-5866(03)00174-6)
- Xiong L, Sun W, Yang Y et al (2011) Heterogeneous photocatalysis of methylene blue over titanate nanotubes: effect of adsorption. *J Colloid Interface Sci* 356:211–216. <https://doi.org/10.1016/j.jcis.2010.12.059>
- Yuan-Shan W, Zhi-Yan P, Jian-Min L et al (2007) Bioleaching of chromium from tannery sludge by indigenous *Acidithiobacillus thiooxidans*. *J Hazard Mater* 147:319–324

Chapter 12

Functionalized Ionic Liquids for the Photodegradation of Dyes



Dipesh S. Patle, Vijay Khajone, Pundlik R. Bhagat, Arvind K. Jaiswal, and
Sushil Kumar

Contents

| | | |
|------|--|-----|
| 12.1 | Introduction | 392 |
| 12.2 | Ionic Liquids | 393 |
| 12.3 | Functionalization of Ionic Liquids | 395 |
| 12.4 | Applications of IL in Wastewater Treatment | 397 |
| 12.5 | Degradation of Dyes Using Functionalized Ionic Liquids | 398 |
| 12.6 | Case Study: Photodegradation of Organic Dyes, Methylene Blue, and Congo Red Using a Polymer-Supported Ionic Liquid Fe-Porphyrin Complex | 398 |
| | 12.6.1 Synthesis of a Polymer-Supported Ionic Liquid Fe-Porphyrin Complex | 398 |
| | 12.6.2 Photodegradation of Methylene Blue and Congo Red | 402 |
| | 12.6.3 Possible Mechanism | 405 |
| 12.7 | Conclusions | 406 |
| | References | 406 |

Abstract From the last few decades, environmental pollution is one of the major problems of the modern world. Increased industrialization has caused a serious problem of water pollution as it has led to the discharge of toxic and hazardous chemicals into the water bodies. Dyes are the main class of organic compounds that pollute the water. Hence, their effective removal is inescapable. The presence of metal ions is also a serious problem. Due to low volatility, chemical stability, and chelating abilities of ionic liquids, the application of functionalized ionic liquids can effectively reduce the amount of these pollutants.

In this chapter, the properties of ionic liquids which make them suitable for wastewater treatment are presented, and design ability of the functionalized ionic

D. S. Patle · A. K. Jaiswal · S. Kumar (✉)
Department of Chemical Engineering, Motilal Nehru National Institute of Technology,
Allahabad, Prayagraj, Uttar Pradesh, India
e-mail: dipesh-patle@mnnit.ac.in

V. Khajone · P. R. Bhagat (✉)
School of Advance Science, Vellore Institute of Technology, Vellore, Tamil Nadu, India

liquids/task-specific ionic liquids provides better opportunities to change the structures in cation and anion to achieve functionalized ionic liquid for specific pollutant removal. Therefore, recent applications of functionalized ionic liquids for the treatment of metal ions and different dyes are discussed. Later, a case study on the photodegradation with possible mechanisms of organic dyes, namely, methylene blue and congo red using a synthesized polymer-supported ionic liquid Fe-porphyrin complex is presented. Catalyst loadings of 10 mg and 12.5 mg at constant time of 60 min are found to be a better choice for the photodegradation of methylene blue and congo red dyes, respectively. The highest photodegradations of methylene blue and congo red are found to be ~78% and ~99%, respectively.

Keywords Wastewater treatment · Functionalized ionic liquids · Photodegradation · Organic dyes · Polymer supported ionic liquid iron porphyrin

12.1 Introduction

Approximately 7,00,000 tons of dyes are manufactured worldwide annually; wherein about 60% is azo dye out of which 10–15% of azo dyes is passed in the water system (Langhals 2004). Azo dyes are classified as acidic, basic, disperse, reactive, direct, and solvents/food dyes. An azo dye which is derived from benzidine, $C_{12}H_{12}N_2$ is the main segment of carcinogenicity. Textile industries use a huge amount of freshwater for dyeing and processing, which discharge large amount of chemical pollutants like organic surfactants, dyes, dispersants, alkalis, acids, solvents, and various salts into the water bodies. The presence of dyes in water creates acute aesthetic and aquatic problems by disturbing the photosynthetic reaction due to light penetration. So, it is essential to focus on wastewater treatment technologies for its reuse and recycle. From the view of an environment, severe problems such as toxicity to water bodies and foremost to carcinogenic and mutagenic effects on humans are created by the textile-based industries (Dalvand et al. 2011; Du et al. 2017). The removal/treatment of dyes from polluted wastewater is comparatively more significant than the other soluble polluted compounds, which also add the portion of biochemical oxygen demand (Holkar et al. 2016). Many methods exist to eradicate harmful dyes from wastewater such as coagulation, an electrochemical process, membrane separation process, chemical oxidation, adsorption, reverse osmosis, and biodegradation. But most of these processes are not so acceptable due to additional chemical demand, producing large amount of secondary by products with their disposal problem and monetary disadvantages. A massive amount of such dyes in wastewater is nonbiodegradable because of their complex and stable molecular structures.

The drawback with the conventional biological methods (Shankar et al. 1999) is the treatment period. Treatment period typically varies from 1 day to 6 days. In

addition, traditional processes (physical and chemical) are found to be comparatively expensive and may also lead to other secondary pollution due to the requirement of additional chemicals (Oller et al. 2011). Conventional biological procedures in association with physical/chemical processes to obtain improved decolorization of effluents may generally be costly and limited applicable. The adsorption processes using suitable adsorbents (activated carbons, charcoals, clays, diatomaceous earth, microbial biomass, compost, unmodified and modified lignocellulose, etc.) for the wastewater treatment have disadvantage of regeneration, which also increases the cost of the process. At times, it demands a very long time, and it may be ineffective for low concentrations of pollutants. Oxidation can be used to decolorize the dye effluent using various oxidizing agents such as hydrogen peroxide and ozone activated with Fe(II) salts. However, the pollutant removal mechanisms involve flocculation, and contaminants are shifted from the wastewater to the sludge, which further demands disposal in landfill (Boczkaj and Fernandes 2017; De Lima et al. 2017). Hence, the abovementioned techniques may not provide sustained solution with ecological point of view. Very recently, electrochemical treatment methods have achieved a good position as effective and efficient treatment technologies for dye effluents. However, the application of electrochemical techniques warrants a higher investment in equipment and energy requirement (Vaghela et al. 2005; Butler et al. 2011; Gautam et al. 2019).

In the recent years, researchers have used ionic liquids for various applications such as biocatalytic transformation, chemical synthesis, electrochemistry, analytical chemistry, and separation processes, because of the green characteristics of ionic liquids (Wasserscheid and Keim 2000; van Rantwijk et al. 2003; Pandey 2006; Hernández-Fernández et al. 2015). Main advantages of ionic liquids are the better possibilities of reusing and relatively easy recovery of ionic liquids. Therefore, application of ionic liquids effectively reduces the amount of waste generated during treatment process. The photodegradation of dye molecules using ionic liquids (ionic liquids), also regarded as green solvents, has advantageous over other processes with the view of environment protection. However, ionic liquids are still quite expensive. Hence, regeneration and recycling of ionic liquids are important to make a technology economically viable (Fernández et al. 2010). The scheme to reduce the amount of pollutants from industrial effluents using ionic liquids and potential sources of environmental release is presented in Fig. 12.1.

12.2 Ionic Liquids

An ionic liquid is a molten salt comprising of positive charged ions, cations and negative charged ions, anions having melting point below 100 °C. Combination of bulky and asymmetrical cations such as imidazolium, pyrrolidinium, and pyridinium and evenly shaped symmetrical anions such as halides, triflate, and nitrate lowers the lattice energy which is accounted for low melting points. Ionic liquids are also known as liquid electrolytes, room temperature molten salts, low temperature molten

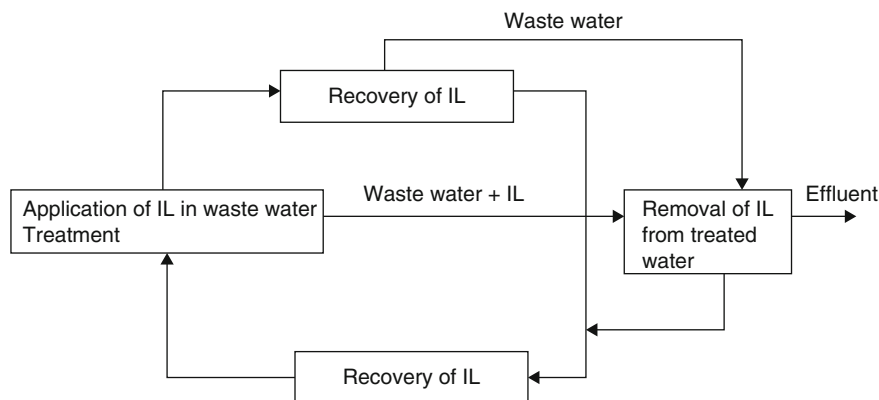
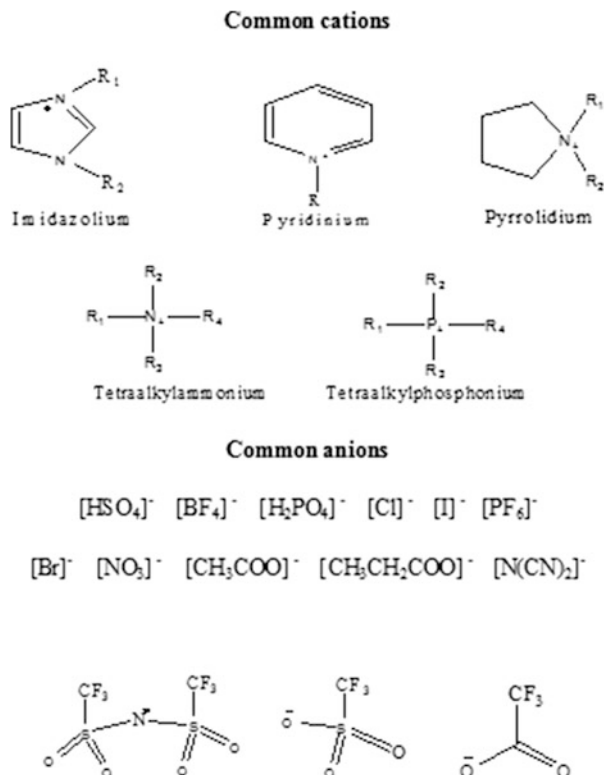


Fig. 12.1 The scheme to reduce the amount of pollutants from industrial effluents using ionic liquids (IL)

salts, ambient temperature molten salts, ionic melts, ionic fluids, fused salts, liquid salts, ionic glasses, or neoteric solvents (Wilkes 2002). Room temperature ionic liquids are salts which are in liquid state at or below room temperature. The structures of common cations and anions of ionic liquids are presented in Fig. 12.2. Ionic liquids are gaining worldwide acknowledgement from researchers as well as people in the industries for a large number of applications (Heintz and Wertz 2006).

Depending on the cation and anion, the characteristics of ionic liquids, e.g., viscosity, solubility, and cloud point, may differ. The main benefit of ionic liquids is the provision of the replacement of anion that enables developing compounds with characteristics necessary for specific application. These tuned salts are referred to as task-specific ionic liquids/functionalized ionic liquids. Moreover, non-volatility, non-flammability, and better thermal stability make ionic liquids very attractive for industrial applications. Ionic liquids also have excellent features for removal of organic pollutants and metal ions because of its low volatility, chemical stability, and chelating abilities (Domanska and Rekaewek 2009; Egorov et al. 2010; Regel-Rosocka and Wisniewski 2011). Ionic liquids consist of loosely coordinating bulky ions with the polarities comparable to alcohols. In addition to negligible vapor pressure, ionic liquids are nonexplosive and nonflammable. Ionic liquids have application in fields such as electrochemical, photo-degradation of organic compounds, catalysis and/or reaction media, drug delivery, biotransformation, solar cells, and various areas of separations (Patel and Lee 2012). The tailored ionic liquids used in reaction media and separation processes are reported to show better activity, selectivity, yields, stability, and environmental safety than conventional solvents (Dietz 2006; Han and Row 2010; Bollin and Viamajala 2012). An overview of physical properties such as density and viscosity of selected ionic liquids used in separations are presented in Table 12.1 (Han and Row 2010). The design ability of the functionalized ionic liquids/task-specific ionic liquids provides better

Fig. 12.2 Structure of common cations and anions of ionic liquids. (Sun and Armstrong 2010)

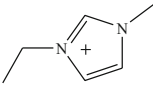
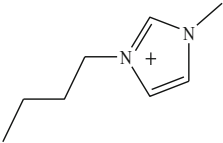
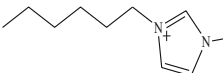
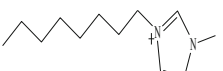
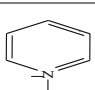
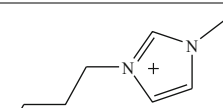
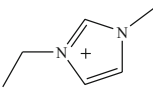


opportunities to change the structures in cation and anion, and the length of the side chain can also be altered to the organic cation to achieve tailored/ functionalized ionic liquid of special properties.

12.3 Functionalization of Ionic Liquids

The chemo-physical properties of ionic liquids depend on the cation-anion combination and the length of alkyl chain. The functionality of ionic liquids also has a strong effect on the properties. Thus, the synthesis of functionalized ionic liquids is generally performed by the integration of functional groups into the cation of ionic liquid. Till date, mostly, the imidazolium cations are functionalized, and a few functionalized anions are known. Imidazolium cations can be modified using functionalized groups such as alkyl halides, hydroxyl groups, carboxylic groups, thiol groups, alkene groups, diene groups, and so on (Ye and Shreeve 2004; Fei et al. 2005). Using the quaternization method, most of the functional groups directly added imidazolium moiety and give the desired functionalized ionic liquids. Certain functionalities require other synthetic routes to be connected to the imidazole

Table 12.1 Physical properties of ionic liquids at 25 °C

| Cation | Anion | Abbreviation | Melting Point °C | Density g ml ⁻¹ | Viscosity cP |
|--|---|--|------------------|----------------------------|--------------|
|  | [BF ₄] ⁻ | [C ₂ mim][BF ₄] | 6 | 1.248 | 66 |
| | [PF ₆] ⁻ | [C ₂ mim][PF ₆] | 58–62 | 1.373 | 450 |
|  | [BF ₄] ⁻ | [C ₄ mim][BF ₄] | -82 | 1.208 | 233 |
| | [PF ₆] ⁻ | [C ₄ mim][PF ₆] | 10 | 1.373 | 400 |
| | [CF ₃ SO ₃] ⁻ | [C ₄ mim][CF ₃ SO ₃] | 16 | 1.290 | 90 |
| | [Tf ₂ N] ⁻ | [C ₄ mim][Tf ₂ N] | -8 | 1.404 | 48 |
|  | [BF ₄] ⁻ | [C ₆ mim][BF ₄] | -82 | 1.075 | 211 |
| | [PF ₆] ⁻ | [C ₆ mim][PF ₆] | -61 | 1.304 | 800 |
|  | [BF ₄] ⁻ | [C ₈ mim][BF ₄] | -79 | 1.11 | 440 |
| | [Cl] ⁻ | [C ₈ mim][Cl] | 0 | 1.000 | 16,000 |
|  | [Tf ₂ N] ⁻ | [C ₁ pyr][Tf ₂ N] | 0 | 1.44 | 39 |
|  | [Br] | [C ₄ mim][Br] | 65–75 | 1.3 | 1486.49 |
| | [N(CN) ₂] | [C ₄ mim][N(CN) ₂] | -6 | 1.06 | 334 |
| | [CH ₃ COO] | [C ₄ mim][CH ₃ COO] | -20 | 1,02 | 440 |
|  | [C ₄ SO ₃] | [C ₂ mim][C ₄ SO ₃] | 1–7 | 1.17 | 180.8 |

Han and Row (2010)

C = alkyl group; mim = methyl imidazolium; pyr = pyridinium

backbone (Liddle and Arnold 2005). The imidazolium salts with SiOMe₃ groups can also be synthesized with greater yield using direct quaternization. The hydrophilicity of these imidazolium salts may be controlled on the surfaces of Si/SiO₂ by anion exchange (Gao et al. 2004).

Less attention was given on the synthesis of pyridinium-based functionalized ionic liquids rather than imidazolium systems. Pyridinium-based ionic liquids are successfully functionalized as the nitrile salt, 1,2,4-substitute-triazolium salts, and phosphazene-based ionic liquids. Other low melting salts have also been formed using quaternization of pyrazine and pyrimidine with alkyl and polyfluoroalkyl halides. Functionalized ammonium ionic liquids, also known as ammonium salts, have been synthesized with ether groups. The ammonium salts show enhancement in cathodic and anodic stability and provide larger electrochemical window (Zhao 2007).

12.4 Applications of IL in Wastewater Treatment

Ionic liquids have excellent features for extraction of metal ions/organic pollutants from aqueous solutions because of its low volatility, chemical stability, and chelating abilities. In this section, few recent studies are discussed particularly extraction of heavy metals/others from wastewater using functionalized and modified ionic liquids as presented in Table 12.2. Major findings of the study appeared in the literature are presented in this table.

Table 12.2 Few selected studies on the wastewater treatment using ionic liquids

| Pollutants | Treated by | Major findings | Reference |
|---|--|--|--------------------------|
| Heavy metals (Cr, Cu, Cd, Ni, Pb, and Zn) | Ammonium and phosphonium-based ionic liquids (Ionic liquids) | The removal of heavy metals (Cu, Ni, and Zn) was achieved $\geq 90\%$ | Fuerhacker et al. (2012) |
| Lead [Pb(II)] | 1-Butyl-3-methylimidazolium bis(trifluoromethylsulfonyl) imide (C4) and 1-hexyl-3-methylimidazolium bis (trifluoromethylsulfonyl) imide (C6) | These ionic liquids are modified using silica sorbents by direct immobilization on silica surface. The effect of sorbent dosage, pH, time of contact, sorbate concentration, and temperature is considered | Saleem et al. (2014) |
| Phthalic acid | [TBP][CF ₃ SO ₃], [OMPYR][BF ₄] and [C4DMIM][CF ₃ SO ₃] | The ionic liquids are found to be possible solvent for the treatment of organic effluent-rich water and wastewater | Pilli et al. (2014) |
| Phenol and phenolic compounds | Trioctylphosphine oxide 90% (Cyanex – 923) with room temperature ionic liquids, RTIL | RTIL encapsulated polymer microcapsules prepared using styrene and divinylbenzene as adsorbent can be effectively employed for the adsorption of phenol and other phenolic compounds | Archana et al. (2016) |
| Cu ²⁺ , Ni ²⁺ , Pb ²⁺ , Cd ²⁺ , Ag ⁺ | Dendritic ionic liquids, four ionic liquids based on Tf ₂ N ⁻ and BF ₄ ⁻ anions | Extraction of Cu ²⁺ , Pb ²⁺ and Ag ⁺ cations is achieved up to 98% | Hayouni et al. (2018) |
| Mercury (Hg) | Polymer membrane incorporating ionic liquids [thiosalicylate (TOMATS) or salicylate (TOMAS)] | TOMATS has given better results. A PIM made of 50% cellulose triacetate, 30% TOMATS, and 20% nitrophenyl octyl ether as a plasticizer enabled the effective transport of Hg | Sergi et al. (2019) |
| Phenolic compounds | Ionic liquid, 1-ethyl-3-methyl imidazolium cyanoborohydride | The process conditions such as temperature, time, and phase volume ratio of ionic liquid and phenol concentration are optimized for its extraction from wastewater | Mathews et al. (2019) |

12.5 Degradation of Dyes Using Functionalized Ionic Liquids

Ionic liquids have found the recent applications in fields such as electrochemical, photo-degradation of organic compounds, catalysis and/or reaction media, drug delivery, biotransformation, and various areas of separations (Patel and Lee 2012). In this section of the chapter, recent and selected studies have been presented in Table 12.3 for the degradation of various dyes such as methyl orange, methylene blue, rhodamine B, indigo blue, and Sudan III using the functionalized ionic liquids. Applicable ionic liquids are also assisted by incorporating different nanoparticles such as Ag and TiO₂. It is clear from Table 12.3 that ionic liquids can be effectively used for the effective removal of the dyes. The following section describes a case study on the photodegradation of organic dyes, namely, methylene blue and congo red, using a polymer-supported ionic liquid Fe-porphyrin complex.

12.6 Case Study: Photodegradation of Organic Dyes, Methylene Blue, and Congo Red Using a Polymer-Supported Ionic Liquid Fe-Porphyrin Complex

In this case study, a polymer-supported ionic liquid Fe-porphyrin complex was synthesized using the procedure described below. Ionic liquid complex was tested for the photodegradation of the organic dyes, namely, methylene blue and congo red. Results were analyzed using several characterization techniques.

12.6.1 Synthesis of a Polymer-Supported Ionic Liquid Fe-Porphyrin Complex

Synthesis of Poly 1-(4-(sec-butyl) benzyl)-3-(3-formyl-4-hydroxybenzyl)-1H-benzo[d]imidazol-3-ium chloride, 1-A

For the synthesis of a polymer-supported ionic liquid Fe-porphyrin complex, firstly, equal moles of poly 1-(4-s-butyl) benzyl)-1H-benzo[d]imidazole, 0.02 mol/5.284 g and 5-(chloromethyl)-2-hydroxybenz-aldehyde, 0.02 mol/3.411 g were taken and mixed in the round bottle flask of 100 mL with acetonitrile of 25 mL. The complete reaction mixture was agitated 24 h using a magnetic stirrer at ambient temperature. After completion of reaction, a new compound was formed and washed using a solvent, diethyl ether to acquire white powder form of 1D (Balange et al. 2017, 2018). The yield and melting point of the resultant compound were determined as 68.99% and 180–198 °C, respectively.

Table 12.3 Recent studies on degradation of dyes using functionalized ionic liquids

| Type of dye | Ionic liquids | Major findings | Reference |
|--|--|---|---------------------------|
| Anionic dyes (methyl orange, eosin yellow, and orange G) | Imidazolium-based ionic liquids [C4mim][PF6], [C6mim][PF6], [C6mim][BF4], and [C8mim][PF6] | The extraction efficiencies of methyl orange, eosin yellows, and orange G are found as 85–99%, almost 100% and 69%, respectively, in tested water under the optimized conditions | Pei et al. (2007) |
| Dyes (methyl blue and chromium ions) | Hydrophobic poly(ionic liquid) of poly(3-ethyl-1-vinylimidazolium bis(trifluoromethanesulfonyl)imide) (PVI-TFSI) | The maximum adsorbed efficiencies for Cr (VI) and methyl blue are 98.0% and 97.6%, respectively, and maximum adsorption capacities of PVI-TFSI are 476.2 and 17.9 mg/g for methyl blue and Cr(VI), respectively | Hao et al. (2013) |
| Methyl orange (MO) and rhodamine B (RhB) Dyes | 1-Butyl-3-methylimidazolium tetrafluoroborate, [Bmim]BF ₄ with Degussa P25 TiO ₂ | This paper presents new insights of photocatalysis mechanism, which is occurring on functional group, TiO ₂ and the design for enhancement of photocatalytic performance | Qi et al. (2013) |
| Set of textile dyes (chloranilic acid, indigo blue, and sudan III) | Ionic liquids (phosphonium- and imidazolium-based) and an inorganic (aluminum sulfate) or organic salt (potassium citrate) | Authors have revealed that a proper IL and salt can be used to extract these dyes to the IL-rich phase in a single step process | Ferreir et al. (2014) |
| Azo dye (trypan blue) | Ionic liquid-assisted hydrothermal synthesis of TiO ₂ nanoparticles; ionic liquid: [BMI]CH ₃ SO ₃ | Ionic liquid-assisted TiO ₂ nanoparticles exhibited the excellent photocatalytic activity for the photodegradation of dye and trypan blue and also reduce the amount of Cr + 6 to Cr + 3 | Ravishankar et al. (2015) |
| Methyl orange (MO), methylene blue (MB) and rhodamine B (RhB) | Synthesized silver chloride nanoparticles and the ionic liquid trihexyl(tetradecyl) phosphonium chloride | The degradation efficiencies are found to be 98.4% for MO, 98.6% for MB, and 99.9% for RhB in 1 h | Rodríguez et al. (2017) |

(continued)

Table 12.3 (continued)

| Type of dye | Ionic liquids | Major findings | Reference |
|---------------------------------|---|--|--------------------|
| Anionic azo dyes, methyl orange | Silver nanostructures in ionic liquid media (1-butyl-3-methylimidazolium tetrafluoroborate) | Results confirmed that Ag nanostructures using silver nitrate incorporated in ionic liquid media have shown good photocatalytic efficiency for the degradation of dyes | Park et al. (2019) |

¹H NMR (400 MHz, DMSO-d₆): δ 0.52 (s, 1H), 0.74 (br. 1H), 1.08 (br. 1H), 1.29 (s, 1H), 1.92 (s, 1H), 5.65 (s, 4H), 7.36 (br. 6H), 7.73 (br. 1H), 10.13 (d, 2H, J = 8.97 Hz), 15.79 (br. 1H). ¹³C NMR (100 MHz, DMSO-d₆): 190.77, 161.74, 159.18, 136.94, 135.46, 131.29, 129.18, 127.15, 122.94, 118.64, 114.49, 49.76. FT-IR – (KBr, v/cm⁻¹): 3377.36, 3018.60, 2926.01, 1654.92, 1612.49, 1558.48, 1487.12, 1444.68, 1371.39, 1282.66, 1249.87, 1188.15, 1151.50, 1016.49, 929.69, 842.89, 744.52, 698.23, 632.65, 540.07, 497.63, 424.34.

Synthesis of 3-(2-carboxyethyl)-1-(3-formyl-4-hydroxybenzyl)-1H-benzo[d]imidazol-3-ium bromide, 1-B

The synthesis of 3-(2-carboxyethyl)-1-(3-formyl-4-hydroxybenzyl)-1H-benzo[d]imidazol-3-ium bromide was carried out according to the procedure given in (Muskarwar et al. 2013; Khiratkar et al. 2016) with slight modification. 5-(1-H-benzo[d]imidazole-1-yl) methyl-2-hydroxybenzaldehyde (BMSA), 7.56 g/30 mmol was stirred for 1 h in toluene solution of 50 ml at 60 °C. Then, 3-bromopropionic acid of 6.08 g/40 mmol in toluene was added drop wise for 30 min and stirred for next 14 h at 85 °C. After this, the whitish solid product was obtained, after the decantation of toluene and washing with ethyl acetate, 3 × 20 mL and diethyl ether, 3 × 25 mL with yield of 73.33%, and melting point of 205 °C.

¹H NMR (400 MHz, DMSO-d₆): δ 2.63 (s, 2H), 4.33 (s, 2H), 5.35 (s, 2H), 6.67 (s, 1H), 7.15 (s, 1H), 7.29 (s, 1H), 7.50 (d, 1H, J = 19.52 Hz), 7.75 (s, 1H), 9.24 (s, 1H), 9.58 (s, 1H), 9.88 (s, 1H), 10.55 (s, 1H), 12.32 (1H, br), 15.58 (1H, br), ¹³C NMR (100 MHz, DMSO-d₆): 190.97, 172.31, 161.49, 161.32, 142.40, 142.57, 136.53, 129.55, 127.12, 126.01, 125.24, 122.90, 118.48, 116.31, 114.47, 114.34, 113.51, 65.36, 49.56, 33.21, 15.63. FT-IR – (KBr, v/cm⁻¹): 3360, 3120, 1720, 1560, 1440, 1249, 1184, 1128, 989, 823, 744, 626, 495.

Synthesis of 1,1'1''-(((20-(5-((3-(4-(sec-butyl)benzyl)-1H-benzo[d]imidazole-3-ium-1-yl)methyl)-2-hydroxyphenyl)porohyrin-5,10,15-triyl)tris(4-hydroxybenzene-3,1-diyl))tris(methylene))tris(3-(2-carboxyethyl)-1H-benzo[d]imidazole-3-ium) tribromide chloride, (PSILPP) ligand 1-C

1-(4-(sec-butyl)benzyl)-3-(3-formyl-4-hydroxybenzyl)-1H-benzo[d]imidazol-3-ium chloride, **1-A** of 1.01 g/2.5 mmol and 3-(2-carboxyethyl)-1-(3-formyl-4-hydroxybenzyl)-1H-benzo[d]imidazol-3-ium bromide, and **1-B** of 3.039 g/7.5 mmol were mixed thoroughly in propionic acid, 20 mL at 60 °C for 30 min.

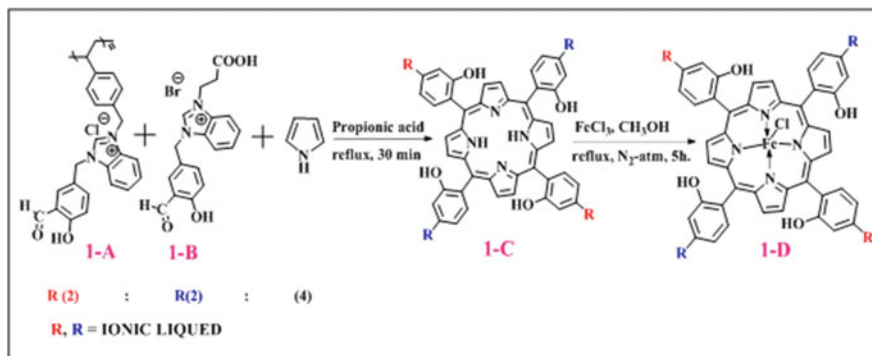


Fig. 12.3 Synthesis of polymer-supported ionic liquid Fe-porphyrin complex

To the mixture, pyrrole of 0.67 g/10 mmol in propionic acid of 15 mL was fed gradually for 30 min with controlled stirring for next 60 min at 130–140 °C. The purple solid product was then obtained. This was separated by removal of 2/3 propionic acid using rotary evaporator and finally washing with methanol followed by diethyl ether, 3 × 25 mL. The NH protons inside the ring of porphyrins acquired acidic character and therefore can get deprotonated to provide porphyrin to ions (Rabbani et al. 2016; Min et al. 2019). %Yield = 71.99% and melting point = above 250 °C were found.

$^1\text{H NMR}$ (400 MHz, DMSO- d_6): δ -1.006 (s, 2H), 0.05(t, 5H, $J = 7.62$ Hz), 0.24 (s, 2H), 1.21(q, 3H, $J = 7.88$ Hz), 1.54(s, 3H), 1.99(q, 2H, $J = 6.1$ Hz), 3.74(q, 3H, $J = 7.21$ Hz), 4.72(brs, 5H), 6.17(s, 7H), 6.57(m, 9H), 6.69(q, 4H, $J = 3.17$ Hz), 6.84 (q, 7H, $J = 3.00$ Hz), 6.98(d, 4H, $J = 8.58$ Hz), 7.07(q, 4H, $J = 3.19$ Hz), 7.10(s, 5H), 8.49(s, 6H), 8.86(s, 2H), 12.21(s, 2H). FT-IR - (KBr, v/cm^{-1}): 3026, 2929, 1712, 1610, 1560, 1502, 1438, 1330, 1255, 1182, 991, 827, 744, 601, 464.

Synthesis of 1,1'1''-(((1⁹-(5-((3-(4-(*sec*-butyl)benzyl)-1H-benzo[d]imidazole-3-ium-1-yl)methyl)-2-hydroxyphenyl)-1²,1³-dihydro-1¹²H,3²H-1¹ λ^2 -1(12,3)-1 λ^2 -5,8-(azeno)pyrrolo[1,2-b][1]zinc[2,1]diazacycloundecina-3(5,2)-pyrrolacycloheptaphan-5-ene-14,2,4-triyl)tris(4-hydroxybenzene-3,1-diyl)tris(methylene))tris(3-(2-carboxyethyl)-1H-benzo[d]imidazole-3-ium) tribromide chloride, polymer supported ionic liquid iron porphyrin complex 1-D

Polymer-supported ionic liquid iron porphyrin complex was successfully prepared and characterized by the different methods. The complex ligand **1-C** of 0.903 g/0.5 mmol and FeCl_3 of 0.097 g/0.6 mmol were charged to methanol and stirred initially for 30 min at atmospheric temperature. Later, above mixture was subjected to reflux at a temperature of 75 °C for 5 h in the inert atmosphere of nitrogen. The synthesized product was then isolated by periodic washing using methanol, and it was dried in the oven for 2 h at a temperature of 80 °C. Finally, a purple color powder of polymer-supported ionic liquid iron porphyrin complex was obtained as given in Fig. 12.3 with yield of 79.93% and melting point of above 250 °C.

FT-IR – (KBr, v/cm^{-1}): 3248, 1714, 1608, 1562, 1506, 1438, 1259, 1189, 1132, 993, 829, 746, 592, 505, 422.

12.6.2 Photodegradation of Methylene Blue and Congo Red

The synthesized polymer-supported ionic liquid iron porphyrin catalyst was used to photodegrade the two azo dyes, methylene blue and congo red under the simulated light and normal air at specific values of pH. The photodegradation results are shown in Figs. 12.4 and 12.5. The process parameters used in photodegradation were optimized to maximize the degradation. In the process of optimization, photodegradation of dyes in visible light was investigated by changing one variable, and remaining variables were kept constant. After getting one optimum parameter, next parameter study was carried out keeping fixed other variables to find optimum photodegradation. First, the photodegradation of methylene blue using this catalyst with different quantities was optimized under simulated light at temperature of 25 °C. The results are presented in Table 12.4 as serial numbers 1–5 and Fig. 12.4, 1B.

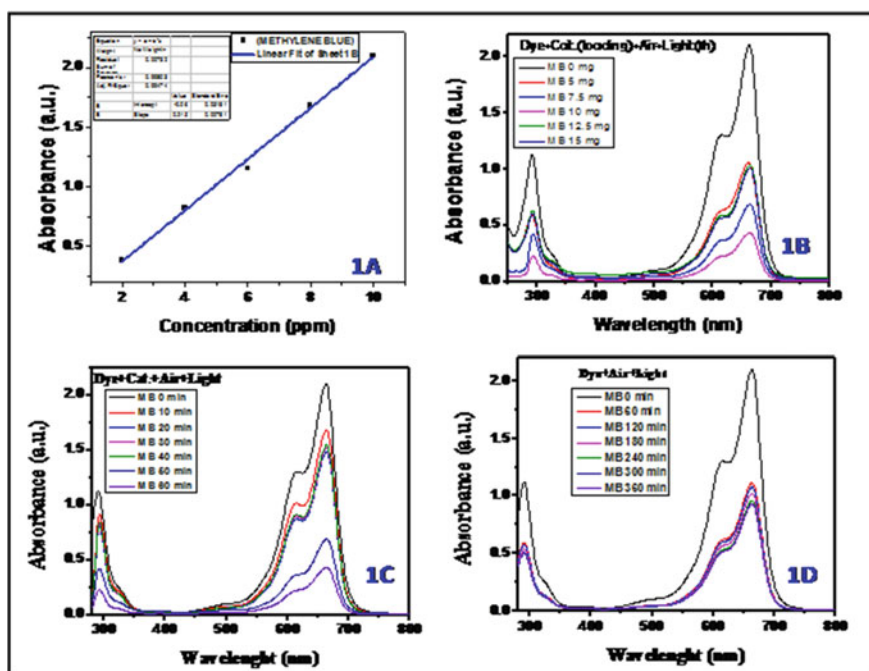


Fig. 12.4 Methylene blue, MB dye (A) R-square value, (B) catalyst loading, (C) time variation of 10 mg catalyst and atmospheric air, and (D) time variation of atmospheric air. (Carried out at pH of ~5 in the presence of 5 W LED light)

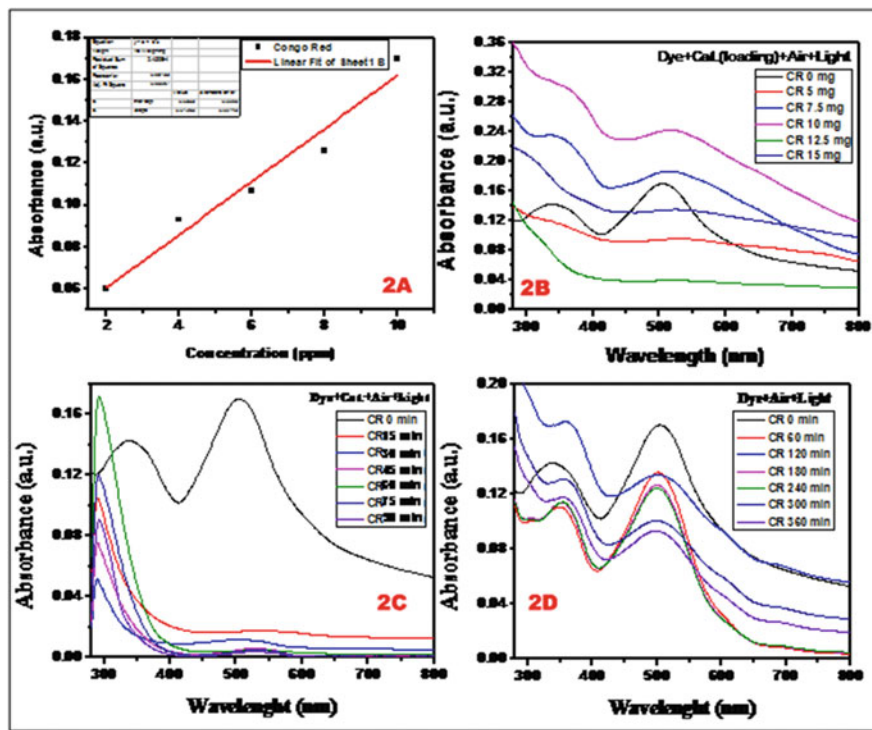


Fig. 12.5 Congo red, CR dye (A) R-square value, (B) catalyst loading, (C) time variation of 12.5 mg catalyst and atmospheric air, and (D) time variation of atmospheric air. (Carried out at pH of ~ 5 in the presence of 5 W LED light)

It was found from Table 12.4 as serial number 12 and Fig. 12.4, 1D that only 22.42% of methylene blue was degraded in 60 min without using catalyst, under atmospheric air irradiation. On the other hand, 46.78% degradation efficiency of methylene blue was obtained with 5 mg catalyst as shown in Table 12.4, serial number 1 and Fig. 12.4, 1B. The improvement in the degradation efficiencies was observed as 65.31% and 77.76% with higher catalyst loadings of 7.5 mg and 10 mg, respectively, as given in Table 12.4, serial numbers 2–3 and Fig. 12.4, 1B. Comparatively less improvement was observed in photodegradation of methylene blue with the catalyst loading above 10 mg as shown in Table 12.4, serial numbers 4–5, and Fig. 12.4, 1B. This implies that the photo-induced electrons and holes are produced at lesser rate with high catalyst loadings and leads to a limiting factor for degradation. Catalyst loading of 10 mg is found to be a better choice for the photodegradation of methylene blue.

The photodegradation of congo red using polymer-supported ionic liquid iron porphyrin with different amounts of catalyst at atmospheric temperature of 25 °C under simulated sunlight was studied as given in Table 12.5 from serial numbers 1–5 and Fig. 12.5, 2B. Without catalyst, 21% of congo red was only able to degrade

Table 12.4 Total optimum conditions of methylene blue dye degradation with or without polymer-supported ionic liquid Fe-porphyrin complex catalyst (10 ppm and 25 mL)

| S. no. | Catalyst (ILPSFePc) (mg) | Air | Time (Min) | % Degradation |
|--------|--------------------------|------|------------|---------------|
| 1 | 5 | Atm. | 60 | 46.78 |
| 2 | 7.5 | Atm. | 60 | 65.31 |
| 3 | 10 | Atm. | 60 | 77.76 |
| 4 | 12.5 | Atm. | 60 | 77.92 |
| 5 | 15 | Atm. | 60 | 78.11 |
| 6 | 10 | Atm. | 10 | 21.38 |
| 7 | 10 | Atm. | 20 | 27.31 |
| 8 | 10 | Atm. | 30 | 28.88 |
| 9 | 10 | Atm. | 40 | 30.69 |
| 10 | 10 | Atm. | 50 | 68.26 |
| 11 | 10 | Atm. | 60 | 78.09 |
| 12 | – | Atm. | 60 | 22.42 |
| 13 | – | Atm. | 120 | 30.45 |
| 14 | – | Atm. | 180 | 51.01 |
| 15 | – | Atm. | 240 | 54.34 |
| 16 | – | Atm. | 300 | 55.25 |
| 17 | – | Atm. | 360 | 56.15 |

Table 12.5 Optimization of parameters for degradation of congo red dye with or without polymer-supported ionic liquid Fe-porphyrin complex catalyst (25 mL of 10 ppm)

| S. no. | Catalyst (ILPSFePc) (mg) | Air | Time (Min) | % Degradation |
|--------|--------------------------|------|------------|---------------|
| 1 | 5 | Atm. | 60 | 41.7 |
| 2 | 7.5 | Atm. | 60 | –8.41 |
| 3 | 10 | Atm. | 60 | 51.76 |
| 4 | 12.5 | Atm. | 60 | 76.05 |
| 5 | 15 | Atm. | 60 | 78.21 |
| 6 | 12.5 | Atm. | 15 | 41 |
| 7 | 12.5 | Atm. | 30 | 54.52 |
| 8 | 12.5 | Atm. | 45 | 68.05 |
| 9 | 12.5 | Atm. | 60 | 77.64 |
| 10 | 12.5 | Atm. | 75 | 98.82 |
| 11 | 12.5 | Atm. | 90 | 99.11 |
| 12 | – | Atm. | 60 | 21 |
| 13 | – | Atm. | 120 | 22.76 |
| 14 | – | Atm. | 180 | 25.88 |
| 15 | – | Atm. | 240 | 27.64 |
| 16 | – | Atm. | 300 | 41.17 |
| 17 | – | Atm. | 360 | 45.29 |

under atmospheric air irradiation in 60 min, whereas 41.7% removal was accomplished with 5 mg of catalyst as presented in Table 12.5 and Fig. 12.5, 2B. The increased removal was noticed at higher loadings of the catalyst, where -8.41% and 51.76% degradation were observed with catalyst loadings of 7.5 mg and 10 mg, respectively, as represented in Table 12.5, serial numbers 2–3, and Fig. 12.5, 2B. The negative value of degradation efficiencies may be attributed to the formation of few chromophore groups during the photodegradation. Similar findings were obtained by Kharazi et al. (2018); Khajone et al. (2019).

The rate of improvement was enhanced with 12.5 mg photocatalyst but found lesser thereafter, in serial numbers 4–5 of Table 12.5 and Fig. 12.5, 2B, which means that the photodegradation rate can be controlled by the production rate of photo-induced electrons and holes at these higher catalyst dosages. Next, the influence of duration was also influenced on photodegradation of congo red using the optimized catalyst loading of 12.5 mg in 25 mL at 10 ppm concentration. The progress in the degradation efficiencies was detected from 41% to 98.82% with respect to duration from 15 min to 75 min as presented in Table 12.5, s. no. 6–10. However, there was no appreciable enhancement with more duration, Table 12.5 at s. no. 11. It was found that there was no significant degradation in absence of photocatalyst as given in Table 12.5, s. no. 12–17.

12.6.3 Possible Mechanism

The possible mechanism of the dye degradation by polymer-supported ionic liquid iron porphyrin catalyst is given in Fig. 12.6. When exposed to replicated sunlight,

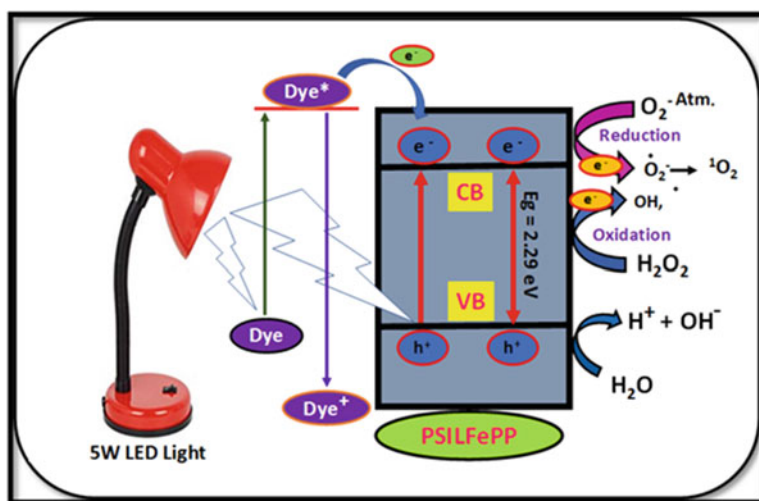
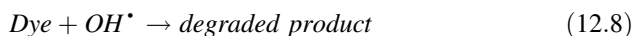
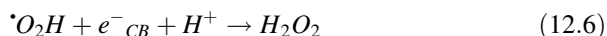
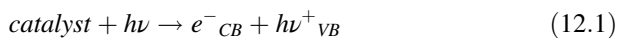


Fig. 12.6 Plausible mechanism for dye degradation by polymer-supported ionic liquid Fe-porphyrin complex (PSILFePP)

electrons could reduce O_2 to $O_2^{\cdot -}$ and the OH^- and OH^\cdot radicals could be formed with the photo-generated holes. More radicals are generated due to the higher separation efficacy of electron–hole pairs in the developed photocatalyst. These generated radicals such as $^\cdot OH$ and $O_2^{\cdot -}$ and 1O_2 were found to be responsible for the photodegradation of methylene blue and congo red. Equations (12.1, 12.2, 12.3, 12.4, 12.5, 12.6, 12.7, and 12.8) illustrate the creation of radicals.



12.7 Conclusions

This study presents the recent applications of functionalized ionic liquids for the removal of metal ions and different dyes. An up-to-date review of the recent articles is presented in the first part. Later, a case study focusing on the application of a polymer-supported ionic liquid Fe-porphyrin complex for the photodegradation of organic dyes, namely methylene blue and congo red, is presented. It was observed that a polymer-supported ionic liquid Fe-porphyrin complex could be effectively used for the removal of organic dyes. This may pave a way for the efficient removal of the organic pollutants from the wastewater.

Acknowledgments The authors acknowledge SIF DST-VITFIST, the SEM facility at SBST, and RGEMS (VIT, Vellore) for allowing them to use the analytical instruments.

References

- Archana V, Meera KM, Begum S, Anantharaman N (2016) Studies on removal of phenol using ionic liquid immobilized polymeric micro-capsules. Arab J Chem 9:371–382. <https://doi.org/10.1016/j.arabjc.2013.03.017>
- Balinge KR, Khiratkar AG, Bhagat PR (2017) Polymer supported Zn-salen complexes: an effective one-pot oxidative esterification of aldehydes to carboxylic esters. J Mol Liq 242:1085–1095. <https://doi.org/10.1016/j.molliq.2017.07.105>

- Balinge KR, Khiratkar AG, Muskawar PN, Thenmozhi K, Bhagat PR (2018) Facile access to polymer supported zinc–salen complex: highly efficient heterogeneous catalyst for synthesizing hydantoin, thiohydantoin and Schiff bases in aqueous medium. *Res Chem Intermed* 44:2075–2097. <https://doi.org/10.1007/s11164-017-3215-x>
- Boczkaj G, Fernandes A (2017) Wastewater treatment by means of advanced oxidation processes at basic pH conditions: a review. *Chem Eng J* 32:608–633. <https://doi.org/10.1016/j.cej.2017.03.084>
- Bollin PM, Viamajala S (2012) Reactive extraction of triglycerides as fatty acid methyl esters using Lewis acidic chloroaluminate ionic liquids. *Energy Fuels* 26:6411–6418. <https://doi.org/10.1021/ef301101d>
- Butler E, Hung YT, Yeh RL, Suleiman Al Ahmad M (2011) Electrocoagulation in wastewater treatment. *Water SA* 3:495–525. <https://doi.org/10.3390/w3020495>
- Dalvand A, Gholami M, Joneidi A, Mahmoodi NM (2011) Dye removal, energy consumption and operating cost of electrocoagulation of textile wastewater as a clean process. *Clean-Soil Air Water* 39:665–672. <https://doi.org/10.1002/clen.201000233>
- De Lima LB, Pereira LO, de Moura SG, Magalhães F (2017) Degradation of organic contaminants in effluents-synthetic and from the textile industry-by Fenton, photocatalysis, and H₂O₂ photolysis. *Environ Sci Pollut Res* 24(7):6299–6306. <https://doi.org/10.1007/s11356-016-6973-x>
- Dietz M (2006) Ionic liquids as extraction solvents: where do we stand? *Sep Sci Technol* 41:2047–2063. <https://doi.org/10.1080/01496390600743144>
- Domanska U, Rekawek A (2009) Extraction of metal ions from aqueous solutions using Imidazolium based ionic liquids. *J Solut Chem* 38:739–751. <https://doi.org/10.1007/s10953-009-9402-7>
- Du C, Xue Y, Wu Z (2017) Microwave-assisted one-step preparation of macadamia nut shell-based activated carbon for efficient adsorption of reactive blue. *New J Chem* 41:15373–15383. <https://doi.org/10.1039/C7NJ03208K>
- Egorov VM, Djigailo DI, Momotenko DS, Chernyshov DV, Torocheshnikova II, Smirnova SV, Pletnev IV (2010) Task-specific ionic liquid trioctylmethylammonium salicylate as extraction solvent for transition metal ions. *Talanta* 80(3):1177–1182. <https://doi.org/10.1016/j.talanta.2009.09.003>
- Fei Z, Zhao D, Geldbach TJ, Scopelliti R, Dyson PJ, Antonijevic S, Bodenhausen G (2005) *Angew Chem Int Ed* 44:5720. <https://doi.org/10.1002/anie.200500207>
- Fernández JF, Neumann J, Thöming J (2010) Regeneration, recovery and removal of ionic liquids. *Curr Org Chem* – in press, Alexander K (ed), (InTech) ISSN 1385-2728
- Ferreir AM, Coutinho JAP, Fernandes AM, Freire MG (2014) Complete removal of textile dyes from aqueous media using ionic-liquid-based aqueous two-phase systems. *Sep Purif Technol* 128:58–66. <https://doi.org/10.1016/j.seppur.2014.02.036>
- Fuerhacker M, Haile TM, Kogelnig D, Stojanovic A, Keppler B (2012) Application of ionic liquids for the removal of heavy metals from wastewater and activated sludge. *Water Sci Technol* 65(10):1765–1773. <https://doi.org/10.2166/wst.2012.907>
- Gao Y, Twamley B, Shreeve JM (2004) *Inorg Chem* 43:3406. <https://doi.org/10.1021/ic049961v>
- Gautam K, Kamsonlian S, Kumar S (2019) Removal of reactive black 5 dye from wastewater using electro-coagulation: equilibrium isotherms and kinetic study. *J Water Chem Technol*. <https://doi.org/10.1515/zpch-2017-1044>
- Han D, Row KH (2010) Recent applications of ionic liquids in separation technology. *Molecules* 15:2405–2426. <https://doi.org/10.3390/molecules15042405>
- Hao M, Zhiguo J, Kong J (2013) Hydrophobic poly(ionic liquid) for highly effective separation of methyl blue and chromium ions from water. *Polymers* 5:1203–1214. <https://doi.org/10.3390/polym5041203>
- Hayouni S, Robert A, Maes C, Conreux A, Marin B, Mohamadou A, Bouquillon S (2018) New dendritic ionic liquids (DILs) for the extraction of metallic species from water. *New J Chem* 42:18010–18020. <https://doi.org/10.1039/C8NJ01921E>

- Heintz A, Wertz C (2006) Ionic liquids: a most promising research field in solution chemistry and thermodynamics. *Pure Appl Chem* 78:1587–1593. <https://doi.org/10.1351/pac200678081587>
- Hernández-Fernández F, de los Ríos PJ, Mateo-Ramírez AF, Godínez C, Lozano-Blanco LJ, Moreno JJ, Tomás-Alonso F (2015) New application of supported ionic liquids membranes as proton exchange membranes in microbial fuel cell for waste water treatment. *Chem Eng J* 279:115–119. <https://doi.org/10.1016/j.cej.2015.04.036>
- Holkar CR, Jadhav AJ, Pinjari DV, Mahamuni NM, Pandit AB (2016) A critical review on textile wastewater treatments: possible approaches. *J Environ Manage* 182:351–366. <https://doi.org/10.1016/j.jenvman.2016.07.090>
- Khajone VB, Balinge KR, Patle DS, Bhagat PR (2019) Synthesis and characterization of polymer supported Fe-phthalocyanine entangled with carboxyl functionalized benzimidazolium moiety: a heterogeneous catalyst for efficient visible-light-driven degradation of organic dyes from aqueous solutions. *J Mol Liq* 288:111032. <https://doi.org/10.1016/j.molliq.2019.111032>
- Kharazi P, Rahimi R, Rabbani M (2018) Study on porphyrin/ZnFe₂O₄@polythiophene nanocomposite as a novel adsorbent and visible light driven photocatalyst for the removal of methylene blue and methyl orange. *Mater Res Bull* 103:133. <https://doi.org/10.1016/j.materresbull.2018.03.031>
- Khiratkar AG, Muskawar PN, Bhagat PR (2016) Polymer-supported benzimidazolium based ionic liquid: an efficient and reusable Brønsted acid catalyst for Biginelli reaction. *RSC Adv* 6:105087–105093. <https://doi.org/10.1039/C6RA23781A>
- Langhals H (2004) Color chemistry. Synthesis, properties and applications of organic dyes and pigments. By Heinrich Zollinger, Wiley Online Library. Liddle ST, Arnold PL *Organometallics*. 24, 2597 <https://doi.org/10.1002/anie.200385122>
- Liddle ST, Arnold PL (2005) Synthesis of heteroleptic cerium(III) anionic amido-tethered N-heterocyclic carbene complexes. *Organometallics*. 24:2597–2605. <https://doi.org/10.1021/om050061b>
- Mathews C, Bhosale VK, Kulkarni PS, Kamble SP (2019) Removal of phenol from organic system using ionic liquids. *Curr Environ Eng* 6:1. <https://doi.org/10.2174/2212717806666190408154507>
- Min KS, Kumar RS, Lee JH, Kim KS, Lee SG, Son YA (2019) Synthesis of new TiO₂/porphyrin-based composites and photocatalytic studies on methylene blue degradation. *Dyes Pigments* 160:37–47. <https://doi.org/10.1016/j.dyepig.2018.07.045>
- Muskawar PN, Kumar SS, Bhagat PR (2013) Carboxyl-functionalized ionic liquids based on Benzimidazolium cation: study of Hammett values and catalytic activity towards one-pot synthesis of 1-amidoalkyl naphthols. *J Mol Liq* 380:112–117. <https://doi.org/10.1016/j.molcata.2013.09.026>
- Oller I, Malato S, Sa'nchez-Pe'rez JA (2011) Combination of advanced oxidation processes and biological treatments for wastewater decontamination-a review. *Sci Total Environ* 409:4141–4166. <https://doi.org/10.1016/j.scitotenv.2010.08.061>
- Pandey S (2006) Analytical applications of room-temperature ionic liquids: a review of recent efforts. *Anal Chim Acta* 556:38–45. <https://doi.org/10.1016/j.aca.2005.06.038>
- Park H, Shamim AH, Nallal M, Park S, Park KH (2019) Synthesis of silver nanostructures in ionic liquid media and their application to photodegradation of methyl orange. *Nanomater Nanotech* 9:1–9. <https://doi.org/10.1177/1847980419836500>
- Patel DD, Lee JM (2012) Applications of ionic liquids. *Chem Rec* 12:329–355. <https://doi.org/10.1002/tcr.201100036>
- Pei YC, Wang JJ, Xuan XP, Fan J, Fan M (2007) Factors affecting ionic liquids based removal of anionic dyes from water. *Environ Sci Technol* 41:5090–5095. <https://doi.org/10.1021/es062838d>
- Pilli SR, Mohanty K, Banerjee T (2014) Extraction of Phthalic Acid from Aqueous Solution by Using Ionic Liquids: A Quantum Chemical Approach. *International Journal of Thermodynamics* 17(1):42–51. <https://doi.org/10.5541/ijot.482>

- Qi L, Yu J, Jaroniec M (2013) Enhanced and suppressed effects of ionic liquid on the photocatalytic activity of TiO₂. *Adsorption* 19:557–561. <https://doi.org/10.1007/s10450-013-9478-7>
- Rabbani M, Heidari-Golafzani M, Rahimi R (2016) Synthesis of TCP/PP/ZnFe₂O₄@ZnO nanohollow sphere composite for degradation of methylene blue and 4-nitrophenol under visible light. *Mater Chem Phys* 179:35–41. <https://doi.org/10.1016/j.matchemphys.2016.05.005>
- Ravishankar TN, Sureshkumar K, Dupont J, Ramakrishnappa T, Nagaraju G (2015) Ionic liquid-assisted hydrothermal synthesis of TiO₂ nanoparticles and its applications towards the photocatalytic activity and electrochemical sensor. *J Exp Nanosci* 10. <https://doi.org/10.1080/17458080.2015.1014870>
- Regel-Rosocka M, Wisniewski M (2011) Ionic liquids in separation of metal ions from aqueous solutions, applications of ionic liquids in science and technology, Prof. Scott Handy (ed), (InTech) ISBN: 978-953-307-605-8. <https://doi.org/10.5772/23909>
- Rodríguez CB, Rodríguez PI, Corchero R, Rodil R, Rodil E, Arce A, Soto A (2017) Photocatalytic degradation of methyl orange, methylene blue and rhodamine B with AgCl nanocatalyst synthesised from its bulk material in the ionic liquid [P6 6 6 14]Cl. *Water Sci Technol* 75 (1–2):128–140. <https://doi.org/10.2166/wst.2016.499>
- Saleem S, Saqib ANS, Mujahid A, Hanif M, Mustafa G, Mahmood T, Waseem A, Khan AR (2014) Extraction of Pb(II) from water samples by ionic liquid-modified silica sorbents. *Desalin Water Treat* 52:40–42. <https://doi.org/10.1080/19443994.2014.922497>
- Sergi D, Gemma E, Claudia F (2019) System for mercury preconcentration in natural waters based on a polymer inclusion membrane incorporating an ionic liquid. *Journal of Hazardous Materials* 371:316–322. <https://doi.org/10.1016/j.jhazmat.2019.03.017>
- Shankar M, Sekaran G, Sadullah S, Ramasami T (1999) *J Chem Tech Biotechnol* 74:337. [https://doi.org/10.1002/\(SICI\)1097-4660\(199904\)74:4<337::AID-JCTB39>3.0.CO;2-U](https://doi.org/10.1002/(SICI)1097-4660(199904)74:4<337::AID-JCTB39>3.0.CO;2-U)
- Sun P, Armstrong DW (2010) Ionic liquids in analytical chemistry. *Anal Chim Acta* 661:1–16. <https://doi.org/10.1016/j.aca.2009.12.007>
- Vaghela SS, Jethva AD, Mehta BR, Dave SP, Ramachandria G (2005) *Environ Sci Technol* 39:2848. <https://doi.org/10.1021/es035370c>
- van Rantwijk F, Madeira LR, Sheldon RA (2003) Biocatalytic transformations in ionic liquids. *Trends Biotechnol* 21. [https://doi.org/10.1016/S0167-7799\(03\)00008-8](https://doi.org/10.1016/S0167-7799(03)00008-8)
- Wasserscheid P, Keim W (2000) Ionic liquids: new “solutions” for transition metal catalysis. *Angew Chem Int Ed* 39:3772–3789. [https://doi.org/10.1002/1521-3773\(20001103\)39:21<3772::AID-ANIE3772>3.0.CO;2-5](https://doi.org/10.1002/1521-3773(20001103)39:21<3772::AID-ANIE3772>3.0.CO;2-5)
- Wilkes JS (2002) A short history of ionic liquids—from molten salts to neoteric solvents. *Green Chem* 4:73–80. <https://doi.org/10.1039/b110838g>
- Ye C, Shreeve JM (2004) *J Org Chem* 69:8561. <https://doi.org/10.1021/jo048383x>
- Zhao D (2007) Design, synthesis and applications of functionalized ionic liquids, (Thesis) M.Sc. in Chemistry, Xinan Petroleum University, Nanchong, China et de nationalité chinoise. <https://doi.org/10.5075/epfl-thesis-3531>

Chapter 13

Photocatalytic Degradation of Chlorophenols and Antibiotics from Wastewater



Cristina Orbeci, Constantin Bobirică, and Liliana Bobirică

Contents

| | | |
|--------|---|-----|
| 13.1 | Introduction | 412 |
| 13.2 | Refractory Organic Compounds: Chlorophenols and Antibiotics | 413 |
| 13.3 | Advanced Oxidation Process Fundamentals | 414 |
| 13.4 | Photocatalytic Degradation of Chlorophenols and Antibiotics from Wastewater | 418 |
| 13.4.1 | Materials and Methods | 418 |
| 13.4.2 | Results and Discussion | 420 |
| 13.5 | Conclusions | 425 |
| | References | 426 |

Abstract In recent years, refractory organic compounds have attracted increasing attention due to the difficulties with which they are removed from waste effluents. The use of advanced oxidation processes alone or in combination with biological processes in wastewater treatment plants represents viable alternatives for removing refractory organic contaminants. Of the advanced oxidation processes, photocatalytic oxidation seems to have the highest potential and therefore has been intensively tested for the removal of many types of refractory organic contaminants. Therefore, the objective of this work is to explore the potential of photocatalytic oxidation for the removal of chlorophenols and antibiotics from wastewater. Several types of photocatalytic membranes have been tested. The experimental results revealed that the rate of photocatalytic degradation is higher in the case of cobalt (Co)-doped TiO₂/polymer membrane comparative with that of TiO₂/Ti for both 4-chlorophenol and 2,4-dichlorophenol, regardless of their concentration. Moreover, the degradation rate of 4-chlorophenol is higher than that of 2,4-dichlorophenol, regardless of the type of photocatalytic membrane used. Regarding the photocatalytic degradation of the antibiotics studied, by using the new obtained TiO₂/sisal fiber membrane, the photocatalytic degradation after 120 minutes of

C. Orbeci (✉) · C. Bobirică · L. Bobirică

Department of Analytical Chemistry and Environmental Engineering, University Politehnica of Bucharest, Bucharest, Romania

© The Editor(s) (if applicable) and The Author(s), under exclusive license to Springer Nature Switzerland AG 2021

411

Inamuddin et al. (eds.), *Water Pollution and Remediation: Photocatalysis*, Environmental Chemistry for a Sustainable World 57, https://doi.org/10.1007/978-3-030-54723-3_13

irradiation is 98% for ampicillin, 96% for tetracycline, and 90% for erythromycin, regardless of their concentration.

Keywords Refractory organic contaminants · Photocatalytic oxidation · Chlorophenols · Antibiotics · Wastewater

13.1 Introduction

A wide range of organic contaminants can reach different water bodies mainly due to leakage from contaminated or intensively fertilized soils and industrial wastewater discharges as well as from leakage of hazardous compounds from various deposits (Simion et al. 2015; Orbeci et al. 2014). Many of these organic contaminants are known to have a strong negative impact, even at very low concentrations, both on the aquatic life of the affected system and on other entities such as humans and animals coming in different ways in contact with it. Thus, the organic contaminants can potentially be carcinogens, mutagens, or endocrine disruptors for the organisms with that they come into contact (Yadav et al. 2019; Omar et al. 2018).

The effluents from the industry of dyes, surfactants, preservatives, medicines, and pesticides contain many chemical residues and solvents that are used or produced during the manufacturing process such as phenols and their derivatives, antibiotics, and azo dye compounds. The effective treatment of these industrial effluents involves an in-depth knowledge of the actual manufacturing process, as well as of the effluent composition and its variation in time, from both qualitatively and quantitatively standpoint (Houria et al. 2014).

At present, there is a wide range of wastewater treatment technologies based on different physical, chemical, and biological processes. The choice of the optimal treatment method is made according to the composition of the wastewater to be treated, but in many situations, it is considered to obtain a high technical–economic efficiency. Therefore, cheaper and less time-consuming technologies are preferred.

If the wastewater contains refractory organic compounds, the conventional biological treatment processes cannot successfully be applied due to the reduced biodegradability manifested by these organic contaminants. Usually, in this situation, technologies based on advanced oxidation processes are preferred. Due to the high oxidation potential of these processes, all organic matter is mineralized and thus eliminated from the treated water. Therefore, choosing the optimal advanced oxidation process that offers high technical–economic efficiency represents a challenge for many specialists working in the field of wastewater treatment.

13.2 Refractory Organic Compounds: Chlorophenols and Antibiotics

Phenols and their derivatives are the most common and abundant pollutants in industrial effluents such as effluents derived from chemical and petrochemical plants, textile, paint, and pesticide factories. They are usually used as intermediates in the synthesis of a wide range of products such as antiseptics, pesticides, dyes, polymers, drugs, and cosmetics. Their presence in water bodies, especially chlorophenols which are the largest group of phenols used by industry, induces a high pollutant potential due to both their harmful effect on aquatic life and carcinogenic and mutagenic effect to humans. Moreover, it is well-known that phenols at concentration lower than 1 $\mu\text{g/L}$ alter both taste and odor of the water (Grzechulska-Damszel 2009; Michałowicz and Duda 2007; Ye et al. 2007; USEPA 2002).

The largest part of the population is exposed to very low concentrations of chlorophenols (of the order of magnitude of parts per trillion) through drinking water that has been subject to disinfection with chlorine. But the most exposed persons are those who work directly with these compounds either in their manufacture or their use as pesticides. For example, in timber manufacture, a mixture of chlorophenols is used for the preservation of wood. In this case, the major way in which humans are exposed to chlorophenols is through the skin, when the chlorophenols from the treatment of wood come into contact with the skin. Chlorophenols can enter the human body by ingestion along with the food, through dermal contact by skin absorption, or by air. They accumulate mainly in the liver and kidneys and less in the brain, muscles, and fat (von Stackelberg 2013; White 1992). An admissible human daily dose of 2-chlorophenol without inducing carcinogenic effects is 5 $\mu\text{g/kg}$ of body weight, while for 2,4-dichlorophenol, 2,4,6-trichlorophenol, and pentachlorophenol, the dose is 3 $\mu\text{g/kg}$ of body weight (USEPA 1982).

The health effects of chlorophenols are in direct proportion with their degree of chlorination. An acute exposure to low-phenol chlorination results in muscle spasms, twitching, tremors, weakness, ataxia, convulsions, and collapse (White 1992). Consequently, it is necessary to have a close monitoring of them in water bodies.

Pharmaceutical compounds have raised increasing concerns over the past years due to their effects on the environment. Recently, such compounds like antibiotics, analgesics, and steroids have been detected in several public water systems from the United States of America, several European countries, and Australia. Many pharmaceutical products are used in both human and veterinary medicine and finally, are released into the environment through metabolic processes. Typically, wastewater treatment plants cannot completely remove these compounds, and, therefore, many of them are discharged into the environment where they can affect the microbial community, leading to the disruption of the natural elemental cycles (Dodson et al. 2011; Kümmerer 2009a; Wick et al. 2009; Kaniou et al. 2005).

Antibiotics can be metabolized by humans and animals to a lesser or greater extent depending on the organism of each individual. In this respect, they can be eliminated in the wastewater in different quantities depending on both the dose used and the rate of excretion thereof (Kümmerer 2009b; Alexy et al. 2004; Bound and Voulvoulis 2004). Studies on tetracycline, ampicillin, and erythromycin have highlighted the toxicity they have on bacteria and algae in natural systems even at very low concentrations. Because these antibiotics have low biodegradability, and therefore high persistence in the environment, they have high bioaccumulation potential (Alaton et al. 2004). In addition, these can favor the emergence of antibiotic-resistant microorganisms, which can lead to an increase in the number of infections for which new and more powerful antibiotics are needed (Rozas et al. 2010).

13.3 Advanced Oxidation Process Fundamentals

Advanced oxidation processes are based on the nonselective reaction of hydroxyl free radicals ($\text{HO}\bullet$) with organic contaminants, leading to their degradation (Petrovic et al. 2011; Pera-Titus et al. 2004).

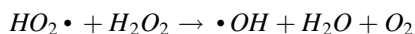
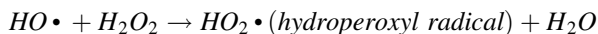
Although there are several ways by which the strong oxidant $\text{HO}\bullet$ radicals can be generated in situ in the system, the photochemical or photocatalytic processes are the most used of them. Often, it is not necessary a complete mineralization of the organic contaminants, but only a transformation of them into biodegradable organic intermediates which, further, can be degraded in a biological process (Wang and Wang 2007).

Advanced oxidation processes can be classified as non-photochemical, such as Fenton or Fenton-like processes, ozone, and ozone/hydrogen peroxide, and photochemical involving different combinations between ozone (O_3) and hydrogen peroxide (H_2O_2), on the one hand, and ultraviolet (UV) radiation and various semiconductors, on the other hand. Depending on the type of phases involved in the photocatalytic process, they can also be classified into homogeneous and heterogeneous (Ortiz de la Plata et al. 2010; Papić et al. 2009).

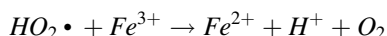
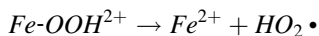
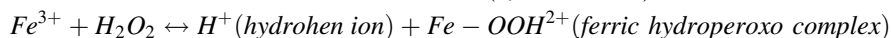
In the ultraviolet radiation/hydrogen peroxide (UV/ H_2O_2) process the hydroxyl radicals are generated through direct photolysis resulting in two $\text{HO}\bullet$ radicals (Orbeci et al. 2016):



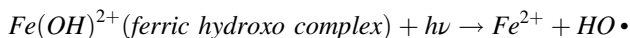
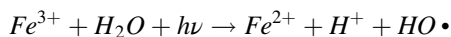
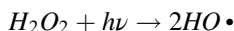
However, at higher concentrations, H_2O_2 can also react with the hydroxyl radicals by the following reactions (Orbeci et al. 2016), which highlights the importance of establishing the optimal H_2O_2 concentration:



In the Fenton process, hydroxyl radicals are generated by a catalytic mechanism in which ferrous (Fe^{2+}) and ferric (Fe^{3+}) ions play an essential role (Borghini et al. 2015; Muñoz et al. 2006; Andreozzi et al. 1999; Benitez et al. 1999; Bossmann et al. 1998). The main reactions are the following:



In the photo-Fenton process, through direct H_2O_2 photolysis and the interaction of UV radiation with the iron ions in the system, more $HO\bullet$ radicals are formed (Ferreira et al. 2015; Pignatello et al. 2006; Sun and Pignatello 1973):



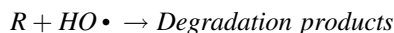
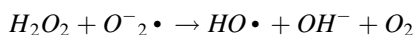
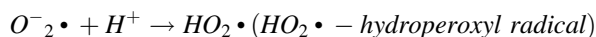
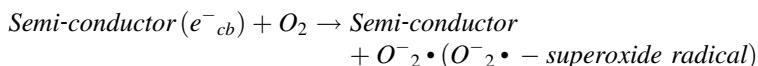
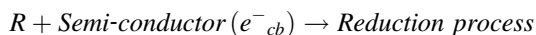
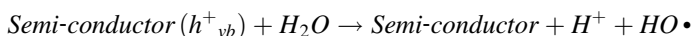
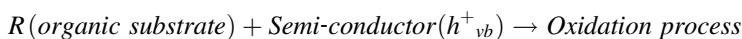
As it was described above, the combination of H_2O_2 and UV radiation with Fe^{2+} or Fe^{3+} ions leads to producing more $HO\bullet$ radicals comparative to the conventional Fenton method or photolysis, which subsequently leads to increases of the rate of the degradation of refractory organic pollutants (Orbeci et al. 2014; Ramírez-Sosa et al. 2013; Klavarioti et al. 2009). In the Fenton reaction, Fe^{3+} ions are accumulated in the system, and the reaction does not take place until all Fe^{2+} ions are consumed. Fe^{2+} ions are photochemical regenerated through the photoreduction of Fe^{3+} ions in the photo-Fenton reaction (de Luna et al. 2013). The newly generated Fe^{2+} ions react with H_2O_2 and generate the $HO\bullet$ radicals and Fe^{3+} ions. Recent studies revealed that conducting the Fenton reaction in the visible or near-ultraviolet radiation field leads to a better degradation of the organic contaminants (Herney-Ramirez et al. 2010). In this respect, compounds such as 4-chlorophenol (Ortiz de la Plata et al. 2010; Untea et al. 2006), nitrobenzene (Rocha et al. 2013), and herbicides (Lofrano et al. 2009) were effectively degraded. It was pointed out that Fenton and photo-Fenton processes offer better performance in acidic conditions, namely, at a pH value of the aqueous solution between 2.5 and 4. This may be due to the fact that at pH lower than 2.5, on the one hand, $(FeOH)^{2+}$ ions react much slower with H_2O_2 , and on the other hand, H^+ ions compete for $HO\bullet$ radicals, leading to a decrease in the degradation efficiency. At pH higher than 4, both the formation of Fe (II) complexes and precipitation of ferric oxyhydroxides lead also to decrease in the degradation efficiency (de Oliveira et al. 2015; Manenti et al. 2015; Ortega-Gomez et al. 2015).

The oxidative degradation process is also influenced by the presence of other active chemical species in the system that could interact with the catalyst in different ways. In this respect, reductive species enhance the oxidation process because these reduce Fe^{3+} to Fe^{2+} and therefore intensify the formation of $\text{HO}\cdot$ radicals. Acid-like species lower the pH of the system, forming stable complexes with Fe^{3+} or Fe^{2+} ions which lead to a marked decrease in the oxidation process. The presence of some inorganic ionic species in the system can modify the efficiency of the process in different ways. In this respect, anions such as chloride (Cl^-), sulfate (SO_4^{2-}), and dihydrogen phosphate (H_2PO_4^-) could, on the one hand, form ferric complexes that are nonreactive and, on the other hand, could decrease the decomposition rate of H_2O_2 . Moreover, they can react with $\text{HO}\cdot$ radicals, forming their own radicals such as $\text{Cl}_2^-\cdot$, $\text{SO}_4^-\cdot$, and $\text{H}_2\text{PO}_4^-\cdot$ that are less reactive than $\text{HO}\cdot$ radicals (Untea et al. 2006).

Photocatalysis is currently one of the most studied oxidative processes used mainly for the decontamination of gaseous and aqueous systems. Its degradation mechanism involves the development of a set of redox (oxidation–reduction) reactions under the action of light in the presence of a semiconductor that leads to the degradation of organic contaminants (Ahmed et al. 2010; Zanjanchi et al. 2009). The photocatalytic reaction mechanism of semiconductors can be explained by the following equations (Parida et al. 2012):



(e^-_{cb} – electrons in the conduction band; h^+_{vb} – positive holes in the valence band)



The semiconductor is excited by photons ($h\nu$) to such a magnitude as to produce electrons in its conduction band (e^-_{cb}) and holes in its valence band (h^+_{vb}). These charge carriers are able to induce redox reactions with both water and organic contaminants. The resulted positive holes are highly oxidant and are able to oxidize

both organic contaminants and water which leads to the formation of hydroxyl radicals ($HO\bullet$) (Hanel et al. 2010; Munter et al. 2001).

A wide range of oxide semiconductors such as TiO_2 , ZnO , ZrO_2 , WO_3 , and Fe_2O_3 ; non-oxide semiconductors such as ZnS , MoS_2 , and CdS ; or doped semiconductors such as $ZnS-CuS-CdS$, $ZnS-WS_2-CdS$, C_3N_4-CdS , $g-C_3N_4-Au-CdS$, $Pd-Cr_2O_3-CdS$, and carbon spheres/ CdS have been tested for removing of a large spectrum of refractory organic compounds from wastewater. Of all these semiconductors or photocatalysts, titanium dioxide (TiO_2) in the anatase form remains the most popular one used in photocatalytic processes due to the advantages it offers such as high oxidizing ability, photodurability, nontoxicity, mechanical robustness, and low cost (Byrne et al. 2018; Wei et al. 2016; Mansourpanah et al. 2009).

TiO_2 or other photocatalysts can be used either in suspension or deposited on a membrane (Mozia 2010; Li et al. 2009; Lim et al. 2009). The photocatalytic membrane reactors are preferred because, on the one hand, they solve the problems regarding the separation of the photocatalyst from the system and, on the other hand, have the advantage of continuous operation (Mozia 2010). A wide range of organic, inorganic, and metallic materials were used to prepare photocatalytic membranes. In this respect, the most popular organic materials used to prepare photocatalytic membranes are polyamide, polyethersulfone, polyvinylidene fluoride, polyurethane, polyethylene terephthalate, polyacrylonitrile, and polytetrafluoroethylene (Argurio et al. 2018). The most common materials used to prepare ceramic photocatalytic membranes are aluminum oxide (Al_2O_3), titanium dioxide (TiO_2), zirconium dioxide (ZrO_2), silicon dioxide (SiO_2), and some mixes between them (Teik-Thye and Ron 2016).

Advanced oxidation processes have a number of advantages in the wastewater treatment, namely:

- High degradation rates of organic compounds from aqueous phase, without transferring pollutants into another phase.
- High reactivity of $OH\bullet$ radicals that react with almost all pollutants from water.
- During oxidation processes, heavy metals could precipitate as hydroxides and can be removed in a subsequent stage.
- $OH\bullet$ radicals facilitate the disinfection during the wastewater/water treatment simultaneously with the organic compounds' degradation.
- Theoretically, no other new organic compounds with higher toxicity are produced.

13.4 Photocatalytic Degradation of Chlorophenols and Antibiotics from Wastewater

13.4.1 Materials and Methods

The chlorophenols used were 4-chlorophenol and 2,4-dichlorophenol, crystalline powder of analytical grade. The characteristics of the two chlorophenols are shown in Table 13.1. The antibiotics used were ampicillin, erythromycin, and tetracycline, crystalline powder of pharmaceutical grade. Their characteristics are shown in Table 13.2.

The hydrogen peroxide stock solution of 30% (w/w) was of analytical grade. The degradation process was studied by monitoring the changes in the concentration of both chlorophenols and antibiotics, also called as organic substrate, as a function of irradiation time by chemical oxygen demand (COD) analysis. A molar ratio of H_2O_2 /organic substrate of 1.5 was used throughout all experiments. All experiments were performed at pH 3. The samples taken from the reactor were contacted with manganese dioxide (MnO_2) to decompose the unreacted H_2O_2 . Next, the samples were filtered and analyzed through the standard method of chemical oxygen demand. The analysis was performed using a Digester DK6. The pH was measured using a Jenway 370 pH-meter.

The experiments were performed by using synthetic solutions of both chlorophenols and antibiotics. The initial concentration of chlorophenols was equivalent to a chemical oxygen demand value of 100 mg O_2 /L, 200 mg O_2 /L, and 300 mg O_2 /L, whereas the initial concentration of antibiotics was 300 mg O_2 /L and 900 mg O_2 /L.

A reactor equipped with different photocatalytic membranes, with UV lamp coaxially positioned with the photocatalytic membranes, and with continuous recirculation facility was used throughout all experiments. The reactor volume was

Table 13.1 Characteristics of chlorophenols


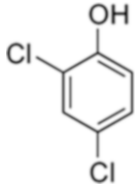
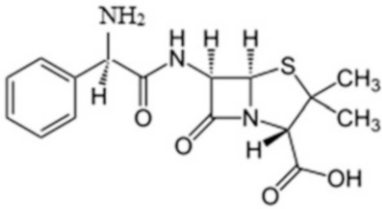
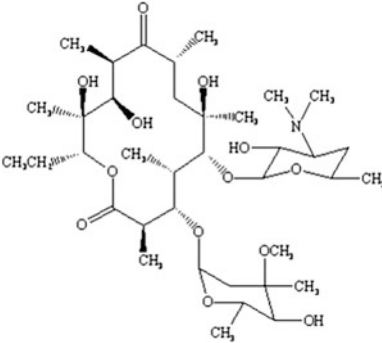
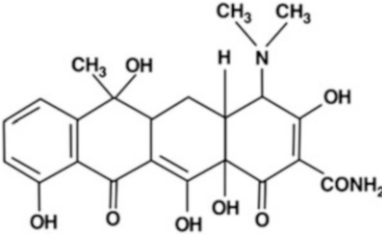
| Chlorophenol | Chemical formula | Molecular mass (g/mol) | Structure |
|--------------------|---|------------------------|--|
| 4-Chlorophenol | $\text{C}_6\text{H}_5\text{ClO}$ | 128.55 |  |
| 2,4-Dichlorophenol | $\text{C}_6\text{H}_4\text{Cl}_2\text{O}$ | 163 |  |

Table 13.2 Characteristics of antibiotics

| Antibiotics | Chemical formula | Molecular mass (g/mol) | Structure |
|--------------|-----------------------|------------------------|--|
| Ampicillin | $C_{16}H_{19}N_3O_4S$ | 349.41 |  The chemical structure of Ampicillin is shown. It features a central beta-lactam ring fused to a five-membered thiazolidine ring. The thiazolidine ring has two methyl groups attached to the carbon atom adjacent to the sulfur atom. The beta-lactam ring has an amide group (-NH-) attached to the carbon atom adjacent to the nitrogen atom. The amide group is further substituted with a phenylacetamido group (-CH2-C6H5). |
| Erythromycin | $C_{37}H_{67}NO_{13}$ | 733.93 |  The chemical structure of Erythromycin is shown. It is a complex macrolide antibiotic consisting of a 14-membered macrolide ring and a 14-membered lactone ring. The macrolide ring is substituted with several methyl groups, hydroxyl groups, and a dimethylamino group. The lactone ring is substituted with a methyl group and a hydroxyl group. |
| Tetracycline | $C_{22}H_{24}N_2O_8$ | 444.44 |  The chemical structure of Tetracycline is shown. It is a tetracycline antibiotic consisting of a tetracyclic core. The core is substituted with several methyl groups, hydroxyl groups, and a dimethylamino group. The structure is highly complex and contains multiple stereocenters. |

1.5 L, the power of the UV lamp was 120 W, and the working solution was continuously recirculated during the irradiation time at a flow rate of 1 L/min.

The photocatalytic membranes titanium dioxide/titanium (TiO_2/Ti) and cobalt (Co)-doped TiO_2 /polymer were kindly supplied by B.I.T. s.r.l (Milan, Italy). The photocatalytic membrane TiO_2 /sisal fiber was prepared by impregnating the support material, namely, the sisal fiber, in a suspension of TiO_2 -sodium silicate. The deposition of TiO_2 on the sisal fiber was performed layer upon layer. The sodium silicate solution was used as binder agent. After impregnation, the obtained photocatalytic TiO_2 /sisal fiber membrane was exposed to air for 2 days in order to remove the excess slurry and to dry completely. Finally, the photocatalytic TiO_2 /sisal fiber membrane was rolled in a cylindrical shape and then washed in distilled water.

13.4.2 Results and Discussion

Photocatalytic Degradation of Chlorophenols

The photocatalytic activity of the two membranes, namely, TiO_2/Ti and cobalt (Co)-doped $\text{TiO}_2/\text{polymer}$, was tested for the two types of chlorophenols, namely, 4-chlorophenol and 2,4-dichlorophenol, at three different values of their equivalent concentration in the initial solution, namely, 100 mg O_2/L , 200 mg O_2/L , and 300 mg O_2/L . The experimental results obtained are presented in Figs. 13.1 to 13.3. As can be seen from Fig. 13.1 and Fig. 13.2, the reaction time to a complete mineralization increases with increasing the concentration of chlorophenol in the initial solution, regardless of the type of chlorophenol and the photocatalytic membrane used.

The obtained results can be explained by the fact that between the initial concentration of the organic substrate and the reaction rate, there is an inversely proportional dependence, so that the higher the initial concentration of chlorophenol, the lower the overall reaction rate. The explanation is that at constant light intensities and irradiation times, as the initial concentration of chlorophenol increases, more and more organic molecules are adsorbed on the surface of the TiO_2 photocatalyst, while the number of $\text{HO}\cdot$ radicals formed on its surface remains constant. This causes a decrease in the ratio of the number of $\text{HO}\cdot$ radicals and the number of organic molecules, which is reflected in lower degradation efficiencies.

Regarding the photocatalytic efficiency of the studied membranes, from Fig. 13.1 to Fig. 13.2 it can be observed that the rate of photocatalytic degradation is higher in

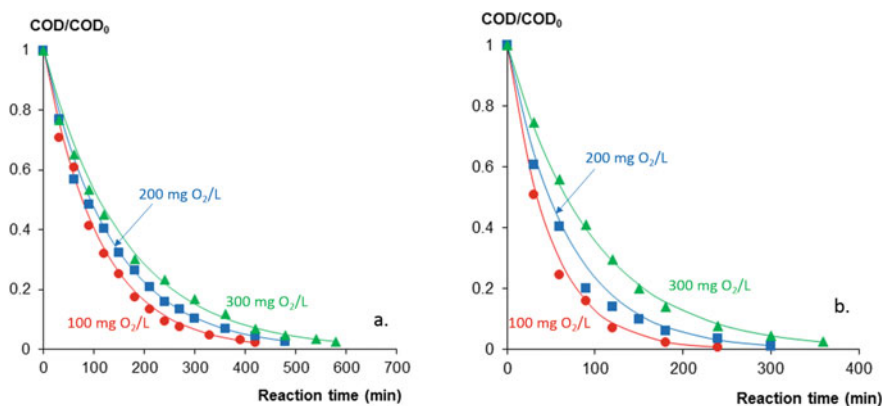


Fig. 13.1 Kinetics of 4-chlorophenol degradation as a function of its initial concentration; a. 4-chlorophenol/ $\text{H}_2\text{O}_2 = 1.5$, $\text{pH} = 3$, TiO_2/Ti membrane; b. 4-chlorophenol/ $\text{H}_2\text{O}_2 = 1.5$, $\text{pH} = 3$, cobalt (Co)-doped $\text{TiO}_2/\text{polymer}$ membrane. The reaction (irradiation) time until a complete mineralization is reached increases with the initial concentration of chlorophenol. The mineralization of aqueous solutions of chlorophenol occurs faster if cobalt (Co)-doped $\text{TiO}_2/\text{polymer}$ membrane has been used. COD, chemical oxygen demand at reaction time t ; COD_0 , initial chemical oxygen demand

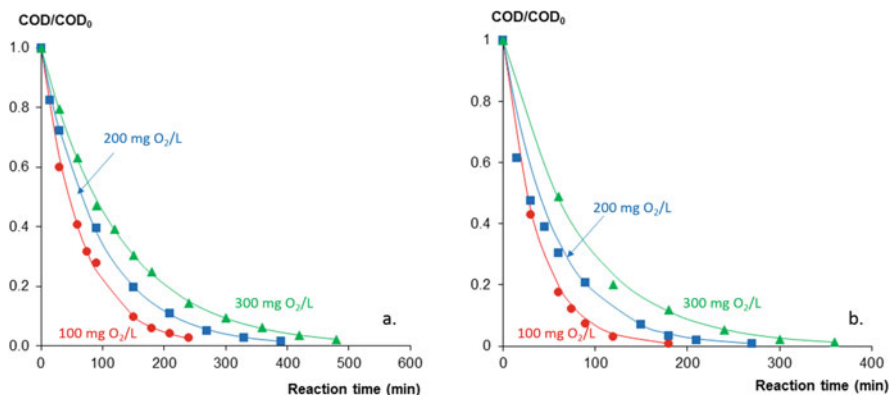
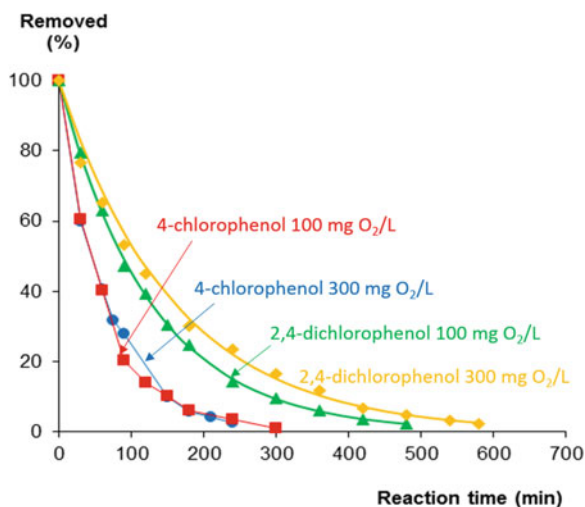


Fig. 13.2 Kinetics of 2,4-chlorophenol degradation as a function of its initial concentration; a. 2,4-chlorophenol/ $\text{H}_2\text{O}_2 = 1.5$, $\text{pH} = 3$, TiO_2/Ti membrane; b. 2,4-chlorophenol/ $\text{H}_2\text{O}_2 = 1.5$, $\text{pH} = 3$, cobalt (Co)-doped TiO_2 /polymer membrane. The rate of mineralization of 2,4-dichlorophenol aqueous solution depends on the initial concentration of chlorophenol and on the photocatalytic membrane used. Increasing the initial concentration of chlorophenol leads to an increase in irradiation time until complete mineralization. Also, the use of cobalt (Co)-doped TiO_2 /polymer membrane increases the mineralization rate. COD, chemical oxygen demand at reaction time t ; COD_0 , initial chemical oxygen demand

Fig. 13.3 The removal degree of organic substrate as a function of reaction time. The complete mineralization of 4-chlorophenol occurs much faster than complete mineralization of 2,4-dichlorophenol. The faster mineralization in the case of 4-chlorophenol is due to the differences between the two chlorophenols in terms of their characteristics. The number and the position of the chlorine atoms on the aromatic ring of the chlorophenols influence their oxidation efficiency



the case of cobalt (Co)-doped TiO_2 /polymer membrane than that of TiO_2/Ti for both 4-chlorophenol and 2,4-dichlorophenol. These results can be explained by the fact that doping the transition metal cobalt (Co) into TiO_2 lattice leads to obtaining a narrow band gap due to the spin exchange interactions which leads the enhancement of photocatalytic activity.

Increasing the reaction time to a complete mineralization in the case of 2,4-dichlorophenol, regardless of its concentration in the initial solution, compared to that of 4-chlorophenol (Fig. 13.3), can be correlated with the difference between the characteristics of the two organic compounds. As can be seen from Fig. 13.3, for a complete mineralization of 4-chlorophenol of 100 mg O₂/L equivalent concentration in the initial solution, approximately 250 minutes of irradiation is required, while for the same equivalent concentration, approximately 300 minutes of irradiation is required for 2,4-dichlorophenol. At an equivalent concentration of 300 mg O₂/L, approximately 500 minutes of irradiation is necessary for 4-chlorophenol and approximately 600 minutes of irradiation for 2,4-dichlorophenol.

It is known that for the chlorinated phenols, the oxidation efficiency is different as a function of the number and the position on aromatic ring of the chlorine atoms. In this respect, it is expected that the oxidation rate, and subsequently the degradation efficiency, decreases with the increase of the number of chlorine atoms on the aromatic ring. This decrease may be associated with the decrease in the number of favorable positions in which the attack of the hydroxyl radicals could have occurred most probably due to their occupation by the chlorine atoms.

Photocatalytic Degradation of Antibiotics

The sisal fiber used to prepare the new photocatalytic membrane TiO₂/sisal fiber has been tested to determine whether it has its own catalytic activity. The tests were performed by using an ampicillin solution at a chemical oxygen demand equivalent concentration of 300 mg O₂/L. In this respect, the reactor was operated first by using only ampicillin solution at pH 3 and at a H₂O₂/ampicillin molar ratio of 1.5, and then, it was operated by using the same solution of ampicillin and the sisal fiber material without any impregnation with TiO₂. As can be seen from Fig. 13.4, there is no clear distinction between the results obtained with and without sisal fiber. These results indicate that the degradation degree of approximately 50% after 120 minutes of reaction obtained for ampicillin in the two experiments was due solely to the oxidizing action of the H₂O₂ introduced into the reaction medium.

The photocatalytic activity of the TiO₂/sisal fiber membrane was tested for the same ampicillin solution, the results being presented in Fig. 13.5 comparative to those obtained in the experiments in which sisal fiber was used without any impregnation with TiO₂. As can be seen in Fig. 13.5, there is a clear distinction between the results obtained with TiO₂/sisal fiber membrane and those obtained with sisal fiber without any impregnation with TiO₂. In this respect, after 120 minutes of reaction, the degradation degree of ampicillin in the presence of TiO₂/sisal fiber membrane is 100%, whereas, for the same reaction time, the degradation degree of ampicillin in the presence of only sisal fiber is 49%. These results confirm the photocatalytic role of the TiO₂ deposited on the sisal fiber.

The new photocatalytic TiO₂/sisal fiber membrane, whose photocatalytic activity was demonstrated in the experiments presented above, was used for degradation of different types of antibiotics, namely, ampicillin, erythromycin, and tetracycline, at

Fig. 13.4 Evaluation of the photocatalytic activity of the supporting material (sisal fiber). Note that there is no definite difference between the results obtained in the presence or in the absence of sisal fiber. Therefore, the degradation of ampicillin occurs only due to the hydrogen peroxide added to the reaction medium. COD, chemical oxygen demand at reaction time t ; COD_0 , initial chemical oxygen demand

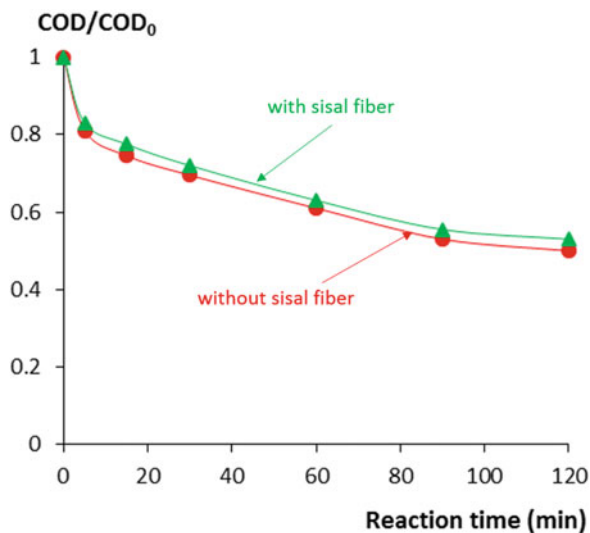
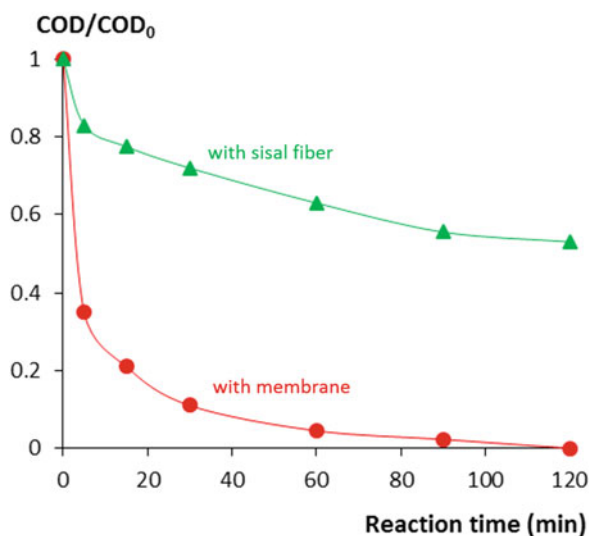


Fig. 13.5 Photocatalytic activity of both sisal fiber and TiO_2 /sisal fiber. Note that there is a clear difference between the results obtained with TiO_2 /sisal fiber membrane and sisal fiber without impregnation with TiO_2 . The results highlight the photocatalytic role of TiO_2 . COD, chemical oxygen demand at reaction time t ; COD_0 , initial chemical oxygen demand



two different chemical oxygen demand equivalent concentrations, namely, 300 mg O_2/L and 900 mg O_2/L . The obtained results were comparatively presented in Fig. 13.6 and Fig. 13.7.

As can be seen in Fig. 13.6, there is no such difference between the degrees of degradation of the studied antibiotics according to their initial concentration in the solution, even if the second concentration is three times higher than the first one. These results indicate a very good photocatalytic activity of the TiO_2 /sisal fiber membrane and the possibility to use it even for high concentration of these types of antibiotics in the solution. On the contrary, it seems that there is some difference in

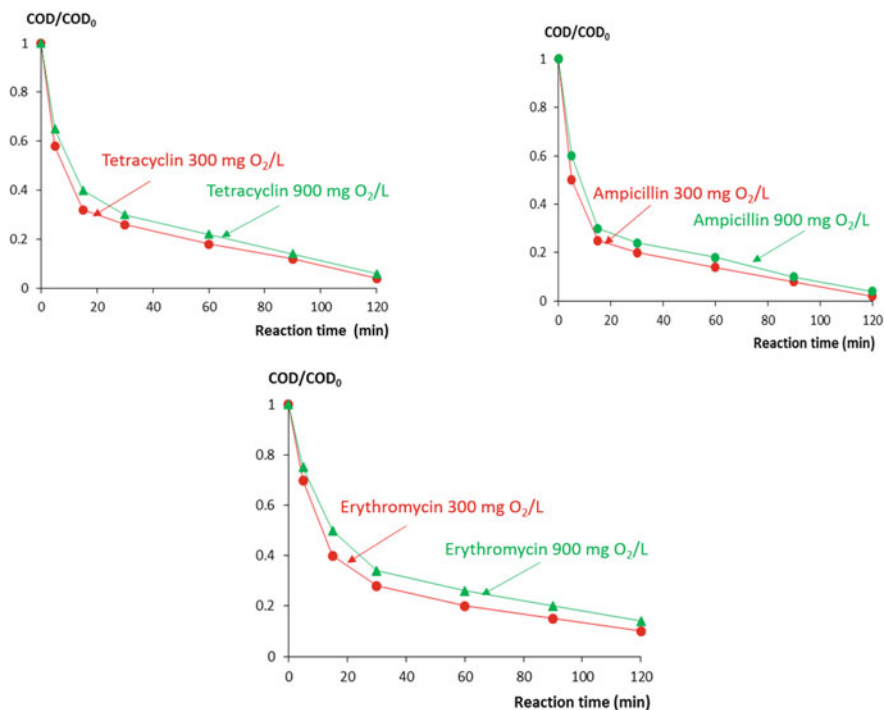


Fig. 13.6 Photocatalytic degradation of studied antibiotics as a function of their chemical oxygen demand equivalent concentration in the initial solution. Note that there is no noticeable difference in photocatalytic degradation efficiency for the two concentrations of antibiotics, regardless of the antibiotic used. The results highlight the photocatalytic potential of the new photocatalytic TiO₂/sisal fiber membrane used. COD, chemical oxygen demand at reaction time t ; COD₀, initial chemical oxygen demand

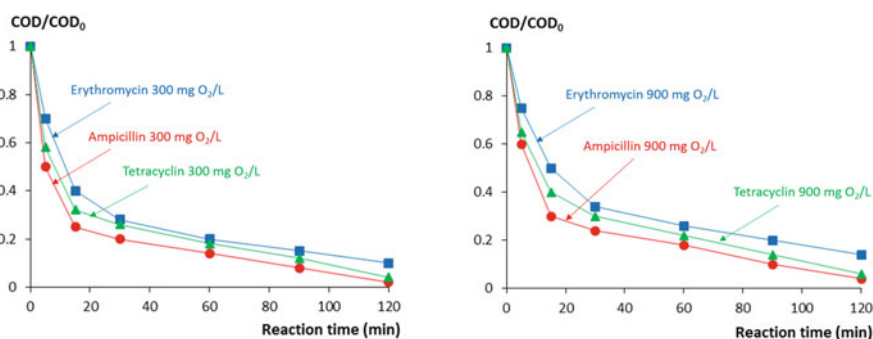


Fig. 13.7 Comparative photocatalytic degradation of the three types of studied antibiotics. Note that erythromycin shows a lower rate of degradation than the other two antibiotics studied. The lower rate of degradation is most likely due to the complex structure and much higher molecular weight of erythromycin compared to ampicillin and tetracycline. COD, chemical oxygen demand at reaction time t ; COD₀, initial chemical oxygen demand

the degree of degradation depending on the type of antibiotic. Regarding the degree of degradation depending on the type of antibiotic presented in Fig. 13.7, ampicillin and tetracycline show after 120 minutes of reaction approximately the same degree of degradation, but, for the same reaction time, the degree of degradation of erythromycin is slightly lower. In this respect, after 120 minutes, the degree of degradation for ampicillin is 98% for 300 mg O₂/L and 96% for 900 mg O₂/L, for tetracycline is 95% for 300 mg O₂/L and 96% for 900 mg O₂/L, and for erythromycin is 90% for 300 mg O₂/L and 86% for 900 mg O₂/L.

The experimental results also revealed that the overall oxidation process follows two successive stages. Thus, in the first stage, which is represented by the interval of 0–15 minutes of reaction, the oxidation of the antibiotics takes place with a high reaction rate, being minimum in the case of erythromycin, for which an oxidation degree of 60% for 300 mg O₂/L and 50% for 900 mg O₂/L was obtained. In the second stage, which is represented by the interval of 15–120 minutes of reaction, the reaction rate is much lower. This behavior can be attributed to organic intermediates formed as a result of the oxidation, which are more resistant, especially in the final phase of the oxidation process. In general, it can be concluded that the degree of oxidation decreases in the following order: ampicillin>tetracycline>> erythromycin. This behavior can be explained by the fact that the latter has a more complex structure and a higher molecular mass as it was presented in Table 13.1. The examination of the membrane after the tests indicates a small deterioration of the sisal fiber substrate or the TiO₂ layer, the shape and general appearance remaining largely the same as the original support.

13.5 Conclusions

The advanced oxidation processes can be applied to remove a large spectrum of refractory compounds due to the high oxidation potential they have. The oxidation potential can be considerably intensified by various combinations between oxidants and catalysts. One of the promising emerging advanced oxidation process technologies that can be effectively used for industrial applications, including wastewater treatment, is photocatalysis. Choosing the right photocatalyst as well as establishing optimal working conditions can lead to the achievement of high degradation efficiencies of refractory organic contaminants from wastewater.

The experimental results obtained in this work on the photocatalytic degradation of refractory compounds from the class of chlorophenols and antibiotics have highlighted that the degradation rate of 4-chlorophenol is higher than that of 2,4-dichlorophenol. It is also revealed that, in the case of photocatalytic degradation of the antibiotics, the degree of oxidation decreases in the following order: ampicillin > tetracycline >> erythromycin. The rate of the photocatalytic oxidation process of both 4-chlorophenol and 2,4-dichlorophenol is higher for the cobalt (Co)-doped TiO₂/polymer membrane than that of TiO₂/Ti. The new obtained TiO₂/sisal fiber

membrane showed that it has a high photocatalytic activity, obtaining almost complete mineralization of the antibiotics studied in only 2 hours of irradiation.

Acknowledgments Authors recognize the financial support from R&D Team Leader of B.I.T. s.r.l., Milan (Italy), and of Professor Ignazio Renato Bellobono, who generously offered the testing installation.

References

- Ahmed S, Rasul MG, Martens WN, Brown R, Hashib MA (2010) Heterogeneous photocatalytic degradation of phenols in wastewater: a review on current status and developments. *Desalination* 261:3–18. <https://doi.org/10.1016/j.desal.2010.04.062>
- Alaton IA, Dogruel S, Baykal E, Gerone G (2004) Combined chemical and biological oxidation of penicillin formulation effluent. *J Environ Manag* 73:155–163. <https://doi.org/10.1016/j.jenvman.2004.06.007>
- Alexy R, Kumpel T, Kümmerer K (2004) Assessment of degradation of 18 antibiotics in the closed bottle test. *Chemosphere* 57:505–512. <https://doi.org/10.1016/j.chemosphere.2004.06.024>
- Andreozzi R, Caprio V, Insola A, Marotta R (1999) Advanced oxidation processes (AOP) for water purification and recovery. *Catal Today* 53:51–59. [https://doi.org/10.1016/S0920-5861\(99\)00102-9](https://doi.org/10.1016/S0920-5861(99)00102-9)
- Argurio P, Fontananova E, Molinari R, Drioli E (2018) Photocatalytic membranes in photocatalytic membrane reactors. *Processes* 6:162. <https://doi.org/10.3390/pr6090162>
- Benitez FJ, Beltran-Heredia J, Acero JL, Rubio FJ (1999) Chemical decomposition of 2,4,6-trichlorophenol by ozone, Fenton's reagent, and UV radiation. *Ind Eng Chem Res* 38:1341–1349. <https://doi.org/10.1021/ie980441f>
- Borghi AA, Silva MF, Al Arni S, Converti A, Palma MSA (2015) Doxycycline degradation by the oxidative Fenton process. *J Chem*. <https://doi.org/10.1155/2015/492030>
- Bossmann SH, Oliveros E, Göb S, Siegwart S, Dahlen EP, Payawan L, Straub M, Wörner M, Braun AM (1998) New evidence against hydroxyl radicals as reactive intermediates in the thermal and photochemically enhanced Fenton reactions. *Chem A Eur J* 102:5542–5550. <https://doi.org/10.1021/jp980129j>
- Bound JP, Voulvoulis N (2004) Pharmaceuticals in the aquatic environment - a comparison of risk assessment strategies. *Chemosphere* 56:1143–1155. <https://doi.org/10.1016/j.chemosphere.2004.05.010>
- Byrne C, Subramanian G, Pillai SC (2018) Recent advances in photocatalysis for environmental applications. *J Environ Chem Eng* 6:3531–3555. <https://doi.org/10.1016/j.jece.2017.07.080>
- de Luna MDG, Briones RM, Su C-C, Lu M-C (2013) Kinetics of acetaminophen degradation by Fenton oxidation in a fluidized-bed reactor. *Chemosphere* 90:1444–1448. <https://doi.org/10.1016/j.chemosphere.2012.09.003>
- de Oliveira D, Martini William S, Santos Mellina DR, Matos Maria Auxiliadora C, da Rocha Lilian L (2015) Caffeine oxidation in water by Fenton and Fenton-like processes: effects of inorganic anions and ecotoxicological evaluation on aquatic organisms. *J Braz Chem Soc* 26(1):178–184. <https://doi.org/10.5935/0103-5053.20140237>
- Dodson LG, Vogt RA, Marks J, Reichardt C, Crespo-Hernández CE (2011) Photophysical and photochemical properties of the pharmaceutical compound salbutamol in aqueous solutions. *Chemosphere* 83:1513–1523. <https://doi.org/10.1016/j.chemosphere.2011.01.048>
- Ferreira GF, Maniero MG, Guimarães JRC (2015) Degradation of sucralose by peroxidation assisted with ultraviolet radiation and photo-Fenton. *Int J Eng Technol* 7:438–444. <https://doi.org/10.7763/IJET.2015.V7.833>

- Grzechulska-Damszel J (2009) Removal of organic impurities from water using a reactor with photoactive refill. *Int J Photoenergy* 9:1–6. <https://doi.org/10.1155/2009/304712>
- Hanel A, Moren P, Zaleska A, Hupka J (2010) Photocatalytic activity of TiO₂ immobilized on glass beads. *Physicochem Problems Mineral Proces* 45:49–56
- Herney-Ramirez J, Vicente MA, Madeira LM (2010) Heterogeneous photo-Fenton oxidation with pillared clay-based catalysts for wastewater treatment: a review. *Appl Catal B Environ* 98:10–26. <https://doi.org/10.1016/j.apcatb.2010.05.004>
- Kaniou S, Pitarakis K, Barlagianni I, Poullos I (2005) Photocatalytic oxidation of sulfamethazine. *Chemosphere* 60:372–380. <https://doi.org/10.1016/j.chemosphere.2004.11.069>
- Klavarioti M, Mantzavinou D, Kassinos D (2009) Removal of residual pharmaceuticals from aqueous systems by advanced oxidation processes. *Environ Int* 35:402–417. <https://doi.org/10.1016/j.envint.2008.07.009>
- Kümmerer K (2009a) Antibiotics in the aquatic environment – a review – part I. *Chemosphere* 75:417–434. <https://doi.org/10.1016/j.chemosphere.2008.11.086>
- Kümmerer K (2009b) Antibiotics in the aquatic environment – a review – part II. *Chemosphere* 75:435–441. <https://doi.org/10.1016/j.chemosphere.2008.12.006>
- Li JH, Xu YY, Zhu LP, Wang JH, Du CH (2009) Fabrication and characterization of a novel TiO₂ nanoparticle self-assembly membrane with improved fouling resistance. *J Membr Sci* 326:659–666. <https://doi.org/10.1016/j.memsci.2008.10.049>
- Lim LLP, Lynch RJ, In SI (2009) Comparison of simple and economical photocatalyst immobilisation procedures. *Appl Catal A Gen* 365:214–221. <https://doi.org/10.1016/j.apcata.2009.06.015>
- Teik-Thye L, Ron G (2016) Combined photocatalysis – Separation processes for water treatment using hybrid photocatalytic membrane reactors. In: Dionysiou DD, Puma GL, Ye J, Schneider J, Bahnemann D (eds) *Photocatalysis: applications*, RSC Energy and Environmental Series No. 15. Royal Society of Chemistry, Cambridge
- Lofrano G, Rizzo L, Grassi M, Belgiorno V (2009) Advanced oxidation of catechol: a comparison among photocatalysis, Fenton and photo-Fenton processes. *Desalination* 249:878–883. <https://doi.org/10.1016/j.desal.2009.02.068>
- Manenti DR, Soares PA, Módenes AN, Espinoza-Quiñones FR, Boaventura RAR, Bergamasco R, Vilar VJP (2015) Insights into solar photo-Fenton process using iron(III)–organic ligand complexes applied to real textile wastewater treatment. *Chem Eng J* 266:203–212. <https://doi.org/10.1016/j.cej.2014.12.077>
- Mansourpanah Y, Madaeni SS, Rahimpour A, Farhadian A, Taheri AH (2009) Formation of appropriate sites on nanofiltration membrane surface for binding TiO₂ photo-catalyst: performance, characterization and fouling-resistant capability. *J Membr Sci* 330:297–306. <https://doi.org/10.1016/j.memsci.2009.01.001>
- Houria M, Mahfoud HM, Youcef T, Abdeltif A (2014) Physico-chemical characterization of industrial effluents from the town of Ouargla (south East Algeria). *Energy Procedia* 50:255–262. <https://doi.org/10.1016/j.egypro.2014.06.031>
- Michałowicz J, Duda W (2007) Phenols – sources and toxicity. *Pol J Environ Stud* 16:347–362
- Moza S (2010) Photocatalytic membrane reactors (PMRs) in water and wastewater treatment. A review. *Sep Purif Technol* 73:71–91. <https://doi.org/10.1016/j.seppur.2010.03.021>
- Muñoz I, Rieradevall J, Torrades F, Peral J, Domènech X (2006) Environmental assessment of different advanced oxidation processes applied to a bleaching Kraft mill effluent. *Chemosphere* 62:9–16. <https://doi.org/10.1016/j.chemosphere.2005.04.044>
- Munter R, Preis S, Kallas J, Trapido M, And Veressinina Y (2001) Advanced oxidation processes (AOPs): water treatment technology for the twenty-first century, *Kemia-Kemi*, vol 28, pp 354–362
- Omar ML, Alharbi, Basheer AA, Khattab RA, Ali I (2018) Health and environmental effects of persistent organic pollutants. *J Mol Liq* 263:442–453. <https://doi.org/10.1016/j.molliq.2018.05.029>

- Orbeci C, Nechifor G, Stanescu R (2014) Removing toxic compounds from wastewater. *Environ Eng Manag J* 13:2153–2158. <https://doi.org/10.30638/eemj.2014.238>
- Orbeci C, Modrojan C, Dancila AM (2016) Degradation of pharmaceutical effluents by photo-assisted techniques. *Rev Chim* 67:166–170
- Ortega-Gomez E, Ballesteros Martin MM, Carratala A, Fernandez Ibanez P, Sanchez Perez JA, Pulgarin C (2015) Principal parameters affecting virus inactivation by the solar photo-Fenton process at neutral pH and mu M concentrations of H₂O₂ and Fe²⁺/(³⁺). *Appl Catal B Environ* 174:395–402. <https://doi.org/10.1016/j.apcatb.2015.03.016>
- Ortiz de la Plata GB, Alfano OM, Cassano AE (2010) Decomposition of 2-chlorophenol employing goethite as Fenton catalyst. I. Proposal of a feasible, combined reaction scheme of heterogeneous and homogeneous reactions. *Appl Catal B Environ* 95:1–13. <https://doi.org/10.1016/j.apcatb.2009.12.005>
- Papić S, Vujević D, Koprivanac N, Šinko D (2009) Decolourization and mineralization of commercial reactive dyes by using homogeneous and heterogeneous Fenton and UV/Fenton processes. *J Hazard Mater* 164:1137–1145. <https://doi.org/10.1016/j.jhazmat.2008.09.008>
- Parida K, Mishra KG, Dash SK (2012) Adsorption of toxic metal ion Cr(VI) from aqueous state by TiO₂-MCM-41: equilibrium and kinetic studies. *J Hazard Mater* 241-242:395–403. <https://doi.org/10.1016/j.jhazmat.2012.09.052>
- Pera-Titus M, García-Molina V, Baños MA, Giménez J, Esplugas S (2004) Degradation of chlorophenols by means of advanced oxidation processes: a general review. *Appl Catal B Environ* 47:219–256. <https://doi.org/10.1016/j.apcatb.2003.09.010>
- Petrovic M, Radjenovic J, Barcelo D (2011) Advanced oxidation processes (AOPs) applied for wastewater and drinking water treatment. *Eliminat Pharm Holistic Appr Environ* 1:63–74
- Pignatello JJ, Oliveros E, MacKay A (2006) Advanced oxidation processes for organic contaminant destruction based on the Fenton reaction and related chemistry. *Crit Rev Environ Sci Technol* 36:1–84. <https://doi.org/10.1080/10643380500326564>
- Ramírez-Sosa DR, Castillo-Borges ER, Méndez-Novelo RI, Sauri-Riancho MR, Barceló-Quintal M, Marrufo-Gómez JM (2013) Determination of organic compounds in landfill leachates treated by Fenton-adsorption. *Waste Manag* 33:390–395. <https://doi.org/10.1016/j.wasman.2012.07.019>
- Rocha EMR, Mota FS, Boaventura RAR (2013) Comparative analysis of trace contaminants in leachates before and after a pre-oxidation using a solar photo-Fenton reaction. *Environ Sci Pollut Res* 20:5994–6006. <https://doi.org/10.1007/s11356-013-1608-y>
- Rozas O, Contreras D, Mondaca MA, Pérez-Moya M, Mansilla HD (2010) Experimental design of Fenton and photo-Fenton reactions for the treatment of ampicillin solutions. *J Hazard Mater* 177:1025–1030. <https://doi.org/10.1016/j.jhazmat.2010.01.023>
- Simion VA, Cretescu I, Lutic D, Luca C, Poullos I (2015) Enhancing the Fenton process by UV light applied in textile wastewater treatment. *Environ Eng Manag J* 14:595–600. <https://doi.org/10.30638/eemj.2015.065>
- Sun Y, Pignatello JJ (1973) Photochemical reactions involved in the total mineralization of 2,4-D by Fe³⁺/H₂O₂/UV. *Environ Sci Technol* 7(2):304–310. <https://doi.org/10.1021/es00039a010>
- U.S (2002) Environmental Protection Agency (USEPA), Toxicological review of phenol (CAS no. 108-95-2) in support of summary information on the Integrated Risk Information System (IRIS). In: MA Barron (Ed.), Washington, DC.
- U.S (1982) Environmental Protection Agency (USEPA), Exposure and Risk Assessment For Chlorinated Phenols
- Uteua I, Orbeci C, Tudorache E (2006) Oxidative degradation of 4-chlorophenol from aqueous solution by photo-Fenton advanced oxidation process. *Environ Eng Manag J* 5:661–674. <https://doi.org/10.30638/eemj.2006.053>
- von Stackelberg K (2013) A systematic review of carcinogenic outcomes and potential mechanisms from exposure to 2,4-D and MCPA in the environment. *J Toxicol*:371610. <https://doi.org/10.1155/2013/371610>

- Wang H, Wang J (2007) Electrochemical degradation of 4-chlorophenol using a novel Pd/C gas-diffusion electrode. *Appl Catal B Environ* 77:58–65. <https://doi.org/10.1016/j.apcatb.2007.07.004>
- Wei XN, Wang HL, Li ZD, Huang ZQ, Qi HP, Jiang WF (2016) Fabrication of the novel core-shell MCM-41@mTiO₂ composite microspheres with large specific surface area for enhanced photocatalytic degradation of dinitro butyl phenol (DNBP). *Appl Surf Sci* 372:108–115. <https://doi.org/10.1016/j.apsusc.2016.03.047>
- White GC (1992) Chlorine Dioxide. In: White GC (ed) *White's handbook of chlorination and alternative disinfectants*, Wiley. Van Nostrand Reinhold, New York, pp 980–1045
- Wick A, Fink G, Joss A, Siegrist H, Ternes TA (2009) Fate of beta blockers and psycho-active drugs in conventional wastewater treatment. *Water Res* 43:1060–1074. <https://doi.org/10.1016/j.watres.2008.11.031>
- Yadav M, Gupta R, Kumar SR (2019) Chapter 14 - green and sustainable pathways for wastewater purification. In: *Advances in water purification techniques, meeting the needs of developed and developing countries*, pp 355–383. <https://doi.org/10.1016/B978-0-12-814790-0.00014-4>
- Ye C, Zhou Q, Wang X, Xiao J (2007) Determination of phenols in environmental water samples by ionic liquid-based headspace liquid-phase microextraction coupled with high-performance liquid chromatography. *J Sep Sci* 30:42–47. <https://doi.org/10.1002/jssc.200600256>
- Zanjanchi MA, Golmojeh H, Arvand M (2009) Enhanced adsorptive and photocatalytic achievements in removal of methylene blue by incorporating tungstophosphoric acid–TiO₂ into MCM-41. *J Hazard Mater* 169:233–239. <https://doi.org/10.1016/j.jhazmat.2009.03.080>

Index

A

Aazam, E., 31
Abe, R., 346
Advanced oxidation processes (AOP), vi, 2, 19,
21, 139, 148, 149, 189–210, 217, 283,
362, 370–373, 381, 412, 414–417, 425
Ahirwar, S., 88, 89
Ahmadi, A., 233
Ahmed, A.A.A., 231
Ahmed, I., 285
Ahunbay, M.G., 273
Al-Anbari, R., 127
Alawa, B., 189–210
Albanis, T.A., 125, 128
Alfaifi, B.Y., 338
Ali, T.T., 32
Amaechi, I.C., 32
Ambaye, T.G., vi, 215–235
Anandan, S., 64
Anirudhan, T.S., 31
Anjali, G., 370
An, L., 32
An, T., 227, 342
Antibiotics, vii, 15, 17, 26, 54, 64, 70, 104–106,
411–426
Archana, V., 397
Archer, R., 18
Ates Genceli, E., 372
Aydoghmish, S.M., 32
Ayekoe, P.Y., 32

Azo dye, vi, 25, 27, 32, 34, 36, 102, 119–140,
169, 170, 176, 204, 207, 209, 324, 364,
365, 392, 399, 400, 402, 412

B

Babar, S., 59, 60
Bacterial disinfection, 56, 217, 219–235
Bagheri, M., 133
Bahnemann, D., 379
Bai, H., 220
Bai, Y., 343
Bajpai, D., 368
Balasubramanian, S., 247–275
Balta, Z., 32
Balu, S., 60, 61, 132
Bao, L., 88
Bao, Y., 65, 68, 343
Barnes, R.J., 219
Barrera-Mota, K., 344
Barrera-Salgado, K.E., 285
Basu, S., 32
Bayahia, H., 338
Behnjady, M.A., 159, 169
Beydoun, D., 301
Bhagat, P.R., 391–406
Bhatia, V., 30
Bi-compounds, 334–340, 343, 348
Bobiric, L., 411–426
Bobirică, C., 411–426

Bodson, C.F., 32
 Bokare, A.D., 285
 Boutamine, Z., 163, 179

C

Carbonaceous nanocomposites, 106, 107, 135, 139
 Carbon quantum dots, vi, 81–107
 Cavitation, vi, 149, 150, 152, 154, 170–172, 176, 179, 180, 191–198, 201, 208, 210
 Chadi, N.E., 164
 Chae, S., 301
 Chahkandi, M., vi, vii, 283–309, 321–349
 Chakma, S., vi, 189–210
 Chandra, R., 364
 Chang, P.Y., 65–67
 Channei, D., 33
 Chatchai, P., 31
 Chatel, G., 179
 Chen, C.Y., 127
 Chen, F., 31, 33
 Chen, J., 64
 Chen, K., 65, 68, 343
 Chen, L., 285
 Chen, W., 93
 Chen, X., 298
 Chen, Y., 17, 18, 31, 32
 Cheng, B.Y., 348
 Cheng, L., 298
 Choi, W., 285
 Christensen, P., 217
 Chuangchote, S., vi, 2–40
 Costa, C.R., 372
 Costa, D.J., 31
 Cuéllar, E.L., 331, 344
 Cuprous oxide (Cu₂O), 9, 63–71, 92, 93, 297, 299, 300, 324, 348
 Czech, B., 30

D

Dalhatou, S., 165, 173
 Dang, X., 342
 De Gisi, S., 369
 Degradation, 4, 55, 82, 120, 149, 190, 217, 263, 285, 322, 362, 398, 414
 Deng, F., 102
 Deng, J., 90, 228, 229
 Devi, N.R., 89
 Dhir, A., 30
 Di, J., 104
 Di Iaconi, C., 373

Di Mauro, A., 33
 Djaja, N.F., 32
 Dogruel, S., 372
 Dong, G., 348
 Dong, X., 106
 Dong, Y., 88
 Dowla, B.M.R.U., 33
 Du, M., 32
 Dükkancı, M., 161
 Duonghong, D., 298

E

Electrically driven, 248, 251, 256
 Electrolysis, 248, 251, 255, 257–259, 262, 266, 267, 274
 Elhalil, A., 30
 Entezari, M.H., 285, 304, 305, 337, 339, 344
 Environmental impact, 382
 Eren, Z., 160, 169
 Espinoza-Quiñones, F.R., 372

F

Fahimirad, B., 134
 Fan, L., 341, 342
 Fang, T., 31
 Fassi, S., 163
 Feng, C., 102
 Feng, H., 344
 Feng, J., 60
 Fenton, 5, 6, 24, 25, 177, 190, 191, 200–204, 210, 285, 308, 370, 372, 373, 414, 415
 Fe₂O₃, 31, 33, 35, 36, 58–63, 70, 71, 106, 125, 130, 132–134, 296, 300, 323, 417
 Ferkous, H., 162, 169, 176
 Ferreir, A.M., 399
 Ferrioxalate, 192, 202, 204
 Forward osmosis, vi, 248, 251, 255, 256, 259, 260, 262, 272, 274, 275
 Francony, A., 156
 Fuerhacker, M., 397
 Fujishima, A., 56
 Fujito, H., 348
 Functionalized ionic liquids, vii, 391–406

G

Gamshadzei, E., 63
 Gao, M., 301
 Ghasemian, S., 232
 Ghernaout, D., 231
 Ghodbane, H., 159, 169, 176

Ghows, N., 285
Gokul, P., 134
Gomez, J.J., 342, 348
Gong, A.S., 217
Gopalakrishnan, D., 90
Graphene quantum dots, 84, 90–93, 95, 97–99,
106, 107, 303
Graphitic carbon nitride (g-C₃N₄), 32, 56, 105,
130, 224, 292, 323, 417
Green technologies, 233
Grun, M., 88
Guelfi, D.R.V., 31
Gültekin, I., 176
Guo, A.J., 348
Guo, J., 344
Guo, W., 332
Guo, X., 99, 344
Guzman-Duque, F., 160

H

Habiba, K., 106
Hamdaoui, O., 147–180
Han, M., 342
Hao, H., 133
Hao, L., 342
Hao, M., 399
Hasija, V., 32, 53–71
Hayouni, S., 397
Heitmann, A.P., 32
Heterogeneous photocatalysis, vi, 2, 3, 7, 8, 10,
11, 24, 25, 27, 29–37, 39, 120, 285, 287,
288, 290, 308
Heterojunction, vi, vii, 57–60, 64–66, 68, 71,
86, 94, 95, 102, 103, 105, 129, 130, 133,
136, 218, 224, 225, 292, 297–301, 305,
323, 334, 339–347
Homem, V., 285
Hosseini-Sarvari, M., 297
Houshyar, Z., 373
Hsieh, S.H., 348
Hu, C., 229
Hu, T., 343
Hu, W., 105
Hu, X.Y., 30, 37
Hu, Y., 300
Huang, G., 227, 228
Huang, J., 224
Huang, W.L., 327
Huang, Y., 342
Huo, Y., 345
Hybrid membrane processes, 370

Hydroxyl radical, 4–6, 9–12, 25, 55, 64, 83,
103, 125, 133, 134, 149, 151, 155, 167,
168, 170, 173, 175, 177, 178, 217, 218,
228, 230, 232, 285, 323, 375, 415, 422

I

Ibrahim, I.M., 129
Ievskaya, Y., 64
Imae, T., 95
Ince, N.H., 157, 158, 160, 169
Induja, M., 65, 66
Industrial wastewater, 4, 120, 200, 234, 267,
375, 381, 412
Inoue, M., 170
Intaphong, P., 344
Ion-exchangeable semiconductors, 301–304
Islam, M.K., 380
Iwase, A., 348

J

Jagannatha, R.B., 30
Jaiswal, A.K., 391–406
Jeong, S.Y., 345
Jia, T., 344
Jia, Y., 228
Jiang, R., 343
Jiang, Y., 156
Jing, L., 343
Jonjana, S., 342
Joseph, J.M., 157
Joshi, B., 348
Journet, C., 88

K

Kadirova, Z.C., 33
Kamat, P.V., 133
Kang, M., 298
Kang, Y., 298, 342
Kanwal, M., 31
Kapitonov, A.N., 95
Kapoor, A., vi, 247–275
Kavitha, E., 247–275
Ke, J., 103, 348
Keerthi, S.V., 370
Kemacheevakul, P., vi, 2–40
Khairy, M., 32
Khajone, V.B., 391–406
Khan, L., 348
Kharazi, P., 405

- Khare, N., 344
Khavar, A.H.C., 31
Khodam, F., 304
Kim, H., 348
Kim, I., 17, 18
Kim, I.S., 368
Kim, J.W., 301
Kongjao, S., 372
Konstantinou, I.K., 125, 128
Koohgard, M., 297, 298
Kovacova, M., 106
Kucharska, M.A., 373
Kumar, A., 58
Kumar, S., 306, 391–406
Kundu, S., 98
Kurt, U., 372
- L**
Lachheb, H., 128
Lai, C.W., 88
La Motta, E.J., 233
Larson, S., 348
Leather industries, 13, 14, 62, 121, 265, 364, 365
Lee, K.S., 300, 303
Le Marechel, A.M., 170
Lewis, K., 18
Li, G., 225
Li, H., 92, 93, 102, 106
Li, J., 285, 297, 298, 344
Li, L., 219
Li, Q., 219
Li, R., 300, 342, 345
Li, X., 59, 323, 324
Li, Y., 219
Li, Z., 306, 344
Liang, J., 228, 229
Liang, Q., 343
Liang, Y., 88, 345
Lin, L., 30
Lin, X., 343
Lins, T., 372
Liquid membrane, 250, 255, 269–271
Liu, B., 62, 65, 217, 305
Liu, F., 91
Liu, J., 106
Liu, Q., 221, 225
Liu, R., 88, 99, 100
Liu, S., 343
Liu, X., 342
Liu, Y., 30, 61, 69
Louangsouphom, B., 32
- Lucas, M., 369
Luo, J., 272
Lv, Y., 344
- M**
Ma, C.Y., 170
Ma, X., 306
Ma, Z., 343
Maeda, K., 300
Mahanthappa, M., 32
Mahjoub, A.R., 133
Mahmoodi, N.M., 137
Majcen-Le-Marechal, A., 157
Malato, S., 378
Malefane, M.E., 32
Man, Y., 344
Mandal, S., 130
Manga Raju, I., 31
Manivel, A., 127
Mant, C., 367
Mark, G., 170
Marugán, J., 229
Mathew, S., 137
Mathews, C., 397
Matsunaga, T., 217
Mbiri, A., 31
Mechanistic aspects, 292–306
Mehta, V.N., 95
Membrane, 16, 54, 90, 120, 190, 218, 249, 347, 369, 392, 417
Membrane bioreactors, 248, 252, 262, 269, 270, 369, 370
Membrane solvent extraction, 252, 255, 262, 269–271
Meng, P., 300
Meng, X., 325
Mera, A.C., 344
Merouani, S., vi, 147–180
Metal oxide, vi, 8, 9, 27, 29, 34, 36, 37, 39, 53–71, 83, 90, 106, 120, 125, 129, 134–136, 206, 217, 223, 228, 286, 292, 294–297, 307, 308
Mi, Y., 342
Milojevic-Raki, M., 61
Min, Z., 68, 69
Minero, C., 158
Mirhoseini, F., 33
Mirmasoomi, S.R., 31
Módenes, A.N., 373
Moholkar, V.S., 194, 198, 203
Monga, D., 32
Moniz, S.J.A., 348

- Morales-Torres, S., 137
Morphology, vii, 56, 61–63, 66, 95, 101, 104, 128, 132, 218, 219, 224, 233, 235, 292, 325, 328–330, 332, 334, 336–338, 345, 347
Moumeni, O., 161, 175
Muñoz-Batista, M.J., 220
- N**
Naciri, Y., 32
Naik, B., 348
Nanocomposites, 31–33, 35, 36, 58–60, 62, 64, 65, 71, 86, 96, 102–107, 121, 129–137, 139, 219, 323, 343, 347
Nanofiltration, 251, 255–258, 262, 266, 268, 272–274
Nanomaterials, vi, 25, 84–86, 89, 94, 106, 107, 215–235, 283–309, 334, 345–347
Narayanan, S., vii, 359–382
Naumczyk, J.H., 373
Ni, M., 342
Nie, X., 222
Niu, F., 342, 344
Non-porous, 250–252, 256
Noorjahan, C.M., 368
- O**
Okitsu, K., 162, 172
Onyancha, D., 368
Opoku, F., 285
Orbeci, C., vii, 411–426
Organic dyes, vii, 3, 13, 19–23, 25, 27, 29, 30, 32, 34, 36–39, 120, 398–405
Organic pollutants, vi, 1–39, 54, 66, 104, 105, 149, 151, 191, 192, 198, 201, 217, 219–221, 227, 230, 232–234, 285, 297, 303, 307, 324, 362, 364, 373–376, 378, 394, 397, 406, 415
Oudghiri-Hassani, H., 344
Ozonation, 4, 5, 7, 14, 16, 23–25, 39, 127, 190, 217, 230, 285, 370
- P**
Pan, D., 31, 93, 99
Pan, J., 86
Pant, B., 60, 62, 63
Paquin, F., 348
Park, H., 399
Park, J.W., 298
Park, S.Y., 92, 94
Patil, S.M., 134
Patle, D.S., vii, 391–406
Paula, C.H.R., 32
Pei, Y.C., 399
Peng, B., 348
Peng, J., 91
Peng, X., 226
Persistent organic pollutants (POP), vi, 3, 12, 19–21, 24, 26, 28, 30, 31, 33, 35, 37–39
Personal care products (PPCP), vi, 3, 12, 13, 15–18, 23, 24, 26, 28, 30, 33, 35, 37–39
Petrella, A., 138
Pétrier, C., 156, 163
Photocatalysis, 3, 55, 83, 120, 167, 190, 217, 285, 322, 362, 399, 416
Photocatalyst, 3, 55, 82, 120, 206, 217, 285, 322, 371, 405, 417
Photocatalytic oxidation, vii, 34, 125, 219, 222
Photocatalytic reactor, vii, 3, 38, 39, 347, 377–382
Photodegradation, vi, vii, 27, 36, 55, 56, 58, 60–62, 64, 66, 102–105, 107, 125–128, 130, 132–140, 285, 287, 288, 297, 303–305, 326–328, 362, 376, 391–406
Photolysis, 3, 4, 9, 190–192, 198–200, 210, 285, 308, 414, 415
Phuong, N.M., 31
Phuruangrat, A., 344
Pillai, V.K., 90
Pilli, S.R., 397
P-N heterojunctions, 65, 68, 297, 301
Point of use device, 248
Pollutant load, 363
Polymer supported ionic liquid iron porphyrin, 401, 402
Poonguzhali, E., 247–275
Porous, 31, 35–37, 56, 58, 61, 64, 65, 71, 102, 104, 224, 248, 250–254, 256, 258, 261, 269, 296, 327
Posa, V.R., 136
Prabhakar, S., 247–275
Prasad, M.N.V., 18
Prasanna, A., 95
Preethi, V., 372
Pressure driven, 251, 256–258, 262, 268
Process intensification, 176–180
- Q**
Qi, L., 399
Qin, X., 88
- R**
Raizada, P., vi, 53–71, 82–107, 119–140
Ramawami, S., 274
Ran, R., 344

- Rani, B.J., 348
 Rasoulnezhad, H., 31
 Rath, P.C., 69
 Ratova, M., 344
 Rauf, A., 348
 Ravidhas, C., 345
 Ravishankar, T.N., 32, 399
 Rayaroth, M.P., 161, 170
 Reddy, P.V.L., 228
 Refractory organic contaminants, 425
 Rehorek, A., 158
 Remediation, vi, 1–39, 53–71, 219, 229, 275, 283–309, 321–349
 Ren, B., 60
 Reverse osmosis, 21, 148, 248, 249, 251, 254–259, 261–268, 272–276, 369
 Rivera-Utrilla, J., 285
 Rodríguez, C.B., 399
 Rosu, M.C., 137
- S**
- Sabumon, P.C., 370
 Sahoo, D.P., 306
 Saini, A., 82–107
 Saini, R., 82–107
 Sajjadi, S., 31
 Salabat, A., 33
 Saleem, S., 397
 Saleh, R., 32
 Sanchez, L., 221
 Santhosh, C., 58
 Santos, L., 285
 Sarkar, P., 274
 Sarkar, S., 88, 95
 Sauer, T.P., 372
 Scholz, W., 369
 Schrank, S.G., 372
 Sehati, S., 304
 Senthil, R.A., 32
 Sergi, D., 397
 Serpone, N., 167
 Shakoori, A.R., 368
 Shandilya, P., vi, 82–107, 119–140
 Sharma, S., 55, 344
 Shen, G., 305
 Shen, T., 94
 Shetty, R., 30
 Shinde, D.B., 90
 Shi, S., 298
 Shi, X., 343
 Shin, Y., 98
 Singh, P., 53–71, 82–107, 119–140
- Singla, R., 159
 Sivagami, K., 373
 Sivakumar, V., 344
 Size enhanced ultrafiltration, 268, 269, 275
 Solar-light, 26, 29, 33, 38, 55, 56, 70, 82, 86, 96, 104, 105, 125, 127–129, 132, 133, 138, 206, 304, 305, 307, 329–331, 333, 335, 337, 339, 345–347, 362
 Solar photocatalysis, 359–382
 Soltani, T., 344
 Song, L., 342
 Song, Z., 366
 Sonolysis, 149, 150, 161, 166, 178, 191–196, 198, 205, 207–210
 Sonoreactors, 180
 Spasiano, D., 301, 374, 379
 Srivastava, S., 368
 Stephenson, J., 348
 Sudhaik, A., 82–107
 Sudrajat, H., 68, 70
 Sun, F., 32
 Sun, H., 227
 Sun, L., 227
 Sun, M., 304
 Sun, Y.P., 86, 89
 Sundarapandiyani, S., 372
 Suslick, K.S., 152
 Synthetic dyes, 19, 121, 155, 171–173
- T**
- Taamallah, A., 162, 168, 176
 Tabasideh, S., 31
 Takashima, T., 306
 Tang, C., 344
 Tang, L., 97, 300
 Tannery wastewater, 362, 364–373, 381
 Tezcanli-Guyer, G., 157, 158
 Thabit, M., 33
 Thakur, V.K., 53–71
 Thakuret, I.S., 368
 Theerthagiri, J., 62
 Tian, Y., 65, 66, 68
 Tripathi, A., vii, 359–382
 Tseng, I., 65, 67
 Tyszczyk-Rotko, K., 30
- U**
- Ultrafiltration, 231, 251, 254–258, 261, 262, 265, 268–270, 273, 275
 Ultrasound, vi, 149, 153–155, 157–159, 161, 163–165, 169, 170, 172, 174, 175, 178–

180, 191, 192, 195–197, 199, 204, 207,
209, 308, 334
Umrao, S., 98
Upadhyay, P., 189–210
Up-conversion, vi, 86, 92, 96, 102–105, 107

V

Vaccari, M., 215–235
Vaiano, V., 30
Vajnhandl, S., 170
Valappil, M.O., 90
van der Bruggen, B., 258
van Hullebusch, E.D., 215–235
Vankar, P., 368
Venkatesan, R., 338, 345
Vinodgopal, K., 133
Voncina, D.B., 157

W

Wang, A., 159
Wang, B., 342
Wang, C., 292
Wang, F., 88, 100, 101, 105
Wang, H., 139
Wang, J., 59, 104
Wang, K., 226, 342
Wang, L., 32, 303
Wang, N., 61
Wang, S., 59, 222, 300
Wang, W., 217, 224, 225, 227
Wang, W.J., 218
Wang, X., 61
Wang, Y., 95, 343–345
Wastewater, 4, 59, 120, 148, 190, 217, 248,
347, 360, 392, 412
Wastewater treatment, v, vi, 4, 6, 21, 38, 39, 59,
120, 134, 149, 190, 210, 230, 233, 251,
253, 255, 259, 261–263, 265, 267, 269,
271–275, 360, 362, 367, 368, 372, 373,
375, 378, 381, 382, 392, 393, 397, 412
Water purification, vi, 57, 64, 81–107, 137,
218, 268, 275
Water recovery and recycle, 265
Water splitting, vii, 56, 64, 259, 284–286, 292,
294–298, 300, 302, 305, 324, 325, 328,
329, 331, 338, 345–348, 371
Wei, C., 219
Wei, Y., 31, 304
Weidong, H., 344
Wen, F., 294
Wetchakun, N., 342

Wo, B., 348
Wu, D., 223
Wu, N., 222
Wu, S., 345
Wu, T., 233, 326, 344
Wu, Z., 130

X

Xia, D., 225
Xiao, J., 88
Xiaoxia, L.I.U., 345
Xie, Z., 105
Xin, Y., 304
Xing, J., 129
Xing, X., 233
Xiong, J., 327, 328, 342, 344
Xu, C., 298
Xu, D., 300
Xu, L., 60
Xu, P., 342
Xu, X., 86–88, 300
Xue, Y., 304

Y

Yan, L., 342
Yan, S., 59
Yan, T., 342
Yang, H., 222, 304
Yang, T., 285
Yang, W., 302
Yang, Y., 101, 306
Yang, Z., 88
Yao, G., 285
Ye, J., 304
Ye, L., 327
Yi, C., 30
Yi, X.H., 299
Ying, H., 348
Yu, H., 96
Yu, J., 340
Yu, K., 285
Yuan, S., 65
Yuan-Shan, W., 368
Yuxue Zhou, P.L., 344

Z

Zakaria, W., 32
Zargazi, M., vi, vii, 283–309, 321–349
Zhang, B.L.W., 344
Zhang, C., 330

- Zhang, J., 65, 343
Zhang, J.-J., 32
Zhang, K., 326, 344
Zhang, L., 329
Zhang, Q., 104
Zhang, W., 304
Zhang, X., 221
Zhang, Y., 65, 345
Zhang, Z., 104, 285, 325
Zhao, G.Q., 128
Zhao, H., 285, 305
Zhao, Y., 348
Zhu, H., 97
Zhu, J., 56
Zhu, Q., 327, 348
Zhu, R., 343
Zhu, Y., 88, 329
Zong, L., 332, 333
Z-scheme, 57, 61, 62, 68, 86, 104, 105, 125,
126, 130, 132, 133, 135, 225, 297–300,
305, 306, 340, 343
Z-scheme photocatalyst, 86, 104, 125
Zuo, P., 88
Zuo, S., 64, 66, 67